Materials Chemistry Principal Investigators' Meeting

DoubleTree by Hilton Gaithersburg and Virtual

August 6-8, 2024

Program and Abstracts

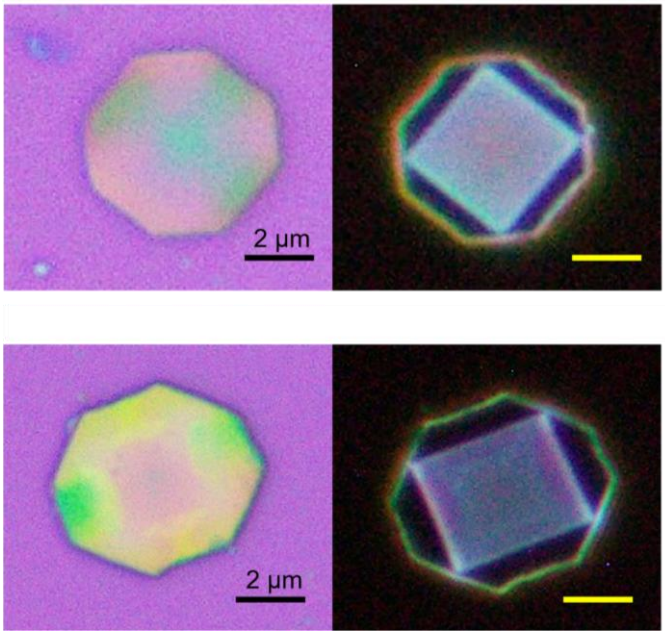

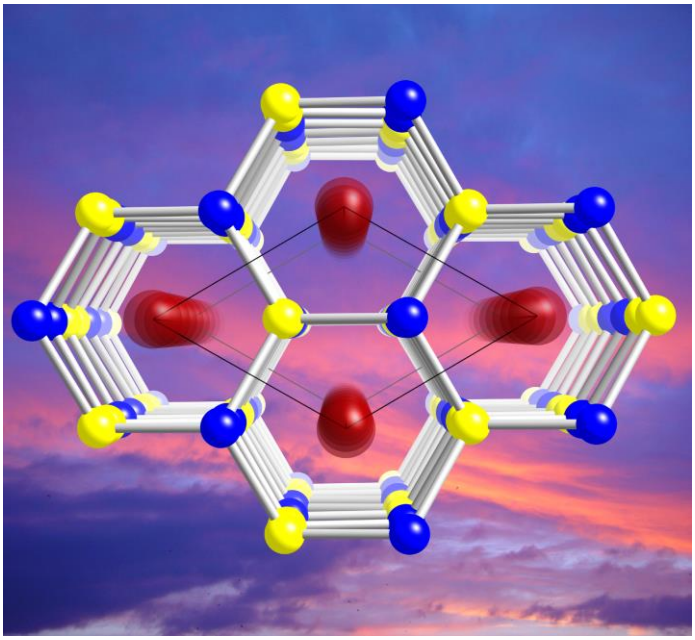

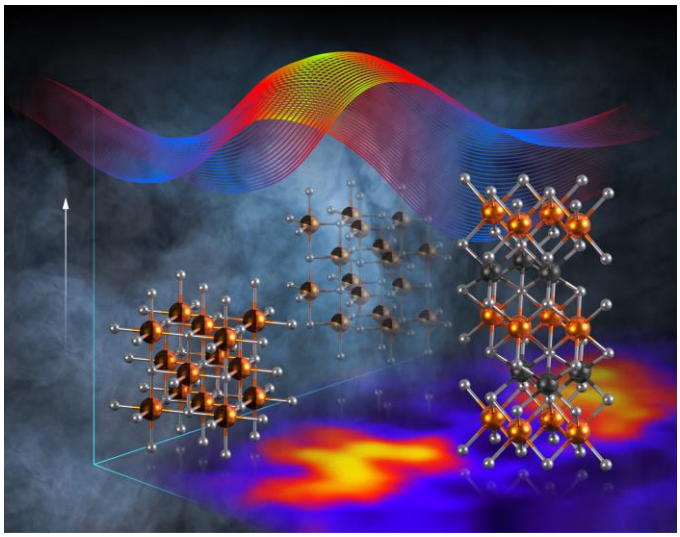

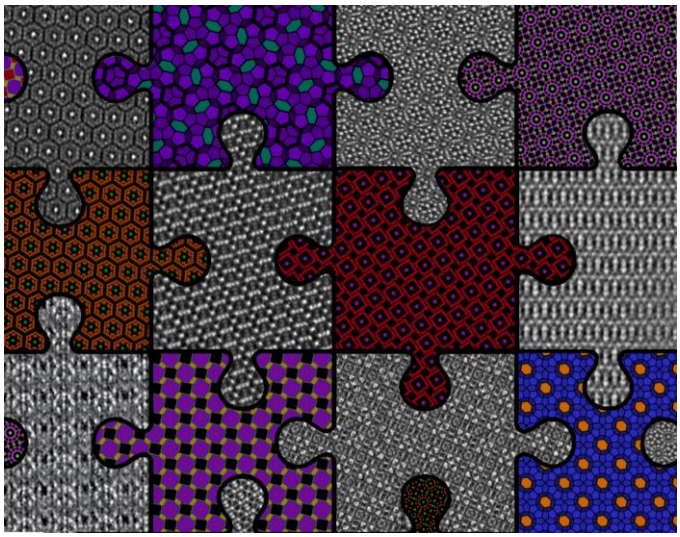

U.S. DEPARTMENT OF ENERGY | Office of Science

Office of Basic Energy Sciences
Materials Sciences and Engineering Division

On the Cover

Top Left: First demonstration of solution phase grown lead perovskite (Pb) – lead-free double perovskite (Na-Sb and Na-In) epitaxial lateral heterostructures. **Left**: optical microscope images; **Right**: photoluminescent images (under 375 nm UV excitation). Unique crystal growth mechanism of lead-free double perovskites was unveiled in this work.
Letian Dou, Purdue University

Top Right: Projection of the hexagonal crystal structure of the ternary bismuthide BaLiBi, established from single-crystal X-ray diffraction methods. In the structure of this compound, the Bi atoms (blue spheres) and Li atoms (yellow spheres) each form a hexagonal close packing array, with the Ba atoms (red spheres) occupying the available octahedral voids. In the absence of direct Bi–Bi bonding, the BaLiBi formula can be partitioned according to the fully-ionic approximation as $[Ba^{2+}][Li^{+}][Bi^{3-}]$, suggesting an electron-balanced composition. If the covalent character of the Bi–Li interactions is emphasized, as in the picture with the white cylinders connecting the two types of atoms, the chemical bonding can be rationalized as $Ba^{2+}(LiBi)^{2-}$, i.e., as layered Zintl phase.
Svilen Bobev, University of Delaware

Bottom Left: Artistic illustration of energy landscape for controlled synthesis of ternary magnesium tungsten nitrides. Thermodynamically stable layered 'rocksaline' structure, and two metastable cubic rocksalt and hexagonal BN-like structures have been synthesized at $MgWN_2$ composition using bulk and film methods. Polymorphic transformation between the rocksalt and 'rocksaline' polymorphs has been demonstrated using rapid thermal annealing.
Andriy Zakutayev, National Renewable Energy Laboratory

Bottom Right: Jigsaw puzzle of transmission electron microscopy TEM images and crystal structure models of predicted and discovered unconventional inorganic clathrates with T-Pn tetrahedral frameworks and A guest atoms, where A = Rb, Cs, Ba; T = Zn, Cd, Cu, Au; Pn = P, As, Sb, and related sodalite-type structures. Image credit: Frank Cerasoli (UC Davis), Oleg Lebedev (CNRS, France).
Davide Donadio, University of California, Davis

Foreword

This document is a collection of long abstracts for basic research projects that were included as either presentations or posters in the recent Principal Investigators' (PI) Meeting of the Materials Chemistry program, sponsored by the Materials Sciences and Engineering (MSE) division of Basic Energy Sciences (BES) in the U.S. Department of Energy's (DOE) Office of Science (DOE SC). The meeting took place August 6-8, 2024, in Gaithersburg, MD, as a primarily in-person meeting with a hybrid option for virtual participation. The return to in-person meetings following the global COVID-19 pandemic ended a four-year period (2020-2024) during which the biennial Materials Chemistry PI meeting was either cancelled (2020) or held entirely as a virtual meeting via the internet (2021, 2023). The use of a hybrid format with a virtual option allowed participation in the meeting by a few Principal Investigators who were unable to travel to the meeting site, and thus nearly all projects currently supported by the BES Materials Chemistry program were represented at the 2.5-day meeting.

This is one of a series of Principal Investigators' Meetings organized regularly by BES. The purpose of the meeting is to bring together all the Principal Investigators with currently active projects in the Materials Chemistry program for the multiple purposes of raising awareness among PIs of the overall program content and of each other's research, encouraging exchange of ideas, promoting collaboration and stimulating innovation. The meeting also provides the DOE Program Managers and MSE/BES management an opportunity to get a comprehensive overview of the program on a periodic basis and to identify program needs and potential new research directions.

The Materials Chemistry program supports basic research in the chemical synthesis and discovery of new materials. The major programmatic focus is on the discovery, design and synthesis of novel functional materials with an emphasis on the use of chemistry for synthesis and control of structure, composition, dynamics, and collective properties. A common objective is to elucidate the complex relationships between a material's functional properties and its chemical synthesis, composition, atomic and molecular structure, higher-order morphology, and material dynamics in an operational environment. A distinctive feature of the program is the emphasis on the discovery, synthesis, and characterization of new materials and the manipulation of materials' structure across a range of length scales beyond molecular scale and time scales beyond milliseconds using chemistry.

We would like to thank all the meeting attendees for their active participation and for sharing their ideas and new research results. And special thanks to the following session moderators for their contributions to productive discussions: Susan Sinnott, Penn State

University; Xueli (Sherry) Zheng, SLAC National Accelerator Laboratory; Gabriel Veith, Oak Ridge National Laboratory; Sarah Tolbert, University of California, Los Angeles; Joe Kolis, Clemson University; and May Nyman, Oregon State University. Sincere thanks also go to Teresa Crockett of BES/MSE for organizing the meeting and to Jody Crisp (administrative lead) and Andrew Fowler (technical lead) and their colleagues at the Oak Ridge Institute for Science and Education (ORISE) for their excellent work providing all the logistical support for the meeting.

Christopher Chervin
Craig Henderson
Program Managers, Materials Chemistry
Materials Sciences and Engineering Division
Basic Energy Sciences, Office of Science
U.S. Department of Energy

Table of Contents

Agenda

Tuesday, August 6, 2024		
7:00 – 8:30 AM	Breakfast	
8:30 – 8:50 AM	Opening Remarks	BES Materials Chemistry Program Managers
Technical Session A: Macromolecular Transformations		
8:50 – 9:10 AM	**A1** – Unlocking Chemical Circularity in Recycling by Controlling Polymer Reactivity Across Scales	Helms LBNL
9:10 – 9:30 AM	**A2** – Polyolefin Upcycling Through Dehydrogenation and Functionalization	Winey UPenn
9:30 – 9:50 AM	**A3** – Elastomeric Miktoarm Star Polymers: Theory and Experiment	Bates (Fredrickson) UCSB
9:50 – 10:10 AM	**A4** – Autooxidation Mechanisms and Methods for Plastics Upcycling	Hermans Wisconsin
10:10 – 10:30 AM	**A5 –** Precision Deconstruction and Upcycling of Polymers by Tailored Ionic Liquids	Saito ORNL
10:30-10:50 AM	BREAK	
Technical Session B: Material Design for Function		
10:50– 11:10 AM	**B1** – Two-Dimensional Chalcogenide Nanomaterials	Cui SLAC/Stanford
11:10 – 11:30 AM	**B2** – Inorganic/Organic Nanocomposites	Xu LBNL

11:30 – 11:50 AM	**B3** – Hybrid Halide Perovskites: Novel Materials with Contraindicated Properties	Seshadri UCSB
11:50 – 12:10 PM	**B4** – New Paradigms for Controlling Molecular and Ion Transport in Precise, Tight and Reconfigurable Polymer Networks	Sing (Braun) UIUC
12:10 – 12:45 PM	Lunch Break and Working Session	
12:45 – 1:15 PM	Materials Chemistry Program Update Presentation	
Technical Session C: Redox Active Materials		
1:15 – 1:30 PM	**C1** – Using Nanoporous Materials to Understand Kinetic Constraints in Pseudocapacitive Energy Storage	Tolbert UCLA
1:30 – 1:45 PM	**C2** – Liquid-Metal Electrodes for Low-Cost and Low Temperature Solid State Batteries for Long Duration Energy Storage	Hatzell Princeton
1:45 – 2:00 PM	**C3** – Porous, Lightweight, and Semiconducting Chalcogel as High Energy Density Electrode for Lithium-ion and Sodium-ion Batteries	Islam Jackson State
2:00 – 2:15 PM	**C4** – Understanding Interfacial Chemistry and Cation Order-Disorder in Mixed-Phased Complex Sodium Metal Oxide Cathodes for Sodium Ion Batteries	Xiong Boise State
2:15 – 2:30 PM	**C5** – Enabling Energy-Dense Grid Scale Batteries with Earth Abundant Materials	Amanchukwu Univ of Chicago
2:30 – 2:50 PM	Break	
Technical Session D: Energy Flow in Materials		
2:50 – 3:05 PM	**D1** – High Electron Affinity Conjugated Polymers: Synthesis, Electron Transport and Discovery of New Class of Two-Dimensional Organic Solid-State Materials	Jenekhe Univ of Washington

3:05 – 3:20 PM	**D2** – Energy Flow in Polymers with Mixed Conduction Pathways	Segalman (Virtual) UCSB
3:20 – 3:35 PM	**D3** – New Synthetic Approaches Towards Atomically Precise π–d Conjugated Materials	Xiao Univ of Washington
3:35 – 3:50 PM	**D4** – High Efficiency Biomimetic Organic Solar Cells	Baldo MIT
3:50 – 4:05 PM	**D5** – Design Exciton and Spin Functionalities in Halide Perovskite Epitaxial Heterostructures	Dou Purdue
4:05 – 6:00 PM	Poster Session I (see below)	
6:00 – 7:30 PM	Dinner Break	
7:30 – 9:00 PM	Poster "After Hours" – Poster from Session I will remain on display, but will be unmanned, for additional viewing.	
Poster Session I	**I-1** – Thin Film Platforms to Advance Scientific Frontiers in Solid State Energy Storage	Rubloff Maryland
Poster Session I	**I-2** – Designing Efficient Nanostructured Polymer Electrolytes Using Tapered Block Polymers - Joint Experiment and Theory Effort in Controlled Interface Design	Hall (Epps) Ohio State (Univ Delaware)
Poster Session I	**I-3** – Direct Reduction of Metal Oxides to Metals for Electrowinning and Energy Storage	Kempler Oregon
Poster Session I	**I-4** – Polyelectrolyte-Grafted Nanochannels for Enhanced Electromechanical Energy Conversion	Das Maryland
Poster Session I	**I-5 –** Designing Chemical Disorder in Solid-State Superionic Conductors	Kim Stevens Institute
Poster Session I	**I-6 –** Elucidating the Electrochemically Enhanced Surface Diffusion Mechanism in Materials for Clean Energy	Papa Lopes ANL

Poster Session I	**I-7 –** Understanding Structure, Phase Behavior, and Physical Properties of Polysulfamides and Polysulfamates using Simulations, Experiments, and Machine Learning	Jayaraman Delaware
Poster Session I	**I-8 –** Facilitating Ionic and Electronic Conduction in Radical Polymers through Controlled Assembly	Savoie (Boudouris) Purdue
Poster Session I	**I-9 –** Charging and Polarization of Organic Semiconductors in Energy Efficient Circuits and Energy Capture Models	Bragg (Katz) Johns Hopkins
Poster Session I	**I-10 –** Multi-Metalloporphyrin Synthetic Polymers for Long-Range Charge Transport	Moore Illinois
Poster Session I	**I-11 –** Shaping Symmetry and Molding Morphology of Triply-Periodic Assemblies via Molecular Design and Processing of Block Copolymers	Grason Massachusetts
Poster Session I	**I-12 –** Molecular and Network Design of Liquid Crystal Elastomer Elastocalorics	Ostermann (Davidson) Princeton
Poster Session I	**I-13 –** Directed Synthesis of New Actinide Containing Oxides, Fluorides and Chalcogenides	Zur Loye South Carolina
Poster Session I	**I-14 –** Kinetic Synthesis of Metastable Nitrides	Zakutayev NREL
Poster Session I	**I-15 –** Hierarchical Hybrid Multifunctional Materials through Interface Engineering	Poudeu Michigan
Poster Session I	**I-16 –** Unraveling the Mysteries of the Platinum Group Elements	Schurko Florida
Poster Session I	**I-17 –** Intermetallic Reactivity: From Frustrated Bonding to Mechanisms for Intergrowth and Modular Functionality in Metals and Alloys	Fredrickson Wisconsin
Poster Session I	**I-18 –** Solid State NMR Spectroscopy for Advanced Energy Materials	Huang (Rossini) Iowa State (Ames Lab)
Poster Session I	**I-19 –** Additive-Assisted Preparation of Multinary Halides	Saparov Oklahoma
Poster Session I	**I-20** – Compositional Control of Fundamental Electronic and Magnetic Properties of Ordered Layered Multi-element MXenes	May (Gogotsi) Drexel

Poster Session I	**I-21** – Novel 2D Materials and Structures via Janus Manipulation	Kong MIT
Poster Session I	**I-22** – Transforming Critical Materials Separation using Precision Control	Ivanov (Jansone-Popova) ORNL
Poster Session I	**I-23** – Designing Photoresponsive Nanosponges for Efficient and Reversible Capture and Release of Carbon Dioxide	Liu CSU-LA
Poster Session I	**I-24** – Understanding the Impact of Intrinsic Structural Vacancies on Reversible Fluoride Insertion	Melot USC
Poster Session I	**I-25** – Intrinsically Porous Polyoxometalate-Based Frameworks for Critical Metal Recovery	Peng Missouri-Kansas City
Poster Session I	**I-26** – Effect of local order on polaron and exciton delocalization in rigid D-A copolymers	Stringelin (Salleo) Georgia Tech (Stanford)
Poster Session I	**I-27** – Broadening Accessibility & Training To Emerging Researchers for Innovative Energy Storage (BATTERIES)	So CSU-Chico
Poster Session I	**I-28** – Center for STrain Optimization for Renewable Energy (STORE)	Tolbert UCLA

Wednesday, August 7, 2024		
7:00 – 8:30 AM	Breakfast	
8:30 – 8:35 AM	Opening Remarks	BES Materials Chemistry Program Managers
Technical Session E: New Material Design Approaches I		
8:35 – 8:55 AM	**E1** – Harnessing the catalytic promise of molybdenum chalcogenides to enable aqueous zinc sulfur batteries	Marschilok BNL
8:55 – 9:15 AM	**E2** – A New Paradigm for Water Splitting in Layered Materials by Modulation of Catalyst Oxidation State	Zdilla Temple
9:15 – 9:35 AM	**E3** – Precision Synthesis and Assembly of Ionic and Liquid Crystal Polymers	Xu (Nealey) ANL
9:35 – 9:55 AM	**E4** – Molecular Mechanisms of Moisture-Driven DAC within Charged Polymers	Wade Northern Arizona
9:55 – 10:15 AM	**E5** – Exploration of Radial Conjugation Pathways in Pi-Electron Materials	Tovar Johns Hopkins
10:15 -10:35 AM	BREAK	
Technical Session F: Materials Chemistry @ Interfaces		
10:35 – 10:55 AM	**F1** – New Cooperative Adsorbents and Regeneration Methods for the Efficient Removal of Carbon Dioxide from Air	Long LBNL
10:55 – 11:15 AM	**F2** – Fundamental Mechanisms Driving Efficiency of CO2 Capture Using Mineral Looping	Weber ORNL
11:15 – 11:35 AM	**F3** – Fundamental Studies of Charge Transfer in Quantum Confined Nanostructure Heterojunctions and Applications to Solar Energy Conversion	Jin Wisconsin

11:35 – 11:55 PM	**F4 –** Understanding the interfaces for high energy batteries using anions as charge carriers	Ji Oregon State
11:55 – 12:15 PM	**F5 –** Materials and Interfacial Chemistry for Next-Generation Electric Energy Storage	Manthiram UT-Austin
12:15 – 12:55 PM	Lunch Break and Working Session	
12:55 – 1:20 PM	Materials Chemistry Program Update Presentation (during lunch)	
Technical Session G: New Materials Design Approaches II		
1:20 – 1:35 PM	**G1** – Permanent Magnets Featuring Heavy Main Group Elements for Magnetic Anisotropy	Freedman MIT
1:35 – 1:50 PM	**G2** – Design and Validation of Defect-Resistant Multinary Chalcogenide Semiconductors for Energy Conversion	Mitzi Duke
1:50 – 2:05 PM	**G3** – Passive and Enhanced Capture and Conversion of CO_2 by d/f0 Molecules and Materials	Nyman Oregon State
2:05 – 2:20 PM	**G4** – Modifying the Surfaces and Interiors of Porous Solids for Energy Science	Cohen UCSD
2:20 – 2:35 PM	**G5** – Development of Recyclable Thermosets for Additive Manufacturing	Chowdhury NM Tech
2:35 – 2:55 PM	Break	
Technical Session H: Material Discovery		
2:55 – 3:10 PM	**H1** – Rational Synthesis of Superconductors	Kanatzidis ANL
3:10 – 3:25 PM	**H2** – Converting Metal–Organic Liquids into Microporous Glasses via Non-Equilibrium Syntheses	Mason Harvard

3:25 – 3:40 PM	**H3** – Multi-Length Scale Synthesis of Silicon Materials	Klausen Johns Hopkins
3:40 – 3:55 PM	**H4 –** A synergistic computational and experimental approach for unprecedented III-IV and II-VI clathrates	Donadio UC-Davis
3:55 – 4:10 PM	**H5 –** New Superconducting Materials	Cava Princeton
4:10 – 6:00 PM	**Poster Session II (see below)**	
6:00 – 7:30 PM	Dinner Break	
7:30 – 9:00 PM	Poster "After Hours" – Poster from Session II will remain on display, but will be unmanned, for additional viewing.	
Poster Session II	**II-1** – Discovering Dopable, Next Generation Defect Tolerant Hybrid Semiconductors	Neilson Colorado State
Poster Session II	**II-2** – Design, Discovery, and Synthesis Science of Porous Frameworks using Fast and Modular Heterophase Assembly	Salehi-Khojin Univ Illinois-Chicago
Poster Session II	**II-3** – Reversible Electrochemical Capture/Release of Carbon Dioxide Mediated by Electrostatically-Enhanced Charge Transfer	Dawlaty USC
Poster Session II	**II-4** – Modulating Complex Chemical Conv ersion with Multi-site Electrocatalyst for Energy Dense Liquids	Cheng Univ. Tennessee
Poster Session II	**II-5** – Molecular Mo Sulifide Clusters for H2-Evolution: Surface Immobilization and Water Solubility, Composition-Function Relationships, and Probes of Mechanisms	Donahue Tulane
Poster Session II	**II-6** – Largely pi-Extended Molecular Systems: Porphryins Fused with PAHs	Wang North Texas
Poster Session II	**II-7** – Li-ion Battery Critical Metal Recycling Using Sugars	Amarasekara PVSU
Poster Session II	**II-8** – Uncovering Intrinsic Transport and Magnetic Properties of Two-Dimensional Electrically Conducting Metal-Organic Frameworks	Oppenheim (Dincă) MIT

Poster Session II	**II-9** – Symmetry Breaking for the Synthesis of Nanostructured Porous Materials	Matzger Michigan
Poster Session II	**II-10** – Expanding iClick to Link Metal Ions in Multidimensional Metallopolymers and Materials Synthesis	Veige Florida
Poster Session II	**II-11 –** Kinetically trapped Poly(pseudo)rotaxane Networks	Ke Dartmouth
Poster Session II	**II-12 –** Electric field-controlled solid sorbent for direct air capture	James (White) Princeton
Poster Session II	**II-13 –** Hybrid metal oxocluster-based soft materials: design principles and emergent properties	Nyman Oregon State
Poster Session II	**II-14** – Novel Strategies for Direct Air Capture and Conversion of CO2 Using Dual-Function Materials	Kuila NCA&T
Poster Session II	**II-15 –** Crystal Growth and Quantum Phases of Frustrated Rare Earth Oxides	Kolis Clemson
Poster Session II	**II-16 –** Kinetics and Thermodynamics of Gaseous Mixtures in Nano-Confined Environments	Thonhauser Wake Forest
Poster Session II	**II-17 –** Experimental Investigation of the Control Mechanism of X-ray Induced Structural and Chemical Synthesis at Extreme Conditions	Pravica UNLV
Poster Session II	**II-18 –** The Role of Local Structure and Dynamics on Proton and Hydroxide Transport in Ion-Conducting Polymers	Winey UPenn
Poster Session II	**II-19 –** Uncovering the mechano-electro-chemo mechanism of fresh Li in sulfide based all solid-state batteries through operando studies	Zhu Northeastern
Poster Session II	**II-20–** New Horizons In Thermal And Charge Transport In Complex Narrow Gap Semiconductors	Dravid Northwestern
Poster Session II	**II-21 –** Molecular Insights into Structure and Function of Doping in Hybrid Metal Halides for the Rational Design of Optoelectronic Materials	Gangishetty Mississippi State
Poster Session II	**II-22 –** Epitaxially-Fused Quantum Dot Superlattices with Collective Electronic and Magnetoelectronic Properties	Law UC-Irvine

Poster Session II	**II-23 –** Understanding Solid-Solution-Reaction vs. Solid-Phase-Transformation Competition of Complex Conversion Materials Dominated by Interfacial Kinetics	Lin Catholic U. of America
Poster Session II	**II-24 –** Materials and Interfacial Chemistry for Next Generation Electrical Energy Storage	Cheng (Dai) ORNL
Poster Session II	**II-25 –** Ionic - Dipolar Inetractions in Poly(Ionic Liquids)	Urban Clemson
Poster Session II	**II-26 –** Emerging Properties through Controlled Phase Transformations for High Energy Sodium Ion Batteries	Xiong Boise State
Poster Session II	**II-27 –** Nature-Derived Materials for Redox Flow Batteries	Hematian UNC-Greensboro
Poster Session II	**II-28** – Solid State Chemistry of Novel Pnictides with Complex Structures	Bobev Univ of Delaware

Thursday, August 8, 2024		
Technical Session I: Mechanisms		
7:00 – 8:30 AM	Breakfast	
8:30 – 8:45 AM	**I1** – Spatio-Temporal Dynamics of CO2 Capture by Sorbents: Multimodal, In-Situ and Operando Measurements	Farha Northwestern
8:45 – 9:00 AM	**I2** – When Covalent Organic Frameworks Meet Cross-coupling Reactions: Directed Synthesis, Mechanistic Investigation, and Energy Application	Li Clark Atlanta
9:00 – 9:15 AM	**I3** – Understanding Degradation Mechanisms of Aminopolymers	Pang LLNL
9:15 – 9:30 AM	**I4** – Fundamental Understanding of Electrochemical – Mechanical Driven Instability of Sodium Metal	Mukherjee Purdue
9:30 – 9:45 AM	**I5** – Impacts of Dynamic Bonding on the Properties of Porous Materials	Brozek Oregon
9:45 – 10:00 AM	**I6** – Multi-scale Study of Self-Healing Polymers to Enhance Carbon Dioxie Removal	Ma Vermont
10:00 – 10:20 AM	Break	
Technical Session J: Structure of Materials		
10:20 – 10:35 AM	**J1** – Chemo-Mechanically Driven In Situ Hierarchical Structure Formation in Mixed Conductors	Perry (Virtual) Univ. Illinois
10:35 – 10:50 AM	**J2** – Understanding Flow Cell Porous Electrodes as Active Materials for Electrochemical Transformations	Aziz Harvard
10:50 – 11:05 AM	**J3** – Pore Space Engineering and Functionalization in Porous Metal-Organic Framework Materials	Feng UC-Riverside

11:05 – 11:20 AM	**J4** – Probing the Hydrogen Bonded Networks and Ion Interactions in Deep Eutectic Solvents (DESs) through Solute Molecules	Suarez CUNY
11:20 – 11:35 AM	**J5** – Multidimensional Phase Maps for the Accelerated Synthesis and Study of Metastable Materials	Brutchey USC
11:35 – 11:45 AM	**BES Program Manager Comments and Closeout of Meeting**	
11:45 AM	**Adjourn**	

Laboratory
Abstracts

Materials and Interfacial Chemistry for Next-Generation Electrical Energy Storage

Sheng Dai, Albina Borisevich, Craig A. Bridges, Lei Cheng, Parans Paranthaman, Bishnu Prasad Thapaliya, and Xiao-Guang Sun

Keywords: Energy storage, Interfacial chemistry, SEI, CEI, Electrode materials

Research Scope

The overarching goal of this project is to establish a comprehensive understanding of fundamental chemistry principles, with a focus on tailoring the chemical composition, functionality, and architecture of electrodes and electrolytes. This knowledge will play a pivotal role in achieving stable electrode/electrolyte interfaces and promoting high ionic conduction, thus driving advancements in the field of next-generation energy storage. To accomplish this overarching goal, the project is organized around three specific aims:

1. Design Locally Concentrated Ionic Liquid Electrolytes: This involves the strategic combination of ionic liquids and molecular solvents to create stable and ionically conducting solid electrolyte interphase (SEI) layers. Our aim is to investigate how heterogeneous environments created by high concentration ionic-liquid electrolytes can be fine-tuned to comprehend the components that stabilize reactive interfaces at both low and high voltages.

2. Control of SEI Formation via Interfacial Synthesis: We will explore the molecular construction of interfacial structures through electrochemical functionalization and autonomous layer-by-layer synthesis methods, with the ultimate goal of deciphering descriptors to tailor the stability of electrode interfaces.

3. Tailor Interfacial and Ion-Storage Chemistry through Organic Framework Materials: In this aspect of the project, we will focus on designing organic framework polymers to impact interfacial structures and energy storage mechanisms. Specifically, we will investigate the utility of 2D layered organic polymers in controlling these critical aspects.

Recent Progress

a) Accomplished stable and uniform SEI and CEI [1-3]

Our project has previously explored two primary avenues for introducing fluorine to the cathode surface. The first method involves high-temperature fluorination, a solid-state synthesis approach, or direct fluorination using F_2 gas for transition metal oxides.[4-6] The second approach, termed solution-mediated fluorination, utilizes fluorinated solvents or additives.[7,8] Leveraging the

advantages of fluorine chemistry at battery interfaces, such as forming a robust SEI, aiding in oxygen retention within the crystal lattice, enhancing capacity, and improving cycling stability, cathode fluorination has garnered significant attention as a unique technique for surface functionalization. However, existing fluorination methods have their limitations, including challenges in controlling sample morphology and the use of highly reactive fluorinating agents such as XeF_2 or elemental F_2 gas. In the current funding period, we have achieved a breakthrough by developing a novel ECF method. This method draws inspiration from emerging electrochemical organic synthesis and extends it to solid-state chemistry. ECF offers several advantages over conventional fluorination techniques, including rapid reaction kinetics, conformal synthesis, and easily controllable parameters, resulting in the creation of an amorphous LiF surface layer on electrodes in lithium-ion-containing electrolytes.

b) Characterizing SEI and electrolytes[9,10]

Employing operando small angle neutron scattering (SANS) and ex-situ X-ray photoelectron spectroscopy (XPS), we demonstrated that FSI^- anion based ionic liquid electrolyte led to the formation of more stable SEI at relatively high cell potentials. SEI formed at high cell potentials reduce the parasitic reaction at interface during cell operation at much lower potential. Our investigation was carried out using SANS while a battery cell was in operation. Notably, our experiments revealed that the use of the 0.5 M LiFSI/1-ethyl-3-methylimidazolium bis(fluorosulfonyl)imide (EMIm.FSI) electrolyte led to the formation of lithium-rich reduction products at relatively high cell potentials, resulting in a more favorable and stable SEI. Both operando neutron scattering and ex-situ XPS demonstrated that the FSI^- anion could chemically react at the open cell voltage (OCV) and could also be electrochemically reduced at relatively high cell voltages (approximately 2 V).

c) Next generation electrode materials[11-19]

We have made significant strides in the development of promising anode materials for lithium-ion batteries, specifically Wadsley-Roth phased niobates with open and interconnected crystallographic shear structures.[20,21] To address the inherent low electrical conductivity limitations, we have successfully synthesized a novel doped material, $Mo_{1.5}W_{1.5}Nb_{14}O_{44}$ (MWNO), through an ionothermal-synthesis-assisted doping strategy.[11,12] Neutron powder diffraction and aberration-corrected scanning transmission electron microscopy were employed to characterize the crystal structure of MWNO, revealing the full occupation of Mo^{6+}-dopant at the t1 tetrahedral site. Ultraviolet–visible diffuse reflectance spectroscopy, density functional theory (DFT) computation, and electrochemical impedance spectroscopy were further used to characterize electronic structures and their correlations to ion transport. We have also expanded our research efforts to construct organic electrode architectures.[15-19]

References

1. B. P. Thapaliya, T. Wang, A. Y. Borisevich, H. M. M. Meyer Iii, X. G. Sun, M. P. Paranthaman, C. A. Bridges, and S. Dai, *In Situ Ion-Exchange Metathesis Induced Conformal LiF Surface Films on Cathode (NMC811) as a Cathode Electrolyte Interphase*, Advanced Functional Materials **33**, 2302443 (2023).
2. B. P. Thapaliya, S. Misra, S. Z. Yang, C. J. Jafta, H. M. Meyer, P. Bagri, R. R. Unocic, C. A. Bridges, and S. Dai, *Enhancing Cycling Stability and Capacity Retention of NMC811 Cathodes by Reengineering Interfaces via Electrochemical Fluorination*, Advanced Materials Interfaces **9**, 10 (2022).
3. B. P. Thapaliya, A. Y. Borisevich, H. M. Meyer, X. G. Sun, C. A. Bridges, and S. Dai, *Conformal LiF Stabilized Interfaces via Electrochemical Fluorination on High Voltage Spinel Cathodes (approximate to 4.9 V) for Lithium-Ion Batteries*, Advanced Materials Interfaces **9**, 10 (2022).
4. Z. A. Qiao, S. S. Brown, J. Adcock, G. M. Veith, J. C. Bauer, E. A. Payzant, R. R. Unocic, and S. Dai, *A Topotactic Synthetic Methodology for Highly Fluorine-Doped Mesoporous Metal Oxides*, Angewandte Chemie-International Edition **51**, 2888-2893 (2012).
5. B. P. Thapaliya, E. C. Self, C. J. Jafta, A. Y. Borisevich, H. M. Meyer, C. A. Bridges, J. Nanda, and S. Dai, *Synthesizing High-Capacity Oxyfluoride Conversion Anodes by Direct Fluorination of Molybdenum Dioxide (MoO_2)*, ChemSusChem **13**, 3825-3834 (2020).
6. H. Zhou, R. E. Ruther, J. Adcock, W. Zhou, S. Dai, and J. Nanda, *Controlled Formation of Mixed Nanoscale Domains of High Capacity Fe_2O_3-FeF_3 Conversion Compounds by Direct Fluorination*, ACS Nano **9**, 2530-2539 (2015).
7. X. G. Sun, C. Liao, L. Baggetto, B. K. Guo, R. R. Unocic, G. M. Veith, and S. Dai, *Bis(fluoromalonato)borate (BFMB) anion based ionic liquid as an additive for lithium-ion battery electrolytes*, Journal of Materials Chemistry A **2**, 7606-7614 (2014).
8. Y. Li, S. Wan, G. M. Veith, R. R. Unocic, M. P. Paranthaman, S. Dai, and X. G. Sun, *A Novel Electrolyte Salt Additive for Lithium Ion Batteries with Voltages Greater than 4.7 V*, Advanced Energy Materials **7**, 1601397 (2016).
9. C. J. Jafta, X. G. Sun, H. L. Lyu, H. Chen, B. P. Thapaliya, W. T. Heller, M. J. Cuneo, R. T. Mayes, M. P. Paranthaman, S. Dai, and C. A. Bridges, *Insight into the Solid Electrolyte Interphase Formation in Bis(fluorosulfonyl)Imide Based Ionic Liquid Electrolytes*, Advanced Functional Materials **31**, 13 (2021).
10. J. Fan, T. Wang, C. A. Bridges, A. Y. Borisevich, C. A. Steren, P. Li, B. P. Thapaliya, C. L. Do-Thanh, Z. Yang, Y. Yuan, and S. Dai, *Entropy stabilized cubic $Li_7La_3Zr_2O_{12}$ with reduced lithium diffusion activation energy: studied using solid-state NMR spectroscopy*, RSC Advances **13**, 19856-19861 (2023).
11. R. Tao, T. Zhang, S. Tan, C. J. Jafta, C. Li, J. Liang, X. G. Sun, T. Wang, J. Fan, Z. Lu, C. A. Bridges, X. Suo, C. L. Do-Thanh, and S. Dai, *Insight into the Fast-Rechargeability of a Novel $Mo_{1.5}W_{1.5}Nb_{14}O_{44}$ Anode Material for High-Performance Lithium-Ion Batteries*, Advanced Energy Materials **12**, 16 (2022).
12. R. Tao, T. Zhang, X. G. Sun, C. L. Do-Thanh, and S. Dai, *Ionothermally Synthesized Nanoporous $Ti_{0.95}W_{0.05}Nb_2O_7$: a Novel Anode Material for High Performance Lithium Ion Batteries*, Batteries & Supercaps **6**, 10 (2023).
13. J. Fan, T. Wang, B. P. Thapaliya, M. Li, C. L. Do-Thanh, T. Kobayashi, I. Popovs, Z. Yang, and S. Dai, *Construction of Nitrogen-abundant Graphyne Scaffolds via Mechanochemistry-*

Promoted Cross-Linking of Aromatic Nitriles with Carbide Toward Enhanced Energy Storage, Small **19**, e2205533 (2023).
14. T. Wang, J. A. Gaugler, M. J. Li, B. P. Thapaliya, J. T. Fan, L. Q. Qiu, D. Moitra, T. Kobayashi, I. Popovs, Z. Z. Yang, and S. Dai, *Construction of Fluorine- and Piperazine-Engineered Covalent Triazine Frameworks Towards Enhanced Dual-Ion Positive Electrode Performance*, ChemSusChem, 7 (2022).
15. J. Fan, T. Wang, Y. Yuan, C.-L. Do-Thanh, X. Suo, Z. Yang, H. Chen, and S. Dai, *Mechanochemically Assisted Synthesis of High-Entropy Layer-Structured Dittmarite Analogues*, ACS Applied Energy Materials **5**, 3290-3297 (2022).
16. J. Fan, T. Wang, B. P. Thapaliya, L. Qiu, M. Li, Z. Wang, T. Kobayashi, I. Popovs, Z. Yang, and S. Dai, *Fully Conjugated Poly(phthalocyanine) Scaffolds Derived from a Mechanochemical Approach Towards Enhanced Energy Storage*, Angew Chem Int Ed Engl **61**, e202207607 (2022).
17. J. Fan, T. Wang, H. Chen, Z. Wang, B. P. Thapaliya, T. Kobayashi, Y. Yuan, I. Popovs, Z. Yang, and S. Dai, *Mechanochemistry Driven Construction of Aza fused π-Conjugated Networks Toward Enhanced Energy Storage*, Advanced Functional Materials **32**, 7 (2022).
18. J. Fan, X. Suo, T. Wang, Z. Wang, C.-L. Do-Thanh, S. M. Mahurin, T. Kobayashi, Z. Yang, and S. Dai, *Mechanochemistry-driven phase transformation of crystalline covalent triazine frameworks assisted by alkaline molten salts*, Journal of Materials Chemistry A **10**, 14310-14315 (2022).
19. Z. Yang, T. Wang, H. Chen, X. Suo, P. Halstenberg, H. Lyu, W. Jiang, S. M. Mahurin, I. Popovs, and S. Dai, *Surpassing the Organic Cathode Performance for Lithium-Ion Batteries with Robust Fluorinated Covalent Quinazoline Networks*, ACS Energy Letters **6**, 41-51 (2020).
20. B. Guo, X. Yu, X.-G. Sun, M. Chi, Z.-A. Qiao, J. Liu, Y.-S. Hu, X.-Q. Yang, J. B. Goodenough, and S. Dai, *A long-life lithium-ion battery with a highly porous $TiNb_2O_7$ anode for large-scale electrical energy storage*, Energy & Environmental Science **7**, 2220-2226 (2014).
21. R. Tao, G. Yang, E. C. Self, J. Liang, J. R. Dunlap, S. Men, C. L. Do-Thanh, J. Liu, Y. Zhang, S. Zhao, H. Lyu, A. P. Sokolov, J. Nanda, X. G. Sun, and S. Dai, *Ionic Liquid-Directed Nanoporous $TiNb_2O_7$ Anodes with Superior Performance for Fast-Rechargeable Lithium-Ion Batteries*, Small **16**, e2001884 (2020).

List of top ten publications during the past 2 years:

1. J. Fan, T. Wang, Y. Yuan, A. Borisevich, C.-L. Do-Thanh, Z. Yang, and S. Dai, *Lattice engineering of high-entropy olivine-type lithium metal phosphate as high-voltage cathodes*, Applied Physics Letters **124** (2024).

2. B. P. Thapaliya, T. Wang, A. Y. Borisevich, H. M. M. Meyer Iii, X. G. Sun, M. P. Paranthaman, C. A. Bridges, and S. Dai, *In Situ Ion-Exchange Metathesis Induced Conformal LiF Surface Films on Cathode (NMC811) as a Cathode Electrolyte Interphase*, Advanced Functional Materials **33**, 2302443 (2023).

3. Z. Wang, B. P. Thapaliya, I. Popovs, Y. Wang, T. Wang, J. Chen, M. A. Arnould, S. M. Mahurin, and S. Dai, *Facile Strategy to Prepare Poly(ionic liquid)-Coated Solid Polymer Electrolytes through Layer-by-Layer Assembly*, ACS Applied Materials & Interfaces **15**, 51806-51814 (2023).

4. R. Tao, T. Zhang, S. Tan, C. J. Jafta, C. Li, J. Liang, X.-G. Sun, T. Wang, J. Fan, Z. Lu, C. A. Bridges, X. Suo, C.-L. Do-Thanh, and S. Dai, *Insight into the Fast-Rechargeability of a Novel Mo1.5W1.5Nb14O44 Anode Material for High-Performance Lithium-Ion Batteries*, Advanced Energy Materials **12**, 2200519 (2022).

5. B. P. Thapaliya, S. Misra, S. Z. Yang, C. J. Jafta, H. M. Meyer, P. Bagri, R. R. Unocic, C. A. Bridges, and S. Dai, *Enhancing Cycling Stability and Capacity Retention of NMC811 Cathodes by Reengineering Interfaces via Electrochemical Fluorination*, Advanced Materials Interfaces **9**, 10 (2022).

6. B. P. Thapaliya, A. Y. Borisevich, H. M. Meyer, X. G. Sun, C. A. Bridges, and S. Dai, *Conformal LiF Stabilized Interfaces via Electrochemical Fluorination on High Voltage Spinel Cathodes (approximate to 4.9 V) for Lithium-Ion Batteries*, Advanced Materials Interfaces **9**, 10 (2022).

7. J. Fan, T. Wang, B. P. Thapaliya, L. Qiu, M. Li, Z. Wang, T. Kobayashi, I. Popovs, Z. Yang, and S. Dai, *Fully Conjugated Poly(phthalocyanine) Scaffolds Derived from a Mechanochemical Approach Towards Enhanced Energy Storage*, Angew Chem Int Ed Engl **61**, e202207607 (2022).

8. J. Fan, T. Wang, H. Chen, Z. Wang, B. P. Thapaliya, T. Kobayashi, Y. Yuan, I. Popovs, Z. Yang, and S. Dai, *Mechanochemistry Driven Construction of Aza fused π-Conjugated Networks Toward Enhanced Energy Storage*, Advanced Functional Materials **32**, 7 (2022).

9. C. A. Bridges, M. L. Martins, C. J. Jafta, X. G. Sun, M. P. Paranthaman, J. Liu, S. Dai, and E. Mamontov, *Dynamics of Emim+ in [Emim][TFSI]/LiTFSI Solutions as Bulk and under Confinement in a Quasi-liquid Solid Electrolyte*, The Journal of Physical Chemistry B **125**, 5443-5450 (2021).

10. C. J. Jafta, X. G. Sun, H. L. Lyu, H. Chen, B. P. Thapaliya, W. T. Heller, M. J. Cuneo, R. T. Mayes, M. P. Paranthaman, S. Dai, and C. A. Bridges, *Insight into the Solid Electrolyte Interphase Formation in Bis(fluorosulfonyl)Imide Based Ionic Liquid Electrolytes*, Advanced Functional Materials **31**, 13 (2021).

Transforming Critical Materials Separation using Precision Control

Alex Ivanov (ORNL), Ilja Popovs (ORNL), Albina Borisevich (ORNL), De-en Jiang (Vanderbilt University), Santa Jansone-Popova (ORNL)

Keywords: rare-earth separations, lanthanides, X-ray absorption spectroscopy, chemical bonding, *f*-block elements

Research Scope

Our current research is focused on the precise manipulation of donor atom distances to the metal center in lanthanide complexes through ligand structural modifications, allowing for targeted affinity towards specific lanthanides. Our goal is to investigate the fundamental interactions between donor atoms and metal ions within the first coordination sphere, and to identify ligand design principles and key structural descriptors that influence selectivity across the trivalent lanthanide series.

Recent Progress

Lanthanide rare-earth metals are ubiquitous in modern technologies[1-5], but we know little about chemistry of the 61st element, promethium (Pm)[6], a lanthanide that is radioactive and inaccessible. Despite its importance[7,8], Pm has been conspicuously absent from the experimental studies of lanthanides, impeding our full comprehension of the so-called lanthanide contraction phenomenon: a fundamental aspect of the periodic table that is quoted in general chemistry textbooks. In our recent research work, we demonstrate a stable chelation of the ^{147}Pm radionuclide (half-life of 2.62 years) in aqueous solution by the newly synthesized organic diglycolamide ligand (Figure 1). The resulting homoleptic Pm^{III} complex is studied using synchrotron X-ray absorption spectroscopy and quantum chemical calculations to establish the coordination structure and a bond distance of promethium. These fundamental insights allow a complete structural investigation of a full set of isostructural lanthanide complexes, ultimately capturing the lanthanide contraction in solution solely based on experimental observations. Our results show accelerated shortening of bonds at the beginning of the lanthanide series, which can be correlated to the separation trends shown by diglycolamides[9-11].

In summary, after almost eight decades since the discovery of the element Pm, its coordination complex has been synthesized and characterized in solution using modern synchrotron spectroscopy tools. The determined Pm–O bond distance of 2.476(16) Å is in line with quantum chemical investigations and originates from a σ-type donation of electron density from the ligands to the primarily 5*d* vacant orbitals of Pm. Finally, this previously inaccessible piece of information allowed us to complete structural studies of a full lanthanide set of isostructural complexes in solution, ultimately establishing and confirming the lanthanide contraction phenomenon solely

based on the experimental structural data. These results are expected to contribute to our fundamental understanding and prediction of the coordination chemistry of lanthanides and scarce *f*-block elements, with pertinence to emergent rare-earth element separations and radiopharmaceutical technologies.

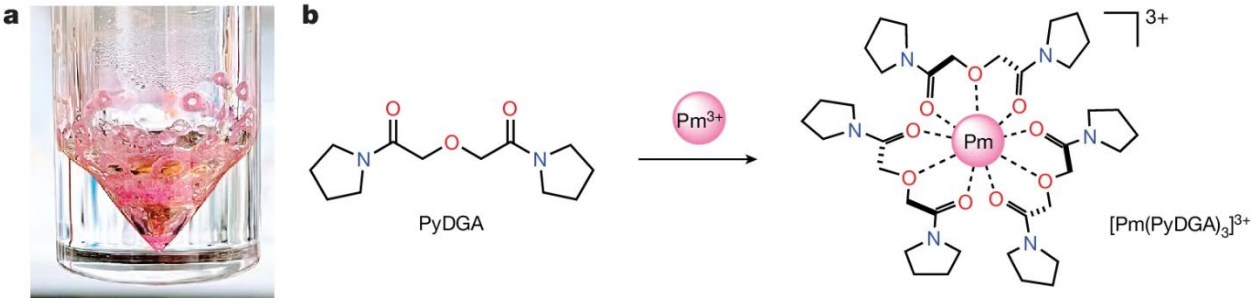

Figure 1. Preparation of Pm^{III} and its chelation by the multidentate ligand PyDGA in an aqueous solution. **a**, Photograph of purified Pm^{III} compound prepared in this study. The depicted pink-coloured $^{147}Pm(NO_3)_3 \cdot nH_2O$ ($n < 9$) solid residue was obtained after several purification steps and used in a Pm^{III} complexation. **b**, Each PyDGA ligand molecule consists of two amide carbonyl oxygen groups and one ether oxygen atom, enabling high aqueous solubility. This chelator coordinates with the promethium cation in a tridentate fashion to form the 1:3 complex by providing nine metal-binding O donor atoms in the first coordination sphere of Pm^{III}.

References

1. Cheisson, T. and Schelter, E. J. Rare earth elements: Mendeleev's bane, modern marvels. *Science* **363**, 489–493 (2019).

2. Cockell, C. S. et al. Space station biomining experiment demonstrates rare earth element extraction in microgravity and Mars gravity. *Nat. Commun.* **11**, 5523 (2020).

3. Cotruvo, J. A. The chemistry of lanthanides in biology: recent discoveries, emerging principles, and technological applications. *ACS Cent. Sci.* **5**, 1496–1506 (2019).

4. Kostelnik, T. I. and Orvig, C. Radioactive main group and rare earth metals for imaging and therapy. *Chem. Rev.* **119**, 902–956 (2019).

5. Liddle, S. T., Mills, D. P. and Natrajan, L. S. *The Lanthanides and Actinides: Synthesis, Reactivity, Properties and Applications* (World Scientific Publishing Europe Ltd, 2021).

6. Marinsky, J. A., Glendenin, L. E. and Coryell, C. D. The chemical identification of radioisotopes of neodymium and of element 61. *J. Am. Chem. Soc.* **69**, 2781–2785 (1947).

7. Cantrill, S. Promethium puzzles. *Nat. Chem.* **10**, 1270–1270 (2018).

8. Elkina, V. and Kurushkin, M. Promethium: to strive, to seek, to find and not to yield. *Front. Chem.* **8**, 588 (2020).

9. Sasaki, Y., Sugo, Y., Suzuki, S. and Tachimori, S. The novel extractants, diglycolamides, for the extraction of lanthanides and actinides in HNO_3–*n*-dodecane system. *Solvent Extr. Ion Exch.* **19**, 91–103 (2001).

10. Ellis, R. J. et al. 'Straining' to separate the rare earths: how the lanthanide contraction impacts chelation by diglycolamide ligands. *Inorg. Chem.* **56**, 1152–1160 (2017).

11. Baldwin, A. G. et al. Outer-sphere water clusters tune the lanthanide selectivity of diglycolamides. *ACS Cent. Sci.* **4**, 739–747 (2018).

Publications

1. D. M. Driscoll, F. D. White, S. Pramanik, J. Einkauf, B. Ravel, D. Bykov, S. Roy, R. T. Mayes, L. Delmau, S. Schrell, T. Dyke, A. Miller, M. Silveira, S. van Cleve, R. Copping, S. Davern, S. Jansone-Popova, I. Popovs, and A. S. Ivanov, Observation of a promethium complex in solution, *Nature*, 629, 819-823 (2024).

2. S. Pramanik, S. Kaur, I. Popovs, A. S. Ivanov, and S. Jansone-Popova, Emerging Rare Earth Element Separation Technologies, *Eur. J. Inorg. Chem.,* e202400064 (2024).

3. M. Toro-González, N. Akingbesote, A. Webb, B. Sanders, A. S. Ivanov, S. Jansone-Popova, I. Popovs, P. Benny, R. Perry, and S. Davern, Development of 225 Ac-doped Biocompatible Nanoparticles for Targeted Alpha Therapy, *J. Nanobiotechnology*, 22, 306 (2024)

4. Th. D. N. Reddy, A. S. Ivanov, D. M. Driscoll, S. Jansone-Popova, and D. Jiang, Changes in nitrate binding with lanthanides in BLPhen complexes, *J. Mol. Liq.*, 387, 122573 (2023).

5. K. R. Johnson, D. M. Driscoll, J. T. Damron, A. S. Ivanov, and S. Jansone-Popova. Size Selective Ligand Tug of War Strategy to Separate Rare Earth Elements. *JACS Au*, 3, 584-591 (2023)

6. T. Liu, A. S. Ivanov, I. Popovs, S. Jansone-Popova, and D. Jiang. N-oxide ligands for selective separations of lanthanides: insights from computation. *RSC Advance*, 13, 764-769 (2023)

7. C. Do-Thanh, H. Luo, and S. Dai, A perspective on task-specific ionic liquids for the separation of rare earth elements. *RSC Sustainability*, 1, 1168-1176 (2023)

8. D. M. Driscoll, H. Liu, B. Reinhart, I. Popovs, V. Bocharova, S. Jansone-Popova, D. Jiang, and A. S. Ivanov, Noncoordinating outer-sphere nitrate ion modulates supramolecular clustering of lanthanides in nonpolar media. *J. Phys. Chem. Lett.*, 13, 12076-12081 (2022)

Rational Synthesis of Superconductors

Mercouri G. Kanatzidis, Materials Science Division, Argonne National Laboratory
Duck Young Chung, Materials Science Division, Argonne National Laboratory

Program Scope

This project focuses on predicting and creating new superconductors and novel quantum materials through a comprehensive range of proposed materials using the principles and techniques of solid-state chemistry. Our FWP's core endeavor ultimately seeks to address several key scientific questions connected to our objectives: (1) will dimensional reduction synthesis methods produce low-dimensional structures with desired electronic structures exhibiting tunable electronic correlations?, (2) what chemical principles and reaction mechanisms contribute to the formation of heterolayered structures made up of two distinct layers, and what is the nature of their interaction?, and (3) can electronically induced symmetry-breaking distortions be detected in low-dimensional compounds, and is it possible to prompt them to superconduct via external approaches such as doping, alloying, or high pressure? To answer these questions, this FWP will apply a powerful new approach that significantly enhances control of the integration of materials synthesis, structural probes, electronic spectroscopy, and theoretical analysis. Our synthesis program fuels further synergies with experimentalists and theorists at ANL to apply sophisticated techniques such as transport, magnetization, heat capacity, x-ray and neutron scattering, and theory to understand the behavior of the new materials.

Recent Progress

- *New Synthesis Methodology for Improved Material Discovery*

– We demonstrated a new materials design rule for altering reaction pathways and composition/dimensionality control, by using a two-component flux where one component serves as an effective medium and the other as a tuning knob by varying their ratios.
  – The key innovations and implications in the current work are that: 1) the new chemistry demonstrated provides a generic approach for successful exploratory synthesis 2) the method is highly efficient for rapid discovery because of only two determining synthetic parameters and 3) rational control of dimensionality and building block can be achieved with tunable solubility which is highly effective for complex multiple-anion systems.
  – The chemical systems we explored so far include complex heterostructures with intergrown layers such as *A*(Ba)-*M*-*Q*(O) (*Q* = S or Se, *A* = Na, K, or Rb, *M* = Cu or Ag), $[Sr_2Mn_{1-x}O_2][Cu_{2-y}Li_yQ_2]$, $[Sr_2NiO_2][Cu_2Se_{2-x}S_x]$, $[Ba_3Fe_2O_5][Ag_2Se_2]$, $Li_6[CoSeO_2][Cu_2Se_2]$, K-Ni-S family by oxidation state control such as β-$K_2Ni_3S_4$, $K_2Ni_2S_3$, KNi_4S_2, $K_4Ni_9S_{11}$, and tunable direct gap semiconductors, $Sr(Ag_{1-x}Li_x)_2Se_2$.[1-4] More than 70 new compounds with novel magnetic, metallic and semiconducting characteristics were discovered, published in *Nature*, *Nature Synthesis*, *JACS* and *Angew. Chem.*

- *A new rational approach to effectively stacking heterolayered structures*

- Targeting 2D heterolayers by vertically stacking chemically different layers is a synthesis challenge. We can achieve rapid stacking of oxide layers and chalcogenide layers with precise composition control.
- Our contribution to the development of a new synthesis-science framework for novel materials especially in the challenging class of heterolayered compounds has the following implications: 1) a generic approach for designing novel heterolayered structures 2) highly efficient for rapid discovery because of only two determining synthetic parameters (basicity and temperature) and 3) a universal crystal growth scheme for heterolayers.
- We designed a new heterolayered superconductor and stabilized $[KPbNi_5S_2][KNi_2S_2]$. $KPbNi_5S_2$ is weak antiferromagnetic, while KNi_2S_2 is superconducting below T_c = 0.8 K. However, upon intercalation, $[KPbNi_5S_2][KNi_2S_2]$ showed a T_c of 2.4 K. This 3-fold increase suggests possible interplay between magnetism and superconductivity.

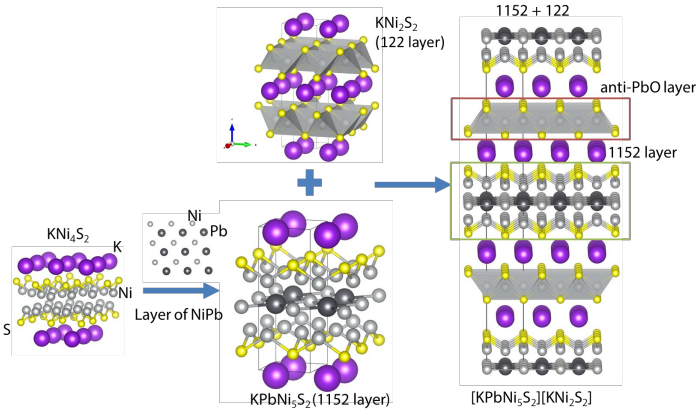

Figure 1: Formation of $[KPbNi_5S_2][KNi_2S_2]$.

- *Exploration of novel intermetallic compounds*

- We applied this new synthetic strategy in Y-Fe-Si system using mixed In/Sn fluxes, observed the phase evolution controlled only by the flux ratio (Figure 2). With mixed In/Sn flux, YSi_2 layers can be inserted to $Y_4Fe_2Si_8$ and $Y_5Fe_4Si_{14}$ ternaries, forming two heterolayered homologous series compounds $[Y_4Fe_2Si_8][nYSi_2]$ (Figure 2b and c) and $[Y_5Fe_4Si_{14}][nYSi_2]$ (Figure 2a), where n = 0, 1. We have discovered over 10 new compounds in the RE-Fe-Si (or Ge) (RE= rare earth metals) systems, which exhibit a broad range of properties such superconductivity, heavy fermion, topological behaviors.

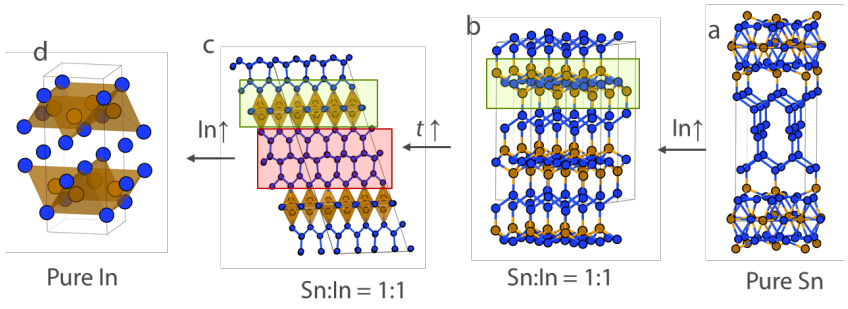

Figure 2. Crystal structures and phase evolution for ternaries of Y-Fe-Si synthesized using mixed In/Sn fluxes at 1000 ºC for a) $Y_9Fe_4Si_{22}$ in Sn flux, b) $YFe_{1-x}Si_2$ in a flux of Sn/In = 1:1, c) heterolayered Y_4FeSi_8 for longer reaction time of b, and d) YFe_2Si_2 in In flux.

Future Plans

1. We will target heterolayers with Ni^{3+} in Ruddlesden-Popper type oxide layers at higher temperatures and then use hydride reduction[5,6] to obtain $[Sr_2Se][Sr_2Ni_2O_4]$ from $[Sr_2Se][Sr_2Ni_2O_6]$ post-synthetically. We also plan to dope the Sr site with Na or K to form $[Sr_{2-x}A_xSe][Sr_2Ni_2O_4]$ (A = Na or

K; x = 0-0.6) to obtain samples with Ni oxidation state varying from +1 to +1.3. Such doping will allow us to obtain the optimal electron filling level for Ni. In addition, partially replacing Sr with Ba in the final sample [AE_2Se][$AE_2Ni_2O_4$] may add the ability to tune the chemical pressure to induce changes in their physical properties

2. We will also perform exploratory synthesis work using mixed metal fluxes to find new superconductors and/or quantum material with novel quantum states in the RE-Fe-Si (or Ge) and A(AE)-Ag-Se systems.
3. High-pressure can alter the electronic structure of materials and lead to dramatic changes in the properties, such as enhancing electron-phonon coupling such that superconductivity can emerge.[8] The semiconductor candidates for high pressure study include $(BaI)_2Se_2$, $(SrI)_2Se_2$, $BaSe_2$, $SrSe_2$ and $BaSe_3$, all containing Se-Se bonds.

References

1. Zhou, X.; Wilfong, B.; Chen, X.; Laing, C.; Pandey, I. R.; Chen, Y.-P.; Chen, Y.-S.; Chung, D.-Y.; Kanatzidis, M. G. $Sr(Ag_{1-x}Li_x)_2Se_2$ and $[Sr_3Se_2][(Ag_{1-x}Li_x)_2Se_2]$ Tunable Direct Band Gap Semiconductors. *Angewandte Chemie International Edition* **2023**, *62*, e202301191.
2. Zhou, X.; Malliakas, C. D.; Yakovenko, A. A.; Wilfong, B.; Wang, S. G.; Chen, Y.-S.; Yu, L.; Wen, J.; Balasubramanian, M.; Wang, H.-H.; Chung, D. Y.; Kanatzidis, M. G. Coherent approach to two-dimensional heterolayered oxychalcogenides using molten hydroxides. *Nature Synthesis* **2022**, *1*, 729.
3. Zhou, X.; Kolluru, V. S. C.; Xu, W.; Wang, L.; Chang, T.; Chen, Y.-S.; Yu, L.; Wen, J.; Chan, M. K. Y.; Chung, D. Y.; Kanatzidis, M. G. Discovery of chalcogenides structures and compositions using mixed fluxes. *Nature* **2022**, *612*, 72.
4. Zhou, X.; Mandia, D. J.; Park, H.; Balasubramanian, M.; Yu, L.; Wen, J.; Yakovenko, A.; Chung, D. Y.; Kanatzidis, M. G. New Compounds and Phase Selection of Nickel Sulfides via Oxidation State Control in Molten Hydroxides. *Journal of the American Chemical Society* **2021**, *143*, 13646.
5. Hayward, M. A.; Green, M. A.; Rosseinsky, M. J.; Sloan, J. Sodium Hydride as a Powerful Reducing Agent for Topotactic Oxide Deintercalation: Synthesis and Characterization of the Nickel(I) Oxide LaNiO2. *Journal of the American Chemical Society* **1999**, *121*, 8843.
6. Li, D.; Lee, K.; Wang, B. Y.; Osada, M.; Crossley, S.; Lee, H. R.; Cui, Y.; Hikita, Y.; Hwang, H. Y. Superconductivity in an infinite-layer nickelate. *Nature* **2019**, *572*, 624.
7. Androulakis, J.; Peter, S. C.; Li, H.; Malliakas, C. D.; Peters, J. A.; Liu, Z.; Wessels, B. W.; Song, J.-H.; Jin, H.; Freeman, A. J.; Kanatzidis, M. G. Dimensional Reduction: A Design Tool for New Radiation Detection Materials. *Advanced Materials* **2011**, *23*, 4163.
8. Ashcroft, N. W.; Mermin, N. D. *Solid state physics*; Cengage Learning, 2022.

New Cooperative Adsorbents and Regeneration Methods for the Efficient Removal of Carbon Dioxide from Air

Jeffrey R. Long,[1,2] Wibe A. de Jong,[1] Hanna M. Breunig,[1] Sean D. Lubner[1,3]

[1]Lawrence Berkeley National Laboratory, [2]University of California, Berkeley, [3]Boston University

Keywords: carbon removal, direct air capture, polyamine, metal−organic framework, solar energy

Research Scope

The direct air capture (DAC) of CO_2 is a promising negative emissions technology that could help stave off the direct effects of anthropogenic climate change. Because of the ultra-dilute concentration of CO_2 in air, DAC materials must exhibit high CO_2 sorption capacities, rapid sorption kinetics, high selectivity and stability to humid and oxygen-rich streams. We have discovered that a molecular polyamine demonstrates DAC with record-breaking capacities over double that of the next leading sorbent. Our goal is to develop a new class of robust polyamine absorbents that, alongside DAC, demonstrate long-term oxidative stability in air and thermal stability throughput sorbent regeneration. We are further utilizing such absorbent properties within a custom and operationally simple DAC device capable of passive adsorption and solar energy-driven regeneration with minimal energy consumption and labor participation.

Recent Progress

Phase-Change Polyamine Absorbents. Diamine-appended MOFs of the type diamine–Mg_2(dobpdc) (dobpdc^{4-} = 4,4'-dioxidobiphenyl-3,3'-dicarboxylate) and related frameworks have been shown to cooperatively adsorb CO_2 from air to form ammonium carbamate chains. The one-dimensional pores of these MOFs template chain formation, endowing the materials with high selectivity and separation capacities for CO_2.[1-3] However, the gravimetric CO_2 separation capacities achievable with such materials are fundamentally limited as a result of the supporting metal–organic structures. We hypothesized that light-weight molecular polyamines containing a rigid core and multiple pendant amine groups could absorb CO_2 to form a hydrogen-bonded three-dimensional ammonium carbamate network. We previously reported that the molecular triamine 1,3,5-tris(aminomethyl)benzene (TriH) readily captures CO_2 via a phase

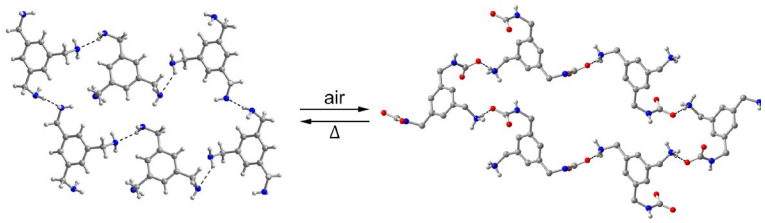

Figure 1. Single-crystal x-ray diffraction structures of TriH and $TriHCO_2$. Upon air exposure, TriH absorbs CO_2 to form a porous hydrogen-bonded ammonium carbamate network with a structure resembling a honeycomb net.

transition to yield $TriHCO_2$, a crystalline and porous ammonium carbamate network (Figure 1). *In situ* powder x-ray diffraction and infrared spectroscopy analyses revealed that the phase transformation from TriH to $TriHCO_2$ is complete within one hour. Breakthrough analyses reveal that TriH exhibits exceptionally high gravimetric CO_2 capacities over a wide range of climate-relevant temperatures (10 to 40 °C) and relative humidities (0% to 80%). TriH demonstrates increased gravimetric CO_2 capacities at high relative humidities, low temperatures, and high flow rates, reaching capacities as high as 8.89 mmol CO_2/g TriH, which is the largest gravimetric capacity measured to date for any solid adsorbent under DAC conditions. Periodic DFT calculations of CO_2 chemisorption by TriH under humid conditions revealed that water mediates ammonium carbamate hydrogen bond formation, which serves as a thermodynamic driving force for CO_2 binding. More broadly, these results highlight the prospect of developing a new class of tunable molecular polyamines for carbon capture from air.

Passive Direct Air Capture of CO_2. Conventional DAC technologies often include significant system complexity and energy costs to overcome slow CO_2 diffusion, adsorption kinetics, and material regeneration[4,5] which contribute to high costs ($500−800/$t_{CO2}$)[6] and high energy requirements (7−10 GJ/t_{CO2}).[7,8] We recently designed and demonstrated an operationally simple, completely passive DAC device that is energetically maintained with inexpensive and ubiquitous solar energy. Our simple device achieves passive DAC by aligning the carbon capture cycle with the natural day-night cycle (Figure 2). Sunlight is captured and converted into heat for the desired system temperature with a compound parabolic concentrator without active tracking. Our prototype utilized an amine-appended MOF for passive DAC system integration, capturing 16.4 g CO_2/100 g in a 30-day field test without human intervention. A complete techno-economic analysis of a DAC process using this device predicts a capture potential of 10 Gt_{CO2}/year at selected location using less than 1% of global land at a levelized cost as low as $90/$t_{CO2}$, less than the "Carbon Negative Shot" 2030 goal ($100/$t_{CO2}$) established by the U.S. DOE.[9] Cost sensitivity suggests that adsorbent performance can impact system-level performance by as much as 80%. Therefore, future efforts will also focus on improving sorbent capture capacity and operational durability and testing the device with next-generation adsorbents.

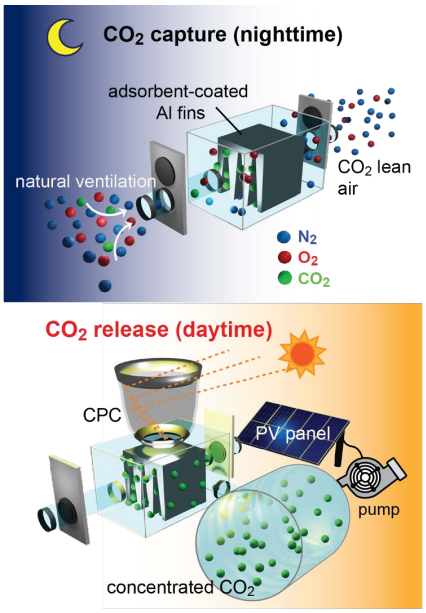

Figure 2. Illustration of completely passive DAC of CO_2 driven only by solar energy. At night, natural ventilation flows ambient air (CO_2-rich) into the DAC unit. The CO_2 in air is taken up by the cooperative adsorbent. In the daytime, the captured CO_2 is desorbed by solar heating and collected by solar power-driven equipment.

References

1. T. M. McDonald, J. A. Mason, X. Kong, E. D. Bloch, D. Gygi, A. Dani, V. Crocellà, F. Giordanino, S. O. Odoh, W. S. Drisdell, B. Vlaisavljevich, A. L. Dzubak, R. Poloni, S. K. Schnell, N. Planas, K. Lee, T. Pascal, L. F. Wan, D. Prendergast, J. B. Neaton, B. Smit, J. B. Kortright, L. Gagliardi, S. Bordiga, J. A. Reimer, and J. R. Long, *Cooperative Insertion of CO_2 in Diamine-Appended Metal–Organic Frameworks*, Nature **519**, 303–308 (2015).
2. R. L. Siegelman, T. M. McDonald, M. I. Gonzalez, J. D. Martell, P. J. Milner, J. A. Mason, A. H. Berger, A. S. Bhown, and J. R. Long, *Controlling Cooperative CO_2 Adsorption in Diamine-Appended Mg_2(dobpdc) Metal–Organic Frameworks*, J. Am. Chem. Soc. **139**, 10526–10538 (2017).
3. E. J. Kim, R. L. Siegelman, H. Z. H. Jiang, A. C. Forse, J.-H. Lee, J. D. Martell, P. J. Milner, J. M. Falkowski, J. B. Neaton, J. A. Reimer, S. C. Weston, and J. R. Long, *Cooperative Carbon Capture and Steam Regeneration with Tetraamine-Appended Metal–Organic Frameworks*, Science **369**, 392–396 (2020).
4. D. W. Keith, G. Holmes, D. S. Angelo, and K. Heidel, *A Process for Capturing CO_2 from the Atmosphere*. Joule **2**, 1573–1594 (2018).
5. K. S. Lackner, *Capture of Carbon Dioxide from Ambient Air*, Eur. Phys. J. Special Topics **176**, 93–106 (2009).
6. S. Deutz, and A. Bardow, *Life-Cycle Assessment of an Industrial Direct Air Capture Process Based on Temperature–Vacuum Swing Adsorption*, Nature Energy **6**, 203–213 (2021).
7. C. Clifford, From Milligrams to Gigatons: Startup That Sucks Carbon Dioxide from the Air is Building a Big Plant in Iceland. CNBC (2022). https://www.cnbc.com/2022/06/28/climeworks-carbon-dioxide-removal-company-building-iceland-plant.html
8. K. Lebling, H. Leslie-Bole, Z. Byrum, and L. Bridgwater. *6 Things to Know About Direct Air Capture*, World Resources Institute, (2022). https://www.wri.org/insights/direct-air-capture-resource-considerations-and-costs-carbon-removal/
9. J. Kerry, and G. McCarthy, *The Long-Term Strategy of the United States – Pathways to Net-Zero Greenhouse Gas Emissions by 2050*, (2021). https://unfccc.int/documents/308100

Publications

1. K. M. Jablonka, Q. Ai, A. Al-Feghali, S. Badhwar, J. D. Bocarsly, A. M. Bran, S. Bringuier, L. C. Brinson, K. Choudhary, D. Circi, S. Cox, W. A. de Jong, M. L. Evans, N. Gastellu, J. Genzling, M. V. Gil, A. K. Gupta, Z. Hong, A. Imran, S. Kruschwitz, A. Labarre, J. Lála, T. Liu, S. Ma, S. Majumdar, G. W. Merz, N. Moitessier, E. Moubarak, B. Mouriño, B. Pelkie, M. Pieler, M. C. Ramos, B. Ranković, S. G. Rodriques, J. N. Sanders, P. Schwaller, M. Schwarting, J. Shi, B. Smit, B. E. Smith, J. Van Herck, C. Völker, L. Ward, S. Warren, B. Weiser, S. Zhang, X. Zhang, G. A. Zia, A. Scourtas, K. J. Schmidt, I. Foster, A. D. White, and B. Blaiszik, *14 Examples of How LLMs Can Transform Materials Science and Chemistry: A Reflection on a Large Language Model Hackathon*, Digit. Discov. **2**, 1233–1250 (2023). doi: 10.1039/D3DD00113J.
2. A. K. Gupta, M. Stulajter, Y. Shaidu, J. B. Neaton, and W. A. de Jong, *Equivariant Neural Networks Utilizing Molecular Clusters for Accurate Molecular Crystal Binding Energy Predictions*, manuscript under review.
3. A. J. Huang, A. K. Gupta, H. Z. H. Jiang, H. Zhuang, M. B. Wenny, R. A. Klein, H. Kwon, W. A. de Jong, J. A. Reimer, C. M. Brown, and J. R.; Long, J. R. *Cooperative Carbon Dioxide Capture from Air with a Molecular Triamine Network Solid*, manuscript under revision.
4. J. Zeng, H. Tsai, H. W. Lim, M. N. Dods, Z. Zhu, H. Albers, A. Huang, M. Ye, H. Furukawa, H. Breunig, J. R. Long, R. S. Prasher, and S. D. Lubner, *Completely Passive Capture of Carbon Dioxide from Air*, manuscript under review.

Elucidating the Electrochemically Enhanced Surface Diffusion Mechanism in Materials for Clean Energy

Pietro Papa Lopes, Materials Science Division, Argonne National Laboratory

Keywords: electrochemistry, durability, dissolution, redeposition, surface diffusion

Research Scope

The process of surface diffusion in electrochemical environments is an important step in understanding changes to materials structure and composition, particularly for materials where its functional properties are dictated by its surface properties, e.g. electrocatalysts. Despite its significance, a deep understanding of the mechanism of surface diffusion in electrochemical media, which can be orders of magnitude greater than in gas-phase, remains elusive. This project focuses on deriving an understanding of surface diffusion processes in electrochemistry as it relates to dissolution and redeposition events at the nanoscale. By establishing the factors contributing to the rates of dissolution/redeposition such as surface orientation, adsorbate species, electrode potential, pH, nature of ion species, and temperature, we will be able to not only gain insights on how to control the rates of surface diffusion, but also how to reconstruct and regenerate materials surfaces. To achieve these goals, we employ the use of well-defined materials such as single crystal surfaces with selected surface orientation and composition such as Iridium to create well-defined interfaces in aqueous-based electrolytes, that serve both as a "blank" canvas for tracking changes to surface morphology, as well as to elucidate the role of defects in directing dissolution and redeposition events. The findings from this project will help us understand how dissolution and redeposition steps contribute to materials degradation rates and mechanisms[1], enhancing our knowledge about strategies to control, at the materials level, the durability of clean energy systems such as fuel cells, electrolyzers, and batteries.

Recent Progress

To understand the process of dissolution and the factors controlling it, we need to establish the adsorption processes and the key surface species forming on the electrode surface as a function of the electrode potential and pH. We have continued our investigation to extend the study of surface speciation and dissolution to cover different pH ranges, namely neutral (pH 7) and alkaline (pH 13), for Ir(111), Ir(100), and Ir(110) surfaces. Within the potential window between 0 and 1V vs RHE we have identified three key adsorption species, namely H_{upd} (under potential deposition, upd), OH_{ad} (adsorbed, ad), and O_{ad}. Furthermore, we found that there is an overlap between H_{upd} desorption and OH_{ad} adsorption at the same potential, as well as OH_{ad} transitioning to O_{ad}, which confirms theoretical surface energetic calculations[2]. Adsorption trends across different surfaces

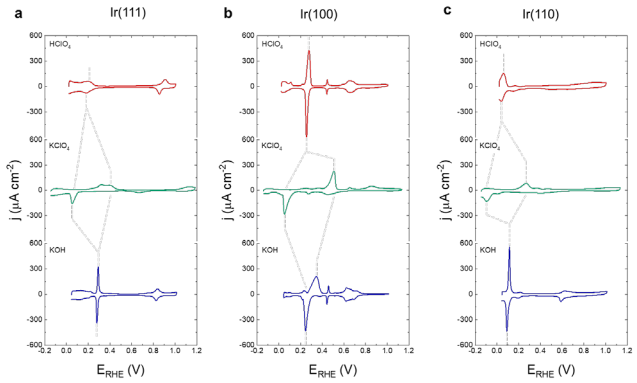

Figure 1. Cyclic voltammograms for: a) Ir(111), b) Ir(100), and c) Ir(110) in 0.1 M $HClO_4$ (pH = 1, top), $KClO_4$ (pH = 7, middle), and KOH (pH = 13, bottom) electrolytes, at 0.05 V s^{-1}. Dashed lines highlight the adsorption potential splitting due to slower water splitting in neutral media

highlight the formation of adsorbate layers at different surface sites (atop and interstitial) that are allowed in (100) but are not easily observed on (111) and (110) surface. Most importantly, however, when changing the electrolyte pH as shown in Figure 1, there is a stark contrast in the adsorption signature across all surfaces, particular at neutral pH. It is well-known that breaking H-OH bond in water is a slow reaction, impacting the rates of H_2 evolution in alkaline media, for example[3,4]. However, OH_{ad} formation in acidic media depends upon water bond breaking, while H_{upd} formation in alkaline media also depends on water bond breaking which are relatively fast processes as suggested by the adsorption signatures in Figure 1. In contrast, the adsorption/desorption peaks in neutral pH show a large potential splitting, meaning a large positive potential shift for the H_{upd} desorption and OH_{ad} and O_{ad} adsorption, and a large negative potential shift for the reverse steps. These results indicate that not only water splitting is a slow process controlling the rates of surface species formation, but that H_2O-H^+ and H_2O-OH^- adducts help with water splitting in more extreme pH environments, a surprising result but that is in line with molecular dynamic studies of the hydrogen bond network in aqueous systems[5]. These bond-breaking dynamics are further modulated by the nature of the alkali cation, which have been shown to influence the adsorption energetics and kinetics[6].

To further characterize the adsorbate species present at the interface we have deployed the use of Shell-Isolated Nanoparticle Enhanced Raman Spectroscopy (SHINERS) over Ir(hkl) surface, which can provide unique spectroscopic evidence for the formation of the adsorbate layers and sub-layers and their evolution as a function of electrode potential. As shown in Figure 2, there is clear evidence for the formation of Ir-H bonds with vibrational signature around ~1550 cm^{-1} and ~2100 cm^{-1} at 0.04 V, while Ir-OH can also be observed (peak at ~1100 cm^{-1}) along with Ir-H at 0.19 V, confirming the co-adsorption of these species. Further work is ongoing to determine the surface speciation when transition between metal and metal oxide is occurring, as formation of Ir-O-Ir can be seen around 0.9 V will have implications to the nature of the Iridium oxide used for O_2 evolution reaction as well as on the dissolution mechanism.

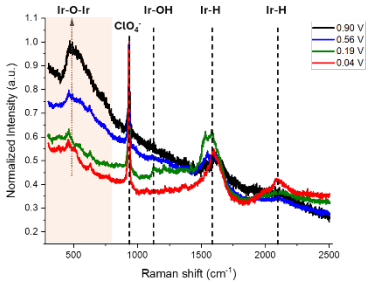

Figure 2. SHINERS results of surface adsorbate species formed on Ir(111) surfaces in 0.1 M $HClO_4$ electrolyte at various electrode potentials.

References

1. P. P. Lopes, *A Framework for the Relationships between Stability and Functional Properties of Electrochemical Energy Materials*, ACS Materials Au **3**, **1**, 8-17 (2023).

2. K. Klyukin, A. Zagalskaya, V. Alexandrov, *Ab Initio Thermodynamics of Iridium Surface Oxidation and Oxygen Evolution Reaction*, Journal of Physical Chemistry C **122**, 29350–29358 (2018).

3. R. Subbaraman, D. Tripkovic, D. Strmcnik, K.-C. Chang, M. Uchimura, A. P. Paulikas, V. R. Stamenkovic, N. M. Markovic, *Enhancing Hydrogen Evolution Activity in Water Splitting by Tailoring Li+-Ni(OH)2-Pt Interfaces*, Science, **334**, **6060**, 1256-1260, (2011).

4. D. Strmcnik, M. Uchimura, C. Wang, R. Subbaraman, N. Danilovic, D. V. Vliet, A. P. Paulikas, V. R. Stamenkovic, N. M. Markovic, *Improving the hydrogen oxidation reaction rate by promotion of hydroxyl adsorption*, Nature Chemistry, **5**, 300–306 (2013).

5. P. Gilli, G. Gilli, *Hydrogen Bond Models and Theories: The Dual Hydrogen Bond Model and its Consequences*, Journal of Molecular Structure, **972**, 2-10, (2010).

6. P. P. Lopes, D. Strmcnik, J. S-Jirkovsky, J. G. Connell, V. R. Stamenkovic, N. Markovic, *Double layer effects in electrocatalysis: The oxygen reduction reaction and ethanol oxidation reaction on Au(111), Pt(111) and Ir(111) in alkaline media containing Na and Li cations.* Catalysis Today **262**, 41–47 (2016).

7. F. Sugimura, N. Sakai, T. Nakamura, M. Nakamura, K. Ikeda, T. Sakai, N. Hoshi, *In situ observation of Pt oxides on the low index planes of Pt using surface enhanced Raman spectroscopy*, Physical Chemistry Chemical Physics, 19, 27570-27579, (2017).

8. F. Bizzotto, H. Ouhbi, Y. Fu, G. K. H. Wiberg, U. Aschauer, M. Arenz, *Examining the Structure Sensitivity of the Oxygen Evolution Reaction on Pt Single-Crystal Electrodes: A Combined Experimental and Theoretical Study*, ChemPhysChem, **20**, **22**, 3154-3162, (2019).

Publications

1. P. P. Lopes, *A Framework for the Relationships between Stability and Functional Properties of Electrochemical Energy Materials*, ACS Materials Au **3**, **1**, 8-17 (2023).

Precision synthesis and assembly of ionic and liquid crystalline polymers

Paul Nealey*, Juan J de Pablo*, Matthew Tirrell*, and Jie Xu[+]

Materials Science Division*, and Nanoscience and Technology[+], Argonne National Laboratory, Lemont, Illinois 60439, USA

Keywords: precision synthesis, self-assembly, hetero-charged polymers, nanostructured polyelectrolytes, mixed conductors

Research Scope

This project advances the discovery of new principles towards a fundamental understanding of the chemistry, physics, and materials science of charged nanostructured and functional polymer and soft matter systems, both at equilibrium and far from equilibrium. Our approach relies on the synthesis of polymers with precise composition and sequence, as well as the processing these new materials through controlled molecular self- and directed self-assembly. Molecular self-assembly, with basic tenets derived from biology, is arguably the most promising strategy for imparting structure and function to materials at the molecular, meso-, and macro-scale and for developing functional soft and biomolecular materials; information encoded into the building blocks introduces specific and controllable intra- and intermolecular interactions to drive assembly with hierarchical structure. Because the assembly, structure, and dynamics of functional polymer and soft matter systems are complicated, a unifying concept and defining strength of our overall project is the combination of experiment, autonomous laboratories, theory, computation, and data driven approaches to accelerate materials discovery and design. Our effort and progress reported below is organized along three interrelated thrusts: Thrust 1: Fundamental Investigation of Water Absorption and Ion Transport Mechanisms in Homopolymer and Block Copolymer Electrolytes, Thrust 2: High-Throughput Robotic Experimentation and Computation for Designing Mixed Conducting Polymers, and Thrust 3: Hybrid Coacervation, Surface Interactions and Their Modification with Polyampholytes. Fundamental materials and principles discovered in his project will impact a wide array of energy technologies, ranging from fuel cells, electrolyzers, and desalination, to energy storage, energy-efficient devices, neuromorphic computing, and electrochemical sensors, to antifouling coatings for separation membranes.

Recent Progress

For this DOE/BES Materials Chemistry Principal Investigators' Meeting, we will focus on our new research Thrust 2. Our objective is to elucidate the fundamental concepts necessary to achieve efficient ion conductivity and electronic charge mobility in solid-state mixed-conducting polymers. Our design strategy focuses on three key criteria: 1) balancing segmental dynamic mobility for ion transport with ordered π-conjugation for electron/hole transport in a single polymer design, 2) achieving dual-continuous pathways for ion and electron transport within one assembled microstructure, and 3) rapidly extracting the formulation-structure-properties relationships to develop design principles. Preliminary results from each of these areas are described below.

The influence of click-chemistry for the side-chain functionalization on the ionic-conducting properties. We developed a synthetic strategy suitable for high-throughput design and synthesis of mixed conductors. Our study examined the impact of linkage chemistry, side chain length, side chain polarity, and the position of polar groups on ion transport and aggregation in polymerized ionic liquids. We discovered that polymers with click chemistry linkages exhibited a 10-fold decrease in ionic conductivity at 30°C due to ionic aggregation from changes in side chain polarity (Figure 1a). Adding three ethylene glycol groups at various positions indicated that ionic conductivity depends on overall side chain polarity, not the position of the polar group (Figure 1b). This study demonstrates click chemistry can be a good synthetic tool for high-throughput synthesis and provides insights into ion transport mechanisms in polymerized ionic liquids, with potential applications for mixed conductors.

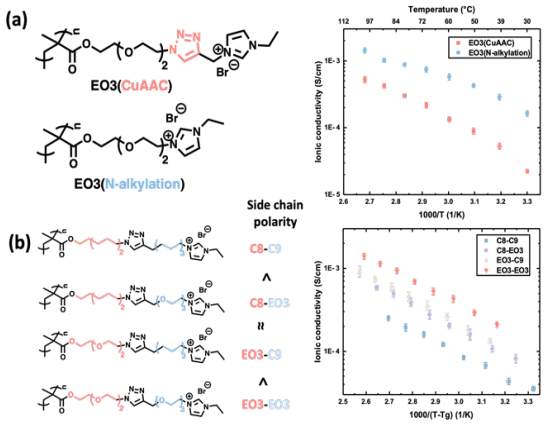

Figure 1. (a) Chemical structure and ionic conductivity for with/ without click chemistry; (b) Chemical structure and T_g normalized conductivity for polymers with different side chain polarity.

Nanostructured morphology achieved with conjugated polymer and ionic polymer blends. We hypothesize that confinement of mixed-conducting polymers into percolated nanostructures can enhance the chain dynamics and enable multi-scale conjugated polymer ordering which are all desirable for ion transport and electronic charge transport in one assembled microstructure[2, 3]. In Figure 2, we used the conjugated polymer and ionic polymer phase separation method to form such percolated nanostructures in mix-conducting polymers (Figure 2). In the future, we will investigate how such assembled nanostructured morphology influence the ion and electron transport within the materials.

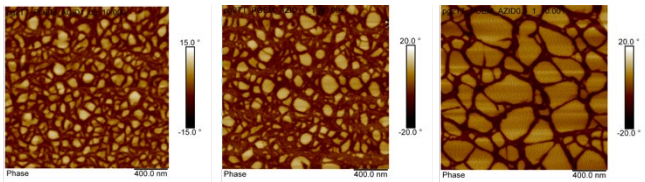

Figure 2. Nanoscale percolated nanostructures in blending systems by phase separation.

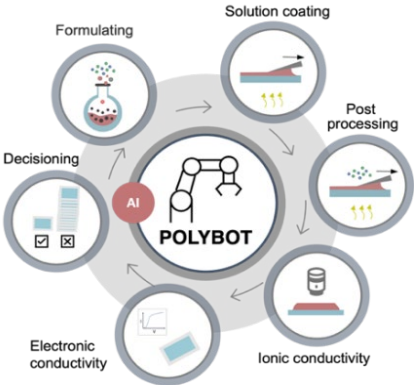

Figure 3. Robotic and machine learning tools to enable rapid exploration.

High-Throughput robotic experimentation platform for mix-conductors. To employ the "materials genome" approach for extracting design principles of mixed-conducting polymers, we are developing a high-throughput robotic experimentation platform integrated with machine learning[4]. This automated platform can synthesize, process, and fabricate mixed conductors into devices. The electronic and ionic conductivity will be measured using electrical impedance spectroscopy (EIS) and organic electrochemical transistors (OECT). This approach allows us to explore a vast chemical design space for achieving mixed conductors with a single polymer design and an assembled microstructure.

References

1. N. Li, Y. Dai, Y. Li, S. Dai, J.Strzalka, Q. Su, N. D. Oliveira, Q. Zhang, P. B. J. S. Onge, S. R.-Gagne, Y. Wang, X. Gu, J. Xu, S. Wang. A universal and facile approach for building multifunctional conjugated polymers for human-integrated electronics. Matter 4, 3015 (2021).
2. J. Xu, S. Wang, G.-J. N. Wang, C. Zhu, S. Luo, L. Jin, X. Gu, S. Chen, V. R. Feig, J.W.F. To, S. Rondeau-Gagné, J. Park, B. C. Schroeder, C. Lu, J. Y. Oh, Y. Wang, Y.-H. Kim, H. Yan, R. Sinclair, D. Zhou, G. Xue, B. Murmann, C. Linder, W. Cai, J. B.-H. Tok, J. W. Chung, Z. Bao, Highly stretchable polymer semiconductor films through the nanoconfinement effect, Science, 355, 59, (2017).
3. J. Xu, HC. Wu, C. Zhu, A, Ehrlich, L. Shaw, M. Nikolka, S. Wang, F. Molina-Lopez, X. Gu, S. Luo, D. Zhou, Y. Kim, G. Wang, K. Gu, V. R. Feig, S. Chen, Y. Kim, T. Katsumata, Y. Zheng, H. Yan, J. W. Chung, J. Lopez, B. Murmann, Z. Bao, Multi-scale ordering in highly stretchable polymer semiconducting films, Nature Materials, 18 (6), 594-601 (2019)
4. A. Vriza, H. Chan, J, Xu, Self-driving laboratory for polymer electronics, Chemistry of Materials 35 (8), 3046-3056 (2023)

Publications

5. 1. L. Zhang, C. Liu, H. Cao, A. J. Erwin, D. D. Fong, A. Bhattacharya, L. Yu, L. Stan, C. Zou, M. V. Tirrell, H. Zhou, W. Chen, Redox Gating for Colossal Carrier Modulation and Unique Phase Control, Adv. Mater. 36, 2308871 (2024).
6. 2. G. A. Vásquez-Montoya, T. Emeršič, N. Atzin, A. Tavera-Vázquez, A. Mozaffari, R. Zhang, O. Guzmán, A. Snezhko, P. F. Nealey, J. J. de Pablo, Control of liquid crystals combining surface acoustic waves, nematic flows, and microfluidic confinement, Soft Matter 20, 397–406 (2024).
7. 3. X. Tang, N. Atzin, A. Mozaffari, S. Das, N. L. Abbott, J. J. de Pablo, Generation and Propagation of Flexoelectricity-Induced Solitons in Nematic Liquid Crystals, ACS Nano 18, 10768–10775 (2024).
8. 4. R. J. Sánchez-Leija, J. A. Mysona, J. J. de Pablo, P. F. Nealey, Phase Behavior and Conformational Asymmetry near the Comb-to-Bottlebrush Transition in Linear-Brush Block Copolymers, Macromolecules 57, 2019–2029 (2024).
9. 5. J. A. Mysona, P. F. Nealey, J. J. de Pablo, Machine Learning Models and Dimensionality Reduction for Prediction of Polymer Properties, Macromolecules 57, 1988–1997 (2024).
10. 6. Y. Qiao, Q. He, H.-H. Huang, D. Mastropietro, Z. Jiang, H. Zhou, Y. Liu, M. V. Tirrell, W. Chen, Stretching of immersed polyelectrolyte brushes in shear flow, Nanoscale 15, 19282–19291 (2023).
11. 7. N. Atzin, A. Mozaffari, X. Tang, S. Das, N. L. Abbott, J. J. de Pablo, Minimal Model of Solitons in Nematic Liquid Crystals, Phys. Rev. Lett. 131, 188101 (2023).
12. 8. Y. N. Fang, A. M. Rumyantsev, A. E. Neitzel, H. Liang, W. T. Heller, P. F. Nealey, M. V. Tirrell, J. J. de Pablo, Scattering Evidence of Positional Charge Correlations in Polyelectrolyte Complexes, Proc. Natl. Acad. Sci. 120, e2302151120 (2023).
13. 9. K. C. Stevens, M. V. Tirrell, Structure and properties of bottlebrush polyelectrolyte complexes, J. Polym. Sci. in press (2024).
14. 10. H. He, H. Liang, M. Chu, Z. Jiang, J. J. de Pablo, M. V. Tirrell, S. Narayanan, W. Chen, Transport Coefficient Approach for Characterizing Non-equilibrium Dynamics in Soft Matter, Proc. Natl. Acad. Sci. in press (2024).

Enabling Durability in Adsorbents for Negative Carbon Emissions (ENDURANCE)

Simon H. Pang, Materials Science Division, Lawrence Livermore National Laboratory

Wade A. Braunecker, Materials, Chemical, and Computational Science Directorate, National Renewable Energy Laboratory

Christopher W. Jones, School of Chemical & Biomolecular Engineering, Georgia Institute of Technology

Nicholas A. Strange, SLAC National Accelerator Laboratory

Keywords: direct air capture, CO_2 capture, oxidative degradation mechanism, aminopolymer, polymer mobility

Research Scope

Our objective is to enable discovery of next-generation durable adsorbents for CO_2 direct air capture (DAC) by elucidating foundational molecular and physical phenomena and structure-property-performance relationships underpinning adsorbent degradation and durability. In this phase, we focus on oxidative degradation of amine-based adsorbents due to the plethora of companies aiming to deploy this technology commercially despite lacking the fundamental understanding of the science of durability. Our research highlights the combined impact of polymer chemistry and molecular mobility, influenced by the local adsorbed species, on the relevant degradation mechanism and kinetic effects observed in the literature.

Recent Progress

Oxidative degradation mechanisms. We have developed a comprehensive oxidation reaction network for the prototypical aminopolymer used in DAC, poly(ethylenimine), (Figure 1) generally applicable to oxidative degradation of other aminopolymers.[1] This reaction network consists of three major types of events that lead to inactivation or loss of amines: (1) radical propagation, (2) alkylhydroperoxide decomposition leading to C–C bond cleavage and formation of amides, and (3) CO_2-catalyzed C–N bond cleavage and formation of imines. The latter two types of events lead to formation of additional radical species that can propagate

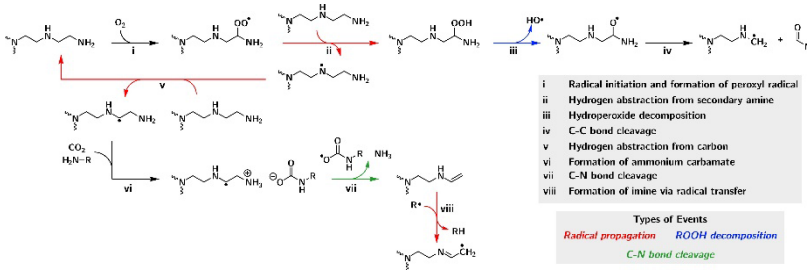

Figure 1. Proposed reaction network for poly(ethylenimine) oxidation, illustrating three types of reaction events that control the overall rate of aminopolymer degradation and the products formed.

through the reaction network or initiate new radicals, similar to the basic autooxidation scheme observed for other types of polymers.[2]

Our proposed reaction network explains the discrepancy in the impact of CO_2 on degradation kinetics reported in the literature. Early studies using flue gas concentrations of CO_2 suggested that CO_2 had a protective effect on amines, minimizing sorbent degradation and improving sorbent lifetime.[3] However, our recent studies have suggested that atmospheric concentrations of CO_2 lead to accelerated sorbent degradation by shuttling protons and reducing the free energy barrier for C–N bond cleavage.[4] We hypothesized that higher concentrations of CO_2—implying larger quantities of adsorbed CO_2—would reduce polymer mobility, leading to slower radical propagation kinetics and overall reducing the rate of degradation as observed in prior studies. A series of accelerated oxidation experiments varying the CO_2 concentration and temperature of oxidation and ab initio metadynamics simulations of the free energy barriers for key reactions at different CO_2 loading confirmed this hypothesis. Figure 2 shows a conceptual summary of the CO_2-dependent kinetic regimes for aminopolymer oxidation.

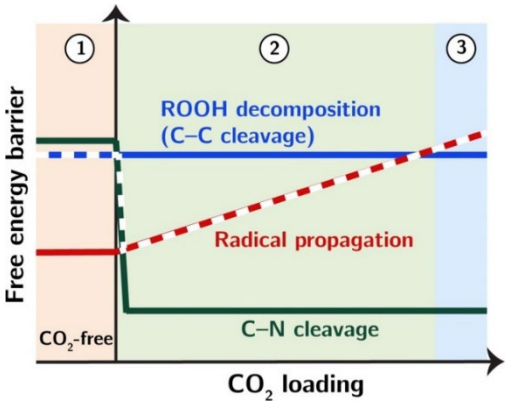

Figure 2. Schematic illustration of the kinetic dependence of key aminopolymer oxidation-driving reactions on CO_2 loading.

Methods for measuring mobility. As demonstrated, polymer and amine mobility is a critical factor for understanding the oxidative degradation of aminopolymers. Our team has developed experimental and computational methods for assessing mobility of aminopolymers confined within nanoporous supports, including techniques based on incorporation of an aggregation-induced emission fluorescent probe,[5, 6] NMR relaxometry,[7] and enhanced sampling with grand-canonical Monte Carlo simulations using machine learning-derived reaction potentials (Figure 3).[8] In addition to the study described above, these techniques have been used to probe the hypothesis that introduction of hydroxyl groups into the aminopolymer system improves durability due to hydrogen bonding interactions, which reduces the mobility of the polymer. We demonstrated that hydrogen bonds from the hydroxyl to the amine were stronger and persisted significantly longer than hydrogen bonds in between amines, and that the persistence of these hydrogen bonds led to reduced polymer mobility and chain dynamics, presumably leading to reduced rate of radical propagation reactions and suppressing degradation.[9]

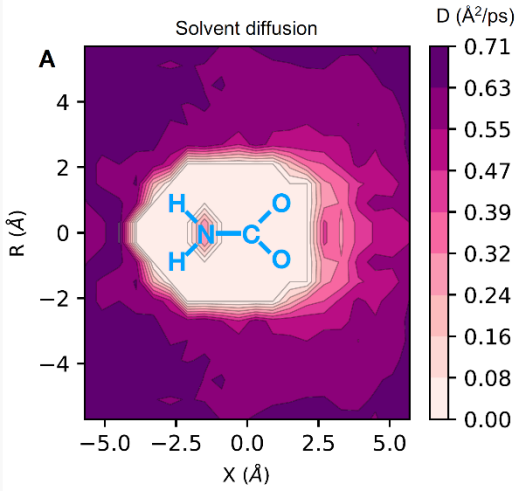

Figure 3. Two-dimensional colormap of solvent dynamics around a bound CO_2 in liquid ammonia, demonstrating the reduction in mobility upon CO_2 adsorption.

References

1. S. Li, Y. Guta, M. F. Calegari Andrade, E. Hunter-Sellars, A. Maiti, A. J. Varni, P. Tang, C. Sievers, S. H. Pang, C. W. Jones, *Competing Kinetic Consequences of CO_2 on the Oxidative Degradation of Branched Poly(ethylenimine)*, submitted.
2. G. Gryn'ova, J. L. Hodgson, M. L. Coote, *Revising the mechanism of polymer autooxidation*, Org. Biomol. Chem. **9**, 480–490 (2011).
3. A. Heydari-Gorji, A. Sayari, *Thermal, Oxidative, and CO_2-Induced Degradation of Supported Polyethylenimine Adsorbents*, Ind. Eng. Chem. Res. **51**, 6887-6894 (2012).
4. Y. A. Guta, J. S. Carneiro, S. Li; G. Innocenti, S. H. Pang, M. A. Sakwa-Novak, C. Sievers, C. W. Jones, *Contributions of CO_2, O_2 and H_2O to the Oxidative Stability of Solid Amine Direct Air Capture Sorbents at Intermediate Temperature,* ACS Appl. Mater. Interfaces **15**, 46790–46802 (2023).
5. H. Correll, N. Leick, R. E. Mow, G. A. Russell-Parks, S. H. Pang, T. Gennett, W. A. Braunecker, *Fluorescent Probe of Aminopolymer Mobility in Bulk and in Nanoconfined Direct Air CO_2 Capture Supports*, J. Phys. Chem. C **126**, 10419–10428 (2022).
6. G. A. Russell-Parks, N. Leick, M. A. T. Marple, N. A. Strange, B. G. Trewyn, S. H. Pang, W. A. Braunecker, *Fundamental Insight into Humid CO_2 Uptake in Direct Air Capture Nanocomposites Using Fluorescence and Portable NMR Relaxometry,* J. Phys. Chem. C **127**, 15363–15374 (2023).
7. E. Hunter-Sellars, J. D. Kerr, H. V. Eshelman, Z. A. Pollard, A. J. Varni, M. A. Sakwa-Novak, M. A. T. Marple, S. H. Pang, *Oxidation of Supported Amines for CO_2 Direct Air Capture: Assessing Impact on Physical Properties and Mobility via NMR Relaxometry*, Macromol. Chem. Phys. (2024), accepted.
8. M. F. Calegari Andrade, S. Li, T. A. Pham, S. A. Akhade, S. H. Pang, *Machine Learning Demonstrates the Impact of Proton Transfer and Solvent Dynamics on CO_2 Capture in Liquid Ammonia*, Chem. Sci. (2024), accepted.
9. S. Li., M. F. Calegari Andrade, A. J. Varni, G. A. Russell-Parks, W. A. Braunecker, E. Hunter-Sellars, M. A. T. Marple, S. H. Pang, *Enhanced Hydrogen Bonding via Epoxide-functionalization Restricts Mobility in Poly(ethylenimine) for CO_2 Capture,* Chem. Comm. **59**, 10737–10740 (2023).

Publications

1. M. F. Calegari Andrade, S. Li, T. A. Pham, S. A. Akhade, S. H. Pang, *Machine Learning Demonstrates the Impact of Proton Transfer and Solvent Dynamics on CO_2 Capture in Liquid Ammonia*, Chem. Sci. (2024), accepted.
2. E. Hunter-Sellars, J. D. Kerr, H. V. Eshelman, Z. A. Pollard, A. J. Varni, M. A. Sakwa-Novak, M. A. T. Marple, S. H. Pang, *Oxidation of Supported Amines for CO_2 Direct Air Capture: Assessing Impact on Physical Properties and Mobility via NMR Relaxometry*, Macromol. Chem. Phys. (2024), accepted.
3. Y. A. Guta, J. S. Carneiro, S. Li; G. Innocenti, S. H. Pang, M. A. Sakwa-Novak, C. Sievers, C. W. Jones, *Contributions of CO_2, O_2 and H_2O to the Oxidative Stability of Solid Amine Direct Air Capture Sorbents at Intermediate Temperature,* ACS Appl. Mater. Interfaces **15**, 46790–46802 (2023).
4. S. Li., M. F. Calegari Andrade, A. J. Varni, G. A. Russell-Parks, W. A. Braunecker, E. Hunter-Sellars, M. A. T. Marple, S. H. Pang, *Enhanced Hydrogen Bonding via Epoxide-functionalization Restricts Mobility in Poly(ethylenimine) for CO_2 Capture,* Chem. Comm. **59**, 10737–10740 (2023). Front cover article.
5. J. S. Carneiro, G. Innocenti, H. J. Moon, Y. Guta, L. Proaño, C. Sievers, M. A. Sakwa-Novak, E. W. Ping, C. W. Jones, *Insights into the Oxidative Degradation Mechanism of Solid Amine Sorbents for CO_2 Capture from Air: Roles of Atmospheric Water*, Angew. Chem. Int. Ed. **135**, e202302887 (2023).
6. G. A. Russell-Parks, N. Leick, M. A. T. Marple, N. A. Strange, B. G. Trewyn, S. H. Pang, W. A. Braunecker, *Fundamental Insight into Humid CO_2 Uptake in Direct Air Capture Nanocomposites Using Fluorescence and Portable NMR Relaxometry,* J. Phys. Chem. C **127**, 15363–15374 (2023).
7. S. Li, M. R. Céron, H. V. Eshelman, A. J. Varni, A. Maiti, S. A. Akhade, S. H. Pang, *Probing the Kinetic Origin of Varying Oxidative Stability of Ethyl- vs. Propyl-spaced Amines for Direct Air Capture*, ChemSusChem **16**, e2022019 (2023).

Solid State NMR Spectroscopy for Advanced Energy Materials

Rana Biswas, Wenyu Huang, Takeshi Kobayashi, Frederic A. Perras, Aaron J. Rossini, Javier Vela

Ames National Laboratory, Ames, Iowa, USA

Keywords: materials characterization, semiconductor materials, 2D materials, porous materials, NMR spectroscopy

Research Scope

The overarching goal of the Ames National Laboratory materials solid-state nuclear magnetic resonance (SSNMR) spectroscopy program is to advance the science of nanomaterials by revealing the link between material properties and the structures of their bulk, interfaces, and defects. Nanomaterials will fulfill current and future societal needs related to optoelectronic devices, energy storage and conversion, quantum information, sensing, and separations/purifications. To advance the science and applications of nanomaterials, analytical techniques capable of probing the molecular structure of surfaces, defects, and disordered systems are required. Our team develops SSNMR methods that exploit dynamic nuclear polarization (DNP) or fast magic angle spinning (MAS) to enhance NMR sensitivity and resolution, enabling atomic-level structure determination. Relationships between structure and properties can then be formed for semiconductor nanocrystals (NC) and disordered 2D materials (**Figure 1**). We also apply DFT calculations to model the structure of materials, their NMR signatures, and predict properties.

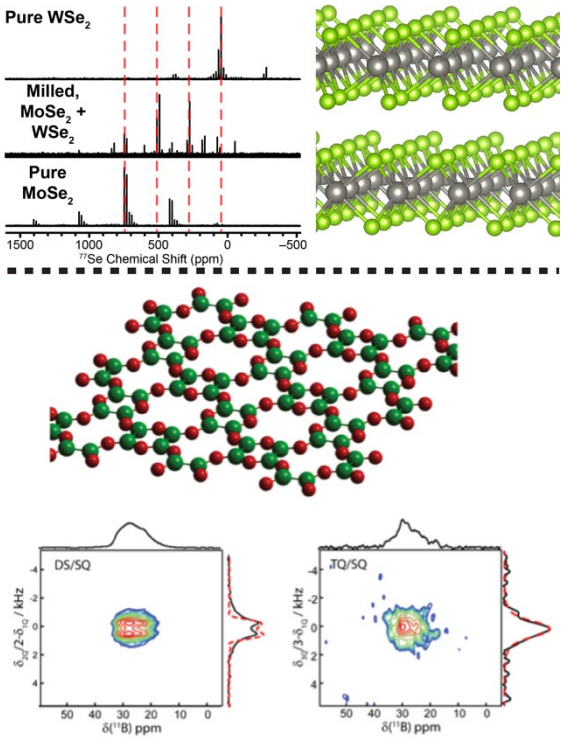

Figure 1. (upper) ^{77}Se SSNMR spectra of WSe_2, ball-milled WSe_2 and $MoSe_2$, and $MoSe_2$. Lines denote isotropic chemical shifts. The structure of the MSe_2 (M = W, Mo) sheets is shown to the right. (lower) Boron monoxide structural model determined from DQ-SQ and TQ-SQ ^{11}B homonuclear correlation SSNMR spectra.

Recent Progress

Synthesis and Structure Determination of Semiconductor Materials. The optoelectronic properties of semiconductor NCs and 2D materials are controlled by their bulk structures and their

surface chemistry. For these reasons, we have been developing SSNMR spectroscopy methods to determine the atomic structure of semiconductor materials. For example, we have used ^{1}H and ^{29}Si SSNMR experiments to create structural models of 2D silicon nanosheets.[R1] We used ^{1}H detected ^{35}Cl solid-state NMR experiments to confirm the presence of terminal Cl atoms on the silicon sheets (Figure 1).[P1] DFT calculations suggest that chlorine substitution can be used to tune the band gap. We have demonstrated solution-phase approaches for synthesis of lead chalcohalides.[P2] Notably, mixed iodide and bromide phases exhibited high stability to moisture and oxygen. ^{207}Pb SSNMR spectra demonstrate extensive halide alloying. We demonstrated methods to acquire ^{77}Se SSNMR spectroscopy of the 2D transition metal dichalcogenides (TMDC) WSe_2 or $MoSe_2$.[R3,P3] ^{77}Se SSNMR spectroscopy was used to elucidate the molecular-level alloying within mixed TMDC materials prepared by ball-milling (Figure 1).[P3] We have used cluster DFT calculations to model the structures and NMR spectra of CdSe NC surfaces.[P4] These calculations confirm the presence of {100} and {111} surface facets on spheroidal CdSe NCs.[R4,P4] Fast MAS ^{15}N SSNMR experiments were used to show that hybrid organic-inorganic MXene materials feature amido and imido ligands bound to the MXene sheets.[P5]

*Structural Characterization of Porous 2D Materials***.** Porous 2D materials have myriad applications for gas storage and separation, sensing, and batteries. Boron monoxide (BO) was first reported in 1940, yet its structure has remained a mystery despite numerous investigations. We have applied ^{11}B NMR experiments to show that BO is made up of turbostratic 2D nanosheets composed of interconnected B_4O_2 rings (Figure 1).[P6] This study confirms the existence of a new type of boron-based 2D material that could have exciting properties, much like hexagonal boron nitride and borophene. We recently demonstrated a general strategy that uses the multi-component Ugi reaction to post-synthetically modify any imine-based covalent organic framework (COF) material.[R5] This strategy was used to introduce diglycolic acid (DGA) groups into COF materials.[P7] ^{13}C SSNMR characterization techniques confirmed incorporation of modified linkers in the COF materials. The DGA-COF materials exhibited high adsorption capacity for REE ions, with reversible binding.

Sensitivity-Enhanced SSNMR Spectroscopy. As a cross-cutting thrust, we develop dynamic nuclear polarization (DNP) and ^{1}H-detected, fast magic angle spinning (MAS) techniques to increase sensitivity and open up the periodic table to SSNMR spectroscopy experiments. We recently showed DNP was applicable to TMDC materials. Interestingly, with DNP we were able to see distinct ^{77}Se NMR signals attributed to TMDC surfaces.[P4] Ball milling of inorganic and organic network solids was shown to create stable free radicals, which can potentially be used as polarization sources in DNP experiments.[P8] We recently demonstrated novel approaches for ^{1}H detection of wideline solid-state NMR spectra of spin-$^{3}/_{2}$ quadrupolar nuclei such as ^{35}Cl, ^{63}Cu and ^{81}Br.[P1, P9] This method has allowed us to study partially Cl-terminated 2D silicon and semiconductors nanoparticles.[P1, P9] Our group has developed the AMES-Fit software program that can automatically fit the multi-field SSNMR spectra of quadrupolar nuclei and increase the potential reach of the methods developed within this research program.[P10]

References

1. B.J. Ryan, Y. Wang, M.P. Hanrahan, U. Ramesh, R.D. Nelson, C. Nyameky, B.S. Whitehead, C. Huang, J. Wang, L.T. Roling, E.A. Smith, A.J. Rossini, M.G. Panthani, *Silicene, Silicane, or Siloxene? Characterizing Silicon Nanosheets from Deintercalated Calcium Disilicide*, Chem. Mater., **32**, 795-804 (2020).

2. A. Volkov, J. Mi, K. Lalit, P. Chatterjee, D. Jing, S.L. Carnahan, Y. Chen, S. Sun, A.J. Rossini, W. Huang, and L.M. Stanley, *General Strategy for Incorporation of Functional Group Handles into Covalent Organic Frameworks via the Ugi Reaction*, J. Am. Chem. Soc., **145**, 6230-6239 (2023).

3. E. Gi, Y. Chen, X.R. Wang, S.L. Carnahan, S. Rahman, E. A. Smith, A.J. Rossini, and J. Vela. *Chemical-Induced Slippage in Bulk WSe_2*. J. Phys. Chem. Lett., **13**, 10924−10928 (2022).

4. Y. Chen., R.W. Dorn R.W., M.P. Hanrahan, L. Wei, R. Blome-Fernández , A.M. Medina-Gonzalez, M.A.S. Adamson, A.H. Flintgruber, J. Vela, A.J. Rossini, *Revealing the Surface Structure of CdSe Nanocrystals by Dynamic Nuclear Polarization-Enhanced 77Se and 113Cd Solid-State NMR Spectroscopy*., J. Am. Chem. Soc., **143**, 8747-8760 (2021).

Publications

1. R.W. Dorn, B.J. Ryan, M.V. Dodson, R. Biswas, M.G. Panthani, and A.J. Rossini, *Chlorination of Hydrogenated Silicon Nanosheets Revealed by Solid-State Nuclear Magnetic Resonance Spectroscopy*, Chem. Mater., **35**, 539–548 (2023).
2. A.N. Roth, Y. Chen, A. Santhiran, J. Opare-Addo, E. Gi, E.A. Smith, A.J. Rossini, and J. Vela. *Designing Complex Pb3SBrxI4−x Chalcohalides: Tunable Emission Semiconductors Through Halide-Mixing*, Chem. Sci., **14**, 12331−12338 (2023).
3. S.L. Carnahan, E. Gi, M. Wagner, A. Santhiran, E. Amerongen, I.Z. Hlova, O. Dolotko, V.P. Balema, H. Yin, J.Q. Geisenhoff, A. Schimpf, J. Vela, A.J. Rossini. *Structural Studies of Alloyed and Nanoparticle Transition Metal Dichalcogenides by Selenium-77 Solid-State Nuclear Magnetic Resonance Spectroscopy*, ChemRxiv, doi:10.26434/chemrxiv-2024-rgsrh (2024).
4. R. Biswas, Y. Chen, J. Vela, A.J. Rossini. *Relativistic DFT Calculations of Cadmium and Selenium Solid-State NMR Spectra of CdSe Nanocrystal Surfaces*, ACS Omega, **8**, 44362-44371 (2023).
5. C. Zhou, D. Wang, F. Lagunas, B.A. Atterberry, M. Lei, H. Hu, Z. Zhou, A.S. Filatov, D.-e. Jiang, A.J. Rossini, R.F. Klie, D.V. Talapin. *Hybrid organic–inorganic two-dimensional metal carbide MXenes with amido- and imido-terminated surfaces*, Nature Chemistry, **15**, 1722–1729 (2023).
6. F.A. Perras, H. Thomas, P. Heintz, R. Behera, J. Yu, G. Viswanathan, D. Jing, S. A. Southern, K. Kovnir, L. Stanley, and W. Huang, *The Structure of Boron Monoxide*, J. Am. Chem. Soc., **145**, 14660–14669 (2023).
7. P. Chatterjee, A. Volkov, J. Mi, M. Niu, S. Sun, A.J. Rossini, L. Stanley, W. Huang. *Efficient Capture and Release of the Rare-Earth Element Neodymium in Aqueous Solution by Recyclable Covalent Organic Frameworks*, J. Am. Chem. Soc., **146**, DOI:10.1021/jacs.4c06609 (2024).
8. S.L. Carnahan, K. Riemersma, I.Z. Hlova, O. Dolotko, S.J. Kmiec, S.N.S. Lamahewage, S.W. Martin, J.F. Wishart, T. Dubroca, V.P. Balema, A.J. Rossini. *Formation of Stable Radicals by Mechanochemistry and Their Application for Magic Angle Spinning Dynamic Nuclear Polarization Solid-State NMR Spectroscopy*, J. Phys. Chem. A, **128**, 3635-3645 (2024).
9. S. Lamahewage, B.A. Atterberry, R. Dorn, E. Gi, M.R. Kimball, J. Vela., J Bluemel, A.J. Rossini. *Accelerated Acquisition of Wideline Solid-State NMR Spectra of Spin 3/2 Nuclei by Frequency-Stepped Indirect Detection Experiments*, Phys. Chem. Chem. Phys., **26**, 5081-5096 (2024).
10. F.A. Perras, A.L. Paterson, *Automatic Fitting of Multiple-Field Solid-State NMR Spectra*, Solid State Nucl. Magn. Reson., **131**, 101935 (2024).

Precision Deconstruction of Polymers by Tailored Ionic Liquids

Tomonori Saito, Jeffrey Foster, Ilja Popovs, Sheng Dai, Bobby Sumpter, Changwoo Do, Oak Ridge National Laboratory, Robert Davis, The University of Virginia

Keywords: Polymer Deconstruction, Organocatalysts, Mixed Plastics, Condensation Polymers, Polymer Upcycling

Research Scope

Condensation polymers comprise ~30% of global plastics production. Although there has been some progress on chemically recycling condensation polymers, most condensation polymers are not recycled because of the difficulty in depolymerization to pure building blocks in an energy efficient manner. New processes and catalysts are needed to lower the energy requirements and temperature for deconstruction of condensation polymers. Ionic liquids (ILs) hold great potential to address these challenges due to their unique physical and chemical properties, including good miscibility with polymers, high thermal stability, low vapor pressure, tailorable functionality, and catalytic activity. Thus, *the overarching goal of this project is to unravel the fundamental principles for precise deconstruction of condensation polymers using ionic liquids as both solvent and organocatalyst while establishing approaches for their reconstruction* (Figure 1). To achieve the overarching goal, the following three specific aims are pursued. **Aim 1**: Develop low energy depolymerization pathways for condensation polymers by tailoring functionality, structure, and composition of ionic liquids as solvents and catalysts. **Aim 2**: Develop design principles for ionic liquid organocatalysts that generate well-defined deconstructed intermediates. **Aim 3**: Understand and control the product selectivity in the deconstruction of mixed streams of condensation polymers using designed ILs and unravel the pathways for reconstruction. This project is delivering the fundamental knowledge to establish the design principles for energy efficient polymer deconstruction and lay a versatile platform for polymer reconstruction with tailored composition, topology, and functionality.

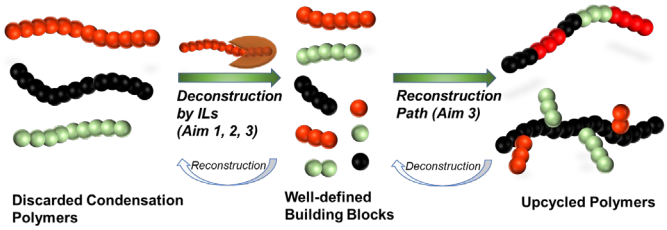

Figure 1. Deconstruction and reconstruction of condensation polymers by tailored ionic liquids

Recent Progress

We have designed and investigated various IL-based catalysts to understand the impact of nucleophilicity and reactivity of ILs on the kinetics of deconstruction (Aim 1).[1] We identified a

critical role of anion and proton in IL-based organocatalyst and developed a highly efficient and versatile protic IL/protic ionic salt organocatalyst, TBD:TFA, for selective glycolysis of poly(ethylene terephthalate) (PET), poly(carbonate) (PC), poly(urethane) (PU), poly(amide) (PA), and their mixed waste streams into valuable monomers (Aim, 2, 3). All electron DFT calculations and MD simulations coupled with kinetic experiments revealed the importance of interaction energy of TBD:TFA itself and minimized interaction energy to the polymer for its efficient deconstruction. The exceptional efficiency of TBD:TFA allowed for selective glycolysis of PET, PC, PU, PA, and their variety of mixed waste streams into respective monomers (Figure 2), where no other reported catalysts can deconstruct such broad range of condensation polymers. The structural stability among carbonate, urethane, ester, and amide functional groups in PC, PU, PET, and PA, respectively, provides a distinctively different rate of deconstruction that allows selective and sequential deconstruction.

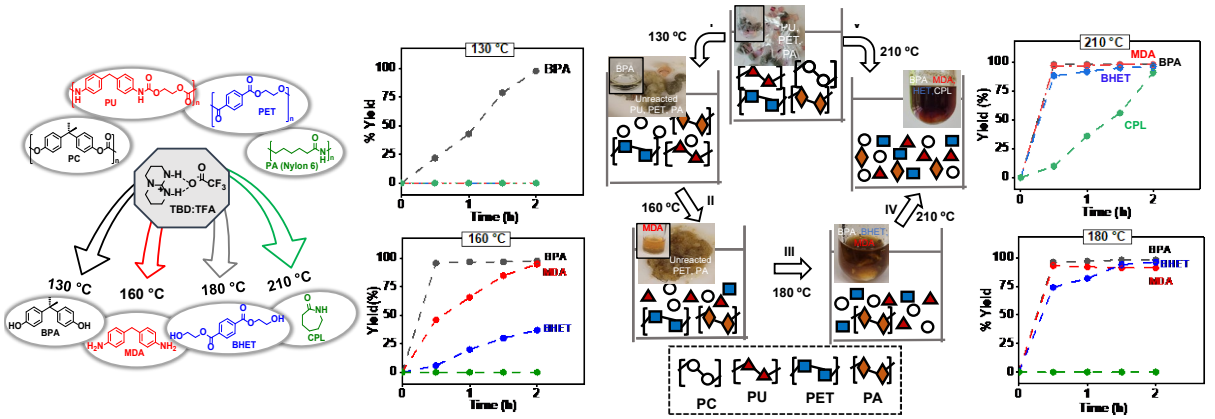

Figure 2. Quantitative deconstruction of PC (black), PU (red), PET (blue), and PA (green) to yield BPA, MDA, BHET, and CPL, respectively, and their sequential deconstruction[1]

The resulting solvolysis products using tailored ILs represent new starting points for plastics production beyond being used for conventional monomers, and provide valuable building blocks for advanced upcycled materials. To demonstrate such an upcycling path, we developed an efficient deconstruction of PET into various α,ω-dialkenenyl terephthalates via organocatalyzed transesterification by ω-unsaturated alcohols (Aim 2), followed by a demonstration of their polymerization into new upcycled polymers using acyclic diene metathesis polymerization under mild temperature conditions (Aim 3).[2] To deeply understand the fundamental kinetics of these transesterification reactions, the reaction kinetics of model compounds were also investigated. Combined with DFT calculation, it revealed that the vicinal -OH of the glycol effectively increased the concentration of the intermediate during reaction, resulting in acceleration of the overall transesterification rate (Aim 1).[3] Furthermore, small-angle neutron scattering revealed the chain conformation of PET in different solvent conditions through the Kratky plot (Aim 2). We also reported a versatile strategy to chemically upcycle PE and PP into fatty acids and surfactant products such as soaps and detergents (Aim 3).[4]

References

1. M. Arifuzzaman, B. G. Sumpter, Z. Demchuk, C. Do, M. A. Arnould, M. A. Rahman, P.-F. Cao, I. Popovs, R. J. Davis, S. Dai, and T. Saito, Selective deconstruction of mixed plastics by a tailored organocatalyst, *Mater. Horiz.*, 10, 3360–3368 (2023).
2. J. C. Foster, J. Zheng, M. Arifuzzaman, M. A. Rahman, J. T. Damron, C. Guan, I. Popovs, and T. Saito, Closed-loop recycling of semi-aromatic polyesters derived from PET, *Cell Rep. Phys. Sci.* 4*,* 101734 (2023)
3. P. Kumar, B. G. Sumpter, T. Saito, and R. J. Davis, Importance of hydrogen bonding in Base-Catalyzed transesterification reactions with vicinal diols, *J. Catal.* 430, 115246 (2024)
4. Z. Xu, N. E. Munyaneza, Q. Zhang, M. Sun, C. Posada, P. Venturo, N. A. Rorrer, J. Miscall, B. G. Sumpter, and G. Liu, Chemical upcycling of polyethylene, polypropylene, and mixtures to high-value surfactants, *Science* 381, 666–671 (2023)

Publications

1. J. Zheng, M. Arifuzzaman, X. Tang, X. C. Chen, and T. Saito, Recent development of end-of-life strategies for plastic in industry and academia: Bridging their gap for future deployment, *Mater. Horiz.*, 10, 1608–1624 (2023). Journal Back Cover, *Materials Horizons Outstanding Review 2023*
2. M. Arifuzzaman, B. G. Sumpter, Z. Demchuk, C. Do, M. A. Arnould, M. A. Rahman, P.-F. Cao, I. Popovs, R. J. Davis, S. Dai, and T. Saito, Selective deconstruction of mixed plastics by a tailored organocatalyst, *Mater. Horiz.*, 10, 3360–3368 (2023). Journal Front Cover
3. Z. Xu, N. E. Munyaneza, Q. Zhang, M. Sun, C. Posada, P. Venturo, N. A. Rorrer, J. Miscall, B. G. Sumpter, and G. Liu, Chemical upcycling of polyethylene, polypropylene, and mixtures to high-value surfactants, *Science* 381, 666–671 (2023).
4. J. C. Foster, J. Zheng, M. Arifuzzaman, M. A. Rahman, J. T. Damron, C. Guan, I. Popovs, and T. Saito, Closed-loop recycling of semi-aromatic polyesters derived from PET, *Cell Rep. Phys. Sci.* 4*,* 101734 (2023)
5. P. Kumar, B. G. Sumpter, T. Saito, and R. J. Davis, Importance of hydrogen bonding in Base-Catalyzed transesterification reactions with vicinal diols, *J. Catal.* 430, 115246 (2024)
6. S. Kim, M. A. Rahman, M. Arifuzzaman, D. B. Gilmer, B. Li, J. K. Wilt, E. Lara-Curzio, and T. Saito, Closed-loop additive manufacturing of upcycled commodity plastic through dynamic crosslinking, *Sci. Adv.* 8, eabn6006 (2022).

Lunch time discussion: Use of Neutrons and Neutron Facilities to Understand Materials Chemistry of Energy Storage and Conversion

Gabriel M. Veith – Oak Ridge National Laboratory

Keywords: Neutron scattering, batteries, energy storage

Research Scope

This lunch time presentation will discuss the use of neutron scattering to investigate physical processes important to energy storage. Neutrons can do so much more than diffraction. Indeed, this presentation will focus on the use of small angle and ultra small angle neutron scattering to understand polymer aggregation and agglomeration during materials synthesis. Figure 1 shows a representation of this aggregation and agglomeration for a polyimide binder as a function of shear. The structure of the polymer shifts and evolves under shear causing new arrangements with significant impact on the resulting battery chemistry. Similar changes are expected for other polymer materials under shear causing intrinsic changes to polymer structure and dynamics.

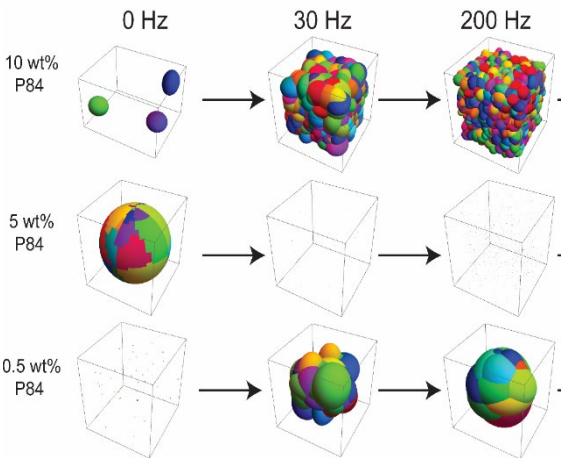

Schematic representation of polymer aggregates and their evolution during shear

Additional examples will include the use of neutron reflectivity to probe buried interfaces *in situ*. These interfaces include all solid-state Li-metal/solid electrolytes and interfaces formed between polymers and solid electrodes. The data will demonstrate how the interfaces form, evolve and mediate transport during energy storage applications.

Finally, quasi-elastic neutron scattering will be used to understand molecular motion and the resulting effect of ceramic cathode particles on the transport and energy storage properties of next generation solid state batteries.

References

X. Chelsea Chen, Charles Soulen, Mary K. Burdette-Trofimov, Xiaomin Tang, Changhao Liu, Luke Heroux, Mathieu Doucet, Madhusudan Tyagi, Gabriel M. Veith, *Origin of rate limitations in solid-state polymer batteries from constrained segmental dynamics within the cathode,* Cell Reports Physical Sciences, **4**(16) pg 101538 (2023).

Katie L Browning, Andrew S Westover, James F Browning, Mathieu Doucet, Robert L Sacci, Gabriel M Veith, *In Situ Measurement of Buried Electrolyte–Electrode Interfaces for Solid State Batteries with Nanometer Level Precision,* ACS Energy Letters, **8**, pg. 1985-1991 (2023).

Mary K. Burdette-Trofimov, Beth L. Armstrong, Rachel J. Korkosz, J. Landon Tyler, Rebecca D. McAuliffe, Luke Heroux, Mathieu Doucet, David T. Hoelzer, Nihal Kanbargi, Amit K. Naskar, and Gabriel M. Veith, Understanding the physical chemistry of PVDF binder with silicon, graphite, and NMC materials and the influence on cycling performance, ACS Applied Materials & Interfaces, **14**(20), pg 23322-23331 (2022).

Mary K. Burdette-Trofimov, Beth L. Armstrong, Luke Heroux, Mathieu Doucet, Robert L. Sacci, and Gabriel M. Veith, Structure and dynamics of small polyimide oligomers with silicon as a function of aging, Soft Matter, **17(**33), pg. 7729-7742 (2021).

Gabriel M. Veith, Katie L. Browning, Mathieu Doucet, James F. Browning, *Solid Electrolyte Interphase Architecture Determined Through Neutron Scattering,* Journal of the Electrochemical Society, **186**, pg. 060523 (2021).

M. K. Burdette-Trofimov, Beth L. Armstrong, Ryan P. Murphy, Luke Heroux, Mathieu Doucet, Stephen E. Trask, Alexander M. Rogers, Gabriel M. Veith, Role of low molecular weight polymers on the dynamics of silicon anodes during casting , ChemPhysChem, **22**(11), pg. 1049-1058 (2021).

M. K Burdette-Trofimov, Beth L. Armstrong, Alexander Rogers, Luke Heroux, Mathieu Doucet, Guang Yang, Nathan Phillip, Michelle Kidder, Gabriel M. Veith, *Understanding binder-silicon interactions during slurry processing*, Journal of Physical Chemistry C, **124**(24), pg 13479-13494 (2020).

Katie L. Browning, Robert L. Sacci, Mathieu Doucet, James F. Browning, Joshua Kim, Gabriel M. Veith, *The Study of the Binder Polyacrylic Acid and its Role in Concomitant Solid-Electrolyte Interphase Formation on Si Anodes,* ACS Materials and Interfaces, **12**(8), 10018-10030 (2020).

Katie L. Browning, James F. Browning, Mathieu Doucet, Norifumi L. Yamada, Gao Liu, Gabriel M. Veith, *Role of conductive binder to direct solid–electrolyte interphase formation over silicon anodes,* Physical Chemistry Chemical Physics, **21**(31), pg 17356-17365 (2019).

Brian Shen, Beth L. Armstrong, Mathieu Doucet, Luke Heroux, James F. Browning, Michael Agamalian, Michael; Wyatt E. Tenhaeff, Gabriel M. Veith, *Shear Thickening Electrolyte Built from Sterically Stabilized Colloidal Particles*, ACS Materials and Interfaces, **10** (11), pp 9424–9434 (2018).

Fundamental Mechanisms Driving Efficiency of CO_2 Capture Using Mineral Looping

PI: Juliane Weber[1]
Co-Is: Lawrence M. Anovitz[1], Jose L. Bañuelos[2], Jacquelyn N. Bracco[3], Andrew G. Stack[1], Vitalii Starchenko[1], Ke Yuan[1]
[1] Chemical Sciences Division, Oak Ridge National Laboratory
[2] University of Texas, El Paso
[3] City University of New York, Queens College
Keywords: Carbon capture, metal oxide, interfacial chemistry, direct air capture

Research Scope

The overarching goal of this project is to understand and control the chemical reactions that govern hydroxylation and carbonation processes during direct air capture of CO_2 using MgO. MgO-based mineral looping promises to be a cost-effective ($46-159/t$CO_2$) [1,2] process to remove CO_2 from the atmosphere at the gigaton scale. Despite previous research on MgO for CO_2 adsorption [3], there is a lack of understanding of reaction pathways at ambient conditions and in the presence of humidity. This FWP is divided into three specific aims focused on major knowledge gaps that currently prevent the implementation of MgO-based mineral looping: 1) What are the chemical reactions that control the rate and extent of reaction of MgO with CO_2 at ambient conditions and varying humidity? 2) What are the mechanisms of reaction-induced fracturing during MgO hydration? 3) What are the roles of impurities in affecting the hydroxylation, carbonation, and oxide regeneration?

Recent Progress

We would like to highlight progress over the past year in three different areas:

1) **Phase Selection and Carbonation Efficiency**

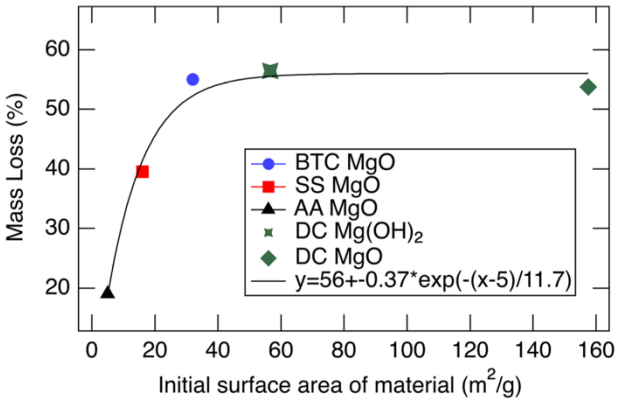

Figure 1: Mass loss [%] as measured by TGA-MS of MgO with different surface areas (m^2/g).

Several types of MgO nanoparticles of varying morphology and surface area were obtained or synthesized. After heating to 450°C to remove adventitious CO_2, samples were carbonated at 1 atm pCO_2 at room temperature and reaction extent was analyzed using Thermogravimetric Analysis with Mass Spectrometry (TGA-MS). What we find is that the reaction extent increases with surface area increase until a threshold value of 40 m^2/g. Both MgO and $Mg(OH)_2$ show comparable carbonation efficiencies.

In addition, relative humidities were varied and higher carbonation was observed at humidities over 40%. By integrating the MS signal from mass 18 (H_2O) and mass 44 (CO_2), an indication of the relative water and CO_2 contents in the phases was determined. Increasing water vapor leads to increasing CO_2 in the product. In summary, elevated humidity (>40% R.H.) increases carbonation of MgO and is equal to carbonation efficiency of $Mg(OH)_2$.

2) **Mechanistic Understanding of Reaction-Induced Fracturing**

The transformation from MgO to $Mg(OH)_2$ is accompanied by a 110% volume increase, which leads to reaction-induced fracturing. MgO single crystals were reacted in liquid water and vapor at temperatures of up to 150°C, showing formation of blisters at major defect lines. In addition, the formation of $Mg(OH)_2$ led to fracturing of the single crystal MgO. Our transmission electron microscopy observations showed MgO dissolution features which indicate a dissolution-reprecipitation process. We combined the experimental evidence with phase field modeling [3], which shows that changes in surface energies and external conditions may result in a transition from a film to a non-uniform coverage. We propose that surface area enhancement via reactive fracturing can help to overcome surface passivation.

3) **Increased Carbonation of MgO by Hydration in the Presence of Iron**

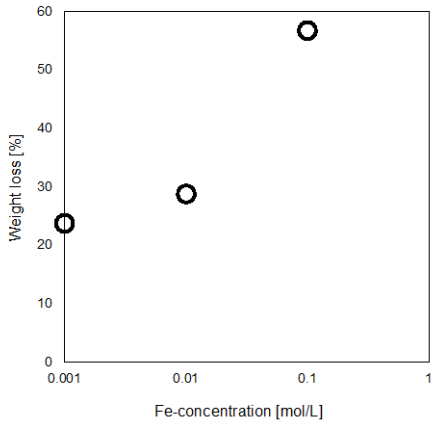

Fig. 2: Mass loss [%] determined by TGA-MS as function of iron concentration during hydroxylation.

We investigated the effect of dissolved iron on the rates and extent of MgO hydroxylation and subsequent carbonation reactions to determine if this might have a beneficial or detrimental effect. Iron is a common component of groundwater and the precursor rock to create the MgO and expected to be present in a mineral looping process for direct air capture. Iron in solution was observed to buffer the pH during hydroxylation and in case of low surface area single crystals, prevented $Mg(OH)_2$ formation and led to γ-FeOOH (lepidocrocite) formation. For powder experiments, Fe-bearing $Mg(OH)_2$ formation was observed. Subsequent carbonation experiments of MgO powders hydrated in the presence of dissolved iron (forming $(Fe,Mg)OH_2$) at 1 atm pCO_2 and 100% relative humidity showed increased carbonation. The carbonation product was nesquehonite, which has a desirable $Mg:CO_3$ ratio of 1:1. We hypothesize that increased Fe^{3+} content led to vacancy formation increasing the carbonation extent. We are currently working on testing this hypothesis using synchrotron-based time resolved XRD.

In summary, our recent results highlight pathways to increase carbonation of MgO by introducing iron during carbonation, increasing surface area of particle to ~40 m^2/g using reaction-induced fracturing and carbonation at elevated humidity (>40% R.H.).

References

1. N. McQueen, P. Kelemen, G. Dipple, P. Renforth, J. Wilcox, *Ambient weathering of magnesium oxide for CO_2 removal from air*, Nature Communication, **11**, 3299 (2020).
2. O. Akeeb, L. Wang, W. Xie, R. Davis, M. Alkaswawi, S. Toan, *Post-combustion CO_2 capture via a variety of temperature ranges and material adsorption process: A review*. Journal of Environmental Management, **313**, 115026, (2022).
3. Y. Hu, Y. Guo, J. Sun, H. Li, W. Liu, *Progress in MgO sorbents for cyclic CO_2 capture: a comprehensive review*. Journal of Materials Chemistry A, **7**(35), 20103, (2019).
4. T. Q. Ansari, H. Huang, S.-Q. Shi, *Phase field modeling for the morphological and microstructural evolution of metallic materials under environmental attack*. npj Comput. Mater. 7, (2021)
5. H.S. Santos, H. Nguyen, F. Venâncio, D. Ramteke, R. Zevenhoven, P. Kinnunen. *Mechanisms of Mg carbonates precipitation and implications for CO_2 capture and utilization/storage*. Inorganic Chemistry Frontiers, **10** (9), 2507-2546 (2023).

Publications

1. Weber, J., Starchenko, V., Yuan, K., Anovitz, L.M., Ievlev, A.V., Unocic, R.R., Borisevich, A.Y., Boebinger, M.G. and Stack, A.G., 2023. Armoring of MgO by a Passivation Layer Impedes Direct Air Capture of CO_2. *Environmental Science & Technology*, *57*(40), pp.14929-14937. https://doi.org/10.1021/acs.est.3c04690
2. Bracco, J.N., Camacho Meneses, G., Colón, O., Yuan, K. , Stubbs, J.E., Eng, P.J., Wanhala, A.K., Einkauf, J.D., Boebinger, M.G., Stack, A.G. and Weber, J., *ACS Appl. Mater. Interfaces*, **2024**, 16, 1, 712-722. DOI: 10.1021/acsami.3c14823

Organic/inorganic Nanocomposites

Ting Xu, Yi Liu, Robert O. Ritchie, Miquel Salmeron, Gregory Su, Jie Yao

Lawrence Berkeley National Laboratory

Keywords: mobility-based synthesis, pseudo bonds, polymer entanglements, dielectrics;

Research Scope

The long-term impact of nanocomposites rests upon our ability to modulate their chemistry and structures across the atomic-nanoscopic-microscopic-macroscopic hierarchy and the abundant interfaces across each length scale. We aim to identify design rules to (1) synergize multi-component blends' thermodynamics and system mobility to program kinetic pathways of hierarchical nanocomposite synthesis; (2) design and synthesize single component nanocomposites (SCCs) by programming polymer entanglements to form pseudo bonds; and (3) guided by machine learning, develop efficient polymer chemistry, e.g. topochemical polymerization or sulfur fluoride exchange (SuFEx) reaction, for use in functional hybrid materials. Programmatically, our team efforts focus on three types of nanocomposites in parallel: multi-component supramolecular nanocomposites, SCCs based on polymer-grafted nanoparticles (PGNPs), and new dielectrics for high temperature electrostatic energy storage.

Recent Progress

1. **Mobility-guided synthesis of multi-component supramolecular nanocomposites** Assembling molecules across the atomic-to-macroscopic structural hierarchy is analogous to a multi-step chemical reaction with many parallel and sequential steps. The reaction mixture evolves continuously, and we cannot define "reactant" identity, concentration, pair interactions and, thus, overall enthalpic contributions. Kinetically, the "reactants" differ in size, shape, diffusivity, and diffusion modes. Geometric confinements and repulsive interactions elevate energy barriers for interfacial diffusion. When self-assembly proceeds across a nano-to-micro-to-macro sequence of growth, there is not enough system mobility to organize preformed nanostructures. We introduced a new nanomaterial design with two key elements: (1) to utilize the ability of entropy-driven assemblies to accommodate variations in reactant composition and pair interactions during processing and integration and (2) to match the system mobility with the necessary diffusion of the building blocks to form targeted structures. To validate the mobility-guided nanomaterial synthesis, we synthesized high-performance barrier materials composed of >200 stacked nanosheets (>100 nm in sheet thickness) with defect density < 0.056 μm^{-2} and ~ 98% efficiency in controlling the defect type in <30 minutes; as well as technologically relevant barrier performance against VOCs, water, and oxygen with programmable lifecycle.

2. **Program pseudo bonds in SCCs by tailoring polymer conformation/entanglements** Nanoscale chain entanglements provide a facile route to form pseudo bonds beyond covalent ones and secondary interactions and can access composites with circular lifecycle. We hypothesize that modulating local curvature of organic/inorganic interfaces tailors the radial and lateral organization of the grafted polymers to form pseudo bonds. Here we tested the hypothesis by probing how SCCs dissipate energy under external stress from the microscopic to nanoscopic scale. At all length scales, mechanical properties of SCCs exhibit a non-linear dependence of composition that can be directly attributed to the curvature dependent local chain organizations in both radial and lateral directions. The grafted glassy polymers can exhibit behaviors of either brittle or ductile materials by modulating local chain organizations and the percolation threshold. Present studies clearly demonstrated the feasibility to tailor pseudo bond strength and directionality and introduced an emerging framework to engineer functional SCCs.

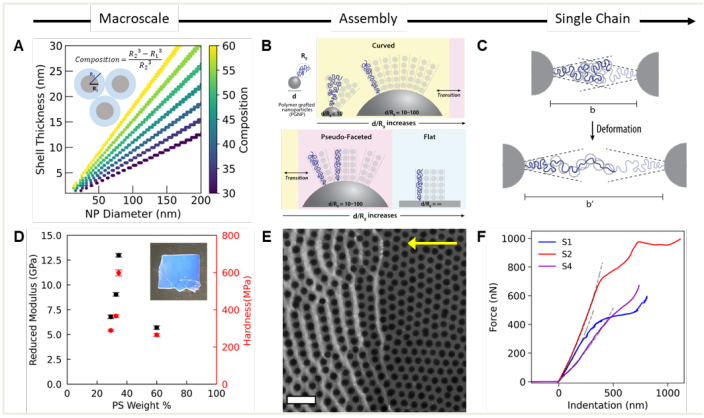

Figure 1. Rational SCC design based by programming polymer entanglements to form pseudo bonds.

3. **Develop efficient polymer chemistry for functional composites** We integrated machine learning with sulfur(VI) fluoride exchange (SuFEx) click chemistry to rapidly identify and synthesize polysulfates for high-temperature electrostatic energy storage. We show that conjugated, flexible and stable sulfate (–O-SO_2-O–) linkages in aromatic polymers overcome the inverse relationship between T_g and bandgap (E_g) and realized polymer dielectrics, with concurrent high T_g (158–230 °C) and E_g (3.9–4.4 eV) along with breakdown strength (≥700 MV/m). We further analyzed a library of > 40,000 polysulfates and discovered a high T_g polysulfate with record-high discharged energy density with over 90% efficiency at 200 °C.

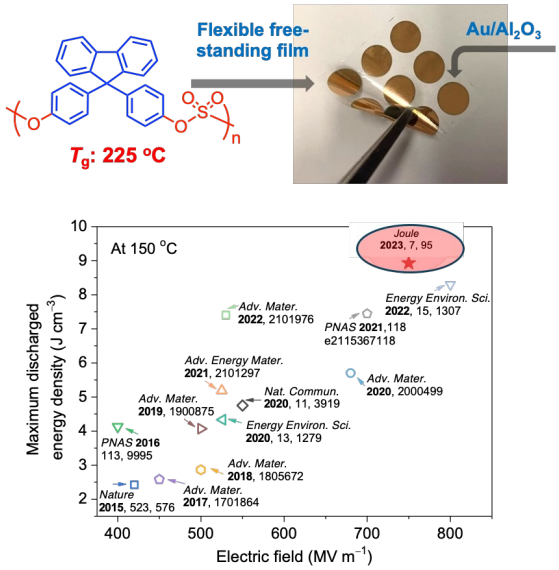

Figure 2. Design polysulfates for high-T dielectrics

Publications

1. E Vargo, L Ma, H Li, Q Zhang, J Kwon, KM Evans, X Tang, VL Tovmasyan, Jasmine Jan, Ana C Arias, Hugo Destaillats, Ivan Kuzmenko, Jan Ilavsky, Wei-Ren Chen, William Heller, Robert O Ritchie, Yi Liu, Ting Xu, Functional composites by programming entropy-driven nanosheet growth, Nature 623, 724 (2023).

2. H. Li, E. Vargo, Z. Xie, L. Ma, P. F. Pieters, S. Shelton, A. P. Alivisatos, T. Xu, Y. Liu, Multilaminate Energy Storage Films from Entropy-Driven Self-Assembled Supramolecular Nanocomposites, Advanced Materials, 2401954 (2024).

3. Z. Xie, K. Le, H. Li, X. Pang, T. Xu, V. Altoe, L. M. Klivansky, Y. Wang, Z. Huang, S. W. Shelton, X. Gu, P. Liu, Z. Peng, Liu, Y. "Interfacial Engineering Using Covalent Organic Frameworks in Polymer Composites for High-Temperature Electrostatic Energy Storage", Adv. Funct. Mater. 34, 2314910 (2024)

4. M. Senarathna, H. Li, S. D. Perera, J. Torres-Correas, S. D. Diwakara, S. R. Boardman, Y. Liu, R. A. Smaldone, R. A. "Highly Flexible Dielectric Films from Solution Processable Hydrazone-linked Covalent Organic Frameworks", Angew. Chem. Int. Ed. 62, e202312617 (2023).

5. H. Li, B. S. Chang, H. Kim, Z. Xie, A. Lainé, L. Ma, T. Xu, C. Yang, J. Kwon, S. W. Shelton, L. M. Klivansky, V. Altoé, B. Gao, A. M. Schwartzberg, Z. Peng, R. O. Ritchie, T. Xu, M. Salmeron, R. Ruiz, K. B. Sharpless, P. Wu, Y. Liu, *High-Performing Polysulfate Dielectrics for Electrostatic Energy Storage Under Harsh Conditions*, Joule **7**, 95 (2023).

6. H. Li, Z. Xie, C. Yang, J. Kwon, A. Lainé, C. Dun, A.V. Galoustian, X. Li, P., J. J. Urban, Z. Peng, M. Salmeron, R. O. Ritchie, T. Xu, Y. Liu, Flexible all-organic nanocomposite films interlayered with in situ synthesized covalent organic frameworks for electrostatic energy storage, Nano Energy, 113, 108544 (2023).

7. A Lainé, R Parmar, M Amati, L Gregoratti, G Su, T Xu, M Salmeron, Damage-free X-ray spectroscopy characterization of oxide thin films, Applied Surface Science 634, 157335 (2023).

7. S. Neumann, J. Kwon, C. Gropp, L. Ma, R. Giovine, T. Ma, N. Hanikel, .K. Wang, T. Chen, S. Jagani, R. O Ritchie, T. Xu, O. M Yaghi, The propensity for covalent organic frameworks to template polymer entanglement, Science 383, 1337 (2024).

8. J. Schwartz, Z. Di, Y. Jiang, J. Manassa, J. Pietryga, Y. Qian, M. Cho, J. L Rowell, H. Zheng, R. D Robinson, J. Gu, A. Kirilin, S. Rozeveld, P. Ercius, J. A Fessler, T. Xu, M. Scott, R. Hovden, Imaging 3D chemistry at 1 nm resolution with fused multi-modal electron tomography, Nature Communications 15, 3555 (2024).

Kinetically Controlled Synthesis of Metastable Nitride Materials

Andriy Zakutayev, National Renewable Energy Laboratory

Keywords: ion exchange, thin film, layered, ternary, perovskite, ferroelectric

Research Scope

The goal of this program is to understand selective synthesis of new metastable nitride materials with desired structures and useful properties. This program aims to answer the following scientific question: "*how to synthesize metastable materials by surpassing kinetic energy barriers under non-equilibrium conditions*?" The hypothesis is that metastable ternary nitrides can be obtained by a kinetically controlled synthesis approach through intermediate energy states that are related to the metastable product. The approach consists of two kinetically controlled synthesis methods: 1) cation-exchange reactions controlled by composition; and 2) crystallographic transformation from precursor to product, controlled by structure. Examples of nitride materials classes studied in the past two years include multivalent ternary nitrides (e.g., layered 'rockseline' $MgMoN_2$, cation-ordered wurtzite Zn_3WN_4, cation-disordered rocksalt $CaZrN_2$, metastable wurtzite nitride ferroelectric alloys (e.g., $Al_{1-x}Sc_xN$, $Al_{1-x}B_xN$), perovskites-structured nitrides (e.g., $LaWN_3$), and binary Cu-based phosphides (e.g., Cu_3P). The two expected outcomes of this program are a fundamental understanding of non-equilibrium kinetically controlled synthesis pathways for nitrides and other inorganic materials chemistries, and the discovery of new nitride materials that could impact energy applications.

Recent Progress

(1) Multivalent ternary nitride compounds

The primary focus of this project remains on the kinetically controlled synthesis of multivalent ternary nitride materials [1], defined as containing two metal cations with a nitrogen anion in equal amounts and charge balanced stoichiometry [2]. Highlights of recent research accomplishments include: (a) Discovery, measurement, and explanation of a hidden synthesis pathway to thin films of thermodynamically stable layered ternary nitride $MgMoN_2$ (Fig.1), with an extension to layered materials with other cation chemistry and stoichiometries (e.g., $MgTa_2N_3$, $MgWN_2$) – in *Nature Synthesis*; (b) Bulk low-temperature synthesis of cation-ordered Zn_3WN_4 semiconductor via heterovalent solid-state metathesis from Li_6WN_4 precursor – published in *Chemical Science*; (c)

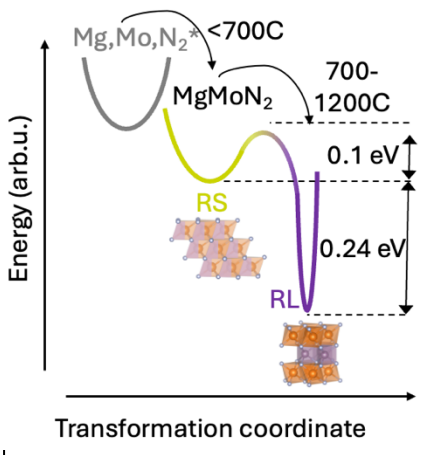

Figure 1. Measured and calculated synthesis pathway for $MgMoN_2$: from elemental precursors, via a metastable disordered 3D state, to a stable ordered 2D-layered structure.

Synthesis of Ternary Nitrides, $CaZrN_2$ and $CaHfN_2$ by metathesis reaction in excess Ca_3N_2, with pathways revealed by in-situ XRD at a synchrotron, and explained by collaborative calculations – published in *Journal of American Chemical Society*; and (d) Bulk and film synthesis pathways to ternary $MgWN_2$ and Mg_3WN_4 in rocksalt, rockseline, h-BN type crystal structures – published and highlighted on the cover of *Journal of Materials Chemistry C*. The follow up research on $ScTaN_2$ with 'rockseline' (layered rocksalt/nickeline) structure is ongoing and will be submitted soon. These recent synthesis examples of multivalent ternary nitride, in both bulk powder and thin film forms, emphasize generality of the kinetically controlled reaction pathways, and build on our prior research in this project [3][4].

(2) Metastable nitride wurtzite ferroelectric alloys

This project also synthesized and characterized metastable nitride alloys with wurtzite structure, in collaboration with other programs, such as the NSF DMREF. This research is timely because of the discovery of ferroelectric switching in $Al_{1-x}Sc_xN$ wurtzite metastable heterostructural alloys [5], with potential applications in energy-efficient nonvolatile memories compatible with Si microelectronics [6]. Selected recent published results include: (a) Development of a simultaneous nucleation and growth model to describe the anomalously abrupt switching measurement results in (Al,Sc)N ferroelectrics – published in *Materials Horizons*; (b) Using this new model to elucidate the effects of the (Al,B)N crystal surface termination on asymmetric polarization reversal as a function of time during electrical measurements – published in *Journal of the American Ceramic Society*. This experimental project also collaborated with theoretical scientists to (c) predict new material candidates such as $MgSiN_2$ and Mg_2PN_3, and distil underlying design principles for wurtzite-type ferroelectrics – published in *Matter*, and (d) reveal a new ferroelectric switching mechanism in alloys with wurtzite structure, that is individual rather than collective in nature – published in *Science Advances*. These results emphasize the relevance of our current and prior basic materials chemistry research on (Al,Sc)N ferroelectric [7][8] to energy-related applications.

(3) Other materials

In addition to the two directions described above, this project continued some research in perovskite-structured nitrides that we discovered earlier [9][10], as well as other pnictide materials such as Cu-based phosphides that we studied in prior years [11][12], with a primary focus on their property measurements. For example, we (a) demonstrated that structural, optoelectronic and magnetic properties of thin film $LaWN_3$ are highly sensitive to cation stoichiometry, with a follow up research publication on $GdWN_3$ under review, and (b) showed that $Cu_{3-x}P$ is an intrinsic semimetal, resolving a long-standing literature debate whether it is a semiconductor or a metal. These examples illustrate the transitivity of the multivalent ternary nitride research to other crystal structures and other materials chemistries.

References

[1] Sun, W., Bartel, C.J., Arca, E., Bauers, S.R., Matthews, B., Orvañanos, B., Chen, B.R., Toney, M.F., Schelhas, L.T., Tumas, W. and Tate, J., A map of the inorganic ternary metal nitrides. *Nature materials*, *18*(7), pp.732-739 (2019)

[2]. Zakutayev, A., Bauers, S.R. and Lany, S. Experimental synthesis of theoretically predicted multivalent ternary nitride materials. *Chemistry of Materials*, *34*(4), pp.1418-1438 (2022)

[3] Todd, P. K., Fallon, M. J., Neilson, J. R., & Zakutayev, A. Two-step solid-state synthesis of ternary nitride materials. *ACS Materials Letters*, *3*(12), 1677-1683. (2021).

[4] Zakutayev, A. Synthesis of Zn2NbN3 ternary nitride semiconductor with wurtzite-derived crystal structure. *Journal of Physics: Condensed Matter*, *33*(35), 354003 (2021).

[5] Fichtner, S., Wolff, N., Lofink, F., Kienle, L. and Wagner, B. AlScN: A III-V semiconductor based ferroelectric. *Journal of Applied Physics*, *125*(11), p.114103 (2019)

[6] Casamento, J., Baksa, S. M., Behrendt, D., Calderon, S., Goodling, D., Hayden, J., ... & Maria, J. P. Perspectives and progress on wurtzite ferroelectrics: Synthesis, characterization, theory, and device applications. *Applied Physics Letters*, *124*(8). (2024).

[7] Yazawa, K., Mangum, J.S., Gorai, P., Brennecka, G.L. and Zakutayev, A. Local chemical origin of ferroelectric behavior in wurtzite nitrides. *Journal of Materials Chemistry C*, *10*(46), pp.17557-17566 (2022)

[8] Yazawa, K., Drury, D., Zakutayev, A., & Brennecka, G. L. Reduced coercive field in epitaxial thin film of ferroelectric wurtzite Al0. 7Sc0. 3N. *Applied Physics Letters*, *118*(16). (2021).

[9] Talley, K.R., Perkins, C.L., Diercks, D.R., Brennecka, G.L. and Zakutayev, A., Synthesis of $LaWN_3$ nitride perovskite with polar symmetry. *Science*, *374*(6574), pp.1488-1491 (2021)

[10] Sherbondy, R., Smaha, R.W., Bartel, C.J., Holtz, M.E., Talley, K.R., Levy-Wendt, B., Perkins, C.L., Eley, S., Zakutayev, A. and Brennecka, G.L., High-Throughput Selection and Experimental Realization of Two New Ce-Based Nitride Perovskites: $CeMoN_3$ and $CeWN_3$. *Chemistry of Materials*, *34*(15), pp.6883-6893 (2022)

[11] Crovetto, A., Kojda, D., Yi, F., Heinselman, K.N., LaVan, D.A., Habicht, K., Unold, T. and Zakutayev, A. Crystallize it before it diffuses: Kinetic stabilization of thin-film phosphorus-rich semiconductor CuP_2. *Journal of the American Chemical Society*, *144*(29), pp.13334-13343 (2022)

[12] Willis, J., Bravić, I., Schnepf, R.R., Heinselman, K.N., Monserrat, B., Unold, T., Zakutayev, A., Scanlon, D.O. and Crovetto, A., Prediction and realisation of high mobility and degenerate p-type conductivity in CaCuP thin films. *Chemical Science*, *13*(20), pp.5872-5883 (2022)

Publications (10 most relevant)

1. Rom, C. L., Smaha, R. W., Knebel, C. A., Heinselman, K. N., Neilson, J. R., Bauers, S. R., & Zakutayev, A. Bulk and film synthesis pathways to ternary magnesium tungsten nitrides. *Journal of Materials Chemistry C*, *11*(34), 11451-11459 (2023).

2. Rom, C. L., O'Donnell, S., Huang, K., Klein, R. A., Kramer, M. J., Smaha, R. W., & Zakutayev, A. Low-temperature synthesis of cation-ordered bulk Zn_3WN_4 semiconductor via heterovalent solid-state metathesis. *Chemical Science* 15, 9709-9718 (2024).

3. Rom, C. L., Novick, A., McDermott, M. J., Yakovenko, A. A., Gallawa, J. R.... Zakutayev A., & Neilson, J. R. Mechanistically Guided Materials Chemistry: Synthesis of Ternary Nitrides, CaZrN2 and $CaHfN_2$. *Journal of the American Chemical Society*, *146*(6), 4001-4012. (2024).

4. Zakutayev, A., Jankousky, M., Wolf, L., Feng, Y., Rom, C. L., Bauers, S. R., ... & Stevanovic, V. Synthesis pathways to thin films of stable layered nitrides. *Nature Synthesis, in press arXiv:2406.17492 (2024)*

5. Yazawa, K., Hayden, J., Maria, J. P., Zhu, W., Trolier-McKinstry, S., Zakutayev, A., & Brennecka, G. L. Anomalously abrupt switching of wurtzite-structured ferroelectrics: simultaneous non-linear nucleation and growth model. *Materials Horizons*, *10*(8), 2936-2944 (2023).

6. Yazawa, K., Drury, D., Hayden, J., Maria, J. P., Trolier-McKinstry, S., Zakutayev, A., & Brennecka, G. L. Polarity effects on wake-up behavior of Al0.94B0.06N ferroelectrics. *Journal of the American Ceramic Society*, *107*(3), 1523-1532 (2024).

7. Lee, C. W., Din, N. U., Yazawa, K., Brennecka, G. L., Zakutayev, A., & Gorai, P. Emerging materials and design principles for wurtzite-type ferroelectrics. *Matter*, *7*(4), 1644-1659 (2024).

8. Lee, C. W., Yazawa, K., Zakutayev, A., Brennecka, G. L., & Gorai, P. (Switching it up: New mechanisms revealed in wurtzite-type ferroelectrics. *Science Advances*, *10*(20), eadl0848 2024).

9. Smaha, R. W., Mangum, J. S., Leahy, I. A., Calder, J., Hautzinger, M. P., Muzzillo, C. P., ... & Zakutayev, A. Structural and optoelectronic properties of thin film $LaWN_3$. *Physical Review Materials*, *7*(8), 084411 (2023).

10. Crovetto, A., Unold, T., & Zakutayev, A. Is $Cu_{3-x}P$ a Semiconductor, a Metal, or a Semimetal?. *Chemistry of Materials*, *35*(3), 1259-1272 (2023).

University
Abstracts

Enabling energy-dense grid scale batteries with earth abundant materials

Chibueze Amanchukwu
Neubauer Family Assistant Professor of Molecular Engineering
Pritzker School of Molecular Engineering
The University of Chicago

Keywords: molten salts, dual-ion batteries, solvent-free electrolytes, lithium intercalation, anion intercalation

Research Scope

The need for energy dense and cheap long duration grid scale batteries requires new battery chemistries. Dual ion batteries are a class of batteries that eschew the use of transition metals and can use earth abundant carbons as both anode and cathode. This battery chemistry operates through cation intercalation at the anode and anion intercalation at the cathode [1,2]. Furthermore, the active species are hosted in the electrolyte (instead of the cathode in Li-ion) [3]. Current electrolytes use high salt concentration (to increase capacity) or ionic liquids (to increase the electrochemical working window). However, high salt concentration electrolytes still contain organic solvents which are vulnerable thermally and detract from the energy density [4]. Unfortunately, ionic liquid organic cations suffer from undesired co-intercalation [5,6]. Here, we focus on the discovery of novel low melting solvent-less alkali-based molten salt electrolytes for next generation batteries. First, we study their physicochemical properties especially the influence of anion identity on melting transition and ionic conductivity. Secondly, we explore their influence on fundamental electrochemical reactions such as electrodeposition, cation, and anion intercalation. Our focus on fundamental understanding of molten salt properties and subsequent electrochemical behavior is of great interest for the development of next generation battery chemistries and electrochemical processes such as electrocatalysis and beyond.

Recent Progress

We have reported in a previous publication (listed below) a low-melting alkali cation-based molten salt electrolyte for lithium metal battery applications. We have investigated the electrochemical properties of this $Li_{0.3}K_{0.35}Cs_{0.35}FSA$ electrolyte with graphite anodes and cathodes to study its behavior in dual-graphite batteries (*manuscript in preparation*). Cation intercalation studies (Figures 1b and 1c) have shown that despite the presence of three different alkali cations in the electrolyte, only Li^+ appears to intercalate at a cutoff potential of 0.01 V vs. Li/Li^+. Furthermore, the FSA^- anion can also intercalate into graphite cathodes and form a stage-1 graphite intercalation compound at an upper cutoff potential of 5.2 V vs Li/Li^+ (Fig 2a and 2b). Further work will focus on understanding the differences in cation/anion intercalation behavior in small molecule electrolytes and molten salt electrolytes to elucidate the role of the solvent in such a process. We

are also exploring binary molten salts with a common cation as a dual-ion battery electrolyte to study the co-intercalation of multiple anions and how the physicochemical properties can be tuned to alter electrolyte performance. These investigations will help unlock a new generation of molten salt electrolytes that can enable high-performing dual-ion batteries.

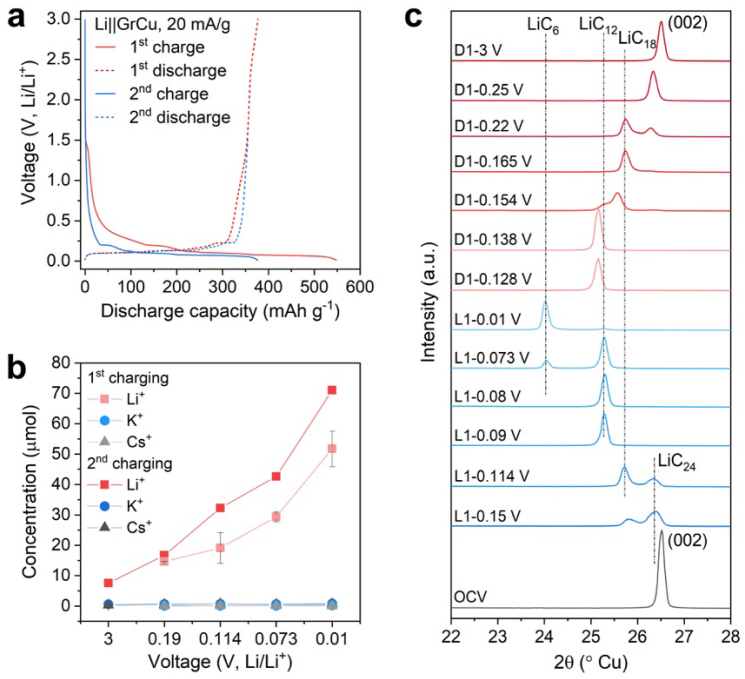

Figure 2. a) Charge-discharge profiles of cation intercalation into a graphite on copper (GrCu) anode, b) inductively coupled plasma-mass spectrometry results that quantify the Li^+, K^+, and Cs^+ present in intercalated GrCu, c) X-ray diffractograms that show the presence of LiC_x compounds in GrCu

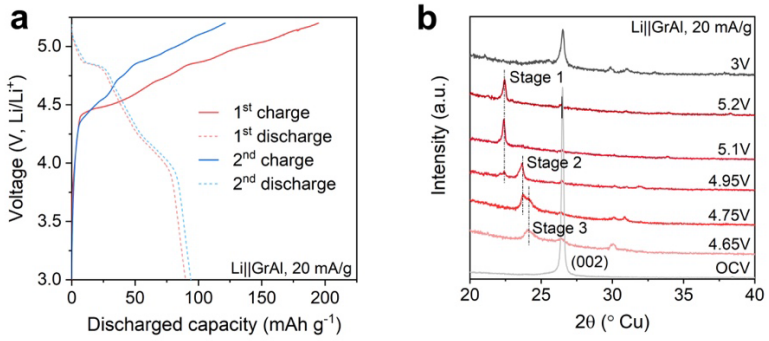

Figure 3. a) Charge-discharge profiles of anion intercalation into a graphite coated on aluminum GrAl) cathode, b) x-ray diffractograms of anion intercalation into GrAl, which show stage-1 formation at an upper cutoff potential of 5.1 V and 5.2 V vs. Li/Li^+

References

[1] K. V Kravchyk, M. V Kovalenko, *Rechargeable Dual-Ion Batteries with Graphite as a Cathode: Key Challenges and Opportunities*, Adv Energy Mater. **9** 1901749 (2019).

[2] L. Zhang, H. Wang, X. Zhang, Y. Tang, *A Review of Emerging Dual-Ion Batteries: Fundamentals and Recent Advances*, Adv Funct Mater. **31** (2021).

[3] A. Kotronia, H.D. Asfaw, C.W. Tai, M. Hahlin, D. Brandell, K. Edström, *Nature of the Cathode-Electrolyte Interface in Highly Concentrated Electrolytes Used in Graphite Dual-Ion Batteries*, ACS Appl Mater Interfaces. **13** 3867–3880 (2021).

[4] L. Xiang, X. Ou, X. Wang, Z. Zhou, X. Li, Y. Tang, *Highly Concentrated Electrolyte towards Enhanced Energy Density and Cycling Life of Dual-Ion Batter*y, Angewandte Chemie International Edition. **59** 17924–17930 (2020).

[5] S. Rothermel, P. Meister, G. Schmuelling, O. Fromm, H.W. Meyer, S. Nowak, M. Winter, T. Placke, *Dual-graphite cells based on the reversible intercalation of bis(trifluoromethanesulfonyl)imide anions from an ionic liquid electrolyte*, Energy Environ Sci. **7** 3412–3423 (2014).

[6] X. Tong, X. Ou, N. Wu, H. Wang, J. Li, Y. Tang, X.Y. Tong, X.W. Ou, N.Z. Wu, H.Y. Wang, J. Li, Y.B. Tang, *High Oxidation Potential ≈6.0 V of Concentrated Electrolyte toward High-Performance Dual-Ion Battery*, Adv Energy Mater. **11** 2100151 (2021).

[7] H. Adenusi, G.A. Chass, S. Passerini, K. V Tian, G. Chen, H. Adenusi, G. Chen, G.A. Chass, K. V Tian, S. Passerini, *Lithium Batteries and the Solid Electrolyte Interphase (SEI)—Progress and Outlook*, Adv Energy Mater. **13** 2203307 (2023).

Publications

1. M.C. Vu, P. Mirmira, R.J. Gomes, P. Ma, E.S Doyle, H.S. Srinivasan, and C.V. Amanchukwu, *Solvent-free low melting alkali-based molten salt electrolytes for lithium metal batteries*, Matter **7** 4357–4375 (2023).
2. M.C. Vu, H.S. Srinivasan, P. Mirmira, E.S. Doyle, and C. V. Amanchukwu, A transition-metal-and-solvent-free dual-graphite battery for long duration storage. To be submitted.

Li-Ion Battery Critical Metal Recycling Using Sugars

PI: Ananda S. Amarasekara, Prairie View A&M University, Texas
Keywords: regeneration; cathode material; hydroxy-acids; hydrothermal; pyrolysis

Research Scope

High purity sources of critical metals are of the utmost importance for our national economic security and transition to renewable energy. With the wide use of Li-ion batteries for energy storage, disposal or recycling of used batteries is becoming an important environmental concern and a critical research challenge. The electrode coating of common Li-ion batteries black material (LiBBM) is composed of valuable Li, Ni, Mn and Co critical metal containing compounds mixed with graphite carbon. While complete leaching of metals can be achieved by using mineral acids; the use of large quantities of strong acids can impose many challenges, including neutralization and disposal of acids. On the other hand, the use of organic chelating agents like hydroxy-acids can significantly improve the leaching and recovery of spent cathode active materials. The current work is based on the hypothesis that, ***sugars can be used in leaching, given that Ni, Mn and Co complexes in LiBBM catalyzes in-situ oxidation of sugars to hydroxy-acids and these carboxylic acids can selectively chelate and extract critical metals from LiBBM under mild hydrothermal conditions.*** Furthermore, we proposed that, pyrolysis could be used to burn off the hydroxy-acid ligands, regenerating the active cathode material. The proposed two step oxidative-leaching followed by pyrolysis process is shown in figure 1.

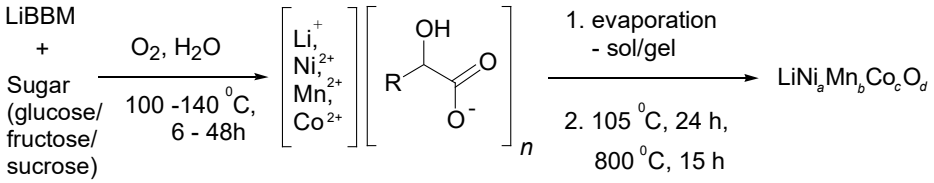

Figure 1. Leaching of Li, Ni, Mn and Co from LiBBM using aqueous sugar solutions *via* in-situ generated hydroxy-acids and recovery of lithium nickel manganese cobalt oxide ($LiNi_aMn_bCo_cO_d$) by pyrolysis of metal-hydroxy acid chelate gel.

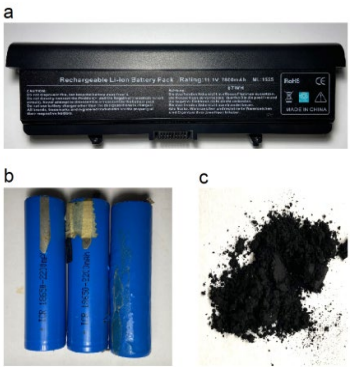

Recent Progress

LiBBM was collected from a spent DELL 1525 laptop battery as shown in the Figure 2. The spent battery was first discharged by immersing in a 10 % aq. sodium chloride solution for 5 days and then opened to remove 18650 Li-ion cells. Cathode and anode black electrode coatings were gathered by sonication of copper and aluminum foil electrodes in hot-water.

Figure 2. a. spent DELL 1525 laptop battery
b. 18650 Li-ion cells. c. LiBBM collected after sonication, filtration and drying

Extraction of Li, Ni, Mn and Co from LiBBM with aq. sugar solutions under oxygen

Li, Ni, Mn and Co metals were hydrothermally extracted with aqueous sugar solutions under oxygen and air atmospheres. Glucose, fructose and sucrose were tested as sugars in water at 100-140 °C, under reflux and in high pressure stainless steel reaction vessels with Teflon sleeves. Leaching of metals to aqueous solutions *via* the oxidation of sugars were tested under a wide range of conditions and a selected set of results using glucose and fructose are shown in Table 1.

Sugar	**Oxidative leaching conditions**	**Leaching Percentage (w/w) %**
Glucose	Air, reflux, 100 ^{0}C, 48 h	Li = 39 %, Ni = 18 % Mn = 16 %, Co = 12 %
Glucose	O_2, 75 psi, 140 ^{0}C, 6 h	Li = 99 %,Ni = 88 % Mn = 86 %,Co = 89 %
Fructose	O_2, 75 psi, 140 ^{0}C, 6 h	Li = 88 %, Ni = 85 % Mn = 82 %,Co = 83 %

Table 1. Hydrothermal extraction of Li, Ni, Mn and Co from LiBBM using sugar solutions

Regeneration of lithium nickel manganese cobalt oxide from leachate solution

First, the leachate solution was evaporated on a steam bath to form a pink-purple sol-gel of the mixed metal-hydroxy acid chelate, which was then dehydrated in an oven. Next, transferred to an alumina crucible, pyrolyzed and sintered at 800 °C resulting a black powder as shown in figure 3. The regenerated lithium nickel manganese cobalt oxide was analyzed for Li, Ni, Mn and Co using ICP-OES and also by XRF and XRD. The Li, Ni, Mn, Co and O (w/w) % composition of the regenerated lithium nickel manganese cobalt oxide is comparable to the empirical formula of lithium nickel manganese cobalt oxide in original LiBBM.

In conclusion, aqueous sugar solutions under a high pressure oxygen atmosphere can be used to leach out Li, Ni, Mn and Co from spent Li-ion battery coatings through the oxidation of sugars. The use of glucose and O_2 at 75 psi, 140 °C, 6 h., yielded the highest Li, Ni, Mn, and Co extraction efficiencies. Furthermore, Li, Ni, Mn, and Co oxide cathode material could be regenerated by drying the leachate solution to a sol-gel and pyrolysis at 800 °C.

Figure 3. Regenerated lithium nickel manganese cobalt oxide ($LiNi_aMn_bCo_cO_d$) after pyrolysis of chelate in an alumina crucible at 800 °C.

Publications Supported by this BES Project

[1]. A. S. Amarasekara, A. B. Shrestha. *Facile Recovery of Lithium as Li_2CO_3 or Li_2O from alpha-Hydroxy-Carboxylic Acid Chelates through Pyrolysis and the Decomposition Mechanism*. Journal of Analytical and Applied Pyrolysis. **2024**, https://doi.org/10.1016/j.jaap.2024.106471

[2]. A. S. Amarasekara, H. N. K. Herath, D. Wang. *Two step Synthesis of poly(Lactic-co-Glycolic acid) from Glycerol by Spent Li-Ion Battery Electrode $LiNi_xCo_yMn_zO_2$/C Catalyzed Oxidation to Lactic, Glycolic Acid Mixture and p-TsOH - $SnCl_2$ Catalyzed Polymerization*. Chemical Papers. **2024**. https://doi.org/10.1007/s11696-024-03449-8

[3]. A. S. Amarasekara, L. J. Leday, D. Wang. *Microwave Assisted Extraction of Lithium from Hectorite Clay. Geo System Engineering*. **2024**. https://doi.org/10.1080/12269328.2024.2338087

[4]. A. S. Amarasekara, D. Wang, A. B. Shrestha. *Efficient Leaching of Metal Ions from Spent Li-Ion Battery Combined Electrode Coatings Using Hydroxy Acid Mixtures and Regeneration of Lithium Nickel Manganese Cobalt Oxide. Batteries.* **2024**, *10*(6), *170,* https://doi.org/10.3390/batteries10060170

Materials Chemistry: Understanding Flow Cell Porous Electrodes as Active Materials for Electrochemical Transformations

Michael J. Aziz (Harvard) – Jennifer A. Lewis (Harvard) – Chris H. Rycroft (University of Wisconsin-Madison) – Shmuel M. Rubinstein (Hebrew University)

Keywords: porous electrodes – 3D printing – confocal microscopy – numerical modeling

Research Scope

We aim to develop a fundamental understanding of the mechanisms occurring within flow cell porous electrodes during operation. In the fabrication effort we aim to fabricate porous electrodes with systematically varied architectures to understand the effect of microstructure on performance. In the characterization effort we aim to utilize *operando* electrochemical fluorescence microscopy in these materials to provide a time-resolved mapping of the state-of-charge (SOC) and velocity field over three spatial dimensions ("4D imaging"). In the modeling effort we aim to understand how electrode microstructure impacts performance by simulating reactive flow in the electrode, where the solid surfaces are explicitly modeled. Ultimately, we aim to unify these research threads to develop new design principles for porous electrodes.

Recent Progress

We developed an electrode fabrication pathway, termed "print-and-plate," in which a graphene nanocomposite ink is extruded through a 30 mm nozzle, then successively plated with nickel and gold (Figure 1) to afford sub W sq^{-1} sheet resistance and high porosity. This fabrication approach enables varied lattice architecture to investigate the relationship between structure and performance. [1]

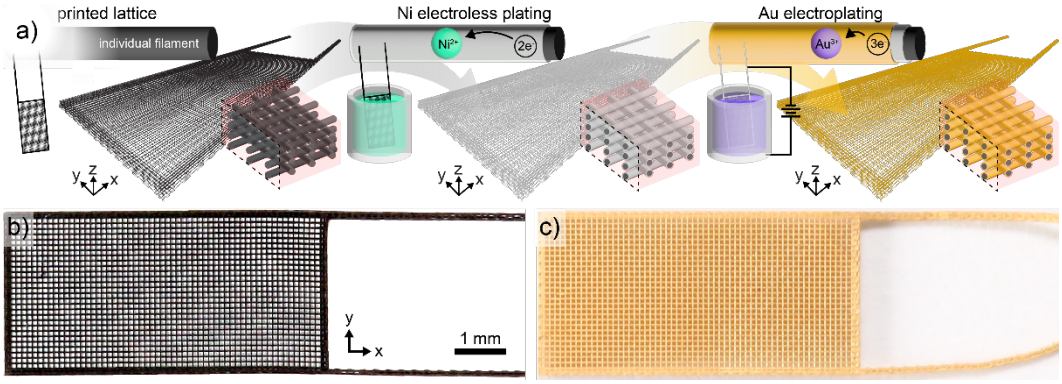

Figure 1. Print-and-plate electrode fabrication. a) schematic of electrode processing, printed graphene nanocomposite (left) is plated in Ni (electroless, center) followed by gold (electroplate, right); a representative nanocomposite lattice b) before metal plating and c) after Au electroplating. From [2].

This is achieved by electrochemical fluorescence microscopy using an anthraquinone disulfonic acid (AQDS) negolyte;[2] reduction to H_2AQDS affords fluorescence,[3] enabling direct and real-time visualization of concentration fields. A challenge has been conversion of raw fluorescence data

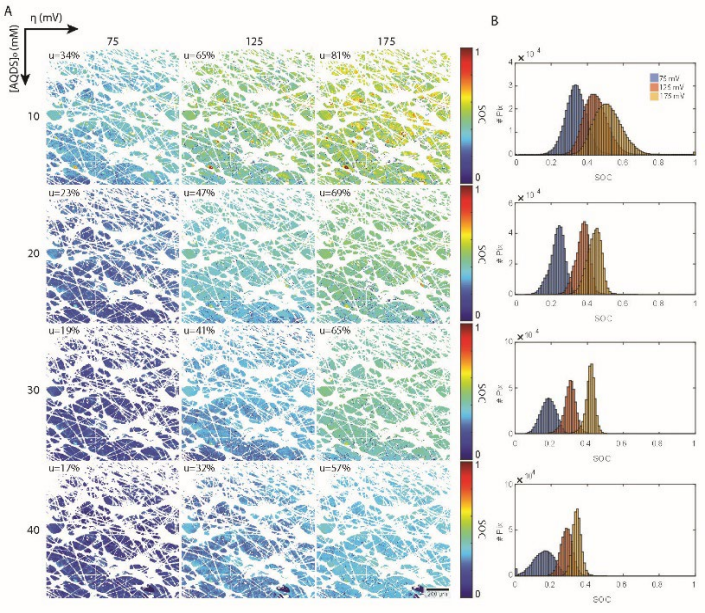

Figure 2. Quantitative 2D SOC mapping in a carbon paper electrode. a) SOC map at 12 operating conditions (4 concentrations x 3 voltages) b) Pixel distribution vs. SOC for each operating condition. From [1].

into a quantitative state-of-charge (SOC) map: shadowing effects, background fluorescence, the spatially-dependent optical transfer function, and non-fluorescent AQDS-H_2AQDS dimers complicate analysis.[4] We have recently achieved a major milestone by developing and calibrating a 2D image processing procedure that converts pixel fluorescence to SOC in a commercial carbon paper electrode (Figure 2). We have applied the same processing pathway to print-and-plate electrodes, mapping SOC in 3 dimensions via confocal fluorescence microscopy (Figure 3a).

Our modeling efforts have extended our simulation code from 2D to 3D, overcoming numerous technical challenges. We can now simulate at 2.5 mm resolution the entire electrode of Figure 3. Importantly, our print-and-plate SOC maps experimentally validate our simulations at the level of individual *z*-slices (Figure 3a-b) and of the total 3D volume, where global experimental and simulated average SOC values (0.19 and 0.22, respectively) are in good agreement. Additional modeling work has included the development of two techniques to speed convergence to steady state: iterative up-sampling and the Nernst model. Using these advancements, we are now developing a data-driven, hierarchical approach to a mesoscale model for larger systems. After building a library of unit cell geometries, we input their statistical properties into a coarse-grained model at the larger scale.

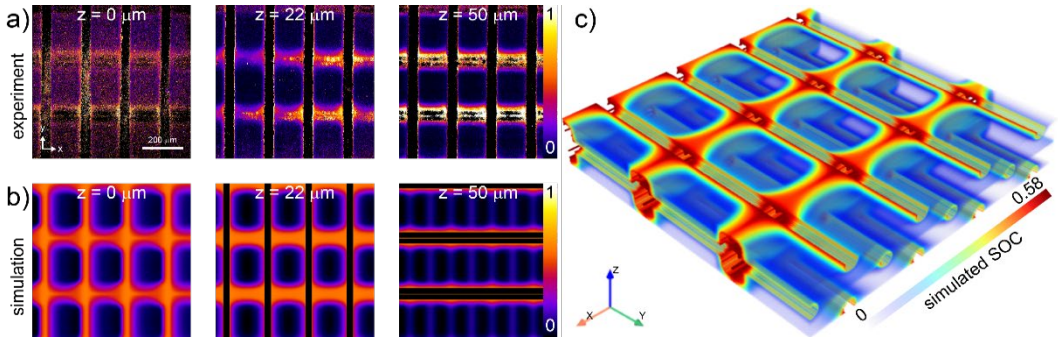

Figure 3. Quantitative 3D SOC mapping in experimental and simulated print-and-plate electrodes. a) slices of a confocal *z*-stack mapping the state of charge through a print-and-plate lattice; b) corresponding slices from a simulated electrode of the same dimensions and same conditions; c) volume view of the simulated lattice. Flow is in the positive *x* direction. Figure adapted from [2].

References

1. G.M. Gratson, M. Xu and J.A. Lewis, *Microperiodic Structures: direct writing of three-dimensional webs*, Nature **428**, 386 (2004).

2. B. Huskinson, M.P. Marshak, C. Suh, S. Er, M.R. Gerhardt, C.J. Galvin, X. Chen, A. Aspuru-Guzik, R.G. Gordon and M.J. Aziz, *A metal-free organic-inorganic aqueous flow battery*, Nature **505**, 195 (2014).

3. A.A. Wong, M.J. Aziz, and S.M. Rubinstein, *Direct visualization of electrochemical reactions and comparison of commercial carbon papers in operando by fluorescence microscopy using a quinone-based flow cell*, ECS Transactions **77**, 153 (2017).

4. L. Tong, Q. Chen, A.A. Wong, R. Gomez-Bombarelli, A. Aspuru-Guzik, R.G. Gordon, and M.J. Aziz, *UV-Vis spectrophotometry of quinone flow battery electrolyte for in-situ monitoring and improved electrochemical modeling of potential and quinhydrone formation*, Phys. Chem. Chem. Phys. **19**, 31684 (2017).

Publications

[1] A. M. Graf, T. Cochard, K. Amini, M.S. Emanuel, S.M. Rubenstein, and M.J. Aziz, *Quantitative Local State of Charge Mapping by Operando Electrochemical Fluorescence Microscopy in Porous Electrodes*, Submitted (2024). https://github.com/memanuel/qefsm

[2] D. M. Barber, S. Edgar, M. S. Emanuel, M. D. Nelwood, B. Y. Ahn, T. Cochard, J. Platero, B. Roman-Manso, K. Amini, C. H. Rycroft, S. Rubinstein, M. J. Aziz, J. A. Lewis, *Print-and-plate electrodes as active materials for electrochemical transformations,* Submitted (2024)

Biomolecular Interactions in Organic Semiconductors

M.A. Baldo, ***Research Laboratory of Electronics, MIT***
T. Van Voorhis, ***Dept. of Chemistry, MIT***
Keywords: Exciton fission, Organic Semiconductors, Solar cells

Research Scope

Silicon solar cells dominate the global photovoltaic market, due to their high efficiencies and low manufacturing costs. It has been proposed that the performance and adoption of silicon solar cells can be further improved by supplementing conventional single junction cells with singlet exciton fission to generate two electrons from each blue and green photon in sunlight[1]. We demonstrate an increase in the power conversion efficiency of crystalline silicon solar cells by coupling to singlet exciton fission in tetracene (Tc). The transfer of Tc triplet excitons to silicon is mediated by an interfacial layer of zinc phthalocyanine. A thin layer of aluminum oxide is used to passivate the silicon solar cell and reduce defect states and losses at the silicon interface. Using a shallow junction crystalline silicon microwire solar cell to efficiently extract charge carriers from the silicon surface, the peak efficiency of charge generation per photon absorbed in Tc is (138 ± 6)%, comfortably surpassing the conventional quantum efficiency limit of a silicon solar cell. Singlet fission enhanced silicon solar cells can exceed the efficiency of traditional silicon technologies while exhibiting the simplicity and practical advantages of a single junction architecture.

Recent Progress

In 1979, the well-known physical chemist D.L. Dexter proposed an intriguing vision for the future of solar energy: the combination of a silicon cell and molecular singlet exciton fission[1]. Unfortunately, Dexter's proposal had a *major* weakness. Since 1979, it has proved impossible to couple molecular triplet excited states to silicon. The conventional approach (also known as Dexter energy transfer) requires simultaneous transfer of an excited state's electron and hole from the donor to the acceptor. But for reasons that remain debated but may be related to silicon's indirect gap, Dexter transfer is apparently ineffective when the acceptor is silicon.

We have recently overcome this long-standing challenge by demonstrating a new energy transfer pathway at silicon interfaces[2]. Based on our prior studies of oxide interfaces[3,4], we engineered new material combinations to perform an initial charge transfer to silicon, followed by a sequential transfer of the remaining charge carrier. The energy of the intermediate charge-separated state must lie between the triplet energy and the bandgap of silicon. This is achieved with a thin layer of an electron donating material, zinc phthalocyanine (ZnPc). The second component of our interface is a thin passivation layer necessary to prevent the transferred charge carriers from immediately recombining at the silicon surface, while still enabling carrier tunneling. Aluminum oxide (AlO_x) is commonly used to passivate silicon solar cells. In this work, we use approximately 1-nm-thick layers of AlO_x to both passivate the silicon surface and maintain charge tunneling across the interface[5].

The measured external quantum efficiency (EQE) spectra of a Si n^+-p microwire (MW) device before and after Tc and ZnPc deposition are presented in Fig. 1. After deposition of Tc/ZnPc, we see a positive contribution corresponding to the absorption spectrum of Tc, with a maximum EQE increase from 81.6% to 87.9% at 520 nm. The measured J-V curves of the devices also show that depositing ZnPc and Tc on the n^+-p MW devices results in an enhancement in the short-circuit current density, with negligible decrease in the open-circuit voltage and fill factors, confirming that the role of the molecular materials in this cell architecture is primarily excitonic in nature, and other than increased charge injection, decoupled from the operation of the junction itself. As expected p^+-n MW devices exhibit shadowing in the EQE spectra from absorption of Tc, confirming that the device performance enhancements observed in the n^+-p devices are not due to enhanced antireflective effects. Figure 1C shows fits of Tc absorption to the EQE, yielding a sensitization efficiency of $\eta_{Tc} = (138 \pm 6)\%$, where 200% is the maximum theoretical enhancement possible for a photocurrent doubling process.

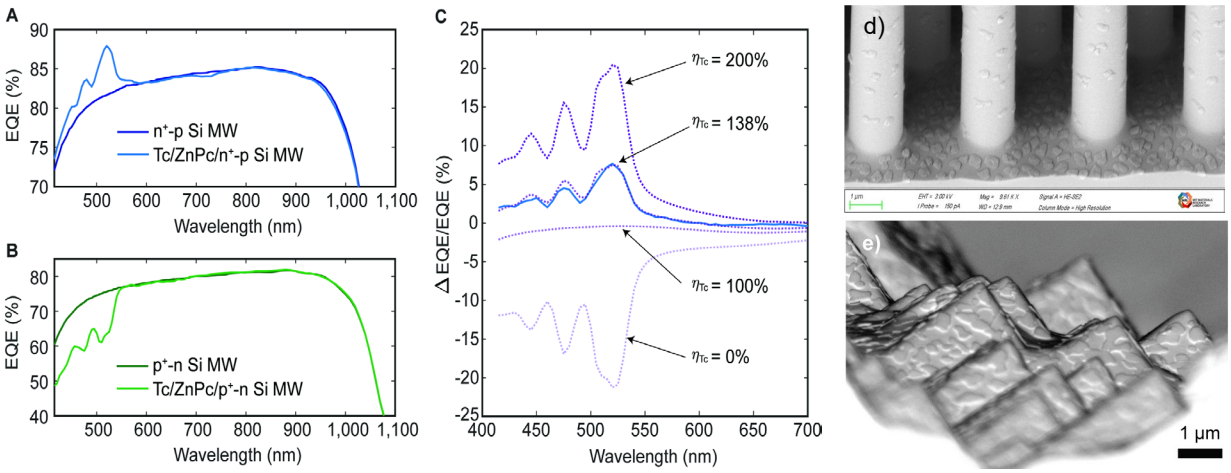

Figure 1. Device External Quantum Efficiencies. (**A**) Measured external quantum efficiency (EQE) spectra of n^+-p Si MW cells before and after Tc and ZnPc deposition. (**B**) Measured EQE spectra of p^+-n Si MW cells before and after Tc and ZnPc deposition. (**C**) Simulation fits of the percentage difference enhancement after organic deposition (ΔEQE/EQE) of the n^+-p Si MW cells presented in (A). The dotted lines represent simulated differential EQE at different Tc sensitization efficiencies (η_{Tc}). The solid line is data for the Tc/ZnPc/n^+-p Si MW device shown in (A). **(D,E)** Scanning electron micrographs of the microwire devices and planar cells. Note the Tc morphology consisting of <1000nm islands.

In conclusion, we demonstrate efficient coupling between a silicon solar cell and singlet exciton fission in Tc, finally realizing the solar cell concept first proposed by D.L. Dexter in 1979[1]. Control over the crucial interface between Tc and silicon is established by assuming sequential charge transfer mediated by a thin layer of ZnPc. The resulting observation of more than one electron per photon in a silicon solar cell provides the foundation for a new solar photovoltaic technology capable of accelerating the global adoption of renewable energy.

References

1 Dexter, D. L. Two Ideas On Energy-Transfer Phenomena - Ion-Pair Effects Involving The OH Stretching Mode, And Sensitization of Photo-Voltaic Cells. *J. Lumines.* **18-9**, 779-784 (1979). https://doi.org:10.1016/0022-2313(79)90235-7

2 Nagaya, N., Lee, K., Perkinson, C. F., Li, A., Lee, Y., Zhong, X., Lee, S., Weisburn, L. P., Baikie, T. K., Bawendi, M. G., Voorhis, T. V., Tisdale, W. A., Kahn, A., Seo, K. & Baldo, M. A. Exciton Fission Enhanced Silicon Solar Cell. *submitted* (2024).

3 Einzinger, M., Wu, T., Kompalla, J. F., Smith, H. L., Perkinson, C. F., Nienhaus, L., Wieghold, S., Congreve, D. N., Kahn, A., Bawendi, M. G. & Baldo, M. A. Sensitization of silicon by singlet exciton fission in tetracene. *Nature* **571**, 90-94 (2019). https://doi.org:10.1038/s41586-019-1339-4

4 Nagaya, N., Perkinson, C. F., Li, A., Voorhis, T. V., Tisdale, W. A. & Baldo, M. A. Trap-mediated energy transfer at interfaces between tetracene and silicon. *unpublished* (2024).

5 Nagaya, N., Perkinson, C. F., Li, A., Bawendi, M. G., Voorhis, T. V., Tisdale, W. A. & Baldo, M. A. Dynamic passivation at tetracene - silicon interfaces. *unpublished* (2024).

Publications

1. Dong-Gwang Ha, Ruomeng Wan, Changhae Andrew Kim, Ting-An Lin, Luming Yang, Troy Van Voorhis, Marc Baldo & Mircea Dinca, "Exchange controlled triplet fusion in metal–organic frameworks", Nature Materials, Volume 21, 1275, (2022), DOI: https://doi.org/10.1038/s41563-022-01368-

Solid-State Chemistry of Novel Pnictides with Complex Structures

Svilen Bobev

Department of Chemistry and Biochemistry, University of Delaware, Newark DE 19716

Keywords: New Materials, Synthesis, Thermoelectrics, Topological Behavior, Zintl Phases

Research Scope

Our program is focuses on synthetic and structural work of novel materials, stepping up the research efforts in the creation of new crystalline forms of matter for energy production and conversion. Specifically, we work on Zintl phases, which in recent years, have established themselves as promising candidates for thermoelectric applications. Owing to their narrow bandgaps, Zintl phases exhibit reasonably high electrical conductivity, while their complex crystal structures and/or presence of heavy elements yield low thermal conductivity. All of the above provide for a favorable combination of transport properties, beneficial for high thermoelectric performance. From a more fundamental point of view, the structure-property relationships derived from our work can be further used for developing a rationale for the synthesis of other new compounds, as well as for tuning of properties of existing ones.

Recent Progress

In the past, while studying ternary and quaternary pnictides with complex structures, we have often discovered unreported binary Zintl pnictides, such as Nd_3Bi_7 and Ba_5P_4, among others.[1,2] Recently, over the course of our studies in various Ba–*M*–Sb ternary systems,[3-8] crystals of the $Ba_{16}Sb_{11}$ phase were identified. Full crystallographic data for $Ba_{16}Sb_{11}$ are not available in the literature. The existence of the phase was only indicated in a 1997 publication by *Corbett et al*,[9] and the structure was assigned as isotypic with $Ca_{16}Sb_{11}$ based on powder X-ray diffraction. Here we briefly recount the results from the synthesis, structural and symmetry analysis from single-crystal X-ray diffraction studies of $Ba_{16}Sb_{11}$. We provide evidence that the structural disorder in this Zintl phase is different compared to the $Ca_{16}Sb_{11}$ archetype. We also identified monoclinic crystals of $Ba_{16}Sb_{11}$, where the structural disorder is alleviated—the fully ordered monoclinic structure is with space group $P2_1$, different from the previously assigned one with the tetragonal space group $P\bar{4}2_1m$.[9]

The "16–11" family of compounds can potentially be large, and although the structure of the $Ca_{16}Sb_{11}$ archetype has been known for over 25 years, surprisingly little structural work has been published concerning other $A_{16}Pn_{11}$ members. From a survey of the literature, it appears that only two more "16–11" phases, $Eu_{16}Pn_{11}$ (*Pn* = Sb, Bi), have been structurally characterized via single-crystal X-ray diffraction methods.[10] All three compounds adopt the $Ca_{16}Sb_{11}$ structure type and crystallize in the tetragonal space group $P\bar{4}2_1m$ (No. 113). All other "known" members of the family are only presumed to be isotypic. On this note, assigning the $Ba_{16}Sb_{11}$ structure as isotypic with $Ca_{16}Sb_{11}$ can be easily justified from periodic trends, although in this case, the Ba-compound

does not mirror the chemistry of the Ca-based compound with the same empirical formula. Specifically, the vast majority of the collected single-crystal XRD data can be indexed in a tetragonal cell with periodicity constants $a \approx 13.6$ Å and $c \approx 12.4$ Å, the subsequent solution and refinements in space group $P\bar{4}2_1m$, although adequate, show that the crystal structure is much more disordered compared to that of $Ca_{16}Sb_{11}$. For the best crystals, there was clear evidence of reflections that could be indexed based on a lower monoclinic symmetry and with unit cell twice the size of the tetragonal one. Subsequent structure solutions and refinements indicated that working with the space group $P2_1$ (No. 4) leads to the same "average" atomic arrangement, where, importantly, all crystallographic positions are fully occupied and positional/occupation disorder is non-existent.

Unlike $Ca_{16}Sb_{11}$, the monoclinic crystal structure of $Ba_{16}Sb_{11}$ exhibits no crystallographic disorder and perfectly satisfies the Zintl concept as far as the count of valence electrons is concerned. There are 32 crystallographically independent Ba sites and 22 Sb sites, all occupying general 2*a* positions. Unsurprisingly, the structural motifs in both monoclinic and tetragonal models of the $Ba_{16}Sb_{11}$ are nearly identical. The monoclinic structure can be viewed as an ordered version of the disordered tetragonal one (in lower symmetry and twice as large unit cell volume, of course). Therefore, the very same structural motifs can be distinguished—square prisms and antiprisms formed by Ba atoms and centered by Sb atoms (Figure 1). They are arranged in columns and repeat in the following sequence: $\{[Sb18Ba_8]_{prism}$–$[Sb14Ba_8]_{antiprism}$–$[Sb11Ba_8]_{antiprism}$–$[Sb5Ba_8]_{prism}$–$[Sb2Ba_8]_{antiprism}$–$[Sb10Ba_8]_{antiprism}\}$ (marked as {ABCDEF}), as shown in the figure. The asymmetric unit of $Ba_{16}Sb_{11}$ consists of four such parallel slabs, which can be broken into two pairs with two shifted antiparallel columns in each described by {ABCDEF}–{FEDCBA}–{DEFABC}–{CBAFED} repeats. Relatively short Ba–Ba distances connect these parallel slabs, with the shortest being 3.717 Å between two pairs of face-sharing antiprisms containing an Sb–Sb bond, making a ladder-like structural arrangement. There are two Sb–Sb dimers per unit cell (or one per doubled formula unit). Therefore, despite the complexity, the monoclinic structure of $Ba_{16}Sb_{11}$ poses no problem for the Zintl concept, which allows us to rationalize it as follows: $2\times Ba_{16}Sb_{11} = (Ba^{2+})_{32}(Sb^{3-})_{20}[Sb_2]^{4-}$. This charge-balanced way of partitioning the valence electrons hints at intrinsic semiconducting behavior, which is also indicated by our electronic structure calculations.

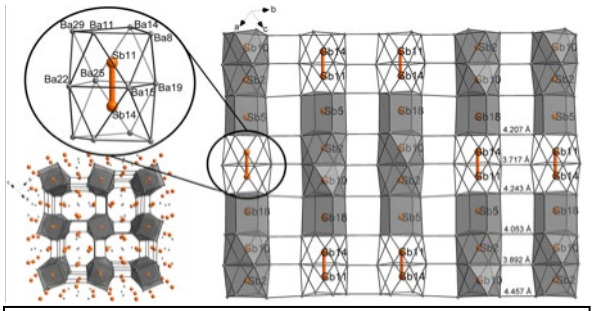

Fig. 1 Crystal structure of $Ba_{16}Sb_{11}$ viewed as an array of face-shared prism–antiprisms. The enlarged portion shows two antiprism hosting a Sb_2 dimer. Barium atoms are shown in grey, and antimony atoms are shown in orange.

References

1. A. Ovchinnikov, J. P. A. Makongo, and S. Bobev, *Yet Again, New Compounds Found in Systems with Known Binary Phase Diagrams. Synthesis, Crystal and Electronic Structure of Nd_3Bi_7 and Sm_3Bi_7*, Chem. Comm. **54**, 7089 (2018).

2. J.-A. Dolyniuk, H. He, A. S. Ivanov, A. I. Boldyrev, S. Bobev, and K. Kovnir, *Ba and Sr Binary Phosphides: Synthesis, Crystal Structures, and Bonding Analysis*, Inorg. Chem. **54**, 8608 (2015).

3. H. He, S. Stoyko, and S. Bobev, *New Insights into the Application of the Valence Rules in Zintl Phases—Crystal and Electronic Structures of $Ba_7Ga_4P_9$, $Ba_7Ga_4As_9$, $Ba_7Al_4Sb_9$, $Ba_6CaAl_4Sb_9$, and $Ba_6CaGa_4Sb_9$*, J. Solid State Chem. **236**, 116 (2016)

4. S. Bobev, J. Hullmann, T. Harmening, and R. Pöttgen, *Novel Ternary Alkaline-earth and Rare-earth Metal Antimonides from Gallium or Indium Flux. Synthesis, Structural Characterization and ^{121}Sb and ^{151}Eu Mössbauer Spectroscopy of the Series $A_7Ga_8Sb_8$ (A = Sr, Ba, Eu) and $Ba_7In_8Sb_8$*, Dalton Trans. **39**, 6049 (2010).

5. B. Saparov, H. He, X. Zhang, R. Greene, and S. Bobev, *Synthesis, Crystallographic and Theoretical Studies of the New Zintl Phases $Ba_2Cd_2Pn_3$ (Pn = As, Sb), and the Solid Solutions $(Ba_{1-x}Sr_x)_2Cd_2Sb_3$ and $Ba_2Cd_2(Sb_{1-x}As_x)_3$*, Dalton Trans. **39**, 1063 (2010).

6. B. Saparov, and S. Bobev, *Isolated $[ZnPn_2]^{4-}$ Chains in the Zintl Phases Ba_2ZnPn_2 (Pn = As, Sb, Bi)—Synthesis, Structure and Bonding*, Inorg. Chem. **49**, 5173 (2010).

7. S.-Q. Xia, and S. Bobev, *Zintl Phase Variations Through Cation Selection. Synthesis and Structure of $A_{21}Cd_4Pn_{18}$ (A = Eu, Sr, Ba; Pn = Sb, Bi)*, Inorg. Chem. **47**, 1919 (2008).

8. S.-Q. Xia, B. Saparov, and S. Bobev, *Synthesis, Structure and Bonding of the Zintl Phase $Ba_3Cd_2Sb_4$*, Inorg. Chem. **47**, 11237(2008).

9. E. A. Leon-Escamilla, W.-M. Hurng, E. S. Peterson, and J. D. Corbett, *Synthesis, Structure, and Properties of $Ca_{16}Sb_{11}$, a Complex Zintl Phase. Twelve Other Isotypic Compounds Formed by Divalent Metals and Pnictogens*, Inorg. Chem. **36**, 703 (1997).

10. J. Y. Chan, M. M. Olmstead, H. Hope, and S. M. Kauzlarich, *Synthesis, Structure, and Properties of $Eu_{16}Sb_{11}$ and $Eu_{16}Bi_{11}$*, J. Solid State Chem. **155**, 168 (2000).

Publications

1. M. O. Ogunbunmi, and S. Bobev, *Exploiting the Fraternal Twin Nature of Thermoelectrics and Topological Insulators in Zintl Phases as a Tool for Engineering New Efficient Thermoelectric Generators,* J. Mater. Chem. C. **11**, 8337 (2023).

2. Y. Wang, and S. Bobev, *Synthesis and Crystal structure of the Zintl phases NaSrSb, NaBaSb and NaEuSb,* Materials **16**, 1428 (2023).

3. M. O. Ogunbunmi, and S. Bobev, *The Electronic and Thermoelectric Transport Properties of Zintl Pnictides,* Encycl. Inorg. Bioinorg. Chem. **9**, 1 (2023).

4. Z. Hu, J. Deng, H. Li, M. O. Ogunbunmi, X. Tong, Q. Wang, D. Graf, W. R. Pudelko, Y. Liu, H. Lei, S. Bobev, M. Radovic, Z. Wang, and C. Petrovic, *Robust Three-dimensional Type-II Dirac Semimetal State in SrAgBi*, npj Quantum Mater. **8**, 20 (2023).

5. A. Ovchinnikov, and S. Bobev, *Crystal and Electronic Structure of the Ternary Zintl Bismuthide BaLiBi*, Z. Anorg. Allg. Chem. **e202300128** (2023).

6. S. Baranets, A. Ovchinnikov, S. M. Gayomi K. Samarakoon, and S. Bobev, *Synthesis, Crystal and Electronic Structure of the Zintl phase $Ba_{16}Sb_{11}$. A Case Study Uncovering Greater Structural Complexity via Monoclinic Distortion of the Tetragonal $Ca_{16}Sb_{11}$ Structure Type*, Z. Anorg. Allg. Chem. **e202300148** (2023).

7. K. Gosh, and S. Bobev, *Synthesis, Crystal and Electronic Structure of the Zintl phase $Sr_{21}Cd_4Sb_{18}$*, Solids **4**, 344 (2023).

8. S. M. Gayomi K. Samarakoon, A. Ovchinnikov, S. Baranets, and S. Bobev, *Ba_5Sb_8: The Highest Homologue of the Family of Binary Semiconducting Barium Antimonides Ba_nSb_{2n-2} ($n > 2$)*, Inorganics **12**, 3 (2024).

9. S. R, Watts, L. M. Wingate, S. Bobev, and S. Baranets, *Completing the Ba–As Compositional Space: Synthesis and Characterization of Three New Binary Zintl Arsenides, Ba_3As_4, Ba_5As_4, and $Ba_{16}As_{11}$*, Crystals **14**, 570 (2024).

10. M. Ishtiyak, S. R, Watts, B. Thipe, F. Womack, P. Adams, X. Bai, D. Young, S. Bobev, and S. Baranets, *Advancing Heteroanionicity in Zintl Phases: Crystal Structures, Thermoelectric and Magnetic Properties of Two Quaternary Semiconducting Arsenide Oxides, $Eu_8Zn_2As_6O$ and $Eu_{14}Zn_5As_{12}O$*, Inorg. Chem. *in print* (2024).

New paradigms for controlling molecular and ion transport in precise, tight and reconfigurable polymer networks

Paul Braun, Christopher Evans, Ken Schweizer, Charles Sing, Materials Research Laboratory, University of Illinois Urbana-Champaign, Urbana, IL 61801

Keywords: penetrant transport, ion transport, polymer networks, dynamic covalent chemistry, vitrimers

Research Scope

The theme of this effort is to understand the fundamental science of carefully-designed polymer networks that are crosslinked with topology-conserving dynamic covalent bonds, and their promise as a new class of materials for selective ion and liquid separations. We envision that, by functionalizing the dynamic crosslinking groups to tune interactions with diffusing species, molecular motion is facilitated or controlled by a coupled combination of network rearrangements and strand dynamics. The fundamental challenge lies in understanding how the multiple tunable length and time scales characteristic of the structure and dynamics of these rubbery, supercooled, and glassy matrices can couple to dynamic bond exchange kinetics to greatly amplify differences of the activated diffusion constant of related families of molecules and ions. We explore this issue via a deeply integrated experiment-simulation-theory effort focused on how controllable physicochemical factors such as the network structural relaxation time, ratio of network mesh to penetrant size, penetrant shape, dynamic bond kinetics, and specific interactions between molecules with polymer strands or crosslinks, determine the absolute and relative magnitudes of molecular and ion transport. The work is organized into two complementary and tightly integrated efforts: Chemical Control of Local Dynamics in Vitrimers which addresses foundational knowledge of how dynamic covalent bonds impact *e.g.* segmental dynamics, bond exchange processes relevant to transport of guest molecules in polymer networks, and Dynamic Bond Facilitated Transport in Networks which specifically examines the transport of species that either reversibly react/interact or are trapped in crosslinked networks.

Recent Progress

A major unresolved question for molecular diffusion in polymers is the influence of heavy crosslinking in dense networks that can have mesh sizes approaching that of a molecular penetrant such as aromatic fluorescent dyes. Mesh confinement effects are much less explored as a size selective sieving mechanism compared to more rigid frameworks[1,2] or polymers of intrinsic microporosity.[3,4] Moreover, crosslinking can dramatically slow down polymer segmental relaxation in a crosslink fraction, temperature, and chemistry dependent manner,[5] which will strongly impact penetrant activated transport in a manner that depends on penetrant size and the degree of coupling of its activated hopping motion with polymer segmental dynamics.

We investigate aspects of this overarching question by probing molecular diffusion in densely crosslinked networks, using an integrated experiment-theory-simulation approach that allows us to understand how the molecular details of the penetrant with the surrounding network govern penetrant transport.[5-10] In one example, our team used a model permanent poly(n-butyl acrylate) polymer network to study how penetrant size, temperature, and crosslink fraction can profoundly affect penetrant diffusion. Agreement between simulation, theory, and experiment (Fig. 1a) indicates that local chemical detail is largely 'self-averaged',[5] so conclusions drawn from coarse-grained models are relevant for experiments. The relationship between penetrant transport, mesh confinement, penetrant size, polymer Kuhn length, electrostatics, and segmental relaxation was subsequently explored in simulation and theory, indicating that confinement effects are of secondary importance relative to crosslink-induced slowing down of segmental relaxation and activated penetrant hopping.[6,7,11] Further investigation using the same models and experimental systems demonstrated that molecular shape becomes important for transport in the deeply supercooled regime for larger penetrants (Fig. 1b),[8] with a competition between the coupling of penetrant motion to molecular shape and the presence of strong penetrant-network interactions and mesh confinement.[9]

Figure 1. (a) Apparent dimensionless slopes k_{cross} determined from experiment, simulation, and theory penetrant diffusion constant and hopping rate results plotted as $\log(1/D_p)$ versus penetrant-segment size ratio d/σ for various temperatures (b) Theoretically predicted mean alpha times for the dyes BTBP and TBRb of the same volume but different shape studied experimentally (representative models shown schematically) as a function of $T_g(f_{cross})/T$. (c) Comparison of experimental and theoretical segmental relaxation times for ethylene vitrimers as a function of $T_g(f_{cross})/T$ for 4 crosslinking fractions, along with the corresponding polymer melt prediction.

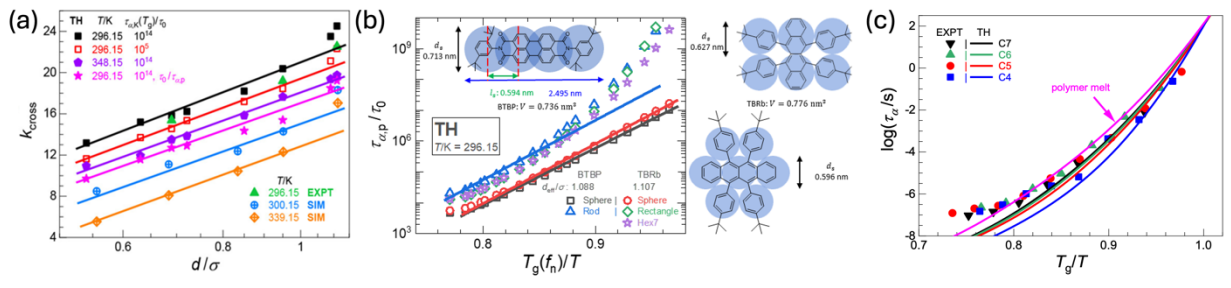

The local dynamics of vitrimers and the effect on penetrant transport were studied for networks composed of precise ethylene linkers and dynamic boronic ester bonds.[10,12] First, theory and simulation provide molecular-level insight into how dynamic bond exchange influences the activated polymer segment relaxation (Fig. 1c).[13,14] The timescales for these two processes exhibit strong coupling and non-Arrhenius behavior at temperatures approaching T_g, consistent with experiments.[15] Penetrant diffusion constants were measured where the molecules either do or do not participate in bond exchange processes.[10,12,16] Initial results indicate that transport of the former couples strongly to bond kinetics, and can be impeded by slow bond exchange.[13,14]

References

1. C. A. Trickett, A. Helal, B. A. Al-Maythalony, Z. H. Yamani, K. E. Cordova, and O. M. Yaghi, *The chemistry of metal-organic frameworks for CO2 capture, regeneration and conversion*, Nat Rev Mater **2** 17045 (2017).
2. S. S. Yuan, X. Li, J. Y. Zhu, G. Zhang, P. Van Puyvelde, and B. Van der Bruggen, *Covalent organic frameworks for membrane separation*, Chem Soc Rev **48**, 2665 (2019).
3. C. G. Bezzu, M. Carta, A. Tonkins, J. C. Jansen, P. Bernardo, F. Bazzarelli, and N. B. McKeown, *A Spirobifluorene-Based Polymer of Intrinsic Microporosity with Improved Performance for Gas Separation*, Adv Mater **24**, 5930 (2012).
4. P. M. Budd, E. S. Elabas, B. S. Ghanem, S. Makhseed, N. B. McKeown, K. J. Msayib, C. E. Tattershall, and D. Wang, *Solution-processed, organophilic membrane derived from a polymer of intrinsic microporosity*, Adv Mater **16** 456 (2004).
5. B. Mei, T. W. Lin, G. S. Sheridan, C. M. Evans, C. E. Sing, and K. S. Schweizer, *How Segmental Dynamics and Mesh Confinement Determine the Selective Diffusivity of Molecules in Crosslinked Dense Polymer Networks*, ACS Cent Sci **9**, 508 (2023).
6. B. Mei, T. W. Lin, C. E. Sing, and K. S. Schweizer, *Self-Consistent Hopping Theory of Activated Relaxation and Diffusion of Dilute Penetrants in Dense Crosslinked Polymer Networks*, J Chem Phys **158**, 184901 (2023).
7. T. W. Lin, B. Mei, K. S. Schweizer, and C. E. Sing, *Simulation Study of the Effects of Polymer Network Dynamics and Mesh Confinement on the Diffusion and Structural Relaxation of Molecular Penetrants*, J Chem Phys **159,** 014904 (2023).
8. B. Mei and K.S. Schweizer, *Penetrant Shape Effects on Activated Dynamics and Selectivity in Polymer Melts and Networks Based on Self-Consistent Cooperative Hopping Theory,* Soft Matter **19**, 8744 (2023).
9. T.W. Lin and C.E. Sing, *Effect of Penetrant-Polymer Interactions and Shape on the Motion of Molecular Penetrants in Dense Polymer Networks,* J Chem Phys **160,** 114905 (2024).
10. J. Huang, N. Ramlawi, G. S. Sheridan, C. Chen, R. H. Ewoldt, P. V. Braun, and C. M. Evans, *Dynamic Covalent Bond Exchange Enhances Penetrant Diffusion in Dense Vitrimers*, Macromolecules **56**, 1253 (2023).
11. B. C. Mei, T. W. Lin, G. S. Sheridan, C. M. Evans, C. E. Sing, and K. S. Schweizer, *Structural Relaxation and Vitrification in Dense Cross-Linked Polymer Networks: Simulation, Theory, and Experiment,* Macromolecules **55**, 4159 (2022).
12. J. Huang, G. S. Sheridan, C. Chen, N. Ramlawi, R. H. Ewoldt, P. V. Braun, and C. M. Evans, *Reversible Reactions, Mesh Size, and Segmental Dynamics Control Penetrant Diffusion in Ethylene Vitrimers*, ACS Macro Lett. **12**, 901-907 (2023).
13. B. Mei, C.M. Evans, and K.S. Schweizer, *Force-Level Self-Consistent Theory of Structural Relaxation, Bond Exchange Times, and the Glass Transition in Polymeric Vitrimers,* Macromolecules **57**, 3242 (2024).
14. T.-W. Lin, S. Dutta, B. Mei, K.S. Schweizer, and C.E. Sing, *Simulations of Glassy and Crosslink Dynamics in Vitrimer Networks*, In Preparation (2024).
15. B. Soman, K.S. Schweizer, and C.M. Evans, *Rheological and Dielectric Measurements Connect Vitrimer Dynamics Across Nine Order of Magnitude,* Macromolecules **56,** 166 (2023).
16. S. Jang, E. I. Hernandez-Alvarez, C. Chen, B. B. Jing, C. Shen, P. V. Braun, A. Schleife, C. M. Schroeder, and C. M. Evans, *Control of Lithium Salt Partitioning, Coordination, and Solvation in Vitrimer Electrolytes*, Chem. Mater. **35**, 8039-8049 (2023).

Team Publications (2023-present)

1. B. Soman, K. S. Schweizer and C. M. Evans, *Fragile Glass Formation and Non-Arrhenius upturns in Ethylene Vitrimers Revealed by Dielectric Spectroscopy*, Macromolecules **56**, 166 (2023).
2. B. Mei, T.-W Lin, G. S. Sheridan, C. M. Evans, C. E. Sing and K. S. Schweizer, *How Segmental Dynamics and Mesh Confinement Determine the Selective Diffusivity of Molecules in Crosslinked Dense Polymer Networks*, ACS-Central Science **9**, 505 (2023).
3. C. Chen, S. Du, J. M. Taylor, J. Huang, C. M. Evans, and P. V. Braun, *Visualizing Ion Transport in Polymer via Ion-chromic Indicators*, ACS Macro Letters **12**, 86 (2023).
4. B. Mei, T.-W. Lin, C. E. Sing and K. S. Schweizer, *Self-Consistent Hopping Theory of Activated Relaxation and Diffusion of Dilute Penetrants in Dense Crosslinked Polymer Networks,* J. Chemical Physics **158**, 184901 (2023).
5. J. Huang, N. Ramlawi, G. S. Sheridan, C. Chen, R. H. Ewoldt, P. V. Braun, and C. M. Evans, *Dynamic Covalent Bond Exchange Enhances Penetrant Diffusion in Dense Vitrimers*, Macromolecules **56**, 1253 (2023).
6. T. W. Lin, B. Mei, K. S. Schweizer, and C. E. Sing, *Simulation Study of the Effects of Polymer Network Dynamics and Mesh Confinement on the Diffusion and Structural Relaxation of Molecular Penetrants*, J Chem Phys **159,** 014904 (2023).
7. B. Mei and K.S. Schweizer, *Penetrant Shape Effects on Activated Dynamics and Selectivity in Polymer Melts and Networks Based on Self-Consistent Cooperative Hopping Theory,* Soft Matter **19**, 8744 (2023).
8. B. Mei, C.M. Evans, and K.S. Schweizer, *Force-Level Self-Consistent Theory of Structural Relaxation, Bond Exchange Times, and the Glass Transition in Polymeric Vitrimers,* Macromolecules **57**, 3242 (2024).
9. B. Soman, K.S. Schweizer, and C.M. Evans, *Rheological and Dielectric Measurements Connect Vitrimer Dynamics Across Nine Order of Magnitude,* Macromolecules **56,** 166 (2023).
10. J. Huang, G. S. Sheridan, C. Chen, N. Ramlawi, R. H. Ewoldt, P. V. Braun, and C. M. Evans, *Reversible Reactions, Mesh Size, and Segmental Dynamics Control Penetrant Diffusion in Ethylene Vitrimers*, ACS Macro Lett. **12**, 901-907 (2023).

Impacts of Dynamic Bonding on the Properties of Porous Materials

Assist. Prof. Carl K. Brozek, University of Oregon, Department of Chemistry and Biochemistry

Keywords: labile, metal-organic frameworks, phase changes, soft modes

Research Scope

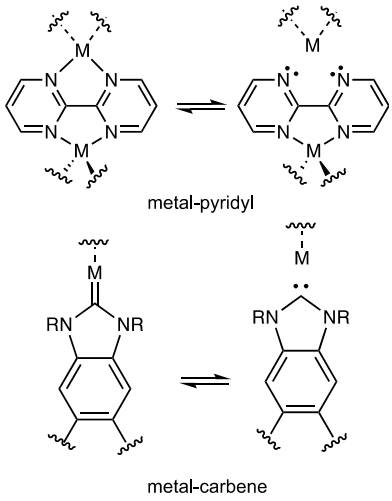

Fig. 1: Reversible metal-ligand bonds in coordination polymers.

Metal-ligand (ML) bonds dictate the properties of metal complexes and coordination materials. Subtle differences in the geometries and energetics of ligand fields surrounding metal ions govern the optical, electronic, magnetic, and catalytic properties and overall stability of the resulting complexes.[1–3] While enthalpy favors ML bond formation, entropy drives their dissociation such that all ML bonds exist to varying degrees in dynamic equilibria between bound and unbound states (**Fig. 1**). This bond lability impacts the mechanisms of transition metal catalysis[4–6] and enables the self-healing behavior observed in coordination polymers.[7–10] Among traditional solid-state materials, the earliest examples of ferroelectric phase-change behavior were documented to involve a special class of ML phonons,[11–13] now termed "soft modes", that drive the phase change by distorting atomic positions from one phase to another. In other words, dynamic equilibria of metal-ligand bonds exist in coordination complexes ranging from small molecules to extended solids, and yet dynamic bonding in materials bridging the gap between the molecular and solid-state divide remains an open frontier.[14,15] Metal-organic frameworks (MOFs, **Fig. 2**), also termed 3D porous coordination polymers, are a compositionally tunable class of materials. Their secondary building units (SBUs) can be altered to yield either isostructural or entirely new materials. To date, nearly 100,000 MOFs have been synthesized and over 500,000 structures have been predicted, all of which contain ML bonds.[16] Considering the fundamental lability of ML bonds, it follows that MOFs and other CPs should also exhibit similar behavior to molecules and nonporous solids and that bond lability should strongly influence MOF behavior.

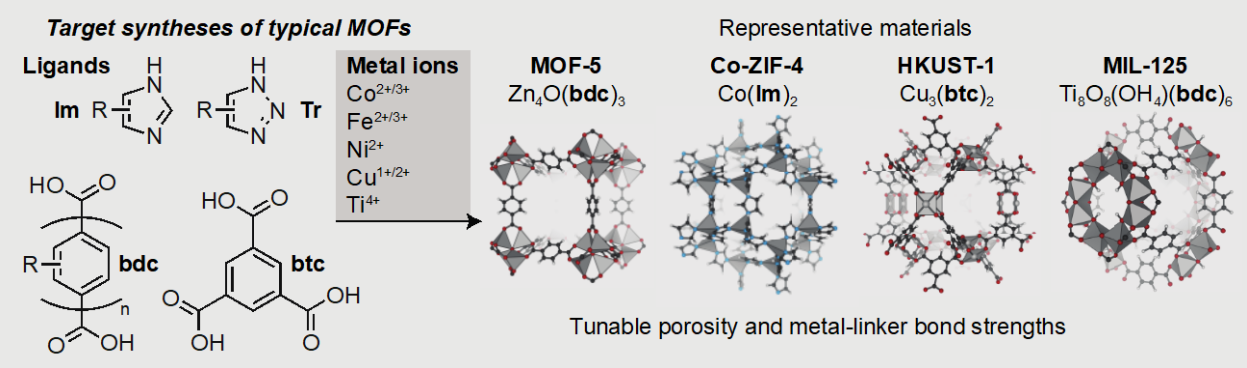

Fig. 2: Representative MOF materials with example ligands and metal ions.

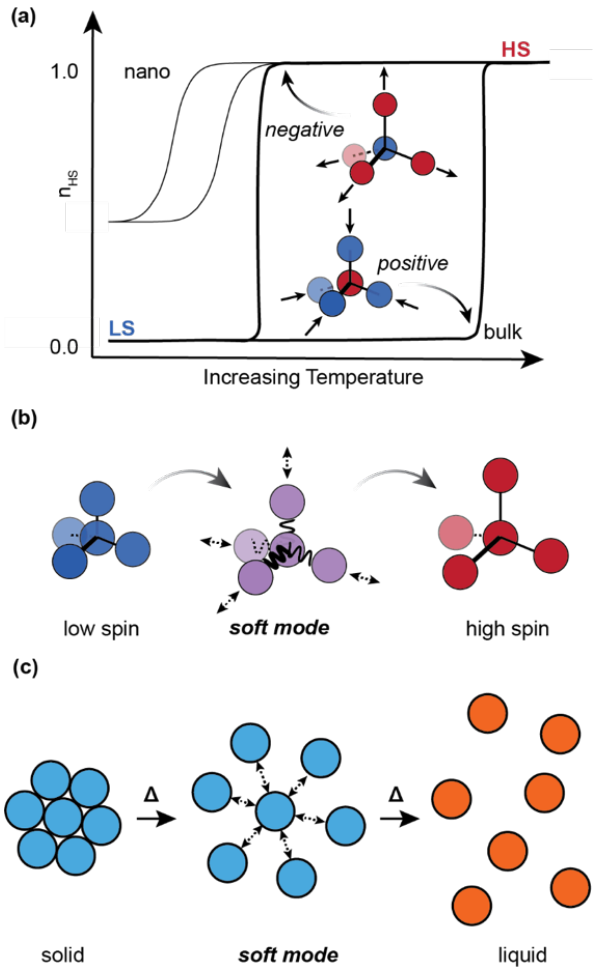

Fig. 3. Representation of bonding and hysteresis phenomena in spin crossover behavior. (a) The fraction of HS sites as a function of temperature in bulk versus nanoparticles. (b) Depiction of soft modes that convert LS to HS sites and (c) a soft mode driving a solid-to-liquid melting phase change.

This project identifies signatures of dynamic bonding in porous materials and studies its influence on electronic, photophysical, and magnetic properties. With these insights, previously unexplained behavior in porous materials can be understood in terms of fundamental microscopic principles developed in our lab that will also provide design guidelines for leveraging dynamic bonding to access new energy materials.

Recent Progress

Size reduction offers a synthetic route to tunable phase change behavior. Preparing materials as nanoparticles causes drastic modulations to critical temperatures (T_c), hysteresis widths, and the "sharpness" of first-order versus second-order phase transitions. A microscopic picture of the chemistry underlying this size dependence in phenomena ranging from melting to superconductivity remains debated. As a case study with broad implications, our recent studies indicate that size-dependent spin crossover (SCO) (**Fig. 3**) in nanocrystals of the MOF Fe(1,2,3-triazolate)$_2$ arises from metal-linker bonds becoming more labile in smaller particles. In comparison to the bulk material, differential scanning calorimetry indicates a ~30-40% reduction in T_c and ΔH in the smallest particles. Variable-temperature vibrational spectroscopy reveals a diminished long-range structural cooperativity, while X-ray diffraction evidences an over three-fold increase in the thermal expansion coefficients. This "phonon softening" provides a molecular mechanism for designing size-dependent behavior in framework materials and for understanding phase changes in general.

References

1 L. Guo, D. E. Ellis, B. M. Hoffman and Y. Ishikawa, *Ligand Substitution Effect on Electronic Structure and Optical Properties of Nickel Porphyrazines*, Inorg. Chem., **35**, 5304 (1996).

2 T. Ishii, S. Tsuboi, G. Sakane, M. Yamashita and B. K. Breedlove, *Universal spectrochemical series of six-coordinate octahedral metal complexes for modifying the ligand field splitting*, Dalton Trans., 680 (2009).

3 Z. Yang, M. Corso, R. Robles, C. Lotze, R. Fitzner, E. Mena-Osteritz, P. Bäuerle, K. J. Franke and J. I. Pascual, *Orbital Redistribution in Molecular Nanostructures Mediated by Metal–Organic Bonds*, ACS Nano, **8**, 10715 (2014).

4 D. Cremer and E. Kraka, *Generalization of the Tolman electronic parameter: the metal–ligand electronic parameter and the intrinsic strength of the metal–ligand bond*, Dalton Trans., **46**, 8323 (2017).

5 J. Bould, O. Tok, V. Passarelli, M. G. S. Londesborough and R. Macías, *Ligand Lability Driven by Metal-to-Borane Pseudorotation: A Mechanism for Ligand Exchange*, Inorg. Chem., **59**, 17958 (2020).

6 K. Zhao, S. Liu, Y. Li, X. Wei, G. Ye, W. Zhu, Y. Su, J. Wang, H. Liu, Z. He, Z. Zhou and S. Sun, *Insight into the Mechanism of Axial Ligands Regulating the Catalytic Activity of Fe–N $_4$ Sites for Oxygen Reduction Reaction*, Adv. Energy Mater., **12**, 2103588 (2022).

7 K. A. Williams, A. J. Boydston and C. W. Bielawski, *Main-chain organometallic polymers: synthetic strategies, applications, and perspectives*, Chem. Soc. Rev., **36**, 729 (2007).

8 K. A. Williams, D. R. Dreyer and C. W. Bielawski, *The Underlying Chemistry of Self-Healing Materials*, MRS Bull., **33**, 759 (2008).

9 A. Winter and U. S. Schubert, *Synthesis and characterization of metallo-supramolecular polymers*, Chem. Soc. Rev., **45**, 5311 (2016).

10 D.-P. Wang, J.-C. Lai, H.-Y. Lai, S.-R. Mo, K.-Y. Zeng, C.-H. Li and J.-L. Zuo, *Distinct Mechanical and Self-Healing Properties in Two Polydimethylsiloxane Coordination Polymers with Fine-Tuned Bond Strength*, Inorg. Chem., **57**, 3232 (2018).

11 K. McCash, B. K. Mani, C.-M. Chang and I. Ponomareva, *The role of mechanical boundary conditions in the soft mode dynamics of $PbTiO_3$*, J. Phys.: Condens. Matter, **26**, 435901 (2014).

12 M. P. Jiang, M. Trigo, I. Savić, S. Fahy, É. D. Murray, C. Bray, J. Clark, T. Henighan, M. Kozina, M. Chollet, J. M. Glownia, M. C. Hoffmann, D. Zhu, O. Delaire, A. F. May, B. C. Sales, A. M. Lindenberg, P. Zalden, T. Sato, R. Merlin and D. A. Reis, *The origin of incipient ferroelectricity in lead telluride*, Nat. Commun., **7**, 12291 (2016).

13 S. Badola, S. Mukherjee, B. Ghosh, G. Sunil, G. Vaitheeswaran, A. C. Garcia-Castro and S. Saha, *Lattice dynamics across the ferroelastic phase transition in Ba_2ZnTeO_6: a Raman and first-principles study*, Phys. Chem. Chem. Phys., **24**, 20152 (2022).

14 J.-C. Lai, X.-Y. Jia, D.-P. Wang, Y.-B. Deng, P. Zheng, C.-H. Li, J.-L. Zuo and Z. Bao, *Thermodynamically stable whilst kinetically labile coordination bonds lead to strong and tough self-healing polymers*, Nat. Commun., **10**, 1164 (2019).

15 C. Li and J. Zuo, Self-Healing Polymers Based on Coordination Bonds, Adv. Mater., **32**, 1903762 (2020).

16 C. W. Jones, *Metal–Organic Frameworks and Covalent Organic Frameworks: Emerging Advances and Applications*, JACS Au, **2**, 1504 (2022).

Publications

1. K. Fabrizio, K. N. Le, S. B. Andreeva, C. H. Hendon, C. K. Brozek, *Determining Optical Band Gaps of MOFs*. ACS Mater. Lett. **4**, 457 (2022).
2. J. McKenzie, K. N. Le; D. J. Bardgett, K. A. Collins, T. Ericson, M.K. Wojnar, J. Chouinard, S. Golledge, A. F. Cozzolino, D. C. Johnson, C. H. Hendon, C. K. Brozek, *Conductivity in Open-Framework Chalcogenides Tuned via Band Engineering and Redox Chemistry*. Chem. Mater. **34**, 1905 (2022).

3. J. McKenzie, P. A. Kempler, C. K. Brozek, *Solvent-Controlled Ion-Coupled Charge Transport in Microporous Metal Chalcogenides*. Chem. Sci. **13**, 12747 (2022).
4. K. Fabrizio, C. K. Brozek, *Size-dependent Thermal Shifts to MOF Nanocrystal Optical Gaps Induced by Dynamic Bonding*. Nano Lett **23**, 905 (2023).
5. F. Fabrizio, S. B. Andreeva, K. Kadota, C. K. Brozek, *Guest-Dependent Bond Flexibility in UiO-66, a 'Stable' MOF*. Chem. Commun. **59**, 1309 (2023).
6. K. Kadota, T. Chen, E. Gormley, C. H. Hendon, M. Dincă, C. K. Brozek, *Electrically Conductive [Fe_4S_4]-based Organometallic Polymers*. Chem. Sci. **14**, 11410 (2023).
7. E. Svensson Grape, A. M. Davenport, C. K. Brozek, C. K. *Dynamic metal-linker bonds in metal-organic frameworks*. *Dalton Trans.* **53**, 1935 (2024).
8. A. M. Davenport, C. R. Marshall, K. Kadota, S. Dunning, A. B. Andreeva, S. Horike, C. K. Brozek, *Size-Dependent Spin Crossover and Bond Flexibility in Metal-Organic Framework Nanoparticles* J. Am. Chem. Soc. *Under Revision* (2024)
9. J. McKenzie, C. H. Hendon, C. K. Brozek, *Tunable Interlayer Interactions in Two-Dimensions Van Der Waals Frameworks* Adv. Mater. *Under Revision* (2024)

Multidimensional Phase Maps for the Accelerated Synthesis and Study of Metastable Materials

Richard L. Brutchey

Department of Chemistry, University of Southern California, Los Angeles, CA 90089, USA

Keywords: synthesis science; phase maps; data driven; metastability

Research Scope

The "materials by design" approach successfully identified a vast number of materials with wide ranging properties. However, a bottleneck exists in the next step of the process: the Edisonian and by-hand nature of materials synthesis. We are addressing this bottleneck by combining our long-standing expertise in *chimie douce* (soft chemistry) methods with multivariate analyses via data-driven learning to accelerate predictive phase determination. We are extending thermodynamic phase diagrams into multidimensional "phase maps" that capture both thermodynamic and kinetic factors. The phase map correlates the effects of statistically significant experimental variables (beyond temperature and composition) on phase determination. Our focus is two-fold: (i) establishing methods for synthesizing specific thermodynamic phases in complex phase diagrams, and (ii) gaining new insights into accessing metastable phases across a variety of materials systems.

Recent Progress

Achieving the synthesis of a phase-pure material is traditionally done using the one-variable-at-a-time (OVAT) approach, where only one variable is changed at a time while all other variables are held constant.[1,2] This one-dimensional approach is not only time and labor intensive, but inefficient in revealing potentially important higher-order interactions between experimental variables and their effects on synthetic outcomes. Deep learning techniques can map multidimensional variable space, but they require large datasets that are not feasible when novel chemistry is being performed and/or done in a low-throughput manner.[3,4] Trained classification algorithms can handle both sparse data sets and categorical variables, such as phase, making it a tractable solution to this problem.

Example #1: The Cu-Se phase diagram is complex and contains many different crystal structures, in addition to several metastable structures that are not found on the thermodynamic phase diagram.[5-7] Consequently, being able to rationally navigate this complex phase space poses a significant challenge. We demonstrated that *chimie douce* synthesis methods combined with classification algorithms can enable predictive phase navigation. We constructed a surrogate model from 80 reactions exploring four variables: C-Se bond strength of a diselenide precursor, time, temperature, and solvent composition. The reactions in the surrogate model resulted in 11 distinct copper selenide phases or phase combinations (**Fig. 1a**). These data were used to train a classification algorithm that predicted phase with a 96% accuracy; the resulting decision tree provided chemical insight into how the experimental variables affect phase and prescribed synthetic conditions for the isolation of specific phases. For example, the metastable wurtzite-like $Cu_{2-x}Se$ polymorph forms at higher temperatures and high volumetric ratios of oleylamine to octadecene, which transitions into umangite Cu_3Se_2 within a small window of slightly lower

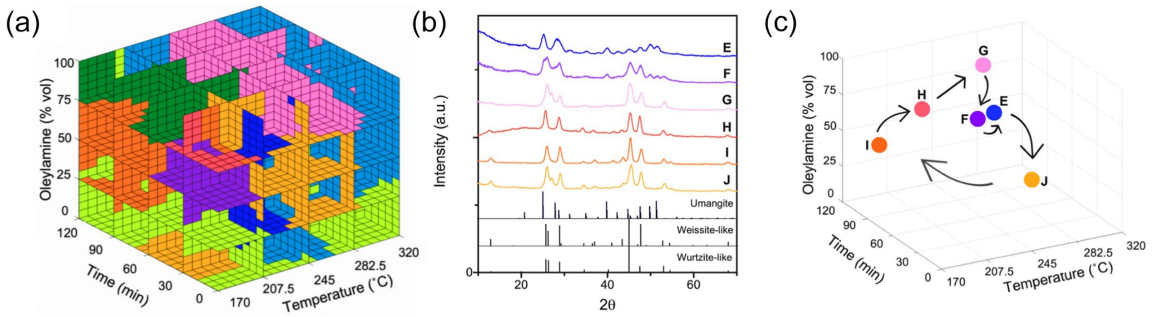

Fig. 1 (a) Cu-Se phase map where each color represents a different phase or combination of phases. (b) Powder XRD patterns of phases and phase combinations that result in the (c) sub-region of the phase map that is bound by the area of lower temperatures and higher volumetric ratios of oleylamine.

temperatures and shorter reaction times. The phase map shows the transition into another metastable weissite-like $Cu_{2-x}Se$ phase at longer reaction times, with a very small temperature difference of 2-3 ˚C separating umangite Cu_3Se_2 from weissite-like $Cu_{2-x}Se$ (**Fig. 1b,c**). This highlights the power of phase maps; we can isolate two phase-pure metastable materials within a complex variable space, where a temperature difference of only a few degrees separates three distinct phases. This would be nearly impossible to pinpoint using traditional, Edisonian methods.

Example #2: Given our ability to synthetically direct phase using phase maps, it is now of interest to prescriptively define other material features within a given crystal phase. For example, it is important to be able to synthesize nanocrystals with a specific size, minimized size distribution, and well-defined shape for catalytic applications.[8,9] To accomplish such a complex goal, we coupled a classifier algorithm with a multivariate Bayesian optimization to synthesize monodisperse rock salt CoO nanocrystals with defined size and shape. Upon compiling data from 72 reactions for the surrogate model, 10 unique crystal phases or phase combinations were observed, including the target rock salt CoO phase, metastable wurtzite CoO, metallic fcc Co, Co_2C, and phase combinations thereof. Within the rock salt CoO portion of the phase map, nanocrystal size, polydispersity, and shape purity were then jointly optimized *via* Bayesian optimization (**Fig. 2**).

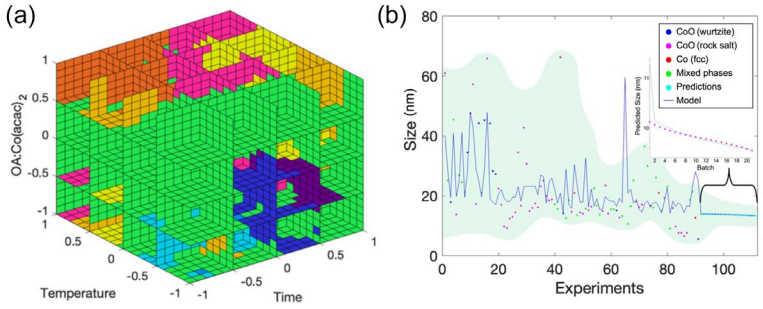

Fig. 2 (a) Phase map for the synthesis of rock salt CoO, indicated in the green phase space. (b) Bayesian optimization to minimize CoO nanocrystal size and predicted size distribution shown behind in green.

The reaction conditions at the multiobjective optimum were predicted to produce a product with a size of 9.8 ± 4.4 nm and a cuboidal particle morphology. The experimental validation of this prediction was performed in triplicate and the averaged results were in good agreement with the predicted responses, yielding cuboidal rock salt CoO nanoparticles with a size of 6.6 ± 2.9 nm, as assessed by automated TEM image analysis (N = 36,000). This contrasts the CoO nanocrystals synthesized under unoptimized conditions, which had an average size of 65 ± 40 nm with nine distinct shapes.

References

1. Cao, B.; Adutwum, L. A.; Oliynyk, A. O.; Luber, E. J.; Olsen, B. C.; Mar, A.; Buriak, J. M. How To Optimize Materials and Devices via Design of Experiments and Machine Learning: Demonstration Using Organic Photovoltaics. *ACS Nano* **2018**, *12*, 7434-7444.
2. Williamson, E. M.; Sun, Z.; Mora-Tamez, L.; Brutchey, R. L. Design of Experiments for Nanocrystal Syntheses: A How-To Guide for Proper Implementation. *Chemistry of Materials* **2022**, *34*, 9823-9835.
3. Braham, E. J.; Davidson, R. D.; Al-Hashimi, M.; Arróyave, R.; Banerjee, S. Navigating the Design Space of Inorganic Materials Synthesis Using Statistical Methods and Machine Learning. *Dalton Transactions* **2020**, *49*, 11480-11488.
4. Brown, K. A.; Brittman, S.; Maccaferri, N.; Jariwala, D.; Celano, U. Machine Learning in Nanoscience: Big Data at Small Scales. *Nano Letters* **2020**, *20*, 2-10.
5. Glazov, V. M.; Pashinkin, A. S.; Fedorov, V. A. Phase Equilibria in the Cu-Se System. *Inorganic Materials* **2000**, *36*, 641-652.
6. Lord, R. W.; Fanghanel, J.; Holder, C. F.; Dabo, I.; Schaak, R. E. Colloidal Nanoparticles of a Metastable Copper Selenide Phase with Near-Infrared Plasmon Resonance. *Chemistry of Materials* **2020**, *32*, 10227-10234.
7. Hernández-Pagán, E. A.; Robinson, E. H.; La Croix, A. D.; Macdonald, J. E. Direct Synthesis of Novel $Cu_{2-x}Se$ Wurtzite Phase. *Chemistry of Materials* **2019**, *31*, 4619-4624.
8. Li, Z.; Ji, S.; Liu, Y.; Cao, X.; Tian, S.; Chen, Y.; Niu, Z.; Li, Y. Well-Defined Materials for Heterogeneous Catalysis: From Nanoparticles to Isolated Single-Atom Sites. *Chemical Reviews* **2020**, *120*, 623-682.
9. Tao, A. R.; Habas, S.; Yang, P. Shape Control of Colloidal Metal Nanocrystals. *Small* **2008**, *4*, 310-325.

Publications

1. Karadaghi, L. R.; Williamson, E. M.; To, A. T.; Forsberg, A. P.; Crans, K. D.; Perkins, C. L.; Hayden, S. C.; LiBretto, N. J.; Baddour, F. G.; Ruddy, D. A.; Malmstadt, N.; Habas, S. E.; Brutchey, R. L. Multivariate Bayesian Optimization of CoO Nanoparticles for CO_2 Hydrogenation Catalysis. *Journal of the American Chemical Society* **2024**, *146*, 14246-14259.
2. Williamson, E. M.; Brutchey, R. L. Using Data-Driven Learning to Predict and Control the Outcomes of Inorganic Materials Synthesis. *Inorganic Chemistry* **2023**, *62*, 16251-16262.
3. Williamson, E. M.; Sun, Z.; Tappan, B. A.; Brutchey, R. L. Predictive Synthesis of Copper Selenides using a Multidimensional Phase Map Constructed with a Data-Driven Classifier. *Journal of the American Chemical Society* **2023**, *145*, 17954-17964.
4. Williamson, E. M.; Sun, Z.; Mora-Tamez, L.; Brutchey, R. L. Design of Experiments for Nanocrystal Syntheses: A How-To Guide for Proper Implementation. *Chemistry of Materials* **2022**, *34*, 9823-9835.
5. Williamson, E. M.; Ghrist, A.; Karadaghi, L. R.; Smock, S. R.; Barim, G.; Brutchey, R. L. Creating Ground Truth for Nanocrystal Morphology: A Fully Automated Pipeline for Unbiased Transmission Electron Microscopy Image Analysis. *Nanoscale* **2022**, *14*, 15327-15339.
6. Cottingham, P.; Brutchey, R. L. Temperature-Dependent Behavior in the Local Structure of $BaTiO_3$ Nanocrystals. *CrystEngComm* **2022**, *24*, 5400-5404.

Elucidating the Link Between Alkali Metal Ions and Reaction-Transport Mechanisms in Cathode Electrodes for Alkali-ion Batteries

Ö. Özgür Çapraz[1,2]

[1]The School of Chemical Engineering, Oklahoma State University, Stillwater, Oklahoma

[2]Chemical, Biochemical and Environmental Engineering, University of Maryland Baltimore County, Baltimore, Maryland

Keywords: Alkali Metal-Ion Batteries, Structural & Interfacial Instabilities, Chemo-Mechanics

Research Scope

The main objective of our study is to identify the intrinsic relationship between the role of alkali metal ions and electrochemically driven mechanical stability and kinetic properties of battery materials. The overall question is, "What is the role of alkali metal ions in the electrochemical and mechanical behavior of cathode electrodes? The program investigates structural interfacial instability mechanisms on electrode materials for alkali-metal ion batteries. In situ / operando mechanical measurements were conducted to elucidate deformation mechanisms in the electrode during cycling in alkali metal ion chemistries. The mechanical measurements were supported by chemical, morphological, and structural characterizations via microscopy, diffractometry, and spectroscopy tools. The abstract here reports the progress of the project in the last two years. Our studies investigated structural and interfacial instabilities in electrode materials for alkali-metal ion batteries. We also focused on how type-of-alkali-metal ions (Li, Na, and K-ions), the transition metals in cathode structure (Ni vs Mn), and higher state-of-(dis)charge impact structural instabilities in the electrode. Operando mechanical tools were coupled with chemical characterization via XPS to monitor the role of electrolyte chemistry in the formation of cathode-electrolyte interface layers. Furthermore, we studied the chemo-mechanical stability of the binders in the composite electrodes. In addition to interfacial and structural characterization, the program investigated the rate-dependent mechanical instabilities in the cathode electrodes.

Recent Progress

Impact of Transition Metals on Chemo-Mechanical Instabilities in Prussian Blue Analogues (PBAs): PBA cathodes suffer from poor cycle life associated with chemo-mechanical instabilities[1]. Here, the electrochemical performance and associated chemo-mechanical instabilities in potassium nickel hexacyanoferrate (KNHCF) -based and potassium manganese hexacyanoferrate (KMHCF) are investigated by conducting electrochemical, mechanical, and chemical characterizations. KMHCF experienced a much faster capacity fade than KNHCF when cycled under the same electrochemical conditions. DIC measurements showed that both cathodes undergo similar nominal reversible strain generation. XPS measurements found a richer organic layer compounds on the surface of KMHCF cathodes compared to KNHCF ones after cycles. The study was published in Advanced Energy Materials.

Impact of Alkali-ion Intercalation into Cobalt Oxide Cathode: Intercalation of larger alkali metal ions is expected to cause severe structural instabilities such as plastic deformation and loss in crystallinity. [2] In the first two years of the project, we reported the governing mechanism behind the crystalline to amorphous phase transformation in iron phosphate cathodes upon intercalation of Na and K-ions by utilizing digital

image correlation (DIC) with structural analysis. Shortly, the study indicated that the strain rate, rather than the absolute value of strain, plays a critical role in the amorphization of the crystalline electrode. [3] In the last two years, in situ DIC tool was coupled with electrochemical techniques to probe deformation mechanisms in cobalt oxide cathodes, a layered metal oxide structure, during the intercalation of Li, Na, and K ions. While insertion of Li ions leads to contraction, intercalation of larger Na-ion causes expansions in the cathode. In the case of K-ion, the expansions were large enough to cause irreversible damage to the electrode. The study points to a way to control mechanical deformations during ion intercalation by utilizing their unique interactions with the host structure. The study was published in ACS Applied Engineering Materials.

Chemo-Mechanical Instabilities in Lithium Cobalt Oxide at Higher State-of-Charge: The practical charge capacity of transition metal oxide cathodes is limited due to severe chemo-mechanical instabilities at higher charge voltage and state-of-charge conditions. [4] Here, in-situ stress and strain measurements were conducted on the lithium cobalt oxide (LCO) cathode via a multi-beam stress sensor (MOSS) and DIC, respectively. The LCO undergoes a compressive stress generation when charged up to 4.2 V, and surface fractures on the LCO particles were detected by SEM. LCO cathode experienced significantly large contractions (negative strains) when charged up to 4.65 V, where intergranular crack formation and phase transformation were detected on the LCO particles via SEM and XRD, respectively. Overall, the study bridges complicated structural deformations with in-situ analysis of mechanical degradations in layer metal oxide cathodes charged at higher voltages. We are currently preparing a manuscript for submission.

Probing the Formation of Cathode-Electrolyte Interphase on Lithium Iron Phosphate Cathodes: The formation of cathode-electrolyte interphase (CEI) and its impact on the chemo-mechanical stabilities of cathodes are not well understood yet. [5,6] To address this gap, we utilized operando DIC combined with Cyro XPS to probe dynamic chemical and mechanical deformations on the $LiFePO_4$ cathodes during cycling in Li chemistry. We investigated the impact of the different anionic salt species (PF_6^-, ClO_4^-, and $TFSI^-$) in organic liquid electrolytes on the CEI formation mechanisms. Unexpected mechanical deformations were detected when cycled in $LiPF_6$-based electrolytes. The formation of fluorinated compounds on the surface of the electrode was captured by Cryo XPS on the onset of an increase in impedance and positive strain generation during the first charge in $LiPF_6$-electrolytes. The study was published in ACS Applied Material and Interphases.

Mechanical Stability of Binders for Composite Electrodes: Electrode undergoes volumetric expansions upon insertion of larger alkali metal ions, such as K-ions. [7] *Integrity of the composite electrode relies on the flexibility and chemical stability of binders. Here, we investigated the* chemo-mechanical properties of the PVDF and PEDOT: PSS binders. Strain generation in the composite graphite electrode during the first potassiation was associated with intercalation-induced structural changes and the formation of the solid-electrolyte interphase. DIC measurements showed that PEDOT: PSS/CB binder provides good mechanical integrity during potassium intercalation into graphite electrodes, even when the electrode expands 23%. This study was published in Advanced Energy Materials.

References

1- A. J. Zhou, W. J. Cheng, W. Wang, Q. Zhao, J. Xie, W. X. Zhang, H. C. Gao, L. G. Xue, J. Z. Li, Hexacyanoferrate-Type Prussian Blue Analogs: Principles and Advances Toward High-Performance Sodium and Potassium Ion Batteries. Adv. Energy Mater., **11**, 2000943 (2021)

2- T. Jin, H. Li, K. Zhu, P. F. Wang, P. Liu, L. Jiao, Polyanion-Type Cathode Materials for Sodium-Ion Batteries. Chem. Soc. Rev. **49**, 2342– 2377 (2020)

3- B. Ozdogru, Y. Cha, B. Gwalani, V. Murugesan, M. Song, and Ö. Ö. Çapraz, In Situ Probing Potassium-ion Intercalation-induced Amorphization in Crystalline Iron Phosphate Cathode Materials, Nano Letters, **21**, 18, 7579–7586, (2021).

4- J. Li, C. Lin, W. Weng, Y. Qiu, P. Chen, K. Yang, W. Huang, Y. Hong, J. Li, M. Zhang, C. Dong, W, Zhao, Z. Xu, X. Wang, K. Xu, J. Sun, F. Pan. Structural origin of the high-voltage instability of lithium cobalt oxide. Nat Nanotechnol. **16** (5):599-605. (2021)

5- J. C. Hestenes, L. E. Marbella, "Beyond Composition: Surface Reactivity and Structural Arrangement of the Cathode Electrolyte Interphase" ACS Energy Letters, **8**, 4572, (2023)

6- W. Fu, D. Kim, F. Wang, G. Yushin, Stabilizing Cathodes and Interphases for Next-Generation Li-Ion Batteries. J Power Sources, **561**, 232738 (2023)

7- T. Hosaka, K. Kubota, A. S. Hameed, S. Komaba, Research Development on K-Ion Batteries. Chemical Reviews, **120**, 14, 6358–6466 (2020).

Publications supported by this Project in the past two years

- B. Ozdogru, V. Murugesan, and Ö. Ö. Çapraz, Rate-Dependent Electrochemical Strain Generation in Composite Iron Phosphate Cathodes in Li-ion Batteries, Journal of Materials Research, **37**, 3237–3248 (2022).
- D. A. Gribble, Z. Li, B. Ozdogru, E. McCulfor, Ö. Ö. Çapraz and V. Pol, Mechanistic Elucidation of Electronically Conductive PEDOT:PSS Binder for a Potassium-ion Battery Graphite Anode: Electrochemical, Mechanical, and Thermal Safety Aspects, Advanced Energy Materials, **12**, 2103439 (2022).
- B. Bal, B. Ozdogru, D. Nguyen, Z. Li, V. Murugesan and Ö. Ö. Çapraz, Probing the Formation of Cathode-Electrolyte Interface on Lithium Iron Phosphate Cathodes via In Operando Mechanical Measurements, ACS App. Mater. Interfaces, **15**, 36, 42449–42459, 2023.
- Z. Li*, B. Ozdogru*, B. Bal, M. Bowden, A. Choi, Y. Zhang, H. Wang, V. Murugesan, V. G. Pol and Ö. Ö. Çapraz, The Role of Transition Metals on Chemo-Mechanical Instabilities in Prussian Blue Analogues For K-ion Batteries: The Case Study on KNHCF vs KMHCF, Advanced Energy Materials, **13**, 32, 2301329, 2023.
- M. Wable, B. Marckx and Ö. Ö. Çapraz, The Linkage Between Electro-Chemical Mechanical Instabilities in Battery Materials, JOM, **76**, 1099-1109, 2024.
- B. Bal and Ö. Ö. Çapraz, Impact of Alkali Metal-ion Intercalation on Mechanical Deformations in Cobalt Oxide Cathodes, ACS Appl. Eng. Mater, in press, 2024.

Development of Recyclable Thermosets for Additive Manufacturing

Sanchari Chowdhury, Youngmin Lee, and John McCoy, New Mexico Institute of Mining and Technology

Keywords: Recycling, Thermosets, Plasmonic, Photothermal, Diels-Alder

Research Scope:

The widespread use of thermosets such as epoxy generates immense amounts of waste. Due to their irreversible network structure, the recycling of epoxies is considered challenging. [1, 2]The goal of this project is to develop reversible thermosetting polymers/photothermal nanoparticles composites which can be recycled simply using solar light and are suitable for additive manufacturing. To develop sustainable recyclable epoxy, we incorporated Diels–Alder reactions in off-the-shelf epoxy reagents to develop a recyclable thermoset which can be reversibly liquified at higher temperature and solidified upon cooling.[1] We incorporated photothermal nanoparticles into the Diels–Alder (DA) modified epoxy, which strongly absorbs solar light to generate heat inside the polymer to efficiently drive the DA reactions for solar light enhanced recycling. [2]These studies have shown strong potential of developing reversible epoxy/photothermal nanoparticles composites for the applications of solar light enhanced recycling as well as light mediated additive manufacturing.

Additionally, our studies highlight the fundamental need to understand nanoscale temperature distribution in the polymer matrix due to photothermal heating and its effect on the reaction kinetics of Diels–Alder reactions.

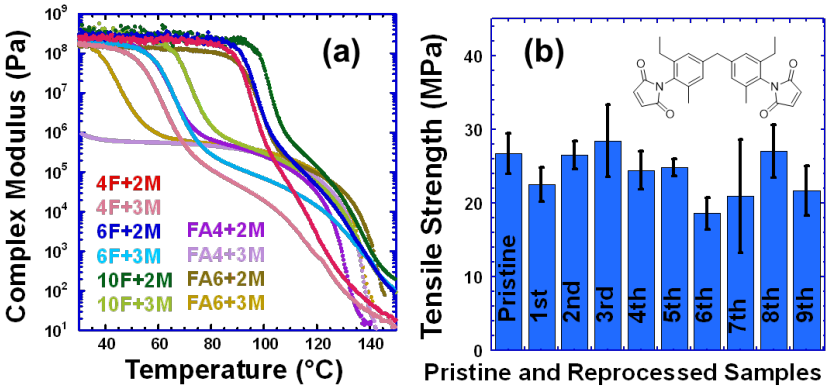

Figure 1: (a) Complex modulus of different reversible epoxy samples. The number in sample codes represents the number of furan or maleimide functional groups per precursor molecule. FA4 and FA6 has branched structure while 4F, 6F, and 10F has a linear backbone with grafted furan groups on the backbone. Compared to 2M, 3M has twice greater molar mass with flexible aliphatic structure. (b) Tensile strengths of pristine and recycled reversible epoxy.

Recent Progress:

In the past 3 years, major progress was made in two main aspects: 1) Varied the molecular design of furan and maleimide precursors to control the thermomechanical behavior of the reversible epoxy as well as suppress side reactions to achieve broad range of recyclable thermoset elastomers from soft elastomers to hard elastomers. 2) We developed photothermal nanoparticles/ reversible epoxy composites which can be successfully recycled using solar light.

I. Tuning the Chemistry of Epoxy using Diels–Alder Reactions:

We designed the functionality, molecular architecture, and molecular weights of furan and maleimide precursors to control the thermomechanical behavior of the reversible epoxy such as viscoelastic moduli, glass transition temperature, and de-gel temperature via the retro-Diels–Alder.[2] (Figure 1 (a)) Most importantly, we found a formulation of thermoreversible epoxy where

the final product shows competitive mechanical properties to a conventional epoxy but still shows flow-like properties at high temperature for reprocessing. We developed a detailed understanding of the effect of side reactions such as maleimide homopolymerization which causes irreversible crosslinking in the network leading to loss of the recyclability.[3] We demonstrated several strategies to reduce the effect of the side reaction such as varying the stoichiometric ratio of furan and maleimide, incorporating a free radical inhibitor such as hydroquinone, and varying the molecular weight and functionality of the maleimide precursors. Notably, by tuning the design of maleimide precursors we could recycle thermosets as high as 9 times without compromising its mechanical properties significantly. (Figure 1 (b))

II. Applications of Photothermal Nanoparticles to Recycle Reversible Epoxy using Solar Light:

For the first time, we demonstrated a complete cycle of liquifying, reprocessing and reshaping of thermosets modified by DA reactions using solar light. We incorporated photothermal nanoparticles such as carbon black (CB) and refractory plasmonic titanium nitride nanoparticles (TiN NPs) into reversible epoxy without altering its chemical formulation and thermomechanical properties (Figures 2(a) and 2(b)). We developed theoretical and experimental understandings to optimize the loading and the dispersion of both kinds of nanoparticles to maximize their light absorption and consequently heat generation. These photothermal nanoparticles strongly absorb sunlight to generate heat inside the polymer to efficiently drive the reversible reactions, facilitating liquification and recycling of reversible thermosets using sunlight. (Figure 2(c)).

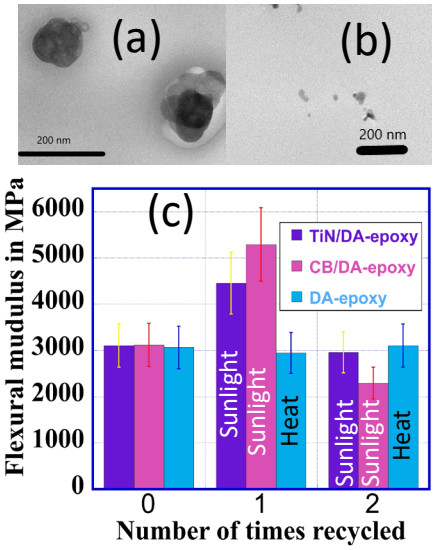

Figure 2. TEM images of (a) DA-epoxy/0.5 wt.% carbon black and (b) DA-epoxy/0.5 wt.% titanium nitride. (c) Flexural modulus of pristine and recycled samples of DA-epoxy, DA-epoxy/TiN and DA-epoxy/CB samples. Sunlight based recycling was under 1000mW/cm^2. Temperature is 140°C for both heat and light-based recycling.

Future Work:

Our future work involves understanding the effect of nanoscale temperature distribution due to photothermal heating under different light on the reaction kinetics of Diels–Alder reactions. This is important for designing processing conditions and developing recyclable thermosets/photothermal nanoparticles composites without compromising the desirable properties of thermosets. We aim to pursue the following studies in future (i)*Combined theoretical and experimental investigation of light induced photothermal heating and spatial heat distribution in different reversible epoxy/nanoparticle composite matrix with nanoscale resolution.* (ii) *Understanding the reaction kinetics of Diels–Alder Reactions and side Reactions associated with the carefully designed precursors and correlate that with photothermal heat generation by nanoparticles. (iii) Study the effect of photothermal nanoparticles on additive manufacturing and recycling of the reversible epoxy and understand the mechanical properties of the final structure in correlation with their processing conditions and feedstock properties.*

References:

1. Jin, Y.; Lei, Z.; Taynton, P.; Huang, S.; Zhang, W., Malleable and Recyclable Thermosets: The Next Generation of Plastics. *Matter* **2019,** *1* (6), 1456-1493.
2. Mojtabai, K. D.; Lindholm, S. J.; McReynolds, B. T.; Penners, N.; McCoy, J. D.; Chowdhury, S.; Lee, Y., Diels–Alder Augmented Epoxies with Plasmonic Nanoparticle Fillers for Efficient Photothermal Depolymerization. *ACS Applied Polymer Materials* **2022,** *4* (4), 2703-2711.
3. McReynolds, B. T.; Mojtabai, K. D.; Penners, N.; Kim, G.; Lindholm, S.; Lee, Y.; McCoy, J. D.; Chowdhury, S., Understanding the Effect of Side Reactions on the Recyclability of Furan–Maleimide Resins Based on Thermoreversible Diels–Alder Network. *Polymers* **2023,** *15* (5), 1106.

Publications:

1. Mojtabai, K. D.; Lindholm, S. J.; McReynolds, B. T.; Penners, N.; McCoy, J. D.; Chowdhury, S.; Lee, Y., Diels–Alder Augmented Epoxies with Plasmonic Nanoparticle Fillers for Efficient Photothermal Depolymerization. ACS Applied Polymer Materials , **4** (4), 2703-2711,2022.

2. McReynolds, B. T.; Mojtabai, K. D.; Penners, N.; Kim, G.; Lindholm, S.; Lee, Y.; McCoy, J. D.; Chowdhury, S., Understanding the Effect of Side Reactions on the Recyclability of Furan and Maleimide Resins Based on Thermoreversible Diels-Alder Network. Polymers-Basel, **15** (5), 1106, 2023.

3. McReynolds, B.; Chowdhury, S.; McCoy, J. D.; Lee,Y.; Determining the Reaction Kinetics and Thermodynamics of a Diels–Alder Network Using Dynamic Gel Criteria, Macromolecules, 57, 12, 5620–5628,2024

4. De Silva, K.-G.-G. C.; Finale, M.; Chowdhury, S., Plasmon mediated deposition of Ni on titanium nitride nanoparticles: Applications in enhanced photoreduction of bicarbonate. Materials Research Bulletin **152**, 111834,2022.

5. De Silva, KGG.C.; Helsel, N.; Jeyashangararaj, H.S.; Choudhury, P. and Chowdhury, S. "Plasmon assisted synthesis of TiN-supported single-atom nickel catalysts" *Discover Nano***19**, 50 (2024). https://doi.org/10.1186/s11671-024-03992-z

MOF-Polymer Hybrids for Energy Science

Seth M. Cohen, University of California, San Diego

Keywords: Metal-organic frameworks, oligomers, phosphines, polymers, surfaces

Research Scope

This project in Materials Chemistry is focused on combining metal-organic frameworks (MOFs) and polymers into unique hybrid materials with emergent properties. This program is pursuing two primary avenues in MOF-polymer composites. The proposed studies will build on innovative findings from our research program:

- In ***Specific Aim 1***, we will expand our pioneering studies on 'polyMOFs', a new class of porous solids. polyMOFs are MOF-like materials that are derived from polymeric, rather than molecular, organic building blocks. polyMOFs have unique features and represent a molecular level integration of MOFs and polymers. The experiments proposed in ***Specific Aim 1*** represent the next step in the translation of polyMOFs to energy applications.

- In ***Specific Aim 2***, we will expand on our recent findings in the self-assembly of polymer-coated MOF nanoparticles. We have discovered that MOF nanoparticles coated with a polymer 'corona' can self-assemble into unprecedented freestanding particle monolayers. In ***Specific Aim 2***, we seek to expand the generality and test the utility of these fascinating, thin film MOF-polymer hybrids.

This continuing research program satisfies two research goals of the Office of Basic Energy Sciences: (a) the fabrication and characterization of new materials; and (b) the understanding and control of chemical reactivity..

Recent Progress

Progress on our project has taken several interesting avenues, opening up new chemistry at the interface metal-organic frameworks (MOFs), polymers, and new materials. Some of these efforts have since spun off into separate programs, while other discoveries are core to the ongoing efforts in this project.

As part of our core studies on MOF-polymer hybrid materials, we have made significant progress on new polyMOF and oligoMOF materials, understanding their interrelationship, and their unique properties. In the last several years, we have published two studies on oligoMOFs, MOF materials made from dimeric, trimeric, etc. ligand systems. In particular, we have begun to map out how these

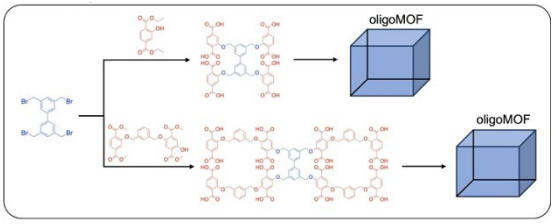

Figure 1. OligoMOFs made from branched ligands.

tethered systems modulate MOF synthesis and structure.[1] We have also established that highly branched tetrameric and octameric ligand systems can for polyMOFs (Figure 1), demonstrating the versatility and vast potential of these systems.[2] In still unpublished work, we have shown that the tether between ligating groups can be functionalized, provide sites for MOF pore tuning via direct modulation or postsynthetic modification (PSM). A manuscript is presently in preparation describing these new findings.

Our studies on polymer-coated MOF particles also continues to progress. We have investigated the effect of polymer molecular weight and composition on the formation of self-assembled MOF monolayers (SAMMs).[3] We have also published a tutorial article to aid others in the synthesis and study of SAMMs.[4]

Perhaps most interesting, we have used organic dyes modified with metal ligating groups to study the surface of MOFs (Figure 2).[5] The surface chemistry of MOFs is critically important to our studies on MOF-polymer hybrids, including those used to form SAMMs. However, the surface chemistry of MOFs is quite understudied. The system we have established provides an excellent quantitative and qualitative probe of surface chemistry that we plan to expand upon in future studies.

Figure 2. Organic dyes used to investigate the surface of MOFs.

In a departure from our core efforts, this program seeded our first studies on low-valent metal-organic frameworks (LVMOFs). These materials, constructed from low-valent metals and phosphine ligands, defy traditional approaches and thinking in MOF chemistry. We described the first metal-phosphine LVMOFs utilizing unconventional metals for MOFs including Pd(0), Pt(0), and Rh(I). This resulted in two publications, one research article on these new materials[6] and a mini-review on this emerging topic.[7] Not being a core element of our original project, this topic has since established funding from the National Science Foundation, where we continue to make pioneering discoveries.

References

1. R. A. Dodson, J. Park, J. Kim, M. J. Cliffe and S, M. Cohen, *Tethering Effects in Oligomer-Based Metal−Organic Frameworks*, Inorg. Chem. **61**, 12284−12292 (2022).
2. H. Kim and S. M. Cohen, *Metal−Organic Frameworks Constructed from Branched Oligomers*, Inorg. Chem. **63**, 1853-1857 (2024).
3. K. Barcus, P.-A. Lin, Y. Zhou, G. Arya and S. M. Cohen, *Influence of Polymer Characteristics on the Self-Assembly of Polymer-Grafted Metal−Organic Framework Particles*, ACS Nano **16**, 18168-18177 (2022).
4. M. Kang and S. M. Cohen, *Synthesis and Characterization of Self-Assembled Metal-Organic Framework Monolayers using Polymer-coated Particles*, JoVE, e66497 (2024).
5. A. Wang, K. Barcus, and S. M. Cohen, *Quantifying Ligand Binding to the Surface of Metal−Organic Frameworks*, J. Am. Chem. Soc. **145**, 16821−16827 (2023).
6. R. E. Sikma, K. P. Balto, J. S. Figueroa and S. M. Cohen, *Metal–Organic Frameworks with Low-Valent Metal Nodes*, Angew. Chem. Int. Ed. **61**, e202206353 (2022).
7. R. E. Sikma, K. P. Balto, J. S. Figueroa and S. M. Cohen, *Metal–Organic Frameworks with Low-Valent Metal Nodes*, Angew. Chem. Int. Ed. **61**, e202206353 (2022).

Publications

1. M. Kang and S. M. Cohen, *Synthesis and Characterization of Self-Assembled Metal-Organic Framework Monolayers using Polymer-coated Particles*, JoVE, e66497 (2024).

2. H. Kim and S. M. Cohen, *Metal−Organic Frameworks Constructed from Branched Oligomers*, Inorg. Chem. **63**, 1853-1857 (2024).

3. A. Wang, K. Barcus, and S. M. Cohen, *Quantifying Ligand Binding to the Surface of Metal−Organic Frameworks*, J. Am. Chem. Soc. **145**, 16821−16827 (2023).

4. R. E. Sikma, K. P. Balto, J. S. Figueroa and S. M. Cohen, *Metal–Organic Frameworks with Low-Valent Metal Nodes*, Angew. Chem. Int. Ed. **61**, e202206353 (2022).

5. R. E. Sikma and S. M. Cohen, *Metal–Organic Frameworks with Zero and Low-Valent Metal Nodes Connected by Tetratopic Phosphine Ligands*, Angew. Chem. Int. Ed. **61**, e202115454 (2022).

6. D. J. Lee, X. Yu, R. E. Sikma, M. Li, S. M. Cohen, G. Cai and Z, Chen, *Holistic Design Consideration of Metal−Organic Framework-Based Composite Membranes for Lithium−Sulfur Batteries*, ACS Appl. Mater. Interfaces **14**, 34742-34749 (2022).

7. K. Barcus, P.-A. Lin, Y. Zhou, G. Arya and S. M. Cohen, *Influence of Polymer Characteristics on the Self-Assembly of Polymer-Grafted Metal−Organic Framework Particles*, ACS Nano **16**, 18168-18177 (2022).

8. J. Zhu, L. Samperisi, M. Kalaj, J. A. Chiong, J. B. Bailey, Z. Zhang, C.-J. Yu, R. E. Sikma, X. Zou, S. M. Cohen, Z. Huang and F. A. Tezcan, *Metal-hydrogen-pi-bonded organic frameworks*, Dalton Trans. **51**, 1927-1935 (2022).

9. R. A. Dodson, J. Park, J. Kim, M. J. Cliffe and S, M. Cohen, *Tethering Effects in Oligomer-Based Metal−Organic Frameworks*, Inorg. Chem. **61**, 12284−12292 (2022).

Two-Dimensional Chalcogenide Nanomaterials

Yi Cui[1,2], Harold Hwang[1,3], Xueli Zheng[1]

[1]Stanford Institute for Materials and Energy Sciences, SLAC National Accelerator Laboratory, Menlo Park, CA 94025, USA.
[2]Department of Materials Science and Engineering, Stanford University, Stanford, CA 94305, USA.
[3]Department of Applied Physics, Stanford University, Stanford, CA 94305, USA.

Keywords: materials synthesis, materials functionality, materials transformation, twisted epitaxial, three-dimensional superlattice.

Research Scope

Our research emphasizes the design, synthesis, and manipulation of novel heterogeneous two-dimensional (2D) nanomaterials through chemical, electrochemical, and physical methods. Our overarching perspective is that materials synthesis, materials functionality, and materials transformation are fundamentally different on the nanoscale and deeply intertwined. We seek to utilize the structures and properties of novel 2D nanomaterials for new heterogeneous materials synthesis, to create and understand new phenomena arising from the interplay between the heterogeneous materials environment and external stimuli. Herein, we build on our previous joint work and established synergies between Cui, Hwang, and Zheng to discover and rationally control novel 2D nanomaterials, which form a solid foundation for a wide range of applications in novel electronics, photonics, and energy applications. Our research represents an exciting class of 2D nanomaterials and their manipulation, using nanoscale materials chemistry to create heterogeneous 2D systems, which greatly impacts a wide range of DOE BES priorities for materials design and control.

Recent Progress

The quest for materials understanding and control has long propelled scientists to try to tailor new materials with novel functionalities[1]. The advent of two-dimensional (2D) nanomaterials has brought new vigor and vitality into this field, presenting a fascinating platform using exfoliable and re-stackable layered structures[2,3]. Simply by continued exploration utilizing these physical attributes, surprising new developments continue to emerge, such as Moiré superconductors and 2D magnets[4-7]. Building on our extensive collaborations between Cui, Harold, and Zheng, we have achieved significant breakthroughs in 2D materials synthesis, functionality, and their transformations.

Specifically, we synthesized novel heterogenous 2D nanomaterials via intercalations, including engineering intercalation-based interlayers to achieve three-dimensional superlattice and two-dimensional monolayer van der Waals magnets. We report a strategy of interlayer engineering of the magnetic van der Waals crystal Fe_3GeTe_2 by intercalating quaternary ammonium cations into

the van der Waals spacing (**Figure 1a**). Both three-dimensional (3D) van der Waals superlattice and 2D van der Waals monolayer can be formed by using this method based on the amount of intercalant.

To synthesize new atomically thin materials, we utilize the confinement of atoms and molecules inside the van der Waals gaps in layered 2D materials. Ultrathin gold nanodiscs are successfully synthesized by utilizing the epitaxy between two molybdenum disulfide (MoS_2) layers (**Figure 1b**). We expanded the concept of epitaxy to a new regime of "twisted epitaxy" by growing nanometer thick gold (Au) nanodiscs between two MoS_2 substrates with varying mutual crystal orientations. In the twisted epitaxy regime, both MoS_2 substrate layers interact with intermediate Au nanoparticles in an appreciable way and influence their crystallographic orientation and registry. Four-dimensional scanning transmission electron microscopy analysis further reveals a periodic strain variation (<|±0.5%|) in the Au nanodisks associated with the twisted epitaxy, consistent with the Moiré registry of the two MoS_2 twisted layers.

In addition, we studied the response of heterogeneous 2D nanomaterials to external stimuli, such as thermal, light, and strain. Our work on exploring structure changes of 2D hydrogen substituted graphdiyne (HGDY) after thermal stimuli. We investigated the structural changes and their application for HGDY, an emerging 2D carbon-rich material with unique sp/sp^2 carbon atoms after thermal stimuli (**Figure 1c**). Specifically, we developed HGDY as the nanoreactor to synthesize metastable nanomaterials. Here, we developed an ultrafast high-temperature platform with the help of HGDY aerogel. 2D HGDY, sp/sp^2 co-hybridized carbon network, provides high-density sites for supporting metastable nanomaterials. We designed a hydrogen substituted graphdiyne assisted ultra-fast sparking synthesis platform for synthesizing metastable nanomaterials. Our findings are of interest in materials chemistry, low-dimensional carbon materials, high-temperature materials synthesis and processing, batteries, energy science, and systems.

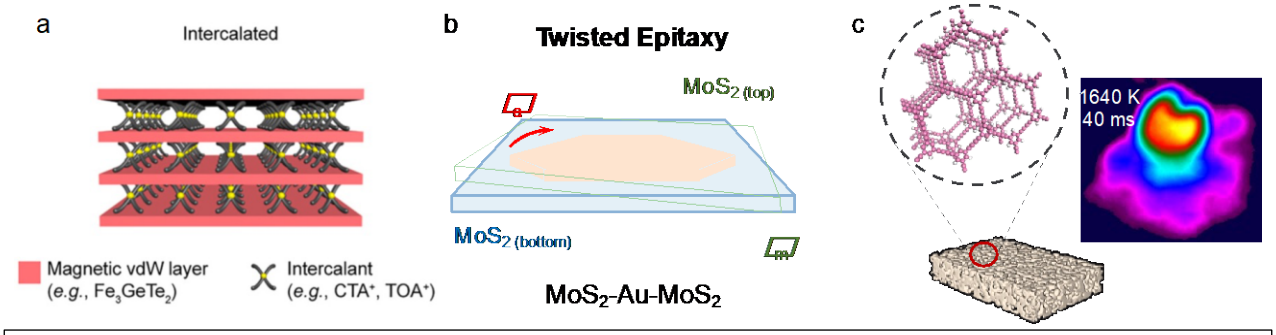

Figure 4. Highlighted recent progress in our research. a, van der Waals magnetic superlattice constructed by intercalation. b, the twisted Au nanodisks encapsulated in the van der Waals spacing of the bilayer MoS_2. θ_m notes the arbitrary rotation angle of the top MoS_2 relative to the bottom one. θ_a notes the twist angle of Au relative to the bottom MoS_2. c, 2D hydrogen substituted graphdiyne after thermal stimuli.

References

1. Nonoselov, K.S., Mishchenko, A., Carvalho, A. & Neto, A.H.C. 2D materials and van der Waals heterostructures. *Science* **353**, aac9439 (2016).
2. Manzeli, S., Ovchinnikov, D., Pasquier, D., Yazyev, O.V. & Kis, A. 2D transition metal dichalcogenides. *Nat. Rev. Mater.* **2**, 17033 (2017).
3. Novoselov, K.S. et al. Two-dimensional atomic crystals. *Proc. Natl. Acad. Sci. U.S.A.***102**, 10451-10453 (2005).
4. Cao, Y. et al. Unconventional superconductivity in magic-angle graphene superlattices. *Nature* **556**, 43-50 (2018).
5. Cao, Y. et al. Correlated insulator behavior at half-filling in magic-angle graphene superlattices. *Nature* **556**, 80-84 (2018).
6. Andrei, E.Y. & MacDonald, A.H. Graphene bilayers with a twist. *Nat. Mater.* **19**, 1265-1275 (2020).
7. Serlin, M. et al. Intrinsic quantized anomalous Hall effect in a moire heterostructure. *Science* **367**, 900-903 (2020).

Publications

1. Y. Cui, J. Wang, Y. Li, Y. Wu, E. Been, Z. Zhang, J. Zhou, W. Zhang, H. Y. Hwang, R. Sinclair, Y. Cui, "Twisted epitaxy of gold nanodisks grown between twisted substrate layers of molybdenum disulfide," ***Science*** 383, 6679, 212-219 (2024).
2. Y. Wu, B. Y. Wang, Y. Yu, Y. Li, H. B. Ribeiro, J. Wang, R. Xu, Y. Liu, Y. Ye, J. Zhou, F. Ke, V. Harbola, T. F. Heinz, H. Y. Hwang, and Y. Cui "Interlayer engineering of Fe_3GeTe_2: From 3D superlattice to 2D monolayer," ***Proceedings of the National Academy of Sciences,*** **121**, 4 (2024).
3. X. Gao, X. Zheng, Y. Ye, H. K. Lee, P. Zhang, A. Cui, X. Xiao, Y. Yang, and Y. Cui, "Lithiophilic Hydrogen-Substituted Graphdiyne Aerogels with Ionically Conductive Channels for High-Performance Lithium Metal Batteries," ***Nano Letters*** 24, 10, 3044-3050 (2024).
4. Y. Wu, D. Li, C. L. Wu, H. Y. Hwang, and Y. Cui "Electrostatic gating and intercalation in 2D materials," ***Nature Reviews Materials*** 8, 41-53 (2023).
5. X. Zheng, X. Gao, R. A. Vilá R, Y. Jiang, J. Wang, R. Xu, R. Zhang, X. Xiao, P. Zhang, L. C. Greenburg, Y. Yang, H. L. Xin, X. L. Zheng, and Y. Cui, "Hydrogen-substituted graphdiyne-assisted ultrafast sparking synthesis of metastable nanomaterials. ***Nature Nanotechnology*** 18, 153-159 (2023).
6. W. J. Kim, M. A. Smeaton, C. Jia, B. H. Goodge, B.-G. Cho, K. Lee, M. Osada, D. Jost, A. V. Ievlev, B. Moritz, L. F. Kourkoutis, T. P. Devereaux, and H. Y. Hwang, "Geometric Frustration of Jahn-Teller Order in the Infinite-Layer Lattice," ***Nature*** 615, 237-243 (2023).
7. T. Wu, B. Liu, C. Liu, J. Wan, A. Yang, K. Liu, F. Shi, J. Zhao, Z, Lu, G. Cheng, A. Pei, H. Y. Hwang, and Y. Cui "Solar-driven efficient heterogeneous subminute water disinfection nanosystem assembled with fingerprint MoS_2," ***Nature Water*** 1, 462-470 (2023).
8. L. C. Greenburg, X. Gao, P. Zhang, X. Zheng, J. Wang, R. A. Vilá, and Y. Cui, "Ni anchored to hydrogen-substituted graphdiyne for lithium sulfide cathodes in lithium-sulfur batteries". ***Nano Letters*** 23, 13, 5967-5974 (2023).
9. Y. Wu, J. Wang, Y. Li, J. Zhou, B. Y. Wang, A. Yang, L.-W. Wang, H. Y. Hwang, and Y. Cui, "Observation of an intermediate state during lithium intercalation of twisted bilayer MoS_2," ***Nature Communications*** 13, 3008 (2022).
10. J. Zhou, Y. Wu, H. Kwon, Y. Li, X. Xiao, Y. Ye, Y. Ma, K. E. Goodson, H. Y. Hwang, and Y. Cui, "Heat Conductor–Insulator Transition in Electrochemically Controlled Hybrid Superlattices," ***Nano Letters*** 22, 5443-5450 (2022).

Thermodynamics, Electroosmosis, and Electrokinetic Energy Generation in Nanochannels Functionalized with Anionic and Cationic Polyelectrolyte Brushes in Presence of Multivalent Counterions

Siddhartha Das (Department of Mechanical Engineering, University of Maryland, Email: sidd@umd.edu**)**

Keywords: Polyelectrolyte brushes; nanochannels; multivalent counterions; electroosmosis; electrokinetic energy; machine learning

Research Scope

The overall scope of this project is to perform extensive atomistic molecular dynamics (MD) simulations [1-11] to understand the effect of multivalent counterions in the conformation and thermodynamics of anionic and cationic polyelectrolyte (PE) brushes and in electroosmotic transport and electrokinetic energy generation in nanochannels grafted with such PE brushes. This project scope is divided into five major objectives. The **first** and **second** objectives are to understand the effect of multivalent counterions in the behavior of brushes and brush-supported water molecules and counterions with the PE brushes being grafted to a single surface (1st objective) or the inner walls of a nanochannel (2nd objective). The **third** and **fourth** objectives are to study the electroosmotic (EOS) transport (third objective) and pressure-driven transport and electrokinetic energy generation (fourth objective) in multivalent-counterion-screened anionic and cationic PE brush grafted nanochannels. The **fifth and the final objective** is to conduct a continuum analysis to model the equilibrium behavior of such brushes and transport in brush-supported nanochannels and compare the findings with all-atom MD simulation results.

Recent Progress

First, we developed unsupervised clustering-based Machine Learning (ML) methods, which use all-atom MD simulation data, for understanding the water-water hydrogen bonding inside the different types of counterions (Na^+, Li^+, Ca^{2+}, and Y^{3+}) screened anionic (poly-acrylic acid or PAA) brush layer [12]. Water-water interactions are represented as distinct clusters [Figs. 1(a)]: as compared to the clusters representing the water-water HBs in the bulk, the edge of the clusters associated with the water-water HBs inside the brush layer gets shortened [Fig. 1(b)] [12]. Also, there is an increase in the water-water HB angle for water-water HBs inside the brush layer [12]. **Second**, our all-atom simulations of the cationic PMETAC [Poly(2-(methacryloyloxy)ethyl trimethylammonium chloride] brushes identify distinct water domains (or first hydration shells) around the $\{N(CH_3)_3\}^+$ and C=O functional groups, as well as around the Cl^- counterion [13]. For example, we identify there is apolar hydration around the $\{N(CH_3)_3\}^+$ group caused by the presence of the methyl groups, while the water molecules around the C=O functional group (due to the partial negative charge on the oxygen atom) demonstrate hydrophilic behavior [as reflected in the corresponding water dipole orientation [Fig. 1(c)] [13]. Furthermore, the Cl^- ion is found to be weakly attracted to the $\{N(CH_3)_3\}^+$ group due to the presence of an intervening water layer between these two species: as a consequence, Cl^- ion is found to have very large mobility inside the brush layer [Fig. 1(d)] [13]. **Third**, in a separate study, we showed that the extent of binding of different halide counterions on the PMETAX brushes vary as $I^- > Br^- > Cl^- > F^-$, i.e., in inverse order as the charge density of these counterions [as confirmed by the PMETA-X RDF or radial distribution function, $g(r)$; see Fig. 1(e)] [14]. Such binding pattern can be explained by noting that the I^- and Br^- ions behave as chaotropic ions (i.e., ions that disrupt the water structure and therefore makes it more favorable for the ions to be away from the water and bind

to the polymer chains), while the Cl^- and F^- ions behave as kosmotropic ions (and hence they prefer to remain in close association with water, thereby demonstrating less binding to the polymer chains) [14]. Also, the specific nature of binding dictates the corresponding water structure around these respective halide ions and the polymer functional group and the corresponding mobility of these ions inside the PMETAX brush layer [14]. **Fourth**, as a separate study, we developed a new Machine Learning method (combining Gaussian fitting based pre-processing of the all-atom MD simulation derived data and unsupervised clustering algorithm) to identify two separate hydration states (one with more structured water and another with less structured water) of the $\{N(CH_3)_3\}^+$ group of the Cl^--ion-screened PMETA brushes [Fig. 1(f)] [15]. We further demonstrate that an increase in the grafting density leads to the prevalence of the hydration state with less structured water molecules [see Fig. 1(g)] [15]. **Finally**, we study the electroosmotic (EOS) transport in nanochannels grafted with PMETAC brushes and identify a massively non-linear increase in the flow strength with applied electric field (2 fold-increase in electric leads to more than 3 fold-increase in the flow strength) caused by the corresponding electric-field-driven deformation of the PMETAC brushes [see Fig. 1(h)].

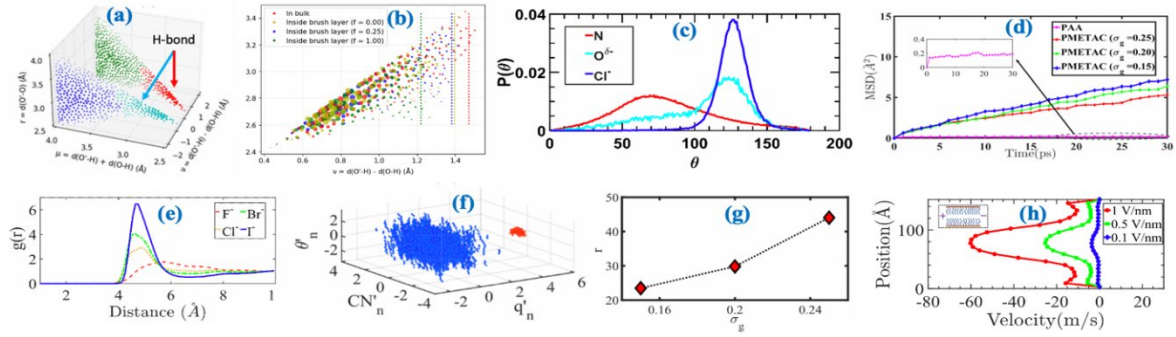

Figure 1. (a) Distribution of (v, μ, r) tupule in form of clusters for water inside the PAA brush layer (with charge fraction, *f*=1) obtained using unsupervised clustering algorithm. The clusters representing the HBs have been identified in (a). Here H, O and O' respectively represent the donor hydrogen, donor oxygen, and acceptor oxygen of any two water molecules forming hydrogen bond. Also, *d*(O'-H), *d*(O-H), and *d*(O-O') respectively represent the acceptor-oxygen-donor-hydrogen distance, donor-oxygen-donor-hydrogen distance, and donor-oxygen-acceptor-oxygen distance [12]. (**b**) Distribution of (v, r) for water in bulk and for water inside the PAA brush layer with *f*=0, *f*=0.25, and *f*=1. The dashed lines indicate the average location (in v) of the edge of hydrogen bond cluster for each of the four cases [12]. **(c)** Probability distribution of the orientation angle of the water dipole for the water in the three separate domains, namely water around the N atom [of the $\{N(CH_3)_3\}^+$ moiety], C=O group, and Cl^- ion of the PMETA-C brushes [13]. **(d)** MSD variation of the counterions inside the PMETAC brush layer (counterions are Cl^- ions) and the PAA brush layer (counterions are Na^+ ions). The results are shown for the PMETAC brush layer with three different grafting density values, while for the PAA brush layer the grafting is σ_g= 1.67 chains/nm^2 (i.e., a grafting density that enables a similar degree of confinement for the solvating water as the PMETAC brush layer with a grafting density of σ_g= 0.25 chains/nm^2). In the inset of **(d)**, the MSD plot for the Na^+ ions inside the PAA brush layer have been magnified [13]. **(e)** RDF of $\{N(CH_3)_3\}^+$-X (X= I^-, Br^-, Cl^-, and F^-) obtained using all-atom MD simulations of the PMETA-X brushes in presence of different halide counterions [14]. **(f)** Data clusters (grafting density, σ_g=0.25 chains/nm^3) obtained by employing the unsupervised ML algorithm on PMETA-C brushes identifying hydration state with more structured water (red cluster) and less structured water (blue cluster) [15]. **(g)** Variation of the ratio of points of the two clusters with σ_g [15]. **(h)** Variation of

References

1. H. S. Sachar, T. H. Pial, P. R. Desai, S. A. Etha, Y. Wang, P. W. Chung, and S. Das, *Densely Grafted Polyelectrolyte Brushes Trigger "Water-in-Salt" like Scenarios and Ultraconfinement Effect*, Matter, **2**, 1509-1521 (2020).
2. H. S. Sachar, T. H. Pial, B. S. Chava, and **S. Das**, *All-atom Molecular Dynamics Simulations of Weak Polyionic Brushes: Influence of Charge Density on the Properties of Polyelectrolyte Chains, Brush-Supported Counterions, and Water Molecules*, Soft Matter, **16**, 7808-7822 (2020).
3. H. S. Sachar, B. S. Chava, T. H. Pial, and S. Das, *All-Atom Molecular Dynamics Simulations of the Temperature Response of Densely Grafted Polyelectrolyte Brushes*, Macromolecules, **54**, 6342-6354 (2021).
4. H. S. Sachar, B. S. Chava, T. H. Pial, and S. Das, *Hydrogen Bonding and its Effect on the Orientational Dynamics of Water Molecules inside Polyelectrolyte Brush-Induced Soft and Active Nanoconfinement*, Macromolecules, **54**, 2011-2021 (2021).
5. H. S. Sachar, T. H. Pial, V. S. Sivasankar, and S. Das, *Simultaneous Energy Generation and Flow Enhancement (Electroslippage Effect) in Polyelectrolyte Brush Functionalized Nanochannels*, ACS Nano, **15**, 17337-17347 (2021).
6. T. H. Pial, H. S. Sachar, and **S. Das**, *Quantification of Mono- and Multivalent Counterion-mediated Bridging in Polyelectrolyte Brushes*, Macromolecules, **54**, 4154-4163 (2021).
7. T. H. Pial, M. Prajapati, B. S. Chava, H. S. Sachar, and **S. Das**, *Charge-Density-Specific Response of Grafted Polyelectrolytes to Electric Fields: Bending or Tilting?* Macromolecules, **55**, 2413-2423 (2022).
8. T. H. Pial and S. Das, *Specific Ion and Electric Field Controlled Diverse Ion Distributions and Electroosmotic Transport in a Polyelectrolyte Brush Grafted Nanochannel*, The Journal of Physical Chemistry B, **126**, 10543-10553 (2022).
9. T. H. Pial, H. S. Sachar, P. R. Desai, and S. Das, *Overscreening, Coion-Dominated Electroosmosis, and Electric Field Strength Mediated Flow Reversal in Polyelectrolyte Brush Functionalized Nanochannels*, ACS Nano, **15**, 6507-6516 (2021).
10. T. H. Pial and S. Das, *Machine Learning Enabled Quantification of the Hydrogen Bonds Inside the Polyelectrolyte Brush Layer Probed Using All-Atom Molecular Dynamics Simulations*, Soft Matter, **18**, 8945-8951 (2022).
11. R. Ishraaq and S. Das, All-atom Molecular Dynamics Simulations of Polymer and Polyelectrolyte Brushes, *Chemical Communications*, **60**, 6093-6129 (2024).
12. A. Bera, T. S. Akash, R. Ishraaq, T. H. Pial, and S. Das, *Hydrogen Bonding Inside Anionic Polymeric Brush Layer: Machine Learning-Driven Exploration of the Relative Roles of the Polymer Steric Effect, Charging, and Type of Screening Counterions*, Macromolecules, **57**, 1581-1592 (2024).
13. R. Ishraaq, T. S. Akash, A. Bera, and S. Das, *Hydrophilic and Apolar Hydration in Densely Grafted Cationic Brushes and Counterions with Large Mobilities*, The Journal of Physical Chemistry B, **128**, 381-392 (2024).
14. R. Ishraaq and S. Das, *All-Atom Molecular Dynamics Simulations of Cationic Polyelectrolyte Brushes in the Presence of Halide Counterions*, Macromolecules, **57**, 3037-3046 (2024).
15. R. Ishraaq, T. S. Akash, and S. Das, *Combined Machine Learning and Molecular Dynamics Reveal Two States of Hydration of a Single Functional Group of Cationic Polymeric Brushes*, Macromolecules, **57**, 5300-5312 (2024).

Publications (in the past 2 years from the work supported by this BES funding)

1. T. H. Pial, M. Prajapati, B. S. Chava, H. S. Sachar, and **S. Das**, *Charge-Density-Specific Response of Grafted Polyelectrolytes to Electric Fields: Bending or Tilting?* Macromolecules, **55**, 2413-2423 (2022).
2. T. H. Pial and S. Das, *Specific Ion and Electric Field Controlled Diverse Ion Distributions and Electroosmotic Transport in a Polyelectrolyte Brush Grafted Nanochannel*, The Journal of Physical Chemistry B, **126**, 10543-10553 (2022).
3. T. H. Pial and S. Das, *Machine Learning Enabled Quantification of the Hydrogen Bonds Inside the Polyelectrolyte Brush Layer Probed Using All-Atom Molecular Dynamics Simulations*, Soft Matter, **18**, 8945-8951 (2022).
4. A. Bera, T. S. Akash, R. Ishraaq, T. H. Pial, and S. Das, *Hydrogen Bonding Inside Anionic Polymeric Brush Layer: Machine Learning-Driven Exploration of the Relative Roles of the Polymer Steric Effect, Charging, and Type of Screening Counterions*, Macromolecules, **57**, 1581-1592 (2024).
5. R. Ishraaq, T. S. Akash, A. Bera, and S. Das, *Hydrophilic and Apolar Hydration in Densely Grafted Cationic Brushes and Counterions with Large Mobilities*, The Journal of Physical Chemistry B, **128**, 381-392 (2024).
6. R. Ishraaq and S. Das, *All-Atom Molecular Dynamics Simulations of Cationic Polyelectrolyte Brushes in the Presence of Halide Counterions*, Macromolecules, **57**, 3037-3046 (2024).
7. R. Ishraaq, T. S. Akash, and S. Das, *Combined Machine Learning and Molecular Dynamics Reveal Two States of Hydration of a Single Functional Group of Cationic Polymeric Brushes*, Macromolecules, **57**, 5300-5312 (2024).
8. R. Ishraaq and S. Das, All-atom Molecular Dynamics Simulations of Polymer and Polyelectrolyte Brushes, *Chemical Communications*, **60**, 6093-6129 (2024).

Molecular and Network Design of Liquid Crystal Elastomer Elastocalorics

PI: Emily C. Davidson (Princeton University)

Keywords: liquid crystal elastomer, liquid crystalline oligomer, elastocaloric effect, supramolecular assembly, crosslinking

Research Scope

Liquid crystal elastomers (LCEs) exhibit a change in structural order in response to external stimuli, with applications ranging from soft robotics to elastocaloric devices. The elastocaloric effect, in which heat is released in response to applied strain and absorbed upon strain relaxation, is of interest for sustainable cooling technologies. Although the elastocaloric effect occurs in shape memory alloys[1] and non-liquid crystalline elastomers,[2,3] LCEs are promising because they undergo a mechanotropic transition between the isotropic and nematic phase, coupling latent heat to mechanical stimulus. However, currently developed LCEs require a large strain ($\lambda = 2$) for a relatively small temperature change ($\Delta T = 3°C$),[4] which is attributed to phase transition broadening arising from internal stress fields[5] and network heterogeneity[6,7] created during crosslinking. To address this limitation, we aim to direct LCE network structure by two design tiers—precise oligomer synthesis and controlled crosslinking—and investigate the relationship between LCE network structure and elastocaloric performance.

Recent Progress

To overcome the inherent dispersity associated with conventional step-growth polymerization, we have leveraged an iterative exponential growth (IEG) strategy[8,9] to synthesize monodisperse oligomers (**Fig 1a**). Our system relies on mesogenic units with orthogonally (de)protectable end groups and a selective copper-mediated alkyne-azide coupling mechanism. Additionally, this method grants sequence control, which we have demonstrated through sequence-defined incorporation of two mesogens (one with a phenyl benzoate core, one modified with a methyl substituent). Through this strategy, we demonstrate the ability to obtain long LC oligomers of low dispersity, which is expected to diminish dispersity-driven heterogeneities in LCEs.

Although oligomers containing the non-methylated core exhibit metastable nematic phases at high cooling rates, crystalline order is thermodynamically preferred. Non-methylated homooligomers exhibit mesogen-mesogen packing with crystalline order, and their correlations on the oligomer lengthscale and hierarchical structures depend on mesogen number. Additionally, heterodimers of alternating sequence pack into nanocylinders which assemble into supramolecular chiral structures with distinct long-range order.

To overcome the limited nematic stability of these oligomers, we have observed long-lived nematic phases in the methylated homooligomers. Additionally, random copolymerization of the methylated mesogen with a flexible carbon spacer suppresses crystallization, compared to either the methylated homopolymer and a polymer incorporating the flexible spacer in a regular sequence (**Fig 1b**). Thus, we have demonstrated two strategies to enhance nematic stability, which we anticipate to persist after network formation. Toward LCEs based on this platform, we are developing the synthesis of tetrafunctional macromers from monodisperse oligomers with asymmetric end groups, using radical-mediated thiol-yne reactions and Sonogashira coupling. These macromers will be leveraged as the precursors to controlled LCE networks. These controlled networks will enable us to elucidate the relationship between network structure and phase transition broadening, allowing us to tailor LCE synthesis for improved elastocaloric performance.

In addition, to design LCEs through controlled crosslinking, we have investigated conventional LCEs. To elucidate how crosslinker concentration (a defect to the nematic order) impacts mechanical crosslinking and the nematic-to-isotropic transition temperature (T_{NI}) in conventional LCEs, we leveraged in situ UV-rheology to monitor network formation. As crosslinker concentration increases, the final storage modulus and T_{NI} increase until the stoichiometric ratio, beyond which both decrease as chain extension becomes more prevalent and the crosslinker acts as a diluent (**Fig 1c**).

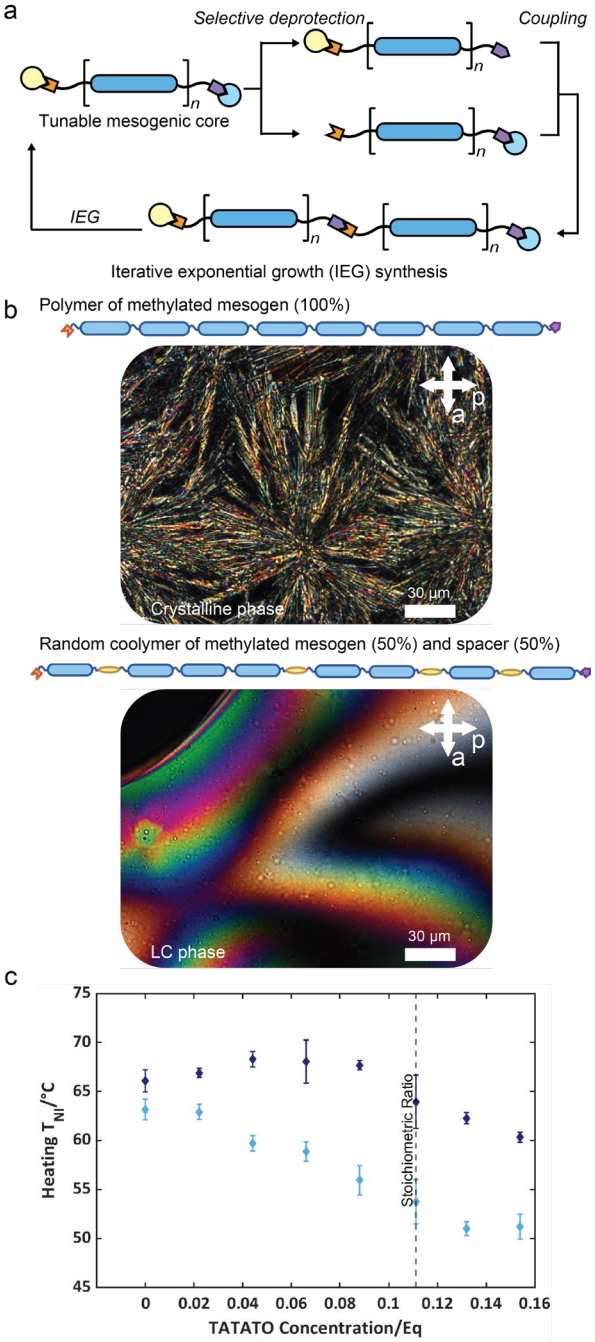

Figure 1. **a**) Iterative exponential growth synthesis scheme. **b**) Polarized optical micrographs of crystalline methylated polymer and liquid crystalline random copolymer of methylated mesogen (blue unit) with flexible spacer (yellow unit). **c**) Change in T_{NI} with TATATO crosslinker concentration in conventional LCEs.

References

1. E. Bonnot, R. Romero, L. Mañosa, E. Vives, and A. Planes, *Elastocaloric Effect Associated with the Martensitic Transition in Shape-Memory Alloys*, Physical Review Letters **100 (12)**, 125901 (2008).
2. C. M. Hartquist, S. Lin, J. H. Zhang, S. Wang, M. Rubinstein, and X. Zhao, *An Elastomer with Ultrahigh Strain-Induced Crystallization*, Science Advances **9 (50)**, eadj0411 (2023).
3. Z. Xie, G. Sebald, and D. Guyomar. *Comparison of Direct and Indirect Measurement of the Elastocaloric Effect in Natural Rubber*, Applied Physics Letters **108 (4)**, 041901 (2016).
4. J. A. Koch, J. A. Herman, and T. J. White, *Elastocaloric Effect in Amorphous Polymer Networks Undergoing Mechanotropic Phase Transitions*, Physical Review Materials **5 (6)**, L062401 (2021).
5. G. Cordoyiannis, A. Lebar, B. Zalar, S. Žumer, H. Finkelmann, and Z. Kutnjak. *Criticality Controlled by Cross-Linking Density in Liquid Single-Crystal Elastomers*, Physical Review Letters **99 (19)**, 197801 (2007).
6. L. Petridis and E. M. Terentjev, *Nematic-Isotropic Transition with Quenched Disorder*, Physical Review E **74 (5)**, 051707 (2006).
7. J. V. Selinger and B. R. Ratna, *Isotropic-Nematic Transition in Liquid-Crystalline Elastomers: Lattice Model with Quenched Disorder*, Physical Review E **70 (4)**, 041707 (2004).
8. J. C. Barnes, D. J. C. Ehrlich, A. X. Gao, F. A. Leibfarth, Y. Jiang, E. Zhou, T. F. Jamison, and J. A. Johnson, *Iterative Exponential Growth of Stereo- and Sequence-Controlled Polymers*, Nature Chemistry **7 (10)**, 810-815 (2015).
9. V. Percec and A. D. Asandei, *Monodisperse Linear Liquid Crystalline Polyethers via a Repetitive 2n Geometric Growth Algorithm*, Macromolecules **30 (25)**, 7701-7720 (1997).

A synergistic computational and experimental approach for unprecedented III-V and II-VI clathrates

Davide Donadio, University of California Davis; Kirill Kovnir, Iowa State University

Keywords: Intermetallic Clathrates, Density Functional Theory, Machine Learning, Materials Discovery

Research Scope

Clathrates are crystal structures that consist of nanometer-size polyhedral cages encapsulating guest atoms or molecules that are not directionally bonded to the framework. These materials have a high potential for energy storage and energy conversion technologies, including batteries and thermoelectrics. In years two and three of this project, the overarching goal has been to further the prediction, synthesis, and characterization of new unconventional inorganic clathrates, exploring the chemical space of transition-metal-stabilized III-V and II-VI clathrates, encapsulating alkali and alkaline-earth elements as guest ions. The discovery of new intermetallic clathrates relies on high-throughput screening by density functional theory and machine learning approaches, which guided synthesis with *in situ* X-ray diffraction characterization. The newly discovered materials undergo an extensive characterization of their electronic and thermal transport properties leveraging both experimental methods and DFT calculations.

Recent Progress

The principles of Zintl electron counting [1] and analogy to other recently discovered materials guided us to the discovery of two "hidden" pseudo clathrates ($Ba_2Zn_5As_6$ and $Ba_2Zn_5Sb_6$) that can be synthesized in a relatively narrow temperature range [2]. This discovery prompted us to explore more systematically the chemical space of intermetallics in search of new intercalation compounds. In this project, we have furthered the development of fast and accurate computational tools to perform such a systematic search of stable ternary and quaternary intercalation compounds. Even assuming a given crystal structure, e.g. type-I clathrate, and knowing that alkali or alkali-earth metals would be incorporated as guests, the chemical decoration of the clathrate framework is usually not known, and its determination is a large-size combinatorial problem that cannot be undertaken with brute-force DFT calculations. We have discovered that machine learning models based on graph neural networks, such as MEGNet and M3GNet [3,4], give the correct energy ordering for different chemical decorations of given compounds. Hence, we have integrated GNN models with a site permutation search with simulated annealing (SPS-SA) Monte Carlo algorithm that allows us to discover the optimal atomic decoration on

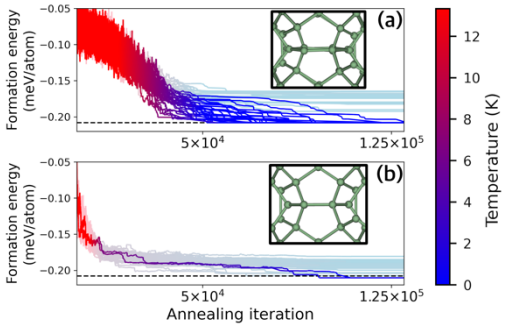

Figure 1. Application of the Site-Permutation Switch with Simulated Annealing algorithm to the superstructural ordering of the $Rb_8Ga_{27}Sb_{19}$ clathrate.

fixed crystalline geometries [5]. This algorithm successfully reproduces the observed superstructural ordering of $A_8T_{27}Pn_{19}$ clathrates [6]. GNN with SPS-SA was applied to compute the energetic stability of chalcogenide clathrates stabilized by noble metals. The electron exact composition with alkaline (A) guests is $A_8M_{4x}E_{25-5x}Ch_{21+x}$. The stability map (Figure 2) allowed us to identify potentially stable compositions, such as $Cs_8Ag_8Hg_{15}S_{23}$ for which synthesis was attempted. Synthesis resulted in the discovery of new compounds with a close to predicted type-I clathrate composition $CsAgHg_3S_4 \approx Cs_6Ag_6Hg_{18}S_{24}$ (Figure 2 right). As opposed to clathrates, where guests are encapsulated in cages, the covalent framework is rearranged such that large 1D channels are filled with Cs atoms.

Based on these predictions, we have also synthesized three polyanionic tellurides, $ABa_6Cu_{31}Te_{22}$ (A = K, Rb, Cs). These are almost charge-balanced compounds that crystallize in a complex structure with a large unit cell (5500 A^3) and extremely low thermal conductivity. These crystals exhibit partial occupancy Cu sites, which can be accounted for in atomistic models by introducing vacancies with the SPS-SA algorithm. We performed a theoretical electronic structure characterization of this system and a full thermoelectric investigation. The ultralow thermal conductivity of $RbBa_6Cu_{31}Te_{22}$ ($k<0.7$ $Wm^{-1}K^{-1}$) across the whole temperature range from 0 to 600 K and favorable electronic properties make these materials very promising thermoelectrics, with an intrinsic $zT \sim 0.2$ that may be improved by doping or defect engineering.

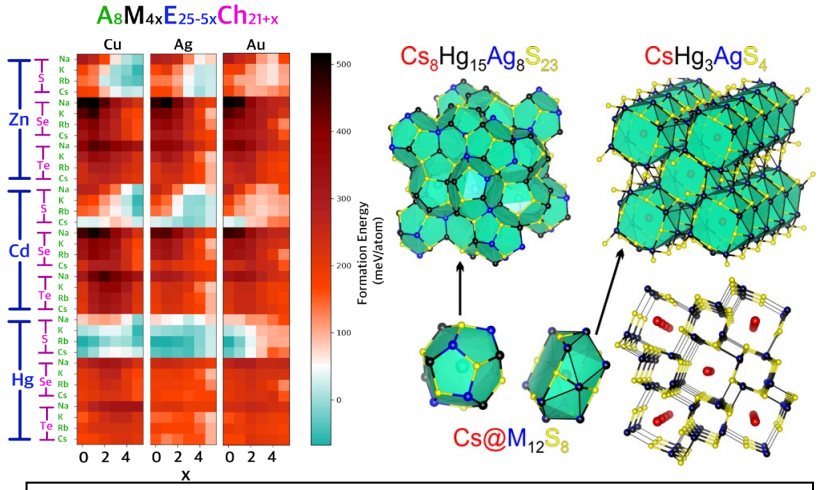

Figure 2. Stability map of the $A_8M_{4x}E_{25-5x}Ch_{21+x}$ family of chalcogenide clathrates (left), predicted clathrate composition, synthesized sodalite-like crystal with a similar stoichiometry.

Finally, we have studied the ordered and disordered phases of $Ba_8Cu_{16}As_{30}$. In situ temperature-dependent powder X-ray diffraction experiments guided synthetic efforts toward the synthesis of the ordered monoclinic and disordered cubic polymorphs with high phase purity. Combined theoretical predictions and experimental observations of both polymorphs reveal that ordering simultaneously enhances the Seebeck coefficient and electronic conductivity by increasing the hole effective mass and reducing scattering, overall enhancing the zT of the ordered phase.

References

1. R. Nesper, *The Zintl-Klemm Concept – A Historical Survey*, Zeitschrift Für Anorganische Und Allgemeine Chemie **640**, 2639 (2014).

2. P. Yox, F. Cerasoli, A. Sarkar, V. Kyveryga, G. Viswanathan, D. Donadio, and K. Kovnir, *New Trick for an Old Dog: From Prediction to Properties of "Hidden Clathrates" Ba2Zn5As6 and Ba2Zn5Sb6*, J. Am. Chem. Soc. **145**, 4638 (2023).

3. C. Chen, W. Ye, Y. Zuo, C. Zheng, and S. P. Ong, *Graph Networks as a Universal Machine Learning Framework for Molecules and Crystals*, Chem. Mater. **31**, 3564 (2019).

4. C. Chen and S. P. Ong, *A Universal Graph Deep Learning Interatomic Potential for the Periodic Table*, Nat Comput Sci **2**, 11 (2022).

5. F. Cerasoli and D. Donadio, *Effective Optimization of Atomic Decoration in Giant and Superstructurally Ordered Crystals with Machine Learning*, J. Chem. Phys. (2024).

6. B. Owens-Baird, J. Wang, S. G. Wang, Y.-S. Chen, S. Lee, D. Donadio, and K. Kovnir, *III–V Clathrate Semiconductors with Outstanding Hole Mobility: Cs $_8$ In $_{27}$ Sb $_{19}$ and* A $_8$ *Ga* $_{27}$ *Sb* $_{19}$ *(* A *= Cs, Rb)*, J. Am. Chem. Soc. **142**, 2031 (2020).

Publications

1. F.T. Cerasoli and D. Donadio, *Effective Optimization of Atomic Decoration in Giant and Superstructurally Ordered Crystals with Machine Learning*, J. Chem. Phys. *in press* (2024).
2. A. Sarkar, F.T. Cerasoli, G. Viswanathan, D. Donadio, and K. Kovnir, *ABa6Cu31Te22 (A = K, Rb, Cs) Featuring Polyanionic Copper−Telluride Frameworks with Ultralow Thermal Conductivity,* ACS Appl. Mater. Interf. *in press* (2024)
3. P. Yox, F. T. Cerasoli, A. Sarkar, G. Amobi, G. Viswanathan, J. Voyles, O. l. Lebedev, D. Donadio, and K. Kovnir, *Organizing Chaos: Boosting Thermoelectric Properties by Ordering the Clathrate Framework of Ba8Cu16As30*, Chem. Mater. **36**, 3925(2024).
4. P. Yox, G. Viswanathan, A. Sarkar, J. Wang, and K. Kovnir, *4.03 - Thermoelectric Materials*, in *Comprehensive Inorganic Chemistry III (Third Edition)*, edited by J. Reedijk and K. R. Poeppelmeier (Elsevier, Oxford, 2023), pp. 45–79.
5. P. Yox, F. Cerasoli, A. Sarkar, V. Kyveryga, G. Viswanathan, D. Donadio, and K. Kovnir, *New Trick for an Old Dog: From Prediction to Properties of "Hidden Clathrates" Ba2Zn5As6 and Ba2Zn5Sb6*, J. Am. Chem. Soc. **145**, 4638 (2023).
6. V. Pecunia et al., *Roadmap on Energy Harvesting Materials*, J. Phys. Mater. **6**, 042501 (2023).
7. J. Jeong, D. Shim, P. Yox, M.-H. Choi, K. M. Ok, K. Kovnir, G. J. Miller, and T.-S. You, *Tuning the Radius Ratio to Enhance Thermoelectric Properties in the Zintl Compounds AM2Sb2 (A = Ba, Sr; M = Zn, Cd)*, Chem. Mater. **35**, 3985 (2023).

Molecular Mo Sulfide Clusters for H_2-Evolution: Surface Immobilization and Water Solubility, Composition-Function Relationships, and Probes of Mechanism

James P. Donahue, Russell H. Schmehl and Alex McSkimming, Department of Chemistry, Tulane University, 6400 Freret Street, New Orleans, LA 70118

Keywords: H_2-evolution, Mo-sulfide clusters, H_2O solubility, composition-function relationships

Research Scope

The primary thrust in this research project is the establishment of composition-H_2 evolving activity correlations in well-defined, atomically precise $[M_3X_7L_3]^+$ clusters (X = chalcogen, L = monoanionic ligand), which serve as models for the metal dichalcogenide (MX_2) class of heterogeneous H_2-evolving catalysts.[1-5] Related objectives include *i*) a computational elucidation of the probable mechanistic pathway for H_2-evolution by $[M_3X_4L_3]^+$ clusters; *ii*) the isolation and characterization of species that are relevant as intermediates in the course of H_2 catalysis; *iii*) the establishment of key electrochemical parameters (*e.g.*, overpotential) in electrocatalytic H_2-evolution by $[M_3X_4L_3]^+$ clusters; *iv*) the development of phosphate-substituted dithiocarbamate ligands for H_2O-solubilization of the cluster catalysts and for immobilization onto metal oxides.

Recent Progress

We have synthesized the suite of triangular cations depicted in **Scheme 1** ([**3a**]$^+$, [**4a**]$^+$, [**5a**]$^+$, [**5b**]$^+$, [**3c**]$^+$, [**4c**]$^+$, [**5c**]$^+$, [**6**]$^+$) by applying and extending known protocols[6-8] and have thoroughly characterized them spectroscopically (NMR, UV-vis, Raman, MS), analytically, and structurally by X-ray crystallography. Under a common photolysis procedure and with a common I^- counteranion, we find overall H_2 turnover numbers rank as [**3a**]$^+$ > [**4a**]$^+$ ≈ [**6**]$^+$ > [**5a**]$^+$ ≈ [**5b**]$^+$ ≈ [**3c**]$^+$ ≈ [**4c**]$^+$ > [**5c**]$^+$. The most important aspect of composition is the $[Mo_3S_7]^{4+}$ core, which, at parity of supporting ligand, is appreciably more active than the corresponding compound with $[Mo_3Se_7]^{4+}$. With the same inorganic $[M_3X_7]^{4+}$ core, clusters having the ^{i}Bu$_2$NCS$_2^{1-}$ supporting ligand are more active for H_2 evolution than complexes with the ^{i}Bu$_2$PS$_2^{1-}$ ligand. At parity of chalcogen core composition and supporting ligand, the Mo_3 cluster is more active than the W_3 cluster. Additionally, counteranion identity plays an unanticipated role, with [**3a**]Cl > [**3a**]I. This observation is attributed to an

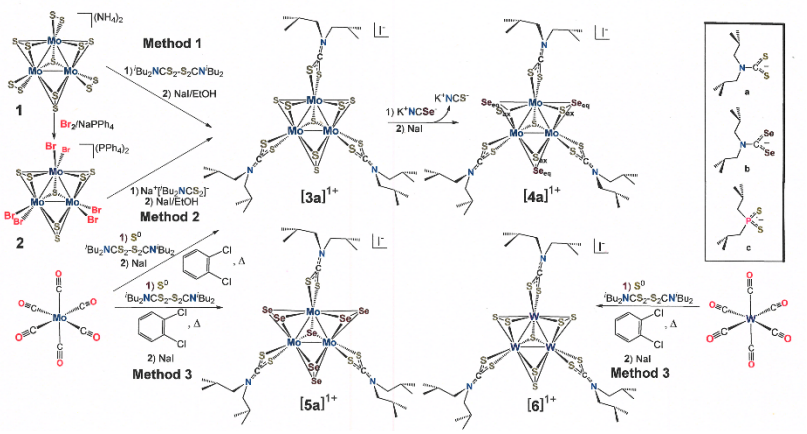

Scheme 1. Syntheses of cluster catalysts undertaken in this work. The supporting ligand is designated by the lowercase letter.

interfering effect of the I^- with some of the e^- transfer intermediaries in the course of photocatalysis. A report describing this work is in an advanced stage of writing.

We have observed that clusters of the formulation $[M_3X_4L_3]^+/[M_3X_4L_4]$ are also active HER catalysts and that they demonstrate immediate activity in contrast to the brief but distinctive incubation period for $[M_3X_7L_3]^+$ clusters that implies they are *pre*catalysts.[9] We have begun to explore possible mechanism(s) for the HER catalysis by these $[Mo_3S_4]^{4+}$ clusters computationally, and a draft mechanism based on these findings is shown in **Scheme 2**. As caveat, we have not, as of yet, located any transition states; consequently, these results are preliminary. Nevertheless, what is quite evident is that, following one electron reduction of the parent DMF adduct ((**a**) → (**b**)), protonation is projected to occur at a μ_2-sulfide, ***not*** Mo. Further one electron reduction and protonation are only *then* expected to yield a Mo hydride. Proton migration across the face of the molecule, which appears energetically reasonable, would then presumably occur to give the *cis*-Mo(H)(SH) arrangement necessary for H_2 evolution (bottom left). Calculations are currently underway to examine other potential pathways and, of course, locate transition states for this putative mechanism. As part of the effort to characterize, where possible, the intermediates in the cycle, we have structurally characterized $[^nBu_4N][Mo_3S_4(S_2CN^iBu_2)_4]$ ((**b**) in **Scheme 2**).

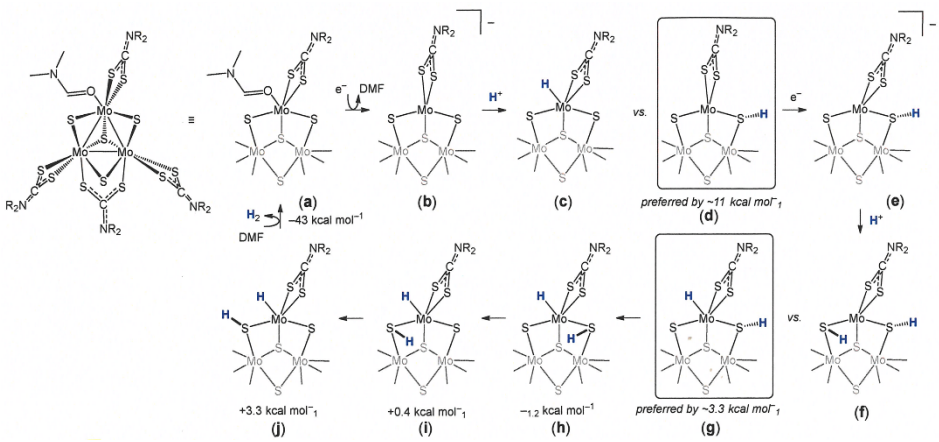

Scheme 2. A putative mechanism for catalyzed H_2 by $[Mo_3S_4]^{4+}$ clusters.

Incorporation of a phosphate/phosphonate group into a ligand design is a strategy to improve H_2O-solubility in a coordination complex. Toward that end, we have synthesized the new diethylphosphonate-substituted dithiocarbamate ligand illustrated in **Figure 1** in its protected disulfide form. Installment of this ligand onto the $[Mo_3S_7]^{4+}$ core results in a cluster that is freely H_2O soluble and is, under the standard photolysis system that we've implemented, our most active H_2-evolving system thus far with the M_3 clusters.

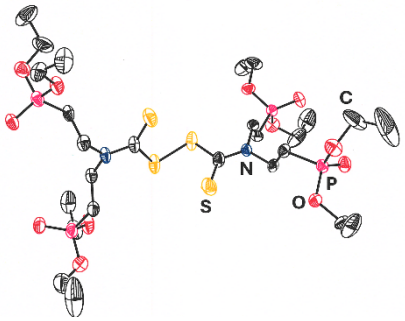

Figure 1. Crystal structure image (50% ellipsoids) of a H_2O-soluble dithiocarbamate ligand in its protected, disulfide form.

References

1. L. M. Maghrabi, N. Singh, K. Polychronopoulou, *A Mini-Review on the MXenes Capacity to Act as Electrocatalysts for the Hydrogen Evolution Reaction,* Int. J. Hydrogen Energ. **51**, 133-166 (2024).

2. S. Li, Z. Luo, S. Wang, H. Cheng, *Atomic Structure and HER Performance of Doped MoS_2: A Mini-Review,* Electrochem. Commun. **155**, 107563 (2023).

3. T. V. Nguyen, M. Tekalgne, T. P. Nguyen, Q. V. Le, S. H. Ahn, S. Y. Kim, *Electrocatalysts Based on MoS_2 and WS_2 for Hydrogen Evolution Reaction: An Overview,* Battery Energy **2**, 20220057 (2023).

4. H. Yu, M. Zhang, Y. Cai, Y. Zhuang, L. Wang, *The Advanced Progress of MoS_2 and WS_2 for Multi-Catalytic Hydrogen Evolution Reaction Systems,* Catalysts **13**, 1148 (2023).

5. V. Sharma, A. Kumar, P. Singh, P. K. Verma, T. Ahamad, S. Thakur, Q. V. Le, V.-H. Nguyen, A. A. P. Khan, P. Raizada, *Advanced Strategies for Modifying the Water Splitting Performance of $MoSe_2$ Photocatalyst: A Critical Review of Recent Progress*, J. Ind. Eng. Chem. **128**, 55-65 (2023).

6. H. Zimmermann, K. Hegetschweiler, T. Keller, V. Gramlich, H. W. Schmalle, W. Petter, W. Schneider, *Preparation of Complexes Containing the $[Mo_3S(S_2)_3]^{4+}$ Core and Structure of Tris-(diethyldithiocarbamato)tris(μ-disulfido)(μ_3-thio)-triangulotrimolybdenum(IV) Iodide,* Inorg. Chem. **30**, 4336−4341 (1991).

7. G. Borgs, H. Keck, W. Kuchen, D. Mootz, R. Wiskemann, H. Wunderlich, *Cubane Type Molybdenum-Halogen-Sulfur-Clusterdithiophosphinates,* Z. Naturforsch. B **46**, 1525-1531 (1991).

8. M. J. Almond, M. G. B. Drew, H. Redman, D. A. Rice, *A New Simple Synthetic Route to M_3Se_7 (M = Mo or W) Core Containing Complexes: Crystal Structure and Characterization of $[M_3\mu_3\text{-}Se)(\mu\text{-}Se_2)_3(dtc)_3]_2Se$*, Polyhedron **19**, 2127-2133 (2000).

9**.** P. R. Fontenot, B. Shan, B. Wang, S. Simpson, G. Ragunathan, A. F. Greene, A. Obanda, L. A. Hunt, N. I. Hammer, C. E. Webster, J. T. Mague, R. H. Schmehl, J. P. Donahue, *Photocataltyic H_2-Evolution by Homogeneous Molybdenum Clusters Supported by Dithiocarbamate Ligands,* Inorg. Chem. **58**, 16458-16474 (2019).

Publications

1. Ragunathan, G.; Mishra, S.; Mague, J. T.; Zhang, X.; Donahue, J. P. *Probing the Limits of Tetraalkylthiuram Disulfide Synthesis by Direct Reaction of Secondary Amines with CS_2: The Structures of $Cy_2NC(S)SSC(S)NCy_2$ and $Cy_2NC(S)SSSSC(S)NCy_2$.* Phosphorus, Sulfur Silicon Relat. Elem. Accepted (2024).

2 Fraker, A.; Donahue, J. P.; McSkimming, A. J. *Bis[tris(di-isobutyldithiocarbamato)-tris(μ_2-disulfido)-(μ_3-sulfido)-trimolybdnum(IV)]$_2$(μ_6-S) THF Solvate.* Acta Crystallogr., Sect. E. **E80**, 472-475 (2024). DOI: 10.1107/S2056989024006522.

Design Exciton and Spin Functionalities in Halide Perovskite Epitaxial Heterostructures

Letian Dou and Libai Huang; Purdue University

Keywords: Halide Perovskites, Heterostructures, Exciton transport, Ultrafast Microscopy

Research Scope

Two-dimensional (2D) organic-inorganic halide perovskites have emerged as an exciting new class of optoelectronic materials, supporting strongly bound excitons with large oscillator strength.[1-8] The large spin–orbit coupling endowed by the heavy elements such as Pb also leads to great potentials for future spintronic and spin-optoelectronic applications.[9-13] These unique properties have inspired substantial research efforts in exploring exciton and spin properties in these materials in recent years. Their unique properties along with highly programmable structures make them great candidates for constructing heterostructures to control the dynamics and transport of both the charge and spin degrees of freedom. However, the current synthesis and characterization methods both lack the necessary precision for controlling the interfaces and interactions, hindering the realization of a "materials-by-design" approach for heterostructures based on 2D halide perovskites.

To bridge this research gap, we plan to develop well-controlled and atomically precise halide perovskite epitaxial heterostructures as a material platform for long-range exciton and spin transport. We will design lateral and vertical heterostructures to form interfacial excitons with long lifetimes and many-body interactions favorable for long-range transport. Furthermore, lattice symmetry and interfacial strain will be tuned synthetically to suppress spin relaxation and to enhance spin transport. The active feedback between materials synthesis and ultrafast microscopy measurements will elucidate structure-property relationship to provide guidelines for designing perovskite heterostructures for optoelectronic and spintronic applications.

Recent Progress

Over the past year, we have carried out fundamental research on the synthesis and optical characterization of novel 2D halide perovskite and heterostructures.

In one of our recent works, we discovered a templating method that enables the growth of 2D perovskite nanowires and heterostructures that exhibit unique optical properties. While 2D perovskite has been widely studied, growth of 1D forms of these layered materials has been challenging. Notably, the structure of layered perovskites has inspired the use of bulky organic spacers with engineered intermolecular interactions. In this regard, we have found organic templating molecules that can break the in-plane symmetry of layered perovskites and induce 1D growth through secondary bonding interactions. Specifically, these molecules introduce in-plane

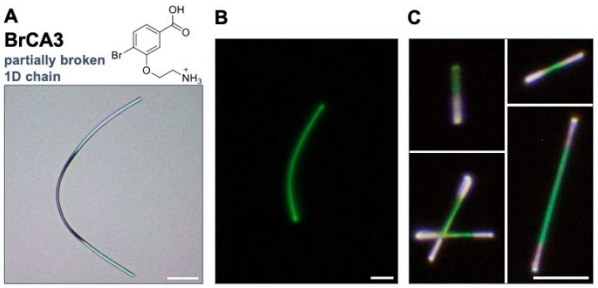

Fig. 1. Molecular templating of 2D perovskite nanowire. (A) Molecular structure of BrCA3. (B) $(BrCA3)_2PbBr_4$ nanowire and (C) $(BrCA3)_2PbBr_4$ - $(BrCA3)_2PbI_4$ heterostructures. Scale bars are 2 μm.

hydrogen bonding that is compatible with both the ionic nature and octahedron spacing of halide perovskites. Nanowires of layered perovskites could be readily assembled in solution facilitated by the formation of 1D H-bonded organic network. For example, we designed a molecular templating cation BrCA3 and grew nanowires of (BrCA3)2PbX4, where BrCA3 is 2-(2-bromo-5-carboxyphenoxy)ethan-1-aminium and X is bromide or iodide (**Fig. 1A**). Interestingly, the carboxylic acid group of BrCA3 inhibited the growth of all crystal facets except [110], which led to one-directional growth of the two-dimensional material. High quality nanowires and epitaxial heterostructures were successfully obtained (**Fig. 1B** and **1C**). These nanowires with tailorable lengths and high-quality cavities provide an ideal platform to study anisotropic excitonic behaviors, light propagation, and lasing in layered perovskites. Our approach highlights the structural tunability of organic-inorganic hybrid semiconductors, which also brings unprecedented morphological control to layered materials. (*Science* 2024)

In another work, we focused on vertical heterostructures of two thin 2D perovskites sheets and examined their twist-angle dependent excitonic properties. Moiré superlattices of 2D materials have recently emerged as a new platform for studying strongly correlated and topological quantum phenomena. 2D organic-inorganic halide perovskites with programmable structures and strongly bound excitons are excellent candidates for creating moiré structures featuring square lattices. Moiré flat bands have been predicted in twisted 2D perovskites; however, their experimental realization is absent owing to a variety of synthetic challenges. In our recent work, we overcome these obstacles via a new synthetic pathway and demonstrate moiré superlattices based on twisted ultra-thin ligand-free 2D hybrid perovskites. Moiré superlattices are clearly visualized through high-resolution transmission electron microscopy (HRTEM) (**Fig. 2a**). Localization of excitons and charge carriers by the moiré potential near a twist angle of 9~11° is observed using both transient photoluminescence microscopy and electrical characterizations, which are excellent agreements with theoretical calculations (**Fig. 2b**). Different from previously reported twisted bilayers, moiré interactions in halide perovskites are long-range (beyond unit-cell-thick sheets), which is likely a result of the strong ionic interactions. Our findings provide a new tunable family of 2D ionic semiconducting materials for exploring moiré flat bands at room temperature. (*Nature Materials* 2024)

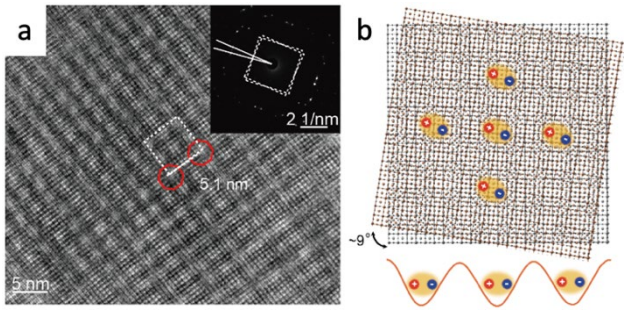

Fig. 2. (a) High-resolution TEM image of twisted ligand-free 2D perovskite bilayers. (b) Illustration of localized moiré excitons in a 9° twisted bilayer heterostructure.

References

(1) Mitzi, D. B.: Synthesis, structure, and properties of organic-inorganic perovskites and related materials. In *Progress in Inorganic Chemistry*; Karlin, K. D., Ed.; John Wiley & Sons, Inc., 2007; pp 1-121.
(2) Dou, L.; Wong, A. B.; Yu, Y.; Lai, M.; Kornienko, N.; Eaton, S. W.; Fu, A.; Bischak, C. G.; Ma, J.; Ding, T.; Ginsberg, N. S.; Wang, L. W.; Alivisatos, A. P.; Yang, P. Atomically thin two-dimensional organic-inorganic hybrid perovskites. *Science* 2015, *349*, 1518-1521.
(3) Blancon, J. C.; Stier, A. V.; Tsai, H.; Nie, W.; Stoumpos, C. C.; Traoré, B.; Pedesseau, L.; Kepenekian, M.; Katsutani, F.; Noe, G. T.; Kono, J.; Tretiak, S.; Crooker, S. A.; Katan, C.; Kanatzidis, M. G.; Crochet, J. J.; Even, J.; Mohite, A. D. Scaling law for excitons in 2D perovskite quantum wells. *Nature Communications* 2018, *9*, 538.
(4) Ishihara, T.; Takahashi, J.; Goto, T. Exciton state in two-dimensional perovskite semiconductor (C10H21NH3)2PbI4. *Solid State Communications* 1989, *69*, 933-936.
(5) Meresse, A.; Daoud, A. Bis(n-propylammonium) tetrachloroplumbate. *Acta Crystallographica Section C* 1989, *45*, 194-196.
(6) Mitzi, D. B.; Feild, C. A.; Harrison, W. T. A.; Guloy, A. M. Conducting tin halides with a layered organic-based perovskite structure. *Nature* 1994, *369*, 467-469.
(7) Papavassiliou, G. C. Three- and low-dimensional inorganic semiconductors. *Progress in Solid State Chemistry* 1997, *25*, 125-270.
(8) Kinigstein, E. D.; Tsai, H.; Nie, W.; Blancon, J.-C.; Yager, K. G.; Appavoo, K.; Even, J.; Kanatzidis, M. G.; Mohite, A. D.; Sfeir, M. Y. Edge States Drive Exciton Dissociation in Ruddlesden–Popper Lead Halide Perovskite Thin Films. *ACS Materials Letters* 2020, *2*, 1360-1367.
(9) Jana, M. K.; Song, R.; Liu, H.; Khanal, D. R.; Janke, S. M.; Zhao, R.; Liu, C.; Valy Vardeny, Z.; Blum, V.; Mitzi, D. B. Organic-to-inorganic structural chirality transfer in a 2D hybrid perovskite and impact on Rashba-Dresselhaus spin-orbit coupling. *Nature Communications* 2020, *11*, 1757.
(10) Long, G.; Jiang, C.; Sabatini, R.; Yang, Z.; Wei, M.; Quan, L. N.; Liang, Q.; Rasmita, A.; Askerka, M.; Walters, G.; Gong, X.; Xing, J.; Wen, X.; Quintero-Bermudez, R.; Yuan, H.; Xing, G.; Wang, X. R.; Song, D.; Voznyy, O.; Zhang, M.; Hoogland, S.; Gao, W.; Xiong, Q.; Sargent, E. H. Spin control in reduced-dimensional chiral perovskites. *Nature Photonics* 2018, *12*, 528-533.
(11) Zhai, Y.; Baniya, S.; Zhang, C.; Li, J.; Haney, P.; Sheng, C.-X.; Ehrenfreund, E.; Vardeny, Z. V. Giant Rashba splitting in 2D organic-inorganic halide perovskites measured by transient spectroscopies. *Science Advances* 2017, *3*, e1700704.
(12) Kagan, C. R.; Mitzi, D. B.; Dimitrakopoulos, C. D. Organic-Inorganic Hybrid Materials as Semiconducting Channels in Thin-Film Field-Effect Transistors. *Science* 1999, *286*, 945.
(13) Lanty, G.; Jemli, K.; Wei, Y.; Leymarie, J.; Even, J.; Lauret, J.-S.; Deleporte, E. Room-Temperature Optical Tunability and Inhomogeneous Broadening in 2D-Layered Organic–Inorganic Perovskite Pseudobinary Alloys. *The Journal of Physical Chemistry Letters* 2014, *5*, 3958-3963.

Publications

1. Wenhao Shao, Jeong Hui Kim, Jeffrey Simon, Zhichen Nian, Sung-Doo Baek, Yuan Lu, Colton B. Fruling, Hanjun Yang, Kang Wang, Jee Yung Park, Libai Huang, Yi Yu, Alexandra Boltasseva, Brett M. Savoie, Vladimir M. Shalaev, Letian Dou*; "Molecular templating of layered halide perovskite nanowires", *Science* 2024, 384, 1000–1006.
2. Shuchen Zhang, Linrui Jin, Yuan Lu, Linghai Zhang, Jiaqi Yang, Qiuchen Zhao, Dewei Sun, Joshua J. P. Thompson, Biao Yuan, Ke Ma, Akriti, Jee Yung Park, Yoon Ho Lee, Zitang Wei, Blake P. Finkenauer, Daria D. Blach, Sarath Kumar, Hailin Peng, Arun Mannodi-Kanakkithodi, Yi Yu, Ermin Malic, Gang Lu, Letian Dou*, Libai Huang*, "Moiré Superlattices in Twisted Two-Dimensional Halide Perovskites", *Nature Materials* 2024, DOI: 10.1038/s41563-024-01921-0.

3. Jee Yung Park, Yoon Ho Lee, Md Asaduz Zaman Mamun, Mir Md Fahimul Islam, Shuchen Zhang, Ke Ma, Aalok Uday Gaitonde, Kang Wang, Seok Joo Yang, Amy Marconnet, Jianguo Mei, Muhammad Ashraful Alam, Letian Dou*; "Electrically induced directional ion migration in two-dimensional perovskite heterostructures", *Matter* 2024, 7, 1817–1832.
4. Linrui Jin, Carlos Mora Perez, Yao Gao, Ke Ma, Jee Yung Park, Shunran Li, Peijun Guo, Letian Dou, Oleg Prezhdo, Libai Huang*; "Superior Phonon-Limited Exciton Mobility in Lead-Free Two-Dimensional Perovskites", *Nano Letters* 2024, 24, 3638–3646.
5. Angana De, Carlos Mora Perez, Aihui Liang, Kang Wang, Letian Dou, Oleg Prezhdo, Libai Huang*; "Tunneling-Driven Marcus-Inverted Triplet Energy Transfer in a Two-Dimensional Perovskite", *Journal of the American Chemical Society* 2024, 146, 4260–4269.
6. Hanjun Yang, Sagarmoy Mandal, Yoon Ho Lee, Jee Yung Park, Han Zhao, Chongli Yuan, Libai Huang, Ming Chen*, Letian Dou*; "Dimensionality Engineering of Lead Organic Chalcogenide Semiconductors" *Journal of the American Chemical Society* 2023, 145, 23963–23971.
7. Ajeet Singh, Biao Yuan, Md. Habibur Rahman, Hanjun Yang, Angana De, Jee Yung Park, Shuchen Zhang, Libai Huang, Arun Mannodi-Kanakkithodi, Timothy J. Pennycook, and Letian Dou*; "Two-Dimensional Halide Pb-Perovskite–Double Perovskite Epitaxial Heterostructures" *Journal of the American Chemical Society* 2023, 145, 19885–19893.
8. Jee Yung Park, Ruyi Song, Jie Liang, Linrui Jin, Kang Wang, Shunran Li, Enzheng Shi, Yao Gao, Matthias Zeller, Simon J. Teat, Peijun Guo, Libai Huang*, Yong Sheng Zhao*, Volker Blum*, Letian Dou*, "Dimensionality-Controlled Organic Semiconductor-Incorporated Perovskite Quantum Wells", *Nature Chemistry* 2023, 15, 1745–1753.
9. Kang Wang, Zih-Yu Lin, Zihan Zhang, Ke Ma, Aidan H. Coffey, Linrui Jin, Harindi R. Atapattu, Yao Gao, Jee Yung Park, Zitang Wei, Blake P. Finkenauer, Chenhui Zhu, Xiangeng Meng, Sarah N. Chowdhury, Zhaoyang Chen, Tauguy Terlier, Yan Yao, Kenneth R. Graham, Alexandra Boltasseva, Tzung-Fang Guo, Libai Huang, Hanwei Gao, Brett M. Savoie, Letian Dou*, "Suppressing Phase Disproportionation in Quasi-2D Perovskite Light-Emitting Diodes", *Nature Communications 2023, 14, 397. (Featured in Editor's Highlight*)
10. Wenhao Shao, Seok Joo Yang, Kang Wang, Letian Dou*; "Light-Emitting Organic Semiconductor-Incorporated Perovskites: Fundamental Properties and Device Applications" *The Journal of Physical Chemistry Letters* 2023, 14, 2034-2046.

Direct Observation of Small Molecules in Smart and Programmable Sponges

Omar K. Farha

o-farha@northwestern.edu

Northwestern University

In this talk, we will explore the fascinating world of metal–organic frameworks (MOFs). MOFs are a class of porous, crystalline materials consisting of metal-based nodes and organic ligands. These components self-assemble into multi-dimensional lattices, distinguishing MOFs from conventional porous materials such as zeolites and activated carbon. The versatility of MOFs stems from the diverse array of molecular building blocks that can be used, allowing for a wide range of properties and applications. Our research has provided a comprehensive understanding of how the physical architecture and chemical properties of MOFs influence their performance in various applications, including storage and separations. One of our recent achievements includes the synthesis of the largest SIFSIX-3-Ni single crystals ever grown. This breakthrough has enabled us to conduct single-crystal X-ray diffraction analyses, allowing for the direct observation of H2O and CO2 dynamics during adsorption and desorption processes. Additionally, we have utilized in situ X-ray scattering methods to uncover long-range and local structural transformations associated with CO2 adsorption within the framework pores. Our findings reveal a temperature-dependent desorption mechanism, further enhancing our understanding of MOF behavior under different conditions. These insights are crucial for the development of smart and programmable sponges, paving the way for advanced material performance in real-world applications.

Pore Space Engineering and Functionalization in Porous Metal-Organic Framework Materials

PI: Pingyun Feng
Department of Chemistry, Materials Science and Engineering
University of California, Riverside, CA 92521

Keywords: Crystalline Porous Materials, Pore Space Partition, Bioisosteric Replacement, Gas Adsorption, Purification and Separation

Research Scope

The research scope centers on developing innovative synthetic and structural concepts and paradigms to create advanced crystalline-porous-materials' platforms. Strong efforts are devoted to synthesizing new materials with functional architectural design and chemical features. Such materials possess multi-modular framework and exceptional tolerance towards isoreticular modular replacement, making precise control of materials' properties possible.[1,2] The synthesized materials have well-defined pore size and geometry that can be tuned in a large range in both small (picometer-level) and large (angstrom-level) increments to target different applications. In addition to serving as adsorbents for gas and energy storage (e.g., C_2H_2),[3] they can improve energy efficiency in large-scale industrial processes such as hydrocarbon purification and separation (e.g., C_2H_2/CO_2, C_2H_4/C_2H_6).[4] Other applications include carbon capture. The project employs innovative synthetic materials-design methods. It combines chemical and solvothermal synthesis, crystal growth and crystal structure analysis, with various property (e.g., thermal and chemical stability) studies. Sorption properties of various gases by these new materials are systematically evaluated to establish composition-structure-property correlations that are used to refine synthetic strategy to optimize porous materials for energy-related applications.

Recent Progress

Multiple significant progresses have been made. Nine manuscripts have been published in the past two years and one is in revision. The following is a brief summary of key achievements during this period.

- Simultaneous Control of Flexibility and Rigidity in Metal–Organic Frameworks

Flexi-MOFs are typically limited to low-connected (<9) frameworks. In this work, we have developed a platform-wide approach capable of creating a family of high-connected materials (collectively called CPM-220) that integrate exceptional framework flexibility with high rigidity. We show that the multi-module nature of the pore-space-partitioned pacs (partitioned acs net) platform allows us to introduce flexibility as well as to simultaneously impose high rigidity in a tunable module-specific fashion. The intermodular synergy has remarkable macro-morphological and sub-nanometer structural impacts. CPM-220 sets multiple precedents and benchmarks on the pacs platform in both structural and sorption properties. They possess exceptionally high benzene/cyclohexane selectivity, unusual C_3H_6 and C_3H_8 isotherms, and promising separation performance for small gas molecules such as C_2H_2/CO_2.

- Pore-Space-Partitioned Metal-Organic Frameworks with Isoreticular Cluster Concept

Trigonal planar $M_3(O/OH)$ trimers are among the most important clusters in inorganic chemistry and are the foundational features of multiple high-impact MOF platforms. In this work, we introduce a concept called isoreticular cluster series and demonstrate that $M_3(O/OH)$, as the

first member of a supertrimer series, can be combined with a higher hierarchical member (double-deck trimer here) to advance isoreticular chemistry. In this work, an isoreticular series of pore-space-partitioned MOFs called M_3M_6 pacs made from co-assembly between M_3 single-deck trimer and M_{3x2} double-deck trimer have been synthesized. The new pacs materials exhibit high surface area and high uptake capacity for CO_2 and small hydrocarbons, as well as selective adsorption properties relevant to separation of industrially important mixtures such as C_2H_2/CO_2 and C_2H_2/C_2H_4.

• Integrative Extreme Pore Tightening and Ultrafine Pore Tuning for Dramatic Amplification of Gas Selectivity in Pore-Space-Partitioned Metal-Organic Frameworks

Ultrafine tuning of MOF structures at sub-angstrom to picometer levels can dramatically improve separation selectivity for gas pairs with subtle differences. However, for MOFs with large-enough pore size, the effect from ultrafine tuning on sorption properties can be muted. In this work, we demonstrate an integrative strategy that couples together extreme pore compression with ultrafine pore tuning. Specifically, we use one module (L1) to shrink pore size to extreme minimum on the pacs platform while retaining porosity. This is followed by using another module (L2) for ultrafine pore turning. This integrative L1-L2 strategy leads to dramatically enhanced C_2H_2/CO_2 selectivity from 2.6 to 20.8 and excellent experimental breakthrough performance.

• Ultrastable Carboxyl-Functionalized Metal-Organic Frameworks for Gas Separation

Isoreticular chemistry, which enables property optimization by changing compositions without changing topology, is a powerful synthetic strategy. One of the biggest challenges facing isoreticular chemistry is to extend it to ligands with strongly coordinating substituent groups such as unbound -COOH, because competitive interactions between such groups and metal ions can derail isoreticular chemistry. In this work, with simultaneous introduction of carboxyl functionalization and pore space partition, we have developed a family of carboxyl-functionalized materials in diverse compositions from homometallic Cr^{3+} and Ni^{2+} to heterometallic Co^{2+}/V^{3+}, Ni^{2+}/V^{3+}, Co^{2+}/In^{3+}, Co^{2+}/Ni^{2+}. Cr-MOF remains highly crystalline in boiling water. Unprecedentedly, Cr-MOF can withstand the treatment cycle with 10 M NaOH and 12 M HCl, allowing reversible inter-conversion between unbound -COOH acid form and $-COO^-$ base form. These materials exhibit excellent sorption properties such as very high uptake capacity for CO_2 (100.2 cm^3/g at 1 bar and 298K) and small hydrocarbon gases (e.g., 142.1 cm^3/g for C_2H_2, 110.5 cm^3/g for C_2H_4 at 1 bar and 298K), high benzene/cyclohexane selectivity (up to about 40), and promising separation performance for gas mixtures such as C_2H_2/CO_2 and C_2H_2/C_2H_4.

• Solvent-free Synthesis of Multi-Module Pore-Space-Partitioned Metal-Organic Frameworks for Gas Separation

The green syntheses using solvent-free methods are generally limited to simple chemical systems with just one inorganic module and one organic module. In this work, we have succeeded in developing a solvent-free method to synthesize complex metal-organic framework materials with multiple modules. Such multi-module materials are more amenable to compositional and geometrical tuning and thus offer more opportunities for property optimization. The synthesis only requires simple mixing of reactants and short reaction time. Highly porous and stable materials can be made without any energy-costing post-synthetic activation.

References

(1) Zhai, Q-G; Bu, X.; Mao, C.; Zhao, X.; Daemen, L.; Cheng, Y.; Ramirez-Cuesta, A. J.; Feng, P., *An Ultra-Tunable Platform for Molecular Engineering of High-Performance Crystalline Porous Materials*, Nat. Commun. **7**, 13645 (2016).
(2) Hong, A. N.; Yang, H.; Bu, X.; Feng, P., *Pore Space Partition of Metal-Organic Frameworks for Gas Storage and Separation.* EnergyChem **4**, 100080 (2022)
(3) Wang, Y.; Jia, X.; Yang, H.; Wang, Y.; Chen, X.; Hong, A.; Li, J.; Bu, X. Feng, P., *A New Strategy for Constructing Pore Space Partitioned MOFs with High Uptake Capacity for C2 Hydrocarbons and CO2*. Angew. Chem. Int. Ed. **59**, 19027 (2020).
(4) Yang, H.; Wang, Y.; Krishna, R.; Jia, X.; Wang, Y.; Hong, A. H.; Dang, C.; Castillo, H. E.; Bu, X.; Feng, P., *Pore-Space-Partition-Enabled Exceptional Ethane Uptake and Ethane-Selective Ethane-Ethylene Separation*. J. Am. Chem. Soc. **142**, 2222 (2020).
(5) Hong, A. N.; Wang, Y.; Chen, Y.; Yang, H.; Kusumoputro, E.; Bu, X.; Feng, P., *Concurrent Enhancement of Acetylene Uptake Capacity and Selectivity by Progressive Core Expansion and Extra-Framework Anions in Pore-Space-Partitioned Metal-Organic Frameworks*. Chem. Eur. J. **29**, e202203547 (2023)
(6) Xiao, Y.; Chen, Y.; Hong, A. N.; Bu, X.; Feng, P., *Solvent-free Synthesis of Multi-Module Pore-Space-Partitioned Metal-Organic Frameworks for Gas Separation*. Angew. Chem. Int. Ed. **62**, e202300721 (2023)

Publications in the past two years

(1) Wang, W.; Yang, H.; Chen, Y.; Bu, X.; Feng, P., *Cyclobutanedicarboxylate Metal–Organic Frameworks as a Platform for Dramatic Amplification of Pore Partition Effect*. J. Am. Chem. Soc. **145**, 17551−17556 (2023)

(2) Chen, Y.; Yang, H.; Wang, W.; Li, X.; Wang, Y.; Hong, A. N.; Bu, X.; Feng, P., *Multi-Modular Design of Stable Pore-Space-Partitioned Metal-Organic Frameworks for Gas Separation Applications*. Small **19**, 2303540 (2023)

(3) Xiao, Y.; Chen, Y.; Wang, W.; Yang, H.; Hong, A. N.; Bu, X.; Feng, P., *Simultaneous Control of Flexibility and Rigidity in Pore-Space-Partitioned Metal–Organic Frameworks*. J. Am. Chem. Soc. **145**, 10980−10986 (2023)

(4) Xiao, Y.; Chen, Y.; Hong, A. N.; Bu, X.; Feng, P., *Solvent-free Synthesis of Multi-Module Pore-Space-Partitioned Metal-Organic Frameworks for Gas Separation*. Angew. Chem. Int. Ed. **62**, e202300721 (2023)

(5) Hong, A. N.; Wang, Y.; Chen, Y.; Yang, H.; Kusumoputro, E.; Bu, X.; Feng, P., *Concurrent Enhancement of Acetylene Uptake Capacity and Selectivity by Progressive Core Expansion and Extra-Framework Anions in Pore-Space-Partitioned Metal-Organic Frameworks*. Chem. Eur. J. **29**, e202203547 (2023)

(6) Xiao, Y.; Hong, A. N.; Chen, Y.; Yang, H.; Wang, Y.; Bu, X.; Feng, P., *Developing Water-Stable Pore-Partitioned Metal-Organic Frameworks with Multi-Level Symmetry for High-Performance Sorption Applications*. Small **19**, 2205119 (2023).

(7) Xiao, Y.; Chen, Y.; Wang, W.; Bu, X.; Feng, P., *Advancing Pore-Space-Partitioned Metal-Organic Frameworks with Isoreticular Cluster Concept*. Angew. Chem. Int. Ed. **63**, e202403698 (2024)

(8) Ajayan, P.; Wang, W.; Chen, Y.; Bu, X.; Feng, P. *Ultrastable Carboxyl-Functionalized Pore-Space-Partitioned Metal-Organic Frameworks for Gas Separation*, Adv. Mater. **36**, in revision (2024)

(9) Xiao, Y.; Yang, H.; Hong, A. N.; Wang, Y.; Bu, X.; Feng, P., In Situ Synthesized Homochiral Spiroborate Ester Metal-Organic Framework with Mono-, Di-, and Trivalent Cations. Chem Asian J. 2022, 17, e202200918 (2022)

(10) Hong, A. N.; Yang, H.; Bu, X.; Feng, P., *Pore Space Partition of Metal-Organic Frameworks for Gas Storage and Separation*. EnergyChem **4**, 100080 (2022).

Modular Intermetallics: Materials Discovery from Chemical Pressure-Derived Principles for the Formation and Morphology of Complex Metallic Structures

Daniel C. Fredrickson and Rie T. Fredrickson, Department of Chemistry, University of Wisconsin-Madison, Madison, Wisconsin

Keywords: Materials design principles, intermetallic phases, modularity in structures, chemical pressure, structure-property relationships

Research Scope

Intermetallic phases offer vast potential for the development of solid state materials, combining an ever expanding structural chemistry with a wide range of properties. The realization of these opportunities, however, is limited by the difficulty of controlling their structures and evaluating structure-properties relationships. An important clue to addressing this problem is the observation that many complex intermetallics are built from units of different parent structures (Figure 1).[1-5] Such intergrowth of different parent phases is reminiscent of MAX phases, where the fusion of ceramic and metallic domains yields materials that combine the temperature- and corrosion-resistance of the former materials type with the machinability of the latter.[6] In this project, we are combining experiment and theory in the development of principles for creating a wider family of intermetallic materials built from units or modules of parent phases, which might bring different functionalities. Toward this end, our objectives are to (1) devise and validate a *theory of modular intermetallic chemistry* for assessing the compatibility of intermetallic structures toward intergrowth with each other and the preferred orientations of their domain interfaces; (2) synthetically realize unprecedented families of modular intermetallics, following the predictions of and providing feedback to this theoretical framework; and (3) evaluate the structure-properties relationships and the potential for new functionality arising from modularity of the new compounds obtained.

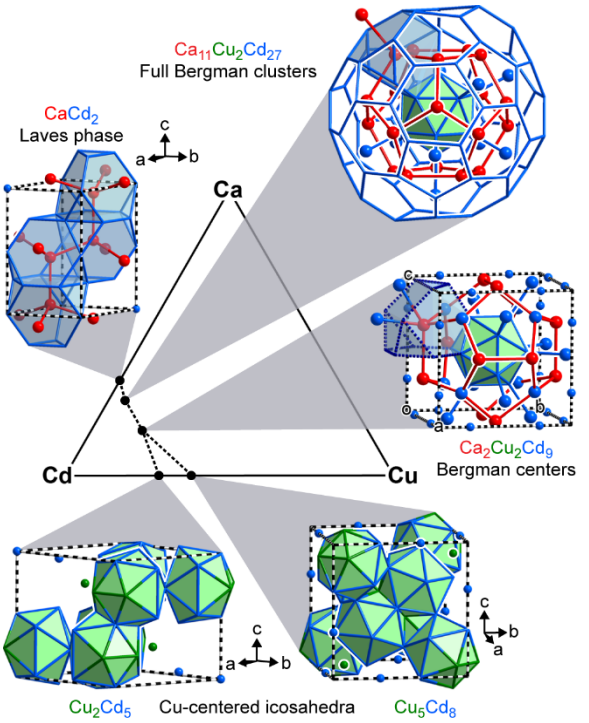

Figure 1. Structures in the Ca-Cu-Cd system, illustrating the construction of complex ternary arrangements from units of simpler ones.

Recent Progress

A key advance has been our development of the *interface nucleus approach* to understanding and anticipating the stability and preferred domain interface orientations in intermetallic intergrowth structures. Drawing on several examples, we noted that parent structure units in complex structure can be linked through a shared collection of atoms, which can be considered as a continuation of either parent. This shared motif is viewed conceptually as a nucleus for the formation of the interface between the two domains. Through a series of DFT-Chemical Pressure (CP) analyses, we demonstrated that favorable intergrowths arise when the interface nuclei in the two parents experience complementary CPs (strong with weak, or positive with negative) at corresponding points (Figure 2).[7] In addition, interfaces between the domains tend to be oriented such that the interface normal is aligned with the vectors of strongest CP complementarity in the interface nuclei.

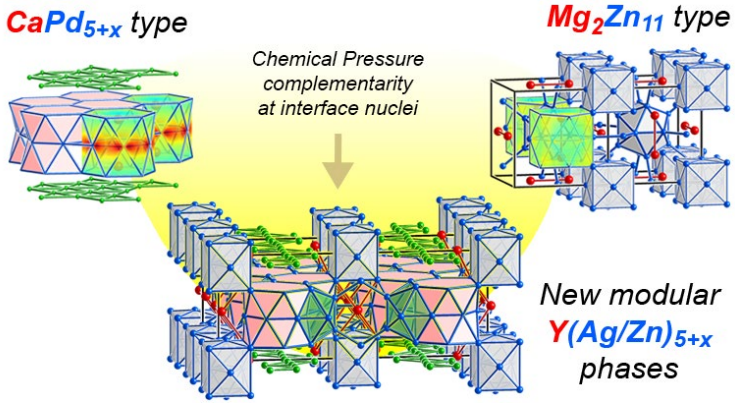

Figure 2. The structure $YAg_{2.44}Zn_{3.17}$ as a lamellar intergrowth of two simpler types stabilized by chemical pressure (CP) compatibility at shared geometrical motifs at the interfaces. Color maps show the CPs acting between the interface nucleus units and their surroundings in the parent structures, with red corresponding to strong positive CP and blue to strong negative CP. Reprinted with permission from Ref. 8. Copyright 2024 American Chemical Society.

These interface nucleus principles are realized in a series of three new Y-Ag-Zn compounds we synthesized: $YAg_{2.79}Zn_{2.80}$, $YAg_{2.44}Zn_{3.17}$, and $YAg_{2.71}Zn_{2.71}$.[8] In these structures, lamellar domains derived from the $CaPd_{5+x}$ type[9] and Mg_2Zn_{11} type[10] alternate (Figure 2), joined by interface nuclei based on double hexagonal antiprisms familiar from the $CaCu_5$ type. The same interface nucleus also underlies a series of $CaCu_5$-/Laves phase-type intergrowths,[11] but with the interfaces running through the nucleus in a perpendicular direction. These differences in the preferred intergrowth direction follow simply the directions of maximum CP complementarity.

Building on these observations, we developed a metric for interface nucleus complementarity (INC) that can be used for screening pairs of structures containing a common geometrical motif for their potential to form intergrowths.[12] By applying this to a series of CP schemes for 15 structure types containing an interface nucleus derived from the σ-phase, we have found that the INC metric can be used in the design of new syntheses, and adapted to create an iterative process for materials discovery. Our recent development of a Machine-Learned model for CP analysis will allow us to apply this approach on a much larger scale.

References

1. Felder, J. B.; Weiland, A.; Hodovanets, H.; McCandless, G. T.; Estrada, T. G.; Martin, T. J.; Walker, A. V.; Paglione, J.; Chan, J. Y. Law and Disorder: Special Stacking Units—Building the Intergrowth $Ce_6Co_5Ge_{16}$. *Inorg. Chem.* **2019**, *58*, 6037-6043.
2. Parthé, E.; Chabot, B. A.; Cenzual, K. Complex structures of intermetallic compounds interpreted as intergrowth of segments of simple structures. *Chimia* **1985**, *39*, 164-174.
3. Grin, Y. N. The Intergrowth Concept as a Useful Tool to Interpret and Understand Complicated Intermetallic Structures In *Modern Perspectives in Inorganic Crystal Chemistry*; Parthé, E., Ed.; Springer Netherlands: Dordrecht, 1992, p 77-96.
4. Fredrickson, D. C.; Lee, S.; Hoffmann, R. Interpenetrating polar and nonpolar sublattices in intermetallics: the $NaCd_2$ structure. *Angew. Chem., Int. Ed.* **2007**, *46*, 1958-1976.
5. Hadler, A. B.; Harris, N. A.; Fredrickson, D. C. New Roles for Icosahedral Clusters in Intermetallic Phases: Micelle-like Segregation of Ca-Cd and Cu-Cd Interactions in $Ca_{10}Cd_{27}Cu_2$. *J. Am. Chem. Soc.* **2013**, *135*, 17369-17378.
6. Dahlqvist, M.; Barsoum, M. W.; Rosen, J. MAX phases – Past, present, and future. *Mater. Today* **2024**, *72*, 1-24.
7. Sanders, K. M.; Gressel, D. G.; Fredrickson, R. T.; Fredrickson, D. C. Toward Predicting the Assembly of Modular Intermetallics from Chemical Pressure Analysis: The Interface Nucleus Approach. *Inorg. Chem.* **2024**, *63*, 6626-6637.
8. Fredrickson, R. T.; Fredrickson, D. C. Interface Nuclei in the Y–Ag–Zn System: Three Chemical Pressure-Templated Phases with Lamellar Mg_2Zn_{11}- and $CaPd_{5+x}$-Type Domains. *Inorg. Chem.* **2024**, *63*, 9252-9264.
9. Kilduff, B. J.; Fredrickson, D. C. Chemical Pressure-Driven Incommensurability in $CaPd_5$: Clues to High-Pressure Chemistry Offered by Complex Intermetallics. *Inorg. Chem.* **2016**, *55*, 6781-6793.
10. Samson, S. Die Kristallstruktur von Mg_2Zn_{11}. Isomorphie zwischen Mg_2Zn_{11} und $Mg_2Cu_6Al_5$. *Acta Chem. Scand.* **1949**, *3*, 835-843.
11. Parthé, E.; Lemaire, R. Structure block stacking in intermetallic compounds. I. The rhombohedral-hexagonal $M_{n+1}X_{5n-1}$ and the monoclinic-hexagonal-trigonal-orthorhombic $M_{n+1}X_{5n+2}$ structure series. *Acta Crystallogr. B* **1975**, *31*, 1879-1889.
12. Gressel, D. G.; Sanders, K. M.; Fredrickson, D. C. Interface Nucleus Compatibility: An Iterative Process for the Discovery of Modular Intermetallics Guided by Chemical Pressure. **2024**, submitted.

Publications

1. Fredrickson, R. T.; Fredrickson, D. C. Chemical Pressure-Derived Assembly Principles for Dodecagonal Quasicrystal Approximants and Other Complex Frank-Kasper Phases. *Inorg. Chem.* **2022**, *61*, 17682-17691.
2. Sanders, K. M.; Van Buskirk, J. S.; Hilleke, K. P.; Fredrickson, D. C. Self-Consistent Chemical Pressure Analysis: Resolving Atomic Packing Effects through the Iterative Partitioning of Space and Energy. *J. Chem. Theory Comput.* **2023**, *19*, 4273-4285.
3. Van Buskirk, J. S.; Kraus, J. D.; Fredrickson, D. C. The Intermetallic Reactivity Database: Compiling Chemical Pressure and Electronic Metrics toward Materials Design and Discovery. *Chem. Mater.* **2023**, *35*, 3582-3591.
4. Kraus, J. D.; Van Buskirk, J. S.; Fredrickson, D. C. The Zintl Concept Applied to Intergrowth Structures: Electron-Hole Matching, Stacking Preferences, and Chemical Pressures in Pd5InAs. *Z. Anorg. Allg. Chem.* **2023**, *649*, e202300125.
5. Sanders, K. M.; Gressel, D. G.; Fredrickson, R. T.; Fredrickson, D. C. Toward Predicting the Assembly of Modular Intermetallics from Chemical Pressure Analysis: The Interface Nucleus Approach. *Inorg. Chem.* **2024**, *63*, 6626-6637.
6. Fredrickson, R. T.; Fredrickson, D. C. Interface Nuclei in the Y–Ag–Zn System: Three Chemical Pressure-Templated Phases with Lamellar Mg_2Zn_{11}- and $CaPd_{5+x}$-Type Domains. *Inorg. Chem.* **2024**, *63*, 9252-9264.
7. Garman, L. C.; Fredrickson, D. C. The Mott-Jones Hamilton Population: Energetics of Fermi Sphere-Jones Zone Interactions in Intermetallic Structures, *J. Phys. Chem. C.* **2024,** accepted.
8. Gressel, D. G.; Sanders, K. M.; Fredrickson, D. C. Interface Nucleus Compatibility: An Iterative Process for the Discovery of Modular Intermetallics Guided by Chemical Pressure, submitted.

Elastomeric Miktoarm Star Polymers: Theory and Experiment

Glenn H. Fredrickson (Principal Investigator)

Materials Research Laboratory, University of California, Santa Barbara, California, United States, 93106

Department of Chemical Engineering, University of California, Santa Barbara, California United States, 93106

Christopher M. Bates (Co-PI)

Materials Research Laboratory, University of California, Santa Barbara, California, United States, 93106

Materials Department, University of California, Santa Barbara, California, United States, 93106

Department of Chemistry and Biochemistry, University of California, Santa Barbara, California, United States, 93106

Keywords: miktoarm star copolymers, bottlebrush copolymers, molecular interactions, thermoplastic elastomers, self-consistent field theory simulations

Research Scope

This research program aims to understand what design rules govern the phase behavior and properties of polymers with complex sequences and architectures, including multiblocks, miktoarm stars, and bottlebrush copolymers. Our approach leverages a combination of expertise in theory/simulation (Fredrickson) and synthetic polymer chemistry/characterization (Bates).

Recent Progress

Thermoplastic elastomers (TPEs) are arguably the most industrially successful type of block copolymer due to their robust mechanical properties and high elasticity. Over 2 million metric tons are produced annually to satisfy multi-billion-dollar market in applications as diverse as the automotive industry, coatings, medical devices, pressure sensitive adhesives, and asphalt modifiers [1,2]. The prototypical example is a linear ABA triblock copolymer with glassy A and rubbery B blocks at service temperatures. Chemical incompatibility drives microphase separation on the nanometer length scale into discrete hard domains with a bridging B matrix. To ensure elasticity, A blocks must remain discrete, which places an upper limit on their volume fraction $f_A \approx 0.3$, beyond which a cylinder-to-gyroid transition renders the material plastic and not elastic.

In a recent study [3], we demonstrated that the mechanical properties of ABC triblock terpolymers improve molecular bridging and associated elasticity relative to symmetric ABA/CBC analogs having similar molecular weights and volume fractions of the B and A/C domains (Figure 1). Up to 98% recovery over 10 cycles was achieved through essentially full chain bridging between discrete hard domains leading to the minimization of mechanically unproductive loops. In addition, the unique phase behavior of ABC triblocks also enables the fraction of hard-block domains to be higher ($f_{hard} = f_A + f_C \approx 0.4$) while maintaining elasticity, which is traditionally only possible with non-linear architectures or highly asymmetric ABA triblock copolymers. These advantages of ABC triblock terpolymers provide a tunable platform to create potentially useful materials that improve our fundamental understanding of chain conformation and structure–property relationships in synthetically accessible block copolymers.

Stabilizing cylindrical phases to higher f_A has been shown to produce stiffer and tougher elastomers, which can be achieved using the miktoarm star architecture [4]. However, many aspects of the self-assembly behavior of miktoarm star polymers are still not well understood [5]. For example, in AB_n miktoarm star polymers, conformational asymmetry can be achieved through either arm-number asymmetry ($n > 1$) or statistical segment length asymmetry ($b_A > b_B$), and it is still unclear how these distinct types of conformational asymmetry affect self-assembly when both are present. Studying this fundamental question remains technically challenging with traditional synthetic techniques that are time-consuming and laborious. In recent work [5], we used self-consistent field theory (SCFT) simulations to gain insights into the role of conformational asymmetry on the equilibrium phase behavior of miktoarm star polymers. Our simulations reveal that the aforementioned two types of conformational asymmetry sometimes have opposing effects on the phase behavior of AB_n miktoarm stars. Subsequently, guided by these SCFT simulations, we synthesized a library of LD_3 and LD_4 miktoarm stars consisting of poly(*rac*-lactide) (L) and poly(dodecyl acrylate) (D) by leveraging the synthetically accessible μSTAR platform developed under DOE support. We were able to obtain well-ordered Frank–Kasper phases such as σ and A15 despite the presence of an inherent distribution in the number of D arms that arises from the μSTAR technique. Interestingly, we experimentally observed a stable A15 mesophase over a wide range of the volume fractions f_L, which quantitatively agrees with the prediction from SCFT simulations that matched experiments. These findings deepen our understanding of the self-assembly of miktoarm star polymers.

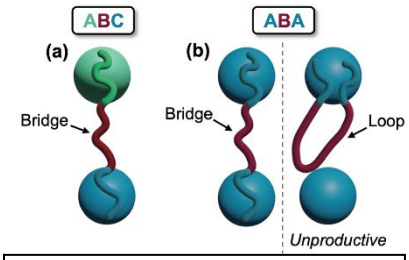

Figure 1: ABC triblock copolymers have improved bridging, reminiscent of miktoarm star polymers, compared to traditional ABA systems.

Another polymeric architecture known as bottlebrush copolymers [6] is an intriguing class of materials that may behave similarly to miktoarm star polymers in many aspects related to

conformational asymmetry but with an easier synthetic strategy. In recent work [7], we used a combination of SCFT simulations and experiments to systematically investigate the self-assembly behavior of conformationally asymmetric A-*stat*-B statistical bottlebrushes with asymmetric statistical segment lengths $b_A > b_B$ (Figure 2). In particular, our SCFT simulations predict the stabilization of the Frank–Kasper A15 phase with A-rich spheres and B-rich matrix at higher f_A compared to their linear counterparts at the same b_A/b_B, which is attributed to the additional conformational asymmetry from the bottlebrush architecture. Furthermore, as the statistical segment length asymmetry increases, order–order phase boundaries shift to larger values of f_A. We find when A side chains with molecular weights roughly less than 1 kg/mol are used, the experimental behavior matches the theoretically predicted equilibrium behavior well, and the Frank–Kasper A15 phase is stabilized in statistical bottlebrush systems. However, when the side chains possess high molecular weights, the complex sphere phases become kinetically inaccessible; nonetheless, a stable hexagonally-packed cylinder phase region is deflected to f_A at least as large as 0.51 when long A and short B chains are used to enhance conformational asymmetry from asymmetric statistical segment lengths $b_A > b_B$. These results reveal unique structure–property relationships that emerge in bottlebrush copolymers, which are both synthetically accessible and potentially useful in a variety of contemporary applications.

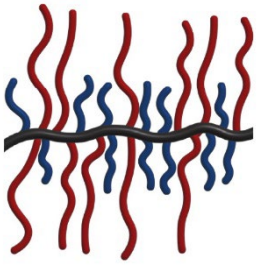

Figure 2: Statistical bottlebrush copolymers also exhibit pronounced conformational asymmetry effects.

References

1. J. G. Drobny, *Handbook of Thermoplastic Elastomers*, 2nd ed., Elsevier, London, UK (2014).

2. N. A. Lynd, F. T. Oyerokun, D. L. O'Donoghue, D. L. Handlin, and G. H. Fredrickson, *Design of Soft and Strong Thermoplastic Elastomers Based on Nonlinear Block Copolymer Architectures Using Self-Consistent Field Theory*, Macromolecules **43**, 3479 (2010).

3. K. R. Albanese, J. R. Blankenship, T. Quah, A. Zhang, K. T. Delaney, G. H. Fredrickson, C. M. Bates, and C. J. Hawker, *Improved Elastic Recovery from ABC Triblock Terpolymers*, ACS Polym. Au **3**, 376–382 (2023).

4. W. Shi, N. A. Lynd, D. Montarnal, Y. Luo, G. H. Fredrickson, E. J. Kramer, C. Ntaras, A. Avgeropoulos, A. Hexemer, *Toward Strong Thermoplastic Elastomers with Asymmetric Miktoarm Block Copolymer Architectures*, Macromolecules **47**, 2037–2043 (2014).

5. K. Watanabe, D. Chen, Y. Zhu, D. Callan, G. H. Fredrickson, and C. M. Bates, *Effect of Conformational Asymmetry on the Self-Assembly Behavior of AB_n Miktoarm Star Polymers*, (to be submitted).

6. Z. Li, M. Tang, S. Liang, M. Zhang, G. M. Biesold, Y. He, S.-M. Hao, W. Choi, Y. Liu, J. Peng, Z. Lin, *Bottlebrush Polymers: From Controlled Synthesis, Self-Assembly, Properties to Applications*, Prog. Polym. Sci. **116**, 101387 (2021).

7. D. Chen, J. R. Blankenship, Y. Zhu, K. R. Albanese, T. Eom, D. Callan, K. T. Delaney, C. M. Bates, and G. H. Fredrickson, *Effects of Conformational Asymmetry and Chain Molecular Weights on the Self-Assembly Behavior of Statistical Bottlebrush Copolymers*, (to be submitted).

Publications

1. D. Chen, M. A. Klatt, and G. H. Fredrickson, *Emergence of Disordered Hyperuniformity in Melts of Linear Diblock Copolymers*, (submitted).

2. K. R. Albanese, J. R. Blankenship, T. Quah, A. Zhang, K. T. Delaney, G. H. Fredrickson, C. M. Bates, and C. J. Hawker, *Improved Elastic Recovery from ABC Triblock Terpolymers*, ACS Polym. Au **3**, 376–382 (2023).

3. J. R. Blankenship, A. E. Levi, D. J. Goldfeld, J. L. Self, N. Alizadeh, D. Chen, G. H. Fredrickson, and C. M. Bates, *Asymmetric Miktoarm Star Polymers as Polyester Thermoplastic Elastomers*, Macromolecules **55**, 4929–4936 (2022).

4. D. Chen, T. Quah, K. T. Delaney, G. H. Fredrickson, *Investigation of the Self-Assembly Behavior of Statistical Bottlebrush Copolymers via Self-Consistent Field Theory Simulations*, Macromolecules **55**, 9324–9333 (2022).

5. R. Xie, I. Lapkriengkri, N. B. Pramanik, S. Mukherjee, J. R. Blankenship, K. Albanese, H. Wang, M. L. Chabinyc, and C. M. Bates, *Hydrogen-Bonding Bottlebrush Networks: Self-Healing Materials from Super-Soft to Stiff*, Macromolecules **55**, 10513–10521 (2022).

6. M. Liu, J. R. Blankenship, A. E. Levi, Q. Fu, Z. M. Hudson, and C. M. Bates, *Miktoarm Star Polymers: Synthesis and Applications*, Chem. Mater. **34**, 6188–6209 (2022).

7. G. H. Fredrickson, S. Xie, J. Edmund, M. L. Le, D. Sun, D. J. Grzetic, D. L. Vigil, K. T. Delaney, M. L. Chabinyc, and R. A. Segalman, *Ionic Compatibilization of Polymers*, ACS Polym. Au **2**, 299–312 (2022).

8. M. L. Le, D. J. Grzetic, K. T. Delaney, K.-C. Yang, S. Xie, G. H. Fredrickson, M. L. Chabinyc, and R. A. Segalman. *Electrostatic Interactions Control the Nanostructure of Conjugated Polyelectrolyte–Polymeric Ionic Liquid Blends*, Macromolecules **55**, 8321–8331 (2022).

9. G. H. Fredrickson and K. T. Delaney, *Field-Theoretic Simulations in Soft Matter and Quantum Fluids*, Oxford University Press, Oxford, UK (2023).

Permanent Magnets Featuring Heavy Main Group Elements for Magnetic Anisotropy

Danna Freedman

Keywords: High-Pressure; Magnetism; Rare-Earth Free; Bismuth; Kinetic

Research Scope

Permanent magnets underpin a vast range of energy technologies, including wind turbines, electric vehicle motors, and regenerative brakes in hybrid vehicles. Improving the performance of the magnets within these applications will have a tremendous impact on energy efficiency, and will lead to the transformative advances that meet core DOE needs. To develop a fundamentally new class of permanent magnet while retaining the properties conferred by rare-earth elements, *we propose combining the two components of a magnetic moment—spin and orbital angular momentum—from two separate elements that are intimately bonded, thus reconstituting these components in a single magnetic moment.*

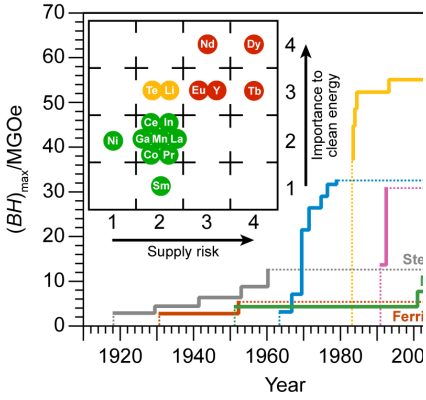

Figure 1** | Plot of the maximum energy product, $(BH)_{max}$, of various industrially relevant permanent magnet materials over the last century. Inset: relationship between the importance of selected elements to the clean energy initiative and their supply risk, highlighting the unfavorable dependence on Nd, Dy, taken from DOE Critical Materials Strategy.* ***Error! Bookmark not defined.,Error! Bookmark not defined.

Recent Progress

Characterization of two new permanent magnet candidates we created: $FeBi_2$ and $MnBi_2$

Our discoveries in the Fe–Bi and Mn–Bi systems demonstrate the promise of this approach. At pressures of ~30 GPa—which is comparable to the pressure found at the core of Mars[1]—we synthesized the first iron–bismuth binary compound, $FeBi_2$,[19] which is a very promising candidate for displaying permanent magnetism. In a parallel direction, we built upon the promise of MnBi—which was for a brief period in the 1950s the most powerful magnet known[1,2,3,4,5]—by exploring the Mn–Bi system under high pressure. At pressures of ~8 GPa, we discovered $MnBi_2$, a new intermetallic compound with the same crystal structure as $FeBi_2$. Both compounds bear striking structural similarities to MnBi, exhibiting linear chains of transition metal atoms along the *c*-axis that are each surrounded by bismuth atoms in antiprism coordination environments (Figure 4). Theoretical studies carried out on $MnBi_2$ by collaborators suggest that it possesses comparable magnetic moments and magnetocrystalline anisotropy to MnBi, greatly spurring our desire to experimentally characterize the magnetic properties of both $FeBi_2$ and $MnBi_2$.[19,20]

To elucidate the magnetic properties of these phases, we developed *in situ* approaches to magnetic characterization. In the first approach, we harnessed X-ray Magnetic Circular Dichroism (XMCD) which is a power spectroscopic technique which interrogates the magnetism of materials. An additional advantage of XMCD is its element specificity which eliminates the possibility of background signals contributing to the observed signal. Our data are necessarily from a ferromagnetic Bi material, which eliminates the potential for Mn-containing impurities. We detected ferromagnetic ordering at 9.4(5) GPa and 10 K (Figure 6). Upon switching from +6 T to 0 T in 1 T increments, the XMCD response did not significantly change, demonstrating $MnBi_2$ exhibits a remnant magnetization nearly equal to magnetization at saturation. Further, the hysteretic signal persists to 300 K. *The aggregate of these data indicate $MnBi_2$ is a room-temperature permanent magnet,* matching theoretical predictions previously executed by the Rondinelli laboratory. One ancillary feature of executing the measurement by measuring the magnetization on the bismuth is we demonstrate that the bismuth is a component of the total magnetic moment thereby supporting our core hypothesis that the orbital moment of bismuth is contributing to the magnetic properties.

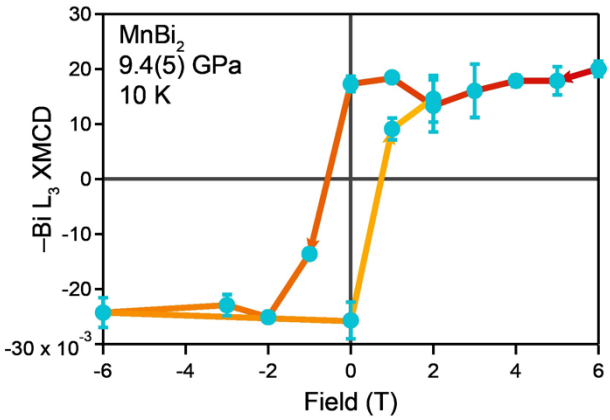

Figure 2 | Field dependence of the integrated XMCD response of the L_3 edge of $MnBi_2$ at 9.4(5) GPa at 10 K, showing a magnetic hysteresis response with a coercivity of ~1 T, suggesting $MnBi_2$ is a permanent magnet.

$FeBi_2$ can be interrogated using NV center magnetometry; data indicate it is a room temp magnet. We expanded upon our work with *in situ* measurements to interrogate the magnetism of $FeBi_2$. We initiated our measurements of $FeBi_2$ mindful of two distinct possibilities for its physical properties, the first, permanent magnetism: $FeBi_2$ features our spin bearing center coupled to the heaviest element stable to radioactive decay, thereby suggesting strong potential for permanent magnetism. The second, superconductivity, $FeBi_2$ features both a pnictide and iron, suggesting potential for it to fall within the alternately named, iron-based superconductors, or pnictide superconductors. *Optically detected magnetic resonance spectroscopy (ODMR) revealed the magnetic dipoles of the $FeBi_2$ in the sample, demonstrating that indeed it is a room temperature magnet*. Variable temperature and variable field studies used to determine the figures of merit of the $FeBi_2$ phase are ongoing. Further, we are currently synthesizing additional samples with larger domains of $FeBi_2$ which will enable higher precision measurements and enable the detection of the orientation of magnetic moment with respect to the crystallographic axes of the compound.

Publications

1. Antonangeli, D.; Morard, G.; Schmerr, N. C.; Komabayashi, T.; Krisch, M.; Fiquet, G.; Fei, Y.; "Toward a mineral physics reference model for the Moon's core." *Proceedings of the National Academy of Sciences of the United States of America* 2015, *112*, 3916–3919.

2. "Bismanol: NOL Develops New Magnetic Material" *Physics Today* 1952, *5*, 8, 19.

3. Adams, E.; Hubbard, W. M.; Syeles, A. M. "A new permanent magnet from powdered manganese bismuthide." *Journal of Applied Physics* 1952, *23*, 1207–1211.

4. Yang, J.; Kamaraju, K.; Yelon, W. B.; James, W. J.; Cai, Q.; Bollero, A. "Magnetic properties of the MnBi intermetallic compound." *Applied Physics Letters* 2001, *79*, 1846–1848.

5. Antropov, V.; Antonov, V.; Bekenov, L.; Kutepov, A.; Kotliar, G. "Magnetic anisotropic effects and electronic correlations in MnBi ferromagnet." *Physical Review B* 2014, *90*, 054404.

6. Williams, T.; Taylor, A.; Christianson, A.; Hahn, S.; Fishman, R.; Parker, D.; McGuire, M.; Sales, B.; Lumsden, M. "Extended magnetic exchange interactions in the high-temperature ferromagnet MnBi." *Applied Physics Letters* 2016, *108*, 192403

Molecular Insights into Structure and Function of Doping in Hybrid Metal Halides for the Rational Design of Optoelectronic Materials

PI: Mahesh K Gangishetty[1], and Co-PI: Neeraj Rai[2]
[1]Department of Chemistry, and Department of Physics & Astronomy, Mississippi State University., Mississippi State 39762
[2]330 Swalm Chemical, Mississippi State University, Mississippi State, MS, 39762.

Keywords: Hybrid metal-halides, metal ion doping, X-ray absorption spectroscopy, X-ray diffraction and exciton diffusion

Research Scope: Doping is an attractive way to achieve desirable optical, electronic, spintronic, and magnetic properties in semiconductors. In lead halide perovskites, various foreign metal ions, including mono, bi, and trivalent ions, have been introduced to improve their optoelectronic properties. [1–3] More specifically, the emission quantum yields and the stability of perovskites and their devices, such as LEDs and solar cells, have been dramatically improved by doping. [3–6] In addition, doping with ferromagnetic ions such as Mn^{2+} and Ni^{2+} has led to exciting new applications in spintronic, nonlinear optics, and quantum information. [1,2] While it is apparent that the dopant ion can bring exceptional properties to perovskites, *a fundamental understanding of their local environment, such as bonding inside the perovskite host and their coordination, is important. Seeking insights into these atomic-level details is not trivial due to the limitations of many traditional techniques. In addition, the dopant ions may be randomly distributed in the lattice. Therefore, we proposed employing state-of-the-art X-ray absorption spectroscopy to probe the local environment of dopant ions. XAS is element-specific, which can provide a complete picture of the oxidation state, coordination, and bonding environment of the element of interest.* By linking this atom-level structural information to their property, we can establish a strong structure-property relationship.
In this report, we demonstrate i) exciton diffusion in 2D Mn^{2+} doped PEA_2PbBr_6 perovskites. From the XRD analyses, we determined that Mn^{2+} ions are occupying an interstitial position, and the transport of excitations is significantly hampered by these dopant ions. ii) By altering the symmetry of Sb^{3+} doped double perovskite using a rigid A-site ion, we produced double perovskite crystals owing to the changes in the degeneracy of their Sb^{3+} excited states.

Recent Progress

Exciton diffusion in Mn^{2+} doped 2D PEA_2PbBr_6 perovskite crystals: In this project, the exciton diffusion in Mn^{2+} doped 2D PEA_2PbBr_6 perovskites was investigated by transient PL microscopy in collaboration with Prof. Ferry Prins at the University of Madrid. These Mn^{2+} doped 2D perovskites were synthesized using the acid precipitation method, and their crystal structure was analyzed using scXRD (**Figure 1a**) and powder XRD. From the powder XRD analysis, we observed a shift in the characteristic diffraction peak to a lower angle with Mn^{2+} doping, which is

typically observed when the dopant ion resides in the interstitial position (**Figure 1b**). The preliminary EXAFS studies support this: the coordination around the Mn^{2+} is < 6, and if the Mn^{2+} substitutes Mn^{2+} sites, one would expect the coordination of 6 (**Figure 1c**). Consequently, the exciton diffusion in perovskite hosts is significantly hampered by the Mn^{2+} doping (**Figure 1d&e**). Most importantly, the results revealed that the distance traveled by the exciton to reach the Mn^{2+} states is larger than the estimated value from the actual Mn% obtained by ICP-MS. We attribute these to either the inhomogeneous distribution of Mn dopant ions or strong exciton-polaron interactions. These studies provided key insights into the exciton dynamics in doped perovskite lattices.

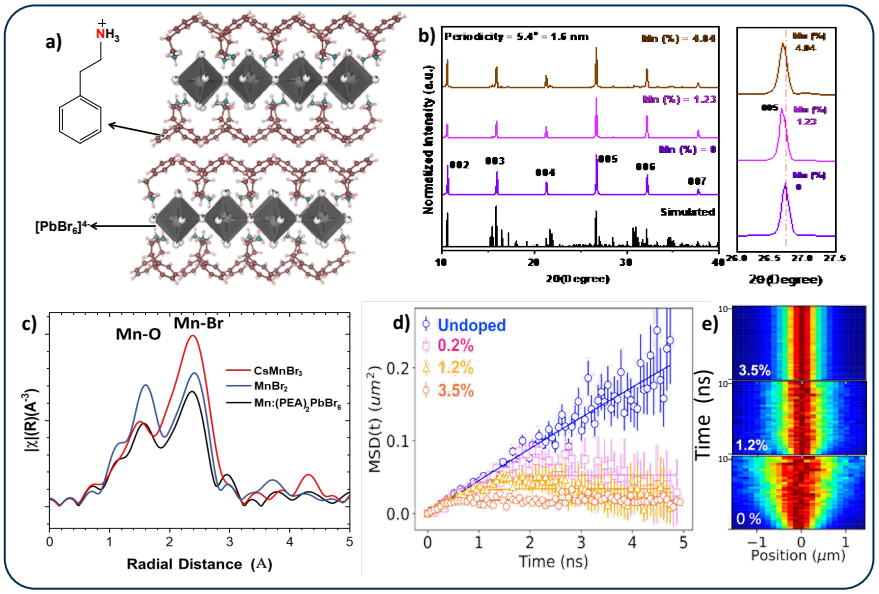

Figure 5 a) Crystal structure of 2D PEA_2PbBr_6, b) powder XRD pattern with and without Mn doping, and the enlarged region showing the peak shift, c) Mn k-edge EXAFS of doped perovskites plotted on R-space showing a decrease in the Mn^{2+}coordination, d) diffusivities of excitonic emission (420 nm), showing a decrease in diffusivities with Mn^{2+} doping, and e) respective 2D plot of exciton diffusion with space, showing narrowing of the diffusion with an increase in Mn doping.

Effect of structural distortions on the emission characteristic of Sb^{3+} dopant ions in double perovskite hosts: Here, we have developed a highly distorted/asymmetric double perovskite system with a triclinic crystal structure in the ground state. We used this distorted system as a host and doped with luminescent Sb^{3+} ions to study the impact of ground state distortions on the excited state behavior of Sb^{3+} ions. Unlike symmetric structures, the distorted hosts can facilitate the formation of multiple self-trapped excitons (STEs) in the dopant ions. Consequently, they can alter the emission from the dopant ions. Supporting this hypothesis, we observed two distinct emission peaks from Sb^{3+} ions when doped in an asymmetric double perovskite host, whereas, in the symmetric lattice, it showed only one peak. This is attributed to the lifting of the degeneracy of A-band emission owing to the formation of two isolated STEs in the excited state of Sb^{3+} ions. Such a phenomenon was never experimentally demonstrated by any other reports. Preliminary computational data also supports this hypothesis. In the excited state, Sb^{3+} ions showed more structural distortion with Sb-X bond elongation along the Z axis and contraction along the XY plane, supporting the experimental data. Overall, this work provides insights into how the optical properties of a dopant ion are dependent on the symmetry of the host lattice.

References

[1] Y. Zhou, J. Chen, O. M. Bakr, and H.-T. Sun, *Metal-Doped Lead Halide Perovskites: Synthesis, Properties, and Optoelectronic Applications*, Chem. Mater. **30**, 6589 (2018).
[2] T. Neumann, S. Feldmann, P. Moser, A. Delhomme, J. Zerhoch, T. van de Goor, S. Wang, M. Dyksik, T. Winkler, J. J. Finley, P. Plochocka, M. S. Brandt, C. Faugeras, A. V Stier, and F. Deschler, *Manganese Doping for Enhanced Magnetic Brightening and Circular Polarization Control of Dark Excitons in Paramagnetic Layered Hybrid Metal-Halide Perovskites*, Nat. Commun. **12**, 3489 (2021).
[3] A. Fakharuddin, M. K. Gangishetty, M. Abdi-Jalebi, S.-H. Chin, A. R. bin Mohd Yusoff, D. N. Congreve, W. Tress, F. Deschler, M. Vasilopoulou, and H. J. Bolink, *Perovskite Light-Emitting Diodes*, Nat. Electron. **5**, 203 (2022).
[4] S. Hou, M. K. Gangishetty, Q. Quan, and D. N. Congreve, *Efficient Blue and White Perovskite Light-Emitting Diodes via Manganese Doping*, Joule **2**, 2421 (2018).
[5] M. K. Gangishetty, S. N. Sanders, and D. N. Congreve, *Mn^{2+} Doping Enhances the Brightness, Efficiency, and Stability of Bulk Perovskite Light-Emitting Diodes*, ACS Photonics **6**, (2019).
[6] S. Feldmann, M. K. Gangishetty, I. Bravić, T. Neumann, B. Peng, T. Winkler, R. H. Friend, B. Monserrat, D. N. Congreve, and F. Deschler, *Charge Carrier Localization in Doped Perovskite Nanocrystals Enhances Radiative Recombination*, J. Am. Chem. Soc. **143**, 8647 (2021).

Publications

[1]. A. S. Kshirsagar,* K. A. Koch, A. S. Kandada, and M. K. Gangishetty,* *Unraveling the Luminescence Quenching Mechanism in Strong and Weak Quantum-Confined CsPbBr3 Triggered by Triarylamine-Based Hole Transport Layers,* JACS Au **4**, 1229 (2024).

Compositional Control of Fundamental Electronic and Magnetic Properties of Ordered Layered Multielemental MXenes

PI: Yury Gogotsi, Co-PI: Steven May

Keywords: MXene, electronic properties, 2D materials, synthesis

Research Scope

MXenes are a family of two-dimensional transition metal carbides, nitrides, and carbonitrides defined by a chemical composition of $M_{n+1}X_nT_x$, that can include a variety of transition metals on the M-site, carbon, nitrogen and/or oxygen on the X-site, and surface functional groups denoted as T_x. This material family is remarkable for its compositional and structural versatility, as the number of layers (n) can range from 1 to 4, and in-plane and out-of-plane M-site ordering can be realized in multi-M MXenes.[1-3] This research project focuses on obtaining new insights into fundamental electronic and magnetic properties of MXenes through control of the M and T_x compositions. Here, we aim to develop new synthetic strategies to realize delaminated MXenes with controllable and uniform surface terminations. Leveraging these and other synthetic approaches, we seek to realize MXenes with long-range magnetic ordering or enhanced magnetic responses. We are also investigating how different surface terminations impact intrinsic electronic transport through measurements on single-flake devices.

Recent Progress

Enhanced magnetic susceptibility in MXenes through dilute Co and Ni incorporation: We have developed an approach for increasing the magnetic response of $Ti_3C_2T_x$ MXene through the incorporation of Ni and Co atoms.[4] The synthesis of Co-$Ti_3C_2T_x$ and Ni-$Ti_3C_2T_x$ was carried out by mixing delaminated $Ti_3C_2T_x$ aqueous dispersions with $CoCl_2$ and $NiCl_2$ salt solutions, respectively. The resultant materials show no signs of transition metal or chloride-based secondary phases for Co:Ti ratios up to 0.075:1, with nanofocused x-ray fluorescence (XRF) mapping confirming a uniform distribution of Co through the MXene flakes (Fig. 1). The room temperature magnetic susceptibility of the Co- and Ni-incorporated $Ti_3C_2T_x$ is enhanced compared to pristine $Ti_3C_2T_x$ by factors of greater than 50 and 10 (Fig. 1). Additionally, the conductivity in Co-$Ti_3C_2T_x$ and Ni-$Ti_3C_2T_x$ remains metallic. We anticipate that this approach can be utilized for incorporation of other transition metal elements with magnetic activity, with implications for applications such as electromagnetic energy absorption.

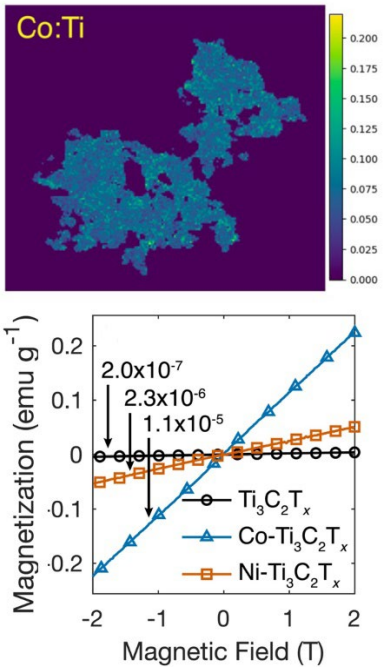

Fig. 1. (top) XRF results showing a uniform distribution of Co within a $Ti_3C_2T_x$ flake. (bottom) Room temperature magnetometry results showing significantly enhanced susceptibility in Co-$Ti_3C_2T_x$ and Ni-$Ti_3C_2T_x$ compared to $Ti_3C_2T_x$. Adapted from Ref. [4].

Delamination of $Ti_3C_2Cl_2$ synthesized using molten salt etching: Conventional synthesis routes for MXenes lead to mixed and inhomogeneous surface terminations as well as related chemistries, which present challenges for stabilizing magnetic order, enhancing electronic conductivity, and mitigating long-term material degradation. Lewis acid molten salt (LAMS) etching has emerged as an alternative synthesis approach that enables uniform halogen terminations.[5,6] We have overcome a significant obstacle to wider-utilization of the LAMS approach by developing a safe and straightforward method for delamination of LAMS-synthesized MXenes using LiCl as the delaminating agent (Fig. 2). $Ti_3C_2Cl_2$ films produced using our approach exhibit high electrical conductivity, are flexible, and are stable against degradation even when exposed to high humidity.[7] The expansion of this approach to other MXenes will dramatically increase the range and stability of MXene chemistries available for research and applications.

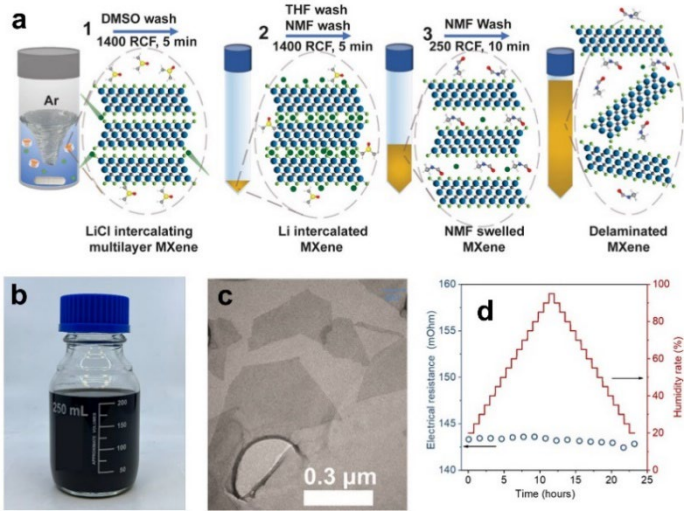

Fig. 2. (a) Schematic of the delamination process. (b) Optical image of a delaminated $Ti_3C_2Cl_2$ solution. (c) Transmission electron micrograph of single-layer $Ti_3C_2Cl_2$ flakes. (d) *In situ* measurement of electronic resistance as a function of relative humidity. Adapted from Ref. [7].

Quantum transport phenomenon in $Ti_3C_2T_x$ single flake measurements: We have used temperature- and magnetic field-dependent electronic transport measurements to confirm the presence of weak localization in metallic $Ti_3C_2T_x$ single flakes. Weak localization emerges in metallic materials owing to quantum interference effects of backscattered electronic wavefunctions. We find that the negative magnetoresistance (MR) exhibits a field- and angle-dependence in agreement with weak localization (Fig. 3), and that the MR magnitude correlates with the onset temperature for the resistance upturn, indicating the role of disorder and defects in magnetotransport. Analysis of the field-dependent MR enables us to extract values of phase coherence lengths. Our study conclusively demonstrates that metallic MXenes can exhibit quantum transport phenomena when probed in the single flake limit that enables intrinsic electronic behavior to dominate.

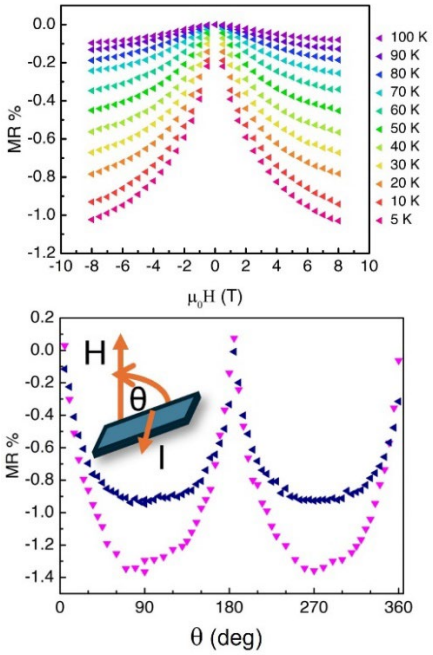

Fig. 3. (top) Magnetoresistance measurements of a multilayer $Ti_3C_2T_x$ single-flake device; (bottom) Angle-dependent measurements from two different samples both showing behavior characteristic of weak localization.

References

1. M. Naguib, M. W. Barsoum, Y. Gogotsi, *Ten Years of Progress in the Synthesis and Development of MXenes*, Advanced Materials **33**, 2103393 (2021).

2. B. Anasori, M. R. Lukatskaya, Y. Gogotsi, *2D metal carbides and nitrides (MXenes) for energy storage*, Nature Reviews Materials **2**, 16098 (2017).

3. A. VahidMohammadi, J. Rosen, Y. Gogotsi, *The world of two-dimensional carbides and nitrides (MXenes)*, Science **372**, eabf1581 (2021).

4. Y. Yang, M. Anayee, A. Pattammattel, M. Shekhirev, R. (John) Wang, X. Huang, Y. S. Chu, Y. Gogotsi, S. J. May, *Enhanced magnetic susceptibility in $Ti_3C_2T_x$ MXene with Co and Ni incorporation*, Nanoscale **16**, 5760 (2024).

5. M. Li, J. Lu, K. Luo, Y. Li, K. Chang, K. Chen, J. Zhou, J. Rosen, L. Hultman, P. Eklund, P. O. A. Persson, S. Du, Z. Chai, Z. Huang, Q. Huang, *Element Replacement Approach by Reaction with Lewis Acidic Molten Salts to Synthesize Nanolaminated MAX Phases and MXenes*, Journal of the American Chemical Society **141**, 4730-4737 (2019).

6. V. Kamysbayev, A. S. Filatov, H. Hu, X. Rui, F. Lagunas, D. Wang, R. F. Klie, D. V. Talapin, *Covalent surface modifications and superconductivity of two-dimensional metal carbide MXenes*. Science **369**, 979 (2020).

7. T. Zhang, K. Shevhuck, R. J. Wang, H. Kim, J. Hourani, Y. Gogotsi, *Delamination of Chlorine-Terminated MXene Produced Using Molten Salt Etching*, Chemistry of Materials **36**, 1998 (2024).

Publications

1. B. E. Sartor, T. Zhang, C. P. Muzzillo, C. Lee, R. Muzzio, Y. Gogotsi, M. O. Reese, A. D. Taylor, *Hierarchical Transparent Back Contacts for Bifacial CdTe PV*, ACS Energy Letters **9**, 1617 (2024).

2. Y. Yang, M. Anayee, A. Pattammattel, M. Shekhirev, R. (John) Wang, X. Huang, Y. S. Chu, Y. Gogotsi, S. J. May, *Enhanced magnetic susceptibility in $Ti_3C_2T_x$ MXene with Co and Ni incorporation*, Nanoscale **16**, 5760 (2024).

3. M. Lounasvuori, T. Zhang, Y. Gogotsi, T. Petit, *Tuning the Microenvironment of Water Confined in $Ti_3C_2T_x$ MXene by Cation Intercalation*, Journal of Physical Chemistry C **128**, 2803 (2024).

4. T. Zhang, K. Shevhuck, R. J. Wang, H. Kim, J. Hourani, Y. Gogotsi, *Delamination of Chlorine-Terminated MXene Produced Using Molten Salt Etching*, Chemistry of Materials **36**, 1998 (2024).

5. I. Roslyk, I. Baginskiy, V. Zahorodna, O. Gogotsi, S. Ippolito, Y. Gogotsi, *Porous Ti_3AlC_2 MAX phase enables efficient synthesis of $Ti_3C_2T_x$ MXene*, International Journal of Applied Ceramic Technology **21**, 2605 (2024).

6. D. Popple, M. Shekhirev, C. H. Dai, P. Kim, K. X. Wang, P. Ashby, B. A. Helms, Y. Gogotsi, T. P. Russell, A. Zettl, *All-Liquid Reconfigurable Electronics Using Jammed MXene Interfaces*, Advanced Materials **35**, 2208148 (2023).

7. T. Zhang, C. E. Shuck, K. Shevchuk, M. Anayee Y. Gogotsi, *Synthesis of Three Families of Titanium Carbonitride MXenes*, Journal of the American Chemical Society **145**, 22374 (2023).

8. Y. Yang, M. Han, C. E. Shuck, R. K. Sah, J. R. Paudel, A. X. Gray, Y. Gogotsi, S. J. May, *Correlating electronic properties with M-site composition in solid solution $Ti_yNb_{2-y}CT_x$ MXenes*, 2D Materials **10**, 014011 (2023).

9. M. Han, C. E. Shuck, A. Singh, Y. Yang, A. C. Foucher, A. Goad, B. McBride, S. J. May, V. B. Shenoy, E. A. Stach, Y. Gogotsi, *Efficient microwave absorption with $V_{n+1}C_nT_x$ MXenes*, Cell Reports Physical Science 3, 101073 (2022).

10. P. P. Michalowski, M. Anayee, T. S. Mathis, S. Kozdra, A. Wojcik, K. Hantanasirisakul, I. Jozwik, A. Piatkowska, M. Mozdzonek, A. Malinowska, R. Diduszko, E. Wierzbicka, Y. Gogotsi, *Oxycarbide MXenes and MAX phases identification using monoatomic layer-by-layer analysis with ultralow-energy secondary-ion mass spectrometry*, Nature Nanotechnology 17, 1192 (2022).

Shaping Symmetry and Molding Morphology of Triply-Periodic Assemblies via Molecular Design and Processing of Block Copolymers

Gregory M. Grason; E. Bryan Coughlin, Polymer Science & Engineering, UMass Amherst
Edwin L. Thomas, Materials Science & Engineering, Texas A&M University

Keywords: supramolecular assembly, triply-periodic networks, 3D multiscale characterization, molecular design principles

Research Scope

This project aims to uncover molecular design rules for block copolymer (BCP) assemblies of triply-periodic network (TPN) phases. While they have been a target of "bottom up" approaches to nanostructured, hybrid materials[R1,R2], the ability to manipulate the tubular network morphology of TPN assemblies beyond the double-gyroid (DG) has advanced relatively little. This project seeks the fundamental knowledge needed for: i) tailorable molecular design that achieves non-canonical TPN symmetries; and ii) unprecedented control over the intra-unit cell morphology of TPN and local network node functionality. Collaborative efforts include advancing theory of molecule-to-TPN morphology map; novel characterization/metrology of sub-domain morphology; and synthesis of precisely defined and labeled BCP for direct imaging of key nano-scale features.

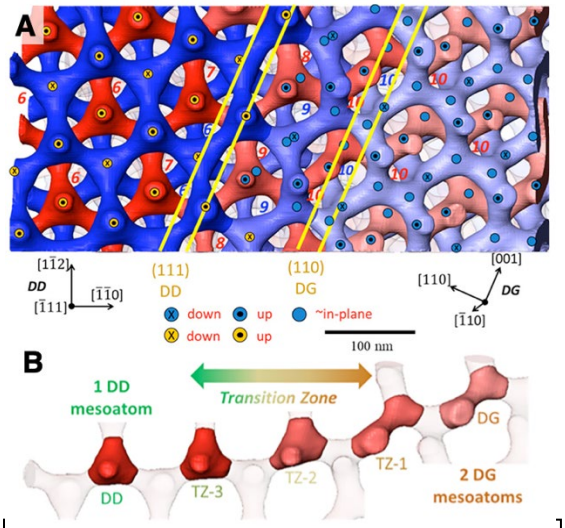

Fig. 1 – (A) Experimental reconstruction of DG to DD transformation in PS-PDMS diblocks. (B) Continuous pairwise fusion sequence of nodal "mesoatoms" .

Recent Progress

Visualizing and quantifying transformations between TPN crystal phases – Most soft matter systems are capable of exhibiting DG as well as double-diamond (DD) intercatenated network cubic network phases, but the specific transformation pathways between distinct crystalline mesostructures have remained obscure[R3-R6]. We used slice-and-view scanning-electron microscope (SVSEM)[R7] tomography to directly image this transformation for an arrested system of polystyrene-*b*-polydimethylsiloxane (PS-PDMS) block copolymers[P6]. We observed, for the first time (Fig. 1), that this transformation remarkably maintains network connectivity and inter-network cantenation across a finite width *gradient zone* . This provides the first spatially resolved view of the "reaction pathway" between the distinct trihedral "mesoatomic" nodal units of DG[P1], fusing along two strut directions, to form tetrahedral mesoatoms of the DD. The observation of a multi-unit cell transition zone opens up important questions about how this size scale might be

tailored to even larger (~multi-micron) sizes, raising the possibility of novel classes of graded network nanomaterials.

Thermodynamic landscape of continuous transitions between TPN crystals - Motivated to understand the observed continuous transformation pathway between DG and DD network crystals, we developed an extension of the medial strong-segregation theory (mSST)[R8] that computes the free energy of BCP networks of essentially *arbitrary arrangement of nodes and connected struts*, which is not possible based on current self-consistent field (SCF) methods. With this approach we computed the free energy landscapes that characterize the symmetry-breaking transformation pathway between DG and DD, which combines a tetragonal strain with a non-affine node-fusion/fission along transverse directions and which models reaction pathways for the 2 DG → 1 DD mesoatoms observed experimentally. These free energy landscapes show that cubic DD is generically an unstable saddle-point that can transform (without barrier) to the lower free energy DG, a thermodynamic feature that has been so far invisible to prior mean-field studies[R9] of the cubic mean-field states alone. We test this strong segregation prediction with SCF-based "computational rheology" studies of the extensional thermodynamics of cubic DD in neat diblock melts, showing DD to be unstable over nearly the entire equilibrium window of ordered phases. These results not only shed direct insight into the optimal pathways between the two canonical cubic network phases of block copolymers, but also imply that formation of widely reported *metastable, kinetically-trapped* DD states in diblocks requires stabilizing factors such blending with additional components or else epitaxially-stabilizing surfaces.

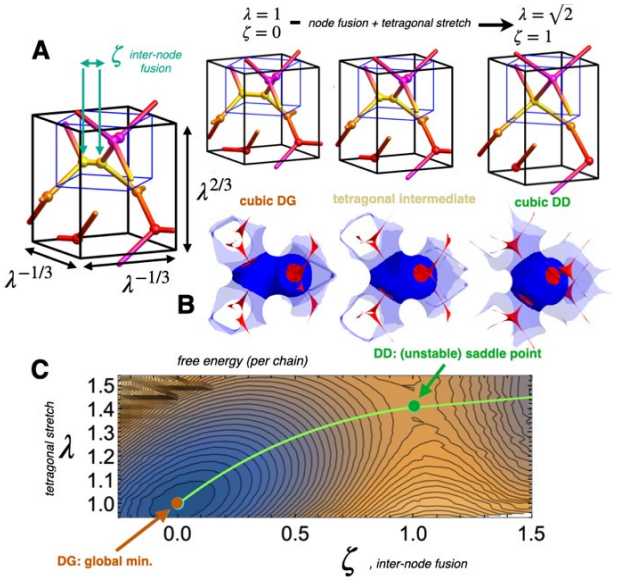

Fig. 2 – (A) Continuous tetragonal transformation of skelal graphs of cubic DG into cubic DD (B) and corresponding chain packing for medialSST model of free energy landscape (C) showing generic unstable mode of DD relative to DG.

Mapping medial chain packing in networks – Current efforts aim to experimentally map sub-domain chain packing in DG and DD networks. Prior theory has pointed to a new motif, known as *medial packing*[R8,P3,P4], that underlies the optimal entropy arrangements of brush-like domains in tubular networks, in which the high-free energy "hotspots" at the core of network domain take form of a twisted, web-like surface[P3]. To test this, we synthesized "host" polystyrene-*b*-polyl(2-vinyl pyridine (PS-P2VP) diblocks (low SEM contrast) and molecular "tags", long PS chains with short oligomeric PDMS (high SEM contrast). SCF predictions are used to guide synthetic design of labeled "tags" and ongoing experimental characterization of hotspot volumes by SVSEM .

References

R1. J.-H. Lee, C.-Y. Koh, J. P. Singer, S.-J. Martin, M. Maldovan, O. Stein, E. L. Thomas, *Ordered Polymer Structures for the Engineering of Photons and Phonons*, Advanced Materials **26**, 532 (2013), DOI: 10.1002/adma.201303456

R2. J. Werner, G. Rodriguez-Calero, H. Abruña, U. Wiesner, *Block copolymer derived 3-D interpenetrating multifunctional gyroidal nanohybrids for electrical energy storage*. Energy & Environmental Science **11**, 1261 (2018), DOI: 10.1039/C7EE03571C

R3. A. Fogden, S. T. Hyde, *Continuous transformations of cubic minimal surfaces* European Physical Journal B **7**, 91 (1999), DOI: 10.1007/s100510050592

R4. A. Squires, R. Templer, J. Seddon, J. Woenckhaus, R. Winter, T. Narayanan, S. Finet, *Kinetics and mechanism of the interconversion of the inverse bicontinuous cubic phases*, Physical Review E **72**, 011502 (2005), DOI: 10.1103/PhysRevE.72.011502

R5. C.-Y. Chu, W.-F. Lin, J.-C. Tsai, C.-S. Lai, S.-C.Lo. H.-L. Chen, T. Hashimoto, *Order-order transition between equilibrium ordered bicontinuous nanostructures of double diamond and double gyroid in stereoregular block copolymer*, Macromolecules **45**, 2471 (2012), DOI: 10.1021/ma202057g

R6. T. Oka, *Transformation between inverse bicontinuous cubic phases of a lipid from a diamond to gyroid*, Langmuir **31**, 2331 (2015), DOI:10.1021/acs.langmuir.5b02180

R7. X. Feng, C. Burke, M. Zhou, H. Guo, K. Yang, A. Reddy, I. Prasad, R.-M. Ho, A. Avgeropolous, G. M. Grason and E. L. Thomas, *Seeing mesoatomic distortions in soft matter crystals of a double gyroid block copolymer*, *Nature* **575**, 175 (2019), DOI: 10.1038/s41586-019-1706-1.

R8. A. Reddy, M. Dimitriyev and G. M. Grason, *Medial packing and elastic asymmetry stabilize the double-gyroid in block copolymers*, Nature Communications **13**, 2629 (2022), DOI: 10.1038/s41467-022-30343-2.

R9. M. W. Matsen, F. S. Bates, *Origins of complex self-assembly in block copolymers,* Macromolecules **29**, 7641 (1996), DOI:10.1021/ma960744q.

Publications (last 2 years)

P1. G. M. Grason and E. L. Thomas, *How does your gyroid Grow: A mesoatomic perspective on supramolecular soft matter crystals*, Phys. Rev. Materials **7** 045603 (2023), DOI: 10.1103/PhysRevMaterials.7.045603 .

P2. X. Feng, M. Dimitriyev and E. L. Thomas, *Soft, Malleable Double Diamond Twin,* Proceedings of the National Academy of Sciences of USA, **120** e221344112 (2023), DOI: 10.1073/pnas.2213441120 .

P3. M. Dimitriyev, A Reddy and G. M. Grason, *Medial packing, frustration and competing network phases in strongly-segregated block copolymers,* Macromolecules **56**, 7184 (2023) DOI: 10.1021/acs.macromol.3c01098.

P4. B. Greenvall, M. Dimitriyev and G. M. Grason, *Chain trajectories, domain shapes and terminal boundaries in block copolymers*, Journal of Polymer Science (2023), DOI: 10.1002/pol.20230748.

P5. W. Shan. V. Subramanian, X. Feng and E. L. Thomas, *The nature of crystallographic defects in noncrystalline tubular network block copolymers*, Giant **17**, 100216 (2024), DOI: 10.1016/j.giant.2023.100216.

P6. W. Shan and E. L. Thomas, *Gradient Transformation of the Double Gyroid to the Double Diamond in Soft Matter*, ACS Nano **18**, 9443 (2024), DOI: 10.1021/acsnano.3c11101.

P7. M. Dimitriyev, X. Feng, E. L. Thomas and G. M. Grason*, Non-affinity of liquid networks and bicontinuous mesophases,* Physical Review Letter*s* **132**, 218201 (2024), DOI: 10.1103/PhysRevLett.132.218201.

P8. M. Hu, H.-G. Seong, M. S. Dimitriyev, W. Hu, Z. Chan, G. M. Grason, T. Emrick and T. P. Russell, *Backbone stitching in bottlebrush copolymer mesodomains and the impact of sidechain crystallization,* submitted (2024).

P9. M. Dimitriyev, B. Greenvall, R. Mathew and G. M. Grason, *Double diamond networks in block copolymer melts: Not even metastable*, to be submitted (2024).

Connecting architecture and dynamics in single ion blends and comb-like polymer electrolytes

Prof. Lisa M. Hall (The Ohio State University) and Prof. Thomas H. Epps, III (University of Delaware)

Keywords: Polymer electrolytes, Glass transition temperature, Ion mobility, Molecular Dynamics simulations, Polymer blends

Research Scope

As proposed, we study the connection between macromolecular chemistry and architecture, nanostructure assembly, small-molecule distributions in nanoscale domains, spatial distributions of chain/segment motion, and ultimate transport properties. Specifically, the current work relates primarily to "Aim 1: Elucidate the relationships between local segmental motion and ion mobility…". We present experimental results on several polymer electrolyte systems and highlights of our semi-generic coarse-grained model, in which a few physically intuitive adjustable variables are used to capture key experimentally observed quantities, such as glass transition temperature (T_g) and cation transference number.

Recent Progress

Poly(oligo-oxyethylene methyl ether methacrylate) (POEM)[1,2] is a promising electrolyte in part due to its comb-like structure; its poly(ethylene oxide) (PEO) side chains complex with Li^+ but do not crystallize easily like linear PEO. To better describe such an architecture, we created a semi-generic coarse-grained model based on Kremer-Grest model[3,4] with angle bending potentials[6] and scaled interactions[5] between polymer beads set to match the side chains to PEO and the backbone to poly(methyl methacrylate) (PMMA) in terms of their Kuhn lengths and densities, along with each homopolymer's approximate T_g.

We also considered, both experimentally and computationally polymer-blend electrolytes, which consist of a single-ion-conducting polymer – poly [lithium sulfonyl(trifluoromethane sulfonyl)imide methacrylate] (PLiMTFSI) and an ion-conducting POEM. We investigated the impact of PLiMTFSI molecular weight (M_n) and ion concentration on the thermal and ion-conduction behavior. Experimental characterization found that at temperatures well above T_g, ion transport could be effectively decoupled from polymer segmental relaxation to realize rapid and highly selective ion conduction. Specifically, Li^+ conductivities approaching 1×10^{-2} S/cm at 150 °C and Li^+ transference number of ~0.9 were realized in this system. The blend is also electrochemically stable with a high limiting current density of 1.8 mA/cm^2 at an electrolyte thickness of 0.05 cm. We attributed the decoupled ion transport to the packing frustration of the glassy PLiMTFSI – sufficient percolating free volume was generated to produce effective ion diffusion pathways. Additionally, this decoupling was tunable as the ion transport could be altered from being closely coupled to the polymer segmental dynamics (Vogel–Tammann–Fulcher-like)

to hopping (Arrhenius-like) by increasing the PLiMTFSI M_n and ion concentration. Simulations of these systems applying the updated model discussed below are ongoing.

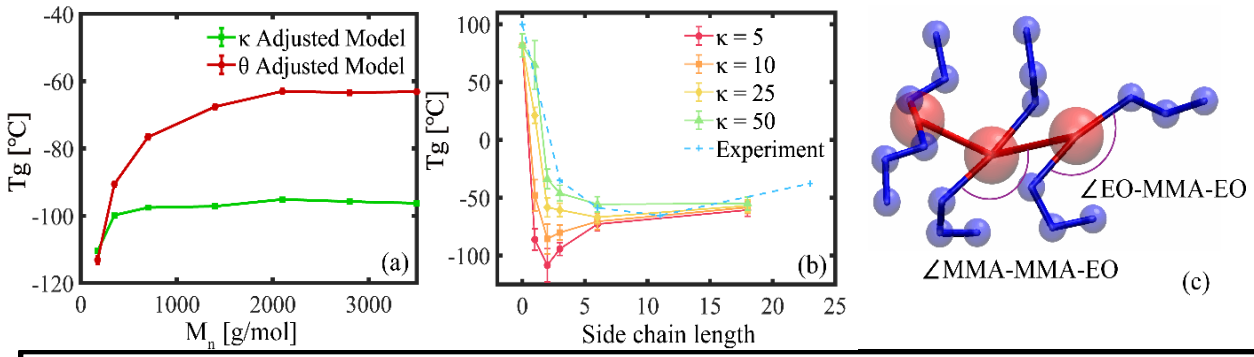

Figure 1. (a) T_g as a function of molecular weight of PEO model with different angle potentials. (b) T_g of POEM as shown in (c), with respect to EO side chain length at different bending potential strengths for EO-MMA-EO and MMA-MMA-EO angles. (c) Snapshot showing a part of POEM chain. Red and blue beads represent PMMA and PEO respectively.

Initial work with the updated simulation model considered salt-doped POEM and captured the impact of M_n and side chain length on T_g and reproduce the T_g trend for POEM with varying side chain length noted in prior experiments. Starting with linear polymers, we compared two strategies to parameterize bending potential to match the Kuhn length and density: adjusting the bond angle (q) at fixed bending strength ($\kappa = 100$) versus adjusting κ (using a much lower value) with a fixed bond angle setting of 180°. We found that M_n has a significant impact on T_g, corresponding to experimental observations, using the q-adjusted model but not the κ-adjusted model, as shown in Figure 1 (a).

We then simulated a comb system representing POEM with the q-adjusted model. The mapping to the Kuhn scale suggests a size difference such that 1 PMMA bead represents 2 repeat units to which 2 smaller PEO beads are attached. Thus, we further added angle potentials between the backbone and side chains, which ensures that each PEO is attached at a different point on the backbone. Figure 1(b) shows the impact of side chain length on T_g with different bending potential strength of MMA-MMA-EO ($q_0 = 90°$) and EO-MMA-EO ($q_0 = 180°$) angle, finding that we can reproduce the experimental trend.

We also studied the impact of ion-monomer interactions (including using an additional Lennard-Jones interaction strength between EO and Li along with a solvation potential, or applying Drude oscillators) on the T_g, domain sizes (for block polymer systems), cation transference number, and cation mobility distributions.

References

1. W. S. Young and T. H. Epps III, *Ionic Conductivities of Block Copolymer Electrolytes with Various Conducting Pathways: Sample Preparation and Processing Considerations*, Macromolecules, **45 (11)**, 4689–4697 (2012).
2. A. M. Elmér and P. Jannasch, *Solid Electrolyte Membranes from Semi-Interpenetrating Polymer Networks of PEG-Grafted Polymethacrylates and Poly(Methyl Methacrylate)*, Solid State Ionics, **177 (5-6)**, 573–579 (2006).
3. K. Kremer and G. S. Grest, *Dynamics of Entangled Linear Polymer Melts: A Molecular-Dynamics Simulation*, J. Chem. Phys., **92 (8)**, 5057–5086 (1990).
4. G. S. Grest, M. D. Lacasse, K. Kremer, and A. M. Gupta, *Efficient Continuum Model for Simulating Polymer Blends and Copolymers*, J. Chem. Phys., **105 (23)**, 10583–10594 (1996).
5. R. J. Lang, W. L. Merling, and D. S. Simmons, *Combined Dependence of Nanoconfined T_g on Interfacial Energy and Softness of Confinement*, ACS Macro Lett., **3 (8)**, 758–762 (2014).
6. R. Everaers, H. A. Karimi-Varzaneh, F. Fleck, N. Hojdis, and C. Svaneborg, *Kremer-Grest Models for Commodity Polymer Melts: Linking Theory, Experiment, and Simulation at the Kuhn Scale*, Macromolecules, **53 (6)**, 1901–1916 (2020).

Publications

1. M. Yang and T. H. Epps III, *Solid-State, Single-Ion Conducting, Polymer Blend Electrolytes with Enhanced Li+ Conduction, Electrochemical Stability, and Limiting Current Density,* Chemistry of Materials **36 (4)**, 1855–1869 (2024)
2. P. M. Ketkar, N. F. Pietra, A. G. Korovich, L. A. Madsen, and T. H. Epps, III, *Role of intra-domain heterogeneity on ion and polymer dynamics in block copolymer electrolytes: An approach for spatially resolving dynamics and ion transport,* Macromolecules, **56 (21)**, 8404-8416 (2023).
3. N. F. Pietra, A. G. Korovich, L. A. Madsen, P. M. Ketkar, and T. H. Epps, III, *Role of intra-domain heterogeneity on ion and polymer dynamics in block copolymer electrolytes: Investigating interfacial mobility and ion-specific dynamics and transport,* Macromolecules, **56 (21)**, 8393-8403 (2023).
4. M. Fan, K.-H. Shen, and L. M. Hall, *Effect of Tethering Anions in Block Copolymer Electrolytes via Molecular Dynamics Simulations*, Macromolecules **55 (17)**, 7945 (2022).

Liquid-metal electrodes for low-cost and low temperature solid state batteries for long duration energy storage

Kelsey B. Hatzell, Princeton University, Andlinger Center for Energy and The Environment

Keywords: Alkali metals, x-ray computed tomography, intermetallic, energy storage

Research Scope

Solid-state sodium-ion batteries (SSSBs) are a promising alternative to Li-ion batteries for their sustainability, low cost and improved safety, ideal for stationary and large-scale energy storage[1]. However, the solid-solid interface within a solid-state battery poses challenges for commercialization. Furthermore, loss of contact at electrode-electrolyte interfaces can drive heterogeneous current focusing inside the cell and accelerate failure. To overcome this challenge, a room-temperature liquid Na-K alloy (NaK) anode was proposed.[2-4] The ability of a liquid electrode to flow helps maintain the electrolyte-anode contact, avoids mechanical stress buildup, and suppresses metal dendrite growth. However, when serving as the Na source for SSSBs, NaK liquid anodes are subject to interfacial liquid-solid phase separation, since interfacial Na ion flux can drive precipitation of Na (upon Na plating) or K metal (upon Na stripping). Such phase separation would result in either contact loss or blockage of Na ion pathways, limiting the actual capacity of NaK anodes[5-6]. Currently such interfacial degradation processes are not well-understood because characterization of solid-state batteries is extremely challenging due to air sensitivity and complex solid-state battery configurations. The non-crystalline nature and high mobility of liquid Na-K alloy pose additional challenges for conventional characterization techniques.

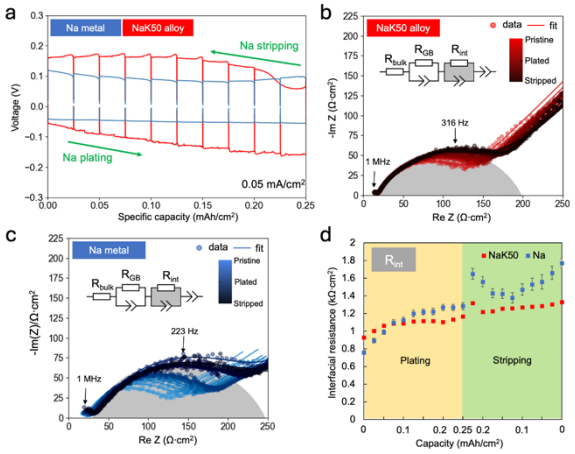

In-situ EIS test during Na plating-stripping on Na and NaK50 working electrodes. **a** Voltage profile of both cells. **b** *In-situ* EIS spectra and equivalent circuit for the NaK50 cell. **c** *In-situ* EIS spectra and equivalent circuit for the Na cell. **d** Interfacial resistance evolution as a function of capacity for both Na and NaK50 cells.

Recent Progress

Over the last year we conducted electrochemistry, diffraction, and x-ray imaging experiments. To probe the interfacial stability of NaK liquid anodes upon electrochemical cycling, Na plating-stripping test with *in-situ* EIS was performed on symmetric cells with Na or NaK50@CC anodes (**Figure 1**). For the convenience of description, the discharge process was referred to as the Na plating process and the charging process was referred to as the Na stripping process, all relative to one side of the two anodes. The NASICON surfaces in contact with NaK liquid were all coated with PEO in this experiment. For this test, the total Na plating-stripping capacity was limited to 0.25 mAh/cm^2 under a constant current density of 0.05 mA/cm^2. According to the phase diagram, no bulk phase transformation is expected for the NaK50 anode at this capacity. *In-situ* EIS results for both cells were fitted with the equivalent circuit drawn as the insets of **Figure 1b** and **41**, which attributed the major semicircle observed in the EIS of both cells to interfacial

charge transfer resistance. Over the whole Na plating-stripping process, both the Na and NaK50 anodes demonstrated slight increase in the interfacial resistance (**Figure 1b** and **1c**), as quantified in **Figure 1d** based on the equivalent circuit. These results show that under small Na plating-stripping capacity, the NaK50 liquid alloy anode maintains the anode-electrolyte interface contact similarly well as Na metal.

Liquid-solid phase separation in NaK liquid anodes upon electrochemical cycling can be directly characterized by non-destructive X-ray computed tomography imaging. *In-situ* XCT was performed on a symmetric NaK50/NASICON/NaK50 cell after Na plating/stripping with a special micro-cell was designed for this purpose. A sintered NASICON electrolyte with a 3 mm diameter was polished to ~ 200 μm thick, with NaK50@C paste applied on both sides as anodes. The cell was cycled to a stage where one anode is Na-stripped and the other is Na-plated then taken to the XCT microscope for 3D imaging. Based on the Na-K phase diagram, NaK50 alloy is more prone to liquid-solid phase separation upon Na plating. Imaging shows that the Na-stripped NaK50 anode is more uniform compared to the Na-plated NaK50 anode side, where large areas with different imaging contrasts can be observed. Future experiments plan to examine the phase segregation with phase contrast x-ray computed tomography.

References

1. Gür, Turgut M. "Review of electrical energy storage technologies, materials and systems: challenges and prospects for large-scale grid storage." *Energy & Environmental Science* 11.10 (2018): 2696-2767.
2. Dunn, Bruce, Haresh Kamath, and Jean-Marie Tarascon. "Electrical energy storage for the grid: a battery of choices." *Science* 334.6058 (2011): 928-935.
3. Ding, Yu, Xuelin Guo, and Guihua Yu. "Next-generation liquid metal batteries based on the chemistry of fusible alloys." *ACS central science* 6.8 (2020): 1355-1366.
4. Guo, X., Zhang, L., Ding, Y., Goodenough, J. B., & Yu, G. (2019). Room-temperature liquid metal and alloy systems for energy storage applications. *Energy & Environmental Science*, *12*(9), 2605-2619.
5. Ding, Y., Guo, X., Qian, Y., & Yu, G. (2020). Low-temperature multielement fusible alloy-based molten sodium batteries for grid-scale energy storage. *ACS central science*, *6*(12), 2287-2293.
6. Koh, H., Hassan, M. H., Lin, S., Wang, L., Stach, E. A., & Detsi, E. (2024). Liquid Na-K alloy is not viable anode material for High-Performance Na-Ion batteries. *Chemical Engineering Journal*, *490*, 151578.

Publications

Two publication in preparation. No published papers.

Nature-Derived Materials for Redox Flow Batteries

Shabnam Hematian

Keywords: Redox Flow Batteries, Perylenequinones, Fungal Metabolites, Multielectron, Organic Electrolytes

Research Scope

Redox flow batteries are a promising technology in the search to find efficient large-scale storage options for the electricity generated by intermittent renewable energy sources such as solar, wind, or hydropower. The battery consists of negative (i.e., anolyte) and positive (i.e., catholyte) electrolytes separated by an ionically conducting membrane. The charging/discharging efficiency and the amount of energy stored in a redox flow battery depends on the properties of the electrolytes. Wide-scale utilization of this technology has been limited by the availability and cost of electrolyte materials as well as loss of capacity over time, particularly those focused on metal-based redox species.[1-3] Organic redox flow batteries are promising alternatives due to their high structural diversity and synthetic tunability.[4-6] This project takes inspiration from Nature by utilizing fungal or plant perylenequinones (PQs) that can be biosynthesized via fermentation or in vitro cultures for energy storage research to improve the efficiency and storage capacity of redox flow batteries.

Using the redox active PQs to create new electrolyte materials enables reactions with a higher number of electrons (i.e., higher charge) as anolyte, catholyte, or both in a symmetric flow battery. In addition to being more efficient, environmentally friendly, and sustainable, the same electrolyte material can be used in both positive and negative components of the battery avoiding cross-contamination and offering promising features such as low cost, an easy manufacturing process, greater stability, and simple recycling post-process which are attractive for the application of large-scale stationary energy storage. Pushing the boundaries of what can be accomplished with these Nature optimized molecules, their performance is determined in a membrane-free setup with two immiscible redox electrolytes. This approach presents the first example of a true symmetric biphasic redox flow battery.

Recent Progress

Our initial studies have been focused on hypocrellin B (**HB, Figure 1**), due to its favorable electrochemical and chemical behavior as well as its stability and accessibility.[7] We have investigated

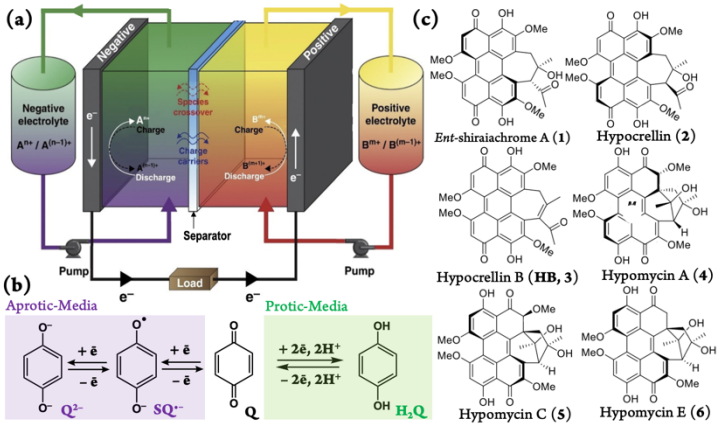

Figure 1. (a) Schematic representation of a redox flow battery, (b) redox reactions of quinones in protic and aprotic solutions, and (c) examples of fungal PQs investigated in our project.

the electrochemical behavior of HB in both acetonitrile (MeCN) and 2-methyltetrahydrofuran (2-MeTHF) along with the counterion dependencies in MeCN using two cations—tetrabutylammonium and lithium—and two anions—hexafluorophosphate and tetra(pentafluorophenyl)borate. Our findings indicate that while the type of anion has minimal influence on the electrochemical behavior of HB, the choice of cation notably affects its 2-electron reduction events.

Our titration experiments demonstrated significant variations in the binding affinities of HB for cations such as lithium across different redox states, i.e., HB, $HB^{\bullet-}$, and HB^{2-}. Additionally, our preliminary findings indicate that the electrochemical behavior of HB in the presence of Li^+ is more stable on a platinum electrode surface as compared to a glassy carbon electrode. This stability may be attributed to the absence of π–π stacking and van der Waals interactions with the electrode surface.

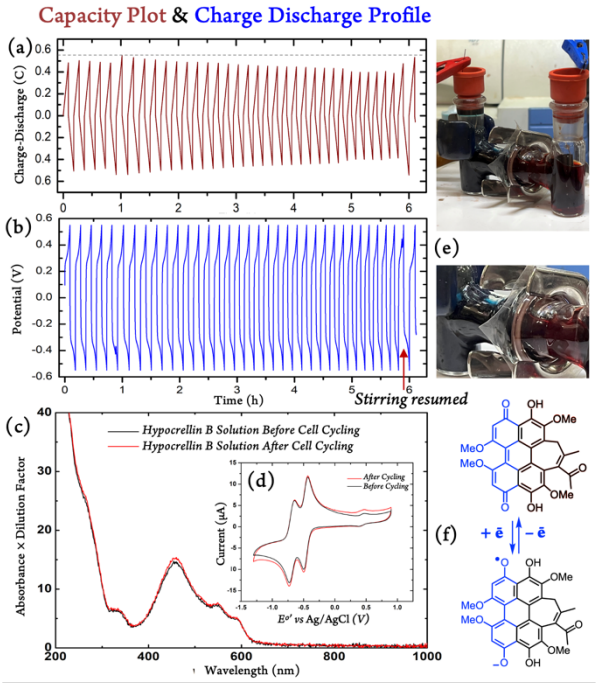

Figure 2. Galvanostatic cycling of 0.9 mM Hypocrellin B in acetonitrile with 200 mM of [(*n*Bu$_4$)N][PF$_6$] in a symmetric H-Cell. Theoretical capacity is 0.69 C. (a) Charge discharge profile; (b) Capacity plot; (c) UV-vis spectra before and after cycling experiment; (d) CV curves before and after cycling experiment. (e) H-cell image containing single electron reduced form (blue) and neutral form (red) of hypocrellin B (HB, f).

We also conducted galvanostatic cycling with potential limitation (GCPL) of HB in a zero-voltage symmetric H-cell, obtaining charge/discharge profiles, and performing UV-vis and electrochemical analyses of the electrolyte before and after cycling (**Figure 2**). The data confirmed the excellent stability and electrochemical reversibility of HB. Furthermore, we carried out galvanostatic full-cell cycling experiments pairing HB with ferrocene or another redox-active organic molecule (2,2′-azino-bis(3-ethylbenzothiazoline-6-sulfonate) diammonium salt; ABTS). We evaluated permeability through a Nafion 117 cation exchange membrane by monitoring UV-vis absorbance of crossed-over concentrations in both sides of H-cells over time. Our initial findings indicate that larger size and the negative sulfonate charge reduce crossover. Ferrocene exhibited the most significant crossover, whereas HB maintained the lowest crossover among the three redox-active compounds, potentially due to its larger size.

With promising results obtained from the static cell cycling, we recently evaluated the HB performance in a zero- voltage symmetric flow cell condition. Throughout the cycling, the cell demonstrated an excellent coulombic efficiency and minimal capacity drop. These findings along with other related discoveries central to the overall performance of PQs will be presented.

References

1. G. L. Soloveichik, *Flow Batteries: Current Status and Trends*, Chem. Rev. **115** (20), 11533 (2015).

2. C. Zhang, L. Zhang, Y. Ding, S. Peng, X. Guo, Y. Zhao, G. He, G. Yu, *Progress and Prospects of Next-Generation Redox Flow Batteries,* Energy Storage Mater. **15**, 324 (2018).

3. B. Huskinson, M. P. Marshak, C. Suh, S. Er, M. R. Gerhardt, C. J. Galvin, X. Chen, A. Aspuru-Guzik, R. G. Gordon, M. J. Aziz, *A Metal-Free Organic–Inorganic Aqueous Flow Battery*, Nature **505** (7482), 195 (2014).

4. X. Fang, Z., Li, Y., Zhao, D., Yue, L. Zhang, X. Wei, *Multielectron Organic Redoxmers for Energy-Dense Redox Flow Batteries,* ACS Materials Letters **4**, 277 (2022).

5. X. Wei, W. Pan, W. Duan, A. Hollas, Z. Yang, B. Li, Z. Nie, J. Liu, D. Reed, W. Wang, V. Sprenkle, *Materials and Systems for Organic Redox Flow Batteries: Status and Challenges*, ACS Energy Lett. **2** (9), 2187 (2017).

6. A. W. Lantz, S. A. Shavalier, W. Schroeder, P. G. Rasmussen, *Evaluation of an Aqueous Biphenol- and Anthraquinone-Based Electrolyte Redox Flow Battery.* ACS Applied Energy Materials **2** (11), 7893 (2019).

7. Z. Y. Al Subeh, A. L. Waldbusser, H. A. Raja, C. J. Pearce, K. L. Ho, M. J. Hall, M. R.; Probert, N. H. Oberlies, and S. Hematian, *Structural Diversity of Perylenequinones is Driven by their Redox Behavior*, J. Org. Chem. **87** (5), 2697 (2022).

Porous, Lightweight, and Semiconducting Chalcogel as High Energy Density Electrode for Li- and Na-ion Batteries

Saiful M. Islam (PI),[1] Chad Risko (Co-PI)[2]
[1]Department of Chemistry, Physics, and Atmospheric Sciences, Jackson State University, Jackson, MS, 39217, USA
[2]Department of Chemistry &; Center for Applied Energy Research, University of Kentucky, Lexington, KY, 40506-0055, USA
Keywords: sodium-sulfide batteries, lithium-sulfide batteries, chalcogel, and chalcocarbogel.

Research Scope

Chalcogenide-based (aero)gel, also known as chalcogel, represents a distinct category of porous, nanoaggregated materials characterized by their highly disordered and amorphous structure.[1] The predominant structural feature within chalcogel nanoparticles is the presence of a polysulfide backbone, which can mimic a sulfur equivalent electrode material for conversion-based Li-ion sulfide batteries.[2] This work explores the use of chalcogels in developing high-energy-density materials for lithium-ion battery electrodes. We have pioneered a novel carbonaceous-metal sulfide gel, "chalcocarbogels," which shows exceptional specific capacity and cyclic stability in both Li-ion and Na-ion batteries.[3] Our findings highlight the potential of chalcogenide-based gels in advancing energy storage technologies.

Recent Progress

Sulfur-based electrodes offer a high theoretical capacity (~1672 $mAh \cdot g^{-1}$) but face practical challenges due to poor cycling stability, low electrical conductivity, and significant dissolution of lithium polysulfide intermediates during charge-discharge cycles.[4] Recently, we investigated chalcogenide-based gels for use as sulfur conversion electrodes in lithium-ion batteries. Chalcogels are porous, semiconducting, nanoaggregated polysulfide-rich materials made from metal-chalcogenide clusters. The synergy of metal-ion-bound polysulfide chains and high-density porosity in these materials offers several advantages for lithium-ion batteries: improved energy density, ion diffusion, charge-discharge cycles, electrical conductivity, reduced polysulfide dissolution, minimal volume change, and ease of structural rearrangement during cycling.

The prospects of chalcogels, as addressed above, inspired us to design and synthesize sulfur-rich chalcogels for use in electrode materials for lithium-sulfide batteries. To this end, we synthesized chalcogels in the Mo-S system with diverse compositions and molecular structures of metal sulfide anionic clusters, which we refer to Mo_2S_{12}, Mo_3S_{13} (Fig. 1) and MoS_9 chalcogels. Additionally, we incorporated diverse 3d transition metals cations into the Mo-S chalcogel matrix, resulting in $M_xMo_2S_{12}$, and $M_xMo_3S_{13}$. To gain structural insights, we analyzed them through electron microscopy and X-ray (including synchrotron X-ray PDF, XANES, and EXAFS) along with AIMD simulations.

These chalcogels demonstrated impressive charge-discharge capacity and stability. For instance, Li/Mo_3S_{13} half-cells initially delivered 1013 $mAh \cdot g^{-1}$ and stabilized at 312 $mAh \cdot g^{-1}$ at a C/3 rate

after 140 cycles, showing sustained performance (Fig. 1).[5] Such high capacity and stability are attributed to the dense polysulfide and stable Mo-S coordination in Mo_3S_{13} chalcogel Incorporating 3d transition metals significantly reduced capacity loss and improved cyclic stability. For example, the Mn-incorporated Mo_3S_{13} gel showed an initial capacity of ~897 $mAh \cdot g^{-1}$ and retained ~571 $mAh \cdot g^{-1}$ after 100 cycles for its $Li/Mn_xMo_3S_{13}$ cell. The higher stability can be attributed to the addition of extra metal ions, which help sulfur remain in the electrode through M-S covalent interactions and form a local structure with smaller chains of polysulfides.

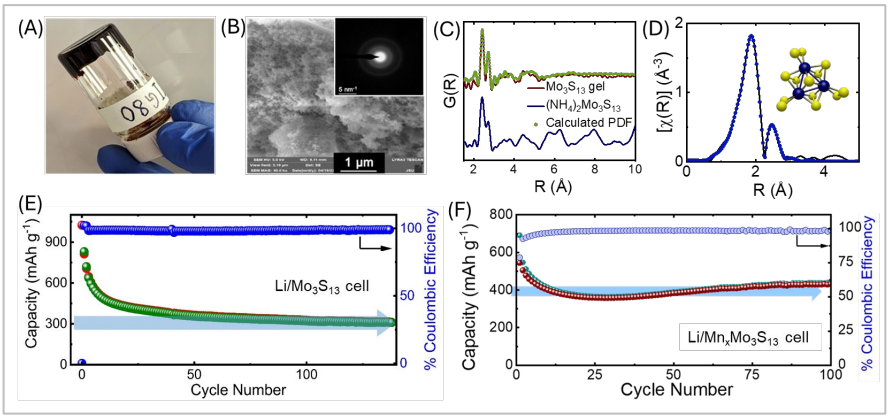

Fig. 1: Synthesis and characterization Mo3S13 chalcogels (A-D), and specific capacity vs cycle number for Li/Mo_3S_{13} (E) and $^*Li/Mn_xMo_3S_{13}$ cells (F). *Islam and Colleagues unpublished work, Jackson State University.

We also integrate graphene oxides into metal sulfides to synthesize amorphous chalcocarbogels, resulting in materials with remarkably high capacity and cyclic stability compared to pure chalcogels. For example, Li/MoSx-GO shows an initial specific capacity of ~1215 $mAh \cdot g^{-1}$ and maintains ~ ~700 $mAhg^{-1}$,[3] while $Li/Fe_{0.5}Mo_3S_{13}$-GO starts at ~696 $mAh \cdot g^{-1}$ and remains between 300-500 $mAh \cdot g^{-1}$ after 700 cycles (Fig. 2). This improvement is likely due to the formation of C-S bonds, which mitigate sulfur dissolution and increase the conductivity of the chalcocarbogel.

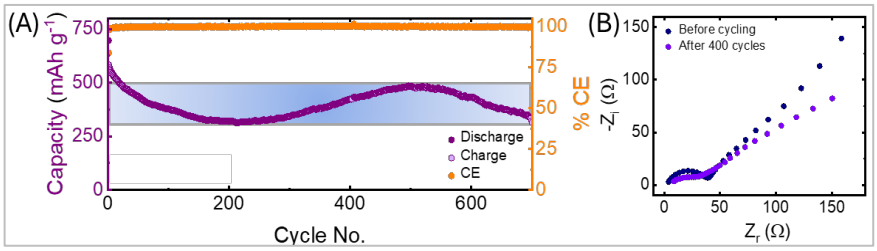

Fig. 2. Specific capacity vs cycle number and EIS (B) of $Li/Fe_xMo_3S_{13}$-GO cell (Islam and Colleagues Unpublished work, Jackson State University).

Overall, supported by this DOE EPSCoR grant, our research has uncovered new chemistry for lightweight, high-capacity, and stable lithium-ion battery electrodes. Future studies will focus on exploring their versatile compositions, understanding their local structure, and elucidating their charge-discharge properties and chemical reactivity during the electrochemical process.

References

(1) Bag, S.; Trikalitis, P. N.; Chupas, P. J.; Armatas, G. S.; Kanatzidis, M. G. Porous Semiconducting Gels and Aerogels from Chalcogenide Clusters. *Science* **2007**, *317* (5837), 490–493.

(2) Doan-Nguyen, V. V. T.; Subrahmanyam, K. S.; Butala, M. M.; Gerbec, J. A.; Islam, S. M.; Kanipe, K. N.; Wilson, C. E.; Balasubramanian, M.; Wiaderek, K. M.; Borkiewicz, O. J.; Chapman, K. W.; Chupas, P. J.; Moskovits, M.; Dunn, B. S.; Kanatzidis, M. G.; Seshadri, R. Molybdenum Polysulfide Chalcogels as High-Capacity, Anion-Redox-Driven Electrode Materials for Li-Ion Batteries. *Chem. Mater.* **2016**, *28* (22), 8357–8365.

(3) Islam, T.; Li, M.; Blanton, A.; Pitton, K. A.; Rao, K. R.; Bayat, S.; Wiaderek, K. M.; Weret, M. A.; Roy, S. C.; Feng, R.; Li, D.; Alam, R.; Nie, J.; Oketola, O.; Pramanik, A.; Guiton, B. S.; Risko, C.; Belharouak, I.; Amin, R.; Islam, S. M. Chalcocarbogels as High-Capacity and Cycle-Stable Electrode Materials for Lithium and Sodium Ion Batteries. *ACS Energy Lett.* **2024**, *9* (1), 1–9. https://doi.org/10.1021/acsenergylett.3c02112.

(4) Zhao, X.; Cheruvally, G.; Kim, C.; Cho, K.-K.; Ahn, H.-J.; Kim, K.-W.; Ahn, J.-H. Lithium/Sulfur Secondary Batteries: A Review. *J. Electrochem. Sci. Technol* **2016**, *7* (2), 97–114.

(5) Islam, T.; Chandra Roy, S.; Bayat, S.; Adigo Weret, M.; Hoffman, J. M.; Rao, K. R.; Sawicki, C.; Nie, J.; Alam, R.; Oketola, O.; Donley, C. L.; Kumbhar, A.; Feng, R.; Wiaderek, K. M.; Risko, C.; Amin, R.; Islam, S. M. Mo3S13 Chalcogel: A High-Capacity Electrode for Conversion-Based Li-Ion Batteries. *ChemSusChem* **2024**, *17* (11), e202400084.

Publication from DOE BES grant:

1. Islam, T.; Li, M.; Blanton, A.; Pitton, K. A.; Rao, K. R.; Bayat, S.; Wiaderek, K. M.; Weret, M. A.; Roy, S. C.; Feng, R.; Li, D.; Alam, R.; Nie, J.; Oketola, O.; Pramanik, A.; Guiton, B. S.; Risko, C.; Belharouak, I.; Amin, R.; Islam, S. M. Chalcocarbogels as High-Capacity and Cycle-Stable Electrode Materials for Lithium and Sodium Ion Batteries. *ACS Energy Lett.* **2024**, *9* (1), 1–9. https://doi.org/10.1021/acsenergylett.3c02112.
2. Islam, T.; Chandra Roy, S.; Bayat, S.; Adigo Weret, M.; Hoffman, J. M.; Rao, K. R.; Sawicki, C.; Nie, J.; Alam, R.; Oketola, O.; Donley, C. L.; Kumbhar, A.; Feng, R.; Wiaderek, K. M.; Risko, C.; Amin, R.; Islam, S. M. Mo3S13 Chalcogel: A High-Capacity Electrode for Conversion-Based Li-Ion Batteries. *ChemSusChem* **2024**, *17* (11), e202400084.

Understanding Structure, Phase Behavior, and Physical Properties of Polysulfamides and Polysulfamates using Simulations, Experiments, and Machine Learning

Arthi Jayaraman, University of Delaware; Ryan Hayward, University of Colorado-Boulder; Quentin Michaudel, Texas A&M University

Keywords: Polysulfamides, Simulations, Experiments, Machine Learning, Semi-crystallinity

Research Scope

The overarching goal of this project is to understand the structure, bulk phase behavior, and physical properties of a new family of polymers — polysulfamides and polysulfamates — with potential as chemically recyclable and high-performance materials. Our goal will be accomplished using synergistic experimental and computational approaches involving polymer synthesis, structure and thermal characterization, molecular modeling, simulations, and machine learning. This project leverages our recent advances in polymer synthesis and SuFEx click chemistry (Quentin Michaudel), our recent development and use of coarse-grained models for polymers exhibiting dominant H-bonding interaction (Arthi Jayaraman), and our expertise in solution and solid-state characterization of polymeric materials, including H-bonding systems (Ryan Hayward) to obtain a fundamental understanding on this new class of polymers that have the potential to serve as sustainable alternatives to analogous commodity polymers.

The specific aims are: ► Specific Aim 1: To understand hydrogen-bonding driven structural ordering of polysulfamides as a function of the molecular structure of the repeat unit. ► Specific Aim 2: To develop machine learning models to automate the classification and interpretation of the structural characterization results. ► Specific Aim 3: To extend the fundamental studies of molecular interactions and chain structure, physical properties, and bulk phase behavior to polysulfamates.

Recent Progress

During this second reporting period the members of the three labs – Jayaraman (Delaware), Hayward (Colorado), and Michaudel (Texas A&M) met as one group once every 2 months (roughly) and continued the efforts on the synthesis (Michaudel), characterization (Hayward), and computational (Jayaraman) tasks listed in the proposal.

In the **Michaudel lab,** Avinash Choudhury (2nd year grad. student) has synthesized a variety of polysulfamides (5) and *N,N'*-disubstituted sulfamides (35) to further elucidate the impact of the backbone/substituents on crystallinity. Polysulfamides and *N,N'*-disubstituted sulfamides are being thoroughly characterized using powder X-ray diffraction, as well as IR and NMR spectroscopies to generalize the trends reported in our previous joint publication with the Jayaraman group (*Macromolecules 2023, 56, 5033*). A collaboration has been initiated with Aaron Rossini (Iowa State University) to investigate the hydrogen bonding in these small and

macromolecules via 1H{14N} and 15N NMR experiments. 5 different samples have already been shipped. These tasks are along the lines of what was proposed for Specific Aim 1. The characterization data will be added to the existing training dataset being used for machine learning model development in the **Jayaraman lab** as proposed in Specific Aim 2. In parallel, Kate Doktor (5^{th} year grad. student) and Srutashini Das (2^{nd} year grad. student) have been developing methods to synthesize polysulfamates as proposed in Specific Aim 3. Two main strategies are being explored and conditions are currently being optimized to increase the molar masses of these polymers that have never been synthesized before. Thus far, 10 structurally different polysulfamates have been synthesized and characterized. The physical properties and recyclability profiles of these unknown polymers are currently analyzed.

For Specific Aim 1, Jay Shah (a 2nd year grad. student in **Jayaraman lab**) has been using atomistic modeling to improve the (older) coarse-grained (CG) model of polysulfamide developed by recent PhD graduate from Jayaraman lab – Zijie Wu (Macromolecules 2023, 56, 5033). Using the older and newly improved CG model Shah has also been studying how blending of two types of polysulfamides affect the extent of positional and orientational order in the assembled state; this tests the hypothesis that blending can be a way to tune the extent of semi-crystallinity. The preliminary blends results have been shared with team members in **Michaudel lab** to guide their experiments under Specific Aim 1.

With regards to Specific Aim 2, in **Hayward lab**, Matthew Ticknor (5th year grad. student) has been generating input data sets for training and testing the machine learning model development described above using DSC, PLOM, and WAXS for semi-crystalline polymers with systematically varying structures (e.g., degree of crystallinity). Since polysulfamides show complex behavior and have not previously been structurally characterized in detail, we have begun with poly(L-lactic acid) (PLLA) as a simpler and more well-studied model system to validate our methodology. Lalit Nagidi and Jay Shah in **Jayaraman lab** have developed new machine learning (ML) workflows for a) calculating the percentage of crystallinity from Differential Scanning Calorimetry (DSC) curves, b) calculating area of image occupied by crystals in polarized optical microscopy (PLOM) images, c) calculating the percentage of crystallinity from Wide Angle X-ray Scattering (WAXS) curves, and d) generating WAXS curves from PLOM images. This collaborative work between is being prepared into a manuscript for submission by August 2024.

Ongoing work in **Hayward lab** is focused on extending the above characterization techniques of PLLA to polysulfamides (Specific Aim 1) and polysulfamates (Specific Aim 3) being synthesized in **Michaudel lab**.

Publications SUPPORTED BY THIS BES PROJECT in the past two (2) years

1. S. Lu and A. Jayaraman* *Pair-Variational Autoencoders for Linking and Cross-Reconstruction of Characterization Data from Complementary Structural Characterization Techniques* JACS Au **3** (9), 2510-2521 (2023)
2. S. Lu, A. Jayaraman*, *Machine Learning for Analyses and Automation of Structural Characterization of Polymer Materials*, Progress in Polymer Science, 101828, (2024)
3. Z. Wu, J. Wu, Q. Michaudel*, A. Jayaraman*, *Investigating hydrogen bond-induced self-assembly of polysulfamides using molecular simulations and experiments*, Macromolecules **56**, *13, 5033–5049 (2023)*

High Electron Affinity Conjugated Polymers: Synthesis, Electron Transport and Discovery of New Class of Two-Dimensional Organic Solid-State Materials

Samson A. Jenekhe
Department of Chemical Engineering and Department of Chemistry
University of Washington, Seattle, WA 98195

Keywords: Conjugated polymers, electron transport, charge transfer complexes, electron-polarons, Peierls instability, ground-state electron transfer.

Research Scope

The two fields of *one-dimensional* organic solid-state materials – molecular charge- transfer complexes and π-conjugated polymers – have progressed in separate parallel directions in the past several decades.[1-8] Among the longstanding grand challenges of the former field is the design and realization of higher-dimensional organic charge-transfer complexes towards stabilization of the metallic state down to low temperatures against Peierls distortions and increase of the critical temperature for ambient-pressure superconductivity.[2,3] Similarly, a central longstanding fundamental challenge in the latter field is the achievement of intrinsic metallic properties in π-conjugated polymers without doping, and here too Peierls instability of one-dimensional materials is the fundamental barrier.[6-8] The overall goal of this project is to enable the discovery of new two-dimensional (2D) organic solid-state materials immune from Peierls instability, by exploring rational design and supramolecular synthesis of charge-transfer (CT) complexes composed of π-conjugated polymer components and investigating the emergent functionalities and collective structural, electronic, and optoelectronic properties of the novel supramolecular materials. Beyond immunity from Peierls distortions, the proposed new supramolecular materials could eliminate the fundamental necessity for doping of π-conjugated polymers as a means of enhancing their electrical and optoelectronic properties and the efficiency of organic electronic and energy conversion devices.

Among our approaches are: to design, synthesize and characterize new n-type π-conjugated polymers with high-electron affinity and tailored backbone topology suitable to explore the fundamental limits of electron-polaron delocalization, stability, and transport as well as the high-EA components for exploring ground-state electron transfer between π-conjugated polymer components;[9] and to combine field-effect and bulk charge transport measurements, optical spectroscopy, density functional theory (DFT) calculations, and thin-film microstructure characterization to quantify and understand effects of degree of polymerization (DP) and electron affinity on electron-polaron delocalization, stability, and transport in n-type π-conjugated polymers.

Recent Progress

Elucidation of Nature of Charge Carriers in n-Doped Conjugated Polymers and Discovery of Super-Nernstian Proton-Coupled Electron Transfer (PCET). Little is currently known and understood about the nature of charge carriers and the evolution of the electronic structure of n-type conjugated polymers upon doping or injection of electrons. Questions such as, are bipolarons or polaron pairs the main charge carriers when the polymers are heavily doped, or what are the optical signatures of the different polaronic species in n-doped conjugated polymers, remain to be

explored. We have recently addressed these questions by using a multiredox π-conjugated polymer, BBL-P[10] (**Fig. 1a**), a derivative of the widely studied n-type conjugated polymer poly(benzimidazo-benzophenanthroline) (BBL), as the model molecular system. We have used various *in-operando* characterization techniques to elucidate the evolution of charge carriers in electrochemically doped conjugated polymer, BBL-P, in aqueous electrolyte. We found that electron-polarons are the charge carriers delocalized over a pro-quinoidal backbone when the polymer is doped (i.e. reduced) to a low to intermediate doping level (0.1 – 1.0 eru, electron transferred per repeat unit). A higher doping level (1.3 eru) results in a mixture of polarons, polaron pairs, and bipolarons, all of which reside on a pro-benzoidal polymer structure. At a very high doping level (1.5 eru), only polaron pairs remained as the charge carriers.[11]

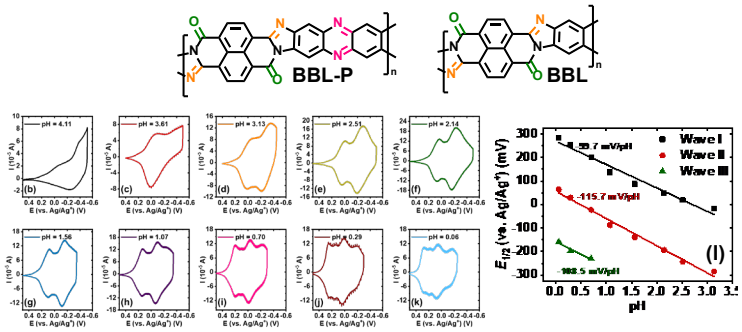

Fig. 1. (a) Molecular structures of BBL and BBL-P; (b – k) pH-dependent cyclic voltammograms of BBL-P in aqueous acidic electrolyte; and (l) Pourbaix diagram of BBL-P thin film.

We also found that the electrochemical response of BBL-P can be tuned by varying the pH of the electrolyte (**Figs. 1b-1k**). In particular, the number of observable quasi-reversible reduction waves increases from one to three as the pH of the electrolyte is lowered from pH > 3 to pH < 1. These results indicate that BBL-P can undergo multiple proton-coupled electron transfer (PCET) processes, each of which correspond to different molecular redox sites on the polymer backbone. Furthermore, we discovered that BBL-P exhibits a ***super-Nernstian PCET response***, featuring two protons per electron transferred as evidenced by the large slopes (-100 to -120 mV/pH) in the Pourbaix diagram (**Fig. 1l**). We similarly found that the parent polymer BBL (**Fig. 1a**) can also exhibit super-Nernstian PCET behavior when electrochemically reduced in aqueous electrolyte, although only 1.5 protons per electron transferred is observed. Our further investigation showed that the observed super-Nernstian PCET response in BBL-P and BBL originates from their unique molecular structures, which feature a series of protonatable redox sites with a gradient of pK_a values embedded directly in the π-conjugated polymer backbone.[11] It is important to highlight that this work demonstrates for the first time that a super-Nernstian proton-coupled electron transfer behavior can be observed in all-organic materials. Proton-coupled electron transfer (PCET), in which a proton is also transferred for every electron transferred, is a fundamental process that lies at the heart of many physical and biological systems such as photosynthesis and respiration, DNA biosynthesis, enzyme operation, water splitting for fuel cells, nitrogen fixation, chemical-/bio-sensors, electrochemical devices, etc.[12-14] Super-Nernstian PCET response has only previously been observed in transition metal oxides and metalloproteins but not in any all-organic material.[12]

References

1. J. B. Torrance, *The difference between metallic and insulating salts of tetracyanoquinodimethone (TCNQ): how to design an organic metal,* Acc. Chem. Res., **12**, 79 (1979).
2. M. R. Bryce, *Recent progress on conducting organic charge-transfer salts,* Chem. Soc. Rev.**, 20**, 355 (1991).
3. D. Jérome, *Organic Conductors: From Charge Density Wave TTF−TCNQ to Superconducting* $(TMTSF)_2PF_6$*,* Chem. Rev., **104**, 5565 (2004).
4. S. Horiuchi, T. Hasegawa, and Y. Tokura, *Molecular Donor–Acceptor Compounds as Prospective Organic Electronics Materials, J. Phys. Soc. Jpn.*, **75**, 051016 (2006).
5. K. P. Goetz, D. Vermeulen, M. E. Payne, C. Kloc, L. E. McNeil, and O. D. Jurchescu, *Charge-transfer complexes: new perspectives on an old class of compounds, J. Mater. Chem. C*, **2**, 3065 (2014).
6. H. Shirakawa, *The Discovery of Polyacetylene Film: The Dawning of an Era of Conducting Polymers (Nobel Lecture),* Angew. Chem. Int. Ed., **40**, 2574 (2001).
7. A. G. MacDiarmid, *"Synthetic Metals": A Novel Role for Organic Polymers (Nobel Lecture).* Angew. Chem. Int. Ed., **40**, 2581 (2001).
8. A. J. Heeger, *Semiconducting and Metallic Polymers: The Fourth Generation of Polymeric Materials (Nobel Lecture), Angew. Chem. Int. Ed.*, **40**, 2591 (2001).
9. K. Xu, H. Sun, T. P. Ruoko, G. Wang, R. Kroon, N. B. Kolhe, Y. Puttisong, X. Liu, D. Fazzi, K. Shibata, C.-Y. Yang, N. Sun, G. Persson, A. B. Yankovich, E. Olsson, H. Yoshida, W. M. Chen, M. Fahlman, M. Kemerink, S. A. Jenekhe, C. Mueller, M. Berggren, and S. Fabiano, *Ground-state electron transfer in all-polymer donor-acceptor heterojunctions*, Nat. Mater., **19**, 738 (2020).
10. S. M. West, D. K. Tran, J. Guo, S. E. Chen, D. S. Ginger, S. A. Jenekhe, *Phenazine-Substituted Poly(benzimidazobenzophenanthrolinedione): Electronic Structure, Thin Film Morphology, Electron Transport, and Mechanical Properties of an n-Type Semiconducting Ladder Polymer*, Macromolecules**, 56**, 2081-2091 (2023).
11. D. K. Tran, S. M. West, E. M. K. Speck, and S. A. Jenekhe, *Observation of Super-Nernstian Proton-Coupled Electron Transfer and Elucidation of Nature of Charge Carriers in a Multiredox Conjugated Polymer*, Chem. Sci., **15**, 7623–7642 (2024).
12. J. M. Mayer, *Bonds over Electrons: Proton Coupled Electron Transfer at Solid–Solution Interfaces,* J. Am. Chem. Soc., **145**, 7050-7064 (2023).
13. M. H. V. Huynh, and T. J. Meyer, *Proton-Coupled Electron Transfer*, Chem. Rev., **107**, 5004-5064 (2007).
14. D. R. Weinberg, C. J. Gagliardi, J. F. Hull, C. F. Murphy, C. A. Kent, B. C. Westlake, A. Paul, D. H. Ess, D. G. McCafferty, and T. J. Meyer, *Proton-Coupled Electron Transfer,* Chem. Rev., **112**, 4016-4093 (2012).

Publications

1. D. K. Tran, S. M. West, J. Guo, S. E. Chen, D. S. Ginger, and S. A. Jenekhe, *Chain Length Dependence of Electron Transport in an n-Type Conjugated Polymer with a Rigid-Rod Chain Topology*, J. Am. Chem. Soc. **146***,* 1435−1446 (2024). Doi: 10.1021/jacs.3c10650.

2. D. K. Tran, S. M. West, E. M. K. Speck, and S. A. Jenekhe, *Observation of Super-Nernstian Proton-Coupled Electron Transfer and Elucidation of Nature of Charge Carriers in a Multiredox Conjugated Polymer*, Chem. Sci. **15**, 7623–7642 (2024). DOI: 10.1039/d4sc00785a.

Understanding the Interfaces for High-Energy Batteries Using Anions as Charge Carriers

Xiulei "David" Ji, Oregon State University

De-en Jiang, Vanderbilt University

Chunsheng Wang, University of Maryland, College Park

Quinton Williams, Howard University

Keywords: Anions, Charge carriers, Iron metal cathode, Anion solid solution, Anionic Redox

Research Scope

The project aims to elucidate the electrochemical reaction mechanisms of an amorphous mixture of lithium salts and an electron source, serving as a cathode for Li-ion batteries (LIBs).[1] We refer to such electrodes as lithium salt composite (LSC) cathode.[2] Our collaborative research focuses on the electrochemical reactivity, the charge storage mechanism, and the ion transport properties of the LSC cathodes. The project investigates three families of electron sources: transition metal particles, nonmetals, and anions of lithium salts.[1,3,4] In the fine mixtures of the electron source and lithium salts, the anodic charging of electrodes converts the electron source into a compound by incorporating the neighboring anions in the solid phase. The **first hypothesis** of this project is that in a fine mixture, the electron source is embedded in the matrix of lithium salts, where their oxidation is charge compensated solely by forming bonds with anions in the immediate vicinity. In other words, the fine mixture serves as a pseudocompound. In such a pseudocompound, there do not exist primary chemical bonds between the electron source and the lithium salts; however, the constituents of this mixture are spatially arranged in such a way that redox chemical reactions proceed within this mixture as if it is a homogeneous compound. Our initial results obtained in this project have supported this basic hypothesis, which unleashes a tremendous potential to discover a great number of new electrodes, considering the assistance the machine learning.[5] The **second hypothesis** is that in the pseudocompounds, the disordered distribution of anions allows the enhanced diffusion of Li-ions and the agility of anions and even the ions formed by oxidizing the electron source. The lack of periodicity of anions distinguishes these composites from the disordered rock-salt electrodes, where the oxide anions are ordered.[6] The ion agility facilitates the unprecedented utilization of the electron source, which is prohibitively difficult to achieve in crystalline compounds.[2]

Recent Progress

In this project, we provide new insights into the active roles of anions regarding the redox reactivity of amorphous solid-state materials. Our initial effort was devoted to the reactivity of iron metal powder—the most affordable cathode active mass, where we discovered that a solid solution of Li_3PO_4 and LiF

provides a unique anionic environment that induces greater redox reactivity of iron metal powder toward a three-electron transfer reaction.[2] Under optimal conditions, the LSC electrode of $Fe/Li_3PO_4/LiF$ exhibits a reversible capacity of 368 mAh/g and specific energy of 940 Wh/kg (FIG. 1), higher than layered oxide cathode materials.[7] Our characterization and computation results suggest that not only Li-ions but iron-ions, phosphate, and fluoride are mobile in the conversion reaction between iron and the iron-salt solid solution. The agility of all ions enhances the utilization of iron metal and the reversibility and reduces polarization.

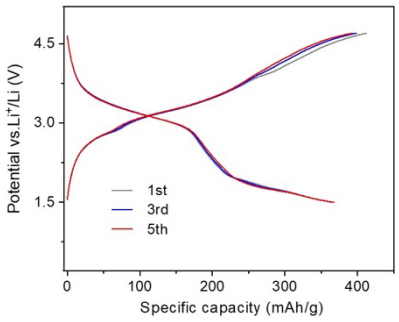

FIG. 1. Charge-discharge profiles of the composite of $Fe/Li_3PO_4/LiF$ at 30 mA/g and at 60 °C.

What species can serve as the electron source of the LSC cathode? Can anions in the common lithium salts serve as electron sources? We hypothesize that a strong binding agent for anions and their oxidized species can facilitate reversible redox reactivity of anions. To test this hypothesis, we selected Cu_2S as a binding agent, a naturally occurring conducting mineral. We discovered the reversible anionic redox reactivity of carbonate and sulfate ions in the composites of $Cu_2S/Li_2CO_3/Li_2SO_4$.[8] Our results show that the interactions between Cu_2S nanodomains and Li_2CO_3/Li_2SO_4 in the amorphous solid-solution matrix transform these common lithium salts into cathode active mass of LIBs. Spectral studies reveal the reversible valence state change of oxygen in carbonate and sulfate upon charging and discharging. The experimental and computation results suggest that Cu_2S is not the primary electron source, but a binding agent to induce the reactivity of carbonate and sulfate and facilitate their reaction reversibility by preventing gas evolution. Interestingly, the anion solid solution of carbonate and sulfate demonstrates a synergistic effect, regarding nearly all aspects of electrochemical properties. Under optimal conditions, the ternary $Cu_2S/Li_2CO_3/Li_2SO_4$ composite exhibits a specific capacity of 247 mAh/g, based on the mass of all materials in the Cu_2S/salt composite, at a voltage of 3.0 V. Our results highlight the opportunities of leveraging anions as both charge carriers and redox centers in the next-generation cathode materials in LIBs.

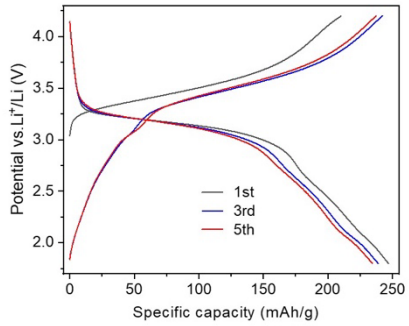

FIG. 2. Initial charge-discharge profiles of the composite of $Cu_2S/Li_2CO_3/Li_2SO_4$ at 30 mA/g.

There are outstanding questions related to the reactivity, conductivity, and reversibility of these lithium-salts-based composite materials. Albeit being composites, their amorphous structures allow them to behave more like homogenous compounds relishing properties that were not possible for crystalline compounds.

References

1. C. Yang, J. Chen, J., X. Ji, T. P. Pollard, X. Lü, C. J. Sun, S. Hou, Q. Liu, C. Liu, T. Qing, Y. Wang, O. Borodin, Y. Ren, K. Xu, and C. Wang, *Aqueous Li-Ion Battery Enabled by Halogen Conversion–Intercalation Chemistry in Graphite,* Nature **569**, 245-250, (2019).
2. M. Yu, J. Wang, M. Lei, M. S. Jung, Z. Zhuo, Y. Yang, X. Zheng, S. Sandstrom, C. Wang, W. Yang, D.-e. Jiang, Tongchao Liu, and X. Ji, *Unlocking Iron Metal as a Cathode for Sustainable Li-ion Batteries by an Anion Solid-Solution,* Science Advances https://www.science.org/doi/10.1126/sciadv.adn4441 (2024).
3. T. C. Gallagher, C. Y. Wu, M. Lucero, S. K. Sandstrom, L. Hagglund, H. Jiang, W. Stickle, Z. Feng, and X. Ji, ***From Copper to Basic Copper Carbonate: A Reversible Conversion Cathode in Aqueous Anion Batteries***, *Angew. Chem. Inter. Ed.* **132**, e202203837 (2022).
4. S. K. Sandstrom, Q. Li, Y. Sui, M. Lyons, C.-W. Chang, R. Zhang, H. Jiang, M. Yu, D. Hoang, W. F. Stickle, H.L. Xin. Z. Feng, D. Jiang, and X. Ji, ***Reversible Cl/Cl⁻ Redox in a Spinel Mn_3O_4 Electrode***, *Chemical Science* **14**, 12645-12652 (2023).
5. N. J. Szymanski, B. Rendy, Y. Fei, R. E. Kumar, T. He, D. Milsted, M. J. McDermott, M. Gallant, E. D. Cubuk, A. Merchant, H. Kim, A. Jain, C. J. Bartel, K. Persson, Y. Zeng, and G. Ceder, *An autonomous laboratory for the accelerated synthesis of novel materials*, Nature **624**, 86-91 (2023).
6. Z. Cai, B. Ouyang, H.-M. Hau, T. Chen, R. Giovine, K. P. Koirala, L. Li, H. Ji, Y. Ha, Y. Sun, J. Huang, Y. Chen, V. Wu, W. Yang, C. Wang, R. J. Clément, Z. Lun, and G. Ceder *In situ formed partially disordered phases as earth-abundant Mn-rich cathode materials,* Nature Energy **9**, 27-36 (2024).
7. M. Manthiram, *A reflection on lithium-ion battery cathode chemistry*, Nature Communications, **11**, 1550, (2020).
8. M. Yu, B. Li, J. Wang, Y. Xu, N. Zhang, M. S. Jung, Z. Xue, Y. Cho, M.-J. Kim, G. Feng, Y. Yang, A. Scida, Y. Sui, Z. Zhuo, M. Lu, A. K. Yadav, K. C. Stylianou, W. Yang, Y. Liu, C. Wang, T. Osborn Popp, C. Wang, T. Liu, X. Zheng, D-e Jiang, and X. Ji, *Unlocking Li_2CO_3-Li_2SO_4 as Cathodes for Li-ion Batteries,* ChemRxiv DOI:10.26434/chemrxiv-2024-732b5, under review (2024).

Publications

1. M. Yu, B. Li, J. Wang, Y. Xu, N. Zhang, M. S. Jung, Z. Xue, Y. Cho, M.-J. Kim, G. Feng, Y. Yang, A. Scida, Y. Sui, Z. Zhuo, M. Lu, A. K. Yadav, K. C. Stylianou, W. Yang, Y. Liu, C. Wang, T. Osborn Popp, C. Wang, T. Liu, X. Zheng, D-e Jiang, and X. Ji, *Unlocking Li_2CO_3-Li_2SO_4 as Cathodes for Li-ion Batteries,* ChemRxiv DOI:10.26434/chemrxiv-2024-732b5, under review (2024).
2. M. Yu, J. Wang, M. Lei, M. S. Jung, Z. Zhuo, Y. Yang, X. Zheng, S. Sandstrom, C. Wang, W. Yang, D.-e. Jiang, Tongchao Liu, and X. Ji, *Unlocking Iron Metal as a Cathode for Sustainable Li-ion Batteries by an Anion Solid-Solution,* Science Advances https://www.science.org/doi/10.1126/sciadv.adn4441 (2024).
3. A.-M. Li, O. Borodin, T. P. Pollard, W. Zhang, N. Zhang, S. Tan, F. Chen, C. Jayawardana, B. L. Lucht, E. Hu, X.-Q. Yang, C. Wang*, Methylation enables the use of fluorine-free ether electrolytes in high-voltage lithium metal batteries*, Nature Chemistry **16**, 922-929 (2024).
4. M. Lei, B. Li, H. Liu, **D.-e. Jiang,** *Dynamic Monkey Bar Mechanism of Superionic Li-ion Transport in $LiTaCl_6$,* **Angew. Chem. Int. Ed. 63**, e202315628. (2024).
5. S. Sandstrom, X. Ji, ***Reversible Halogen Cathodes for High Energy Lithium Batteries*** *Joule* **7**, 13-14 (2023).
6. J. Fortunato, B. Z. Zydlewski, M. Lei, N. P. Holzapfel, M. Chagnot, J. B. Mitchell, H. C. Lu, D. Jiang, D. J. Milliron, and V. Augustyn, *Dual-Band Electrochromism in Hydrous Tungsten Oxide*, *ACS Photonics* **10**, 3409–3418 (2023).

Charge Separation in Polymer Films from Tuned Polarizability and Electroactive Molecule Aggregation for Energy Storage, Utilization, and Conversion

Howard E. Katz, Arthur E. Bragg, and Daniel H. Reich, Johns Hopkins University

Keywords: crystallites, conjugated polymer, charge storage, morphology-dependent photophysics, memristors

Research Scope

Synthesis, growth, and investigation of phase-separated donors and acceptors as charged sites in polarizable media. Diblock polymer and molecular surfactants will be designed with segments interacting with electroactive molecule and polymer matrix moieties to promote dispersion of strongly crystallizable donors and acceptors and formation of nanoscale crystallites in polymer matrices.[1] Strongly crystallizable donors and acceptors will be used to form crystallites in polymer matrices.[2] Spectroscopic signatures of crystallite effects on surrounding polymer matrix material will be uncovered. Composite morphologies will be determined by x-ray diffraction (XRD).

Testing the hypothesis that charge storage in aggregates is stabilized by the combined contributions of intermolecular interactions and local polarizable surroundings.[3] We hypothesize that charges in crystallites will be additionally stabilized by the surrounding polarizable segments[4] separately from any contribution from mixing of frontier orbitals of multiple molecules, while a minimally polarizable matrix, e.g. styrene polymers, adds kinetic stabilization.

Recent Progress

We investigated composites of polystyrene (PS), poly(4-methylstyrene) (P4MS), and poly(4-tert-butylstyrene) (P4TBS) incorporating varying concentrations of the strong electron donor dibenzotetrathiafulvalene (DBTTF) (Figure 1) and the weaker donor 2,8-difluoro-5,11-bis (triethylsilylethynyl)anthradithiophene (diF-TES-ADT). At appropriate concentrations, the molecules formed small, separated crystallites in the polymer matrices. Films of these composites

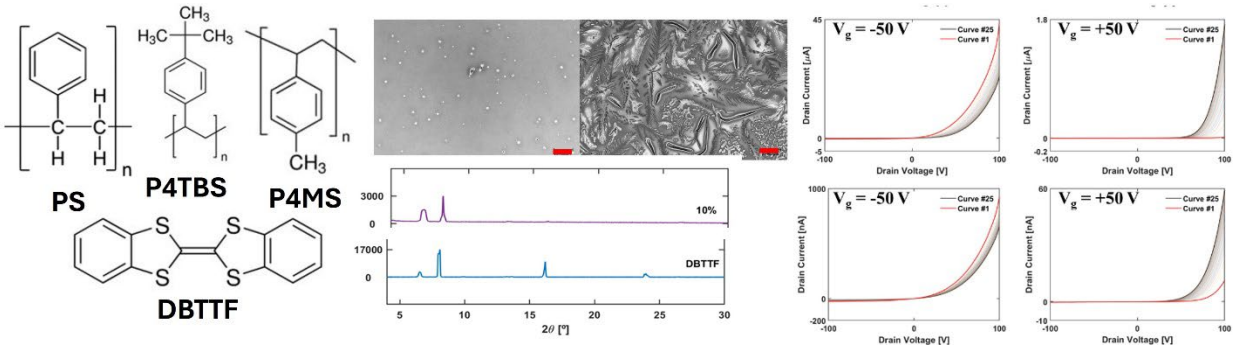

Figure 1. Materials used for memristor project, laser optical microscopy for P4TBS films with 5 wt% (left) and 10 wt% (right) DBTTF, XRD of DBTTF powder and 10 wt% composite, and representative memristor I-V traces for P4MS with 10wt% DBTTF OFET, and P4TBS with 10wt% DBTTF. I_{ds} was measured as V_{ds} was scanned starting in increments of -1 V. 25 consecutive curves were measured following this protocol, with the red scan first, and no pauses between the acquisition of each curve.

were analyzed via laser optical microscopy, x-ray diffraction (XRD), scanning electron microscopy (SEM), and energy-dispersive x-ray spectroscopy (EDS) to confirm the presence and persistence of the small molecule crystallites. Crystallite concentration and morphology was strongly matrix and molecule concentration dependent. The DBTTF crystallites increased the amount of charge stored in the films when they were used as pentacene-based organic field-effect transistor (OFET) dielectrics as evidenced by increased threshold voltage shift induced by static charging.[5,6] Strikingly, a novel and reversible memristor effect[7,8] was uncovered by repeatedly measuring currents versus source-drain voltages over a range that included positive drain voltages and static gate voltages in both accumulation and depletion, outside the normally scanned range for p-channel OFETs. DBTTF greatly increased this effect and stabilized the devices against high gate voltages. P4MS with 10wt% DBTTF OFETs showed a range in maximum current from 20 nA to 44 μA.

We also began an investigation of the effects of incorporating crystalline conjugated monomers in conjugated polymers where the repeat unit is the same as the monomer, focusing specifically on BTTT blended with its polymer PBTTT (Figure 2). Transient absorbance spectroscopy showed that the magnitudes and lifetimes of excited-state features for the composite crystalline region, made apparent by a unique BTTT-induced XRD peak, were greater than those measured from the amorphous region of the same sample, reflecting modifications in polymer electronic interactions arising

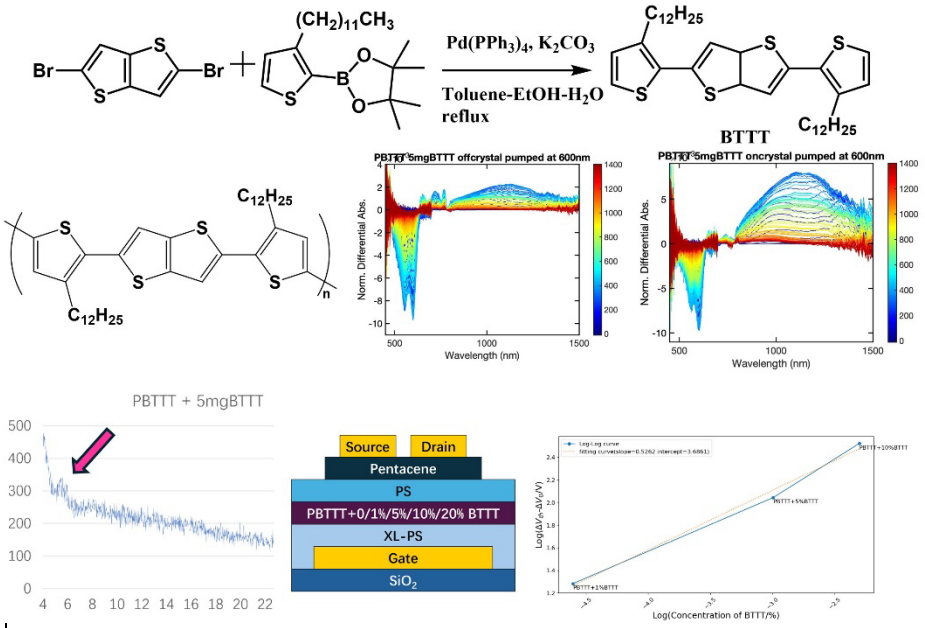

Figure 2. BTTT synthesis and PBTTT structure. Transient absorbance spectroscopy of off- and on-crystallite regions of a PBTTT-BTTT composite; color codes are picosecond delay times. Unique XRD peak for a PBTTT-BTTT composite. OFET multilayer structure and plot of threshold voltage shift vs log of % incorporation of BTTT in the PBTTT middle layer.

from small-molecule impacts on polymer crystalline domains. Threshold voltage shifting from -70 V static charging of a pentacene OFET with a styrene polymer trilayer and PBTTT/BTTT as the middle layer was increased when BTTT was included with the PBTTT, showing that the monomer had charge storage activity that was distinguishable from the polymer alone. Plotting the threshold voltage shift from the static charging against log of BTTT concentration in the PBTTT showed close to a square root dependence, raising the interesting possibility that constant proportions of the BTTT either hold charge themselves or stabilize charge by serving as polarizable near-neighbors, analogous to the kinetics of a dimeric chemical reagent in equilibrium with a pair of monomers that act independently in subsequent chemical reactions.

References

1. P. Kumari, K. Khawas, M. K. Bera, S. Hazra, S. Malik, and B. K. Kuila. *Enhanced Charge Carrier Mobility and Tailored Luminescence of n-Type Organic Semiconductor through Block Copolymer Supramolecular Assembly*, Macromolecular Chemistry and Physics **218,** 1600508 (2017). DOI: 10.1002/macp.201600508.
2. E. P. Bruckner, T. Curk, L. Đordevic, Z. Wang, Y. Yang, R. Qiu, A. J. Dannenhoffer, H. Sai, J. Kupferberg, L. C. Palmer, E. Luijten, and S. I. Stupp. *Hybrid Nanocrystals of Small Molecules and Chemically Disordered Polymers*, ACS Nano **2022**, 16, 8993-9003. DOI: 10.1021/acsnano.2c00266.
3. B. J. Barrett, H.E. Katz, and A.E. Bragg. *Permittivity Threshold and Thermodynamics of Integer Charge-Transfer Complexation for an Organic Donor–Acceptor Pair*, Journal of Physical Chemistry B 127, 2792-2800 (2023). DOI: 10.1021/acs.jpcb.3c00218.
4. T. Lee, Y. Luo, C. Wang, A. Park, E. Zapata-Mercado, K. Hristova, T. Mueller, W.L. Wilson, D.H. Reich, and H.E. Katz. *Effect of Organic Electroactive Crystallites in a Dielectric Matrix on the Electrical Properties of a Polymer Dielectric,* Physical Review Materials **7**, 065003 (2023). DOI: 10.1103/PhysRevMaterials.7.065003.
5. P. Heremans, G. H. Gelinck, R. Muller, K. J. Baeg, D. Y. Kim, and Y. Y. Noh. *Polymer and Organic Nonvolatile Memory Devices*, Chemistry of Materials **23**, 341-358 (2011). DOI: 10.1021/cm102006v.
6. J. C. Hsu, W. Y. Lee, H. C. Wu, K. Sugiyama, A. Hirao, W. C. Chen. *Nonvolatile memory based on pentacene organic field-effect transistors with polystyrene para-substituted oligofluorene pendent moieties as polymer electrets*, Journal of Materials Chemistry **22** (12), 5820-5827 (2012). DOI: 10.1039/c2jm16039k.
7. D. B. Srukove, G. S. Snider, D. R. Stewart, and R. S. Williams. *The missing memristor found*. Nature **453**, 80-83 (2008). DOI: 10.1038/nature06932.
8. Y. Park, K. J. Baeg, and C. Kim. *Solution-Processed Nonvolatile Organic Transistor Memory Based on Semiconductor Blends*, ACS Applied Materials & Interfaces **11**, 8327-8336 (2019). DOI: 10.1021/acsami.8b20571.

Publications

1. T. Lee, Y. Luo, C. Wang, A. Park, E. Zapata-Mercado, K. Hristova, T. Mueller, W.L. Wilson, D.H. Reich, and H.E. Katz. *Effect of Organic Electroactive Crystallites in a Dielectric Matrix on the Electrical Properties of a Polymer Dielectric,* Physical Review Materials **7**, 065003 (2023). DOI: 10.1103/PhysRevMaterials.7.065003.
2. B. J. Barrett, H.E. Katz, and A.E. Bragg. *Permittivity Threshold and Thermodynamics of Integer Charge-Transfer Complexation for an Organic Donor–Acceptor Pair*, Journal of Physical Chemistry B 127, 2792-2800 (2023). DOI: 10.1021/acs.jpcb.3c00218.
3. T. Mukhopadhyaya, T. Lee, C. Ganley, S. Tanwar, P. Raj, L. Li, Y. Song, P. Clancy, I. Barman, S. M. Thon, and H. E. Katz. *Stable High-Conductivity Ethylenedioxythiophene Polymers via Borane-Adduct Doping,* Advanced Functional Materials **32**, 202208541 (2022). DOI: 10.1002/adfm.202208541.
4. C. Chi, Y. Song, T. Lee, A.E. Bragg, D.H. Reich, and H.E. Katz. *2-Aminoanthracene Crystallization in Its Compatible Polystyrene Block: RAFT Synthesis and Enhanced Charge Retention in Pentacene Transistor Gate Dielectrics,* Macromolecules **56**, 8592-8601 (2023). DOI: 10.1021/acs.macromol.3c01130.
5. T. Mukhopadhyaya, J. Wagner, T. D. Lee, C. Ganley, S. Tanwar, P. Raj, L. Li, Y. Song, S. J. Melvin, Y. Ji, P. Clancy, I. Barman, S. Thon, R. Klausen, and H. E. Katz. *Solution-doped donor-acceptor copolymers based on diketopyrrolopyrrole and 3, 3'-bis (2-(2-(2-methoxyethoxy) ethoxy) ethoxy)-2, 2'-bithiophene exhibiting outstanding thermoelectric power factors with p-dopants*, Advanced Functional Materials **34**, 2309646 (2023). DOI: 10.1002/adfm.202309646

Kinetically Trapped Poly(pseudo)rotaxane Networks

Wenlin Zhang, Department of Chemistry, Dartmouth College
Chenfeng Ke, Department of Chemistry, Washington University in St. Louis

Keywords: polyrotaxane hydrogels, slide-ring networks, mechano-responsive, 3D-printing, simulation-aided design.

Research Scope

This proposal aims to introduce a chemical approach to design and develop kinetically trapped polyrotaxane materials with controlled nano-to-macroscale architectures and emergent properties. We plan to introduce a variety of stoppers and speed bumps to diverge the threading and translocation of CD rings, thus kinetically resolving meta-stable polypseudorotaxanes. Covalently crosslinking them will afford new polyrotaxane materials that possess enhanced mechanical robustness, as well as mechano-responsiveness.

Recent Progress

The research team has developed a new strategy to synthesize crystalline-domain-reinforced pro-slide-ring crosslinkers, exploiting them for high throughput synthesis and identifying suitable hydrogels for direct-ink-writing 3D printing.[1]

In this work, a pro-slide-ring crosslinker formed by double-threaded PEGs in γ-CDs (Figure), in which the γ-CD-included segments crystallized as micro-crystalline domains at high concentrations. As such, the pro-slide-ring crosslinker can react with various (meth)acrylate/acrylamide monomers for slide-ring network formation. More excitingly, its rapid gelation and excellent viscoelasticity enable high-throughput synthesis and 3D printing. A spectrum of hydrogels

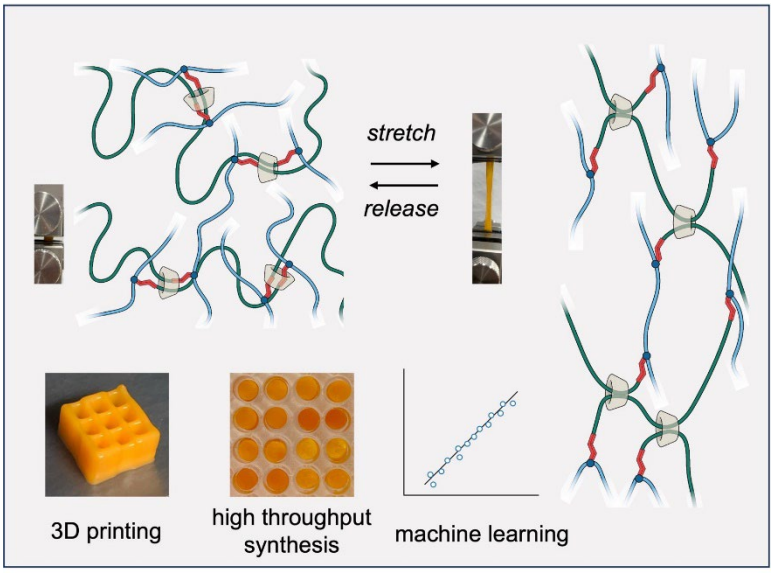

Figure. Illustration of a crystalline-domain-reinforced double-threaded slide-ring network that surpasses the elasticity-toughness trade-off in conventional slide-ring gels. We employed 3D-printable modular crosslinkers that feature rigid crystalline domains and mobile γ-cyclodextrin slide-ring joints to create slide-ring hydrogels. The efficient, high-throughput production of these hydrogels, combined with machine learning-facilitated structure-property elucidation, has led to the identification of superior slide-ring gels suitable for 3Dprinting and the fabrication of capacitive stress sensors.

with various elastic moduli, compressibility, and viscoelasticity were obtained through high-throughput synthesis. We have identified a group of high elasticity and toughness hydrogels, breaking the elasticity-toughness trade-off in conventional slide-ring networks and facilitating additional 3D printability. The structure-property relationship of the hydrogels was clarified with machine-learning algorithms, providing insights into future material designs. We employed 3D printing to construct high-performance capacitive stress sensors, with a significantly enhanced sensitivity measured compared to the molded devices.

To guide experimental exploration of the vast design space of poly(pseudo)rotaxane networks, we also developed a multi-scale computational framework to predict the assembly of cyclodextrin and polymer axles.[2] Our approach employs free energy sampling and atomistic simulations to compute the free energy barrier for cyclodextrin threading across different functional moieties. Together with the predicted free energy landscapes, a lattice approximation for cyclodextrin and polymer diffusion in dilute solutions allows us to construct a kinetic Monte Carlo (kMC) model to predict the linear density and intra-chain distribution of cyclodextrin on polymer axles with functional moieties installed for tuning the threading kinetics. Because the distribution and linear density of cyclodextrin on polymer backbones affect the crystallization in poly(pseudo)rotaxane networks, our multi-scale approach lays the foundation for efficient predictions of the supramolecular structure of functionalized polyrotaxane.

Extending the kinetically controlled method, we also developed mechanically robust 3D-printed polyrotaxane hydrogels by integrating the dynamic covalent network with the noncovalently connected polypseudorotaxane network.[5] Tensile tests showed that the ketoenamine-crosslinked polyrotaxane hydrogels could be stretched to 260% with Young's modulus of 214 kPa. When Förster resonance energy transfer pairs were introduced to the polyrotaxane network, the hydrogel showed strain-dependent emissions, revealing the micro-environment changes. Furthermore, we developed a templated synthesis of urethane-crosslinked α-CDs with nanotubular structures and 3D-printed architectures, using tetraethoxysilane-based telechelic polyethylene glycol as the axle and α-CD as the ring.[6] These crosslinked α-CD polymers selectively adsorbed lycopene from raw tomato juice and protected it from photo- or thermal oxidation.

Publications

1. M. Tang, D. Zheng, J. Samanta, E. H. R. Tsai, H. Qiu, J. A. Read, and C. Ke, *Reinforced double-threaded slide-ring networks for accelerated hydrogel discovery and 3D printing,* Chem **9**, 3515-3531 (2023).
2. C.D. Smith, C. Ke, W. Zhang, *Multi-scale framework for predicting α-cyclodextrin assembly on polyethylene glycol axles*, in preparation.
3. C. A. Boyer, E. Blasco, and C. Ke, "Unleashing the Potential of 3D Printing: Bridging Chemistry and Applications", Small, **19**, 2309837 (2023).
4. C. A. Boyer, E. Blasco, and C. Ke, *Advanced 3D/4D Printing for Functional Materials Innovation,* Advanced Materials Technologies **8**, 2301869 (2023).

5. D. Zheng, M. Tang, and C. Ke, *3D-printed ketoenamine crosslinked polyrotaxane hydrogels and their mechanochromic responsiveness,* Polymer Chemistry **14**, 2159-2163 (2023).
6. M. Zhang, W. Liu, Q. Lin, and C. Ke, *Hierarchically Templated Synthesis of 3D-Printed Crosslinked Cyclodextrins for Lycopene Harvesting*, Small **19**, 2300323 (2023).
7. M. Tang, Z. Zhong., and C. Ke, *Advanced supramolecular design for direct ink writing of soft materials,* Chemical Society Reviews **52**, 1614-1649 (2023).
8. Q. Lin, and C. Ke, *Conductive and anti-freezing hydrogels constructed by pseudo-slide-ring networks*, Chemical Communications **58**, 250-253 (2022).
9. L. Zou, and W. Zhang, *Molecular dynamics simulations of the effects of entanglement on polymer crystal nucleation*, Macromolecules **55**, 4899-4906 (2022).

Direct Reduction of Metal Oxides to Metals for Electrowinning and Energy Storage

Paul A. Kempler,[1,2] Carl K. Brozek,[1,2] Nancy M. Washton,[3] J. David Bazak[3]

1. **Department of Chemistry and Biochemistry, University of Oregon**
2. **Oregon Center for Electrochemistry, University of Oregon**
3. **Pacific Northwest National Laboratory**

Keywords: Electrochemistry, energy storage, nanoparticles, NMR, electrodeposition

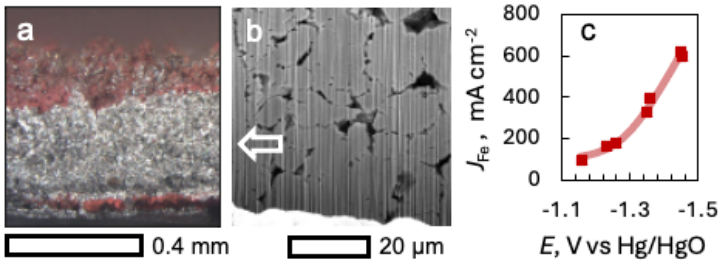

Figure 1 (a) Microscope image of Fe cross section **(b)** Focused ion beam cross section and SEM image of internal porosity of Fe film **(c)** Partial current towards Fe (J_{Fe}) vs electrode potential (E) for iron film reduction after 30 min in 10 M NaOH at 80 °C

Research Scope: Conversion reactions between metal-oxides, metal-hydroxides. and metals are a promising means of directly electrifying industrial production of zinc, iron,[1] and other metals. These reactions are also proposed for low-cost energy storage, particularly for long duration (>20 hours), grid-scale batteries.[2] This project seeks to understand atom-efficient conversion reactions between transition metals and transition metal oxides, with an emphasis on concentrated alkaline electrolytes used in commercialized batteries and electrowinning processes. Although the electrochemical reduction of iron oxides can in principle occur with a minimal quantity of dissolved products in alkaline electrolytes,[3] identifying the dominant reduction pathway is made challenging by the complex chemical equilibria between solid and dissolved metal oxides and hydroxides and our limited understanding of the transport of water and ions in concentrated electrolytes and nanoconfined pores. Our goal is to resolve the mechanism of these multi-electron conversion reactions and uncover new design principles for economical, energy efficient, and emissions-free electrochemical devices.

Our research efforts are focused on three key knowledge gaps: **(1)** We do not yet understand the material properties that limit the reaction rate for metal oxide particles reacting at an electrode surface. **Aim 1** investigates the ways that porosity and particle size limit reactivity and transport during metal-oxide to metal electrowinning. **(2)** Our understanding of cation transport and speciation of dissolved transition metals is primarily based on characterization performed in bulk, dilute electrolytes; we do not sufficiently understand how solvation and reactivity changes in nanoconfined pores present in solids undergoing conversion reactions. **Aim 2** is thus focused on developing new techniques capable of measuring the solvation environment of cations in alkaline, mesoporous metal oxides. **(3)** We have limited understanding of the reactive intermediates present during conversion of metal oxides/metals. **Aim 3** seeks to identify the structure and composition of the microenvironment at a reacting metal/metal-oxide interfaces in concentrated alkaline electrolytes.

Recent Progress: Aim 1) Our recent efforts have focused on monodisperse iron oxides with tunable particle diameter and porosity, prepared using sol-gel methods.[4] With this system of particles, we have

identified the material properties controlling the reaction rate during the multi-electron reduction of insulating Fe_2O_3 to metallic Fe **(Figure 1**). We find that the rate of Fe growth is strongly dependent on the internal porosity of reactant Fe_2O_3 and that sufficiently porous particles support partial current densities towards Fe growth in excess of 500 mA cm^{-2}—in the absence of forced convection within the cell **(Figure 1c**). A differential half-cell reactor was used to measure growth kinetics as a function of electrode potential and electron probe microanalysis was used to resolve the partial current density towards Fe. The limiting current towards Fe formation is substantially diminished for highly crystalline Fe_2O_3 particles **(Figure 2**), which are prepared at a nearly identical distribution of hydrodynamic radii but afford a reduced internal surface area.

These results indicate that the transport of solids through the hydrodynamic boundary layer supports current densities for Fe growth that are consistent with other forms of industrial electrolysis (e.g. alkaline water electrolysis) but the reactivity of the particles is controlled by either surface area or nanoscale transport of water and supporting ions.

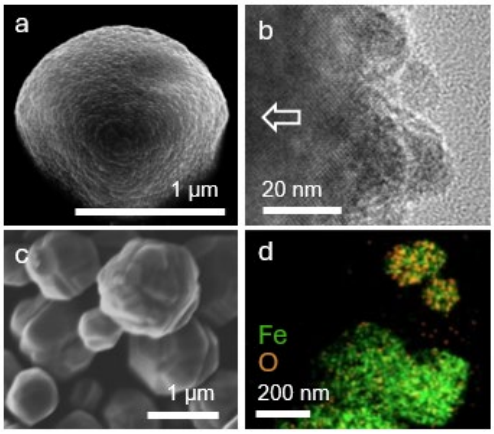

Figure 2 (a) SEM image of Fe_2O_3 particle prepared via sol-gel synthesis. **(b)** TEM image of Fe_2O_3 particle revealing primary particles ~20 nm in diameter. **(c)** SEM image of crystalline Fe_2O_3 particles **(d)** Elemental map of Fe and FeO_x produced via electrochemical reduction of crystalline Fe_2O_3 particles on a Cu TEM grid in 10 M NaOH at 80 °C.

Aim 2: We have conducted detailed characterization of bulk brine dynamics and transport properties. Most recently, our efforts have focused on understanding NMR dynamics for ions solvated within zeolitic imidazolate frameworks with tunable pore sizes and mixed metal/metal-oxide films of varied porosity.[5] Specifically, we used multinuclear NMR for both zinc triazolate and Zn/ZnO wetted pellets, measuring distinct dynamics for ^7Li based on the solvation environment. This validates the general approach of using MOFs and ZIFs as tunable analogues to understand cation dynamics in realistic metal/metal oxide systems used for energy storage.

Aim 3: We have combined *in-situ* Raman and rotating ring-disk electrode characterization (**Figure 3**) in 10 M NaOH with *ex-situ* TEM characterization of individual Fe_2O_3 nanoparticles to resolve the mechanism of direct oxide reduction in concentrated alkaline environments. We find that the reduction proceeds through an pseudomorphic reduction to solid ferrous phase,[6] followed by dissolution and plating of Fe metal within the hydrodynamic boundary layer. *In-situ* Raman reveals the presence of both β-FeOOH (-0.7 V) and Fe_3O_4 (-0.8 V) prior to FeO. Onset of dissolved Fe^{2+} is controlled by the morphology of the Fe_2O_3 particle and no significant Fe^{2+} escapes the boundary layer following the onset of Fe metal formation. A slower, apparent solid-state reduction of Fe_2O_3 is observed for crystalline particles (**Figure 2d**). This mechanistic understanding of Fe_2O_3 reactivity will support design rules for selecting ores for electrowinning and is of fundamental importance for understanding the scalability of electrified pathways for ironmaking.

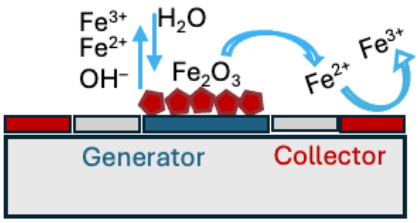

Figure 3 Thin-film rotating ring-disk electrode measurement for measuring dissolved species.

References

1. A. Allanore, H. Lavelaine, G. Valentin, J.P. Birat, and F. Lapicque, *Iron metal production by bulk electrolysis of iron ore particles in aqueous media*. J. Electrochem. Soc. **155**, E125 (2008)
2. W.H. Woodford, S. Burger, M. Ferrara, Y.-M. Chiang *The iron-energy nexus: A new paradigm for long-duration energy storage at scale and clean steelmaking*. One Earth. **5**, 212 (2022)
3. A. Putnis, *Why mineral interfaces matter*. Science. **343,** 1441 (2014)
4. T. Sugimoto, Y. Wang, H. Itoh, A. Muramatsu, *Systematic control of size, shape, and internal structure of monodisperse a-Fe_2O_3 particles*. Colloids and Surfaces. **134**, 265 (1998)
5. R. Banerjee, H. Furukawa, D. Britt, C. Knobler, M. O'Keeffe, and O. M. Yaghi, *Control of Pore Size and Functionality in Isoreticular Zeolitic Imidazolate Frameworks and their Carbon Dioxide Selective Capture Properties*. J. Amer. Chem. Soc. **131**, 3875 (2009)
6. H. Tuysuz, Y. Liu, C. Weidenthaler, and F. Schuth. *Pseudomorphic Transformation of Highly Ordered Mesoporous Co_3O_4 to CoO via Reduction with Glycerol.* J. Amer. Chem. Soc. **130,** 14108 (2008)

Publications

1. B.B. Noble, A. Konovalova, L.J. Moutarlier, Brogden, V. Kempler, P.A. *Electrochemical chlor-iron process for iron*
production from iron oxide and salt water, Joule **8**, 1-14 (2024).

Designing Chemical Disorder in Solid-State Superionic Conductors

Jae Chul Kim, Department of Chemical Engineering & Materials Science, Stevens Institute of Technology

Keywords: Solid electrolyte, Thiophosphates, Li conductors, Noncrystalline, Mechanochemical

Research Scope

The objective of this project is to establish design principles and synthesis guidelines for noncrystalline solids that can expand the frontiers of materials chemistry for energy storage. Specifically, through the rational design approach we aim to develop thiophosphate-based noncrystalline lithium (Li) superionic conductors with high ionic conductivity and excellent electrochemical stability for all-solid-state battery applications. The uniqueness in our approach is to derive the noncrystalline materials from crystalline materials that have the same chemical composition. While the lack of structural descriptors makes it difficult to employ traditional materials chemistry in noncrystalline materials design,[1] we will test the hypothesis that physicochemical properties of crystalline materials (parents) can be inherited in noncrystalline materials (children) if chemical and structural disorder are systematically introduced by mechanochemical reactions. We will investigate how local configurations and compositions of noncrystalline frameworks (e.g., Li coordination, polyanion distribution, and short-range order) dictate macroscopic Li conduction and electrochemical stability with reference to the crystalline phases. Our model system is Li_3PS_4 (LPS) that has multiple crystalline polymorphs with different conductivities and can be prepared as the noncrystalline.

Recent Progress

This is the second year of the five-year project. In the first year, we obtained two different polymorphs of LPS (i.e., β- and γ-LPS) as parent phases to produce amorphous LPS children mechanochemically. Amorphization of the two phases was partially achieved by planetary ball-milling, as observed by x-ray diffraction (XRD) and transmission electron microscopy (TEM). In this year, we used planetary ball-milling more aggressively. While our initial goal of achieving complete amorphization of LPS was yet to be fulfilled, we uncovered an intriguing phenomenon: rather than the insufficient driving force for crystalline-to-noncrystalline phase transformations, fast recrystallization that can occur during high-energy ball-milling hinders achieving complete amorphization. In the process, we found complex interplays between phase stability, local structures, and Li transport properties of LPS manipulated by mechanochemical reactions.

We produced three different LPS for each β- and γ phases: the crystalline, noncrystalline, and re-crystalline. The crystalline LPS parent phase was directly obtained by solid-state reactions, as previously reported.[2,3] The noncrystalline phases were derived by ball-milling the crystalline phases. Subsequent furnace heating after ball-milling led to the re-crystalline phases. We found that high-energy, planetary ball-milling was remarkably efficient to drive the crystalline-to-

noncrystalline phase transformation. A brief mechanochemical activation resulted in significant amorphization for both β- and γ-LPS. It is very surprising to observe a substantial degree of amorphization after 1-min ball-milling for β-LPS and 10-min ball-milling for γ-LPS, while a small amount of crystalline LPS remains in each case. Obtained noncrystalline LPS children phases show higher Li conductivity than their parent phases.

To track the phase ancestry, we heat-treated the noncrystalline children phases to partially recrystallize the parent phases. It should be pointed out that the crystallinity of LPS after recrystallization, as determined by the full-width-half-maximum of the XRD patterns, is lower than the that of the parent phases, suggesting imperfect periodicity and/or mechanical strain present in the re-crystalline phases. Li conductivity values of β-LPS are similar before and after recrystallization (1 X 10^{-4} S/cm) and in good agreement with literature.[4] In contrast, re-crystalline γ-LPS shows substantially improved Li conductivity (4 X 10^{-4} S/cm), the largest value among the known γ-LPS, compared to its parent crystalline γ-LPS (3 X 10^{-6} S/cm).[4]

Though not yet conclusive, we speculate that Li conductivity variation in the LPS family coincides with short- to mid-range atomic arrangements in LPS. We have adopted a mid-range peak area fraction index (MRI) to describe disorderness in a material using the results obtained by pair-distribution function (PDF) analysis.[5] This index is expressed by the fraction of the peak area within 10 Å over the entire peak area up to 30 Å and scales with the disorderness of the material. Figure 1 shows the correlation between the index and ionic conductivity of β- and γ-LPS families. The linear distribution of Li conductivity with respect to the mid-range peak area fraction index indicates their strong correlation. For re-crystalline γ-LPS, it is highly likely that short-range disorder has enabled high Li conductivity. We speculate that implemented short-range disorder can unblock Li conduction pathways that are originally forbidden in the crystalline parent phases,[4] thereby enhancing Li conductivity for the child phases. As the rate of recrystallization depends on nucleation and growth kinetics, short-range disorder can be systematically implemented by controlling recrystallization time and temperature. Our results in this project year propose an unconventional, yet fundamental relationship between local structure and Li conductivity, offering valuable insights into designing solid electrolytes for all-solid-state batteries.

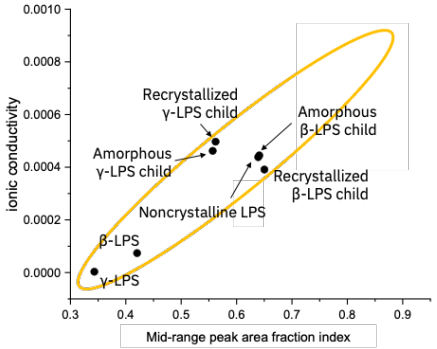

Figure 1. Li conductivity vs. MRI of LPS phases

References

1. G. Biroli, *Machine Learning Glasses*, Nature Physics **16**, p. 373–374 (2020).

2. M. Tachez, J.-P. Malugani, R. Mercier, and G. Robert, *Ionic Conductivity of and Phase Transition in Lithium Thiophosphate Li_3PS_4*, Solid State Ionics **14**, p. 181–185 (1984).

3. Z. Zhang, H. Li, K. Kaup, L. Zhou, P.-N. Roy, L. F. Nazar, *Targeting Superionic Conductivity by Turning on Anion Rotation at Room Temperature in Fast Ion Conductors*, Matter **2**, p. 1667–1684 (2020).

4. Y. Wang, W. D. Richards, S. P. Ong, L. J. Miara, J. C. Kim, Y. Mo, and G. Ceder, *Design Principles for Solid-State Lithium Superionic Conductors*, Nature Materials **14**, p. 1026–1031 (2014).

5. N. Minafra, M. A. Kraft, T. Bernges, C. Li, R. Schlem, B. J. Morgan, and W. G. Zeier, *Local Charge Inhomogeneity and Lithium Distribution in the Superionic Argyrodites Li_6PS_5X (X = Cl, Br, I)*. Inorganic Chemistry **59**, p. 11009–11019 (2020).

Publications

No publications yet. Two papers are in a pipeline.

Multilength-Scale Synthesis of Silicon Materials

Rebekka S. Klausen, PI, Johns Hopkins University

Keywords: polymers, silicon, optoelectronic materials, synthesis, catalysis

Research Scope

This proposal describes the impact of atomic- and molecular-level control of skeletal isomerism and stereoisomerism on the bulk properties of hierarchical silicon- based materials. Inorganic semiconductors, such as those from Group IV or Group III-V of the periodic table, are tetrahedral. In contrast, organic semiconductors, both molecular and polymeric, are comprised of π-conjugated building blocks that are most commonly planar (1- or 2-D). Interest in non-planar conjugated (macro)molecular materials has grown in the last several years, including nanohoops, helicenes, and the PI's research on conjugated polymers inspired by crystalline silicon. Recent advances from the PI's group on controlling relative configuration in stereogenic at Si complex silanes, as well as elucidation of the consequences of skeletal isomerism, will now make possible the first studies of the effect of isomerism on materials properties. Stereochemistry (the arrangement of atoms in space) is a critical factor in the development of non-planar conjugated materials, especially Si-derived, both because of the 3-D structure of tetrahedral semiconductors and for the discovery of fundamental knowledge, as the mechanistic principles and synthetic methods underlying stereoselective organic synthesis do not translate to silicon. The OBJECTIVES of this proposal are to:

(1) Based on the insight that skeletal connectivity controls conformation-dependent absorbance spectra, we will synthesize novel branched and networked (co)polymers to afford extended σ-conjugated pathways.

(2) We will synthesize stereoregular hybrid σ,π-conjugated polymers via stereochemically- defined building blocks, providing the first study of the impact of stereoregularity on bulk properties, with a particular focus on semicrystallinity.

(3) Based on design rules for chemoselective cyclosilane functionalization developed in earlier work, well-defined silicon building blocks will be covalently elaborated to hierarchically structured materials.

Recent Progress

This proposal describes the impact of atomic- and molecular-level control of skeletal isomerism and stereoisomerism on the bulk properties of hierarchical silicon-based materials. We found that isomeric polymers with cyclosilane repeat units absorbed different wavelengths of light, arising from differences in main chain conformation.[1] This insight led to the ability to tune the wavelength of light absorbed by statistical copolymerization of two monomers. We also found that reaction of isomeric cyclosilanes with thioethers afforded hybrid materials in which sulfur acted to couple sigma- and pi-conjugated fragments.[2]

Recent advances[3] from the PI's group make possible the first studies of the effect of silicon-centered stereoisomerism on materials properties. Stereochemistry (the arrangement of atoms in space) is a critical factor in the development of non-planar conjugated materials both because of

the 3-D structure of tetrahedral semiconductors and for the discovery of fundamental knowledge, as the design rules for stereoselective synthesis are distinct for Si vs C-based stereogenic centers, requiring new synthetic strategies.[4,5] A lack of general synthetic strategies also means that there is little known about the relationship between macromolecular stereochemistry (tacticity) and properties in silicon-based materials. Ladder compounds are formed by the consecutive fusion of two or more rings. We have now achieved the synthesis of a three-membered ladder cyclosilane possessing 4 stereogenic-at-silicon centers, as confirmed by X-ray crystallography. This molecule is the most complex molecular silane yet synthesized, consisting of three fused rings, 4 stereogenic centers, and 14 connected Si atoms, synthesized with total atomic precision. An isomer has also been synthesized and characterized crystallographically.

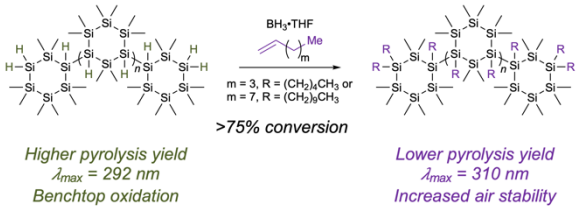

Figure 1. Controlling poly(cyclosilane) properties by hydrosilylation.

Postpolymerization functionalization is a key strategy in the diversification of polymeric materials for the conferral of tailored properties. Poly(cyclosilane)s have an all-silicon backbone and a periodic array of hydrido (Si–H) side chains potentially suitable for postpolymerization functionalization via hydrosilylation. At the same time, classical methods for hydrosilylation employing Pt- or Pd-based catalysts can result in Si–Si bond scission. We demonstrated borane-catalyzed hydrosilylation reactions between α-olefins and small molecules and three skeletally isomeric poly(cyclosilane) architectures.[6] Diastereomeric small molecules (cis or trans isomers) afforded the same products, consisting of a mixture of isomers, indicating that hydrosilylation was not stereospecific. We investigated chemoselectivity for end group versus internal Si–H groups and find that ^{29}Si cross-polarization magic angle spinning (CPMAS) can provide insight on site-selectivity in the functionalization of a complex poly(cyclosilane). We further showed that postpolymerization hydrosilylation, converting oxidatively sensitive Si–H groups to Si–alkyl chains, modulates solubility and physical characteristics, optical properties, pyrolytic reactivity, and air sensitivity. Attachment of long alkyl chains to the poly(cyclosilane)s resulted in a ca. 20-nm red-shift in light absorption, without attaching any unsaturation or other chromophore. This was attributed to a change in poly(cyclosilane) conformation enhancing sigma-conjugation.

References

1. F. Fang, Q. Jiang, R. S. Klausen, *Poly(cyclosilane) Connectivity Tunes Optical Absorbance*, J. Am. Chem. Soc. **144**, 7834 (2022).

2. A. F. Gittens, Q. Jiang, M. A. Siegler, R. S. Klausen, *Conjugation in Isomeric Cyclosilane Thioethers*, Organometallics **41**, 3762 (2022).

3. E. A. Marro, C. P. folster, E. M. Press, H. Im, J. T. Ferguson, M. A. Siegler, R. S. Klausen, *Stereocontrolled Syntheses of Functionalized cis- and trans-Siladecalins*, J. Am. Chem. Soc. **141**, 17926 (2019).

4. Q. Jiang, A. F. Gittens, S. Wong, M. A. Siegler, R. S. Klausen, *Highly selective addition of cyclosilanes to alkynes enabling new conjugated materials*, Chem. Sci. **13**, 7587 (2022).

5. W. Guan, L. Li, Q. Jiang, A. F. Gittens, Y. Wang, L. F. T. Novaes, R. S. Klausen, S. L. Lin, *An electrochemical strategy to synthesize disilanes and oligosilanes from chlorosilanes*, Angewandte Chemie Int. Ed. **135**, e202303592 (2023).

6. M. G. Coschigano, S. L. Gregory, J. Catazaro, A. J. Rossini, R. S. Klausen, *Poly(cyclosilane) Postpolymerization Hydrosilylation*, Macromolecules **57**, 4095 (2024)

Publications

1. M. G. Coschigano, S. L. Gregory, J. Catazaro, A. J. Rossini, R. S. Klausen, *Poly(cyclosilane) Postpolymerization Hydrosilylation*, Macromolecules **57**, 4095 (2024)

2. W. Guan, L. Li, Q. Jiang, A. F. Gittens, Y. Wang, L. F. T. Novaes, R. S. Klausen, S. L. Lin, *An electrochemical strategy to synthesize disilanes and oligosilanes from chlorosilanes*, Angewandte Chemie Int. Ed. **135**, e202303592 (2023).

3. A. F. Gittens, Q. Jiang, M. A. Siegler, R. S. Klausen, *Conjugation in Isomeric Cyclosilane Thioethers*, Organometallics **41**, 3762 (2022).

4. Q. Jiang, A. F. Gittens, S. Wong, M. A. Siegler, R. S. Klausen, *Highly selective addition of cyclosilanes to alkynes enabling new conjugated materials*, Chem. Sci. **13**, 7587 (2022).

5. F. Fang, Q. Jiang, R. S. Klausen, *Poly(cyclosilane) Connectivity Tunes Optical Absorbance*, J. Am. Chem. Soc. **144**, 7834 (2022).

Crystal Growth and Quantum Phases of Frustrated Rare Earth Oxides

Joseph W. Kolis, Department of Chemistry, Clemson University,

Kate Ross, Department of Physics, Colorado State University

Keywords: Quantum Materials, Hydrothermal, Single Crystals, Spin Ice

Research Scope

This project focuses on the exploration of potential quantum materials made of single crystals of three dimensional lattices containing lanthanide ions. Special emphasis is placed on pyrochlore and perovskites as they contain multiple axes of trigonal symmetry leading to possible frustration. Single crystals are often quite useful since higher structural resolution can be obtained and the crystals can be oriented in external magnetic fields. Pyrochlores $A_2B_2O_7$ (A = lanthanide, B = magnetically silent tetravalent ion, Ti, Ge, Sn, Zr, Hf)) are our initial targets because they can act as nonclassical quantum materials like quantum spin ices and are 3-D test beds for quantum spin liquids.[1] Unfortunately the lanthanide oxides are exceptionally refractory and usually require extremely high temperatures to grow single crystals. This commonly leads to lattice defects that jeopardize the measurement of quantum states. Instead we use a unique high temperature hydrothermal technique developed in our labs. This leads to decently sized single crystals at relatively low temperatures (6-700˚C). It eliminates many of the lattice defects and opens the door to the preparation and characterization of quantum materials.[2] The primary goal of this project is to test this hypothesis and use our technique to prepare samples suitable for measurements that could identify quantum behavior. It is our hope that this could open a whole new route to quantum materials.

In addition to the pyrochlores, the perovskites and the double perovskites are also promising materials with potential frustration and quantum properties. In this work we will focus on two preliminary results. One is a completely unexpected outcome that stems from an attempt to form double perovskites. We were surprised to obtain large high quality single crystals of a broad but poorly studied class of minerals called adelites, with the formula $AB(EO_4)(OH)$ with quasi 1-D chains and an acentric space group. In our case we isolated $LnTM(GeO_4)(OH)$ where Ln = La – Sm and TM^{2+} = Mn, Co, Ni, Zn).[3] This large matrix of possibilities provides with an excellent opportunity to study the coupling between d- and f-block magnetic ions in acentric frustrated systems. We are also initiating study of the lanthanide ruthenates. This is in the very early stages and while starting to prepare ruthenium pyrochlores $Ln_2Ru_2O_7$, we stumbled upon perovskites $LnRuO_3$ (Ln = Pr, Nd, Sm) containing S = ½ Ru^{3+}. Although the results are very preliminary they display some very interesting and exciting transport properties.

Recent Progress

The lanthanide pyrochlores contain a magnetically silent tetravalent ion at the B site. and we will focus on some results using Sn^{4+} as the B-site ion. Stannate is the only ion that can form stable cubic pyrochlore phases $Ln_2Sn_2O_7$ for all the lanthanides. $Ce_2Sn_2O_7$ is most challenging from a chemical viewpoint because of the tendency of Ce to oxidize and form a disordered fluorite phase. This is an exciting problem because the Ce^{3+} f^1 state is predicted be a quantum spin liquid via dipole-octupole coupling.[4] Previously reported material was prepared by high temperature methods and displayed considerable chemical instability, changing color and decomposing over time.[5] With effort we were able to make stable crystals that remained intact indefinitely (Fig.a). Detailed neutron scattering experiments suggest strongly that the material is not

a D-O material but rather an ordered dipolar All-In-All-Out (AIAO) spin ice (Fig. b.).[6] Diffuse scattering measurements at SNS and ultralow (20 mK) heat capacity measurements at Los Alamos are planned in the coming months to attempt to trap the quantum spin liquid.[7] These experiments are led by our collaborator, Professor Bruce Gaulin at McMaster University. Since the Pr and Nd stannates are also predicted to display quantum spin behavior,[8] possibly via D-O coupling, we grew single high quality single crystals of them for our collaborators at Oak Ridge (Aczel, Ortiz, Paddison and Calder). Early measurement results are very promising. For example preliminary INS of $Nd_2Sn_2O_7$ does appear to display dipole octupole quantum spin ice behavior.

The adelites LnTM $(GeO_4)(OH)$ (Ln = La – Sm and TM^{2+} = Mn, Co, Ni, Zn) provide a very large matrix of spin states to enable the careful study of magnetic coupling in an anisotropic acentric system. We already have many crystals and these are under investigation to probe the coupling of d- and f-electron ions in quasi 1-D environments. Our initial study of "simple" system of $LaCo(GeO_4)(OH)$ with no f-electrons, we observe at least three magnetic structures with magnetic frustration from intra and interchain coupling (Fig.c.).[3] They show metamagnetic field dependence with cycloidal magnetic vectors and frustration caused by Dzyaloshinski-Moriya coupling. We will use neutron scattering to determine the magnetic structures while also systematically building in more magnetic complexity using other lanthanide and d-block ions.

Finally, we will present some very preliminary results on lanthanide ruthenates with focus on the perovskites, especially $PrRuO_3$ and $NdRuO_3$. In both cases we can prepare small crystals that are fully ordered and stoichiometric. This is significant because Ru^{3+} is notoriously unstable in oxide environments. Early studies on powders display some very interesting behavior, including a ferromagnetic ordering transition at 150K and possible superconducting behavior around 15K.

a) 

b) 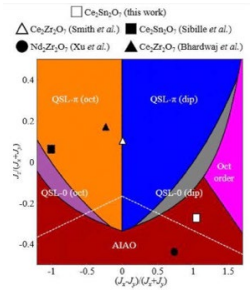

c) 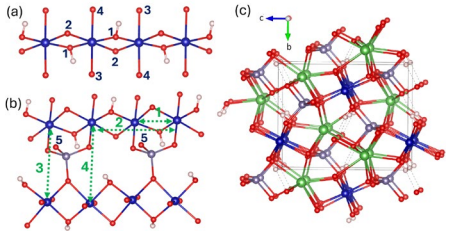

Figure a) large single crystals of Ce_2Sn_2O7. b) The magnetic phase diagram of $Ce_2E_2O_7$ with the stannate placed in the AIAO region. c) the structure of $LaCo(GeO_4)(OH)$

References

1. J.G. Rau and M. J. Gingras *Frustrated quantum rare-earth pyrochlores*. Annual Review of Condensed Matter Physics. **10**, 357-86 (2019).
2. J. W. Kolis and McMillen, C. D. *High Temperature Hydrothermal Synthesis of Inorganic Compounds* Comprehensive Inorganic Chemistry III Reedijik, J.; Poeppelmeier, K. (eds.) Elsevier 2023**.**
3. M. S. Powell, C. D. McMillen, H.-J. Koo, M.-H. Whangbo and J. W. Kolis *Lanthanide-Germanate Adelites, LnCo(GeO$_4$)(OH) (Ln = La-Sm) Containing One-Dimensional Co^{2+} Chains with Unusual Magnetic Structures* Inorg. Chem. (2024) submitted.
4. R.Sabille, E. L'hotel, V. Pomjakushin, C. Baines, T.Fennell and M.Kenzelmann *Candidate quantum spin liquid in the Ce^{3+} pyrochlore stannate Ce$_2$Sn$_2$O$_7$.* Physical Review Letters. **115** 097202 (2015).
5. R. Sibille, N. Gauthier, E. L'hotel, V. Porée, V. Pomjakushin, R.A. Ewings, T.G. Perring, J. Ollivier, A. Wildes, C. Ritter and T.C. Hansen *A quantum liquid of magnetic octupoles on the pyrochlore lattice.* Nature physics. **16**, 546-52. (2020)
6. D.R. Yahne B Plack, R. Schäfer, O. Benton, R. Moessner, M. Powell, J. W. Kolis, C. M. Pasco, A. F. May, M. D. Frontzek, E. M. Smith, B. D. Gaulin, S. Calder and K. A. Ross *Dipolar spin ice regime proximate to an all-in-all-out Néel ground state in the dipolar-octupolar pyrochlore Ce$_2$Sn$_2$O$_7$* Phys. Rev. X **14**, 011005. (2024)
7. E. M. Smith, J. Dudemaine, B. Placke, R. Schäfer, D.R. Yahne, T. DeLazze, A. Fitterman, J. Beare, J. Gauder, C. R. Buhariwalla, and A. Podlesnyak. *Quantum spin ice response to a magnetic field in the dipole-octupole pyrochlore Ce$_2$Zr$_2$O$_7$.* Physical Review B. **108**, 054438. (2023)
8. B.R. Ortiz, P.M. Sarte, G. Pokharel, M.J. Knudtson, S.J. Gomez Alvarado, A.F. May, S. Calder, L. Mangin-Thro, A.R. Wildes, H. Zhou and G. Sala G. *Revisiting spin ice physics in the ferromagnetic Ising pyrochlore Pr$_2$Sn$_2$O$_7$.* Physical Review B. **109**, 134420. (2024)

Publications over 2 years

M. S. Powell, C. D. McMillen, H.-J. Koo, M.-H. Whangbo and J. W. Kolis *Lanthanide-Germanate Adelites, LnCo(GeO$_4$)(OH) (Ln = La-Sm) Containing One-Dimensional Co^{2+} Chains with Unusual Magnetic Structures* Inorg. Chem. (2024) submitted

J.W. Kolis, M. Powell *Hydrothermal Growth of Magnetically Frustrated Crystals: Lanthanide Stannate Pyrochlores as a Prototype* America Assoc. Crystal Growth Tucson AZ August **2023**

D.R. Yahne B Plack, R. Schäfer, O. Benton, R. Moessner, M. Powell, J. W. Kolis, C. M. Pasco, A. F. May, M. D. Frontzek, E. M. Smith, B. D. Gaulin, S. Calder and K. A. Ross *Dipolar spin ice regime proximate to an all-in-all-out Néel ground state in the dipolar-octupolar pyrochlore Ce$_2$Sn$_2$O$_7$* Phys. Rev. X **14**, 011005. (2024)

M. Powell, J.W. Kolis *Hydrothermal synthesis of lanthanide stannate pyrochlores: The curious case of spin-1/2 Ce$_2$Sn$_2$O$_7$* ACS Spring Meeting (2022) Abstract 3662312

J. W. Kolis and McMillen, C. D. *High Temperature Hydrothermal Synthesis of Inorganic Compounds* Comprehensive Inorganic Chemistry III Reedijik, J.; Poeppelmeier, K. (eds.) Elsevier 2023

D.R. Yahne, D. Pereira, L.C. Jaubert, L.D. Sanjeewa, M. Powell, J.W. Kolis, G. Xu, M.J. Gingras,and K.A. Ross, *Understanding Reentrance in Frustrated Magnets: The Case of Er$_2$Sn$_2$O$_7$ Pyrochlore* Phys. Rev. Lett. **127**, 277206. (2021)

Janus 2D Material Platform Enabled by Atomic-Layer Substitution

Jing Kong, Massachusetts Institute of Technology

Keywords: Janus monolayers, atomic-layer substitution, transition metal dichalcogenide

Research Scope

This project aims at using the room-temperature (RT) atomic layer substitution (ALS) strategy developed in our previous DOE BES supported research to continue the development of a variety of revolutionary 2D Janus materials and structures that have never been obtained before. In addition, for the Janus materials/structures that have already been demonstrated by our group, there is a great need to characterize their properties and develop their applications. Our proposed research can be divided into three areas: (1) For the already developed Mo- and W- based, S- or Se- Janus structures, we plan to carry out in depth characterizations and further investigations on the conversion process, so that the reaction can be extended to Te- Janus and 1T' Janus materials; (2) We plan to use our ALS method to develop a set of novel Janus structures based on new TMD host materials and study their interesting properties; (3) based on our current understanding on the ALS process, we propose to extend it to wider range of 2D materials, beyond TMD.

Recent Progress

Under the support of this project, during the past year, we have made the following progress:

1. During the past year, we have explored two different reaction pathways for the Janus conversion, this has led to the same Janus material but with opposite dipole orientations, and we have found the chalcogen type in the starting material has direct influence on the RT-ALS reaction energy barrier and the degree of Janus conversion (Fig. 1). We are currently writing the manuscript and plan to submit it in the near future.
2. We have also worked with Prof. Ju Li (MIT)'s group and Prof. Aaron Lindenberg (Stanford)'s group on the characterization of non-linear optical properties of the Janus 1T' MoSSe via high harmonic generation (HHG), THz emission and second harmonic generation measurements. It was found that indeed 1*T'* MoSSe shows orders of magnitude enhancement in THz nonlinearities (e.g., it has > 50 times higher than 2*H* MoS2 for 18th order harmonic generation; and it shows > 20 times higher than 2*H* MoS2 for terahertz emission). These results confirmed our 2021 theoretical prediction and indicated the potential for the 1T' Janus TMD in nonlinear optical applications such as scalable attosecond sources. These results confirmed our 2021 theoretical prediction and indicated the potential for the 1T' Janus TMD in nonlinear optical applications such as scalable attosecond sources. This work has been published at Nature Communications in 2023.

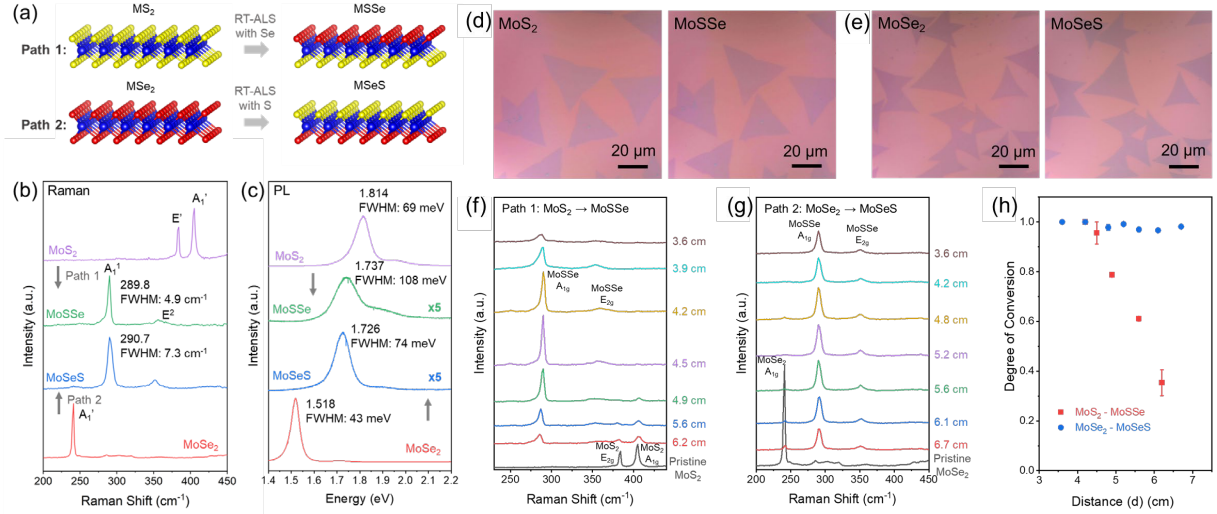

Figure 1. (a) Schematic illustration of the two conversion pathways leading to MoSSe or MoSeS. (b, c) Raman (b) and PL (c) spectra of the starting MoS_2 monolayer and the resulting Janus MoSSe, and starting $MoSe_2$ monolayer and the resulting MoSeS. (d, e) Optical microscope images of the starting MoS_2 monolayer and the resulting Janus MoSSe, and starting $MoSe_2$ monolayer and the resulting MoSeS. (f-h) Distant dependent Raman spectra for the two different paths (f & g) and the degree of conversion as a function of distant d, indicating location dependent conversion rate and a lower reaction barrier for conversion from $MoSe_2$.

3. We have continued our collaborations with Prof. Shengxi Huang's group on the characterizations of MoSSe/MoS_2 heterobilayers, and also worked with Prof. Riichiro Saito in Tohuku University in Japan on the theoretical understandings on the nonlinear optical responses of these heterobilayers optimized by stacking order and strain. From the theoretical calculation, we found that the non-linear susceptibility, χ_2, of the AA stacking MoSSe/MoS_2 is three times as large as AB stacking (AA: 550pm/V; AB: 170pm/V) due to the broken inversion symmetry in AA. Further, a relatively large, two-dimensional strain (0.04) that breaks C_{3v} point group symmetry of the MoSSe/MoS2, enhances the χ_2 values for both AA (900pm/V) and AB (300pm/V) stacking by 1.6 times as large as that without strain. This work has been published in ACS Nano in 2023.

4. We have been collaborating with Dr. Andrey Krayev in Horiba Scientific to characterize these Janus TMD with tip enhanced Raman spectroscopy. We have observed some interesting results, and have been trying to understand the phenomena.

5. During the course of this project, Dr. Nannan Mao, Dr. Tianyi Zhang and Dr. Peng Wu (who have been partially supported by this project) have also carried out collaborations within our own group or outside our group, with several other publications. Even though these progresses are not directly using Janus materials, they are important progresses in the field acknowledging the support of this project.

Publications

List of publications SUPPORTED BY BES DE-SC0020042 (2023-2024):

1. Nannan Mao, Yue Luo, Ming-Hui Chiu, Chuqiao Shi, Xiang Ji, Tymofii S Pieshkov, Yuxuan Lin, Hao-Lin Tang, Austin J Akey, Jules A Gardener, Ji-Hoon Park, Vincent Tung, Xi Ling, Xiaofeng Qian, William L Wilson, Yimo Han, William A Tisdale, Jing Kong, "Giant Nonlinear Optical Response via Coherent Stacking of In-Plane Ferroelectric Layers", Advanced Materials, 2210894, (2023) DOI: https://doi.org/10.1002/adma.202210894
2. Ming-Hui Chiu, Xiang Ji, Tianyi Zhang, Nannan Mao, Yue Luo, Chuqiao Shi, Xudong Zheng, Hongwei Liu, Yimo Han, William L. Wilson, Zhengtang Luo, Vincent Tung, Jing Kong, "Growth of Large-Sized 2D Ultrathin SnSe Crystals with In-Plane Ferroelectricity", Advanced Electronic Materials, 2201031, (2023) DOI: https://doi.org/10.1002/aelm.202201031
3. Yue Luo, Nannan Mao, Dapeng Ding, Ming-Hui Chiu, Xiang Ji, Kenji Watanabe, Takashi Taniguchi, Vincent Tung, Hongkun Park, Philip Kim, Jing Kong, William L Wilson, "Electrically switchable anisotropic polariton propagation in a ferroelectric van der Waals semiconductor", Nature Nanotechnology, (2023) DOI: https://doi.org/10.1038/s41565-022-01312-z.
4. Jiadi Zhu, Ji-Hoon Park, Steven A. Vitale, Wenjun Ge, Gang Seob Jung, Jiangtao Wang, Mohamed Mohamed, Tianyi Zhang, Maitreyi Ashok, Mantian Xue, Xudong Zheng, Zhien Wang, Jonas Hansryd, Anantha Chandrakasan, Jing Kong, Tomás Palacios, "Low thermal budget synthesis of monolayer molybdenum disulfide for silicon back-end-of-line integration on 200 mm platform", Nature Nanotechnology, 18, 456–463 (2023) DOI: https://doi.org/10.1038/s41565-023-01375-6
5. Shuai Fu, Ji-Hoon Park, Hongyan Gao, Tianyi Zhang, Xiang Ji, Tianda Fu, Lu Sun, Jing Kong, Jun Yao, “Two-Terminal MoS2 Memristor and the Homogeneous Integration with a MoS2 Transistor for Neural Networks”, Nano Letters, (2023), 23, 13, 5869–5876. https://doi.org/10.1021/acs.nanolett.2c05007
6. Jiaojian Shi, Haowei Xu, Christian Heide, Changan HuangFu, Chenyi Xia, Felipe de Quesada, Hao Zhou, Tianyi Zhang, Leo Yu, Amalya Johnson, Fang Liu, Enzheng Shi, Liying Jiao, Tony Heinz, Shambhu Ghimire, Ju Li, Jing Kong, Yunfan Guo, Aaron M. Lindenberg, “Giant room-temperature nonlinearities from a monolayer Janus topological semiconductor”, Nature Communications, Volume 14, 4953, Published, 2023, DOI: ttps://doi.org/10.1038/s41467-023-40373-z.
7. Nguyen T. Hung, Kunyan Zhang, Vuong V. Thanh, Yunfan Guo, Alexander A. Puretzky, David B. Geohegan, Jing Kong, Shengxi Huang, Riichiro Saito, “Nonlinear Optical Responses of Janus MoSSe/MoS2 Heterobilayers Optimized by Stacking Order and Strain”, ACS Nano 2023, 17, 20, 19877–19886, https://doi.org/10.1021/acsnano.3c04436
8. Tianyi Zhang, Jiangtao Wang, Peng Wu, Jing Kong, “Vapor Phase Deposition of Two-Dimensional Layered Chalcogenides”, Nature Reviews Materials, Volume 8, 799, Published, 2023, DOI: https://doi.org/10.1038/s41578-023-00609-2.
9. Hongwei Liu, Tianyi Zhang, Peng Wu, Hae Won Lee, Zhenjing Liu, Tsz Wing Tang, Shin-Yi Tang, Ting Kang, Ji-Hoon Park, Jun Wang, Kenan Zhang, Xudong Zheng, Yu-Ren Peng, Yu-Lun Chueh, Yuan Liu, Tomás Palacios, Jing Kong, and Zhengtang Luo, “Boosting Monolayer Transition Metal Dichalcogenides Growth by Hydrogen-Free Ramping during Chemical Vapor Deposition”, Nano Lett. 2024, 24, 27, 8277–8286 https://doi.org/10.1021/acs.nanolett.4c01314

DE-SC0022230-Novel Strategies for Direct Air Capture and Conversion of CO_2 Using Dual-Function Materials

PI-Debasish Kuila, NC A&T State University, Greensboro, NC 27411; dkuila@ncat.edu

North Carolina A&T State University (D. Kuila, A. Prokofjevs, J. Lou); Caltech (W. Goddard)

Keywords: Phosphine Oxide, Phosphine Borane, Cu-Pd Bimetallic, Mixed Matrix Membranes

Research Scope

During the implementation period of this project, we created the infrastructure required for synthesis and characterization of air sensitive compounds in the Department of Chemistry at NCA&T. In collaboration with Goddard's research group at Caltech, we have been screening a number of phosphorus derivatives that could potentially bind CO_2. We are also investigating other CO_2 capture agents such as metal organic frameworks (MOFs) and activated carbons (1, 2). We are also investigating the fabrication of mixed matrix membranes by incorporating phosphine oxide and silica as fillers to separate CO_2 gas from N_2, and O_2 gas mixtures (3). In parallel, we are exploring the effect of various catalysts on electrochemical CO_2 reduction using an H-cell (4).

Recent Progress

Low pKa Borane Phosphines Capture Carbon Dioxide with Exceptional Strength: DFT Predictions Followed by Experimental Validation (*Riasati, Musgrave, Yeboah, Prokofjevs, Goddard III*).

We report a combined computational-experimental study that discovers new anionic borane-phosphines (BoPh) for the efficient capture of CO_2. We used Quantum Mechanics (QM) to predict CO_2 binding for BoPh's with free energies of -12.8 to -24.0 kcal/mol at 300K followed by NMR experimental validation in d_8-THF solution.

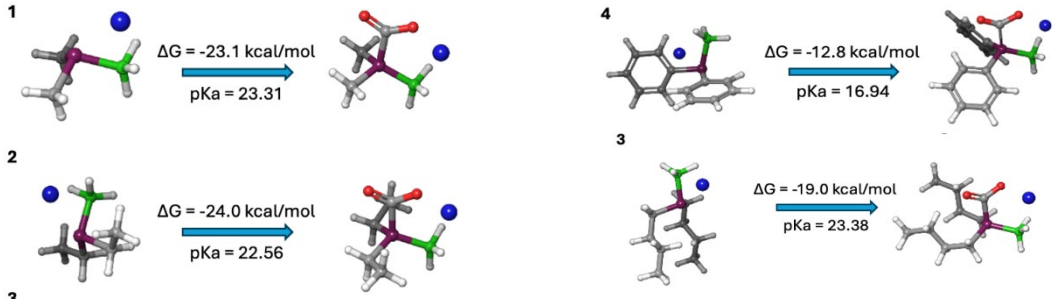

CO_2 Capture using Adsorbents (*Mukherjee, Sarkar, Hassan, Kuila*)

We have synthesized amine incorporated hierarchical metal organic framework (MOF) MIL-101(Cr)/SBA-15, meso/micro-porous composites, with tailored properties for CO_2 capture. The optimized composite i.e., MIL-101(Cr)/SBA-15/PEI-25 showed improved pseudo-equilibrium adsorption capacity of 3.2 mmol/g at 303 K and 1 bar, compared to nascent SBA-15 (0.8 mmol/g) and the MOF, i.e., MIL-101(Cr) (1.3 mmol/g). Such adsorption performance can be attributed to

the basic sites of the impregnated polyethyleneimine (PEI), unsaturated Cr(III) metal sites, and the hierarchical pore structure of the composite which imparts chemical as well physical adsorption forces towards CO_2 uptake.

Electrochemical Reduction of CO_2 to Value added Products Using a Cu-Pd Bimetallic Catalyst (*Gupta, Mukherjee, Das, Goddard, Kuila*)

Reduction of CO_2 at ambient temperature and pressure via electrochemical routes (eCO_2RR) to obtain value-added products is a potential approach towards net zero emission. We report here experimental development of bimetallic Cu-Pd based catalysts for production of formate, methanol, and acetate via eCO_2RR, followed by Quantum Mechanical calculations as a function of applied potential confirming the experiments.

Phosphine Oxide-Based Polyimide Membranes for Separation of CO_2/CH_4 and CO_2/N_2 (*Chowdhury, Lou, Kuila, Mukherjee).*

We prepared mixed matrix membranes (MMMs) using different weight percentages of phosphine oxide-based polysulfone into the polyimide matrix to separate CO_2 gas from N_2, and CH_4. Our preliminary results show that the incorporation of phosphine oxide-based polysulfone into the polyimide matrix improves the separation efficiency of CO_2/CH_4 and CO_2/N_2.

References

1. Mahajan, S. and Lahtinen, M., 2022. Recent progress in metal-organic frameworks (MOFs) for CO2 capture at different pressures. Journal of Environmental Chemical Engineering, 10(6), p.108930.
2. Abuelnoor, N., AlHajaj, A., Khaleel, M., Vega, L.F. and Abu-Zahra, M.R., 2021. Activated carbons from biomass-based sources for CO2 capture applications. Chemosphere, 282, p.131111.
3. Ataeivarjovi, E., Tang, Z. and Chen, J., 2018. Study on CO2 desorption behavior of a PDMS–SiO2 hybrid membrane applied in a novel CO2 capture process. ACS applied materials & interfaces, 10(34), pp.28992-29002.
4. Xiao, C. and Zhang, J., 2021. Architectural design for enhanced C2 product selectivity in electrochemical CO2 reduction using Cu-based catalysts: a review. ACS nano, 15(5), pp.7975-8000.

Publications:

1. Musgrave III, Charles B., Prokofjevs, A., and Goddard III., W.A. "Phosphine Modulation for Enhanced CO_2 Capture: Quantum Mechanics Predictions of New Materials." *The Journal of Physical Chemistry Letters* 13, no. 48 (2022): 11183-11190.
2. Mukherjee, D., Hassan, S., Shajahan, J., Prokofjevs, A. and Kuila, D. “Synergistic Enhancement of CO_2 Capture via Amine Decorated Hierarchical MIL-101 (Cr)/SBA-15 Composites.” *Materials Chemistry and Physics*, 322, 129533, 2024.
3. Riasati, A., Musgrave III, C., Yeboah, N., Prokofjevs, A., and Goddard III., W.A. “Low pKa Borane Phosphines Capture Carbon Dioxide with Exceptional Strength: DFT Predictions Followed by Experimental Validation.” (Communicated to *Science*).
4. Chowdhury, M.J., Lou, J., Kuila, D., Mukherjee, D. “Surface-treated fumed silica in polydimethylsiloxane (PDMS) mixed matrix membrane for CO_2 separation application.” (Communicated to *Separation and Purification Technology*).
5. Gupta, S., Mukherjee, D., Das, T., Goddard III., W.A. Kuila, D. “Electrochemical Reduction of CO_2 to Value added Products Using a Cu-Pd Bimetallic Catalyst”. (to be communicated shortly).

When Covalent Organic Frameworks Meet Cross-coupling Reactions: Directed Synthesis, Mechanistic Investigation, and Energy Application

Xinle Li, Clark Atlanta University

Keywords: Covalent organic frameworks; topochemical polymerization; cross-coupling reaction; mechanochemistry; photocatalysis

Research Scope

This project challenges two primary conventions in the field of covalent organic frameworks (COFs), an emerging class of crystalline porous solids. The first convention is the prevalent reliance on reversible reactions, which severely restricts the inherent chemical stability and structural complexity of COFs. The second convention involves traditional solvothermal synthesis, known for its tediousness, time consumption, and use of toxic solvents. To overcome the first obstacle, our established versatile template directed approach, also known as topochemical synthesis, will enable the synthesis of new sp^2c-COFs through the irreversible reaction, Heck reaction, which is previously considered impractical for COF synthesis. This innovative approach has the potential to revolutionize bulk COF synthesis by allowing precise control over synthetic pathways and facilitating the development of new porous crystalline materials, which hold vast promise for energy applications even under extreme conditions, addressing a significant obstacle to the practical use of COFs. To address the second synthetic limitation, we employ a sustainable alternative—mechanochemistry—to replace conventional thermal energy. This approach aims to establish a transformative toolkit for sustainable, rapid, and scalable COF synthesis. By adopting mechanochemistry, we not only address current bottlenecks but also promote green chemistry principles, leading to significant advancements in COF chemistry.

Recent Progress

I. Template-directed approach: We have pioneered a versatile template-directed approach for the facile preparation of sp^2-carbon conjugated covalent organic frameworks (sp^2c-COFs) through the classic irreversible reaction, Heck reaction. Imine-linked COFs serve as templates for the oriented growth of unsubstituted sp^2c-COFs,[1] resulting in highly crystalline sp^2c-COFs upon template removal. Solid-state ^{13}C NMR and FTIR analyses confirmed the removal of the imine COF template. In addition, the chemical stability of Heck-COF-1 was far superior to the imine COF template. This methodology significantly expands the range of sp^2c-COFs and enhances their utility in energy applications. Notably, Heck-COF-1 demonstrates exceptional efficiency in the oxidative hydroxylation of arylboronic acid, achieving a 99% yield of phenol within 3 hours under blue light irradiation, outperformed most reported imine COFs,[2] benzoxazole COFs,[3] and olefin-linked COFs.[4] We are currently extending the

approach to various unsubstituted sp^2c-COFs and exploring additional photocatalytic applications. More excitingly, this approach can be extended to other types of irrevisble reactions, which hold enorous potential to expand the synthetic toolbox for unprecedended COFs.

II. COF mechanochemistry. As the pioneering group dedicated to COF mechanochemistry in USA,[5] we have developed a green liquid-assisted mechanochemical synthesis of imine-linked COFs, which acted as highly efficient adsorbents for static iodine vapor capture. Unlike traditional solvothermal methods used for COF synthesis, our approach is characterized by its green nature, rapidity, efficiency, and scalability. Beyond bare COF synthesis, we have developed a mechanochemical *in situ* encapsulation strategy that enables the one-step synthesis of metal-encapsulated COFs. Remarkably, the obtained Pd/COF showed exceptional activity and broad substrate scope for the room temperature Suzuki-Miyaura coupling reaction. This mechanochemical *in situ* encapsulation strategy will open tremendous opportunities in developing a wide array of metal/COF hybrids for sustainable catalysis.

References

[1] E. Jin, K. Geng, K. H. Lee, W. Jiang, J. Li, Q. Jiang, S. Irle, D. Jiang, *Angew. Chem. Int. Ed*. 132, 12260-12267 (2020).

[2] X. Yan, H. Liu, Y. Li, W. Chen, T. Zhang, Z. Zhao, G. Xing, L. Chen, *Macromolecules* 52, 7977-7983 (2019).

[3] P.-F. Wei, M.-Z. Qi, Z.-P. Wang, S.-Y. Ding, W. Yu, Q. Liu, L.-K. Wang, H.-Z. Wang, W.-K. An, W. Wang, *J. Am. Chem. Soc*. 140, 4623-4631 (2018).

[4] S. Bi, P. Thiruvengadam, S. Wei, W. Zhang, F. Zhang, L. Gao, J. Xu, D. Wu, J.-S. Chen, F. Zhang, *J. Am. Chem. Soc*. 142, 11893-11900 (2020).

[5] J. Hu, Z. Huang, Y. Liu, *Angew. Chem. Int. Ed*. 62, e202306999 (2023).

Publications

1. Brown, N.; Alsudairy, Z.; Behera, R.; Akram, F.; Chen, K.; Smith-Petty, K.; Motley, B.; Williams, S.; Huang, W.; Ingram, C.; Li, X., Green mechanochemical synthesis of imine-linked covalent organic frameworks for high iodine capture. *Green Chem*. 25, 6287-6296 (2023).
2. Alsudairy, Z.; Brown, N.; Yang, C.; Cai, S.; Akram, F.; Ambus, A.; Ingram, C.; Li, X., Facile Microwave-Assisted Synthesis of 2D Imine-Linked Covalent Organic Frameworks for Exceptional Iodine Capture. *Precis. Chem*. 1, 233-240 (2023).
3. Alsudairy, Z.; Brown, N.; Campbell, A.; Ambus, A.; Brown, B.; Smith-Petty, K.; Li, X., Covalent organic frameworks in heterogeneous catalysis: recent advances and future perspective. *Mater. Chem. Front*. 7, 3298-3331 (2023).
4. Alsudairy, Z.; Zheng, Q.; Brown, N.; Behera, R.; Yang, C.; Hanif Uddin, M.; Saintlima, A.; Middlebrooks, L.; Li, J.; Ingram, C.; Li, X., Microwave-assisted synthesis of mixed-linker covalent organic frameworks enabling tunable and ultrahigh iodine capture. *Chem. Eng. J.* 485, 149135 (2024).
5. Campbell, A.; Alsudairy, Z.; Dun, C.; Akram, F.; Smith-Petty, K.; Ambus, A.; Bingham, D.; Dinadayalane, T.; Ingram, C.; Li, X., Dioxin-Linked Covalent Organic Framework-Supported Palladium Complex for Rapid Room-Temperature Suzuki-Miyaura Coupling Reaction. *Crystal*, 13, 1268 (2023).

Epitaxially-Fused Quantum Dot Superlattices with Collective Electronic and Magnetoelectronic Properties

Matt Law, University of California, Irvine

Keywords: nanocrystals, quantum dots, superlattices, self-assembly, charge transport

Research Scope

Chemically-synthesized colloidal quantum dots (QDs) are promising building blocks for making self-assembled crystalline solids that exhibit emergent collective properties (e.g., electronic, excitonic, magnonic). QD superlattices (SLs) fabricated by controlling self-assembly with near-atomistic precision are an example of heterogeneous, non-ideal, far-from-equilibrium mesoscale systems whose collective electronic behavior is critically dependent on various types of disorder (spatial and energetic) and the properties of interfaces spanning from the atomic to >10 μm length scales. However, existing QD SLs are too defective to allow for electronic miniband formation and charge carrier delocalization over useful distances.[1,2]

The major goals of this project are to fabricate and study QD solids that exhibit electronic minibands and to combine miniband transport with novel electronic and magnetic functionality to create a new class of materials that bring together the unique, size-dependent physics and solution processability of QDs with the excellent charge transport of bulk semiconductors for applications in next-generation electronics and optoelectronics. A series of new synthetic techniques will be deployed to make QD SLs of unprecendented electronic coupling, structural perfection, and energetic order, sufficient to enable minibands to form. Iteration between these synthesis innovations, atomic structural characterization by state-of-the-art electron microscopy, tomography, and X-ray scattering methods, and band structure and transport measurements will provide a dynamic synthesis/structure/property feedback loop for optimizing miniband formation and elucidating how miniband and charge carrier characteristics depend on defects and disorder across multiple length scales. A main outcome of the project will be the development of highly-perfect QD SLs that exhibit delocalized miniband charge transport, high mobility and long diffusion length, tunable doping, and excellent environmental stability. It will result in the first demonstration of emergent miniband transport in a self-assembled material and insights into the relationships between miniband width, carrier characteristics, structural defects, and energetic disorder. This understanding will facilitate the fabrication of several classes of multi-component QD crystals that further enhance the functionality of miniband transport by providing separate low-loss transport channels for electrons and holes and magnetic periodicity that engenders three-dimensional magnonic band gaps and strong magnetotransport and electron-magnon interactions.

Recent Progress

In the first nine months of this new project, we have focused on novel methods to make and characterize highly-ordered PbSe QD SLs. We demonstrated that electrospray deposition (ESD) yields superior oleate-capped SLs. Oleate-capped SLs are normally prepared by drop casting and slowly drying a dispersion of oleate-capped QDs in a volatile nonpolar solvent (e.g., hexane) on the surface of liquid ethylene glycol (EG), but the dropcast QD dispersion spreads

across the EG surface in a complex, turbulent, and irreproducible fashion, resulting in nonuniform films rich in flow defects (QD positional disorder). In contrast, electrospray generates a plume of microscale droplets that impinge gently across the entire EG surface to build up a uniform and continuous layer of concentrated QD dispersion that slowly dries in place without macroscopic liquid flow. We showed that ESD of decane dispersions of oleate-capped PbSe QDs onto the surface of EG produces oleate-capped SL films that are largely free from flow defects and homogeneous over large areas (~20 cm^2). Electron microscopy imaging, grazing incidence small-angle X-ray scattering, and infrared spectroscopy studies indicate that the ESD films have the same superlattice unit cell and surface chemistry as the dropcast films, but the flow defects present in the dropcast films are nearly absent in the ESD films. Unlike dropcast films, the ESD films are continuous and uniform over the entire EG surface and their thickness can be precisely controlled by the sprayed volume. Epitaxially-fused SLs (epi-SLs) made from the ESD films via amine injection or photobase triggering showed unprecendented intra-grain structural perfection. ESD makes possible the reproducible fabrication of extremely high-quality, high-uniformity, and large-area QD SLs. Epi-SLs made by ESD have a much lower concentration of intra-grain structural defects and are therefore the most promising self-assembled system now available for observing the emergence of electronic minibands. The success of the ESD effort puts the project in an excellent position to study miniband formation. A manuscript about the ESD films is now in preparation.

We have worked with our collaborators at UC Davis (Prof. Adam Moule and his student Ethan Field) to characterize the internal structural defects of (dropcast) epi-SL films as a function of film thickness using high-resolution electron tomography carried out at the National Center for Electron Microscopy at LBNL. Tomograms for ~10 epi-SL samples of varying film thickness (40-180 nm) have been reconstructed and we are now in the process of analyzing these massive datasets to determine how epi-SL structural defects depend on film thickness. We observe nearly-perfect necking connectivity (~99%) in the thicker films, demonstrating that unprecedented coupling order and mesoscale atomic coherence is achievable with this materials system.

We have also started making PbS QDs in order to fabricate layered binary PbSe-PbS epi-SLs as described in the proposal. The latest results on the PbSe-PbS QD SLs will be presented.

References

1. K. Whitham, J. Yang, B. H. Savitzky, L. F. Kourkoutis, F. Wise, and T. Hanrath, *Charge transport and localization in atomically coherent quantum dot solids*, Nat. Mater. 15, 557 (2016).
2. A. Abelson, C. Qian, Z. Crawford, G. T. Zimanyi, and M. Law, *High-mobility hole transport in single-grain PbSe quantum dot superlattice transistors*, Nano Lett. 22, 9578 (2022).

Publications

1. G. Kim and M. Law, *Electrospray deposition of PbSe quantum dot superlattices with improved uniformity and structural perfection*, To be submitted.

Understanding Solid-Solution-Reaction vs. Solid-Phase-Transformation Competition of Complex Conversion Materials Dominated by Interfacial Kinetics

Chuan-Fu Lin

The Catholic University of America, Washington DC, 20064

Keywords: Conversion materials, phase separation, solid solutions, Interfacial kinetics.

Research Scope

The scope of this project is to explore the competition between solid-solution reaction vs. solid-state transformation in conversion materials controlled by interfacial kinetics. Conversion materials promised high capacity but failed in reversibility due to the solid-state phase transformation, while it is interesting to note that lithiation often starts with an "intercalation" process. The fundamentals of the competition between conversion vs. intercalation are not clear. We plan to comprehensively study which (and how) kinetic factors, play a critical role in the competition of the "intercalation" and "conversion" reactions. By developing a pristine material platform with thin-film architecture to pursue high reaction homogeneity, we attempt to decouple the nucleation, chemical, mechanical effects on controlling the conversion reaction.

For the case study of conversion material FeOF, there is a wide variation of the onset of conversion reaction across theory and various experimental conditions, as shown in Fig 1 [1-3]. One of the essential hypotheses motivated this proposal is: *Can we control (promote/suppress) the conversion reaction?* For example, using the lithium conducting surface coating as the chemical and mechanical constraints to delay the conversion reactions. This research will facilitate the fundamental knowledge of the energetic competitions between the solid solution phases following the "intercalation" process and the phase transformation following the "conversion" process, which is also a fundamental question in material science.

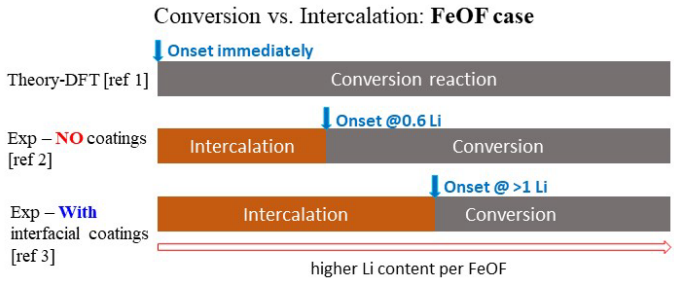

Fig. 1 Wide variation in theoretical prediction and experimental observations of the onsets of conversion reaction.

Recent Progress

First, we developed amorphous to highly crystalline FeF_3 and FeF_2 conversion materials through sputtering deposition technique to study the thresholds of conversion reaction depending on the crystallinity of the conversion materials. An amorphous to crystalline transition is observed for FeF_3 deposited between 250 ~ 400 °C through the technique. It was found that the densities, the lithiation potentials (the onset potentials of conversion reaction) increase with the crystallinity

of the Fe-F based conversion materials. The high-density, crystalline FeF_3 exhibits an observed higher lithiation potential (Δ of ~ 0.43 V) than the low-density, amorphous FeF_3. To interpret the observed potential difference $\Delta E = E_{amorphous} - E_{crystalline} \sim -0.43$ V ($\Delta E < 0$) from amorphous to crystalline FeF_3, it suggests that the difference of chemical potentials for Li accommodation ($\Delta\mu_{Li}$) from amorphous to crystalline $\Delta\mu_{Li} = \mu_{Li\text{-amorphous}} - \mu_{Li\text{-crystalline}} > 0$, which means that the Li accommodation in the amorphous matrix is more difficult than in the crystalline phase. The chemical potential for Li accommodation (μ_{Li}) in the amorphous phase is determined by the ionic chemical potentials (μ_{Li^+}) and the electronic chemical potential (μ_{e^-}) during lithiation in the amorphous matrix, that is, $\mu_{Li} = \mu_{Li^+} + \mu_{e^-}$. The plausible explanation for the decreased lithiation potential for the amorphous phase is the fact that due to the size fluctuations in the amorphous phase facilitating an easier Li^+ accommodation (lowering μ_{Li}), the loss of crystalline periodicity of FeF_3 dominated hinders the accommodation of electronic carriers during the lithiation process (increasing μ_{Li}) [4]. Therefore, the figure depicts the crystallinity dependent lithiation behaviors for FeF_3.

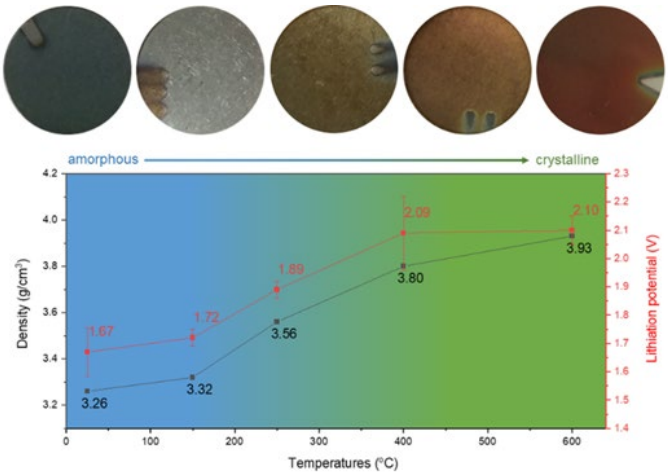

Fig 2. Relationship of the density and lithiation potential of conversion reaction vs. FeF3 thin film's temperatures.

Second, we investigated the nucleation effect on the onsets of conversion reaction by applying the seed coating vs. anti-seed coating. We prepared coated FeF_3 slurry electrodes with 50 nm seed coating (LiF, note: LiF is considered as the seed coating is because LiF is one of the products of the conversion reaction of FeF3) or 50 nm anti-seed coating (LiPON – not the reaction product) and analyzed them using cyclic voltammetry. The CVs reveal that the onset of conversion reaction was promoted with LiF coating by ~ + 0.1 V and the onset of conversion reaction was suppressed/delayed with LiPON thin film coating by ~ - 0.1 V. This agrees with our hypothesis that the pre-existing of the seed coating before the conversion reaction occurs will reduce the nucleation barrier (energy cost) for the formation of the products of the conversion reaction, i.e. promoting the reaction to occur with smaller driving force (higher discharging potential) – the conversion reaction is promoted through a "heterogenous nucleation" process. In comparison, the conversion reaction process of FeF_3 with an anti-seed coating, went through a "homogeneous nucleation" process that costs larger driving force to overcome the energy barriers, therefore, delayed the onset of the conversion reaction.

References

[1] V. L. Chevrier, G. Hautier, Shyue, P. Ong, R. E. Doe, and G. Ceder, "*First-Principles Study of Iron Oxyfluorides and Lithiation of FeOF*" PHYSICAL REVIEW B **87**, 94118, (2013).

[2] K. M. Wiaderek, O. J. Borkiewicz, E. Castillo-Martínez, R. Robert, N. Pereira, G. G. Amatucci, C. P. Grey, P. J. Chupas, and K. W. Chapman, "*Comprehensive Insights into the Structural and Chemical Changes in Mixed-Anion FeOF Electrodes by Using Operando PDF and NMR Spectroscopy*" Journal of the American Chemical Society **135**, 10, 4070–4078. (2013)

[3] C.-F. Lin, X. Fan, A. Pearse, S. Liou, K. Gregorczyk, M. Leskes, C. Wang, SB. Lee, G. Rubloff, and M. Noked, "*Highly Reversible Conversion-Type FeOF Composite Electrode with Extended Lithium Insertion by Atomic Layer Deposition LiPON Protection*" Chemistry of Materials **29**, 20 (2017)

[4] C. Zhu, X. Mu, J. Popovic, K. Weichert, P. A. Van Aken, Y. Yu, and J. Maier, "*Lithium potential variations for metastable materials: Case study of nanocrystalline and amorphous LiFePO4*" Nano Lett., **14** (9), 5342−5349, (2014)

Publications

B. Hoang, V. C. Ferrari, H. Wang, D. M. Stewart, R. Damircheli, C. -F. Lin, "*From Amorphous to Crystalline Thin-Film FeF 3 Conversion Electrodes by Sputtering Deposition*" ACS Applied Energy Materials, **6**, 19, 10005–10011 (2023)

Designing Photoresponsive Nanosponges for Efficient and Reversible Capture and Release of Carbon Dioxide

Dr. Yangyang Liu

California State University, Los Angeles

Keywords: metal-organic frameworks (MOFs), photoresponsive, carbon capture, core-shell MOFs, reversible materials.

Research Scope

Our overarching goal of this project is to develop photoresponsive porous materials that can efficiently capture CO_2 from the air and can be easily regenerated utilizing visible light/sunlight for multiple reversible cycles without sacrificing the overall CO_2 adsorption capacity of the materials. We will design core-shell MOFs with a photoresponsive "gate" for controlled CO_2 capture and release (Figure 1). Upon saturation of CO_2, the release of CO_2 from the materials can be triggered by visible light/sunlight, minimizing the energy required for materials regeneration. This project is expected to discover new materials with high CO_2 capacity, excellent CO_2 selectivity over N_2 and other gases, and outstanding hydrolytic stability, which can maintain their structures and CO_2 adsorption capacity after multiple CO_2 capture/release cycles.

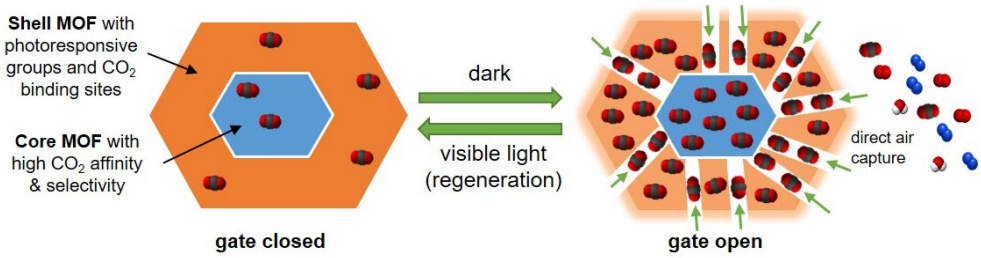

Figure 1. The proposed concept of using photoresponsive core-shell porous materials for reversible CO_2 capture and release driven by visible light.

Recent Progress

This award started in August 2023, and we are currently near the end of our first grant year. During the past year, we developed synthetic routes for V-shaped linkers that are used to synthesize core and shell MOFs. We recruited students from underrepresented groups to our research labs to perform the proposed research at California State University, Los Angeles, and Ames National Laboratory for summer internships. We have negotiated and acquired a breakthrough analyzer coupled with a mass spectrometer, which will be used for studying the CO_2 capture capabilities of designed materials. This crucial instrument expanded the research capabilities of our minority-serving institution.

Four V-shaped linkers were synthesized, purified, and confirmed using ^{1}H NMR. These linkers are used to construct core MOFs.[1-3] The structures of these linkers are outlined in Figure 2a. Two MOFs were synthesized from two of the linkers using solvothermal reactions, and the crystal structure of the MOFs was studied using single-crystal X-ray diffraction, and their phase purity was confirmed using powder X-ray diffraction (Figure 2bc). The surface areas of the MOFs were probed using nitrogen sorption experiments at 77 K, which were 2,555 m^2/g and 3,018 m^2/g, respectively (Figure 2d). The thermal stability of the MOFs was studied by thermogravimetric analysis (TGA). While we are still waiting for the breakthrough analyzer to arrive, we conducted single-component CO_2 adsorption studies for the MOFs and found two MOFs showed excellent CO_2 adsorption and good CO_2/N_2 selectivity at ambient conditions (Figure 2e). Samples were sent to Ames to study the adsorption sites of these materials using in-situ and ex-situ NMRs.

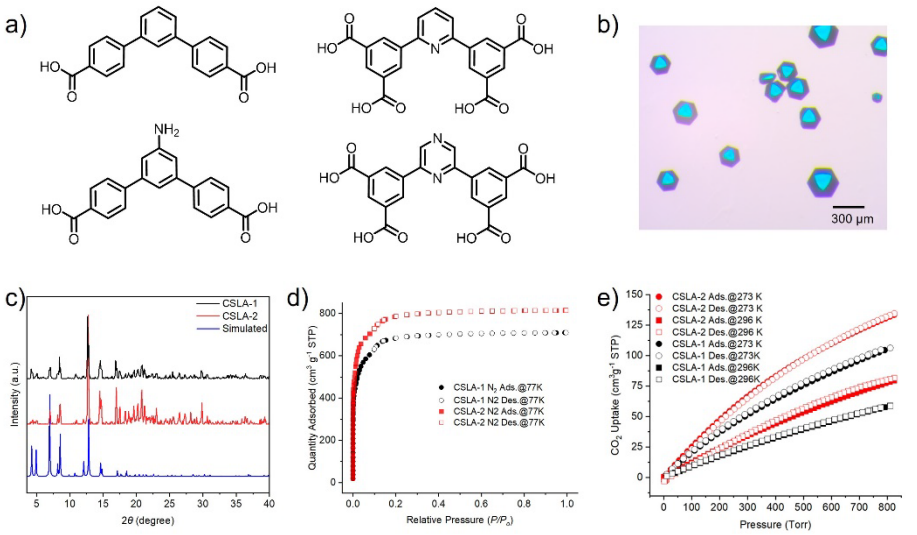

Figure 2. a) The structures of synthesized V-shaped linkers. b) The optical image of an obtained MOF. c) Powder X-ray diffraction patterns of two MOFs compared to the simulated pattern. d) N_2 sorption at 77 K and e) the CO_2 adsorption/desorption isotherms for the two MOFs at 273 K and 296 K up to 1 bar.

The synthetic route was developed and optimized for a photoresponsive linker with azoheteroarenes, which was outlined in Scheme 1.[4-5] These V-shaped linkers are expected to alleviate steric hindrance and facilitate the photoswitching.[6] During this reporting period, we completed the synthesis of the photoresponsive linker, and scale-up is underway. The photoswitching behaviors of this linker under visible light and the construction of shell MOFs using this linker are currently being investigated.

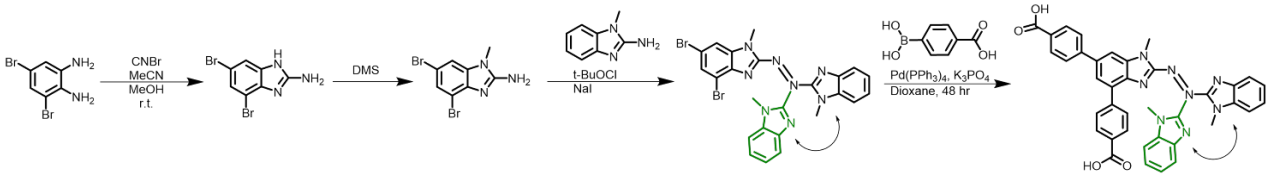

Scheme 1. The synthetic route for the synthesis of photoresponsive linker

References

1. Sun, X.; Li, X.; Yao, S.; Krishna, R.; Gu, J.; Li, G.; Liu, Y., A multifunctional double walled zirconium metal–organic framework: high performance for CO_2 adsorption and separation and detecting explosives in the aqueous phase. *J. Mater. Chem. A* **2020,** *8* (33), 17106-17112.
2. Gu, J.; Sun, X.; Kan, L.; Qiao, J.; Li, G.; Liu, Y., Structural Regulation and Light Hydrocarbon Adsorption/Separation of Three Zirconium–Organic Frameworks Based on Different V-Shaped Ligands. *ACS Appl. Mater. Interfaces* **2021,** *13* (35), 41680-41687.
3. López-Olvera, A.; Zárate, J. A.; Martínez-Ahumada, E.; Fan, D.; Díaz-Ramírez, M. L.; Sáenz-Cavazos, P. A.; Martis, V.; Williams, D. R.; Sánchez-González, E.; Maurin, G.; Ibarra, I. A., SO_2 Capture by Two Aluminum-Based MOFs: Rigid-like MIL-53(Al)-TDC versus Breathing MIL-53(Al)-BDC. *ACS Appl. Mater. Interfaces* **2021,** *13* (33), 39363-39370.
4. Calbo, J.; Weston, C. E.; White, A. J. P.; Rzepa, H. S.; Contreras-García, J.; Fuchter, M. J., Tuning Azoheteroarene Photoswitch Performance through Heteroaryl Design. *J. Am. Chem. Soc.* **2017,** *139* (3), 1261-1274.
5. Kennedy, A. D. W.; Sandler, I.; Andréasson, J.; Ho, J.; Beves, J. E. Visible-Light Photoswitching by Azobenzazoles. *Chem. Eur. J.* **2020**, *26*, 1103-1110.
6. Huang, Q.; Mu, J.; Zhan, Z.; Wang, F.; Jin, S.; Tan, B.; Wu, C., A steric hindrance alleviation strategy to enhance the photo-switching efficiency of azobenzene functionalized metal–organic frameworks toward tailorable carbon dioxide capture. *J. Mater. Chem. A* **2022,** *10* (15), 8303-8308.

Publications

In preparation

Reversible Electrochemical Capture/Release of Carbon Dioxide Mediated by Electrostatically-Enhanced Charge Transfer

Joaquín Rodríguez López, University of Illinois at Urbana-Champaign (Principal Investigator), Veronica Augustyn, North Carolina State University (Co-Investigator), Jahan Dawlaty, University of Southern California (Co-Investigator)

Keywords: CO2 capture and release, electrochemical CO2 capture, Photochemical CO2 release, Direct Air Capture, Capacitive Swing

Research Scope

Direct air capture (DAC) of CO_2 is an emerging technology that presents great challenges due to the dilute nature of CO_2 and the kinetic and energetic underperformance exhibited by current thermochemical processes. The objective of this proposed research is to exploit an energetically-inexpensive electrostatic charge transfer mechanism for the capture and release of CO_2 in a reversible and controllable fashion at modified electrode surfaces. Our concept is based on harnessing the polarizing effect of an electrode surface to capture CO_2. The overarching hypothesis of this project is that modulation of the reactivity of surface-confined CO_2 binding agents will permit the on-demand capture and release of CO_2 for its effective separation from air. This approach improves the functionality of CO_2 capture media through electrochemical methods, creating the opportunity for integration of DAC to renewable energy sources such as solar and wind energy. This proposal introduces an alternative and highly selective energy transfer mechanism for DAC of CO_2 that we hope will dramatically decrease the energetic expenditure compared to state-of-the-art thermochemical approaches. This project aligns with the mission of DOE-BES to lay the foundations of new energy technologies via exploration of basic chemical principles, and it also responds to the Priority Research Directions (PRDs) as outlined in the "Carbon Capture: Beyond 2020 Basic Research Needs" including the identification of new interfacial processes and chemistries with controllable kinetics and stimuli-responsive materials under alternative driving forces.

Recent Progress

In our collaboration, we have followed three synergistic directions to address the challenge of controllable capture and release of CO_2. These three approaches are control via a redox-active capture agent, control via non-Faradaic polarization of the electrochemical double layer, and control of the pH via photoacids and light. The first path is built upon prior knowledge of interaction of quinones with CO_2,[1] where a reduced quinone forms an adduct with CO2 and reversibly releases it upon oxidation. We have extended this concept by tethering several quinones at an electrochemical interface. Our spectroscopic results suggest formation of CO2 adducts at the interface. This will give us a handle in understanding the fundamentals of coupling electron transfer to CO_2 release without the ambiguities arising from solution phase kinetics. In our second path, we have measured that the capacitance of an electrochemical double layer changes in the

presence of CO_2.[2,3] Additional spectroscopic results, including electrochemical surface plasmon resonance (EC-SPR) and Attenuated Total Reflectance (ATR) measurements reveal that CO_2 is localized in the diffuse layer. Since CO_2 changes the capacitance and double layer structure, naturally it led us to hypothesize that the reverse is also true, i.e. change in potential should lead to double layer structure change and affect the CO_2 concentration. Inspired by this hypothesis, we have built a CO_2 flow cell coupled with a CO_2 meter and have demonstrated that applied potential can indeed affect the concentration of the outgoing CO_2. Our third approach is based on the realization that nearly all CO_2 capture equilibria are coupled with protons.[4,5] Often, the capture agent is deprotonated first, enabling the conjugate base to attack and capture CO2. A natural way to reverse this process is by adding acid to the solution, which is costly and inefficient. Instead, we have used photoacid molecules in the sorb mixture and have used light to acidify the solution. We have shown that shining light on the sorb release CO2, and thereby have opened opportunities for using sunlight to reverse CO2 equilibria.

References

1. F. Simeon, M.C. Stern, K.M. Diederichsen, Y. Liu, H. J. Herzog, T. A. Hatton, *Electrochemical and Molecular Assessment of Quinones as CO2-Binding Redox Molecules for Carbon Capture*, J. Phys. Chem. C, 126, **3**, 1389–1399 (2022)
2. C. Liu, K. Landskron, *Design, construction, and testing of a supercapacitive swing adsorption module for CO2 separation*, Chem. Commun., **53**, 3661-3664 (2017)
3. T. B. Binford, G. Mapstone, I. Tempranoa, A. C. Forse, *Enhancing the capacity of supercapacitive swing adsorption CO2 capture by tuning charging protocols*, Nanoscale,**14**, 7980-7984 (2022)
4. M. A. Alfaraidi, B. Kudisch, N. Ni, J. Thomas, T. Y. George, K. Rajabimoghadam, H. Jiang, D. G. Nocera, M. J. Aziz, R.Y. Liu, *Reversible CO2 Capture and On-Demand Release by an Acidity-Matched Organic Photoswitch*. J Am Chem Soc, 145, **49**, 26720-26727 (2023)
5. A. de Vries, K. Goloviznina, M. Reiter, M. Salanne, M.R. Lukatskaya, *Solvation-Tuned Photoacid as a Stable Light-Driven pH Switch for CO2 Capture and Release*, Chem Mater, 36, **3**, 1308-1317 (2024)

Publications

1. D. Cotton, T. Khuu, K. Takematsu, B. Delibas, J. Dawlaty, *Photoinduced Carbon Dioxide Release via a Metastable Photoacid in a Nonaqueous Environment*, Just accepted in J. Phys. Chem. Lett. (2024)
2. B. Delibas, K. Kron, D. Cotton, S. Sharada, J. Dawlaty, *Inferring Energetics of CO2-Aniline Adduct Formation from Vibrational Spectroscopy*, J. Phys. Chem. A, 127, **24**, 5162–5170 (2023)
3. A.R. Siddiqui, J. N'Diaye, K. Martin, A. Baby, J. Dawlaty, V. Augustyn, J. Rodríguez-López, *Monitoring SEIRAS on a Graphitic Electrode for Surface-Sensitive Electrochemistry: Real-Time Electrografting*, Anal. Chem. 96, **6**, 2435–2444 (2024)
4. A.R. Siddiqui, J. N'Diaye, A. Santiago-Carboney, K. Martin, R. Bhargava, J. Rodríguez-López, *Spectroelectrochemical Determination of Thiolate Self-Assembled Monolayer Adsorptive Stability in Aqueous and Non-Aqueous Electrolytes,* Analyst, **149**, 2842-2854. (2024)

Multi-scale Study of Self-Healing Polymers to Enhance Carbon Dioxide Removal

Jihong A. Ma, University of Vermont

Jason E. Bara, University of Alabama

Keywords: Self-Healing Polymers, Polymer Synthesis, Atomistic Simulation, Characterization, Gas Transport

Research Scope

Our overarching objective is to improve the ability to capture carbon dioxide (CO_2) by creating high-performance self-healing (SH) polymers for use in gas separation membranes. This study aims to develop long-lasting, high-performance CO_2 separation systems by gaining an atomistic understanding of the gas transport and SH mechanisms of a group of polyamide ionene (PA-ionene) membranes. These membranes are designed to self-heal when damaged and also to have high CO_2 permeability and selectivity compared to other gases [1]. Our approach involves using advanced material synthesis techniques, high-performance atomistic simulations, and structural and thermomechanical characterization to fully understand the role of each functional group in the membranes' structural characteristics, as well as their mechanical, thermal, and transport properties. Our long-term goal is to establish a comprehensive framework for general high-performance amorphous material advancement for a broader range of applications based on the understanding and protocols developed from the materials studied in this project, from initial material discovery to industrial-level applications.

Recent Progress

We have successfully developed PA-ionene membranes incorporating the spirobisindane (SBI) group, illustrated in Fig. 1. The inclusion of the SBI component is anticipated to create microporosity in the polymers [2], thereby enhancing the permeability of CO_2 due to a higher free fractional volume (FFV). Notably, we have also demonstrated the ability to synthesize self-healing ionic polymers from polystyrene waste [3]. Our exploration of the different components of this polymer has provided insights into their individual roles in its thermomechanical properties.

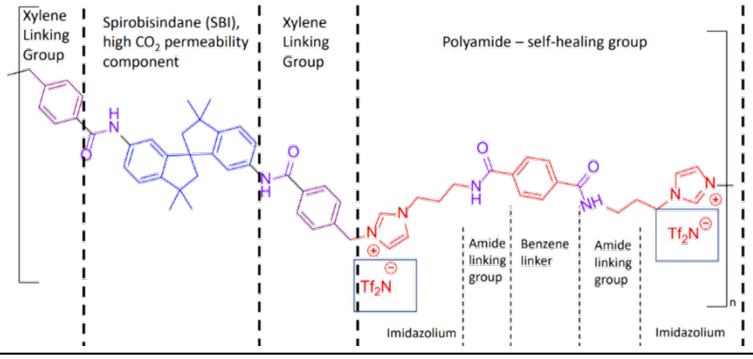

Figure 6. SR-SBI-PA with high permeability SBI segments (blue) and self-healing segments (red) with linking groups (purple).

First, our experimental findings indicate that the PIM-induced SBI renders the membrane brittle and stiff. To address this, we propose the addition of ionic liquids (ILs), such as 1-benzyl-3-methylimidazolium bistriflimide ($[BMIM^+][Tf_2N^-]$). Incorporating additional ILs not only

accelerates the self-healing process but also generally enhances CO_2 permeability without compromising its selectivity against other gases. Our comprehensive investigation into the mechanical and transport performance improvements resulting from the inclusion of ILs involved atomistic simulations and small-angle X-ray spectroscopy (SAXS) to examine the structural variations. Both the molecular dynamics (MD) simulations and SAXS characterization revealed that the added ILs fill up the pores induced by SBI, as depicted in Fig. 2. This indicates that the increased permeability is likely a result of the stronger affinity of ILs with CO_2 gas molecules. A hydrogen bond (H-bond) count between polymer chains, chain-ILs, and ILs from MD simulations reveals that IL interactions are mostly responsible for the self-healing behavior, especially the H-O bonds. Remarkably, the chain configuration and interactions remain largely unaffected by ILs.

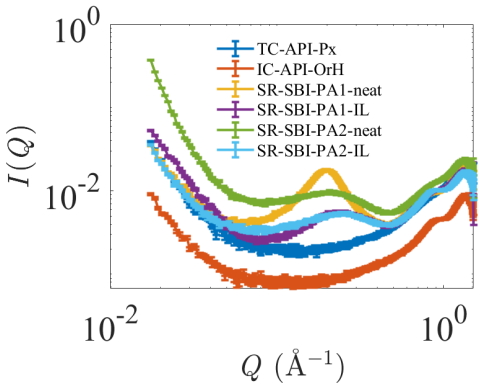

Figure 2 SAXS raw data showing a prominent peak in SR-SBI-PA1-neat system at $Q = 0.16\text{Å}^{-1}$, which is significantly broadened with the addition of ILs. As a comparison, PA systems without the PIM are also measured showing no peaks below $Q = 0.5\text{Å}^{-1}$.

In addition to the role of ILs in self-healing and thermomechanical properties, we also studied the H-bonds between chains by capping the H atoms with methyl groups to eliminate both intrachain and interchain H-bonds. Our MD simulations demonstrated that mechanical properties such as tensile strength and creep rates decrease with this modification, highlighting the significance of H-bonds.

We also investigated the influence of imidazolium on polymer interactions and their affinity with counter ions to understand the energy transfer process. Due to the complex charge distribution in zwitterionic systems, classical MD simulations were not sufficient. Thus, a multi-scale approach engaging density functional tight-binding theories with long-range correction has been developed [4]. This method will be extended to investigate the structural dynamics of PIM-PA-ionenes with Fragment Molecular Orbital methods [5], whose linear-scaling feature allows for highly efficient large-scale full quantum-chemical MD simulations [6].

Additionally, we conducted experimental analyses on the role of linkers. By replacing p-xylyl groups with polyethylene oxide (PEO) linkages we observed faster membrane healing, especially with higher IL concentrations. SAXS of this modified polymer (labeled SR-SBI-PA2) indicated the presence of dispersed pores, possibly due to increased chain flexibility. A more detailed atomistic study will follow up to provide further insights into this structure.

Overall, we have addressed the roles of H-bonds, ILs, imidazolium, and linking groups in the configuration of polymer structures and their physical properties. Our findings indicate that while polymer structures are crucial, they are not the sole determining factor in their thermal and mechanical behaviors. In the next phase of our project, we will focus on studying the affinity of gas molecules with the polymers to confirm the applicability of these conclusions.

References

1. K. E. O'Harra, I. Kammakakam, D. M. Noll, E. M. Turflinger, G. P. Dennis, E. M. Jackson, and J. E. Bara, *Synthesis and Performance of Aromatic Polyamide Ionenes as Gas Separation Membranes*, Membranes **10**, 51 (2020).
2. I. Kammakakam, K. E. O'Harra, J. E. Bara, and E. M. Jackson, *Spirobisindane-Containing Imidazolium Polyimide Ionene: Structural Design and Gas Separation Performance of "Ionic PIMs*," Macromolecules **55**(11), 4790-4802 (2022).
3. Z. Sekhavat Pour, P. S. Shinde, J. E. Bara, Upcycling of Polystyrene Waste to Poly(Ionic Liquid) Materials, submitted to ACS Applied Polymer Materials.
4. V. Q. Vuong, Y. Nishimoto, D. G. Fedorov, B. G. Sumpter, T. A. Niehaus, and S. Irle, *The Fragment Molecular Orbital Method Based on Long-Range Corrected Density-Functional Tight-Binding*, Journal of Chemical Theory and Computation **15**, 3008 (2019).
5. T. Walker, V.-Q. Vuong, S. Irle, J. Ma, Evaluation of density-functional tight-binding methods for simulations of protic molecular ion pairs in gas phase and solution, submitted to the Journal of Computational Chemistry.
6. Y. Nishimoto, H. Nakata, D. G. Fedorov, and S. Irle, *Large-Scale Quantum-Mechanical Molecular Dynamics Simulations Using Density-Functional Tight-Binding Combined with the Fragment Molecular Orbital Method*, The Journal of Physical Chemistry Letters **6**, 5034 (2015).

Publications

Two manuscripts submitted:

Walker, T., Vuong, V.-Q., Irle, S., Ma, J. Evaluation of density-functional tight-binding methods for simulations of protic molecular ion pairs in gas phase and solution, submitted to the Journal of Computational Chemistry.

Sekhavat Pour, Z., Shinde, P. S., Bara, J. E. Upcycling of Polystyrene Waste to Poly(Ionic Liquid) Materials, submitted to ACS Applied Polymer Materials.

Oral presentations:

Buckser, E., Ravula, S., Shinde, P., Bara, J., Ma, J. Effect of Hydrogen Bonds on Thermomechanical Properties of Polyamide Ionene. 03/07/2024, American Physical Society, Minneapolis, MN, USA.

Sabokroozroozbahani, F., Buckser, E., Bara, J., Ma, J. Atomistic Understanding of the Mechanical Behaviors of Polyamide Ionene Self-Healing Elastomers, 06/05/2024, the Platform for Advanced Scientific Computing Conference, Zurich, Switzerland (Invited talk).

Sustainable Materials and Interfacial Chemistry for Next-Generation Electrical Energy Storage

Arumugam Manthiram, University of Texas at Austin

Keywords: sodium batteries, cobalt-free, interface, single crystals, solid-state batteries

Research Scope

With the goal of developing next-generation electrical energy storage systems, this project aims to develop a fundamental understanding of materials and interfacial chemistry, pertaining to sustainable rechargeable battery systems. With a focus on cobalt-free sodium-based batteries, the progress described here presents the critical aspects of cell components for a few cell chemistries. The project currently focuses on (i) delineating the relationships among surface reactivity and particle cracking in layered sodium oxides with advanced electrolytes, (ii) structural modifications to mitigate sodium-ion ordering and enhance cycling stability in sodium cathodes, and (iii) solid-state sodium cells with halide-based composite solid-state electrolytes.

Recent Progress

Origin of capacity fade at high-voltages in P2-type cathodes: P2-type $Na_{2/3}Ni_{1/3}Mn_{2/3}O_2$ (NM12) is a popular sodium layered oxide cathode due to its exceptional air stability and high energy density.[1] When cycled up to 4.3 V vs. Na/Na^+, it has an average discharge voltage of 3.65 V. Above 4 V, the $Ni^{3+/4+}$ redox reaction coincides with a highly unstable P2 – O2 phase transition and a large volume change that results in significant particle cracking. Furthermore, traditional carbonate electrolytes have poor oxidative stability above 4 V that results in increased parasitic surface reactions and exacerbated capacity fade.

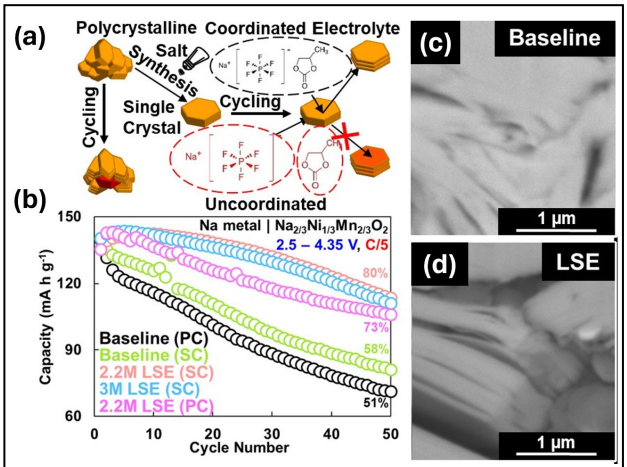

Figure 1. (a) Schematic of methods used to compare degradation mechanisms in NM12 cathode. (b) Cyclability of polycrystalline and single-crystal cathodes with different electrolytes. (c-d) Post-mortem SEM micrographs after 50 cycles in baseline and LSE electrolytes for the single-crystal cathodes.

We were able to systematically delineate the capacity fade to be due to different cracking modes by synthesizing single crystals (SC), which show that roughly 5% of active material becomes isolated within polycrystalline (PC) agglomerates created by the traditional synthesis method. We then paired our single-crystal cathodes with a novel "locally saturated electrolyte" (LSE), the design of which increases the coordination of propylene carbonate with the $NaPF_6$ salt and reduces its reactivity with the NM12 cathode. In **Figure 1a-b**, we show that surface reactivity is the dominant factor in the capacity fade of NM12 above 4 V. This is despite the egregious

particle cracking observed when cycled with both the baseline and LSE electrolytes (**Figure 1c-d**), which has been traditionally blamed for the rapid capacity fade. Instead, we conclude that the primary issue is the increase in exposed and reactive lattice oxygen created by stacking faults generated by the P2 – O2 transition.[2]

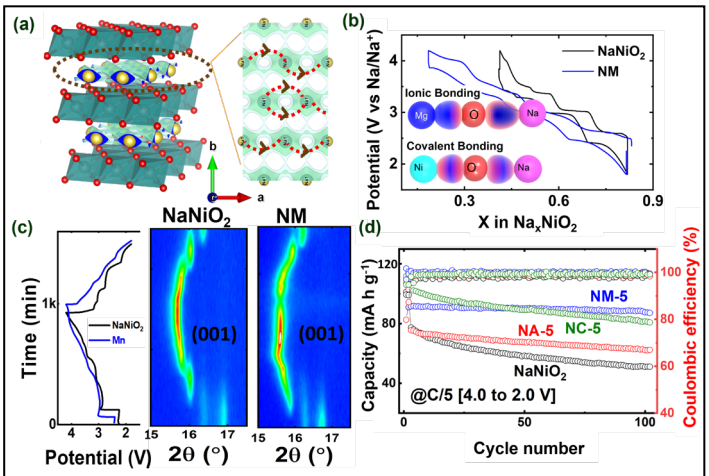

Figure 2. (a) Crystal structure with calculated migration barriers. (b) The enhanced solid-solution behavior in Mg-doped $NaNiO_2$. (c) *Operando* X-ray diffractogram, showing a smooth transition of (001) peaks during cycling. (d) Electrochemical cycling of doped cathodes (NA = 5% Al; NM = 5% Mg, and NC = 5% Co).

Enhanced solid-solution in $NaNiO_2$: O′3-type layered nickel oxides suffer from undesired co-operative Jahn-Teller distortion stemming from low-spin Ni^{3+} ions and undergo multiple biphasic structural transformations during the insertion/extraction of large Na^+ ions.[3] This instability poses a challenge in stabilizing the structural integrity of these cathodes. We investigated systematically the impact of substituting 5% divalent Mg^{2+} or trivalent Al^{3+} or Co^{3+} ions for Ni^{3+} to alleviate Na^+-ion ordering and perturb the Jahn-Teller effect, thereby enhancing structural stability. **Figure 2a** illustrates the structure of $NaNiO_2$. Mg^{2+} substitution reduces the Na^+-ion migration barrier and thereby the lattice strain. This effect is reflected in a smoother charge-discharge profile with more than 30 mA h g^{-1} excess capacity in comparison to undoped $NaNiO_2$ (**Figure 2b**). *Operando* X-ray diffraction data offer structural insights into the reduced ordering. **Figure 2c** illustrates the irreversible phase transformation of these materials and the emergence of a stable and reversible $Na_{0.91}NiO_2$ phase. The incorporation of 5% Mg into $NaNiO_2$ enables a stable solid-solution reaction with 96% capacity retention after 100 cycles (**Figure 2d**).[4]

Aluminum oxychloride solid-state electrolytes: The halide class of solid-state electrolytes (SSEs) are gaining attention owing to their high electrochemical oxidative stability, allowing them to be used in conjunction with high-voltage cathodes. Most halide SSEs employ less-abundant elements like In, Y, and Er.[5] $NaAlCl_4$ is low cost, but it suffers from a low ionic conductivity of ~ 3 x 10^{-6} S cm^{-1}. We have substituted divalent O^{2-} for Cl^- in $NaAlCl_{4-2y}O_y$ through mechanochemical reaction using Na_2O, which increases the ionic conductivity by two orders of magnitude to 1.3 x 10^{-4} S cm^{-1}. Multiple quantum (MQ) MAS NMR spectroscopy further confirms that the oxychloride interface exists as a multiphase layer, as evident from five discrete aluminum sites arising from the possible combinations of aluminum tetrahedrally coordinated to oxygen and chlorine. Solid-state cells assembled with the resulting electrolyte and layered $NaNi_{0.5}Mn_{0.5}O_2$ cathode exhibit a high capacity of 124 mA h g^{-1} with good cycle life.[6]

References

1. D. Lee, J. Xu, and Y. Meng, *An advanced cathode for Na-ion batteries with high rate and excellent structural stability,* Physical Chemistry Chemical Physics **15**, 3304-3312 (2013).
2. J. Darga and A. Manthiram, *Deconstructing the High Voltage Degradation Mechanisms in $Na_{2/3}Ni_{1/3}Mn_{2/3}O_2$ with Single Crystals and Advanced Electrolyte*, Advanced Functional Materials **2408642,** 1-17 (2024).
3. M. H. Han, E. Gonzalo, M. Casas-Cabanas and T. Rojo, *Structural evolution and electrochemistry of monoclinic $NaNiO_2$ upon the first cycling process*, Journal of Power Sources **258**, 266-271 (2014).
4. K. Sada, S. Kmiec, and A. Manthiram, *Mitigating Sodium Ordering for Enhanced Solid Solution Behavior in Layered $NaNiO_2$ Cathodes*, Angewandte Chemie International Edition **63**, e202403865 (2024).
5. H. Kwak, S. Wang, J. Park, Y. Liu, K. Kim, Y. Choi, Y. Mo, and Y. Jung, *Emerging Halide Superionic Conductors for All-Solid-State Batteries: Design, Synthesis, and Practical Applications*, ACS Energy Letters **7**, 1776-1805 (2022).
6. E. Ruoff, S. Kmiec, and A. Manthiram, *Enhanced Interfacial Conduction in Low-cost $NaAlCl_4$ Composite Solid Electrolyte for Solid-state Sodium Batteries*, Advanced Energy Materials **2402091**, 1-15 (2024).

Publications

1. H. Sul, A. Bhargav, and A. Manthiram, *Sodium Trithiocarbonate Cathode for High-performance Sodium-sulfur Batteries*, Journal of Materials Chemistry A **11**, 130–140 (2022).
2. D. Guo, J. Wang, T. Lai, G. Henkelman, and A. Manthiram, *Electrolytes with Solvating Inner Sheath Engineering for Practical Na-S Batteries*, Advanced Materials **35**, 2300841 (2023).
3. Y Ren, T. Lai, and A. Manthiram, *Reversible Sodium-Sulfur Batteries Enabled by a Synergistic Dual-Additive Design*, ACS Energy Letters **8**, 2746–2752 (2023).
4. K. Sada, J. Darga, and A. Manthiram, *Challenges and Prospects of Sodium-ion and Potassium-ion Batteries for Mass Production*, Advanced Energy Materials **13**, 2302321 (2023).
5. J. He, A. Bhargav, L. Su, H. Charalambous, and A. Manthiram, *Intercalation-type Catalyst for Non-aqueous Room-temperature Sodium-sulfur Batteries*, Nature Communications **14**, 6568 (2023).
6. S. Kmiec, P. Vanaphuti, and A. Manthiram, *Solid-state Sodium Batteries with P2-type Mn-based Layered Oxides by Utilizing Anionic Redox*, Journal of Materials Chemistry A **12**, 3006–3013 (2024).
7. J. He, A. Bhargav, J. Lamb, L. Su, J. Okasinski, W. Shin, and A. Manthiram, *Tuning the Solvation Structure with Salts for Stable Sodium-metal Batteries*, Nature Energy **9**, 446–456 (2024).
8. W. Yao, K. Liao, T. Lai, H. Sul, and A. Manthiram, *Rechargeable Metal-sulfur Batteries: Key Materials to Mechanisms*, Chemical Reviews **124**, 4935–5118 (2024).
9. K. Sada, S. Kmiec, A. Manthiram, *Mitigating Sodium Ordering for Enhanced Solid Solution Behavior in Layered $NaNiO_2$ Cathodes*, Angewandte Chemie International Edition **63***,* e202403865 (2024).
10. E. Ruoff, S. Kmiec, and A. Manthiram, *Enhanced Interfacial Conduction in Low-cost $NaAlCl_4$ Composite Solid Electrolyte for Solid-state Sodium Batteries*, Advanced Energy Materials **2402091**, 1–15 (2024).

Dynamic Properties of Nanostructured Porous Materials

Adam J. Matzger; Department of Chemistry and the Macromolecular Science and Engineering Program; University of Michigan; 930 North University Avenue, Ann Arbor, MI 48109-1055

Keywords: MOF, porous materials, activation, coordination chemistry, vibrational spectroscopy

Research Scope

The overarching goal for this project is to develop an enhanced understanding of dynamic phenomena in metal-organic frameworks (MOFs), and to harness this knowledge to explain and optimize MOF creation and behavior.

Recent Progress

Solvent exchange is a critical step in MOF activation that involves replacing synthesis solvents (such as *N,N*-dimethylformamide (DMF)) remaining in the pores with volatile solvents such as ethanol (EtOH) or methanol (MeOH) that facilitate achieving optimal porosity by minimizing structural collapse during guest evacuation.[1,2] In certain MOFs, coordinatively unsaturated sites (CUS) are obtained via the liberation of solvent molecules bound to the metal clusters while preserving the MOF structure. The CUS-bound solvent is more challenging to replace than pore-filled solvent[3] and this has been a major focus of our work under DOE-BES support. During the last project period, we deconvoluted exchange kinetics of CUS-bound solvent and pore-filled solvent in a copper paddlewheel MOF using in situ ^{1}H NMR and Raman spectroscopy.[4] Applying the developed methodology, we have now elucidated the metal-dependent activation conditions of isostructural CUS-MOFs M_2(dobdc)[5–7] with regard to the kinetics and thermodynamics of solvent replacement (Figure 1).

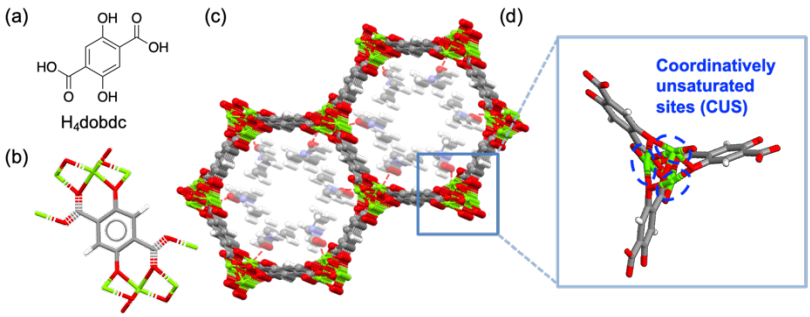

Figure 1. *(a) Chemical structure of H_4dobdc, (b) secondary building units of Mg_2(dobdc) composed of magnesium connected with dobdc, (c) 3D honeycomb structures linked with infinite chains coordinated with DMF, and (d) pentacoordinated metal clusters with 1 vacant site on each metal site.*

To examine solvent exchange rates of M_2(dobdc) (M=Mg, Co, Zn), MOF soaked in DMF was employed to examine solvent exchange with EtOH and MeOH. The change in DMF concentration of the supernatant during solvent exchange was measured via in situ IR spectroscopy. The exchange rate followed the order Mg > Co >> Zn for both EtOH and MeOH. To elucidate exchange rates at metal centers, solvent exchange of single crystal M_2(dobdc) was

observed through in situ Raman spectroscopy. M_2(dobdc) does not display a metal-metal stretching frequency; instead, that of phenolate CO, which coordinates directly to the metal, was measured to monitor the change in metal-solvent interaction indirectly. The relative exchange rates of M_2(dobdc) are Mg > Co >> Zn for both EtOH and MeOH exchange. Comparing the time to reaching equilibrium, MeOH exchange is around 40 times, 60 times, and 3 times faster than EtOH exchange for Mg_2(dobdc), Co_2(dobdc), and Zn_2(dobdc), respectively. This indicates that the solvent exchange of Zn_2(dobdc) is less affected by the exchange solvent, implying that Zn_2(dobdc) obeys a dissociative substitution mechanism, whereas Mg_2(dobdc) and Co_2(dobdc) follow an associative substitution mechanism. Though the exchange rates of Mg_2(dobdc) are too rapid to capture any potential induction time in the solvent exchange mechanism, Zn_2(dobdc) manifests a sigmoidal shape of CUS solvent exchange curve. The sigmoidal curve implies that the solvent replacement of M_2(dobdc) follows a cooperative binding mechanism, which may arise from a high density of CUS subsequently inducing multiple interactions with near neighboring metal sites (perpendicular to the channels in Figure 1).

If it is assumed that the metal-dependent exchange rates in M_2(dobdc) are related to the solvent binding strength, then DMF would be more strongly bound to Zn than other metals. However, it is also possible that the slow exchange at Zn is merely a kinetic phenomenon. To differentiate these possibilities, the reverse direction of solvent exchange was explored and the reverse exchange rates show the same order as the forward solvent exchange rates: Mg > Co > Zn, and also manifest cooperativity. To examine the hypothesis that DMF is most strongly bound to Zn, the thermal release of solvents from the CUS was observed via thermogravimetric analysis coupled to IR (TGA-IR). The release temperatures indicate DMF coordination strength to M_2(dobdc) is Mg > Co > Zn, and therefore the slow exchange rates of Zn_2(dobdc) cannot be attributed to the strong DMF binding affinity to Zn. This trend was similarly observed in the cases of the EtOH and MeOH indicating the solvent binding affinity on M_2(dobdc) follows the order Mg > Co > Zn. To corroborate the experimental ordering observed by TGA, theoretical calculation was undertaken. The binding energy of the solvents follows the same pattern for all metals with DMF > EtOH > MeOH, as observed in the TGA-IR data. The binding energy of individual solvent molecules to Mg_2(dobdc) is calculated to be higher than Zn_2(dobdc), matching the TGA-IR data that Mg_2(dobdc) releases solvents at higher temperatures than Zn_2(dobdc). Therefore, this clarifies that the exchange rates in M_2(dobdc), measured by Raman spectroscopy, are not attributed to the solvent binding strength to the metal; the solvent exchange process is primarily driven by kinetics, while the solvent binding affinity plays a crucial role in solvent removal. Practically, this means strongly bound solvent, as is relevant for vacuum activation, does not necessarily imply that kinetics of exchange at the metal centers are also slow. This has broad implications for numerous applications here CUS-MOFs are employed in separations, gas storage, and catalysis.

References

(1) Dodson, R. A.; Matzger, A. J. Resolvation-Based Damage to Metal–Organic Frameworks and Approaches to Mitigation. *ACS Materials Lett.* **2019**, *1* (3), 344–349.

(2) Dodson, R. A.; Wong-Foy, A. G.; Matzger, A. J. The Metal–Organic Framework Collapse Continuum: Insights from Two-Dimensional Powder X-Ray Diffraction. *Chem. Mater.* **2018**, *30* (18), 6559–6565.

(3) Wright, K. R.; Nath, K.; Matzger, A. J. Superior Metal-Organic Framework Activation with Dimethyl Ether. *Angew. Chem.* **2022**, *61* (52), e202213190.

(4) Woo, H.; Devlin, A. M.; Matzger, A. J. In Situ Observation of Solvent Exchange Kinetics in a MOF with Coordinatively Unsaturated Sites. *J. Am. Chem. Soc.* **2023**, *145* (33), 18634–18641.

(5) Caskey, S. R.; Wong-Foy, A. G.; Matzger, A. J. Dramatic Tuning of Carbon Dioxide Uptake via Metal Substitution in a Coordination Polymer with Cylindrical Pores. *J. Am. Chem. Soc.* **2008**, *130* (33), 10870–10871.

(6) Rosi, N. L.; Kim, J.; Eddaoudi, M.; Chen, B.; O'Keeffe, M.; Yaghi, O. M. Rod Packings and Metal−Organic Frameworks Constructed from Rod-Shaped Secondary Building Units. *J. Am. Chem. Soc.* **2005**, *127* (5), 1504–1518.

(7) J. Geier, S.; A. Mason, J.; D. Bloch, E.; L. Queen, W.; R. Hudson, M.; M. Brown, C.; R. Long, J. Selective Adsorption of Ethylene over Ethane and Propylene over Propane in the Metal–Organic Frameworks M_2(dobdc) (M = Mg, Mn, Fe, Co, Ni, Zn). *Chem. Sci* **2013**, *4* (5), 2054–2061.

Publications

1. Du Bois, D. R.; Matzger, A. J. Metal–Organic Framework Seeding to Drive Phase Selection and Overcome Synthesis Limitations. *Cryst. Growth Des.* **2022**, *22* (11), 6379–6383.
2. Du Bois, D. R.; Wright, K. R.; Bellas, M. K.; Wiesner, N.; Matzger, A. J. Linker Deprotonation and Structural Evolution on the Pathway to MOF-74. *Inorg. Chem.* **2022**, *61* (11), 4550–4554.
3. Suresh, K.; Kalenak, A. P.; Sotuyo, A.; Matzger, A. J. Metal-Organic Framework (MOF) Morphology Control by Design. *Chem. Eur. J.* **2022**, *28* (18), e202200334.
4. Harris, J. T.; de la Garza, G. D.; Devlin, A. M.; McNeil, A. J. Rapid Removal of Poly- and Perfluoroalkyl Substances with Quaternized Wood Pulp. *ACS EST Water* **2022**, *2* (2), 349–356.
5. Wright, K. R.; Nath, K.; Matzger, A. J. Superior Metal-Organic Framework Activation with Dimethyl Ether. *Angew. Chem.* **2022**, *61* (52), e202213190.
6. Crom, A. B.; Strozier, J. L.; Tatebe, C. J.; Carey, C. A.; Feldblyum, J. I.; Genna, D. T. Deinterpenetration of IRMOF-9. *Chem. Eur. J.* **2023**, *29* (70), e202302856.
7. Woo, H.; Devlin, A. M.; Matzger, A. J. In Situ Observation of Solvent Exchange Kinetics in a MOF with Coordinatively Unsaturated Sites. *J. Am. Chem. Soc.* **2023**, *145* (33), 18634–18641.
8. Suresh, K.; Carey, C. A.; Matzger, A. J. Metal–Organic Frameworks (MOFs) Morphology Control: Recent Progress and Challenges. *Cryst. Growth Des.* **2024**, *24* (5), 2288–2300.
9. Woo, H.; Robinson, J. W.; Matzger, A. J. Solvent Exchange Dynamics in M_2(dobdc): An Interplay among Binding Strength, Exchange Kinetics, and Cooperativity. *J. Am. Chem. Soc.* **2024**, *146* (26), 18136–18142.

Design and Validation of Defect-Resistant Multinary Chalcogenide Semiconductors for Energy Conversion

David B. Mitzi (Principal Investigator), Volker Bum (Co-Investigator), Duke University

Keywords: Chalcogenide semiconductors, Structure-property relationship, Density functional theory (DFT), Optoelectronic properties, Photovoltaics

Research Scope: Multinary chalcogenides underlie numerous high-performance energy conversion and electronic devices based on a range of physical processes, including photovoltaic (PV), photoelectrochemical, light emission, non-linear optical, thermoelectric, and phase change phenomena.[1-4] Examples include $CuIn_{1-x}Ga_xSe_2$ (CIGS) (thin-film PV absorber), $Ge_2Sb_2Te_5$ (active phase-change memory and optical disk media), $Bi_{2-x}Sb_xTe_3$ (thermoelectric devices), and $AgGaS_2$ (non-linear optical material). Substantial contemporary research also focuses on Cu_2ZnSnS_4 (CZTS) and related systems, offering prospects of replacing CIGS as an active PV absorber with non-toxic and earth-abundant analogs. An earlier program version focused on a related emerging class of tunable multinary chalcogenides based on I_2-II-IV-X_4 stoichiometry (I, II, and IV refer to oxidation states of the included metals; X is a chalcogen), to develop underlying structural and chemical design rules for these systems and to understand how the resulting crystal structures impact properties, particularly those that relate to more effective solar energy application. The current program uses a synergistic combination of computational and experimental tools to build upon this research, targeting a broader array of structure-property relationships. Specific goals for the program include extending the range of chemical systems that can be predicted and understood by the design rules developed previously, focusing on using these design rules to produce an increased range of relevant property tunability (e.g., bandgap and carrier concentration), and extending the program's property focus to physical phenomena that rely on structural distortions and symmetry breaking (e.g., spin control). Accomplishing these goals will provide foundational materials chemistry understanding for an important semiconductor family, for which important emerging energy-related applications have already been envisioned.

Recent Progress: Several research directions from the project over the last two years will be highlighted. First, to further our understanding of I_2-II-IV-X_4 chalcogenide semiconductors, and to understand the impact of including rare earth (RE) elements in the family, we undertook a hybrid DFT level first-principle computational analysis exploring 18 Eu-containing I_2-II-IV-X_4 (I = Li, Cu, Ag; II = Eu; IV = Si, Ge, Sn; X = S, Se) systems. Total energy calculations agree with the phase stability predictions of the tolerance factor approach from our group's previous work (**Figure 1**),[5] further confirming its reliability as a tool for the prediction of preferred structures among I_2-II-IV-X_4 compounds. The computational work is augmented by experimental synthesis and characterization of one compound among this set, $Cu_2EuSnSe_4$ (CETSe), selected because it

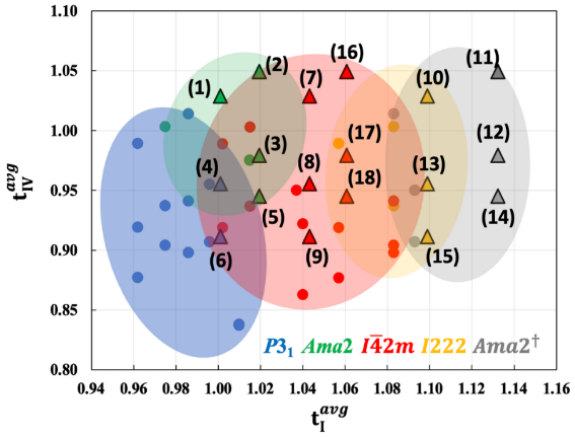

Figure 1. Tolerance factor approach as applied to predict Eu-containing I_2-II-IV-X_4 compounds. Dots represent known structures, and triangles represent Eu compounds. Triangles are color-coded to indicate the predicted structure type according to DFT.

is predicted to show the strongest promise (i.e., suitable band structure) for PV application. X-ray diffraction (XRD) for CETSe samples from solid-state confirms formation in the predicted *Ama*2 space group, and refined lattice parameters from a Pawley fitting of the XRD data fall within 1% of predicted values from computation, affirming the power of DFT for structural prediction within this family. Using diffuse reflectance spectroscopy, we deduced the bandgap for CETSe, ~1.55 eV, consistent with computational prediction of 1.53 eV and well within the ideal range for PV. Furthermore, our broader predictive investigation of the family revealed several prospective systems beyond CETSe for applications from PV to LEDs. This work was recently published in *Chemistry of Materials*.[6] Ongoing study of CETSe films is underway to investigate optoelectronic properties and assess viability for PV application.

Next, to apply and expand upon the experience gained from I_2-II-IV-X_4 chalcogenides, we investigated an analogous I_2-I'-V-X_4 chalcogenide family, incorporating a coupled substitution of an alkali (I' = K, Rb, Cs) and a pentavalent transition metal (V = V, Nb, Ta) for the II and IV sites, respectively. The non-centrosymmetric nature of existing family members led us to hypothesize that incorporation of heavy elements like Ta could result in significant spin-splitting behavior. The 6 new compounds in this set were found to form analogous layered *Ama*2 structures to those of the 3 known K-based members (**Figure 2**), and these experimental structures agree with predicted structures from DFT relaxation. All 9 compounds show strong absorption with bandgaps ranging from 1.2—2.5 eV, suggesting a broad range of potential applications, including PV. Our study finds that the electronic properties (i.e. bandgap) in this series depend primarily upon the identity of the 5+ transition metal ion. Critically, our DFT study finds that the heavy element (e.g. Ta) containing members exhibit significant spin-orbit coupling induced splitting at the conduction band minimum, consistent with our hypothesis and suggesting promise for further study of spin behavior. A manuscript is in preparation for this work. We are further characterizing spin splitting in spin-coated bournonite films using the circularly polarized photogalvanic effect.

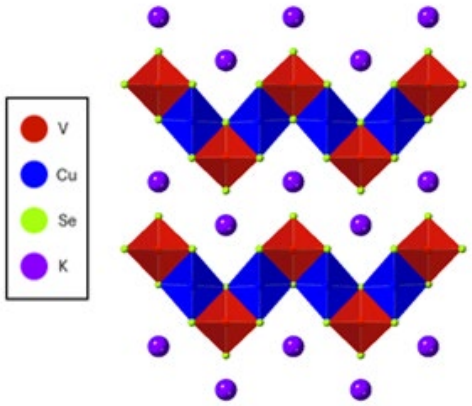

Figure 2. Layered structure of Cu_2KVSe_4, exhibited isostructurally across members of the I_2-I'-V-X_4 family.

References

1. Kanatzidis, M. G. “Discovery-Synthesis, Design, and Prediction of Chalcogenide Phases,” *Inorganic Chemistry* **56**, 3158-3173 (2017).

2. Zakutayev, A. “Brief review of emerging photovoltaic absorbers,” *Current Opinion in Green and Sustainable Chemistry* **4**, 8-15 (2017).

3. Shi, Y.; Sturm, C.; Kleinke, H. “Chalcogenides as thermoelectric materials,” *Journal of Solid State Chemistry* **270**, 273-279 (2019).

4. Eggleton, B. J.; Luther-Davies, B.; Richardson, K. “Chalcogenide photonics,” *Nature Photonics* **5**, 141-148 (2011).

5. Sun, J.-P.; McKeown Wessler, G. C.; Wang, T.; Zhu, T.; Blum, V.; Mitzi, D. B. “Structural Tolerance Factor Approach to Defect-Resistant I_2-II-IV-X_4 Semiconductor Design” *Chemistry of Materials* **32**, 1636-1649 (2020).

6. Wang, T.; McWhorter, T. M.; McKeown Wessler, G. C.; Yao, Y.; Song, R.; Mitzi, D. B.; Blum, V. “Exploration, Prediction, and Experimental Verification of Structure and Optoelectronic Properties in I_2-Eu-IV-X_4 (I = Li, Cu, Ag; IV = Si, Ge, Sn; X = S, Se) Chalcogenide Semiconductors,” *Chemistry of Materials* **36**, 340-357 (2024).

Publications

1. T. Wang, T. M. McWhorter, G. C. McKeown Wessler, Y. Yao, R. Song, D. B. Mitzi, and V. Blum, “Exploration, Prediction, and Experimental Verification of Structure and Optoelectronic Properties in I_2-Eu-IV-X_4 (I = Li, Cu, Ag; IV = Si, Ge, Sn; X = S, Se) Chalcogenide Semiconductors,” *Chemistry of Materials* **36** (1), 340-357 (2024).

2. Y. Kim, H. Hempel, S. P. Harvey, N. A. Rivera, T. Unold, D. B. Mitzi, “Alkali Element (Li, Na, K, and Rb) Doping for $Cu_2BaGe_{1-x}Sn_xSe_4$ Films,” *Journal of Materials Chemistry A*, **11**, 15336 (2023).

3. E. T. Chang, G. Koknat, G. C. McKeown Wessler, Y. Yao, V. Blum, D. B. Mitzi, “Phase Stability, Bandgap Tuning and Rashba Splitting in Selenium-Alloyed Bournonite: $CuPbSb(S_{1-x}Se_x)_3$,” *Chemistry of Materials* **35**, 595-608 (2023).

4. Y. Kim, H. Hempel, T. Unold, D. B. Mitzi, “Ag alloying in $Cu_{2-y}Ag_yBa(Ge,Sn)Se_4$ films and photovoltaic devices,” *Solar RRL* **7**, 2201058 (2023).

5. B. Teymur, Y. Kim, J. Huang, K. Sun, X. Hao, D. B. Mitzi, “Top stack optimization for $Cu_2BaSn(S,Se)_4$ photovoltaic cell leads to improved device power conversion efficiency beyond 6%,” *Advanced Energy Materials* **12**, 2201602 (Oct 2022).

6. B. Teymur, L. Choubrac, H. Hempel, O. Gunawan, T. Unold, D. B. Mitzi, “Influence of Copper Composition in $Cu_2BaSn(S,Se)_4$ Solution-Deposited Films and Photovoltaic Devices with Over 5% Efficiency,” *ACS Applied Energy Materials* **5**, 10645-10656 (Aug 2022).

Multi-Metalloporphyrin Synthetic Polymers for Long-Range Charge Transport

PI: Jeffrey S. Moore, co-PIs: Qian Chen, Charles M. Schroeder, Emad Tajkhorshid

University of Illinois at Urbana-Champaign

Keywords: precision polymers; long-range electron transport; molecular electronics; computational modeling; heme-containing polymers

Research Scope

The main objective of this research is to understand long-range charge transport in multi-metalloporphyrin synthetic polymers. Given their biocompatibility, multifunctionality, processibility, and scalability, metalloporphyrin synthetic polymers hold strong promise for a wide range of applications.[1,2] However, substantial knowledge gaps remain in understanding the self-assembly behavior and charge-transport mechanisms of synthetic polymers that regulate electron and energy flow.[3,4] To bridge these gaps, our research team investigates how electron transport through metalloporphyrin synthetic polymers depends on their sequence, structure, architecture, and redox-active centers. Our work focuses on understanding electron transport in model systems such as single molecules while further extending to charge-transport mechanisms in more complex systems such as self-assembled biomaterials and nanoparticles. Our research methodology integrates cutting-edge computational modeling, organic synthesis, nanoscale structural characterization,[5] and single-molecule/monolayer charge-transport measurements. Our work aims to significantly advance the understanding of long-range electron transport while informing the design of biocompatible, manufacturable materials for applications in energy harvesting, transduction, and storage.

Recent Progress

Our project focuses on advancing the understanding of self-assembly and electron transport mechanisms in metalloporphyrin synthetic polymers. We began by focusing on model peptide systems based on single-molecule designs. The role of amino acid sequence and secondary structure of various peptides on their electron transport behavior was extensively studied using single-molecule experiments and computational modeling methods (**Figure 1a**)[6]. A small library of sequence-defined oligopeptides was designed and synthesized, and the electron-transport properties were measured using the scanning tunneling microscope break junction (STM-BJ) technique[7]. Results from STM-BJ experiments were quantitatively analyzed using Gaussian mixture modeling (GMM), revealing a surprising bimodal molecular conductance distribution for all oligopeptides. Molecular dynamics (MD) simulations and non-equilibrium Green's function-density functional theory (NEGF-DFT) calculations were used to understand experimental data, showing that an extended peptide sequence (primary structure) leads to a low conductance state, whereas a folded conformation (secondary structure) results in a high conductance state. Interestingly, principal components analysis (PCA) revealed that specific intramolecular

hydrogen-bonding between the peptide backbone atoms accounts for the most significant structural variation observed in the MD simulations. These results highlight the critical role of molecular conformation on electron transport in molecules such as peptides with flexible backbones.

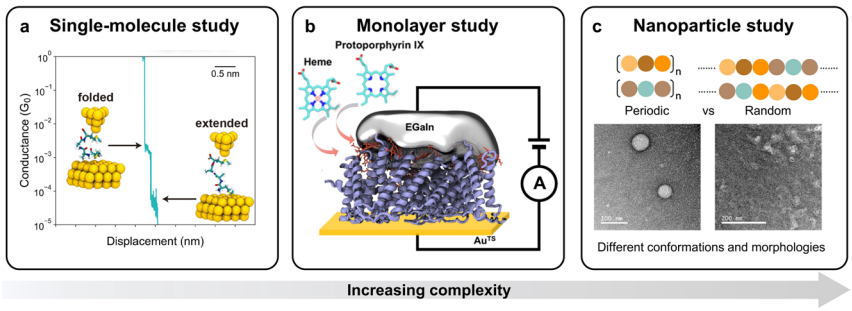

Figure 7. *Our work focuses on understanding the self-assembly and electron transport behavior in precisely defined synthetic polymers, spanning length scales from individual molecules to assembled materials.*

Extending beyond electron transport in molecules with flexible backbones such as peptides, we expanded our work to understand the role of molecular rigidity or shape-persistence on the electronic response of charged ladder-type organic molecules. Here, we synthesized and characterized the electronic properties of shape-persistent ladder molecules, with our results showing that molecular conductance is nearly independent of junction displacement, suggesting that shape-persistent molecules provide a stable route for single-molecule electronic properties[8]. This investigation of shape-persistent ladder molecules further illustrates the critical role of molecular conformation in controlling electron transport in synthetic materials.

Building on our understanding of single-molecule electronic properties, we next explored charge transport in self-assembled monolayers (SAMs) formed from heme-peptides. We designed four sequence-defined heme-binding peptides capable of forming secondary structures (**Figure 1b**). and assembling into well-ordered monolayers. We then quantified the electronic response (voltage-current density) across SAMs using liquid metal soft contact electrodes (eutectic gallium indium alloy, EGaIn)[9]. SAM layer properties were characterized using atomic force microscopy (AFM) and x-ray photoelectron spectroscopy. Monolayer electronic measurements (EGaIn) revealed a staggering >1000-fold increase in current density across the junction upon heme loading while maintaining constant film thickness. By systematically varying the amino acid composition and heme-binding sequence position, we efficiently achieve enhancements in electron transport. Overall, these findings demonstrate the key role of heme in controlling the electronic properties of peptides while providing valuable insights into electron transport at protein-metal interfaces.

We further aimed to understand the self-assembly process of more complex aggregated polymeric systems. Here, we studied the structural and self-assembly properties of nanoparticles consisting of peptide-containing periodic or random polymers (**Figure 1c**). Our results show that polymer sequence has a dramatic effect on the self-assembly behavior of these materials, with periodic repeat sequences giving rise to well-ordered assemblies.[10] Moving forward, we aim to understand and manipulate energy flow within these self-assembled systems to achieve efficient long-range charge transport, which will aid in the development of functional bioelectronic material.

References

1. Wang, F.; Gu, Y.; O'Brien, J. P.; Yi, S. M.; Yalcin, S. E.; Srikanth, V.; Shen, C.; Vu, D.; Ing, N. L.; Hochbaum, A. I.; Egelman, E. H.; Malvankar, N. S. Structure of Microbial Nanowires Reveals Stacked Hemes that Transport Electrons over Micrometers. *Cell* **177**, 361-369.e310, (2019).

2. Yu, J., Horsley, J. R. & Abell, A. D. Peptides as Bio-Inspired Electronic Materials: An Electrochemical and First-Principles Perspective. *Acc. Chem. Res.* **51**, 2237-2246, (2018).

3. Ward, M. D. & Raithby, P. R. Functional Behaviour from Controlled Self-assembly: Challenges and Prospects. *Chem. Soc. Rev.* **42**, 1619-1636, (2013).

4. Lv, Z., Zhou, Y., Han, S.-T. & Roy, V. A. L. From Biomaterial-based Data Storage to Bio-inspired Artificial Synapse. *Mater. Today* **21**, 537-552, (2018).

5. Lyu, Z., Yao, L., Chen, W., Kalutantirige, F. C. & Chen, Q. Electron Microscopy Studies of Soft Nanomaterials. *Chem. Rev.* **123**, 4051-4145, (2023).

6. Samajdar, R; Meigooni, M; Yang, H; Li, J; Liu, X; Jackson, N; Mosquera, M; Tajkhorshid, E; Schroeder, C. Secondary Structure Determines Electron Transport in Peptides. *bioRxiv*. DOI: 10.1101/2024.02.18.578245 (2024)

7. Li, J.; Peng, B.-J.; Li, S.; Tabor, D. P.; Fang, L.; Schroeder, C. M. Ladder-type Conjugated Molecules as Robust Multi-state Single-molecule Switches. *Chem*, (2023). DOI: 10.1016/j.chempr.2023.05.001.

8. Liu, X.; Yang, H.; Harb, H.; Samajdar, R.; Woods, T.; Lin, O.; Chen, Q.; Rodríguez-López, J.; Romo, A.; Assary, R.; Moore, J.; Schroeder, C. Shape-persistent Ladder Molecules Exhibit Nanogap-Independent Conductance in Single-Molecule Junctions. *Chemrxiv*. DOI: 10.26434/chemrxiv-2023-29v0h (2023)

9. Zhao, Z., Soni, S., Lee, T., Nijhuis, C. A. & Xiang, D. Smart Eutectic Gallium–Indium: From Properties to Applications. *Adv. Mater.* **35**, 2203391, (2023).

10. Yu, H.; Kalutantirige, F. C.; Yao, L.; Schroeder, C. M.; Chen, Q.; Moore, J. S. Self-Assembly of Repetitive Segment and Random Segment Polymer Architectures. *ACS Macro Lett.* **11**, 1366-1372, (2022).

Publications

1. Kalutantirige, F. C.; He, J.; Yao, L.; Cotty, S.; Zhou, S.; Smith, J. W.; Tajkhorshid, E.; Schroeder, C. M.; Moore, J. S.; An, H.; Su, X.; Li, Y.; Chen, Q. Beyond Nothingness in the Formation and Functional Relevance of Voids in Polymer Films. *Nat. Commun.* **15**, 2852, (2024).

2. Liu, X.; Yang, H.; Harb, H.; Samajdar, R.; Woods, T.; Lin, O.; Chen, Q.; Rodríguez-López, J.; Romo, A.; Assary, R.; Moore, J.; Schroeder, C. Shape-persistent Ladder Molecules Exhibit Nanogap-Independent Conductance in Single-Molecule Junctions. *Nat. Chem.* Accepted. (2024)

3. Samajdar, R; Meigooni, M; Yang, H; Li, J; Liu, X; Jackson, N; Mosquera, M; Tajkhorshid, E; Schroeder, C. Secondary Structure Determines Electron Transport in Peptides. *Proc. Natl. Acad. Sci. U. S. A.* In Press. (2024)

4. Chen, W.; Zhan, X.; Yuan, R.; Pidaparthy, S.; Yong, A. X. B.; An, H.; Tang, Z.; Yin, K.; Patra, A.; Jeong, H.; Zhang, C.; Ta, K.; Riedel, Z. W.; Stephens, R. M.; Shoemaker, D. P.; Yang, H.; Gewirth, A. A.; Braun, P. V.; Ertekin, E.; Zuo, J.-M.; Chen, Q. Formation and Impact of Nanoscopic Oriented Phase Domains in Electrochemical Crystalline Electrodes. *Nat. Mater.* **22**, 92-99, (2023).

5. Jacobs, M. I., Bansal, P., Shukla, D. & Schroeder, C. M. Understanding Supramolecular Assembly of Supercharged Proteins. *ACS Cent. Sci.* **8**, 1350-1361, (2022).

6. Yu, H.; Kalutantirige, F. C.; Yao, L.; Schroeder, C. M.; Chen, Q.; Moore, J. S. Self-Assembly of Repetitive Segment and Random Segment Polymer Architectures. *ACS Macro Lett.* **11**, 1366-1372, (2022).

7. Chen, W.; Zhan, X.; Yuan, R.; Pidaparthy, S.; Tang, Z.; Zuo, J.-M.; Chen, Q. 4D-STEM Mapping of Nanoscale Structural Ordering in Cathode Materials. *Microsc. Microanal.* **28**, 2608-2609, (2022).

8. Samajdar, R; Meigooni, M; Yang, H; Li, J; Liu, X; Jackson, N; Mosquera, M; Tajkhorshid, E; Schroeder, C. Secondary Structure Determines Electron Transport in Peptides. *bioRxiv*. DOI: 10.1101/2024.02.18.578245 (2024)

9. Liu, X.; Yang, H.; Harb, H.; Samajdar, R.; Woods, T.; Lin, O.; Chen, Q.; Rodríguez-López, J.; Romo, A.; Assary, R.; Moore, J.; Schroeder, C. Shape-persistent Ladder Molecules Exhibit Nanogap-Independent Conductance in Single-Molecule Junctions. *Chemrxiv*. DOI: 10.26434/chemrxiv-2023-29v0h (2023)

Fundamental Understanding of Electrochemical – Mechanical Driven Instability of Sodium Metal

Partha P. Mukherjee (PI, Purdue University), David Mitlin (Co-PI, The University of Texas at Austin), Yu-chen Karen Chen-Wiegart (Co-PI, Stony Brook University)

Keywords: sodium metal, interface instability, heterogeneity, dendrite and solid electrolyte interphase interaction, electro-chemo-mechanics.

Research Scope

Sodium metal electrodes hold tremendous potential to enable next-generation electrochemical energy storage systems due to their high specific capacity (1166 mAh g^{-1}) and low reduction potential (−2.73 V *vs.* standard hydrogen electrode).[1-4] However, developing viable sodium metal electrodes is confronted with critical challenges such as dendrite growth, unstable solid electrolyte interphase (SEI), and dead metal formation.[5-8] While significant focus has been laid on understanding the limitations of electrolyte transport and non-uniform metal morphologies, the underlying electro-chemo-mechanical coupling and sodium-metal/SEI interactions still need to be investigated in detail. To address these knowledge gaps, we develop three interrelated research thrusts investigating the origin and evolution of electrochemical-mechanical driven interfacial instabilities in sodium metal electrodes. These thrusts examine the (i) mechanistic correlation between electrolyte interactions, SEI heterogeneity, and interface evolution, (ii) influence of electro-chemo-mechanical coupling on the sodium morphology and failure mechanism, and (iii) role of collector support chemistry on the metal microstructure and SEI composition. To understand these aspects, a combination of mechanistic modeling, electrochemical experiments, and in situ/operando characterization has been performed.

Recent Progress

As part of the proposed research, three fundamental areas pertaining to the coupled electrochemical-mechanical interactions and morphological stability of sodium metal electrodes were studied. The first thrust was focused on understanding the mechanistic role of electrochemical, transport, and morphological heterogeneities on sodium-metal/SEI interactions and the evolution of interface instabilities. We investigate how SEI-driven heterogeneities can influence transport and reaction kinetics at sodium metal interfaces, forming current and stress hotspots during electrodeposition. The effect of non-uniform mechanical stresses on the distribution of mechanical overpotential, reaction

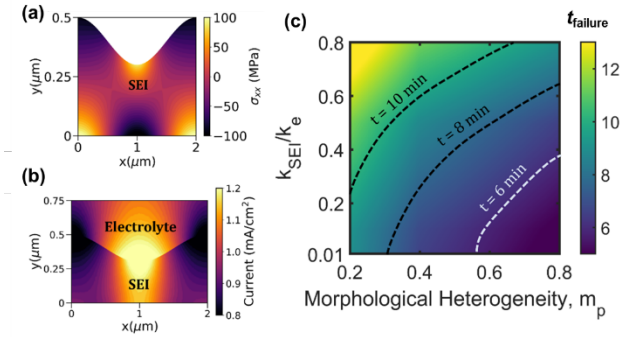

Figure 1. Role of (a) mechanical stress distribution and (b) reaction heterogeneity on the (c) failure onset at the sodium-metal/SEI interface.

heterogeneity, and electrochemical failure has been demonstrated. We develop a comprehensive mapping between the morphological, mechanical, and transport characteristics of the SEI, and the associated mechanistic regimes governing the onset of interface instability (Figure 1). In addition, we reveal that adding fluoroethylene carbonate can induce chemical heterogeneities in the SEI and cause accelerated electrochemical failure. Based on this model system, the correlation between the SEI characteristics, electrolyte interactions, and sodium morphological evolution has been examined.

The second research thrust examined the interrelation between electrochemical-mechanical coupling, electrolyte/SEI interactions, and interface evolution in sodium metal electrodes. The influence of external pressure on the dynamic evolution of sodium metal morphology during electrodeposition and electrodissolution has been captured (Figure 2). We investigate how mechanical stress profiles affect ionic transport in the electrolyte and SEI, and correlate it to different morphological patterns such as film-type, mossy, and fractal. A fundamental relationship has been developed between the mechanical overpotential, reaction current distribution, and the onset of interface instability. Further, we reveal the combined influence of external pressure and mechanical/transport properties of the electrolyte and SEI on the degree of reaction heterogeneity at the sodium metal interface. Under such external pressure conditions, the mechanistic processes leading to hotspot formation, SEI failure, and dendrite growth have been delineated. This study allows deriving mechanistic design guidelines toward achieving stable sodium-metal/SEI interfaces during plating and stripping.

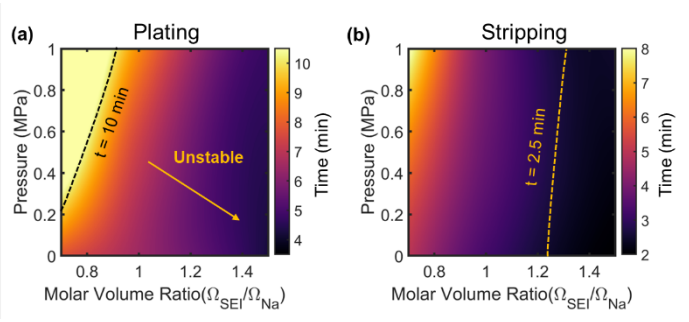

Figure 2. Effect of external pressure on the onset of interface instability during (a) plating and (b) stripping.

The third research thrust involved understanding how the sodium metal microstructure and its SEI are influenced by the collector support chemistry. By using an intermetallic-coated copper current collector as a model sodiophilic support and an unmodified sodiophobic baseline, major differences in the electrodeposit morphology, internal porosity, and evolution of the crystallographic texture of sodium metal have been demonstrated. We reveal that the SEI composition critically depends on the support chemistry and deposition rate through X-ray nanotomography, grazing-incidence wide-angle X-ray scattering, and mesoscale modeling. For instance, while textured sodium hydride and sodium hydroxide are prevalent for the baseline copper current collector, sodium fluoride is dominant for the intermetallic-coated copper current collector. The onset of electrochemical instabilities is also correlated to the chemical evolution of the SEI and the morphological dynamics of the sodium metal.

References

1. Y. Zhao, K. R. Adair, and X. Sun, *Recent developments and insights into the understanding of Na metal anodes for Na-metal batteries*, Energy & Environmental Science, **11**, 2673 (2018).
2. X. Zheng, C. Bommier, W. Luo, L. Jiang, Y. Hao, and Y. Huang, *Sodium metal anodes for room-temperature sodium-ion batteries: Applications, challenges and solutions*, Energy Storage Materials, **16**, 6 (2019).
3. B. Lee, E. Paek, D. Mitlin, and S. W. Lee, *Sodium metal anodes: emerging solutions to dendrite growth*, Chemical reviews, **119**, 5416 (2019).
4. H. Wang, E. Matios, J. Luo and, W. Li, *Combining theories and experiments to understand the sodium nucleation behavior towards safe sodium metal batteries*, Chemical Society Reviews, **49**, 3783 (2020).
5. B. Sayahpour, W. Li, S. Bai, B. Lu, B. Han, Y. Chen, G. Deysher, S. Parab, P. Ridley, G. Raghavendran, L. H. B. Nguyen, M. Zhang, and Y. S. Meng, *Quantitative analysis of sodium metal deposition and interphase in Na metal batteries*, Energy & Environmental Science, **17**, 1216 (2024).
6. S. Sarkar, M. J. Lefler, B. S. Vishnugopi, R. B. Nuwayhid, C. T. Love, R. Carter, and P. P. Mukherjee, *Fluorinated ethylene carbonate as additive to glyme electrolytes for robust sodium solid electrolyte interface*, Cell Reports Physical Science, **4**, 101356 (2023).
7. Q. Liu, L. Zhang, H. Sun, L. Geng, Y. Li, Y. Tang, P. Jia, Z. Wang, Q. Dai, and T. Shen, *In situ observation of sodium dendrite growth and concurrent mechanical property measurements using an environmental transmission electron microscopy–atomic force microscopy (ETEM-AFM) platform*, ACS Energy Letters, **5**, 2546 (2020).
8. W. Liu, P. Liu and D. Mitlin, *Review of emerging concepts in SEI analysis and artificial SEI membranes for lithium, sodium, and potassium metal battery anodes*, Advanced Energy Materials, **10**, 2002297 (2020).

Publications

1. Y. Wang, H. Dong, N. Katyal, B. S. Vishnugopi, M. K. Singh, H. Hao, Y. Liu, P. Liu, P. P. Mukherjee, G. Henkelman, J. Watt, and D. Mitlin, *Intermetallics Based on Sodium Chalcogenides Promote Stable Electrodeposition–Electrodissolution of Sodium Metal Anodes.* Advanced Energy Materials, **13**, 2204402 (2023).
2. P. Liu, D. Yen, B. S. Vishnugopi, V. R. Kankanallu, D. Gürsoy, M. Ge, J. Watt, P. P. Mukherjee, Y. K. Chen-Wiegart, and D. Mitlin, *Influence of Potassium Metal-Support Interactions on Dendrite Growth*. Angewandte Chemie, **62**, e202300943 (2023).
3. A. Singla, K. G. Naik, B. S. Vishnugopi, and P. P. Mukherjee, *Heterogeneous Solid Electrolyte Interphase Interactions Dictate Interface Instability in Sodium Metal Electrodes*, (under review), (2024).
4. S. Sarkar, B. S. Vishnugopi, R. Carter, C. T. Love, J. Watt, D. Mitlin, and P. P. Mukherjee, *Mechanistic Origin of Dendrite Growth through Solid Electrolyte Interphase Heterogeneity in Sodium Metal Anodes*, (under review), (2024).
5. A. Singla, K. G. Naik, B. S. Vishnugopi, and P. P. Mukherjee, *Critical Role of External Pressure on Sodium Electrode Morphology during Plating and stripping*, (under review), (2024).
6. P. Liu, H. Hao, A. Singla, B. S. Vishnugopi, P. P. Mukherjee, J. Watt, and D. Mitlin, *Artificial SEI and CEI based on Aluminum Oxide Promotes Electrochemical Stability in Potassium Metal Batteries*, Angewandte Chemie, e202402214 (2024).
7. V. Raj, K. G. Naik, B. S. Vishnugopi, A. K. Rana, A. S. Manning, S. R. Mahapatra, K. Varun, V. Singh, A. Nigam, J. D. McBrayer, P. P. Mukherjee, N. P. B. Aetukuri, D. Mitlin, *Dendrite Growth—Microstructure—Stress—Interrelations in Garnet Solid-State Electrolyte*. Advanced Energy Materials, **14**, 2303062 (2024).
8. V. Raj, Y. Wang, K. G. Naik, M. Feng, M. Jain, B. S. Vishnugopi, H. Hao, N. B. Schorr, M. Salazar, A. M. Heusser, G. Michalke, S. Kalnaus, J. Watt, J. D. McBrayer, B. Boyce, Y. Qi, P. P. Mukherjee, and D. Mitlin, *Grain Boundary Zirconia-Modified Garnet Solid-State Electrolyte*, (under review), (2024).
9. C. Lo, Y. Wang, V. R. Kankanallu, A. Singla, D. Yen, X. Zheng, K. G. Naik, B. S. Vishnugopi, C. Campbell, V. Raj, C. Zhao, L. Ma, J. Bai, F. Yang, R. Li, M. Ge, J. Watt, P. P. Mukherjee, D. Mitlin, Y. K. Chen-Wiegart, *Interdependence of Support Wettability - Electrodeposition Rate - Sodium Metal Anode and SEI Microstructure*, (under review), (2024).

Discovering Dopable, Next-Generation Defect Tolerant Hybrid Semiconductors

James R Neilson, Department of Chemistry, Colorado State University

Obadiah G Reid, Renewable and Sustainable Energy Institute, University of Colorado Boulder

Keywords: Semiconductor, hybrid perovskite, crystallography, defects

Research Scope

This project seeks to discover new defect tolerant and dopable semiconductors, as these new materials are needed for myriad energy-relevant technologies. In this project, the overarching goal is to discover new hybrid inorganic-organic semiconductors by understanding how entropy manifests and dictates phase behavior. We focus on understanding how materials chemistry, through compositional substitution with organic cations or polyanions, influences the creation and organization of point defects[1] and doping. These goals are accomplished by the synthesis of materials with well-defined compositions, identification of their often-disordered atomistic structures,[2] interrogation of the electronic properties using microwave conductivity and bulk transport,[3] and discovery of composition-structure-property relationships. Selective control over the concentration and mobility of defects *and* carriers has potential to enable new and emerging technologies requiring next-generation semiconductors.

Recent Progress

This year, we highlight recent progress on two subprojects. First, with the goal to influence the concentration and organization of point defects, we discovered new defect-ordered structures relative to the perovskite aristotype through both anion and cation substitution. Secondly, we identified how alloying on a specific site of the perovskite aristotype influences the defect thermochemistry, displacements of the ideal bonding configurations, and the resulting influence on electronic properties.

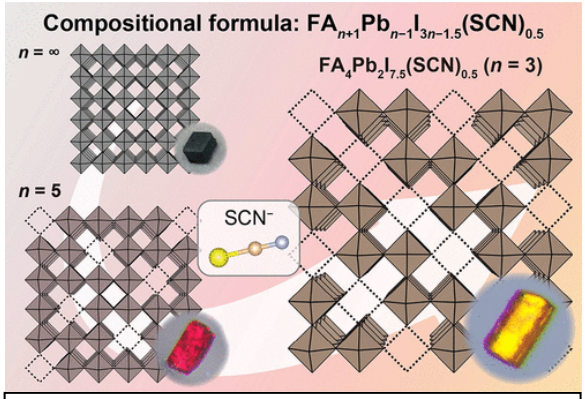

Figure 1: Substitution of SCN^- for I^- with specific stoichiometric ratios yields a homologous series of compounds with ordered of columns of vacancies.

In the first subproject, we discovered how partial replacement of iodine by the pseudohalide, SCN^-, leads to the coalescence and ordering of vacancy defects in $(CH(NH_2)_2)PbI_3$ (i.e., $FAPbI_3$) to yield a new homologous series of compounds, $FA_{n+1}Pb_{n-1}I_{3n-1.5}(SCN)_{0.5}$, as summarized in Figure 1.[4] Isovalent substitution yields vacancy-ordered superstructures to accommodate the steric interactions of the larger SCN^- polyanion. For

a low substitution ratio (1 SCN^- for 30 I^- sites), the compound $FA_6Pb_4I_{13.5}SCN_{0.5}$ crystallizes with ordered columnar Pb vacancies.[5] This specific compound can co-crystalize with $FAPbI_3$ and preserve $FAPbI_3$ in the metastable perovskite crystal structure to near ambient conditions (e.g., $FAPbI_3$ is only stable as perovskite at elevated temperature). Increasing the amount of SCN^- to 6.7% (1 SCN^- for 15 I^- sites) yields a layered crystal structures, with the layers representative of the corrugated (110) slice through the perovskite aristotype.[4] While the substitution of small organic cations with larger organic cations (e.g., *n*-butylammonium for methylammonium) often yields layered crystal structures, some large organic cations accomplish similar vacancy-ordered structures akin to SCN^- substitution. In this project, we identify a defect-ordered perovskite derivative with three-dimensional electronic connectivity and properties comparable to other tin-based perovskites: $(NH_3(CH_2)_7NH_3)_2Sn_3I_{10}$. Understanding how cations and anions substitute into the perovskite structure is vital to understanding how different device-proven additives play a role in the materials chemistry.

In the second subproject, we reveal how composition in perovskite alloys controls the defect thermochemistry. Most hybrid inorganic-organic perovskite-derived devices employ alloyed compositions to tune bandgaps and impart stability. However, fundamental materials chemistry questions underlying the nature of these systems persist. In this project, we have elucidated how alloying in $(CH_3NH_3)_{1-x}Cs_xSnBr_3$ modifies the underlying defect thermochemistry and local distortions that dictate the electronic properties, as summarized in Figure 2.[6] Microwave conductivity experiments across the series of compounds reveals a significant increase in carrier density when comparing $CH_3NH_3SnBr_3$ to $CsSnBr_3$; however, there is a reduction in carrier density for the intermediate compositions. This compositional dependence permits extraction of the average enthalpy and non-configurational entropy per defect that yields carriers (e.g., tin oxidation compensated by tin vacancies). Symmetry-adapted displacement mode analysis of pair distribution functions obtained from synchrotron X-ray total scattering experiments reveals a change in the predominant local displacement mode going from methylammonium-rich to cesium-rich compositions. This change in local bonding displacements explains the observed anomalous transients in time-resolved microwave conductivity studies thought to arise from carrier localization and trapping. Altogether, this recent progress provides new insight into the entropy-rich materials chemistry of hybrid inorganic-organic semiconductors that have significant potential for chemical tunability and functionality.

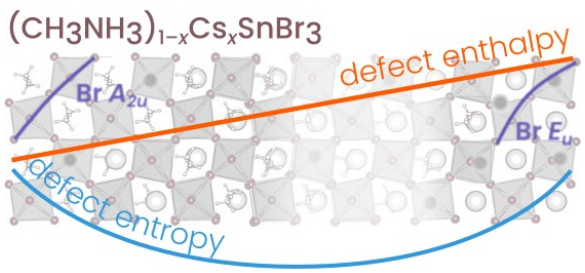

Figure 2: $(CH_3NH_3)_{1-x}Cs_xSnBr_3$ solid solutions reveal the defect thermochemistry and defect-limited carrier mobilities.

References

1. A. Walsh, D. O. Scanlon, S. Chen, X. G. Gong, S.-H. Wei, *Self-Regulation Mechanism for Charged Point Defects in Hybrid Halide Perovskites*. Angew. Chem., **127**, 1811–1814 (2015).
2. E. M. Mozur, J. R. Neilson, *Cation Dynamics in Hybrid Halide Perovskites*, Ann. Rev. Mater. Res., **51**, 269-291 (2021).
3. O. G. Reid, D. T. Moore, Z. Li, D. Zhao, Y. Yan, K. Zhu, G. Rumbles, *Quantitative analysis of time-resolved microwave conductivity data*. J. Phys. D: Appl. Phys., **50**, 493002 (2017).

Publications

4. T. Ohmi, J. R. Neilson, W. Taniguchi, N. Tomoya, H. Teppei, Y. Haruta, M. Saidaminov, T. Fukushima, M. Azuma, Masaki, T. Yamamoto. *$FA_4Pb_2I_{7.5}(SCN)_{0.5}$: n = 3 Member of Perovskite Homologous Series $FA_{n+1}Pb_{n-1}I_{3n-1.5}(SCN)_{0.5}$ with Columnar Defects.* ACS Mat. Lett. **6** 1913–1919 (2024).
5. T. Ohmi, I. W. H. Oswald, J. R. Neilson, N. Roth, S. Nishioka, K. Maeda, K. Fujii, M. Yashima, M. Azuma, T. Yamamoto, *Thiocyanate-Stabilized Pseudo-Cubic Perovskite $CH(NH_2)_2PbI_3$ from Coincident Columnar Defects Lattices,* J. Am. Chem. Soc. **145**(36), 19759-19767 (2023).
6. D. C. Asebiah, E. M. Mozur, A. A. Koegel, A. Nicolson, S. R. Kavanagh, D. O. Scanlon, O. G. Reid, J. R. Neilson, *Defect-Limited Mobility and Defect Thermochemistry in Mixed A-cation Tin Perovskites: $(CH_3NH_3)_{1-x}Cs_xSnBr_3$.* In review (2024).

Passive and Enhanced Capture and Conversion of CO_2 by d/f^0 Molecules and Materials

May Nyman and Tim Zuehlsdorff, Oregon State University; Ahmet Uysal, Argonne National Laboratory

Keywords: DAC, peroxide, transition metals, CO_2, SFG

Research Scope

Designing chemical reactions for carbon dioxide removal (CDR) from air, both point-source (i.e. factory emissions) and direct air capture (DAC) is very important to meet global climate goals. Challenges to CDR material performance include selectivity, capacity, capture rate, stability, and re-usability under a range of conditions, driving opportunities for innovation. High oxidation-state transition metal (TM) and uranyl species (Ti^{IV}, $V/Nb/Ta^{V}$, $Cr/Mo/W^{VI}$ and $U^{VI}O_2^{2+}$) are promising for CO_2 chemisorption, as both additives to point-source CDR media, and as DAC materials.[1-5] These metals drive CO_2 hydration at a solid-air or liquid-air interface, directly bind carbonate, and lower the regeneration temperature of the sorbent matrix. We have identified that metal peroxoanions, or peroxometalates, undergo DAC via chemisorption as solids, converting up to three peroxide ligands to carbonate ligands. All aqueous chemisorption reactions involving $CO_2 \rightarrow CO_3^{2-}$ conversion requires the CO_2 to cross the 1 nm air-liquid interface. Yet, we understand very little about this process. Soluble high oxidation state metal oxoanions can also play an important role in probing this interfacial reaction.

All peroxometalates we have studied in detail (beyond scoping) exhibit increased DAC reactivity with increasing counter cation size, a phenomenon that cannot be readily explained by thermodynamics, spectroscopy or computation. In this overview presentation, I will describe the DAC reaction mechanisms for vanadium and titanium tetraperoxometalates, differentiating the roles of the metal and the alkali counter cation. By vibrational SFG (sum frequency generation) studies, we have made the first observation of CO_2 directly at the air-water interface, exploiting VO_4^{3-} solutions. These studies enable understanding the $CO_2 \rightarrow CO_3^{2-}$ chemisorption reaction. Finally, photogeneration of superoxide from peroxide with concomitant reduction of M^{V} to M^{IV} (M=Nb, Ta) is also affected by the alkali counter cation, and I will discuss characterization of these materials, plus preliminary assessment of the role of photoactivity for carbon capture.

Recent Progress

Peroxometalate DAC. Monitoring DAC of $A_3V(O_2)_4$ (tetraperoxovanadate, A=K,Rb,Cs) enabled isolation of $VO(CO_3)(O_2)_2^{3-}$, revealing the role of vanadium in the DAC mechanism.[6] DFT shows an activation step of forming and breaking a peroxycarbonate intermediate. The peroxovanadates capture 1.5-2 molecules CO_2 per metal center, with a capacity of 4.9 mmol CO_2/g $K_3V(O_2)_4$ for the K-analogue. We synthesized and structurally characterized $A_4Ti(O_2)_4$ (A=Li,Na,K) for the first time (only synthesis reported in 1928[7]), and the K-analogue showed very rapid and high capacity (8.17 mmol CO_2/g $K_4Ti(O_2)_4$, **fig. 1a**). Energy dispersive spectroscopy (SEM-EDX) mapping indicated phase separation (Ti-rich and alkali-rich) for the Li and Na analogues, but not for the fast-reacting K-analogue **fig. 1b**). The least reactive Na-analogue shows

distinct passivation of Ti-rich particle cores with Na-rich shells (**fig. 1c**), an indirect indication of the importance of the Ti in DAC. While Li is not detectable by EDX, mapping oxygen is used for color contrast (**fig. 1d**), and the Li-analogue undergoes phase separation with a Ti-rich surface. The DAC reactivity rates and capacity of the analogues trends K>Li>Na (**fig. 1a**) providing additional evidence of the role of high oxidation state metals in DAC.

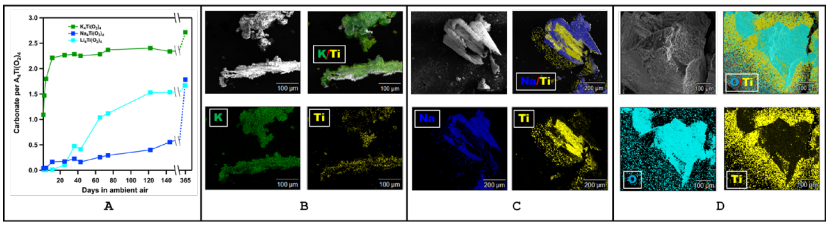

Figure 1. DAC behavior of $Ti(O_2)_4^{4-}$.

Directly observing CO_2 at the air-liquid interface. Prior studies have shown the impact of high oxidation state metals on point source carbon capture using aqueous monoethanolamine or KOH. [1-4] SFG analysis of aqueous VO_4^{3-} and MoO_4^{2-} exposed to CO_2 atmosphere provide opportunity to evaluate mechanisms of vanadate-enhanced CO_2 chemisorption. To our surprise, 0.1 – 1.0 M K_3VO_4 exposed to CO_2 gas produced an intense peak at the 1 nm air-water interface at 2336 cm^{-1}, shifted from the CO_2 vibrational peak in a vacuum (2446 cm^{-1}, **fig. 2a**). Moreover, upon exposure of the CO_2-saturated solution to ambient air produced only a 20% decrease in the CO_2 signal over 2 hours (**fig. 2a**). This suggests that the CO_2 molecules are stably bound to the interface. DFT calculations indicated that bending the CO_2 molecule to ~155° increases the Raman activity (**fig. 2b**), enabling observation of the peak. This also indicates the first step of chemisorption. DFT predicts a $\square_3$ vibration at 2340 cm^{-1}, very close to the observed peak position. At 2M K_3VO_4 concentration, the CO_2 signal disappears and instead chemisorbed carbonate is observed at the interface. We will discuss several hypotheses of the concentration dependent CO_2 surface association, transitioning to CO_3^{2-} chemisorption. **Fig. 2c** illustrates one possible role of vanadate in CO_2 surface binding and O=C=O bending as a first step to chemisorption.

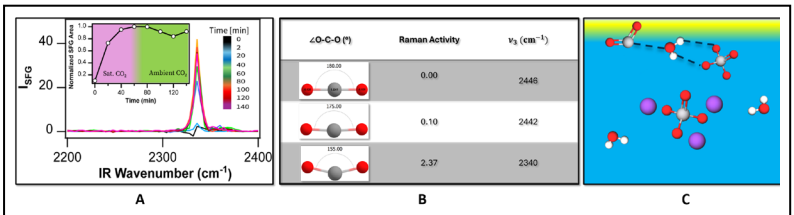

Figure 2. CO_2 observation at the air-$VO_4^{3-}{}_{aq}$ interface.

Photoactivity We are currently endeavoring to exploit photochemistry in order to produce reactive oxygen species that can stabilize via DAC. The ultimate goal is to design DAC materials that activate via sunlight exposure. $A_3M(O_2)_4$ (A=K,Rb,Cs; M=Nb,Ta) presents an opportunity to explore this hypothesis. These materials exposed to ambient light or UV-light turn brown due to reduction of M^V to M^{IV}, along with formation of superoxides. The UV-vis absorption of the pristine materials increases with alkalis size; Cs>Rb>K (**fig. 4**). The Nb/Ta trend is currently unknown, but under investigation. I will present the photoreduction behavior of this series of compounds, along with possible use in carbon capture.

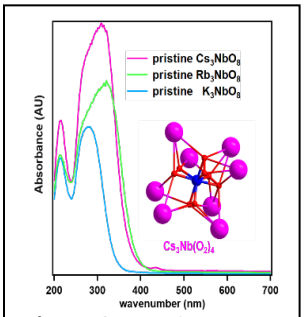

Figure 3. UV-vis spectrum of $A_3Nb(O_2)_4$.

References

(1) U.H. Bhatti, A.K. Shah, J.N. Kim, J.K. You, S.H. Choi, D.H. Lim, S. Nam, Y.H. Park, I.H. Baek, *Effects of Transition Metal Oxide Catalysts on MEA Solvent Regeneration for the Post-Combustion Carbon Capture Process*. ACS Sustain Chem Eng **5**, 5862-5868 (2017).
(2) H.X. Gao, Y.F. Huang, X.W. Zhang, Z.A.S. Bairq, Y.Q. Huang, P. Tontiwachwuthikul, Z.W. Liang, *Catalytic performance and mechanism of SO_4^{2-}/ZrO_2/SBA-15 catalyst for CO_2 desorption in CO_2-loaded monoethanolamine solution*. Appl Energ, **259**, 114179 (2020).
(3) Q.H. Lai, S. Toan, M.A. Assiri, H.G. Cheng, A.G. Russell, H. Adidharma, M. Radosz, M.H. Fan, *Catalyst-$TiO(OH)_2$ could drastically reduce the energy consumption of CO_2 capture*. Nat Commun **9**, 2672 (2018).
(4) D.T. Phan, M. Maeder, R.C. Burns, G. Puxty, *Catalysis of CO_2 absorption in aqueous solution by vanadate and sulfate and their application to post combustion capture*. Int J Greenh Gas Con **36**, 60-65(2015).
(5) D.V. Kravchuk, N.N. Dahlen, S.J. Kruse, C.D. Malliakas, P.M. Shand, T.Z. Forbes, *Isolation and Reactivity of Uranyl Superoxide*. Angew Chem Int Edit **60**, 15041-15048 (2021).
(6) E.G. Ribó, Z. Mao, J.S. Hirschi, T. Linsday, K. Bach, E.D. Walter, C.R. Simons, T.J. Zuehlsdorff, M. Nyman, *Implementing vanadium peroxides as direct air carbon capture materials*. Chem Sci **15**, 1700-1713 (2024).
(7) V.R. Schwarz, H. Giese, *Uber die Peroxyde des Titans, Zirkons, Hafniums und Thoriums*. Zeitschrift für anorganische und allgemeine Chemie **176**, 209-232 (1928).

Publications

1. M. Rashwan, Z. Mao, J.S. Hirschi, T.J. Zuehlsdorff, M. Nyman, Ahmet Uysal, *Direct observation of CO_2 adsorption and binding at the air/aqueous interface*, submitted to PNAS (2024)
2. Z. Mao, M. Rashwan, E. Garrido Ribó, M. Nord, L.N. Zakharov, T.W. Surta, A. Uysal, M. Nyman. *Carbon Dioxide Capture by Niobium Polyoxometalate Fragmentation*. Journal of the American Chemical Society. Published July 8 **https://doi.org/10.1021/jacs.4c06178** (2024).
3. K. Bach, E. Garrido Ribo, J. Hirschi, Z. Mao, L.N. Zakharov, T.J. Zuehlsdorff, M. Nyman, *Tetraperoxotitanates for High Capacity Direct Air Capture of Carbon Dioxide*. Chemistry of Materials, in review. Posted to ChemRxiv: 10.26434/chemrxiv-2024-xb06z (2024).
4. J.S. Hirschi, M. Nyman, T.J. Zuehlsdorff, *Electronic Structure and CO_2 Reactivity of Group IV/V/VI Tetraperoxometalates*. Posted to ChemRxiv: 10.26434/chemrxiv-2024-blwjs, The Journal of Physical Chemistry, in revision (2024).
5. A. Arteaga, T. Arino, G.C. Moore, J.L. Bustos, M.K. Horton, K.A. Persson, J. Li, W.F. Stickle, T.A. Kohlgruber, R.G. Surbella III, M. Nyman, *The Role of Alkalis in Orchestrating Uranyl-Peroxide Reactivity Leading to Direct Air Capture of Carbon Dioxide*. Chemistry–A European Journal, **30**, e2023016872024 (2024).
6. E.G. Ribó, Z. Mao, J.S. Hirschi, T. Linsday, K. Bach, E.D. Walter, C.R. Simons, T.J. Zuehlsdorff, M. Nyman, *Implementing vanadium peroxides as direct air carbon capture materials*. Chemical Science, **15**, 1700-1713 (2024).

Hybrid metal oxocluster-based soft materials: design principles and emergent properties

May Nyman, Oregon State University

Keywords: Nb-POMs, UiO-66 MOFs, SAXS, glasses, nerve-agent degradation

Research Scope

Disordered inorganic or hybrid materials is a large family that includes gels, ionic liquids, glasses, less ordered versions of crystalline counterparts, and even solutions. These materials, especially in comparison to highly-ordered counterparts, offer advantages such as accessible surface area and reactivity (i.e. ion exchangers, catalysts, ion conductors), grain-boundary free interfaces and membranes, conformal surface coatings, and transparency and/or isotropic optical properties. However, disordered/amorphous/solution-based materials are challenging to characterize. The discovery and optimization of functional inorganic and hybrid materials often relies heavily on structure elucidation from single-crystal X-ray diffraction (SCXRD). With such atomic-level information, we can determine what properties we expect a material to possess, and enables explanation of an observed phenomenon. SCXRD can also be the starting point to understanding amorphous or disordered derivatives of crystalline analogues, as well as solutions.

We are investigating oxo-clusters as the foundation for disordered/amorphous materials, to elucidate atomic-level arrangement of matter and function in both solution and glassy solids. Three recent/ongoing studies in this poster presentation include: 1) Niobium-silicate/phosphate gels and related crystal structures from Nb-polyoxometalates (POMs), 2) Cluster-derived nerve agent (simulant) degradation driven by cluster lability, and 3) Top-down acid dissolution of UiO-66 metal organic frameworks (MOFs) leading to new cluster-based materials.

Recent Progress

Niobium-silicate/phosphate gels and glasses. Glass is an extremely important material in advanced technologies (i.e. next generation microelectronics packaging[1]), and glass production is energy intensive, inspiring soft chemistry approaches to glass formation.[2] Niobium oxide is an important glass-forming oxide (or glass ceramic with nanocrystalline domains) due to the high refractive index, mechanical strength, and electrical properties.[3] Glasses with high concentrations of distorted NbO_6 are of particular interest. We have found that certain Nb-POMs can undergo disassembly in the presence of alkalis (and other ions), leading to networks and gels.[4-6] We are using this platform to devise low temperature methods to access niobium-based glassy materials. By introducing carbon dioxide gas (to decrease pH 'gently') to

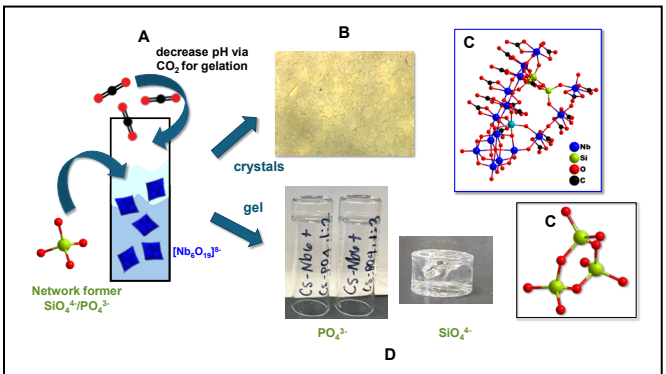

Figure 1. Overview of niobate glass formation.

hexaniobate-silicate/phosphate solutions, glassy materials are obtained, currently with Cs as the alkali for enhanced solubility (**fig. 1a**). By varying the Cs concentration, we can also obtain a crystal structure from the Cs-Nb-SiO_4 oxide matrix (**fig. 1b, 1c**), as a baseline for structural characterization of the glassy materials (**fig. 1d**). We are still trying to obtain an analogous structure from the Cs-Nb-PO_4 system, structurally characterize the glasses using X-ray scattering and multinuclear solid-state NMR, and characterize properties including optical and electrical. Low temperature dehydration without losing transparency is an additional current challenge.

Exploiting cluster lability for nerve agent simulant degradation. Nerve agent (simulants) fluorophosphates can be neutralized by presumed acid or base catalyzed hydrolysis of the P-F bond. The most studied acidic and basic materials are respectively Zr-MOFs[7] and Nb-POMs,[8] where the former possesses an acidic Zr-oxocluster. In a head-to-head comparison of these presumed two disparate reaction mechanisms leading to the same end-product, we show that bond lability is the most important feature of the material substrate for effective DFP (diisopropylfluorophosphate) degradation (**figure 2**). The profound effect of the counter cation for the Nb-POMs on DFP degradation will also be presented.

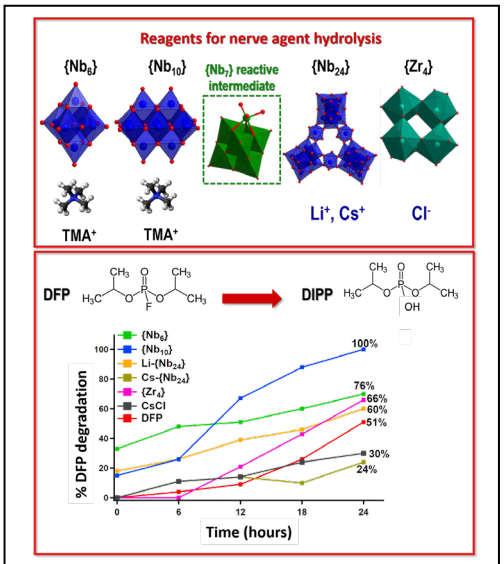

Figure 2. Top: Zr and Nb cluster lability studied (plus their counterions) using DFP degradation as a probe. Bottom: tracking various DFP decomposition times.

Top down dissolution of UiO-66. UiO-66 MOF featuring the $M^{IV}_6(O,OH)_8$ node (M=Zr,[9] Hf,[10] Ce,[11] Th,[12] U,[13] Np,[14] Pu[15]) and benzenedicarboxylate (BDC) linker are amongst the most studied hybrid materials. They are purported to be stable in strong acid, but we have shown the nodes can be completely dissolved in acetic or formic acid (pH 2-4) as intact hexamers (2M acetic acid) or cluster sub-fragments including trimers and dimers (respectively 5 and 10M acetic acid), as determined by SAXS (**fig. 3a-c** for dissolution of Zr-UiO-66). The clusters are separated via metathesis of insoluble, protonated BDC. The dissolved nodes also crystallize new (or prior-reported) cluster-based materials that are representative of the dissolved species, analyzed by SAXS. Formate linked hexamers obtained from dissolved Zr-UiO-66 and Hf-UiO-66 are shown in **figure 3d**, for example.

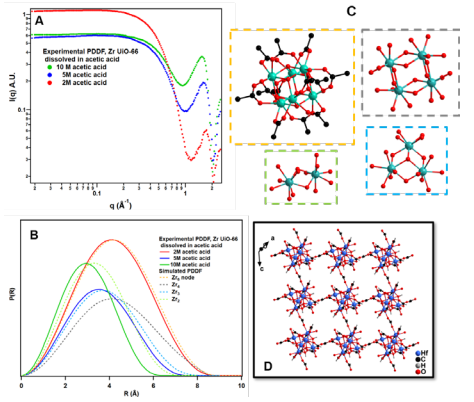

Figure 3. Examples of solution speciation and recrystallization of Zr/Hf UiO-66 nodes.

References

(1) M. Letz, T. Gotschke, F. Wagner, M. Heiss-Chouquet, L. Müller, U. Peuchert, D.Vanderpool. In *Structured glass substrates in wafer- and panel level packaging: Status and recent achievements*, IMAPS 2021 - 54th International Symposium on Microelectronics San Diego CA (2021).
(2) M. Mader, O. Schlatter, B. Heck, A. Warmbold, A. Dorn, H. Zappe, P. Risch, D. Helmer, F. Kotz, B.E. Rapp, *High-throughput injection molding of transparent fused silica glass*. Science, **372**, 182-186 (2021).
(3) Komatsu, T.; Honma, T.; Tasheva, T.; Dimitrov, V. *Structural role of Nb_2O_5 in glass-forming ability, electronic polarizability and nanocrystallization in glasses: A review*. J Non-Cryst Solids **581**, 121414 (2022**)**.
(4) Nyman, M.; Rahman, T.; Colliard, I. Decaniobate: The Fruit Fly of Niobium Polyoxometalate Chemistry. Accounts Chem Res **56**, 3616-3625 (2023).
(5) D. Sures, M. Segado, C. Bo, M. Nyman, *Alkali-Driven Disassembly and Reassembly of Molecular Niobium Oxide in Water*. *J Am Chem Soc* **2018**, *140*, 10803-10813.
(6) T. Rahman, N.P. Martin, J.K. Jenkins, R. Elzein, D.B. Fast, R. Addou, G.S. Herman, M. Nyman, *Nb_2O_5, $LiNbO_3$, and (Na, K)NbO_3 Thin Films from High-Concentration Aqueous Nb-Polyoxometalates*. Inorg Chem **61**, 3586-3597 (2022).
(7) A.M. Plonka, Q. Wang, W.O. Gordon, A. Balboa, D. Troya, W.W. Guo, C.H. Sharp, S.D. Senanayake, J.R. Morris, C.L. Hill, A.I. Frenkel, *In Situ Probes of Capture and Decomposition of Chemical Warfare Agent Simulants by Zr-Based Metal Organic Frameworks*. J Am Chem Soc **139**, 599-602 (2017).
(8) M.K. Kinnan, W.R. Creasy, L.B. Fullmer, H.L. Schreuder-Gibson, M. Nyman, *Nerve Agent Degradation with Polyoxoniobates*. Eur J Inorg Chem, **2014**, 2361-2367 (2014).
(9) J.H. Cavka, S. Jakobsen, U. Olsbye, N. Guillou, C. Lamberti, S. Bordiga, K.P. Lillerud, *A new zirconium inorganic building brick forming metal organic frameworks with exceptional stability.* J Am Chem Soc **130**, 13850-13851 (2008).
(10) S. Jakobsen, D. Gianolio, D.S. Wragg, M.H. Nilsen, H. Emerich, S. Bordiga, C. Lamberti, U. Olsbye, M. Tilset, K.P. Lillerud, *Structural determination of a highly stable metal-organic framework with possible application to interim radioactive waste scavenging: Hf-UiO-66*. Phys Rev B **86**, 125429 (2012).
(11) Lammert, M.; Wharmby, M. T.; Smolders, S.; Bueken, B.; Lieb, A.; Lomachenko, K. A.; De Vos, D.; Stock, N. Cerium-based metal organic frameworks with UiO-66 architecture: synthesis, properties and redox catalytic activity. *Chem Commun* **2015**, *51*, 12578-12581.
(12) C. Falaise, J.S. Charles, C. Volkringer, T. Loiseau*, Thorium Terephthalates Coordination Polymers Synthesized in Solvothermal DMF/H_2O System*. Inorg Chem **54**, 2235-2242 (2015).
(13) C. Falaise, C. Volkringer, J.F. Vigier, N. Henry, A. Beaurain, T. Loiseau, *Three-Dimensional MOF-Type Architectures with Tetravalent Uranium Hexanuclear Motifs (U_6O_8)*. Chem-Eur J **19**, 5324-5331 (2013).
(14) N.P. Martin, J. März, H. Feuchter, S. Duval, P. Roussel, P.N. Henry, A. Ikeda-Ohno, T. Loiseau, C. Volkringer, *Synthesis and structural characterization of the first neptunium based metal-organic frameworks incorporating {Np_6O_8} hexanuclear clusters*. Chem Commun **54**, 6979-6982 (2018).
(15) A.M. Hastings, D. Ray, W. Jeong, L. Gagliardi, O.K. Farha, A.E. Hixon, *Advancement of Actinide Metal-Organic Framework Chemistry via Synthesis of Pu-UiO-66*. J Am Chem Soc **142**, 9363-9371 (2020).

Publications

1. L. Palys, D. Stephen, Z. Mao, S.T. Mergelsberg, D. Boglaienko, Y. Chen, Liu L, Bae Y, Jin B, J.A. Sommers, J.J. De Yoreo, M. Nyman *Cerium Nanophases from Cerium Ammonium Nitrate*. Langmuir **40,** 4350-4360 (2024).
2. J.F. Yin, L. Amidani, J. Chen, M. Li, B. Xue, Y. Lai, K. Kvashnina, M. Nyman, P. Yin, *Spatiotemporal Studies of Soluble Inorganic Nanostructures with X-rays and Neutrons* Angewandte Chemie International Edition, **63** e2023109532024 (2024).
3. M. Nyman, T. Rahman, I. Colliard. *Decaniobate: The Fruit Fly of Niobium Polyoxometalate Chemistry*, Accounts of Chemical Research, **56**, 3616-3625 (2023).
4. M. Amiri, A. Lulich, N.C. Chiu, S. Wolff, D.B. Fast, W.F. Stickle, K.C. Stylianou, M. Nyman, *Bismuth-polyoxocation coordination networks: controlling nuclearity and dimension-dependent photocatalysis*. ACS Applied Materials & Interfaces, **15** 18087-18100 (2023).

5. A. Lulich, M. Amiri, D. Stephen, M. Shohel, Z. Mao, M. Nyman, *Bismuth Coordination Polymers with Fluorinated Linkers: Aqueous Stability, Bi-volatility, and Adsorptive Behavior*. ACS Omega, **8**, 10476-10486 (2023).
6. J.J. Chen, L. Vilà-Nadal, A. Solé-Daura, G. Chisholm, T. Minato, C. Busche, T. Zhao, B. Kandasamy, A.Y. Ganin, R.M. Smith, I. Colliard, J.M. Poblet, M. Nyman, L. Cronin. *Effective storage of electrons in water by the formation of highly reduced polyoxometalate clusters*. Journal of the American Chemical Society. **144**, 8951-8960 (2022).
7. T. Rahman, E. Petrus, M. Segado, N.P. Martin, L.N. Palys, M.A. Rambaran, C.A. Ohlin, C. Bo, M. Nyman. *Predicting the solubility of inorganic ion pairs in water*. Angewandte Chemie International Edition, **61**, e202117839 (2022).
8. T. Rahman, N.P. Martin, J.K. Jenkins, R. Elzein, D.B. Fast, R. Addou, G.S. Herman, M. Nyman. *Nb_2O_5, $LiNbO_3$, and $(Na,K)NbO_3$ Thin Films from High-Concentration Aqueous Nb-Polyoxometalates*. Inorganic Chemistry. **61**, 3586-3597 (2022).
9. J.A. Sommers, L. Palys, N.P. Martin, D.B. Fast, M. Amiri, M. Nyman. *Oxo-Cluster-Based Zr/Hf^{IV} Separation: Shedding Light on a 70-Year-Old Process*. Journal of the American Chemical Society. **144**, 2816-2824 (2022).
10. R.M. Smith, M. Amiri, N.P. Martin, A. Lulich, L.N. Palys, G. Zhu, J.J. De Yoreo, M. Nyman. *Solvent-driven transformation of Zn/Cd^{2+}-deoxycholate assemblies*. Inorganic Chemistry. **10**, 1275-1286 (2022).

Uncovering intrinsic transport and magnetic properties of two-dimensional electrically conducting metal-organic frameworks

Mircea Dincă – Massachusetts Institute of Technology

Julius Oppenheim – Massachusetts Institute of Technology

Keywords: Metal-organic frameworks, electronic conductivity, MOF–polymer composites, ionic conductivity, sensing

Research Scope

This research program focuses on two key areas: (1) exploring the impact of band engineering on the electronic conductivity of two-dimensional metal-organic frameworks (2D MOFs) and (2) investigating the interaction between electronic and ionic conductivities. Band engineering in native MOFs is achieved electronically through redox modifications or sterically through modulation of structural parameters, and in 2D MOF–polymer composites by aligning bands at the heterojunctions. Electron transport may be competitive with ion transport, which can be chemically controlled by modifying ion activity. These findings are applied to enhance the performance of capacitors and chemiresistive sensors.

Recent Progress

The intrinsic transport properties of an electronically conductive two-dimensional metal-organic framework (2D MOF) are dependent upon the band structure of the material (i.e., caused by in-plane conjugation and interlayer stacking), perturbations caused by heterojunctions, and any competing transport via ionic conductivity.[**Ref 1,2**] Recently, we have focused on probing the underlying intrinsic transport properties by systematically modifying 2D MOFs.

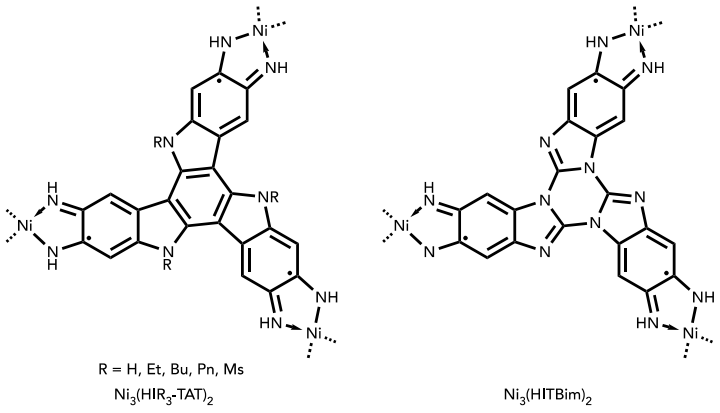

Figure 1: Molecular structure of , $Ni_3(HIH_3\text{-}TAT)_2$ and $Ni_3(HITBim)_2$.

We have recently been investigating the effects of electronic and steric modifications on the electronic conductivity of nitrogen-substituted 2D MOFs.[**Pub 1,2, Ref 3**] In particular, we have compared two isoreticular frameworks, $Ni_3(HIH_3\text{-}TAT)_2$ and $Ni_3(HITBim)_2$, the latter of which possesses an extra nitrogen-atom substitution and does not possess a functionalizable indole (**Figure 1**). We find that $Ni_3(HIH_3\text{-}TAT)_2$ has a bulk conductivity of 44 mS/cm whereas $Ni_3(HITBim)_2$ only displays 0.5 mS/cm (measured as pressed pellets). The additional N-atom substituents in the aromatic core prevent strong in-plane delocalization, causing electronic bands to be flatter (i.e., higher hole/electron effective masses) and the band gap to be larger. Currently, we are working towards new 2D MOFs based on N-substituted ligands as well as ligands with novel connectivity.

We find that the indole moiety of $Ni_3(HIH_3\text{-}TAT)_2$ is susceptible to post-synthetic modification via mesylation, and the resultant material exhibits decreased bulk electronic conductivity and higher transport activation energies. We attribute these changes to an increase in the interlayer π-π packing distance as caused by the bulky mesyl groups. Furthermore, we find that the series of isoreticular frameworks $Ni_3(HIR_3\text{-}TAT)_2$ (where R = ethyl, butyl, pentyl) display progressively larger interlayer stacking distances relative to $Ni_3(HIH_3\text{-}TAT)_2$. As the stacking distance increases, the orbital overlap between layers decreases, and the electronic conductivity decreases.

In order to understand the effects of heterojunctions on 2D MOF transport, we have been investigating 2D MOF–conductive polymer composites. Recently, we have demonstrated new electronically conductive polymers[**Pub 3**] as well as new methodology for constructing MOF–polymer composites.[**Pub 4**] These methodologies have recently proven their general utility in enhancing reversibility and sensitivity response in chemiresistors derived from composites of 2D MOFs, M_3HXTP_2 where M = Co, Cu, Ni and X = NH, O, and a conductive polymer based on 3,4-propylenedioxythiophene (ProDOT) and 2,1,3-benzothiadiazole (BTD). [**Pub 5**] Whereas the pristine 2D MOFs exhibit irreversible gas sensing and low sensing responses for NO_2, the composites exhibit significantly enhanced reversibility and sensing response.

As these 2D MOFs tend to be relatively n-type compared to the chosen polymer, there is a hole injection from the polymers to the 2D MOFs, facilitating desorption kinetics of NO_2, leading to higher sensing reversibility (**Figure 2**). Such idea is further verified by use of the n-type polymer, poly{[*N*,*N*′-*bis*(2-octyldodecyl)-naphthalene-1,4,5,8-*bis*(dicarboximide)−2,6-diyl]-alt-5,5′-(2,2′-bithiophene)} (N2200), which forms composites with 2D MOFs that display diminished response and irreversible kinetics.

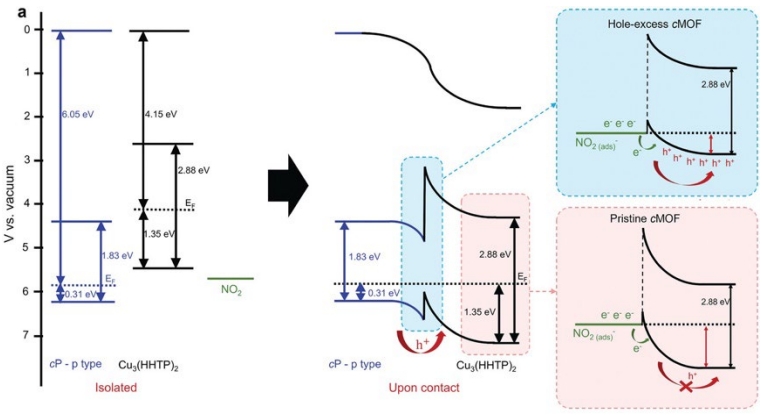

Figure 2: Hole enrichment and its impact on analyte binding.

We have recently been examining the interaction between electronic and ionic conductivity for 2D MOFs. Traditionally, MOFs have either displayed electronic or ionic conductivity, whereas dual electronic-ionic conductors remain rare.[**Ref 4**] Mixed electronic-ionic conductors have been considered to be promising for various applications, particularly as electrode materials for energy storage, sensors, and electrochemical catalysts [**Ref 5**]. The absence of dual conductors may be due to only one transport mechanism being measurable if the impedance through one mechanism is much smaller than the other. Additionally, many of the reported 2D MOFs are neutral species, without mobile counter ions. To gain a deeper understanding of the electronic-ionic interactions, we have focused on understanding the design principles required to make MOFs ionically conductive.[**Pub 6**] As well ion transport within the pores of a MOF is dissimilar to traditional solid-state ionic and bulk solution ionic conductors, we have studied the dynamics and structure of solvent under confinement.[**Pub 7**] We have recently been able to combine these insights by investigating the impact of relative humidity on intrinsic transport within a series of 2D MOFs.

We have found that in arid conditions, transport is dominated by electrons, however as the water content in the pores of the frameworks increases (commensurate with the interlayer stacking distance increasing), the electronic conductivity decreases, and the ionic (proton) conductivity increases. The transition between transport regimes dramatically affects the chemiresistive sensitivity for analytes including NO_2 and NH_3. We are currently analyzing the interaction between electronic and ionic conductivity in the systems that conduct alkali ions, rather than protons.

References

1. L. S. Xie, G. Skorupskii, M. Dincă, *Electrically Conductive Metal–Organic Frameworks*. Chem. Rev. **120**, 8536–8580 (2020).
2. R. A. Kharod, J. L. Andrews, M. Dincă, *Teaching Metal-Organic Frameworks to Conduct: Ion and Electron Transport in Metal-Organic Frameworks.* Annual Review of Materials Research **52**, 103–128 (2022).
3. Y. Lu, Y. Zhang, C.-Y. Yang, S. Revuelta, H. Qi, C. Huang, W. Jin, Z. Li, V. Vega-Mayoral, Y. Liu, X. Huang, D. Pohl, M. Položij, S. Zhou, E. Cánovas, T. Heine, S. Fabiano, X. Feng, R. Dong, *Precise tuning of interlayer electronic coupling in layered conductive metal-organic frameworks.* Nat Commun **13**, 7240 (2022).
4. J. Su, W. He, X.-M. Li, L. Sun, H.-Y. Wang, Y.-Q. Lan, M. Ding, J.-L. Zuo, *High Electrical Conductivity in a 2D MOF with Intrinsic Superprotonic Conduction and Interfacial Pseudo-capacitance.* Matter **2**, 711–722 (2020).
5. B. D. Paulsen, K. Tybrandt, E. Stavrinidou, J. Rivnay, *Organic mixed ionic–electronic conductors.* Nat. Mater. **19**, 13–26 (2020).

Publications

1. A. Y. Su, P. Apostol, J. Wang, A. Vlad, M. Dincă, *Electrochemical Capacitance Traces with Interlayer Spacing in Two-dimensional Conductive Metal–Organic Frameworks*. Angewandte Chemie International Edition **63**, e202402526 (2024).
2. P. Apostol, S. M. Gali, A. Su, D. Tie, Y. Zhang, S. Pal, X. Lin, V. R. Bakuru, D. Rambabu, D. Beljonne, M. Dincă, A. Vlad, *Controlling Charge Transport in 2D Conductive MOFs─The Role of Nitrogen-Rich Ligands and Chemical Functionality.* J. Am. Chem. Soc. **145**, 24669–24677 (2023).
3. G. G. Yang, D.-H. Kim, S. Samal, J. Choi, H. Roh, C. E. Cunin, H. M. Lee, S. O. Kim, M. Dincă, A. Gumyusenge, *Polymer-Based Thermally Stable Chemiresistive Sensor for Real-Time Monitoring of NO2 Gas Emission*. ACS Sens. **8**, 3687–3692 (2023).
4. M. A. Pearson, S. Bhagchandani, M. Dincă, J. A. Johnson*, Mixing ligands to enhance gas uptake in polyMOFs.* Mol. Syst. Des. Eng. **8**, 591–597 (2023).
5. H. Roh, D.-H. Kim, Y. Cho, Y.-M. Jo, J. A. del Alamo, H. J. Kulik, M. Dincă, A. Gumyusenge, *Robust Chemiresistive Behavior in Conductive Polymer/MOF Composites*. Advanced Materials **n/a**, 2312382 (2024).
6. A. Iliescu, J. L. Andrews, J. J. Oppenheim, M. Dincă, *A Solid Zn-Ion Conductor from an All-Zinc Metal–Organic Framework Replete with Mobile Zn2+ Cations.* J. Am. Chem. Soc. **145**, 25962–25965 (2023).
7. M. L. Valentine, G. Yin, J. J. Oppenheim, M. Dincă, W. Xiong, *Ultrafast Water H-Bond Rearrangement in a Metal–Organic Framework Probed by Femtosecond Time-Resolved Infrared Spectroscopy.* J. Am. Chem. Soc. **145**, 11482–11487 (2023).

Chemo-Mechanically Driven In Situ Hierarchical Structure Formation in Mixed Conductors

PI: Nicola H. Perry, UIUC Department of Materials Science & Engineering

Keywords: crystallization, combinatorial films, conductivity, oxygen surface exchange kinetics

Research Scope

In many energy contexts, active materials must exhibit "hierarchical" function – they should perform distinct, yet inter-related tasks at different sites, across disparate length and time scales. To support this heterogeneous function, there is a need to understand and direct formation of corresponding tailored hierarchical architectures. Particularly, oxide mixed ionic and electronic conductors (MIECs) catalyze reactions at their surfaces and selectively transport both ionic and electronic species in the bulk[1]. Ideally, MIECs should adopt hierarchical structures with 1) high surface areas, 2) surface compositions exhibiting high catalytic activity, and 3) microstructural connectivity in the direction needed for fast mass and charge transport. In practice, however, MIECs are typically fabricated at elevated temperatures, leading to coarse, non-directional structures with poisoned (chemically segregated) surfaces[2].

This work therefore hypothesized that a new approach – low-temperature vapor-phase deposition of non-equilibrium thin films plus stimulated chemo-mechanical actuation – would transform homogeneous MIECs into ideal, highly active hierarchical structures in situ. We sought to leverage the intrinsic coupling of contraction upon oxidation, plus the contraction inherent in crystallization, to direct beneficial structure formation from the atomic scale to the nanoscale[3]. Key questions addressed – leveraging pulsed laser deposition, DOE user facilities (XAS, GIXRD), molecular dynamics, impedance spectroscopy, scanning nanobeam diffraction (4D-STEM), and a contact-free high-throughput optical approach – included: 1) how are chemical/structural changes across multiple length scales linked during transformation, 2) which process variables are most significant for directing hierarchical structure evolution and why, and 3) how and why do the ionic transport, electronic transport, and surface reactivity change during transformation?

Recent Progress

We focused on monitoring, understanding, and controlling the emerging hierarchical structure and functional properties in primarily ABO_{3-d} (A=Sr,La,Ba; B=Ti,Ga,Fe,Co,Pr) perovskites. In initial work[4-8], we observed that mild annealing of amorphous films induced both crystallization and oxidation, with consequences for evolving structure across many length scales: increases in cation coordination numbers and valences, complex strain evolution leading to pore formation/hierarchical microstructures, and alignment of neighboring BO_x polyhedra that promoted crystal symmetry increases. The consequences were an orders-of-magnitude increase in hole concentration, rise in hole mobility, and development of an unusual B-site-rich surface composition. These factors gave rise to large increases in *electronic* conductivity and oxygen

surface exchange coefficient (k) during hierarchical transformation. Based on these results, later work focused on a) evaluating evolution of *ionic* conductivity[9] and b) examining the role of oxygen availability at all stages of the transformation in directing structure and property development[7,10-11]. We also advanced a contact-free optical method for monitoring k during crystallization[12-14], which avoids the problematic contribution of metal current collectors to measured catalytic activity, and extended it to spatially resolved measurements of combinatorial film libraries for high-throughput analysis of both crystallization kinetics and k.

We developed a thin-film blocking electrode cell design to isolate changes in ionic vs. electronic conductivity during crystallization. By coupling *in-situ* synchrotron GIXRD with simultaneous ac impedance spectroscopy and dc polarization, we demonstrated that in (La,Sr)(Ga,Fe)O_{3-d} the ionic conductivity increases ~2 orders of magnitude during crystallization, but the electronic conductivity increases much more. Therefore it transforms from a mostly ionic conductor into an electronic conductor, with every ratio of ionic: electronic conductivity accessible in between. Grain boundaries form during crystallization; MD simulations plus activation energy measurements demonstrated that these features appear to hinder ion migration but not electronic transport, partly explaining the transference number evolution. [9]

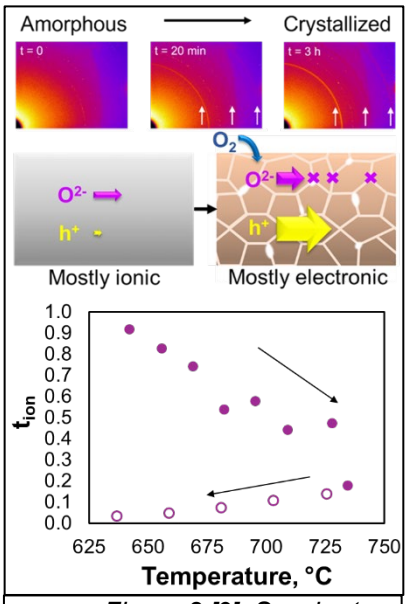

Figure 8 [9]. Synchrotron GIXRD patterns monitoring crystallization; illustration of evolving ionic/electronic transport behavior; ionic transference numbers during crystallization.

We examined the role of oxygen availability during growth and during annealing on structure and property evolution[7,10-11]. During deposition, oxygen pressure impacted initial density, porosity, density change from annealing, and the overall cation ratio (studied by XRR and RBS), with intermediate growth pressures yielding the best k values. During annealing, gas-phase oxygen partial pressure modified the final bond lengths and coordination numbers. Most strikingly, high oxygen chemical potential in the films by solid-state electrochemical pumping yielded faster crystallite nucleation kinetics, as studied by *in-situ* optical analysis and *ex-situ* correlation mapping in 4D-STEM; pumping also changed compositional heterogeneity.

In summary, the hierarchical structures demonstrated exceptional surface catalytic activity[4,6] and high ionic and electronic conductivity[5,9], opening the door to much lower operating temperatures than are possible with conventionally prepared MIECs. Moreover, they served as a platform to develop a fundamental understanding of dynamic, evolving MIEC processing-structure-property relationships, through the amorphous-to-crystalline transformation, guiding low-thermal-budget processing and rational design for energy applications.

References

1. N. H. Perry, and T. Ishihara, *Roles of bulk and surface chemistry in the oxygen exchange kinetics and related properties of mixed conducting perovskite oxide electrodes*, Materials, **9**(10), 858 (2016); H. J. M. Bouwmeester, H. Kruidhof, and A. J. Burggraaf, *Importance of the surface exchange kinetics as rate limiting step in oxygen permeation through mixed-conducting oxides,* Solid state ionics, **72**, 185-194 (1994); P. J. Gellings, and H. J. Bouwmeester, *Ion and mixed conducting oxides as catalysts,* Catalysis Today, **12**(1), 1-101 (1992); U. Balachandran, B. Ma, P. S. Maiya, R. L. Mieville, J. T. Dusek, J. J. Picciolo, J. Guan, S. E. Dorris, and M. Liu, *Development of mixed-conducting oxides for gas separation,* Solid State Ionics **108** (1-4), 363-370 (1998).

2. B. Koo, K. Kim, J. K. Kim, H. Kwon, J. W. Han, and W. Jung, *Sr segregation in perovskite oxides: why it happens and how it exists*, Joule, **2**(8), 1476-1499 (2018); Y. Li, W. Zhang, Y. Zheng, J. Chen, B. Yu, Y. Chen, and M. Liu, *Controlling cation segregation in perovskite-based electrodes for high electro-catalytic activity and durability*, Chemical Society Reviews, **46**(20), 6345-6378 (2017).

3. T. Chen, G. F. Harrington, K. Sasaki, and N. H. Perry*, Impact of microstructure and crystallinity on surface exchange kinetics of strontium titanium iron oxide perovskite by in situ optical transmission relaxation approach*, Journal of Materials Chemistry A, **5**(44), 23006-23019 (2017).

4. T. Chen, G. F. Harrington, J. Masood, K. Sasaki, and N. H. Perry, *Emergence of rapid oxygen surface exchange kinetics during in situ crystallization of mixed conducting thin film oxides*, ACS applied materials & interfaces, **11**(9), 9102-9116 (2019). [supported by this grant]

5. H. B. Buckner, Q. Ma, J. Simpson-Gomez, E. J. Skiba, and N. H. Perry, *Multi-scale chemo-mechanical evolution during crystallization of mixed conducting $SrTi_{0.65}Fe_{0.35}O_{3-\delta}$ films and correlation to electrical conductivity*, Journal of Materials Chemistry A, **10**(5), 2421-2433 (2022). [supported by this grant]

6. E. J. Skiba, T. Chen, and N. H. Perry, *Simultaneous Electrical, Electrochemical, and Optical Relaxation Measurements of Oxygen Surface Exchange Coefficients: $Sr(Ti,Fe)O_{3-d}$ Film Crystallization Case Study*, ACS Applied Materials & Interfaces, **12**(43), 48614-48630 (2020). [supported by this grant]

7. E. J. Skiba, Q. Ma, H. B. Buckner, and N. H. Perry, *Evolution of local ion environments as a function of crystallinity in $Sr(Ti,Fe)O_{3-x}$ films* (in preparation, supported by this grant); and E. J. Skiba, *Relating multiscale structure and chemistry with oxygen exchange kinetics in low-thermal-budget $Sr(Ti,Fe)O_{3-d}$ and high-throughput combinatorial thin films*, PhD Dissertation, UIUC [N. H. Perry: Advisor] (2023).

8. N. Kim, B. J. Blankenau, T. Su, N. H. Perry, and E. Ertekin, *Multisublattice cluster expansion study of short-range ordering in iron-substituted strontium titanate*, Computational Materials Science, **202**, 110969 (2022). [supported partially by this grant]

9. H. B. Buckner, J. Simpson-Gomez, A. Bonkowski, K. Rübartsch, H. Zhou, R. A. De Souza, and N. H. Perry, *Transforming an ionic conductor into an electronic conductor via crystallization: in-situ evolution of transference numbers and structure in $(La,Sr)(Ga,Fe)O_{3-x}$ perovskite thin films,* Advanced Functional Materials, 2401854 (2024). [supported by this grant]

10. E. J. Skiba, Q. Ma, and N. H. Perry, *Impact of gas-controlled oxygen chemical potential on atomic structure evolution during crystallization of $Sr(Ti,Fe)O_{3-x}$ perovskite* (in preparation) [supported by this grant]

11. H. B. Buckner, R. Busch, J. Zuo, and N. H. Perry, *Electrochemical oxygen pumping accelerates crystallization kinetics of perovskite mixed conducting films* (in preparation, supported by this grant); and H. B. Buckner, *Relating charge transport properties to the multi-scale chemo-mechanical evolution of crystallizing mixed conducting oxide thin films*, PhD Dissertation, UIUC [N. H. Perry: Advisor] (2023).

12. H. B. Buckner and N. H. Perry, *In situ optical absorption studies of point defect kinetics and thermodynamics in oxide thin films*, Advanced Materials Interfaces, **6**(15), 1900496 (2019). [supported by this grant]

13. E. J. Skiba and N. H. Perry, *High-Temperature 2D Optical Relaxation Visualizes Enhanced Oxygen Exchange Kinetics at Metal-Mixed Conducting Oxide Interfaces*, ACS Applied Materials & Interfaces, **14**(42), 47659-47673 (2022). [supported by this grant]

14. A. Popescu, E. Skiba, K. Arsky, Y. Malka, and N. H. Perry, *Combinatorial analysis of oxygen surface exchange kinetics and crystallization by 2D optical transmission relaxation on Sr(Ti,Co,Fe)O_{3-x} libraries* (in preparation) [supported by this grant]

Publications (Past 2 Years)

1. H. B. Buckner, J. Simpson-Gomez, A. Bonkowski, K. Rübartsch, H. Zhou, R. A. De Souza, and N. H. Perry, *Transforming an ionic conductor into an electronic conductor via crystallization: in-situ evolution of transference numbers and structure in (La,Sr)(Ga,Fe)O_{3-x} perovskite thin films,* Advanced Functional Materials, 2401854 (2024).

2. J. Lee, H. B. Buckner, and N. H. Perry, *Proton Surface Exchange Kinetics of Perovskite Triple Conducting Thin Films for Protonic Ceramic Electrolysis Cells: $BaPr_{0.9}Y_{0.1}O_{3-\delta}$ (BPY) vs. $Ba_{1-x}Co_{0.4}Fe_{0.4}Zr_{0.1}Y_{0.1}O_{3-\delta}$ (BCFZY)*, Journal of Materials Chemistry A **12**, 15412-15429 (2024).

3. E. J. Skiba and N. H. Perry, *High-Temperature 2D Optical Relaxation Visualizes Enhanced Oxygen Exchange Kinetics at Metal-Mixed Conducting Oxide Interfaces*, ACS Applied Materials & Interfaces, **14**(42), 47659-47673 (2022).

4. E. J. Skiba, *Relating multiscale structure and chemistry with oxygen exchange kinetics in low-thermal-budget Sr(Ti,Fe)O_{3-d} and high-throughput combinatorial thin films*, PhD Dissertation, UIUC [N. H. Perry: Advisor] (2023).

5. H. B. Buckner, *Relating charge transport properties to the multi-scale chemo-mechanical evolution of crystallizing mixed conducting oxide thin films*, PhD Dissertation, UIUC [N. H. Perry: Advisor] (2023).

6. Various publications in preparation for submission, as listed in references section.

Hierarchical Hybrid Multifunctional Materials through Interface Engineering

PI: Dr. Pierre Ferdinand Poudeu; Department of Materials Science and Engineering, University of Michigan; ppoudeup@umich.edu

Co-PI: Dr. Ctirad Uher; Department of Physics, University of Michigan; cuher@umich.edu

Keywords: Electronic defect hybridization; Hierarchical composite materials; hole density optimization; Ultralow thermal conductivity; Degenerate to non-degenerate electronic transport

Research Scope

This project focuses on the development of *stimuli-responsive hybrid multifunctional materials*. We place emphasis on the correlation between (i) the hierarchical structural entanglement of Cu_2Se, a narrow band gap (NBG), with a range of wider band gap semiconductors (WBGS) such as $CuMSe_2$ (M = Al, Ga, In, Fe, Cr) and Cu_4TiSe_4; and (ii) the interactions between native electronic defects within the coexisting phases in the resulting (1-x)Cu_2Se/(x)WBGS *bulk composites*.

Recent Progress

We demonstrate that the nature (type) of native electronic defects in these composites as well as their relative density can be tuned through alteration of the chemistry of the $CuMSe_2$ phase. This affords the ability to leverage the partial solubility between Cu_2Se and $CuMSe_2$ to engineer the carrier density and to modulate Cu^+ ion disorder in the Cu_2Se-matrix, which lead to enhanced thermoelectric properties and superior electrochemical stability. [4-9] For instance, we found that the incorporation of Cr^{3+} into the Cu_2Se crystal lattice in (1-x)Cu_2Se/(x)$CuCrSe_2$ composites facilitates the stabilization of α-Cu_2Se at 300 K leading to a large reduction in the carrier density. Such optimization of the carrier density led to a large (63%) increase in the thermopower and a drastic (46%) reduction in the total thermal

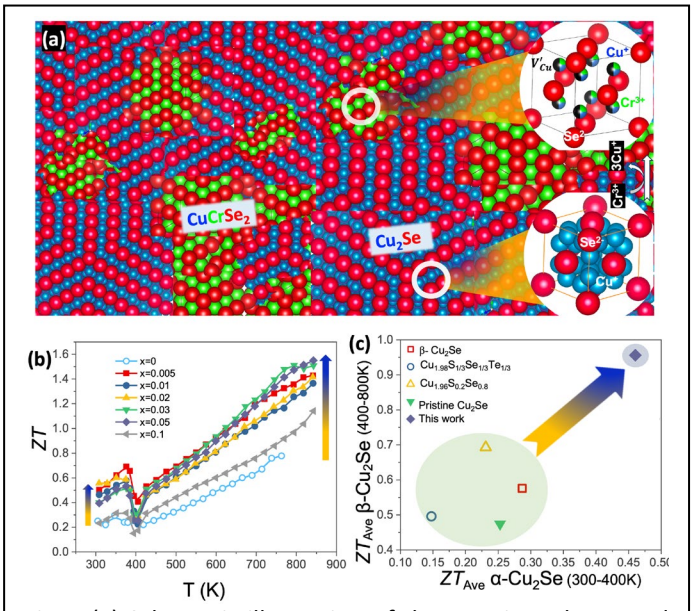

Fig.1: (a) Schematic illustration of the atomic-scale mutual integration between Cu_2Se (CS) and $CuCrSe_2$ (CCS) domains highlighting the generation of *extrinsic* copper vacancies (V'_{Cu}) and the reduction in the density of *intrinsic* copper interstitials (Cu'_i) upon partial dissolution of $CuCrSe_2$ into the Cu_2Se crystal lattice; (b) Temperature dependent ZT; (c) Comparison of the average figure of merit (ZT_{ave}) for both α-Cu_2Se and β-Cu_2Se phases in the (1-x)Cu_2Se/(x)$CuCrSe_2$ composite with x = 0.03 with those of Cu_2Se-based materials from previous work such as β-Cu_2Se, [1] $Cu_{1.98}S_{1/3}Se_{1/3}Te_{1/3}$, [2] and $Cu_{1.96}Se_{0.8}S_{0.2}$. [3]

conductivity resulting in a significant enhancement of the thermoelectric performance in the entire temperature range from 300 K to 773 K. This results in high average ZT values for both α-Cu_2Se (ZT_{ave} = 0.60) and β-Cu_2Se (ZT_{ave} = 0.97). [10]

We also show that for a given $CuMSe_2$ phase, the degree of interactions between the coexisting native electronic defects and their energy distribution within the band gap of the resulting hierarchical composites can be controlled by altering the Cu_2Se:$CuMSe_2$ phase ratio, which also results in the alteration of the degree of structural entanglement of the coexisting phases. For instance, we found that the high degree of intermixing between the coexisting phases for nearly equimolar (1-x)Cu_2Se/(x)$CuMSe_2$ (M = In, Ga) composites, lead to the defect hybridization as probed by a sudden unexpected large increase in the carrier density and electrical conductivity. [5, 7, 9, 11] This ability to engineer the energy distribution of electronic defects in semiconductors to afford the coexistence of degenerate and nondegenerate transport behavior within the resulting composites, which is manifested by unusual temperature dependent electronic transport, can be leveraged for the development of more versatile electronic and optoelectronic devices with superior performance. For instance, the dependence of the carrier density on temperature associated with the non-degenerate behavior in such a semiconductor can be leveraged to design electronic devices with low noise level that can operate under a wide temperature range.

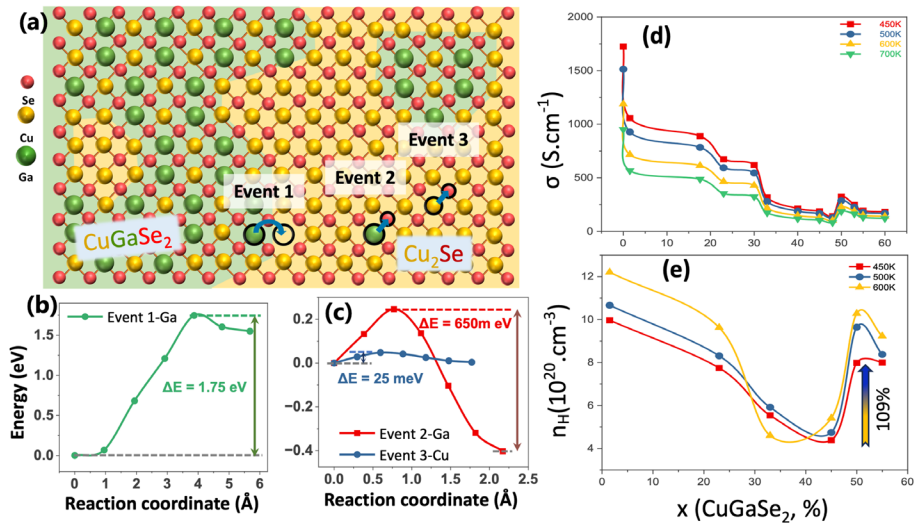

Fig. 2: (a) Schematic illustration of the atomic-scale mutual integration between Cu_2Se (CS) and $CuGaSe_2$ (CGS) domains with coherent interfaces; (b) Energy change of the system as a Ga^{3+} ion migrates across the Cu_2Se/$CuGaSe_2$ interface (event 1). The large energy difference, ΔE, which is the energy barrier to Ga^{3+} migration indicates poor mutual solubility and the stability of the Cu_2Se/$CuGaSe_2$ interface. (b) Change in the energy of the system as Ga^{3+} and Cu^{+} ions migrate within the Cu_2Se phase (events 2 and 3). (d) and (e) Isothermal composition dependent electronic properties of (1-x)Cu_2Se/(x)$CuGaSe_2$ composites 0 ≤ x ≤ 0.6. (d) electrical conductivity showing a gradual drop with the increasing $CuGaSe_2$ content for x ≤ 0.45 and a surprising increase in the conductivity for x = 0.5; (e) A similar trend is observed for the carrier concentration vs $CuGaSe_2$ content suggesting that the change in the electrical conductivity is strongly controlled by the dynamics of electronic defects in the composites.

References

1. H. L. Liu, X. Shi, F. F. Xu, L. L. Zhang, W. Q. Zhang, L. D. Chen, Q. Li, C. Uher, T. Day and G. J. Snyder, *Copper ion liquid-like thermoelectrics*. Nat Mater **11** (5), 422-425 (2012).
2. K. P. Zhao, C. X. Zhu, P. F. Qiu, A. B. Blichfeld, E. Eikeland, D. D. Ren, B. B. Iversen, F. F. Xu, X. Shi and L. D. Chen, *High thermoelectric performance and low thermal conductivity in $Cu_{2-y}S_{1/3}Se_{1/3}Te_{1/3}$ liquid-like materials with nanoscale mosaic structures*, Nano Energy **42**, 43-50 (2017).
3. T. Mao, P. F. Qiu, X. L. Du, P. Hu, K. P. Zhao, J. Xiao, X. Shi and L. D. Chen, *Enhanced Thermoelectric Performance and Service Stability of Cu_2Se Via Tailoring Chemical Compositions at Multiple Atomic Positions*, Adv Funct Mater **30,** (2020)
4. R. M. Lu, T. P. Bailey, C. Uher and P. F. P. Poudeu, *Ultrafine Interwoven Dendritic $Cu_2Se/CuFeSe_2$ Composites with Enhanced Thermoelectric Performance*, ACS Appl Energ Mater **3** (9), 9133-9142 (2020).
5. R. M. Lu, A. Olvera, T. P. Bailey, C. Uher and P. F. P. Poudeu, *Nanoscale Engineering of Polymorphism in Cu_2Se-Based Composites*, ACS Appl Mater Inter **12** (28), 31601-31611 (2020).
6. R. M. Lu, A. Olvera, T. P. Bailey, C. Uher and P. F. P. Poudeu, *$CuAlSe_2$ Inclusions Trigger Dynamic Cu^+ Ion Depletion from the Cu_2Se Matrix Enabling High Thermoelectric Performance*, ACS Appl Mater Inter **12** (52), 58018-58027 (2020).
7. Y. X. Chen, Y. Y. Zhang, R. M. Lu, T. P. Bailey, C. Uher and P. F. P. Poudeu, *Unusual electronic transport in (1-x)Cu_2Se-(x)$CuInSe_2$ hierarchical composites*, Nanoscale Adv **4** (20), 4279-4290 (2022).
8. Y. X. Chen, Y. Y. Zhang, C. Uher and P. F. P. Poudeu, *Carrier Mobility Modulation in Cu_2Se Composites Using Coherent Cu_4TiSe_4 Inclusions Leads to Enhanced Thermoelectric Performance,* ACS Appl Mater Inter **14** (51), 56817-56826 (2022).
9. A. A. Olvera, N. A. Moroz, P. Sahoo, P. Ren, T. P. Bailey, A. A. Page, C. Uher and P. F. P. Poudeu, *Partial indium solubility induces chemical stability and colossal thermoelectric figure of merit in Cu_2Se*, Energ Environ Sci **10** (7), 1668-1676 (2017).
10. Z. Yin, R. M. Lu, T. P. Bailey, C. Uher and P. F. P. Poudeu, *Enhanced Thermoelectric Performance of α- and β- Cu_2Se through Suppression of Hole Density using Extrinsic Copper Vacancies*. *Submitted,*(2024).
11. Z. Yin, Y. Zhang, Y. Huang, J. Schwarz, Z. Xi, C. Uher, R. Hovden, L. Qi and P. F. P. Poudeu, *Native Defects Hybridization and Electronic Transport in Cu_2Se-$CuGaSe_2$ Hierarchical Composites,* Adv Funct Mater, revision submitted (2024).

Publications

1. Zhixiong Yin, Yinying Zhang, Yiqiao Huang, Johnathan Schwarz, Zhucong Xi, Ctirad Uher, Robert Hovden, Liang Qi, Pierre F. P. Poudeu; *Native Defects Hybridization and Electronic Transport in Cu_2Se-$CuGaSe_2$ Hierarchical Composites*; Advanced Functional Materials, **revision submitted** (2024).
2. Zhixiong Yin, Ruiming Lu, Trevor P. Bailey, Ctirad Uher, Pierre F. P. Poudeu, *Enhanced Thermoelectric Performance of α- and β- Cu_2Se through Suppression of Hole Density using Extrinsic Copper Vacancies*, **submitted** (2024).
3. Yiqiao Huang, Pierre FP Poudeu; *Room temperature chemical transformation of SnSe to Ag_2Se nanocrystals via cation exchange*; Materials Advances **5**, 5096 (2024).
4. Y. Chen, Y. Zhang, C. Uher, P.F.P. Poudeu, *Carrier Mobility Modulation in Cu_2Se Composites Using Coherent Cu_4TiSe_4 Inclusions Leads to Enhanced Thermoelectric Performance*, ACS Appl. Mater. Interfaces **14**, 56817–56826 (2022).
5. Y. Chen, Y. Zhang, R. Lu, T.P. Bailey, C. Uher, P.F.P. Poudeu, *Unusual electronic transport in (1− x) Cu_2Se–(x)$CuInSe_2$ hierarchical composites*, Nanoscale Advances **4**, 4279-4290 (2022).

Experimental investigation of the control mechanism of X-ray induced structural and chemical synthesis at extreme conditions

Michael Pravica, Department of Physics and Astronomy, University of Nevada Las Vegas

Keywords: X-ray photochemistry, high pressure, chemistry at extreme conditions, DAC

Research Scope

We harness the highly ionizing, penetrating and focusd properties of hard x-rays to drive novel chemistry in the hopes of synthesizing novel materials. We had the following objectives during our 2 year grant:

•Experimentally and theoretically investigate the mechanism of high-pressure assistance in X-ray induced photochemistry (particularly moderate HP range ≤ 1 GPa)

•Investigate the X-ray flux density dependence of photochemical reactions at HP and identify a lowest value of X-ray flux necessary for their activation

•Expand our previously developed model of X-ray energy dependence of electronic relaxation pathways by studying the L-edge excitation mechanism

•Establish a difference between structural and chemical transformations of ionic compounds at HP induced by monochromatic and white X-rays

•Examine the role of water molecules in the chemical reactivity of ionic salts subjected to X-ray irradiation

•Study the impact of high temperature on photochemical reaction pathways triggered by X-rays

•Demonstrate the universality of X-ray induced photochemistry for novel materials design by developing novel means of HP doping of wide band gap semiconductors and by investigating the main concepts of inner-shell chemistry at HP

•Examine the difference between cation- vs anion-excitation in initiating decomposition and synthesis. (viii)

•Demonstrate that damage be localized in the immediate vicinity of the target metal in larger molecules (e.g. metalloenzymes) for targeting purposes

Recent Progress

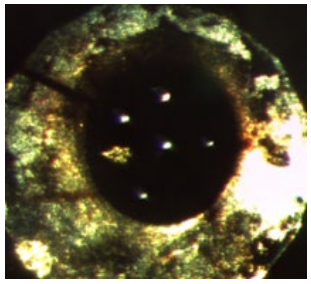

Xray irradiation of a silver salt produced five spots of pure Ag

1. We have demonstrated that the presence of water aids x-ray photochemical reactions at high pressure acting as a mediator for electron transfer.
2. We have created metals by irradiating certain oxalate salts (Ag, Cd, W and Sn) demonstrating widely differing cation-based photochemistry [1-2]. We also have preliminary evidence of irradiating ambient and pressurized samples of a metallic salt with a hydrogenator to produce metals [3]. This may have serious implications for claims of metallic hydrogen [4].
3. We have demonstrated x-ray induced intercalation of oxygen in WO_3 likely via oxygen radicals that react to form O_2 and are then trapped inside the WO_3 lattice. This is important because of the ability to study radical reactions in real time in the solid state and lower the bandgap of a wide band gap material [5].

4. We have demonstrated that, at least for Au, L-edge excitations results in faster decomposition chemistry than K-edge excitations when mixing metal powder with uracil to decompose uracil with x-rays.
5. We have developed a novel means to pressurize samples which will aid *in situ* access and coupling with the pressurized sample.
6. We have successfully damaged large biological molecules using our precision x-ray methods.

Sample (red disk) pressurized inside a diamond.

References

1. M. Pravica , E. Evlyukhin, P. Cifligu, B. Harris, J. J. Koh, N. Chen, Y.Wang, *Chemical Physics Letters* **686,** 183–188 (2017).

2. E. Evlyukhin, E. Kim, D. Goldberger, P. Cifligu, S. Schyck, P. F. Weck and M. Pravica, *Physical Chemistry Chemical Physics* **20**, 18949—18956 (2018),

3. M. Pravica, K. Lipinska-Kalita, Z. Quine, E. Romano, Y. Shen, M. F. Nicola, and W. Pravica, *Journal of Physics and Chemistry of Solids* **67**, 2159–2163 (2006).

4. M. Zaghoo, A. Salamat, and I. F. Silvera, *Physical Review. B* **93**, 155128 (2016).

5. Q. Mi, Y. Ping, Y. Li, B. Cao, B. S. Brunschwig, P. G.. Khalifah, G. A. Galli, H. B. Gray, and N. S. Lewis, *Journal of the American Chemical Society* **134**, 18318−18324 (2012).

Publications

1. “A novel means to generate high pressure,” M. Pravica, P. Cifligu, A. Lua Sanches, T. Maalik, N. Appathurai, and B. Diaz Moreno, *Review of Scientific Instruments* **95**a), 073904 (2024).

2. "Piezochromic Behaviour of 2,4,6-triphenylpyrylium tetrachloroferrate" P. Canasa, D. King, P. Cifligu, A. Lua Sanchez, S. Chen, H. Han, T. Malik, B. Billinghurst, J. Zha, C. Park, G. Rossman, M. Pravica, P. Bhowmik, and E. Evlyukhin *Small Science* 2400106 pp. 1-7 (2024).

3. “The High Pressure Dependence of X-Ray Induced Decomposition of Cadmium Oxalate," A. Sanchez, P. Cifligu, M. Graff, M. Pravica, P. Bhowmik, C. Park, E. Evlyukhin, *AIP Advances* **13**, 105031 (2023).

4. “Experimental demonstration of necessary conditions for X-ray induced synthesis of cesium superoxide,” E. Evlyukhin, P. Cifligu, M. Pravica et al., *Physical Chemistry Chemical Physics*, **25**, 1799–1807 (2023).

Thin Film Platforms to Advance Scientific Frontiers in Solid State Energy Storage

Gary Rubloff, Sang Bok Lee, Paul Albertus, David Stewart (University of Maryland)

and Alec Talin (Sandia National Lab, California)

Keywords: solid state battery, thin films, microfabrication, modeling, diagnostic devices

Research Scope

Work in our previous NEES EFRC demonstrated that precision 3D solid state battery (SSB) structures can achieve high energy-and-power performance.[1]–[4] **Thin film microfabrication**, the workhorse of electronic products, uniquely enables such structures amid a growing set of thin film processes for battery electrodes[5], [6] and electrolytes[7]–[10]. **Continuum and multiscale modeling** play a complementary role in assessing 3D architectures, posing a mesoscale design challenge – spatially, dimensionally, and functionally.

Challenging scientific questions remain largely unanswered in SSBs, from battery materials properties as a function of state of charge to energy band alignment and transport at interfaces, the role of grain boundaries and interfaces, and the coupling of mechanical forces. 3D thin film microfabrication provides an opportunity to create new diagnostic devices to quantify fundamental electrochemical properties and behavior that are otherwise rather inaccessible. This program's ***fundamental hypothesis is that 3D thin film synthesis, microfabrication, and modeling can be used to create electrochemical diagnostic platforms that provide new scientific and mechanistic insights***. By focusing these platforms on specific scientific questions,[11], [12] we anticipate our enhanced understanding will also improve design and modeling of materials, architectures, and systems. We concentrate on 3D vertical SSB's formed on high aspect ratio nanoscaffolds[13], [14] and on multilayer stacks of largely planar SSBs.

Recent Progress (selected examples)

AAO-based SSB architectures. While nanopore arrays formed in anodic Al oxide are excellent architectures for high power/energy SSBs, anodization chemistries limit what pore size and spacings are available. We have developed a high-anodization-voltage process which expands AAO pore diameter from 60nm to 400nm, thereby dramatically increasing electrode mass and energy density. We have also used photolithography and etching of small-pore AAO to create pores with diameters in the micron range. We have published a process sequence using photolithography to define AAO regions, a scheme for fabricating bottomside contacts to the in-pore nanobatteries, and adjustable power and energy by choice of geometric dimensions, all supported by continuum/COMSOL modeling.

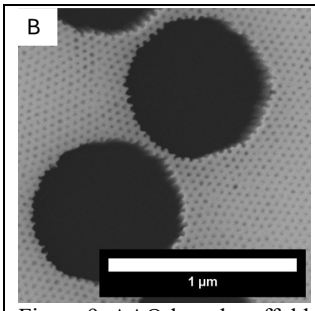

Figure 9. AAO-based scaffolds for 3D-SSB arrays.

Continuum modeling for 3D-SSB architectures. We have completed a fully-coupled electrochemical-mechanical (ECM) model for our AAO-based 3D-SSB structures, revealing high power effects and highlighting where high stresses occur that risk mechanical failure. Results indicate that stress-induced

diffusion drives a more uniform Li distribution in the electrodes, thereby compensating in part for inhomogeneities induced by the 3D structure itself and improving capacity at higher rate.

SSB components platform. We have completed our initial work analyzing and applying this platform (manuscript submitted). While fabricating multiple full SSB cells by thin film techniques, we generate diagnostic devices comprising subsets of materials and interfaces present in the full cells. We develop models to fit the electrochemical impedance spectra (EIS) for the diagnostic device behavior and use this to achieve a physically informed EIS full cell model, revealing which interfaces and materials limit the SSB behavior and providing estimates for permittivity and space charge characteristics at the various interfaces. Given the central role of EIS in battery science, we believe this approach is a very significant step.

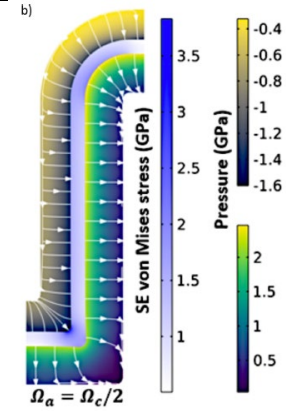

Figure 2. ECM modeling of 3D-SSB stresses

Lateral diffusion platforms. Our goal is to create [Li] lateral concentration gradients and to follow their evolution under applied fields and thermal/mechanical stress, while using spatial diagnostics (XPS, Raman, etc) to map [Li] concentrations. We deploy interdigitated electrode structures (IDEs) to measure EIS locally to extract local ionic and electronic conductivity to correlate with [Li], thus providing crucial parameters for continuum modeling.

We earlier created [Li] gradients laterally by providing a Li source at one end of a patterned V2O5 strip. Two developments have stimulated other options. Our discovery of autolithiation of V2O5 during LiPON sputtering can employ shadow masking to define separated autolithiated regions of the V2O5 as a starting point. We have started collaboration with Celia Polop Jorda et al (Autonomous University of Madrid) using the CMAM facility in Madrid for proton-initiated nuclear reaction analysis and Rutherford backscattering as an ideal way for 3D characterization of [Li] in patterned multi-material structures.

ECM experiments using nano-indenter thin film platform. Following on our earlier successes using Raman to measure local strain in c-Si and 3D polySi structures, we have used nanoindentation to apply controlled forces to thin film ECM test platforms such that the electrochemical response to stress can be obtained. The first embodiment was a lateral battery structure built on a commercial LATP wafer as electrolyte. Thin film V2O5 cathode regions coated with Al contacts were deposited on the LATP and subjected to uniaxial nanoindenter stress while electrochemistry was monitored with a Li anode coupled to the LATP through a PEO layer. The immediate ECM is promising for our goals to determine how the coupling depends on LixV2O5 stoichiometry and phase as well as dynamics of charging rates. Response range ~0.4 mV/MPa.

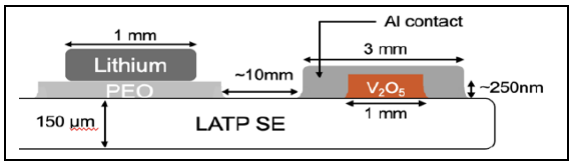

Figure 3. Nanoindenter stress on lateral battery V2O5 cathode

Materials chemistry for SSBs. We have discovered and will exploit the autolithiation mechanism for patterned lithiation of electrode layers. Following on our development of ALD LiPON, we have taken a path to ALD LATP [$Li_{1-x}A_xTi_{2-x}(PO_4)_3$] to achieve markedly higher ionic conductivity in the electrolye, employing supercycling strategies to control low concentration dopants (Al, Ti, Li) crucial for enhanced properties. This has proven successful for ALD Li-Ti-PO4 and is promising for the full LATP material.

References

1. F. Han et al., "*Dielectric capacitors with three-dimensional nanoscale interdigital electrodes for energy storage*," Science Advances, vol. 1, no. 9, 2015, doi: 10.1126/sciadv.1500605.
2. J. W. Long, B. Dunn, D. R. Rolison, and H. S. White, "*Three-dimensional battery architectures*," Chemical Reviews, vol. 104, no. 10, pp. 4463–4492, 2004, doi: 10.1021/cr020740l.
3. G. W. Rubloff and S. B. Lee, "*New science at the meso frontier: Dense nanostructure architectures for electrical energy storage*," Current Opinion in Solid State and Materials Science, vol. 19, no. 4, pp. 227–234, 2015, doi: 10.1016/j.cossms.2014.12.004.
4. J. W. Long, B. Dunn, D. R. Rolison, and H. S. White, "*3D Architectures for Batteries and Electrodes*," Adv. Energy Mater., vol. 10, no. 46, p. 2002457, Dec. 2020, doi: 10.1002/aenm.202002457.
5. N. J. Dudney, "*Thin Film Micro-Batteries*," ECS Interface, 44-48 (2008).
6. N. J. Dudney, "*Solid-state thin-film rechargeable batteries*," Materials Science and Engineering: B, vol. 116, no. 3, pp. 245–249, Feb. 2005.
7. A. C. Kozen, A. J. Pearse, C.-F. Lin, M. Noked, and G. W. Rubloff, "*Atomic Layer Deposition of the Solid Electrolyte LiPON*," Chemistry of Materials, vol. 27, no. 15, pp. 5324–5331, Jul. 2015.
8. E. Kazyak et al., "*Atomic Layer Deposition of the Solid Electrolyte Garnet Li7La3Zr2O12*," Chemistry of Materials, vol. 29, no. 8, pp. 3785–3792, 2017, doi: 10.1021/acs.chemmater.7b00944.
9. J. Li, C. Ma, M. Chi, C. Liang, and N. J. Dudney, "*Solid Electrolyte: the Key for High-Voltage Lithium Batteries*," Advanced Energy Materials, vol. 5, no. 4, pp. 1401408–1401410, Oct. 2014.
10. A. J. Pearse et al., "*Nanoscale Solid State Batteries Enabled by Thermal Atomic Layer Deposition of a Lithium Polyphosphazene Solid State Electrolyte*," Chem. Mater., vol. 29, no. 8, pp. 3740–3753, Apr. 2017, doi: 10.1021/acs.chemmater.7b00805.
11. C. Liu et al., "*An all-in-one nanopore battery array*," Nature Nanotechnology, vol. 9, no. 12, pp. 1031–1039, Nov. 2014.
12. A. J. Pearse, E. Gillette, S. B. Lee, and G. W. Rubloff, "*The reaction current distribution in battery electrode materials revealed by XPS-based state-of-charge mappin*g," Physical Chemistry Chemical Physics, vol. 18, no. 28, pp. 19093–19102, Jul. 2016.
13. A. J Pearse et al., "*Three-Dimensional Solid-State Lithium-Ion Batteries Fabricated by Conformal Vapor-Phase Chemistry*," ACS Nano, vol. 12, no. 5, pp. 4286–4294, 2018, doi: 10.1021/acsnano.7b08751.
14. A. A. Talin et al., "*Fabrication, Testing, and Simulation of All-Solid-State Three-Dimensional Li-Ion Batteries*," ACS Applied Materials and Interfaces, vol. 8, no. 47, pp. 32385–32391, 2016, doi: 10.1021/acsami.6b12244.
15. H. Wang et al., "*Micro-Raman Stress Characterization of Crystalline Si as a Function of the Lithiation State*," ACS Appl. Mater. Interfaces, vol. 15, no. 8, pp. 10752–10760, Mar. 2023, doi: 10.1021/acsami.2c22530.
16. V. C. Ferrari, N. S. Kim, S. B. Lee, G. W. Rubloff, and D. M. Stewart, "*Co-sputtering of lithium vanadium oxide thin films with variable lithium content to enable advanced solid-state batteries*," J. Mater. Chem. A, p. 10.1039.D2TA01021F, 2022, doi: 10.1039/D2TA01021F.
17. A. S. Westover, N. J. Dudney, R. L. Sacci, and S. Kalnaus, "*Deposition and Confinement of Li Metal along an Artificial Lipon-Lipon Interface*," ACS Energy Letters, vol. 4, no. 3, pp. 651–655, Mar. 2019, doi: 10.1021/acsenergylett.8b02542.
18. E. J. Fuller et al., "*Spatially Resolved Potential and Li-Ion Distributions Reveal Performance-Limiting Regions in Solid-State Batteries*," ACS Energy Lett., vol. 6, no. 11, pp. 3944–3951, Nov. 2021, doi: 10.1021/acsenergylett.1c01960.

19. G. Bucci, T. Swamy, S. Bishop, B. W. Sheldon, Y.-M. Chiang, and W. C. Carter, "*The Effect of Stress on Battery-Electrode Capacity*," J. Electrochem. Soc., vol. 164, no. 4, pp. A645–A654, 2017, doi: 10.1149/2.0371704jes.

Publications

1. Zoey Warecki, Victoria Castagna Ferrari, Donald A. Robinson, Joshua D. Sugar, Jonathan Lee, Anton V. Levlev, Nam Soo Kim, et al. "*Simultaneous Solid Electrolyte* Deposition and Cathode Lithiation for Thin Film Batteries and Lithium Iontronic Devices." ACS Energy Letters, April 9, 2024, 9, 5, 2065–74. https://doi.org/10.1021/acsenergylett.4c00674.
2. Yue Qi, Michael W. Swift, Elliot J. Fuller, and A. Alec Talin. "*Interface Potentials inside Solid-State Batteries: Origins and Implications*." MRS Bulletin, **48**, 1239-1246, December 5, 2023. https://doi.org/10.1557/s43577-023-00625-1.
3. Haotian Wang, Yueming Song, Victoria Castagna Ferrari, Nam Soo Kim, Sang Bok Lee, Paul Albertus, Gary Rubloff, and David Murdock Stewart. "*In Situ Raman Mapping of Si Island Electrodes and Stress Modeling as a Function of Lithiation and Size*." ACS Applied Materials & Interfaces **15**, no. 34 (August 30, 2023): 40409–18. https://doi.org/10.1021/acsami.3c06287.
4. Nam Kim, Marco Casareto, Miles Mowbray, Robert Henry, John Hayden, Gary Rubloff, Sang Bok Lee, and Keith E. Gregorczyk. "*On-Wafer Wide-Pore Anodic Aluminum Oxide*." Journal of The Electrochemical Society **170**, no. 6 (June 1, 2023): 063507. https://doi.org/10.1149/1945-7111/acd87b.
5. Yueming Song, Bhuvsmita Bhargava, David M. Stewart, A. Alec Talin, Gary W. Rubloff, and Paul Albertus. "*Electrochemical-Mechanical Coupling Measurements*." Joule **7**, 4, April 2023, S2542435123001137. https://doi.org/10.1016/j.joule.2023.03.001.
6. Zach Levy, Victoria Castagna Ferrari, Pablo Rosas, Mitchell J. Walker, Kalpak Duddella, Micah Haseman, David Stewart, Gary Rubloff, and Leonard J. Brillson. "*Lithium Spatial* Distribution *and Split-Off Electronic Bands at Nanoscale V2O5/LiPON Interfaces*." ACS Applied Energy Materials **6**, 9, March 20, 2023, acsaem.2c03683. https://doi.org/10.1021/acsaem.2c03683.
7. Haotian Wang, Nam Soo Kim, Yueming Song, Paul Albertus, Sang Bok Lee, Gary Rubloff, and David Stewart. "*Micro-Raman Stress Characterization of Crystalline Si as a Function of the Lithiation State*." ACS Applied Materials & Interfaces **15**, no. 8 (March 1, 2023): 10752–60. https://doi.org/10.1021/acsami.2c22530.
8. Elliot J. Fuller, David S. Ashby, Celia Polop, Elena Salagre, Bhuvsmita Bhargava, Yueming Song, Enrique Vasco, et al. "*Imaging Phase Segregation in Nanoscale LixCoO2 Single Particles*." ACS Nano **16**, no. 10 (October 25, 2022): 16363–71. https://doi.org/10.1021/acsnano.2c05594.

Design, Discovery, and Synthesis Science of Porous Frameworks using Fast and Modular Heterophase Assembly

Principal Investigator: Amin Salehi-Khojin, U Illinois at Chicago

Co-Investigators: Ksenija Glusac (UIC), Jordi Cabana-Jimenez (UIC), Santanu Chaudhuri (UIC), Fatemeh Khalili-Araghi (UIC), Russell Hemley (UIC)**,** Laura Gagliardi (U Chicago), Siamak Nejati (U Nebraska-Lincoln).

Keywords: Porous Frameworks, Covalent Organic Frameworks, Molecular layer deposition, liquid organic hydrogen carriers, CO_2 capture and concentration

Research Scops: Porous and crystalline materials, such as Covalent Organic Frameworks (COFs), uniquely combine intrinsic porosity and programmable function via a wealth of chemical functionalities. These critically determine activity and selectivity in electrochemical reactions crucial to meet the targets of the Hydrogen and Carbon Negative Earthshots, such as electrochemical CO_2 capture and concentration (e-CCC), and electrochemical hydrogenation/dehydrogenation of liquid organic hydrogen carriers (e-LOHC). To transcend common practices of growth which limit programmable function, the PIs will demonstrate vapor-phase pathways using scalable Molecular layer deposition to engineer electrode surfaces coated with well-defined thin films that contain molecularly precise functional groups that direct the desired transformations. The precision that can be achieved through this process provides an opportunity to go beyond "single atom catalysts" (SACs), whose chemical simplicity limits the ability to perform advanced electrochemical transformations selectively and efficiently. Growth of these frameworks from the vapor phase could result in molecular assemblies at fast rates and simplified processability. The PIs hypothesize that fulfilling the promise of these materials demands a cross-cutting combination of predictive and in-situ studies of reaction landscapes, to dial in modularity for the desired functionality. This approach will accelerate the discovery of new materials with both transformational properties and sustainable routes of manufacturing.

The core mission of the proposal is to overcome the limitations of current classes of COFs by understanding, predicting, synthesizing, and controlling their structure and surface chemistry with molecular precision and modularity needed to impart transformative electrochemistry for e-CCC and e-LOHC. The proposed approach can be generalized for other frameworks, such as metal-organic and zeolitic imidazolate frameworks. The following goals define our mission:

1. To identify the landscape of synthesizability of COFs for use in the design and synthesis of functional and environmentally benign electrode materials.

2. To develop methodologies for in-situ monitoring and controlling the growth of thin films of complex porous COFs within functional architectures designed for e-CCC and e-LOHC.

3. To demonstrate a massively parallel optimization basis for establishing nano-to-meso-to-microscale porosity and local electronic structure to enhance electrocatalytic stability.

Proposed Research.

The proposal is organized in three Thrusts:

Thrust 1: Synthesis and Characterization of Frameworks

Objective 1. Identify the parameters that govern precursor order on the surface and define the thermodynamics of nucleation.

Milestone: Create a feedback loop between Thrusts 1 and 3 and narrow the processing parameters for the delivery of the selected precursors to the target substrates with the end goal of achieving material order.

Objective 2. Establish the basic knowledge of reaction dynamics for COF synthesis on the surface.

Milestone: Create a feedback loop between Thrust 1 and 3 and narrow down the processing parameters for reaction engineering. The deposition rate for each pair of precursor/linker will be identified.

Objective 3. Establish Field-assisted molecular ordering as a means for directing COF growth.

Milestone: Extend order in the film by using external field bias that regulates the assembly of precursors.

Objective 4. Establish structure-property relationships.

Milestone: Resolve the structure of synthesized COFs with a focus on crystal structure, phase composition, crystallographic orientation, surface chemistry and electronic properties.

Thrust 2. From Design to Function of Frameworks: Translational Impact

Objective 1. Establishing and controlling the functionality of frameworks.

Milestone: Post-synthetic modifications will be established on both planar and 3D substrates for the proposed reactions of e-CCC and e-LOHCs.

Objective 2. Electrochemistry of Post-synthetic modified frameworks.

Milestone: An integrated suite of complementary ex-situ and operando measurements will be performed to efficiently build a comprehensive picture of electrocatalysis process for e-CCC or e-LOHCs.

Thrust 3 (Crosscut). Discovery by Design of Frameworks

Objective 1. Porous Framework Design with Generative AI for Thermodynamic Stability and Synthesizability Predictions.

Milestone: Close the feedback loop between theory and initial experiments with data on reactions of known precursors, pore-scale functionality and stability of 2D COFs; compare and contrast the thermodynamic stability and synthesizability ranking of closely related COFs.

Objective 2. Detailed quantum chemistry for active site design and catalytic performance feedback.

Milestone: Use guidelines to deliver new COFs and validate the predicted reaction dynamics against observed dynamic for e-CCC and e-LOHC reactions.

Unraveling the Mysteries of the Platinum Group Elements

Robert W. Schurko (PI, Florida State University and National High Magnetic Field Laboratory) and Jochen Autschbach (co-I, University of Buffalo)

Keywords: solid-state NMR spectroscopy, platinum group elements, ^{103}Rh NMR, ^{99}Ru NMR, ^{195}Pt NMR, ^{59}Co NMR, ^{55}Mn NMR, ^{35}Cl NMR, relativistic DFT calculations, NBO/NLMO analysis

Research Scope

The goals under the scope of this research include: (1) to develop and apply new protocols for efficient acquisition of solid-state NMR (ssNMR_ spectra of unreceptive isotopes of the PGEs in organometallic and coordination compounds, including candidates such as ^{99}Ru, ^{103}Rh, ^{105}Pd, and ^{195}Pt, as well as nuclides in their ligands; (2) to quantify the nature of σ and π metal-ligand (M-L) covalent donation bonding in relation to NMR tensors using experimental NMR data and first-principles relativistic DFT calculations and subsequent NBO/NLMO analysis; and (3) to use this information to identify non-PGE metals as potential replacements.

Recent Progress

We have designed new protocols for acquiring ultra-wideline (UW) ssNMR spectra[1] of two extremely unreceptive nuclei: ^{103}Rh (I = 1/2)[2] and ^{99}Ru (I = 5/2), for which there are only cursory studies in the literature,[3,4] and have applied them to inorganic and organometallic Rh (**Fig. 1**) and Ru complexes (a publication will be forthcoming on ^{99}Ru, **Fig. 2**). We have also explored SSNMR of key ligand nuclei (*e.g.*, ^{35}Cl, ^{13}C, ^{31}P) and extended our new methods to potential replacement metals (*e.g.*, ^{55}Mn and ^{59}Co UW ssNMR).[5] Spectral simulations were used to extract the chemical shift (CS) and electric field gradient (EFG) interaction tensors, providing the first sets of comprehensive ^{103}Rh and ^{99}Ru ssNMR measurements. We have had recent

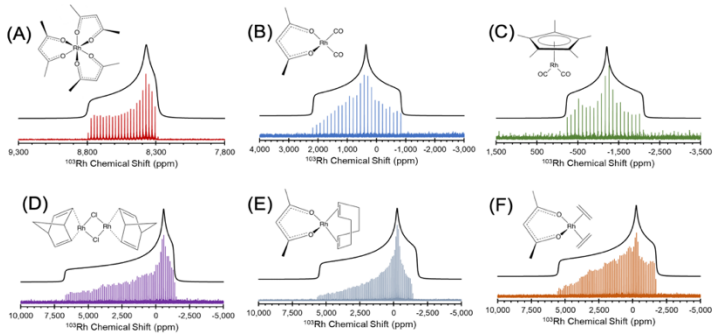

Fig. 1: ^{1}H-^{103}Rh BRAIN-CP NMR spectra acquired at 21.1 T, along with simulated spectra (black traces).

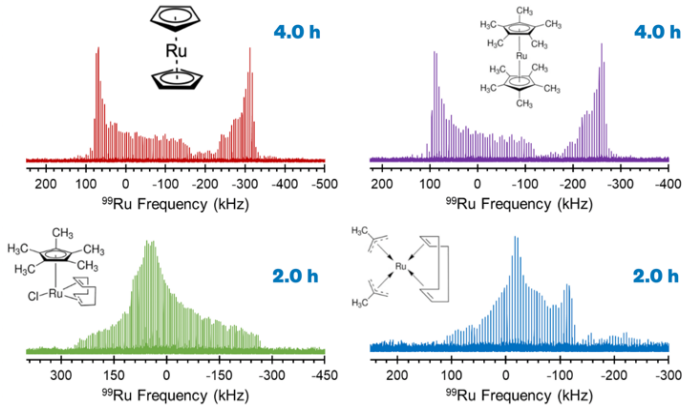

Fig. 2. ^{99}Ru WCPMG NMR spectra acquired at 35.2 T (ν_0 ν_0 (^{99}Ru) = 69.013 GHz, with experimental times in hours.

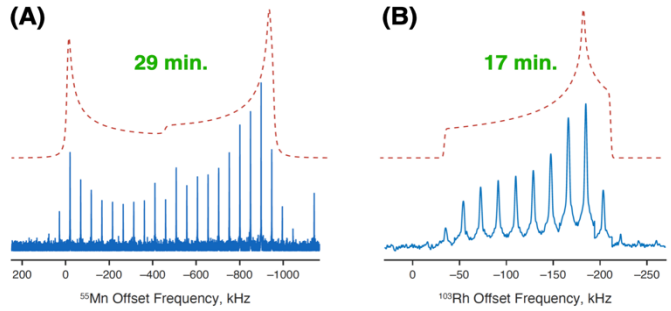

Fig. 3. (**A**) ^{1}H-^{55}Mn PROSPR spectrum of CpMn(CO)$_3$ (14.1 T) and (**B**) ^{1}H-^{103}Rh PROSPR spectrum of Rh(COD)(acac) (18.8 T). Experiment times are shown in green and ideal spectra in red.

success optimizing ^{1}H-^{103}Rh and ^{1}H-^{99}Ru broadband adiabatic inversion cross polarization (BRAIN-CP) methods[6] for efficient acquisition of spectra of these challenging isotopes. Finally, using a method we devised for *indirectly detecting* the spectra of unreceptive nuclides via proximate protons, the ^{1}H-X PROSPR (Progressive Saturation of the Proton Reservoir) technique, we have been able to indirectly detect ^{103}Rh and ^{55}Mn UW ssNMR spectra (**Fig. 3**) with great rapidity in comparison to standard direct detection experiments. This is a promising alternative for experiments on unreceptive nuclides of both PGEs and replacement metals.

Relativistic DFT calculations of the CS and EFG tensors have been carried out, with thorough optimizations revealing the best choices of correlation functional and methodology for achieving the best agreement with experiment. For ^{103}Rh and ^{99}Ru, we found that lattice effects must be taken into account (*e.g.*, clusters *vs*. periodic lattices), relativistic effects must be included to the spin-orbit level, and hybrid DFT functionals work the best (*i.e.*, PBE0). Finally, we have completed NBO/NLMO analyses of molecular orbitals (MOs) and their contributions to the NMR interaction tensors. For instance, the differences in the ^{103}Rh CS tensors among systems, along with the corresponding contributions from the Rh 4*d* shell, π-backbonding MOs from ligands (*e.g.*, Rh–CO), and π MOs of cyclopentadienyl rings, reveal a rich picture of structure and bonding (**Fig. 4**), which we believe is one that will aid in the gaining a deeper understanding of M-L covalent donation bonding.[2] Similar work is published for ^{195}Pt CS tensors[8] and ongoing for ^{99}Ru EFG and CS tensors. Much of this work was enabled by a publication by one of the PIs, which describes the decomposition of contributions to NMR interaction tensors using spin-free LMOs.[9]

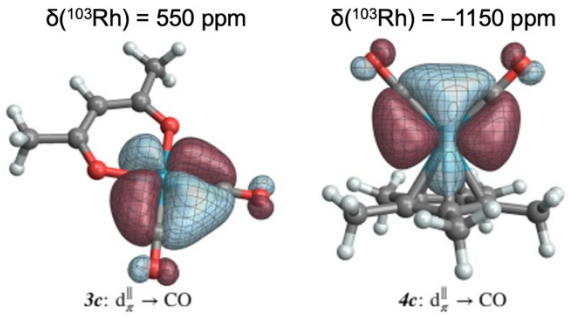

Fig. 4: Isosurfaces for $d_{\pi}^{\parallel}$ M-L bonding MOs in Rh(CO)$_2$(acac) and Rh(CO)$_2$Cp*.

References

1. Schurko, R. W. *Ultra-Wideline Solid-State NMR Spectroscopy*. Acc. Chem. Res. **46**, 1985 (2013)

2. Holmes, S. T.; Schönzart, J.; Philips, A. B.; Kimball, J. J.; Termos, S.; Altenhof, A. R.; Xu, Y.; O'Keefe, C. A.; Autschbach, J.; Schurko, R. W. *Structure and Bonding in Rhodium Coordination Compounds: A ^{103}Rh Solid-State NMR and Relativistic DFT Study*. Chem. Sci. **15**, 2181 (2024)

3. Phillips, B. L.; Houston, J. R.; Feng, J.; Casey, W. H. *Observation of Solid-State Rh-103 NMR by Cross-Polarization*. J. Am. Chem. Soc. **128**, 3912 (2006)

4. Ooms, K. J.; Wasylishen, R. E. *Solid-State Ru-99 NMR Spectroscopy: A Useful Tool for Characterizing Prototypal Diamagnetic Ruthenium Compounds*. J. Am. Chem. Soc. **126**, 10972 (2004)

5. Kimball, J. J.; Altenhof, A. R.; Jaroszewicz, M. J.; Schurko, R. W. *Broadband Cross-Polarization to Half-Integer Quadrupolar Nuclei: Wideline Static NMR Spectroscopy*. J. Phys. Chem. A **127**, 9621 (2023)

6. Harris, K. J.; Lupulescu, A.; Lucier, B. E. G.; Frydman, L.; Schurko, R. W. *Broadband Adiabatic Inversion Pulses for Cross Polarization in Wideline Solid-State NMR Spectroscopy*. J. Magn. Reson. **224**, 38 (2012)

7. Jaroszewicz, M. J.; Altenhof, A. R.; Schurko, R. W.; Frydman, L. *Sensitivity Enhancement by Progressive Saturation of the Proton Reservoir: A Solid-State NMR Analogue of Chemical Exchange Saturation Transfer*. J. Am. Chem. Soc. **143**, 19778 (2021)

8. Batista, P. R.; Ducati, L. C.; Autschbach, J. *Dynamic and Relativistic Effects on Pt-Pt Indirect Spin-Spin Coupling in Aqueous Solution Studied by Ab Initio Molecular Dynamics and Two- vs Four-Component Density Functional NMR Calculations*. J. Chem. Phys. **160**, 114307 (2024)

9. Fernández-Alarcón, A.; Autschbach, J. *Relativistic Density Functional NMR Tensors Analyzed with Spin-Free Localized Molecular Orbitals*. ChemPhysChem **24**, e202200667 (2023)

Publications

1. Fernández-Alarcón, A.; Autschbach, J. *Relativistic Density Functional NMR Tensors Analyzed with Spin-Free Localized Molecular Orbitals*. ChemPhysChem **24**, e202200667 (2023)

2. Holmes, S. T.; Schönzart, J.; Philips, A. B.; Kimball, J. J.; Termos, S.; Altenhof, A. R.; Xu, Y.; O'Keefe, C. A.; Autschbach, J.; Schurko, R. W. *Structure and Bonding in Rhodium Coordination Compounds: A ^{103}Rh Solid-State NMR and Relativistic DFT Study*. Chem. Sci. **15**, 2181 (2024)

3. Kimball, J. J.; Altenhof, A. R.; Jaroszewicz, M. J.; Schurko, R. W. *Broadband Cross-Polarization to Half-Integer Quadrupolar Nuclei: Wideline Static NMR Spectroscopy*. J. Phys. Chem. A **127**, 9621 (2023)

4. Stirk, A. J.; Holmes, S. T.; Souza, F. E. S.; Hung, I.; Gan, Z.; Britten, J. F.; Rey, A. W.; Schurko, R. W. *An Unusual Ionic Cocrystal of Ponatinib Hydrochloride: Characterization by Single-Crystal X-Ray Diffraction and Ultra-High Field NMR Spectroscopy*. CrystEngComm **26**, 1219 (2024)

5. Batista, P. R.; Ducati, L. C.; Autschbach, J. *Dynamic and Relativistic Effects on Pt-Pt Indirect Spin-Spin Coupling in Aqueous Solution Studied by Ab Initio Molecular Dynamics and Two- vs Four-Component Density Functional NMR Calculations*. J. Chem. Phys. **160**, 114307 (2024)

Energy Flow in Polymers with Mixed Conduction Pathways

Rachel A. Segalman and Michael L. Chabinyc - University of California, Santa Barbara

Keywords: Electrostatic Complexation, Mixed Conduction, Coacervate, Battery, Binder

Research Scope

Organic mixed ionic-electronic conducting polymers are emerging as a dominant class of materials finding widespread applications ranging from organic electronics and bioelectronics to electrochemical energy storage devices, where simultaneous conduction of electrons and ions and ion-electron couplings play an important role. While ionic and electronic charge transport demand contradictory design rules, the relationships between chemical structure, mesoscale morphology, processability, and charge transport behavior are critical to future design rules and are still relatively unclear. This project addresses the overarching questions centered around the effect of electronic-ionic charge transport behavior at the molecular scale, mesoscale, and macroscale: 1) How does molecular designs influence stability and charge carrier conductivity within a mixed conductor? 2) How do dielectric environment and local structure affect ion dissociation and ionic conduction? 3) How do the electrostatic interactions within a mixed conductor be leveraged for processing and the corresponding effect of ion and counter-ion identity on them? 4) How are the structure and performance of mixed conductors affected by the method and timescale of processing?

Recent Progress

We have recently demonstrated that complex coacervates formed by electrostatic complexation of conjugated polyelectrolytes (CPEs) with polymeric ionic liquids (PILs), are promising mixed conducting systems with tunable nanoscale morphology, enhanced processability and stretchability, suitable for application as battery binders and stretchable electronics.[1–3] Utilization of such electrostatic complexation allows aqueous processing of otherwise difficult conjugated polymers, leading to the development of novel processing methods, including ionic processability, to reduce the impact of industrial solvent usage.[4,5] Furthermore, high polymer fraction in these complexes allows the formation of conductive thick films and bulk structures. When we examined complexes formed from varying frequency of charged repeat units of CPE and PIL, we have seen reduced structural disorder in highly charged complexes, thereby enhancing its intrachain conjugation and interchain packing (**Figure 1**).[6] In fact, electrical conductivity of any acid-doped complex was found to be

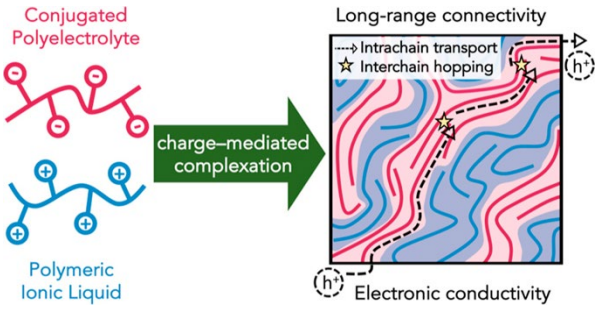

Figure 1. Role of complexation strength on the electronic charge transport properties of semiconducting polymer complexes.

higher than that of an unblended CPE, reaching highest electrical conductivity of ~ 1 S cm^{-1} for 100% charge fraction.

We have shown that polymer-ion interaction strength play a crucial role in striking a balance between salt solvation and cation-selective transport in CPEs for battery applications.[7] In this regard, we have studied a series of cationic functionalized polythiophenes where the cationic pendant unit was systematically varied (**Figure 2**). We found that cation group size and charge localization play a critical role, whereby the more diffusely charged imidazolium effectively has the best overall performance by affording improved electronic conductivity, labile ionic interaction and higher Li^+ transference than the other cationic pendants studied.

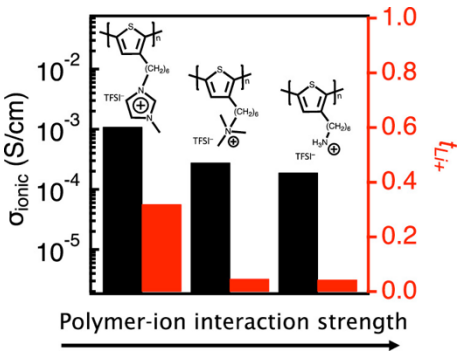

Figure 2. Comparison of ionic conductivity and Li^+ transference for a series of cationic functionalized polythiophenes, where the pendant unit is varied from N-methylimidazolim to trimethyl ammonium to ammonium.

We have also leveraged ion complexation between two polymers with architecturally different backbone chemistry using an anionic CPE and a cationic bottlebrush polymer (BPE), resulting in a soft, elastic conductive polymer complex.[2] With 60% charge fraction in each of CPE and BPE, a much lower charge density in BPE and a 5% volume fraction of the conjugated polymer, the electrical conductivity of acid doped complexes still reached 3×10^{-1} S cm^{-1}, indicating maintenance of effective electronic coupling of the CPE in complex electrostatic environment. More importantly, the complex exhibited significant mechanical properties in their undoped and doped states with strain to break close to 450 and 100%, respectively, demonstrating their suitability for bio-interfacing and stretchable electronics.

We have demonstrated the mixed conducting ability of complex coacervates by application as a dissolution-resistant lithium-ion battery (LIB) binder using $LiFePO_4$ (LFP) electrodes.[1,8] In this regard, we have examined various polythiophene-based polyelectrolyte complexes, with varying side-chain pendants, showing electronic conductivities as high as 0.8 S cm^{-1}, room temperature ionic conductivities above 10^{-4} S cm^{-1} when swollen with an electrolyte and appreciable dry ionic conductivity ($\approx 1 \times 10^{-7}$ S cm^{-1}).[1] As a result, we have observed dramatic reductions in overpotential, improved charge transfer kinetics and enhanced performance at high cycling rates (70% cathode utilization for complex vs. 1.4% for PVDF, at 6C) compared to the electronically and ionically insulating PVDF, which relies on solvent-induced swelling for ion conduction. Complex binders also exhibited significant improvements in initial capacity and long-term capacity retention attributed to their reduced resistance.[8]

References

1. G. Pace, A. Zele, P. Nguyen, R. J. Clément, and R. A. Segalman, *Mixed Ion–Electron-Conducting Polymer Complexes as High-Rate Battery Binders.* Chem. Mater. **35**, 8101–8111 (2023).
2. M. L. Le, I. Lapkriengkri, K. R. Albanese, P. H. Nguyen, C. Tran, J. R. Blankenship, R. A. Segalman, C. M. Bates, and M. L. Chabinyc, *Engineering Soft, Elastic, and Conductive Polymers for Stretchable Electronics Using Ionic Compatibilization.* Chem. Mater. **35**, 7301–7310 (2023).
3. M. L. Le, D. J. Grzetic, K. T. Delaney, K-C. Yang, S. Xie, G. H. Fredrickson, M. L. Chabinyc, and R. A. Segalman, *Electrostatic Interactions Control the Nanostructure of Conjugated Polyelectrolyte–Polymeric Ionic Liquid Blends.* Macromolecules **55**, 8321–8331 (2022).
4. M. L. Le, D. Rawlings, S. P. O. Danielsen, R. M. Kennard, M. L. Chabinyc, and R. A. Segalman, *Aqueous Formulation of Concentrated Semiconductive Fluid Using Polyelectrolyte Coacervation.* ACS Macro Lett. **10**, 1008–1014 (2021).
5. I. McCulloch, M. Chabinyc, C. Brabec, C. B. Nielsen, and S. E. Watkins, *Sustainability considerations for organic electronic products.* Nat. Mater. **22**, 1304–1310 (2023).
6. M. L. Le, C. Warner, R. A. Segalman, and M. L. Chabinyc, *Role of Complexation Strength on the Photophysical and Transport Properties of Semiconducting Charged Polymer Complexes.* Chem. Mater. **35**, 4449–4460 (2023).
7. G. Pace, O. Nordness, P. H. Nguyen, Y-J. Choi, C. Tran, R. J. Clément, and R. A. Segalman, *Tuning Transport via Interaction Strength in Cationic Conjugated Polyelectrolytes.* Macromolecules **56**, 6078–6085 (2023).
8. G. T. Pace, M. L. Le, R. J. Clément, and R. A. Segalman, *A Coacervate-Based Mixed-Conducting Binder for High-Power, High-Energy Batteries.* ACS Energy Lett. **8**, 2781–2788 (2023).

Publications

1. I. McCulloch, M. Chabinyc, C. Brabec, C. B. Nielsen, and S. E. Watkins, *Sustainability considerations for organic electronic products.* Nat. Mater. **22**, 1304–1310 (2023).
2. G. Pace, A. Zele, P. Nguyen, R. J. Clément, and R. A. Segalman, *Mixed Ion–Electron-Conducting Polymer Complexes as High-Rate Battery Binders.* Chem. Mater. **35**, 8101–8111 (2023).
3. M. L. Le, I. Lapkriengkri, K. R. Albanese, P. H. Nguyen, C. Tran, J. R. Blankenship, R. A. Segalman, C. M. Bates, and M. L. Chabinyc, *Engineering Soft, Elastic, and Conductive Polymers for Stretchable Electronics Using Ionic Compatibilization.* Chem. Mater. **35**, 7301–7310 (2023).
4. G. Pace, O. Nordness, P. H. Nguyen, Y-J. Choi, C. Tran, R. J. Clément, and R. A. Segalman, *Tuning Transport via Interaction Strength in Cationic Conjugated Polyelectrolytes.* Macromolecules **56**, 6078–6085 (2023).
5. G. T. Pace, M. L. Le, R. J. Clément, and R. A. Segalman, *A Coacervate-Based Mixed-Conducting Binder for High-Power, High-Energy Batteries.* ACS Energy Lett. **8**, 2781–2788 (2023).
6. M. L. Le, C. Warner, R. A. Segalman, and M. L. Chabinyc, *Role of Complexation Strength on the Photophysical and Transport Properties of Semiconducting Charged Polymer Complexes.* Chem. Mater. **35**, 4449–4460 (2023).
7. A. Agee, T.M. Gill, G. Pace, R. Segalman, & A. Furst, *Electrochemical Characterization of Biomolecular Electron Transfer at Conductive Polymer Interfaces*, Journal of the Electrochemical Society **170(1)** 016509 (2023).
8. D. Yuan, E. Plunkett, P.H. Nguyen, D. Rawlings, M.L. Le, R. Kroon, C. Müller, R.A Segalman, & M.L. Chabinyc, *Double Doping of Semiconducting Polymers Using Ion-Exchange with a Dianion*, Advanced Functional Materials, 2300934 (2023).
9. M. L. Le, D. J. Grzetic, K. T. Delaney, K-C. Yang, S. Xie, G. H. Fredrickson, M. L. Chabinyc, and R. A. Segalman, *Electrostatic Interactions Control the Nanostructure of Conjugated Polyelectrolyte–Polymeric Ionic Liquid Blends.* Macromolecules **55**, 8321–8331 (2022).
10. G. Pace, O. Nordness, K. Asham, R. J. Clément, and R. A. Segalman, *Impact of Side Chain Chemistry on Lithium Transport in Mixed Ion−Electron-Conducting Polymers.* Chem. Mater. **34**, 4672−4681 (2022)

Lone-Pair Driven Phenomena in Optoelectronic Halide Materials

Ram Seshadri and Michael Chabinyc (UCSB), and Mercouri Kanatzidis (Northwestern)

Keywords: Lone Pairs, Semiconductors, Symmetry Breaking, Electronic and Optical Properties

Research Scope

The impact of lone pairs on the electronic properties of halides, including metal halides such as AMX_3 perovskites are studied. Lone pair containing compounds display one of three states,[1] corresponding to lone pairs being: (i) active and ordered, (ii) active and disordered, or (iii) silent and dynamic. Case (iii) is the most intriguing and least well-controlled state with associated anharmonicity that can enhance functionality. The following overarching questions are addressed in this project: (i) What are the consequences of the inverted band structure, with ns^2 states in the valence band, on optical properties? (ii) Can anharmonicity-by-design be deployed in materials with "hidden" lone pairs? (iii) Can we disentangle the highly interrelated aspects of what drives lone pair expression: the nature of the lone pair cation itself, other cations in the structure, and the anion(s)? (iv) How do lone pairs on the M site influence tilting and rotation in all-inorganic AMX_3 perovskites? (v) Can lone pair behavior be driven and controlled by external stimuli? The lone pair ions of interest are depicted in Figure 1. Some accomplishments from this new project are described here.

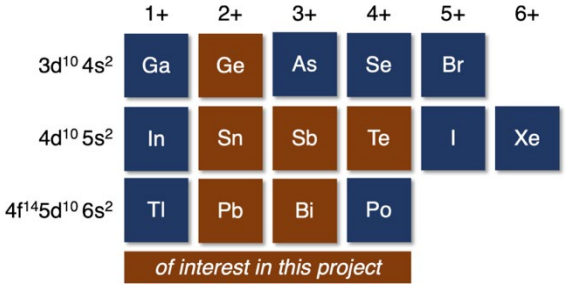

Figure 1: Lone pair ions of interest. Halide compounds — both hybrid and all-inorganic — that contain these ions are the subject of this study.

Recent Progress

Hybrid Iodide Perovskites of Divalent Alkaline Earth and Lanthanide Elements Hybrid halide perovskites $AM^{II}X3$ (where A is an ammonium cation, M is a divalent cation, and X is a halide) have been extensively studied but have only been reported for the divalent carbon group elements Ge, Sn, and Pb. Through rational design rules and low-temperature solid-state synthesis, we have synthesized five new hybrid iodide perovskites centered around divalent alkaline earth and lanthanide elements with the general formula $AM^{II}I_3$ (A = methylammonium [MA] with M^{II} = Sr, Sm, Eu; and A = formamidinium [FA] with M^{II} = Sr, Eu).[2] Significantly, all of our new compounds are free of lone pairs, providing opportunities to make direct comparisons to the crystal and electronic structures of compositions with lone-pair M^{II} cations [*i.e.* Pb(II), Sn(II)]. All five compositions are isostructural with their APbI$_3$ counterparts but exhibit slightly larger lattice parameters, with the MA perovskites crystallizing in the tetragonal $I4/mcm$ space group and the FA perovskites crystallizing in the tetragonal $P4/mbm$ space group.

Alloying Sn and Pb Perovskites on Anion and Cation Sites One of the primary methods for band gap tuning in metal halide perovskites has been halide (I/Br) mixing. Despite widespread usage of this type of chemical substitution in perovskite photovoltaics, there is still little understanding of the structural impacts of halide alloying, with the assumption being the formation of ideal solid solutions. The $FASnI_{3-x}Br_x$ ($x = 0 – 3$) family of compounds provides the first example where the assumption breaks down, as the composition space is broken into two unique regimes ($x = 0 – 2.9$; $x = 2.9 – 3$) based on their average structure with the former having a 3D and the latter having an extended 3D (pseudo 0D) structure. Pair distribution function (PDF) analyses further suggest a dynamic $5s^2$ lone pair expression resulting in increasing levels of off-centering of the central Sn as the Br concentration is increased. These antiferroelectric distortions indicate that even the $x = 0 – 2.9$ phase space behaves as a nonideal solid-solution on a more local scale. Solid-state NMR confirms the difference in local structure yielding greater insight into the chemical nature and local distributions of the FA cation. ramatic quenching of photoluminescence is observed, with $x \geq 1.9$ compounds having no observable PL. Our detailed studies attribute this quenching to structural transitions induced by the distortions of the $[SnBr_6]$ octahedra in response to stereochemically expressed lone pairs of electrons.[3] In a related study, the FA cation in $(Cs_{0.17}FA_{0.83})Pb(Br_{0.2}I_{0.8})_3$ was substituted by seven alternative cations to achieve a slight blue shift in the bandgap, that is typically achieved by increasing bromide content. Among alternative cations, dimethylammonium and acetamidinium induced greater blue shifts at 10% concentration without forming a new low-dimensional second phase.[4]

Polar, Chiral Phase of $CsSnBr_3$ Polar and chiral crystal symmetries confer a variety of potentially useful functionalities upon solids by coupling otherwise noninteracting mechanical, electronic, optical, and magnetic degrees of freedom. We have described two previously unstudied phases of the 3D perovskite, $CsSnBr_3$, which emerge below 85 K due to the expression of Sn(II) lone pairs and their interaction with octahedral tilts.[5] Phase II ($77\ K < T < 85\ K$, space group $P2_1/m$) exhibits ferroaxial order driven by a noncollinear pattern of lone pair-driven distortions within the plane normal to the unique octahedral tilt axis, preserving the inversion symmetry observed at higher temperatures. Phase I ($T < 77$ K, space group $P2_1$) additionally exhibits ferroelectric order due to distortions along the unique tilt axis, breaking both inversion and mirror symmetries. This polar and chiral phase exhibits second harmonic generation from the bulk and a large, intrinsic polarization-electrostriction coefficient along the polar axis ($Q_{22} \approx 1.1\ m^4\ C^{-1}$), resulting in acute negative thermal expansion ($\alpha_V = -9\times10^{-5}\ K^{-1}$) through the onset of spontaneous polarization. Relativistic electronic structure scenarios compatible with reported photoluminescence measurements are discussed. Together, the polar symmetry, small bandgap, large spin-orbit splitting of Sn 5p orbitals, and predicted strain sensitivity of the symmetry-breaking distortions suggest bulk samples and epitaxial films of $CsSnBr_3$ or its neighboring solid solutions as strong candidates for bulk Rashba effects.

References

1. D. H. Fabini, R. Seshadri, and M. G. Kanatzidis, *The Underappreciated Lone Pair in Halide Perovskites Underpins their Unusual Properties*, MRS Bulletin **45**, 467–477 (2020).
2. G. Kent, J. Huang, K. Albanese, A. Zohar, E. Morgan, A. Kallistova, L. Kautzsch, A. Mikhailovsky, P. Vishnoi, R. Seshadri, and A. K. Cheetham, *Hybrid Iodide Perovskites of Divalent Alkaline Earth and Lanthanide Elements*, J. Am. Chem. Soc. **145**, 27850–27856 (2023).
3. A. Balvanz, M. Safdari, M. Zacharias, D. Kim, C. Welton, E. H. Oriel, M. Kepenekian, C. Katan, C. D. Malliakas, J. Even, V. Klepov, G. N. Manjunatha Reddy, R. D. Schaller, L. X. Chen, R. Seshadri, and M. G. Kanatzidis, *Structural Evolution and Photoluminescence Quenching across the $FASnI_{3-x}Br_x$ (x = 0 – 3) Perovskites*, J. Am. Chem. Soc. **146**, 16128–16147 (2024).
4. M. Safdari, D. Kim, A. Balvanz, and M. G. Kanatzidis, *Mitigation of Halide Segregation by Cation Composition Management in Wide Bandgap Perovskites*, ACS Energy Lett. **9**, 3400–3408 (2024).
5. D. H. Fabini, K. Honasoge, A. Cohen, S. Bette, K. M. McCall, C. C. Stoumpos, S. Klenner, M. Zipkat, L. P. Hoang, J. Nuss, R. K. Kremer, M. G. Kanatzidis, O. Yaffe, S. Kaiser, and B. V. Lotsch, *Noncollinear Electric Dipoles in a Polar Chiral Phase of $CsSnBr_3$ Perovskite*, J. Am. Chem. Soc. **146**, 15701–15717 (2024).

Publications

1. G. Kent, J. Huang, K. Albanese, A. Zohar, E. Morgan, A. Kallistova, L. Kautzsch, A. Mikhailovsky, P. Vishnoi, R. Seshadri, and A. K. Cheetham, *Hybrid Iodide Perovskites of Divalent Alkaline Earth and Lanthanide Elements*, J. Am. Chem. Soc. **145**, 27850–27856 (2023).
2. A. K. Cheetham and R. Seshadri, *Artificial Intelligence Driving Materials Discovery? Perspective on the Article: Scaling Deep Learning for Materials Discovery*, Chem. Mater. **36**, 3490–3495 (2024).
3. A. Balvanz, M. Safdari, M. Zacharias, D. Kim, C. Welton, E. H. Oriel, M. Kepenekian, C. Katan, C. D. Malliakas, J. Even, V. Klepov, G. N. Manjunatha Reddy, R. D. Schaller, L. X. Chen, R. Seshadri, and M. G. Kanatzidis, *Structural Evolution and Photoluminescence Quenching across the $FASnI_{3-x}Br_x$ (x = 0 – 3) Perovskites*, J. Am. Chem. Soc. **146**, 16128–16147 (2024).
4. M. Safdari, D. Kim, A. Balvanz, and M. G. Kanatzidis, *Mitigation of Halide Segregation by Cation Composition Management in Wide Bandgap Perovskites*, ACS Energy Lett. **9**, 3400–3408 (2024).
5. D. H. Fabini, K. Honasoge, A. Cohen, S. Bette, K. M. McCall, C. C. Stoumpos, S. Klenner, M. Zipkat, L. P. Hoang, J. Nuss, R. K. Kremer, M. G. Kanatzidis, O. Yaffe, S. Kaiser, and B. V. Lotsch, *Noncollinear Electric Dipoles in a Polar Chiral Phase of $CsSnBr_3$ Perovskite*, J. Am. Chem. Soc. **146**, 15701–15717 (2024).

Broadening Accessibility & Training To Emerging Researchers for Innovative Energy Storage (BATTERIES)

PI: Dr. Monica C. So[1], Associate Professor
Co-PI(s): Drs. Kathleen Meehan[1], Liwen Wan[2], Philip T. Dirlam[3]
1: California State University, Chico, Chico, CA 95929
2: Lawrence Livermore National Laboratory, Livermore, CA 94550
3: San Jose State University, San Jose, CA 95192

Keywords: batteries, porous materials, STEM training

Research Scope

The BATTERIES project addresses two crucial goals in basic energy science research: (1) the development of novel materials for enhancing stability, catalytic activity, and conductivity of lithium-sulfur (Li-S) batteries to meet energy storage demands and (2) the preparation of future STEM scientists from underrepresented minority (URM), first-generation college student (FGCS), and women subpopulations. Although Li-S batteries theoretically have capacities up to four times higher than that of current Li-ion batteries, several challenges related to the dissolution and diffusion of polysulfides limit commercialization of Li-S batteries. To overcome these challenges, a computation-guided experimental approach to investigate three research thrusts (RTs) is being employed:

1. Control of Metal Organic Framework (MOF) pores to stop polysulfide shuttling caused by the dissolution of intermediate lithium polysulfide species in the electrolyte resulting in poor battery cell performance,
2. Determination of potential catalytic effects of conductive MOFs on Li-S electrochemistry, and
3. Quantification of the cycling capability of Li-S batteries containing porous and conductive MOFs.

The outcomes will enable the rational design and control of *electrically* conductive cathode additives and sulfur hosts, as well as *ionically* conductive interlayers in the Li-S battery. To achieve the scientific goals, over one third of students who self-identify as URM, FGCS, and/or female will be recruited at the two participating minority serving institutes. The project's plan for Promoting Inclusive and Equitable Research (PIER) includes:

1. Comprehensive recruitment workshops,
2. An inclusive environment management for research and training of all participants, and
3. Mentorship matching for 22 trainees, including student participants and postdoctoral scholars, providing the participants with unique career development opportunities.

The goal is the retention and graduation of more than 90% of the participants, jumpstarting the careers of two early career scientists, and serving as a role model on techniques to retain and prepare a diverse STEM workforce.

Recent Progress

To address challenges in RT 2 and 3, PI So investigated guest-host interactions within MOFs. These are critical to unlocking the power of extrinsically conductive metal–organic frameworks (MOFs) for electronics applications. One model system involves studying conjugated acceptor 7,7,8,8-tetracyanoquinodimethane (TCNQ) guests within isostructural M-MOF-74 (M = Cu, Mn, Zn, Mg) hosts, To date, however, none have elucidated the nature of these host–guest complexes or proposed conductivity mechanisms in the TCNQ@M-MOF-74 system. Previous studies also failed to address additional fundamental questions, such as: to what extent do open d shells of metal ions in M-MOF-74 influence charge transfer? What role does conjugation play in TCNQ in influencing electrical conductivity? How does oxygen affect the stability of TCNQ? Through what charge transport mechanism does TCNQ induce MOF conductivity? We found an air-free approach to infiltrate isostructural M-MOF-74 with TCNQ. The TCNQ@M-MOF-74 compounds exhibit a striking correlation between their bulk conductivities and the open *d* shell variants (Cu, Mn), arising from TCNQ *p*-doping of the MOFs.[1] Importantly, conjugation of guest molecules is required for inducing electrical conductivity in these systems.

To investigate factors affecting RT2, we employed UiO-66 analogues as catalysts. Namely, UiO-66, UiO-66-NH_2, and UiO-66-NO_2 were employed as catalysts in oxidative desulfurization (ODS) of an organic sulfur-containing compound, dibenzothiophene (DBT). We found that the effects of the electronic environment of the organic linker of the MOFs were the most substantial on the turnover frequency (TOFs) on the ODS of DBT.[2] UiO-66-NO_2 exhibits superior activity, followed by UiO-66, while UiO-66-NH_2 demonstrates the lowest TOFs. The highest catalytic activity of UiO-66-NO_2 is likely due its nitro group functionalized linker which adds electron-withdrawing character. This aids in making the H_2O_2 complex in the reaction more electrophilic. The formation of Zr^{4+} is a major contributor for ODS, as DBT molecules coordinate to the Lewis-acid metal sites on the MOF. Having more electron-withdrawing character on the linker would provide activation of more Lewis acid sites and enable more coordination with DBT, resulting in more efficient ODS. Students' experimental data showed that the appearance of an electron-donating group greatly hindered catalytic activity, indicating the need for electron-withdrawing character for ODS.

To address goals in PIER 2, PI So, co-PI Dirlam, Meehan, and Wan recruited and trained 2 postdoctoral scholars, 1 graduate student, and 12 undergraduate students. As of July 2024, we are mentoring 68% of our intended trainees for the project. Of these, there are 8 women, 4 are underrepresented minorities (URM), and 4 are first-generation college students. Of those trainees, 1 female URM undergraduate[1] and 1 URM and FGCS undergraduate[2] coauthored peer-reviewed manuscripts as first authors and one female postdoctoral scholar second authored one manuscript.

Publications

1. S. M. Angel, N. S. Barnett, A. A. Talin, M. E. Foster, V. Stavila, M. D. Allendorf, M. C. So. *J. Mater. Chem. C,* **12**, 2699 (2024).
2. E. Lucatero, R. Bashiri, M. C. So. *J. Chem. Educ., Accepted* (2024).

Effect of local order on polaron and exciton delocalization in rigid D-A copolymers (DE-SC0024420)

Alberto Salleo (Stanford University), Frank Spano (Temple University), Christine Luscombe (OIST), Natalie Stingelin (Georgia Tech)

Keywords: conjugate polymers, charge transport properties, mechanical stretchability

Research Scope

There is a great interest in semiconducting polymers for a large variety of energy —and DOE-relevant— applications, including for light harvesting and storage, wearable electronics, sensing, self-healing skins, and beyond. Excitons and polarons, i.e. bound electron-hole pairs and free charges respectively, play a fundamental role in the operation of devices used in such applications as they are the vehicles by which energy and electrical current flow. However, gaining a broad, widely applicable understanding of interrelations between intrinsic optoelectronic properties and materials design, macromolecular arrangements across multiple length scales, and assembly, has been challenging due to the fact that most semiconducting polymers are highly heterogeneous systems as a result of their long-chain nature and often high dispersity. Moreover, conjugated polymers are often brittle with poor mechanical properties. Currently, the most common approach to obtaining mechanically robust semiconductors is blending a brittle conjugated polymer in an elastomeric matrix. While successful, this approach dilutes the semiconductor, limiting the amount of current that it can carry, and poses formidable processing challenges. A more elegant and functional approach would be to design conjugated polymers that are intrinsically mechanically robust, a property non-existent in conventional semiconductors which are brittle and exhibit low fracture toughness. An important fundamental materials chemistry question can thus be raised: Are high mechanical robustness and efficient electronic transport mutually exclusive properties of a (single component) polymer semiconductor?

Recent Progress

We started the project with the comparison of two rigid-rod polymer semiconductors, poly(indacenodithiophene-co-benzothiadiazole), p(IDT-BT), and poly(indacenodithiophene-co-benzopyrollodione), p(IDT-BPD), to understand the effect charge carrier intrachain delocalization has on electronic transport. The two polymers were selected because they are structurally both highly disordered (near-amorphous) but they feature charge-carrier mobilities that are orders of magnitude different. Quantum chemical calculations show that p(IDT-BPD) has a significantly lower barrier to backbone torsion than p(IDT-BT) and is thus more likely to have reduced conjugation lengths. We utilize absorption and photoluminescence spectroscopy to characterize energetic disorder and show that p(IDT-BPD) has indeed higher energetic disorder. Charge modulation spectroscopy (CMS) and model calculations are used to show that polarons are substantially delocalized in p(IDT-BT) and occupy near-uniform energetic environments, however, mobility-activated hopping barriers are similar in these two materials. Electronic

structure calculations show that both intrachain and interchain coupling of monomer units is poor enough in p(IDT-BPD) that charge carriers collapse to single IDT units and transport via a through-space tunneling mechanism. Our work, thus, highlights the remarkable charge transport properties of p(IDT-BT) by showing that high mobilities are achievable on device relevant length-scales with only 1D carrier delocalization. Guidelines how p(IDT-BT) can be made mechanically tough in future are given as well.

Publications

1. G. LeCroy, R. Ghosh, P. Sommerville, C. Burke, M. Hesam, K Rozylowicz, C. Cheng, M. Weber, N. Stingelin, A. Troisi, C. Luscombe, F. Spano, and A. Salleo, *Using molecular structure to tune intrachain and interchain charge transport in indacenodithiophene based copolymers*, JACS (accepted)

Probing the hydrogen bonded networks and ion interactions in deep eutectic solvents (DESs) through solute molecules.

PI: Sophia Suarez, Brooklyn College of City University of New York (CUNY)

Keywords: deep eutectic solvents (DESs), nuclear magnetic resonance (NMR) relaxometry, ion conduction, electrolytes, fast field cycling NMR.

Research Scope

In this project we are focused on characterizing the various interactions in deep eutectic solvent (DES) electrolytes based on metallic salts. Through a combination of measurements, we assess the bulk and local dynamics of the ionic species to better understand the various interactions and their effect on dynamics and speciation. Techniques such as nuclear magnetic resonance (NMR) relaxometry as functions of both temperature and frequency allows us to qualitatively isolate and identify the various types of motions. Additionally, by combining NMR with conductivity, viscosity, and density measurements, we can tune these inherent interactions in the materials as a means of enhancing dynamics.

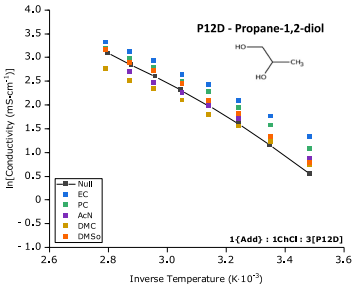

Figure 1. Ionic conductivity dependence on probe solvent type for 1ChCl:3P12D mixture.

Recent Progress

We started with zinc salts ($ZnCl_2$ and $ZnBr_2$) and various hydrogen bond donors (HBD, ethylene glycol, choline chloride) and incorporated various 'probe' solvents (water, ethylene carbonate (EC), propylene carbonate (PC), acetonitrile (AcN)) in varying concentrations. We are especially interested in the hydrogen bonding networks of these electrolytes and the effect they have on the electrolytes' ion transport capabilities. Based on our findings of probe molecule and HBD types being strong determinants of ionic transport, we have since expanded our scope to include additional hydrogen bond acceptors (HBAs), various HBDs and hydrophobic probes solvents. Additional focus variables include probe molecule dipole moment and degree of hydrophobicity, and the range of conformational dynamics of HBDs. Our investigation is ongoing with NMR relaxometry and diffusometry measurements. We expect these results to provide us more understanding of the zinc species types. We are also in the process of incorporating other HBAs including organic salts, thereby allowing us selective views of the interactions between the zinc species and their solvation spheres.

Publications

In the last two years, we have published three manuscripts funded by this grant in peer-reviewed journals. Currently, one manuscript is under review and three are in preparation, all based on work from this project. Asterisk (*) signifies corresponding authorship.

1. M. N. Garaga, L. Murdock, T. Pranto, S. Suarez*, B. C. Benicewicz, and S. G. Greenbaum, NMR investigation of proton transport in polybenzimidazole/polyphosphoric acid membranes prepared via novel synthesis route, J. Power Sources, **575**, 233169 (2023).
2. Fariha Ahmed, Domenec Paterno, Gurneet Singh, **Sophia Suarez***, Ion transport in non-aqueous electrolyte mixtures of zinc chloride deep eutectic solvent (DES) and molecular solvents, Electrochim. Acta, 462, 142784, **2023**.
3. Mounesha N. Garaga*, *Sahana Bhattachary,* Domenec Paterno, **Sophia Suarez**, Steve Greenbaum, Structure and dynamics of ILs-based gel polymer electrolytes and its enhanced conductive properties with the incorporation of Al_2O_3 nanofibers, Electrochim. Acta, 462, 142765, **2023**.

Kinetics and Thermodynamics of Gaseous Mixtures in Nano-Confined Environments

Timo Thonhauser (WFU), Jing Li (Rutgers), Kui Tan (UNT)

Keywords: Metal-organic frameworks, gas mixtures, co-adsorption, kinetics, thermodynamics

Research Scope

Our program investigated the kinetics and thermodynamics of molecular mixtures in nano-confined environments. The nano-confinement can tip the thermodynamic vs. kinetic balance, and current understanding and theory can lead to incorrect predictions for such mixtures [1–4]. This is of particular interest in real-world applications, where gases/vapors are typically mixed or contain impurities and are often exposed to humid conditions. Our approach integrated intensive *in situ* characterization, *ab initio* modeling, and tailored synthesis. Our objectives were (i) to disentangle kinetic from thermodynamic effects by a series of sequential and simultaneous gas loading experiments; (ii) to identify the interactions between gas molecules of the mixture as well as between gas molecules and the host; and (iii) to develop nano-porous materials that are stable in reactive humid mixture environments. Due to their structural diversity, functional flexibility, and design freedom, metal organic frameworks (MOFs) have been the main platform to serve as our nano-confined environments to address our objectives.

Recent Progress

One of our most exciting recent successes concerns the separation and purification of C6 cyclic hydrocarbons (e.g., benzene, cyclohexene, cyclohexane), which represent a critically important process, but the current technologies are extremely energy intensive. Developing adsorptive separation technique to replace thermally driven distillation processes holds great promise to significantly reduce energy consumption. We were able to use a flexible one-dimensional (1D) coordination polymer as an efficient adsorbent to discriminate ternary C6 cyclic hydrocarbons via an ideal molecular sieving mechanism [5]. The compound undergoes fully reversible structural transformation associated with removal/re-coordination of water molecules and between activated and hydrocarbon-loaded forms. It exhibits distinct temperature- and adsorbate-dependent adsorption behavior which facilitates the complete separation of benzene, cyclohexene and cyclohexane from their binary and ternary mixtures, with record-high uptake ratios for C_6H_6/C_6H_{12} and C_6H_{10}/C_6H_{12} in vapor phase and the highest binary and ternary selectivities in the liquid phase. A Combination of *in situ* infrared spectroscopic analysis and *ab initio* calculations provide insight into the host-guest interactions that lead to the difference in adsorption energetics and observed preferential adsorption, and further identified the changes occurring to specific chemical bonds that account for the overall structural transformation.

Another main focus of our research was molecular competition and exchange, which are common steps occurring in many technological processes such as chemical separation, capture, delivery, and release. However, the underlying principle is not fully understood, especially in nano-confined environments where the energetics and kinetics of such processes can deviate from that on flat surfaces. We unraveled the mechanism of a molecular exchange process by studying the displacement of NO by H_2O in Ni-MOF-74 in real-time using *in situ* infrared spectroscopy combined with *ab initio* calculations [6]. We showed that weakly bound H_2O gradually displaces strongly bound NO on the metal sites by first weakening the M–N bond through forming an H-bond and then moving the NO away so that it eventually desorbs. Interestingly, we further found that additional water facilitates this exchange by significantly lowering the kinetic barrier associated with this process as well as the overall energy of the final state. Although our study focuses on Ni-MOF-74, we believe that our finding and explanation of unexpected exchange phenomena—where strongly adsorbed molecules are apparently easily displaced by much weaker bound H_2O—is applicable to a much larger group of frameworks and will be helpful in designing and improving MOFs for real-world applications where humidity is often present.

Through a large number of kinetics/thermodynamics studies of molecululular adsorption in MOFs, we were fortunate to find a case with fundamental relevance for organometallic chemistry. Ferrocene is perhaps the most popular and well-studied organometallic molecule, but our understanding of its structure and electronic properties has not changed for more than 70 years. In particular, all previous attempts of chemically oxidizing pure ferrocene by binding directly to the iron center have been unsuccessful, and no significant change in structure or magnetism has been reported. Using a MOF host, we were able to fundamentally change the electronic and magnetic structure of ferrocene to take on a never-before observed physically stretched/bent high-spin Fe(II) state [7], which readily accepts O_2 from air, chemically oxidizing the iron from Fe(II) to Fe(III). Ferrocene thus becomes an exception to the 18-electron rule for which it has been the prime example, contrary to seven decades of well-accepted ferrocene chemistry. Through a careful analysis of the thermodynamics and kinetics of the ferrocene state change in the presence of oxygen, we were also able to show that the binding of oxygen is reversible, further confirmed through temperature swing experiments. Our analysis is based on combining Mößbauer spectroscopy, extended X-ray absorption fine structure, *in situ* infrared, SQUID, thermal gravimetric analysis, and energy dispersive X-ray fluorescence spectroscopy measurements with *ab initio* modeling.

References

1. H. Wang, M. Warren, J. Jagiello, S. Jensen, S.K. Ghose, K. Tan, L. Yu, T. J. Emge, T. Thonhauser, and J. Li, *Crystallizing Atomic Xenon in a Flexible MOF to Probe and Understand Its Temperature Dependent Breathing Behavior and Unusual Gas Adsorption Phenomenon*, J. Am. Chem. Soc. **142**, 20088 (2020).
2. K. Tan, S. Jensen, H. Wang, L. Feng, K. Wei, H.C. Zhou, J. Li, and T. Thonhauser, *Thermally Activated Adsorption in Metal-Organic Frameworks with a Temperature-Tunable Diffusion Barrier Layer*, Angew. Chem. Int. Ed. **59**, 18468 (2020).
3. K. Tan, S. Jensen, S. Zuluaga, E.K. Chapman, H. Wang, R. Rahman, J. Cure, T.-H. Kim, J. Li, T. Thonhauser, and Y.J. Chabal, *Role of Hydrogen Bonding on Transport of Co-adsorbed Gases in Metal-Organic Framework Materials*, J. Am. Chem. Soc. **140**, 856 (2018).
4. K. Tan, S. Zuluaga, Q. Gong, Y. Gao, N. Nijem, J. Li, T. Thonhauser, and Y.J. Chabal, *Competitive co-adsorption of CO_2 with H_2O, NH_3, SO_2, NO, NO_2, N_2, O_2, and CH_4 in M-MOF-74 (M = Mg, Co, Ni): The role of hydrogen bonding*, Chem. Mater. **27**, 2203 (2015).
5. F. Xie, L. Chen, E. M. Cedeno Morales, S. Ullah, Y. Fu, T. Thonhauser, K. Tan, Z. Bao, and J. Li, *Complete separation of benzene-cyclohexene-cyclohexane mixtures via temperature-dependent molecular sieving by a flexible chain-like coordination polymer*, Nature Commun. **15***, 2240* (2024).
6. H. Pandey, H. Wang, M. V. Alfaro, J. Li, T. Thonhauser, and K. Tan, *Real-time observation of the exchange process between H_2O and NO in the metal–organic framework Ni-MOF-74*, J. Mater. Chem. A **12***, 6880-6884* (2024).
7. S. Ullah, S. Jensen, Y. Y. Liu, K. Tan, H. Drake, G. Y. Zhang, J. J. Huang, J. Klimes, D. M. Driscoll, R. P. Hermann, H. C. Zhou, J. Li, and T. Thonhauser, *Magnetically Induced Binary Ferrocene with Oxidized Iron*, J. Am. Chem. Soc. **145***, 18029-18035* (2023).

Publications

1. F. Xie, L. Chen, E. M. Cedeno Morales, S. Ullah, Y. Fu, T. Thonhauser, K. Tan, Z. Bao, and J. Li, *Complete separation of benzene-cyclohexene-cyclohexane mixtures via temperature-dependent molecular sieving by a flexible chain-like coordination polymer*, Nature Commun. **15***, 2240* (2024).
2. J. Miao, W. Graham, J. Liu, E. C. Hill, L. L. Ma, S. Ullah, H. L. Xia, F. A. Guo, T. Thonhauser, D. M. Proserpio, J. Li, and H. Wang, *An Octacarboxylate-Linked Sodium Metal-Organic Framework with High Porosity*, J. Am. Chem. Soc. **146***, 84-88* (2024).
3. H. Pandey, H. Wang, M. V. Alfaro, J. Li, T. Thonhauser, and K. Tan, *Real-time observation of the exchange process between H_2O and NO in the metal–organic framework Ni-MOF-74*, J. Mater. Chem. A **12***, 6880-6884* (2024).
4. F. Xie, L. Yu, T. Jenkins, J. Shutak, K. Tan, T. Thonhauser, H. Wang, and J. Li, *Nickel Isonicotinate Framework with Optimal Pore Structure for Complete Discrimination of Hexane Isomers*, ACS Mater. Lett. **6***, 43-48* (2023).
5. S. K. Xian, J. J. Peng, H. Pandey, W. Graham, L. Yu, H. Wang, K. Tan, T. Thonhauser, and J. Li, *Simultaneous removal of C_2H_2 and C_2H_6 for C_2H_4 purification by robust MOFs featuring a high density of heteroatoms*, J. Mater. Chem. A **11***, 21401-21410* (2023).
6. L. Yu, J. Zhang, S. Ullah, J. Z. Yao, H. Y. Luo, J. J. Huang, Q. B. Xia, T. Thonhauser, J. Li, and H. Wang, *Separating Xylene Isomers with a Calcium Metal-Organic Framework*, Angew. Chem.-Int. Edit. **62***, 5* (2023).
7. F. Xie, J. Q. Liu, W. Graham, S. Ullah, E. M. C. Morale, K. Tan, T. Thonhauser, H. Wang, and J. Li, *The effect of pore structure in ethane-selective metal-organic frameworks for ethylene purification*, Chem. Eng. J. **473***, 9* (2023).
8. S. Ullah, S. Jensen, Y. Y. Liu, K. Tan, H. Drake, G. Y. Zhang, J. J. Huang, J. Klimes, D. M. Driscoll, R. P. Hermann, H. C. Zhou, J. Li, and T. Thonhauser, *Magnetically Induced Binary Ferrocene with Oxidized Iron*, J. Am. Chem. Soc. **145***, 18029-18035* (2023).
9. S. Ullah, K. Tan, D. Sensharma, N. Kumar, S. Mukherjee, A. A. Bezrukov, J. Li, M. J. Zaworotko, and T. Thonhauser, *CO_2 Capture by Hybrid Ultramicroporous TIFSIX-3-Ni under Humid Conditions Using Non-Equilibrium Cycling*, Angew. Chem.-Int. Edit. **61***, 8* (2022).
10. K. Tan, S. Ullah, H. Pandey, E. M. Cedeno-Morales, H. Wang, K. Y. Wang, H. C. Zhou, J. Li, and T. Thonhauser, *Competitive Adsorption of NH_3 and H_2O in Metal-Organic Framework Materials: MOF-74*, Chem. Mat. **34***, 7906-7915* (2022).

Using Nanoporous and Nanostructured Materials to Understand and Optimize Pseudocapactive Charge Storage

Sarah H. Tolbert, Department of Chemistry & Biochemistry, and Department of Materials Science & Engineering, University of California Los Angeles, Los Angeles, California 90095

Keywords: pseudocapacitors, phase transitions, fast-charging, energy storage, nanomaterials

Research Scope

Fast-charging Li-ion batteries, often called pseudocapacitors due to their capacitor-like chare/discharge kinetics,are necessary for the continued development and universal adoption of electric vehicles and grid-scale energy storage[1,2,3]. Many battery materials have insertion-induced first-order phase transitions which, along with long ion diffusion paths, lead to slow kinetics. [4,5,6,7,8,9,10,11,12] Suppression of these first-order phase transitions has been correlated with fast charging in a number of systems, but the mechanisms behind their suppression remain poorly understood.[13, 14, 15, 16, 17,18] In recent DOE-supported work, we used *operando* synchrotron X-ray diffraction and electrochemical kinetics studies to investigate how nanoscale crystal size and crystallographic disorder can lead to the suppression of first-order insertion-induced phase transitions and mitigate their negative kinetic effects.[19,20] In nanostructured MoS_2 and MoO_2, changes in phase transition behavior were correlated with domain size, disorder, and electrochemical kinetics, overall showing that decreased size and increased disorder are independently capable of altering phase transition behavior. We also investigate a number of materials that do not undergo intercalation-induced first-order phase transitions, including Li_xTiS_2, the nickel-rich cathodes $LiNi_{0.8}Co_{0.1}Al_{0.1}O_2$ (NCA_{811}) and $LiNi_{0.8}Co_{0.1}Mn_{0.1}O_2$ (NCM_{811}), and a disordered rocksalt structured $V_9Mo_6O_{40}$ (VMO) to understand the factors limiting charging speeds in these systems. These materials show pseudocapacitive behavior to larger size, with parameters other than first order phase transitions dominating the kinetics of Li (de)insertion.

Recent Progress

As reported last year, we used MoO_2 and MoS_2 as model tunnel and layered systems, respectively, to investigate how size and disorder can suppress first-order phase transitions.[Error! Bookmark not defined.,Error! Bookmark not defined.] Bulk Li_xMoO_2 undergoes a first-order phase transition, shown by a discontinuous jump in peak position during which there is coexistence of two phases. As the size of the MoO_2 grains decrease, the size of the miscibility gap and the extent of two-phase coexistence decrease until finally, in MoO_2 nanocrystals, the phase transition becomes entirely continuous, solid-solution based. As the miscibility gap shrinks, the rate capabilities improve.[Error! Bookmark not defined.] To understand the role of disorder, we turned to the model layer system MoS_2 made through the thermal sulfurization of MoO_2;

here disorder can be controlled through the temperature at which the sulfurization occurs and size can be controlled by the size of the starting MoO_2.**Error! Bookmark not defined.** *Operando* XRD shows suppression of the Li^+ intercalation-induced 1T-to-triclinic transition in all of the small *or* disordered samples, but not in the large crystalline material. Electrochemical studies indicate that the smaller and more disordered samples outperform their larger and more crystalline counterparts in rate capability and longterm cycling stability, indicating that size and lattice disorder are both effective options for suppressing intercalation-induced phase transitions and introducing pseudocapacitive behavior.

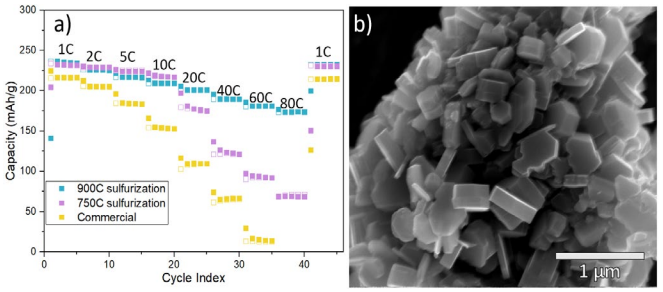

Fig. 3: a) Galvanostatic cycling for TiS_2 sulfurized at different temperatures and for commercial bulk TiS_2. b) SEM of nanosized TiS_2 obtained by sulfurizing TiO_2 nanoparticles

Building on our work with MoS_2, we have investigating TiS_2, which is also layered, but unlike MoS_2, shows fully solid-solution phase behavior upon Li (de)intercalation. When synthesized through the sulfurization of TiO_2, TiS_2 is capable of extraordinarily fast charging/discharging when sulfurized at a high temperature, even though it is relatively large (~500nm) (Fig.3). EDS and XPS indicate that the fastest TiS_2 is close to being stoichiometrically perfect, while the slower nanostructured TiS_2 and commercial bulk have S:Ti ratios below 2:1, suggesting a lack of defects such as interstitial titanium or sulfur vacancies in the high T material. Structural changes in all materials upon Li (de)insertion are identical, indicating that for materials without first-order phase transitions, more perfect materials lead to faster lithium ion diffusion and retention of pseudocapacitive behavior to larger size.

Like TiS_2, many layered cathodes, including NCA and NCM, show solid-solution behavior upon Li insertion/extraction. We have shown that these materials can similarly show pseudocapacitive behavior at sizes up to a few hundred nm, but not all materials are equally fast. To determine what factors most affect (de)insertion kinetics, we varied the molar excess of Li precursor in the synthesis. Higher Li excess significantly improved cation ordering, as measured by X-ray diffraction (Fig. 2a), but create surface impurities that led to higher charge transfer resistance (Fig. 2b,d). Despite the increased resistance, nanoporous NCA with 7.5% Li excess has much enhanced rate capability compared to 5% and 2.5% excess samples (Fig. 2c). This data suggests that fast Li diffusion is the most important parameter for determining

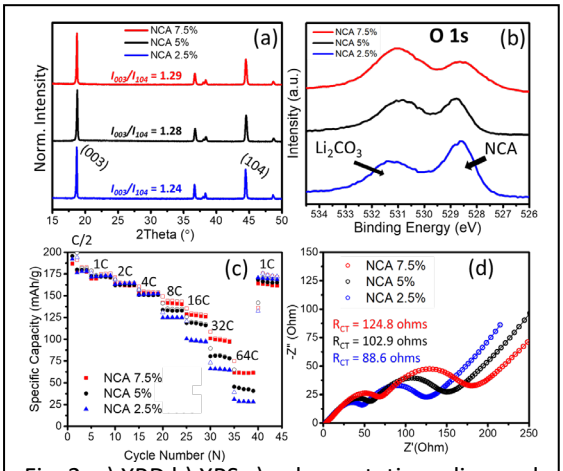

Fig. 2: a) XRD b) XPS c) galvanostatic cycling and d) EIS measurements for nanoporous NCA prepared with different amounts of Li^+ excess

pseudocapacitive behavior, and that some surface limitations can be tolerated in nanoscale materials.

Finally, we examined disordered rocksalt structured VMO and found fast charging and pseudocapacitive behavior in both bulk and nanoscale materials, due to the lack of first order phase transitions and the unique local architecture of both materials.

References

1. P. Simon, Y. Gogotsi; B. Dunn, *Where Do Batteries End and Supercapacitors Begin?* Science ***343***, 1210–1211 (2014).
2. B.E. Conway*, Transition from "Supercapacitor" to "Battery" Behavior in Electrochemical Energy Storage*. J. Electrochem. Soc. **138**, 1539–1549 (1991).
3. B.E. Conway, V. Birss, J. Wojtowicz, *The Role And Utilization of Pseudocapacitance for Energy Storage by Supercapacitors*. J. Power Sources, **66,** 1–14 (1997).
4. M. S. Whittingham, *Lithium Batteries and Cathode Materials*. Chem. Rev. **104**, 4271-4302 (2004).
5. M. Winter, J.O. Besenhard, M.E. Spahr, P. Novák. *Insertion Electrode Materials for Rechargeable Lithium Batteries.* Adv. Mater. **10**, 725-763 (1998).
6. J.N. Reimers, J.R. Dahn, *Electrochemical and In situ X-ray Diffraction Studies of Li Intercalation in Li_xCoO_2*. J. Echem. Soc. **139**, 2-8 (1992).
7. A. Yamada, H. Koizumi, S. Nishimura, N. Sonoyama, R. Kanno, M. Yonemura, T. Nakamura, Y. Kobayashi,. *Room-temperature miscibility gap in Li_xFePO_4.* Nature Mater. **5**, 357-360 (2006).
8. H. Fujimoto, T. Yamaki, K. Shimoda, S. Fujinami, T. Nakatani, G. Kano, M. Kawasaki, Z. Ogumi, T. Abe. Phase Diagram of Li-Graphite Intercalation Compound Formed by the Charge/Discharge Reaction in Li-Ion Battery. J. Electrochem. Soc. 169, 070507 (2022).
9. . M. Fehse, L. Monconduit, F. Fischer, C. Tessier, L. Stievano. Study of the Insertion Mechanism of Lithium into Anatase by Operando X-ray Diffraction and Absorption Spectroscopy. Solid State Ion. 268, 252-255 (2014).
10. . X. Zhang, M. van Hulzen, D.P. Singh, A. Brownrigg, J.P. Wright, N.H. van Dijk, M. Wagemaker, Direct View on the phase evolution in individual LiFePO4 nanoparticles during Li-ion battery cycling. Nat. Comm. 6, 8333 (2015).
11. . G. Oyama, Y. Yamada, R. Natsui, S. Nishimura, A. Yamada. Kinetics of Nucleation and Growth in Two-Phase Electrochemical Reaction of LixFePO4. J. Phys. Chem. C. 116, 7306–7311 (2012).
12. . N. Meethong, Y.-H. Kao, W.C. Carter, Y.-M. Chiang. Comparative Study of Lithium Transport Kinetics in Olivine Cathodes for Li-ion Batteries. Chem. Mater. 22, 1088–1097 (2010).
13. . N. Meethong, H.Y.S. Huang, W. Carter, Y.M. Chiang, Size-Dependent Lithium Miscibility Gap in Nanoscale Li1−xFePO4. Electrochem. Solid State Lett. 10, A134 (2007).
14. . H.-S. Kim, J.B. Cook, S.H. Tolbert, B. Dunn, B. The Development of Pseudocapacitive Properties in Nanosized-MoO2. J. Electrochem. Soc. 162, A5083–A5090 (2015).
15. . J.B. Cook, T.C. Lin, H.-S. Kim, A. Siordia, B. Dunn, S.H. Tolbert, Suppression of Electrochemically Driven Phase Transitions in Nanostructured MoS2 Pseudocapacitors Probed Using Operando X-ray Diffraction. ACS Nano, 13, 1223–1231 (2019).
16. . G.A. Muller, J.B. Cook, H.-S. Kim, S.H. Tolbert, B. Dunn, High Performance Pseudocapacitor Based on 2D Layered Metal Chalcogenide Nanocrystals. Nano Lett. 15, 1911–1917 (2015).
17. . B.K. Lesel, J.B. Cook, Y. Yan, T.C. Lin, S.H. Tolbert, Using Nanoscale Domain Size to Control Charge Storage Kinetics in Pseudocapacitive Nanoporous LiMn2O4 Powders. ACS Energy Lett. 2, 2293–2298 (2017).
18. . W.J.H. Borghols, M. Wagemaker, U. Lafont, E.M. Kelder, F.M. Mulder, Size Effects in the Li4+xTi5O12 Spinel. J. Am. Chem. Soc. 131, 17786–17792 (2009).

19. . D.D. Robertson, H. Cumberbatch, D.J. Pe, Y. Yao, S.H. Tolbert, Understanding How the Suppression of Insertion-Induced Phase Transitions Leads to Fast Charging in Nanoscale LixMoO2. ACS Nano. 18, 996-1012 (2024).
20. . Y. Yao, H. Cumberbatch, D.D. Robertson, M.A. Chin, R. Lamkin, and S.H. Tolbert, On the Interplay between Size and Disorder in Suppressing Intercalation-Induced Phase Transitions in Pseudocapacitive Nanostructured MoS2. Adv. Func. Mater. 2304896 (2023).
21. . Dahn, J.R.; Haering, R.R. Anomalous Bragg Peak Widths in LixTiS2. Solid State Commun. 40, 245-248 (1981).
22. . Fleischmann, S.; Shao, H.; Taberna, P.-L.; Rozier, P.; Simon, P. Electrochemically Induced Deformation Determines the Rate of Lithium Intercalation in Bulk TiS2. ACS Energy Lett. 6, 4173-4178 (2021)

Publications

1. D.D. Robertson, C. Salamat, D.J. Pe, H. Cumberbatch, D.N. Agyeman-Budu, J Nelson Weker, and S.H. Tolbert. "Electrochemically-Formed Disordered Rock Salt ω-$V_9Mo_6O_{40}$ as a Fast-Charging Li-Ion Electrode Material." *Chemistry of Materials*. Under review (2024).
2. D.D. Robertson, H. Cumberbatch, D.J. Pe, Y. Yao, S.H. Tolbert, *Understanding How the Suppression of Insertion-Induced Phase Transitions Leads to Fast Charging in Nanoscale Li_xMoO_2.* ACS Nano. **18**, 996-1012. (2024).
3. Y. Yao, H. Cumberbatch, D.D. Robertson, M.A. Chin, R. Lamkin, and S.H. Tolbert, *On the Interplay between Size and Disorder in Suppressing Intercalation-Induced Phase Transitions in Pseudocapacitive Nanostructured MoS_2.* Adv. Func. Mater. 2304896 (2023).
4. J.B. Cook, J.S. Ko, T.C. Lin, D.D. Robertson, H.-S. Kim, Y. Yan, Y. Yao, B.S. Dunn, S.H. Tolbert, *Ultrafast Sodium Intercalation Pseudocapacitance in MoS_2 Facilitated by Phase Transition Suppression*. ACS Appl. Energy Mater. **6**, 99-108 (2023). DOI: 10.1021/acsaem.2c02368.
5. Y. Yan, M.A. Chin, D.D. Robertson, B.K. Lesel, *S.H. Tolbert, Tuning the Porous Structure in PMMA-Templated Mesoporous MoO_2 for Pseudocapacitive Li-Ion Electrodes*. J. Electrochem. Soc. **169**, 040545 (2022). DOI: 10.1149/1945-7111/ac63f8.
6. Y. Yan, H.S. Kim, J.B. Cook, S. Robbennolt, B. Dunn, S.H. Tolbert, *Mesoporous MoO_2 Thin Films for High Rate Li^+ Storage: Effect of Crystallinity and Porous Structure*. Solid State Sci., **129**, 106890 (2022). DOI: 10.1016/j.solidstatesciences.2022.106890

Exploration of Radial Conjugation Pathways in Pi-Electron Materials

John D. Tovar, PI, Department of Chemistry, Johns Hopkins University; Ramesh Jasti, co-PI, Department of Chemistry, University of Oregon; Miklos Kertesz, co-PI, Department of Chemistry, Georgetown University

Keywords: Pi-electron materials, radial conjugation, delocalization

Research Scope

This project involves hypothesis-driven exploratory research on new manifestations of pi-electronic delocalization relevant to organic electronics via building onto hitherto unused structural subunits that invoke different degrees of aromaticity, conjugation, radical character and strain. Our team consists of three interrelated groups specializing in *pi-conjugated organic electronic systems with unusual properties well beyond the conventional arsenal of organic semiconductors with linear conjugation topologies present on planar pi-electron backbones*. These systems combine unusual bonding patterns, unusual curvatures, and unusual charge states in new ways that have yet to be tapped for emerging electronics applications. Our objectives for this research program are to (1) design and characterize new energy materials that access unusual spin states and pi-electron delocalization in curved carbon structures and (2) examine through-space delocalization as encouraged by mechanical bonding of curved components. Our specific targets in this research are pi-conjugated materials bridged in different ways to cycloparaphenylene (CPP) radially-conjugated units in order to explore how the combination of radial and linear pi-conjugation influences emergent optoelectronic properties. Figure 1 shows two pathways installed during this project.[1,2]

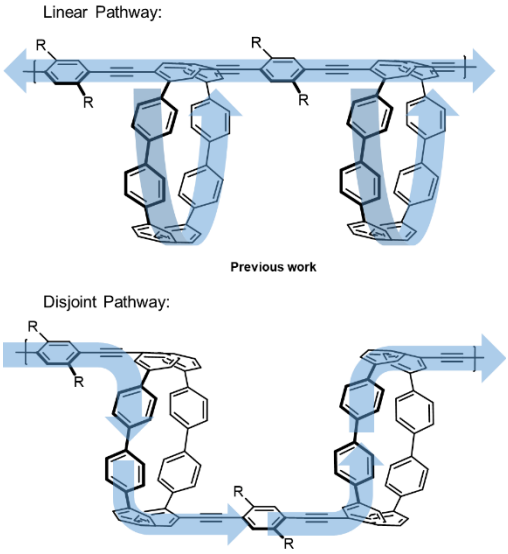

Figure 1. Linear (top) and disjoint (bottom) CPP conjugation pathways.

Recent Progress

CPPs linked with alkene spacers. We diversified the linker chemistry to include arylene vinylene repeat units (as opposed to arylene ethynylene in Figure 1) because alkyne linkages are known to have limited electron delocalization across the polymer backbone, and vinylene polymers are known for their emissive properties and high effective conjugation length. Additionally, we could further tune the polymer properties through co-polymerization with other monomers which allows for the optimization of parameters such as molecular weight and thin-film crystallinity. We have successfully observed (via *in-situ* NMR spectroscopy) the presence of the quinodimethane intermediate during the Gilch polymerization of [8]CPP-PPV.

This is important as it demonstrates for the first time, to our knowledge, a reaction mechanism proceeding through the backbone of an [*n*]CPP and temporarily disrupting aromaticity.

Probing carrier transport through linear-radial hybrids. We prepared disjoint CPP molecules flanked with aryl thiol groups to enable interrogation via break-junction STM measurements.[3] Using this technique, we validated their electrical transport properties. Our preliminary measurements suggest that there are two distinct attachment modes to the disjoint molecular wire: one bridging both sulfur contacts, and one connecting through a sulfur and a direct CPP carbon contact. We recently prepared model systems to further elucidate the nature of these contacts. Importantly, the presence of the conduction – even if of a low magnitude – sheds further light on the impact of the radial conjugation on defining transport.

Impacts of tensile strain. The radial pi-system in CPP is quite strained. By investigating the frontier orbital patterns of two dozen cases, we established the connection to topological insulators by finding that the aromatic ones constitute a trivial topological phase, and the quinonoid ones constitute a non-trivial topological phase. The significance of this insight lead to the discovery of a novel way to control the bandgap of pi-conjugated polymers by external tensile strain, ε (Figure 2).[4] Furthermore, with well-chosen chemical repeat units, extremely low bandgaps for pi-onjugated polymers have become a possibility. This will help in design of new CPP hybrid materials with unusual electronic properties.

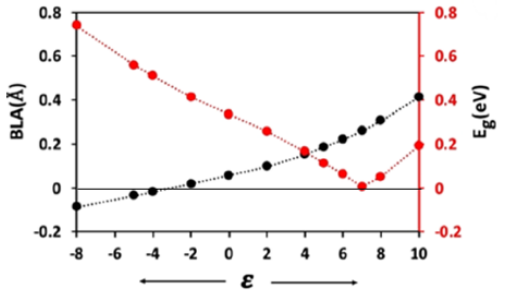

Figure 2. At a critical strain (ε) value the HOMO and LUMO cross and the bandgap (E_g) becomes very small. The correlation with bond length alternation (BLA) is essential.

Advanced CPP intermediates. Our synthetic and computational modeling efforts are continuing on several fronts. CPP synthesis relies on an established but lengthy procedure which unfortunately requires starting from scratch whenever a new substituent is desired. We completed the synthesis of several advanced intermediates towards universally functionalizable CPP monomers which contain different "masking groups" that can be unveiled to yield reactive CPP monomers. We are also continuing the exploration of molecular templating approaches to join two CPP rings non-covalently as a starting point for mechanically conjugated polymers. Computational modeling is also being used to identify new arene units for inclusion to the CPP core that might further extend the extent of radial conjugation throughout the linear-radial pi-conjugted materials, enhance possible open shell radical character throughout these networks,[5] or add elements of anti-aromaticity within the radial pathway.

References

1. G. M. Peters, G. Grover, R. Maust, C. Colwell, H. Bates, W. Edgell, R. Jasti, M. Kertesz, and J. D. Tovar, *Linear and radial conjugation in extended pi-electron systems*, Journal of the American Chemical Society **142**, 2293-2300 (2020).

2. E. Peterson, R. L. Maust, R. Jasti, M. Kertesz and J. D. Tovar, *Splitting the ring: impact of ortho and meta pi conjugation pathways through disjointed [8]cycloparaphenylene electronic materials*, Journal of the American Chemical Society **144**, 4611-4622 (2022).

3. M. S. Hybertsen and L. Venkataraman, *Structure-Property Relationships in Atomic-Scale Junctions: Histograms and Beyond,* Accounts of Chemical Research **49**, 452-460 (2016)

4. R. Bhattacharjee and M. Kertesz, *Continuous Topological Transition and Bandgap Tuning in Ethynylene-Linked Acene Pi-Conjugated Polymers Through Mechanical Strain,* Chemistry of Materials **26**, 1395-1404 (2024)

5. B. C. Streifel, J. L. Zafra, G. L. Espejo, C. J. Gómez-García, J. Casado, and J. D. Tovar, *An unusually small singlet-triplet gap in a quinoidal 1,6-methano[10]annulene due to Baird's 4n pi-electron triplet stabilization*, Angewandte Chemie International Edition **54**, 5888-5893 (2015)

Publications

1. E. Peterson, R. L. Maust, R. Jasti, M. Kertesz and J. D. Tovar, *Splitting the ring: impact of ortho and meta pi conjugation pathways through disjointed [8]cycloparaphenylene electronic materials*, Journal of the American Chemical Society **144**, 4611-4622 (2022).

2. G. Grover, J. D. Tovar, and M. Kertesz, *Quinonoid versus Aromatic π-Conjugated Oligomers and Polymers and Their Diradical Characters*, The Journal of Physical Chemistry C **126**, 5302-5310 (2022).

3. R. Bhattacharjee and M. Kertesz, *Continuous Topological Transition and Bandgap Tuning in Ethynylene-Linked Acene Pi-Conjugated Polymers Through Mechanical Strain,* Chemistry of Materials **26**, 1395-1404 (2024)

7.

Ionic-Dipolar Interactions in Poly(Ionic Liquid)s

Marek W. Urban, Department of Materials Science and Engineering, Clemson University, Clemson SC 29634

Keywords: dipolar-ionic interactions, polymers, poly(ionic liquids) (PILs),

Research Scope

There are three primary objectives of the proposed program: (1) design and synthesize a new platform of PIL copolymers with precisely positioned anion-cation (A-C), dipole-dipole (D-D), dipole-induced dipole (D-ID), and induced dipole-induced dipole (ID-ID) interactions; (2) determine the magnitude of inter- and intra-chain interactions as a function of the position of A-C pair with respect to copolymer backbone and side groups; (3) elucidate the origin of molecular processes that govern A-C, D-D, D-ID, and ID-ID interactions in the presence and absence of alternating current (AC) electric fields (EF).

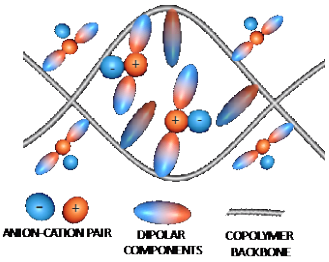

Fig 1. A-C, D-D, D-ID, and ID-ID interactions in a PIL copolymer.

Recent Progress

Although there are ubiquitous interactions within polymer chains governed by dipolar or ionic forces, their origin and magnitude are not well defined. These interactions, encompassing dipole-dipole, dipole-ion, or dipole-induced dipole forces arising from electron distributions around covalently bonded atoms, are critical contributors to mechanical strength, electrical conductivity, or responsiveness to external stimuli, to name just a few.[1-3] To investigate the impact of hydrophobic tail length on PIL interactions, a series of copolymers were synthesized using 1-[(2-methacryloyloxy)propyl]-3-R-imidazolium bis(trifluoromethyl-sulfonyl)imide (Im-R-TFSI) monomers with varying alkyl chain lengths (R = C1-C4) along with 2,2,2-trifluoroethyl methacrylate (TFEMA) (Fig. 2A). These materials were prepared for the first time. The primary motivation was to

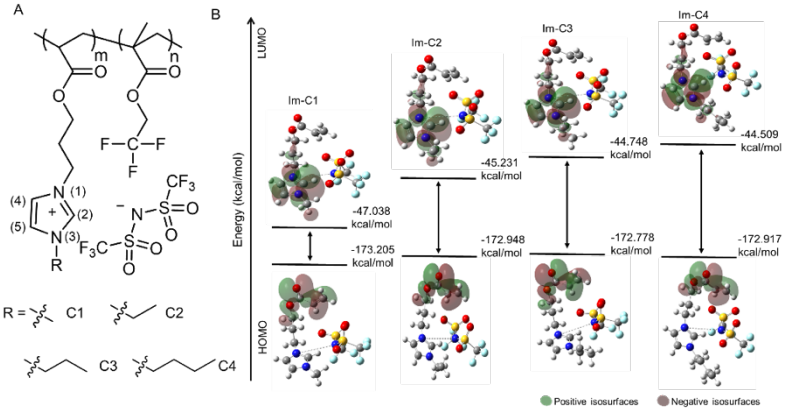

Fig. 2. (A) Repeating unit of p(Im-RTFSI/TFEMA) copolymer (R = C1 (methyl), C2 (ethyl), C3 (propyl), and C4 (butyl); (B) Pictorial representation of HOMO–LUMO energy gaps for highest occupied molecular orbital (HOMO) and lowest unoccupied molecular orbital (LUMO) in Im-C1, Im-C2, Im-C3, and Im-C4 monomers.

maintain the ionic character of monomers by using specific cation-anion pairs while systematically varying hydrophobic tails attached to the cation. The unique discovery was the influence of the length of aliphatic side groups on dipolar and ionic interactions. The energy density changes on the N(3) atom of the Im ring and the C-H tails adjacent to N(3) increase for longer aliphatic tails. At the same time, the LUMO-HOMO energy gaps increase (Fig. 2B). These studies showed that the length of C1-C4 tails affects the electron density distribution of the cation-anion surroundings. Using 2-dimensional correlation (2D COS) FT-IR spectroscopy, dynamics of structural changes were assessed and revealed that longer hydrophobic tails (C2-C4) promote stronger dipolar and van der Waals (vdW) interactions than shorter tails (C1). 2D FT-IR COS measurements identified specific changes in inter-chain distances reflected by molecular vibrations. This behavior was attributed to the flexibility and enhanced segmental mobilities of longer aliphatic tails. MD simulations further confirmed the formation of multi-ion pair clusters in longer aliphatic tail copolymers, thus affecting their electrical responses and self-healing capabilities (Fig. 3). This is also reflected in the energetic contributions of vdW and electrostatic (ES) forces to intra- and inter-chain interactions. These data also showed that inter-chain ES energy is independent of the length of the aliphatic tails. Even more intriguing was how these groups responded to the perturbations; longer aliphatic tails (C2-C4) responded first, followed by the cation-anion pairs, whereas short tails (C1) responded last. In summary, two inter-related events attributed to the length of the aliphatic tails were identified: (1) dipole-dipole C-H (R) ⇔ C-H (R) inter-chain interactions of aliphatic tails and (2) the formation of cation-anion channels. Using physical (electrical and mechanical) and controllable chemical perturbations, ubiquitous dipole-dipole and cation-anion interactions and their dynamics provide favorable environments that impact as conductivity and the ability to recover from external perturbations. Further understanding is crucial for identifying the magnitude of these interactions. Ongoing efforts are underway to test the hypothesis of how perturbations of dipolar forces in the presence of ionic components with variable monomer molar ratios. Also, the way in which the perturbation of copolymers by temperature, pressure, and electric fields influences the dipolar and ionic interactions is examined. By precisely positioning cations in ILs between the spacer and terminal aliphatic ends, these studies also showed how minute chemical changes in aliphatic tails covalently bonded to ionic groups induce significant inter- and intra-chain vdW and polar forces.

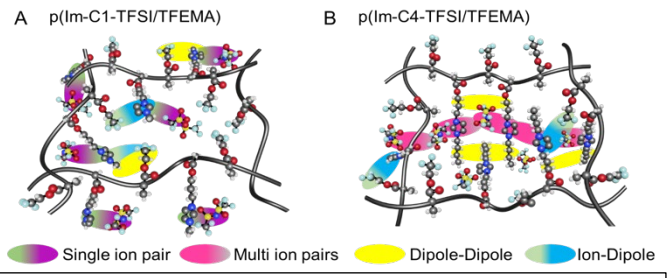

Fig. 3. Pictorial representation of single (p(Im-C1-TFSI/TFEMA)) and multiple (p(Im-C4-TFSI/TFEMA) cation–anion pair channels in the presence of dipole–dipole and ion–dipole interactions.

References

1. M.W. Urban, D. Davydovich, Y.Yang, T. Demir, Y. Zhang, and L. Casabianca, *Key-and-lock commodity self-healing copolymers*. Science **362(6411)**, 220−225 (2018).
2. S. Gaikwad, M.W.Urban, *Ring-and-Lock Interactions in Self-Healable Styrenic Copolymers*, J. Am. Chem. Soc., **145(17)** 9693−9699 (2023).
3. J. Liu and M.W. Urban, *Dynamic Interfaces in Self-Healable Polymers,* Langmuir **40**, 7268−7285 (2024).

Publications

1. J. Liu, S. Biswas, and M.W. Urban, *Dynamics of Dipolar and Ionic Interactions in Self-Healable Poly(ionic liquid) Copolymers,* Macromolecules **57(12**), 5831-5837 (2024).
2. J. Liu and M.W. Urban, *Dynamic Interfaces in Self-Healable Polymers,* Langmuir **40**, 7268−7285 (2024)
3. S. Gaikwad and M.W. Urban, *Fluorophilic Sigma(σ)-Lock Self-Healable Copolymers*, Angew. Chem. Int. Ed. e202405504 (2024).

Pi-Extended Porphyrins: The Impact of Aromatic Heterocycles on the Properties of the Largely Pi-Extended Structures

Hong Wang, Francis D'Souza, Department of Chemistry, University of North Texas

Keywords: Pi-Extended Porphyrins, Aromatic Heterocycles, Oligomers, Charge Transfer/Separation, Transient Spectroscopy

Research Scope

This proposed research aims to develop new synthetic strategies and methods for largely pi-extended porphyrins fused with aromatic heterocycles, which are underdeveloped currently.[1-4] The development of new synthetic methods is the key to facilitate the growth of this field. The purpose of this proposed project is threefold. First, we will develop concise and versatile synthetic methods to fuse heterocycles to porphyrin. Second, we will use these methods to design different types of heterocycle-fused porphyrins including porphyrins fused with phenanthroline-based heteroacenes, porphyrins fused with 5-, 6- and 7-membered N-heterocycles, and porphyrins fused with naphtho-dithiophene, -difuran and -dipyrrole. Third, we will study their optical-, electronic-, and photophysical properties using UV-Vis/fluorescence spectroscopy, cyclic voltammetry, femtosecond and nanosecond transient absorption spectroscopy, and DFT/TDDFT/NICS calculations. The excited-state dynamics including their singlet and triplet states, charge transfer, and charge separation will be studied to identify new systems for energy-related applications. We will identify specific factors influencing their electronic, optical, and aromatic properties in each type of fused system and establish structure-property relationships for future development.

The proposed aromatic heterocycle incorporated pi-extended systems represent novel functional structures in materials science. The synthetic methods developed in this proposal will pave the way to open new opportunities in materials science and will significantly expand the current scope of this emerging field. The success of this project is expected to provide important information on guiding new materials design, leading to new advances in fundamental science.

Recent Progress

We have successfully designed and synthesized a number of novel classes of pi-extended porphyrins including benzoimidazo-isoindoles-,[5,6] naphthodithiophene-,[7] azepine-,[8] (pentacene-6,13-diylidene)dimalononitrile-,[9] and cyclooctatetraene-fused porphyrins.[10] Unprecedented electronic and photophysical propertied have been revealed for these new compounds. For examples, azepine-fused porphyrin displayed unusually short fluorescence lifetime (0.7 ns) and long phosphorescence lifetime (132 ms), noting that the fluorescence and phosphorescence lifetime for conventional free base porphyrins is 9-12 ns and 20-30 ms, respectively. Efficient excited state charge transfer (CT) was unveiled in (pentacene-6,13-diylidene)dimalononitrile-fused porphyrins and cyclooctatetraene-porphyrins. These data suggest unconventional excitation

state dynamics, the investigation of which will advance the basic knowledge in photochemistry, leading to new opportunities in solar energy related applications. In the past two year, we particularly focused on developing and understanding a donor-acceptor molecular system involving benzoimidazo-isoindole-fused porphyrins as the donor and C_{60} as the acceptor, for which an exceptionally long-lived charge separation (CS) state (37.4 □s) (Figure 1, A) was established.[5,6] The exceptionally long-lived CS state was attributed to the formation of ^{3}CT through spin-orbit charge transfer intersystem crossing (SOCT-ISC), which suggest the existence of a new mechanism paradigm for CS and charge combination (CR) dynamics/kinetics/thermodynamics. We have also developed porphyrin oligomers including dimers and trimers based on benzoimidazo-isoindole-fused porphyrins (Figure 1, B & C). While ZnD1-C_{60} exhibited long-lived CS state (~30-40 ms), ZnFBD1 system displayed efficient singlet-singlet energy transfer (>95% efficiency).[6] Interestingly, no charge separation in ZnFBD1-C_{60} system was observed wherein excitation transfer dominated the process. Different scenario occurred in the trimer system. Zn-Trimer-1 showed strong exciton coupling and titration of Zn-rimer-1 with C_{60} suggested cooperativity of the three porphyrin components, which is in sharp contrast to that was observed with ZnD1-C_{60} system. These results showcase the significant impact of heteroatom/heterocycles and the importance of the conjugated π-spacer in governing the energy and electron transfer events.[11,12]

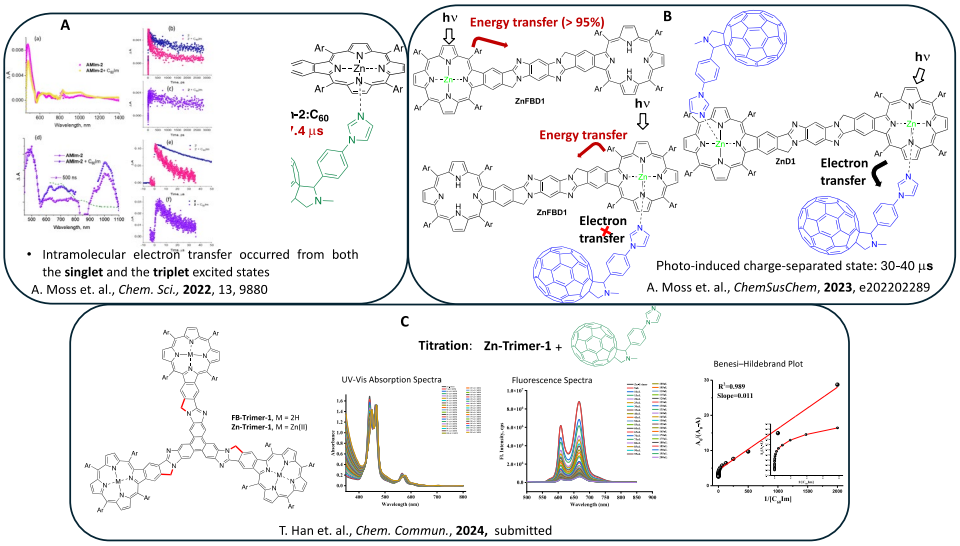

Figure 10 *Benzoimidazol-isoindole-fused porphyrins. A: Monomer, B: Dimer, C:*

We have also started a new research direction to develop covalent organic frameworks derived from pi-extended porphyrins. Our preliminary studies on donor-acceptor COFs have revealed their semiconducting nature with band gaps of 1.54 - 1.63 eV. Exceptionally high optical conductivity (1 S/m - 2 S/m (at 1THz)) was obtained for these COFs using temperature resolved THz-transmission measurements. These preliminary data promise the great potentials to introduce pi-extended porphyrins as building blocks to COFs and other types of polymers.

References

1 X. Wang, G. Sun, P. Routh, D.-H. Kim, W. Huang and P. Chen*, Heteroatom-doped graphene materials: syntheses, properties and applications*, Chem Soc Rev **43**, 7067-7098 (2014).

2 S. Kawai, S. Nakatsuka, T. Hatakeyama, R. Pawlak, T. Meier, J. Tracey, E. Meyer, A. S. Foster, *Multiple heteroatom substitution to graphene nanoribbon*, Sci. Adv. **4**: eaar7181 (2018).

3 X. Y., Wang, X. Yao, A. Narita, and K. *Mullen, Heteroatom-Doped Nanographenes with Structural Precision,* Acc Chem Res **52**, 2491-2505 (2019).

4 C. Hu, D. Liu, Y. Xiao, and L. Dai, *Functionalization of graphene materials by heteroatom-doping for energy conversion and storage,* Progress in Natural Science: Materials International **28**, 121-132 (2018).

5 A. Moss, Y. Jang, J. Arvidson, V. N. Nesterov, F. D'Souza and H.Wang*, Aromatic heterobicycle-fused porphyrins: impact on aromaticity and excited state electron transfer leading to long-lived charge separation*, Chem. Sci. **13**, 9880-9890 (2022).

6 A. Moss, Y. Jang, H. Wang and F. D'Souza, *Porphyrin Dimers with Conjugated Linker Exhibiting Charge-Transfer and Excitonic Coupling Characteristics*, ChemSusChem **16***, e202202289* (2023).

7 C. Cooper, R. Paul, A. Alsaleh, S. Washburn, W. Rackers, S. Kumar, V. N. Nesterov, F. D'Souza, S. A. Vinogradov, H. Wang, *Naphthodithiophene-Fused Porphyrins: Synthesis, Characterization, and Impact of Extended Conjugation on Aromaticity,* Chem. Eur. J. **29**, e202302013. (2023).

8 S. Shaikh, C. Tang, R. Kaswan, F. D'Souza and H. Wang, *Azepine-fused porphyrins: the investigation of unusual excited state kinetics and theromodynamics,* unpublished results.

9 R. Kaswan, S. Washburn, U. Oji, H. Wang and F. D'Souza, *Tetracyanopentacenequinone-Fused Porphyrins: Investigation of the Effects of Cyano Groups on Fully Conjugated Donor and Acceptor*, *Chem. Sci.*, to be submitted (2024).

10 S. Shaikh, A. Alsaleh, C. Tang, F. D'Souza and H. Wang, *COT-Fused Porphyrins: Unusual Ring Dynamics Causing Reversal Trend Charge Transfer*, manuscript *to be submitted* (2024).

11 M. Stepien, E. Gonka, M. Zyla and N. Sprutta*, Heterocyclic Nanographenes and Other Polycyclic Heteroaromatic Compounds: Synthetic Routes, Properties, and Applications*, Chem. Rev. **117**, 3479-3716 (2017).

12 Y. Gu, Z. Qiu, K. Mullen, *Nanographenes and Graphene Nanoribbons as Multitalents of Present and Future Materials Science*, J. Am. Chem. Soc. **144**, 11499-11524 (2022).

Publications

1. T. Han, Y. Jang, J. Arvidson, F. D'Souza, H. Wang, *Optical and photophysical properties of platinum benzoporphyrins with C2v and D2h symmetr,* J. Porphyrins Phthalocyanines **26**, 458-468 (2022).
2. A. Moss, Y. Jang, J. Arvidson, V. N. Nesterov, F. D'Souza and H. Wang, Aromatic Heterobicycle-Fused Porphyrins: Impact on Aromaticity and Excited State Electron Transfer Leading toLong-Lived Charge Separation, Chem. Sci. **13**, 9880-9890 (2022). Highlighted in Inside **Cover Page**. This has been selected by the Editors of Chemical Science for inclusion in the new collection on **Emerging Frontiers in Aromaticity**.
3. A. Moss, D. E. Nevonen, Y. Hu, V. N. Nesterov, V. Nemykin and H. Wang, Unsymmetric Pentacene- and Pentacenequinone-Fused Porphyrins: Understanding the Effect of Cross- and Linear-Conjugation, ACS Phys. Chem. Au **2**, 468-481 (2022).
4. A. Moss, Y. Jang, H. Wang, F. D'Souza, *Porphyrin Dimers with Conjugated Linker Exhibiting Charge-Transfer and Excitonic Coupling Characteristics,* ChemSusChem **16** (8), e202202289 (2023). This has been selected by the Editors of ChemSusChem for inclusion in **Advances in Engineering series**.
5. S. Washburn, R. Kaswan, S. Shaikh, A. Moss, F. D'Souza and H. Wang, *Excited State Charge Transfer in Push-Pull Platinum (II) pi-Extended Porphyrins Fused with Pentacenequinone*, J. Phys. Chem. A. **127** (43), 9040-9051 (2023).
6. C. Cooper, A. Alsaleh, S. Kumar, W. Rackers, V. N. Nesterov, F. D'Souza, S. A. Vinogradov and H. Wang, *Naphthodithiophene-Fused Porphyrins: Synthesis, Characterization, and Impact of Extended Conjugation on Aromaticity*, Chem. Eur. J. **29** (57), e202302013 (2023).
7. S. G. Moorthy, J. Arvidson, R. Meunier-Prest, H. Wang, M. Bouvet, Light Effect on Ammonia Sensing Properties of p-Extended Porphyrin-Phthalocyanine Heterojunction Devices, ACS Sens **9** (2), 883-894 (2024).
8. T. Han, P. Sharma, N. Khetrapal and H. Wang, *Cyclically Conjugated Porphyrin Trimers Linked through Aromatic Heterocycles*, submitted to Chem. Commun. (2024), invited paper for contribution to a Special Anniversary (60th) Collection of Chemical Communications.

Electric field-controlled solid sorbent for direct air capture

Claire White, Princeton University

Keywords: LDH, CO_2, capture, plasma, regeneration

Research Scope

There is a dire need to reduce atmospheric carbon dioxide (CO_2) concentrations due to the known link between the recent rise in CO_2 concentrations and increasing global temperatures [1]. One approach that is being actively pursued to reduce atmospheric CO_2 concentrations is direct air capture (DAC) [2]; however, this approach is currently cost prohibitive using existing technologies due to the challenges of removing dilute amounts of CO_2 from air, part of which is attributed to the large energy demands of sorbent regeneration. Thus, fundamental research is required to create new sorbent materials and explore novel methods of regeneration.

This project seeks to combat the cost and energy limitations of DAC by developing a novel solid sorbent that is actively controlled by an applied electric field during CO_2 capture and material regeneration. By utilizing abundant, inexpensive materials for synthesis of the Ca-based layered double hydroxide (LDH) sorbent, the overall cost is reduced [3], and the use of renewable electricity has the potential to significantly reduce energy demands for material regeneration. The objectives of this project are to: (i) uncover the fundamental chemical processes controlling CO_2 capture and release on Ca-based LDH from dilute CO_2 sources, and the impact of water vapor, (ii) explore how low-temperature plasma (LTP)-generated electric fields affect these chemical processes, (iii) augment capture behavior by tailoring the chemical composition and associated electron density of the LDH, and (iv) determine the viability of electric field-controlled CO_2 release as a means of material regeneration. This project will utilize a synergistic simulation-experiment approach that exploits the predictive power of atomistic simulations with operando X-ray and neutron scattering, and spectroscopy techniques. These high-fidelity simulations will exploit DOE high performance computing resources, while operando experiments will be performed at DOE synchrotron and neutron facilities. These approaches will be complemented by findings from plasma diagnostic tools, and downstream gas phase composition from mass spectrometry.

The potential impact of this project centers on the use of high-voltage electric fields generated by low-temperature plasmas for enhancing DAC, and thus will contribute to increasing its technological feasibility and economic viability. Due to the increase of renewable electricity production in the U.S. and associated intermittency, the use of low-temperature plasmas for CO_2 capture provides an ideal solution that will actively utilize excess electrons during peak production periods.

Recent Progress

The effect of relative humidity (RH) on CO_2 uptake by the sorbent has been investigated. Two sorbent materials were synthesized, $Ca_2Fe(OH)_6Cl{\cdot}2H_2O$ and $Ca_2Al(OH)_6Cl{\cdot}2H_2O$ (denoted CaFeCl and CaAlCl LDH, respectively) using a recently developed environmentally friendly one-pot synthesis method [4]. Figure 1 shows inelastic neutron scattering (INS) data for CaFeCl sample at different relative humidities before and after CO_2 exposure. The low (0%) RH sample had little uptake of CO_2 and showed little change in the INS spectrum. By contrast, the high (100%) RH sample had large uptake of CO_2 (~4 mmol/g) with the spectrum showing loss of modes associated with lattice vibrations and OH units after 11 h of CO_2 exposure, resulting in a spectrum of amorphous H_2O [5]. Subsequent molecular simulations using density functional theory (DFT) found the reaction: $Ca_2Fe(OH)_6Cl{\cdot}2H_2O + 2CO_2 \rightarrow 2CaCO_3 + 0.5Fe_2O_3 + HCl + 4.5H_2O$ to be exothermic based on the formation energies of each species, with $CaCO_3$ confirmed from X-ray diffraction and amorphous Fe_2O_3 assumed as the Fe species based on X-ray photoelectron spectroscopy data. Complementary data using *in situ* X-ray PDF analysis will shed light on the evolution of non-crystalline phases during CO_2 capture.

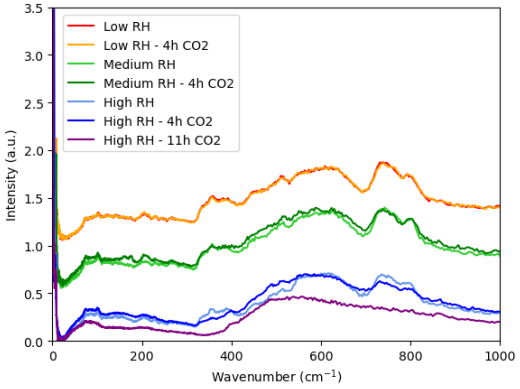

Figure 1. CO_2 dosing CaFeCl LDH at different relative humidity (RH) levels. Measurement temp. of 20K

Following the determination of calcite formation occurring in CO_2 uptake of LDHs at high RH levels, we have also investigated sorption of CO_2 on LDH-derived mixed metal oxides (MMOs) due to the postulated lower binding energy of CO_2 being potentially preferable for cyclability of a DAC sorbent. MMOs form as an amorphous material when an LDH is calcined at ~300-500 °C, whereby the LDH first loses interlayer water molecules at ~100 °C followed by hydroxyl groups at ~275 °C. We have been exploring the behavior of LDH-derived MMOs through *in situ* diffuse reflectance infrared Fourier transform spectroscopy (DRIFTS) coupled with mass spectrometry analysis of gas outflow, and have collected complementary X-ray PDF data. Figure 2 shows the change in DRIFTS spectrum from a baseline CaFeCl MMO spectrum during exposure to dry CO_2. We are currently installing a low-temperature plasma capability to explore regeneration of the sorbent material.

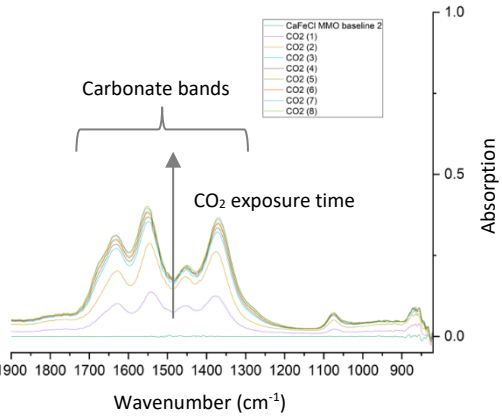

Figure 2. DRIFTS spectrum of net changes to CaFeCl MMO sample during dry CO_2 exposure.

References

1. *Climate Change 2023: Synthesis Report*, IPCC, (2023).
2. N McQueen et al. *A review of direct air capture (DAC): scaling up commercial technologies and innovating for the future* Prog. Energy **3**, 032001 (2021).
3. M. C. Curria and C. E. White, *Synthesis and characterization of Ca-based layered double hydroxides as solid sorbents for carbon capture*, GHGT-15, 1-7, (2021).
4. M. C. Curria and C. E. White, *Mechanistic insights on solution-based green synthesis of phase-pure Ca-based layered double hydroxides from $Ca(OH)_2$*, Cryst. Growth Des. **24**, 56-70 (2024).
5. D. D. Klug et al. *Dynamics and structural details of amorphous phases of ice determined by incoherent inelastic neutron scattering*, Phys Rev. Lett. **83**, 2584-2587 (1999).

Publications

N/A

The Role of Local Structure and Dynamics on Proton and Hydroxide Transport in Ion-Conducting Polymers

Karen I. Winey (PI)[1], Amalie L. Frischknecht[2], Michael A. Hickner[3], Justin G. Kennemur[4]

[1] University of Pennsylvania, [2] Sandia National Laboratories, [3] Michigan State University, [4] Florida State University

Keywords: ring opening metathesis polymerization, proton conduction, hydroxide conduction, atomistic molecular dynamics simulations, IR and NMR spectroscopy

Research Scope

We aim to reveal the local structures and dynamics that underlie fast proton and hydroxide transport in fluorine-free polymers with fully saturated carbon backbones and functional groups tethered to the backbone by phenyl or alkyl linkages. We are developing cyclopentene-based ROMP and functionalization methods to produce terpolymers with either sulfonic acid or quaternary ammonium groups for synergistic comparisons between the proton and hydroxide transport mechanisms. Characterization of these terpolymers at known water contents will include IR and NMR spectroscopies, electrical impedance spectroscopy, and X-ray scattering. Atomistic molecular dynamics simulations will augment our characterization methods with direct comparisons.

Recent Progress

Simulations of Hydrated Terpolymers: We previously showed that a fully sulfonated homopolymer (p5PhSH) had excellent proton conductivity when hydrated due to its morphology of nanophase separated, continuous hydrophilic domains.[1] To improve the mechanical properties of these ROMP-synthesized polymers, we explored reducing the level of sulfonation and introducing short polyethylene segments. In our recent publication[2], we performed atomistic molecular dynamics (MD) simulations on 14 terpolymers containing p5PhSA along with two hydrophobic units, unsulfonated p5Ph segments and p5 segments, **Fig. 1**. Eight compositions form continuous, percolating hydrophilic domains at a water content of 9 waters per sulfonic acid (filled symbols). Water diffusion constants increase linearly with increasing ion content and correlated to the morphological characteristics (fractal dimension, interfacial area per sulfonate group, and water channel width) of these swollen terpolymers. The simulation results suggest that future terpolymer synthesis should focus on polymers with IEC > 2 mmol/g to produce percolated, continuous hydrophilic domains.

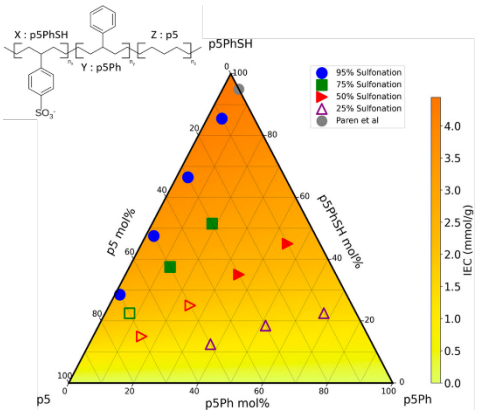

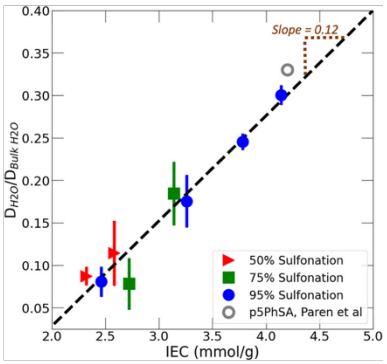

Fig. 1: Terpolymers and ternary phase diagram indicating the X:Y:Z composition simulated at λ = 9. The water diffusion coefficient correlates strongly with IEC.

Experiments and Simulations of Hydrated Copolymers: Copolymers of p5PhSH and p5Ph were prepared by an in-depth study exploring the use of acetyl sulfate as a soft and homogeneous sulfonation method.[3] Our all-atom molecular dynamics simulations find percolated water channels at levels of sulfonation $Y \geq 50\%$ and □ ≥ 6, and the characteristic length scale (d) is in excellent agreement with X-ray scattering, **Fig. 2**.[4] The measured proton conductivity at □ ≥ 6 exceeds 0.10 S/cm when $Y \geq 60\%$. Fractal dimensions from the simulations correlate well with water diffusion coefficients measured by simulations and by ^{1}H NMR. Ongoing work uses IR, NMR and MD simulations to understand how the local environment impacts conductivity.

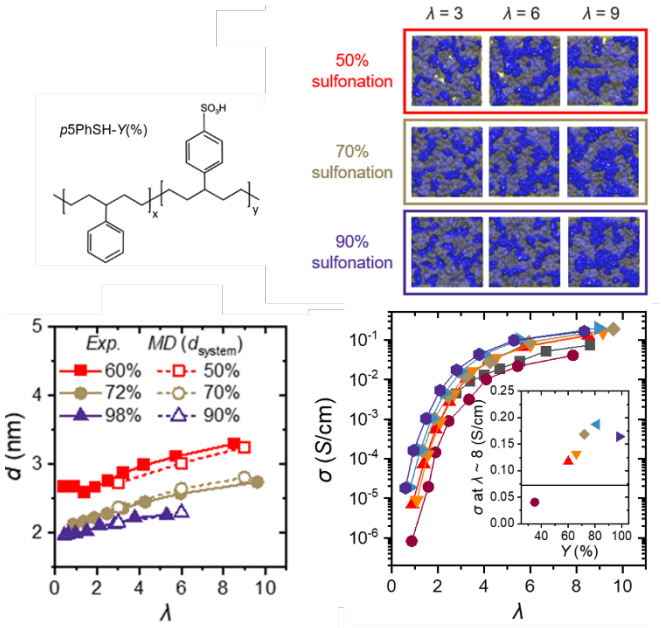

Fig. 2: Chemical structure of copolymers and all atom MD simulations showing percolated structures at λ ≥ 6. Proton conductivity increases with λ.

Polymers for Hydroxide Conductivity: From a cyclopentene functionalized with a carboxylic acid, we have developed a synthetic route to a precise polyethylene with a quaternized ammonium on every 5th carbon, **Fig.3**.[5] This modular system allows the installation of commercially available trialkylamines (R, R', R'') to probe structure and function. Initial all-atom MD simulations find percolated water channels in both the trimethyl and dimethylhexyl compounds at □ ≥ 10.

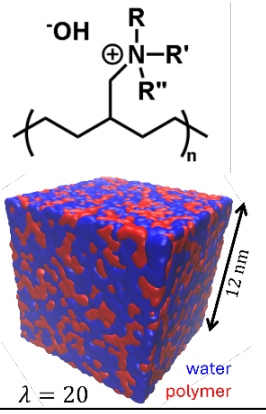

Fig. 3: New polymers for OH- conductivity.

References

1. B. A. Paren, B. A. Thurston, A. Kanthawar, W. J. Neary, A. Kendrick, M. Maréchal, J. G. Kennemur, M. J. Stevens,* A. L. Frischknecht,* and K. I. Winey*, *Fluorine-free Precise Polymer Electrolyte for Efficient Proton Transport: Experiments and Simulations*, Chemistry of Materials, **33**, 6041 (2021).

2. M. Win, K. I. Winey*, and A. L. Frischknecht *, *Morphology-Diffusivity Relationships in Fluorine-free Random Terpolymers for Proton Exchange Membranes*, Macromolecules, **56**, 9905 (2023).

3. C. M. Leo, S. Alonzo, E. Grumbles, J. G. Kennemur*, *Sulfonated aromatic polypentenamers - Scope of the acetyl sulfate reaction*." submitted to Macromolecules on May 2024.

4. S. M. Oh, W. F. Drayer, V. Lee, M. S. Win, C. M. Leo, E. Grumbles, J. G. Kennemur, A. L. Frischknecht*, K. I. Winey*, *Enhanced transport and mechanical properties of fluorine-free random copolymers achieved at optimal sulfonation levels*, manuscript drafted.

5. J. G. Kennemur, N. Z. Singleton *Modular Polypentenamers for Direct Functionalization* US Provisional Patent Appl 63/567,380. Filed: March 19, 2024.

Publications since start of the grant on August 15, 2022

1. M. Win, K. I. Winey*, and A. L. Frischknecht *, *Morphology-Diffusivity Relationships in Fluorine-free Random Terpolymers for Proton Exchange Membranes*, Macromolecules, **56**, 9905 (2023).

2. C. M. Leo, S. Alonzo, E. Grumbles, J. G. Kennemur*, *Sulfonated aromatic polypentenamers - Scope of the acetyl sulfate reaction*." submitted to Macromolecules on May 2024.

3. S. M. Oh, W. F. Drayer, V. Lee, M. S. Win, C. M. Leo, E. Grumbles, J. G. Kennemur, A. L. Frischknecht*, K. I. Winey*, *Enhanced transport and mechanical properties of fluorine-free random copolymers achieved at optimal sulfonation levels*, manuscript drafted.

Polyolefin Upcycling Through Dehydrogenation and Functionalization

Karen I. Winey (PI)[1], E. Bryan Coughlin[2], Raymond J. Gorte[1], Daeyeon Lee[1], Karen I. Goldberg[1], Marisa C. Kozlowski[1], and John M. Vohs[1].

[1] University of Pennsylvania, [2] University of Massachusetts (Amherst)

Keywords: polymer upcycling, dehydrogenation, click chemistry, associating polymers

Research Scope

Our multidisciplinary team endeavors to reduce plastic waste by developing the chemical routes to convert polyethylenes (PEs) into a variety of high-value specialty polymers, **Fig. 1**. Our approach to converting PE waste involves (1) maintaining their high degree of polymerization throughout the conversion and (2) employing energy-efficient and environmentally-friendly reactions. Aim 1 seeks homogeneous and heterogeneous catalysts and reaction conditions to partially dehydrogenate PE (< 5%) with minimal chain scission. Aim 2 explores a variety of synthetic strategies to functionalize carbon-carbon double bonds. Aim 3 works to add chemical functionality directly to PE. This extended abstract focuses on Aim 2 and uses poly(cyclooctene) (PCOE) as a model for partially de-hydrogenated HDPE.

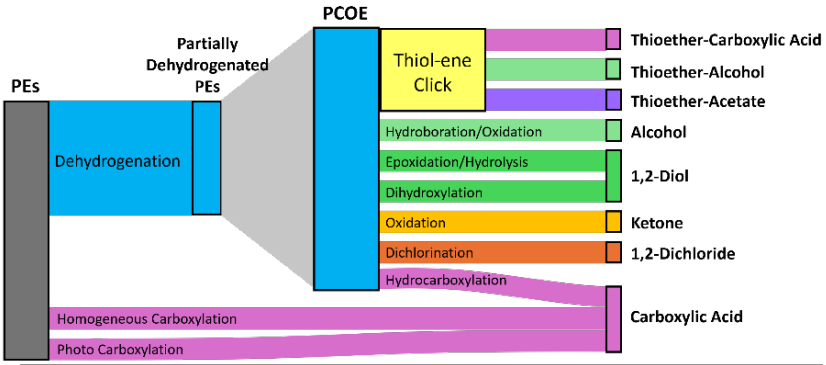

Fig. 1: Project overview illustrating the range of chemistries.

Recent Progress

Thiol-ene Click Reactions. Previously, we demonstrated thiol-ene click chemistry as a means for attaching alcohol groups onto PCOE to generate a linear version of poly(vinyl alcohol) will good adhesive properties.[1] This synthetic route has been expanded to add carboxylic acid[2] and thioacetate functionality.[3] The separation between the backbone and the carboxylic acid functionality as well as the level of functionality were systematically varied to control the rubbery moduli. Electrochemical impedance spectroscopy experiments revealed distinct polymer relaxations for the sulfur linages near the backbone (~ 25 kJ/mol) and the H-bonding relaxation (~ 6 kJ/mol), **Fig. 2**.[4]

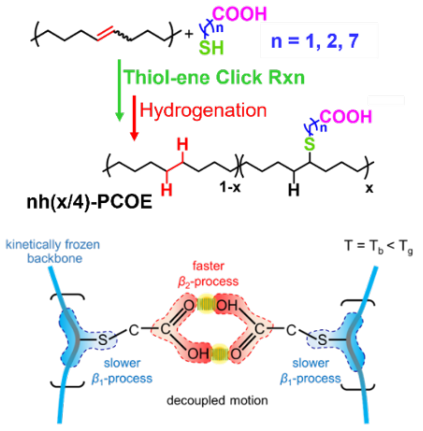

Fig. 2: Acid-functionalized PEs via thiol-ene click reactions.

Hydrocarboxylation Reaction. A palladium catalyst at moderate conditions effectively functionalizes PCOE and the level of carboxylic acid incorporation into the polymer was readily controlled by varying the reaction time.[5] Hydrogenation removes the remaining unsaturation. Consistent with poly(ethylene-*co*-acrylic acid) copolymers, the level of crystallization and the melting temperature decreased with additional acid content.

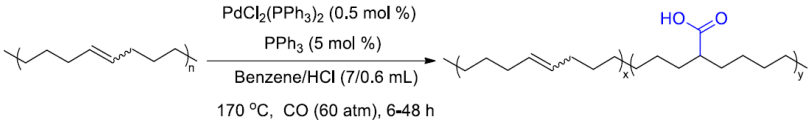

Poly(vinyl alcohol)s and Polydiols. In addition to the thiol-ene click chemistry, we have developed a variety of chemistries to install alcohol functionality on linear PCOE. Using a two-step one-pot method involving hydroboration followed by oxidation and then hydrogenation to remove unsaturation, we achieved levels of OH functionalization (*m*) from 0 to 23%.[6] With increasing -OH content the crystalline structure evolved from orthorhombic to hexagonal packing with a peak at $Q = 0.6$ Å^{-1} indicating the pseudo precise placement of the -OH groups. Interestingly, the measured water contact angle correlates with the -OH content in the amorphous phase, **Fig. 3**. More recently, we have developed synthetic routes to install -OH on adjacent carbons in PCOE via epoxidation followed by acid-catalyzed ring-opening (*erythro*) and via dihydroxylation (*threo*).[7] These linear polyethylene diols have distinct crystal structures and fail to co-crystallize.

N_2O Deconstructs and Installs Ketone Functionality on PCOE. N_2O, a greenhouse gas and a byproduct from nylon monomer synthesis, efficiently deconstructs PCOE while installing carbonyl groups.[8] By balancing the deconstruction and the ketone functionalization, the ketones could be further elaborated to produce functional polymers. The molecular weight and ketone content of the macromonomers are controlled with reaction time. Any remaining alkenes were readily saturated by hydrogenation. Additionally, the level of ketone functionalization is tuned by varying the carbon-carbon double bond content of the starting polymers; this result highlights that the reaction could be compatible with partially dehydrogenated PEs even with low levels of unsaturation.

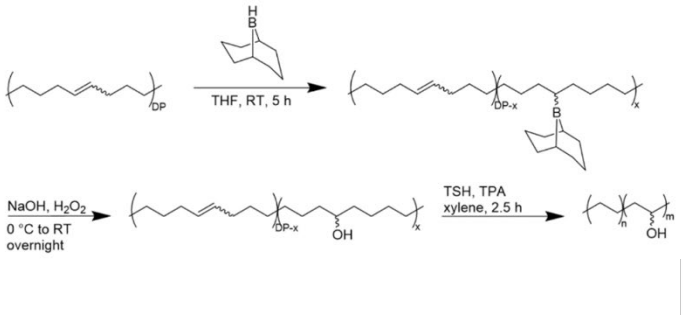

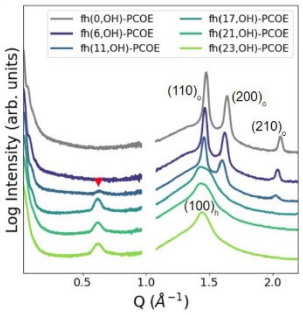

Fig. 3: Linear poly(ethylene-co-vinyl alcohol) from PCOE. X-ray scattering as a function of -OH content.

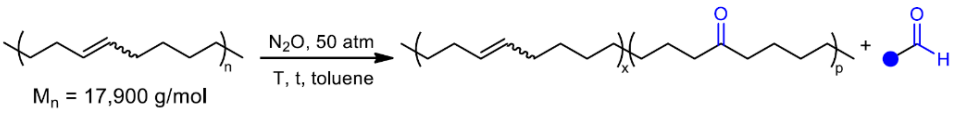

References

1. R. John Chethalen, E. J. Fastow, E. B. Coughlin*, K. I. Winey*, *Thiol–ene click chemistry incorporates hydroxyl functionality on polycyclooctene to tune properties*, ACS Macro Letters **12**, 107 (2023).
2. E. J. Fastow, R. John Chethalen, E. B. Coughlin*, K. I. Winey*, *Thiol-ene click chemistry incorporates carboxylic acid-terminated alkane pendants on polycyclooctene to tune properties*, Giant **17**, 100231 (2024).
3. R. John Chethalen, M. Kim, J. Correa Ruiz, C.-H. Tu, J. Gray, K. I. Winey*, A. Crosby*, E. B. Coughlin*, *Incorporation of thioacetate pendants on a polyalkenamer enables high extensibility*, manuscript drafted.
4. C.-H. Tu, E. J. Fastow, R. John Chethalen, G. Papamokos, E. B. Coughlin, K. I. Winey*, *Coupling-Decoupling between Fast Stickers and Slow Backbones in Associating Polymers with Side-Chain Terminal-Functionalization*, manuscript resubmitted to Macromolecules on July 11, 2024.
5. I. M. Ogbu, E. J. Fastow, W. Zhu, L. A. Wells, R. J. Chethalen, V. Nair, Z. R. Hinton, A. Balzer, W. Hu, E. B. Coughlin, K. I. Winey,* M. C. Kozlowski*, *Hydrocarboxylation of C=C bonds in polycyclooctene: Progress toward valorization of waste polyolefins*. Macromolecules **57**, 5860 (2024).
6. A. N. Radzanowski, E. J. Fastow, C.-H. Tu, J. Votruba-Drzal, V. Nair, K. I. Winey*, E. B. Coughlin*. *Tuning alcohol functionalization and presence of unsaturation of PCOE influence thermal, structural, and surface properties*, manuscript submitted to ACS Macro Letters on June 20, 2024.
7. P. M. Jimenez Antenucci, A. N. Radzanowski, E. J. Fastow, J. Votruba-Drzal, M. Redder, K. I. Winey*, E. B. Coughlin*, M. C. Kozlowski. *Impact of mixed 1,2-diol stereochemistry on thermal and morphological properties of regioregular poly(ethylene-co-vinyl alcohol) analogs*, manuscript in preparation.
8. I. M. Ogbu, C.-H. Tu, E. J. Fastow, J. Votruba-Drzal, K. I. Winey, M. Kozlowski*, *N_2O deconstruction of polycyclooctene to generate ketone-functionalized macromonomers*, manuscript submitted to Polymer Degradation and Stability on June 17, 2024.

Publications since July 2022

4. S. Lee, M. Monai, K. Shen, J. Chang, J. M. Vohs*, R. J. Gorte, *A study of how $LaFeO_3$ and $CaTiO_3$ supports affect the oxidation, hydrogenation, and methane steam reforming activity Pt and Ni catalysts*, Journal of Physical Chemistry C **126**, 11619 (2022).
5. S. Lee, K. Shen, C.-Y. Wang, J. M. Vohs*, R. J. Gorte*, *Hydrogenolysis of n-eicosane over Ru-based catalysts in a continuous flow*, Chemical Engineering Journal **456**, 141030, (2023).
6. R. John Chethalen, E. J. Fastow, E. B. Coughlin*, K. I. Winey*, *Thiol–ene click chemistry incorporates hydroxyl functionality on polycyclooctene to tune properties*, ACS Macro Letters **12**, 107 (2023).
7. E. J. Fastow, R. John Chethalen, E. B. Coughlin*, K. I. Winey*, *Thiol-ene click chemistry incorporates carboxylic acid-terminated alkane pendants on polycyclooctene to tune properties*, Giant **17**, 100231 (2024).
8. C.-Y. Wang, B. T. Ferko, Kai Shen, K. I. Winey, J. M. Vohs*, R. J. Gorte*, *Determination of film thicknesses of metal oxides prepared by atomic layer deposition on SBA-15*, Microporous and Mesoporous Materials **366**, 112945 (2024).
9. I. M. Ogbu, E. J. Fastow, W. Zhu, L. A. Wells, R. J. Chethalen, V. Nair, Z. R. Hinton, A. Balzer, W. Hu, E. B. Coughlin, K. I. Winey,* M. C. Kozlowski*, *Hydrocarboxylation of C=C bonds in polycyclooctene: Progress toward valorization of waste polyolefins*. Macromolecules **57**, 5860 (2024).

10. A. Majumder, A. Radzanowski, C.-Y. Wang, Y. Mu, E. B. Coughlin, R. J. Gorte, J. M. Vohs, D. Lee*, *Modulating the contact angle between non-polar polymers and SiO2 nanoparticles*, revised manuscript resubmitted to Macromolecules on July 5, 2024.
11. C.-H. Tu, E. J. Fastow, R. John Chethalen, G. Papamokos, E. B. Coughlin, K. I. Winey*, *Coupling-Decoupling between Fast Stickers and Slow Backbones in Associating Polymers with Side-Chain Terminal-Functionalization*, revised manuscript resubmitted to Macromolecules on July 11, 2024.
12. I. M. Ogbu, C.-H. Tu, E. J. Fastow, J. Votruba-Drzal, K. I. Winey, M. Kozlowski*, *N_2O deconstruction of polycyclooctene to generate ketone-functionalized macromonomers*, manuscript submitted to Polymer Degradation and Stability on June 17, 2024.
13. A. N. Radzanowski, E. J. Fastow, C.-H. Tu, J. Votruba-Drzal, V. Nair, K. I. Winey*, E. B. Coughlin*. *Tuning alcohol functionalization and presence of unsaturation of PCOE influence thermal, structural, and surface properties*, manuscript submitted to ACS Macro Letters on June 20, 2024.

New Horizons In Thermal And Charge Transport In Complex Narrow Gap Semiconductors

Chris Wolverton, Mercouri G. Kanatzidis, Vinayak P. Dravid

Northwestern University, Evanston, IL

Keywords: thermoelectrics, charge transport, thermal transport, narrow gap semiconductors

Research Scope

The intricate relationship between charge and thermal transport in semiconductors underpins numerous energy-related materials and technologies. Thermoelectric (TE) materials exemplify the fusion of conflicting factors governing thermal and charge transport across complex microstructures. TE materials enable the conversion of waste heat to usable energy, enhancing efficiency and impacting energy demand by addressing significant energy loss as heat. However, achieving high efficiency in TE energy conversion remains challenging. Despite significant progress over the past decade, gaps remain in our understanding of the interplay between charge and thermal transport phenomena. This collaborative project aims to address these gaps through cutting-edge theory-experiment investigations of two critical challenges that promise to advance the science of heat-to-electrical power conversion: 1. Exploring phase stability in high-entropy semiconductors (HESs) and investigating how increased configurational entropy affects electron-phonon coupling and electronic band properties. 2. Investigating discordant atoms in diamondoid semiconductors and examining their impact on thermal transport and electronic properties.

Recent Progress

Our initial research effort focuses on HESs formed through extensive multicomponent ion mixing in rock-salt chalcogenide compounds. Rock-salt chalcogenide compounds offer diverse chemistries and transport behaviors due to adaptable cations and anions in their crystal structures, which provides a model system for the investigation on HESs. HESs, with at least five elements in near-equimolar amounts, exhibits significant configurational entropy, which stabilizes novel solid solutions and results in diverse electronic and thermal transport behaviors. Increased configurational entropy is anticipated to reduce thermal conductivity due to heightened scattering, aiming to decouple this from electronic mobility to enhance thermoelectric efficiency. To understand the nature of HESs, techniques like high-angle annular dark-field imaging, energy dispersive spectroscopy, and energy-loss spectroscopy are used to characterize chemical homogeneity, while atomic-resolution imaging and 4D scanning/transmission electron microscopy enable distinguishing structurally similar phases down to the nanoscale. First-principles density functional theory (DFT) calculations investigate the core effects of high entropy alloys, focusing on their stability and thermoelectric performance.

The ongoing research has led to several discoveries on how entropy engineering affects crystal symmetry, subsequently modifying electronic band structure and microstructure for

optimized transport properties. We demonstrated that crystal symmetry breaking induces the formation of strained polar domain structure in high-entropy metal chalcogenide $PbGeSnSe_{1.5}Te_{1.5}$, which suppresses lattice thermal conductivity. Entropy-engineering through alloying AgSbSeTe enables enhancing crystal symmetry, controlling domain formation and improving valley degeneracy, leading to optimized weighted mobility[1]. This strategy can be extended to general IV-VI systems with temperature-dependent phase transitions. For instance, alloying $LiBiTe_2$ with GeSe introduces disordered occupation and increases configurational entropy. [2] Consequently, room-temperature crystal symmetry increased from the *Pnma* to the *R*3*m* space group, resulting in a multi-valley energy-converged valence band of L and Σ bands, significantly enhancing the thermoelectric figure-of-merit in GeSe-based compounds.

These research efforts have highlighted that high-entropy semiconductors represent a potential class of thermoelectric materials and that their transport properties can be rationally modulated.

Building on these findings, our ongoing and future work will further explore the potential of HESs. Considering the enormous composition space associated with HESs, we will utilize high-throughput DFT to search for new alloys, constructing stability maps for various elemental combinations based on the established Open Quantum Materials Database (OQMD). Machine learning will be employed to predict compositions, facilitating efficient and large-scale exploration of HESs, which will provide suitable candidate systems for further experimental investigations. Moreover, we will extend our research efforts to the second proposed theme: investigating the role of discordant atoms in diamondoid semiconductors on phonon transport and electronic structures.

References

1. Liu, Y.; Xie, H.; Li, Z.; Dos Reis, R.; Li, J.; Hu, X.; Meza, P.; Almalki, M.; Snyder, G. J.; Grayson, M. A.; Wolverton, C.; Kanatzidis, M. G.; Dravid, V. P. *Implications and Optimization of Domain Structures in IV–VI High-Entropy Thermoelectric Materials.* J. Am. Chem. Soc. ***146*** (18), 12620-12635 (2024).
2. Dong, J.; Liu, Y.; Li, Z.; Xie, H.; Jiang, Y.; Wang, H.; Tan, X. Y.; Suwardi, A.; Zhou, X.; Li, J.-F.; Wolverton, C.; Dravid, V. P.; Yan, Q.; Kanatzidis, M. G. *High Thermoelectric Performance in Rhombohedral GeSe-$LiBiTe_2$.* J. Am. Chem. Soc. 2024, ***146*** (25), 17355-17364 (2024).

Publications

1. Dong, J.; Hu, L.; Liu, J.; Liu, Y.; Jiang, Y.; Yu, Z.; Tan, X.; Suwardi, A.; Zhang, Q.; Li, Q.; Li, J.-F.; Dravid, V. P.; Yan, Q.; Kanatzidis, M. G. *Off-Centering of Ge Atoms in $GeBi_2Te_4$ and Impact on Thermoelectric Performance. Adv. Funct. Mater.,* ***34***(18), 2314499 (2024).
2. Liu, Y.; Xie, H.; Li, Z.; Dos Reis, R.; Li, J.; Hu, X.; Meza, P.; Almalki, M.; Snyder, G. J.; Grayson, M. A.; Wolverton, C.; Kanatzidis, M. G.; Dravid, V. P. *Implications and Optimization of Domain Structures in IV–VI High-Entropy Thermoelectric Materials.* J. Am. Chem. Soc. ***146*** (18), 12620-12635 (2024).
3. Li, Z.; Pal, K.; Lee, H.; Wolverton, C.; Xia, Y. *Electron–Phonon Interaction Mediated Gigantic Enhancement of Thermoelectric Power Factor Induced by Topological Phase Transition*. Nano letters, ***24***(19), 5816-5823 (2024).
4. Dong, J.; Liu, Y.; Li, Z.; Xie, H.; Jiang, Y.; Wang, H.; Tan, X. Y.; Suwardi, A.; Zhou, X.; Li, J.-F.; Wolverton, C.; Dravid, V. P.; Yan, Q.; Kanatzidis, M. G. *High Thermoelectric Performance in Rhombohedral GeSe-$LiBiTe_2$.* J. Am. Chem. Soc. 2024, ***146*** (25), 17355-17364 (2024).

New Synthetic Approaches Towards Atomically Precise π–d Conjugated Materials

Dianne J. Xiao, Department of Chemistry, University of Washington, Seattle

Keywords: metal–organic frameworks, conjugated materials

Research Scope

Two-dimensional conjugated metal–organic frameworks (MOFs), which are structurally reminiscent of graphene, have attracted significant recent attention due to their potential to host unique reactivity and physical phenomena, as well as by the presence of well-defined porosity, which enables the rapid transport, storage, and conversion of molecular and ionic guests.[1] The objective of our work is to expand the functional and structural scope of π–d conjugated metal–organic materials beyond existing 2D architectures, as well as to better understand their fundamental formation mechanisms. To accomplish this broader goal, three complementary research directions were undertaken over the past two years: 1) establish synthetic routes to dimensionally reduce 2D frameworks to 0D macrocycles; 2) understand how the properties of extended frameworks change as their structures are truncated and confined to nanoscale dimensions; and 3) understand the formation mechanisms of conjugated metal–organic materials.

Recent Progress

There has been rising interest in down-sizing crystalline porous frameworks to the nanoscale, motivated by the inherent processability and mass transport benefits of nanomaterials. Over the past two years, we have developed routes to achieve nanoscale truncation in an *atomically precise* manner. By replacing the tritopic ligands used in the synthesis of 2D MOFs with ditopic analogues, we have been able to halt in-plane polymerization to exclusively obtain discrete macrocycles. Our ditopic ligands can be combined with both metal cations as well as organic building blocks to achieve fully conjugated macrocycles that resemble fragments of semiconducting MOFs and covalent organic frameworks (COFs) (**Fig. 1**).[2,3]

Despite their dramatically truncated structures, our macrocycles preserve many of the desirable properties of 2D MOFs and COFs, including π-stacked nanochannels and good out-of-plane electrical conductivity. For example, copper macrocycles functionalized with short ethoxy side-chains show a pressed pellet conductivity of 10^{-3} S/cm and a CO_2 surface area of ~200 m^2/g.[2]

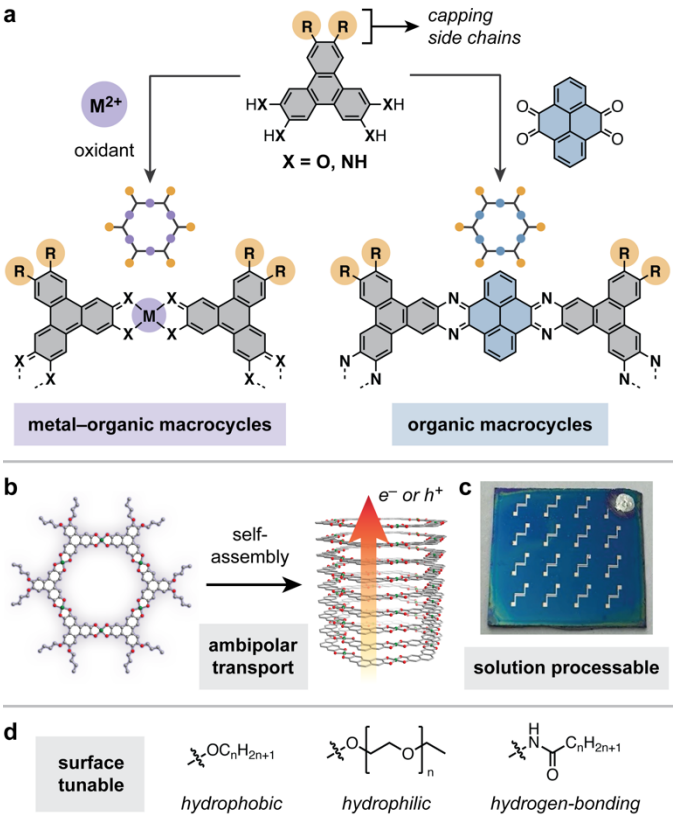

Fig. 1. a) Synthesis, (b) self-assembly, (c) processability and FET device fabrication, and (d) surface tunability of conjugated metal–organic and organic macrocycles.

The molecular nature and nanoscale dimensions of macrocycles provide significant gains in solution processability, surface tunability, and external surface-to-volume ratio. These distinct advantages can be leveraged to introduce new function, facilitate device integration, and overcome transport limitations. For example, copper macrocycles functionalized with long alkyl side chains are fully soluble in organic solvents, enabling the fabrication of thin-film field-effect transistor (FET) devices via straightforward spin-coating methods (**Fig. 1c**). The macrocycles transport both electrons and holes with comparable mobilities of 10^{-3} $cm^2/V{\cdot}s$, a property rarely observed in organic materials. Ongoing work is focused on characterizing thin-film morphology and macrocycle alignment.

Aside from their processability, a second unique advantage of macrocycles is their surface tunability. By altering the side-chain identity, we have been able to create locally hydrophobic, hydrophilic, and hydrogen-bonding environments (**Fig. 1d**). Subtle changes to the macrocycle periphery can lead to profound changes in materials properties and crystal morphology.[4] For example, the electrical conductivity is highly sensitive to peripheral steric bulk, decreasing by three orders of magnitude upon introduction of large neopentyl substituents. Perhaps our most unexpected finding was how dramatically the crystal size increased upon introduction of hydrogen-bonding interactions in the π-stacking direction. Atomic force microscopy (AFM) images of *n*-butoxy substituted copper macrocycles revealed columnar stacks with an average length of only 23(6) nm.[2] In contrast, the amide-functionalized macrocycles crystallize as aggregates of thin microneedles with an average length of ~6(3) μm, more than two orders of magnitude larger.[4] Given the structural similarities between our macrocycles and 2D MOFs, this finding may have implications in the crystallization and growth of 2D frameworks, and work is under way to synthesize stronger hydrogen-bonding motifs. Together, our studies have highlighted how macrocyclic architectures can introduce new function that is not possible in 2D frameworks, as well as serve as model systems to probe out-of-plane charge transport and fundamental formation mechanisms.

References

1. L. S. Xie, G. Skorupskii, M. Dincă, *Electrically Conductive Metal–Organic Frameworks*, Chem. Rev. **120**, 8536 (2020).

2. L. B. Zasada, L. Guio, A. A. Kamin, D. Dhakal, M. Madison, G. T. Seidler, C. K. Luscombe, D. J. Xiao, *Conjugated Metal–Organic Macrocycles: Synthesis, Characterization, and Electrical Conductivity,* J. Am. Chem. Soc. **144**, 4515 (2022).

3. P. H. Le, A. Liu, L. B. Zasada, J. Geary, A. A. Kamin, A. M. Hill, Y. Liu, D. J. Xiao. *Nitrogen-rich conjugated macrocycles: Synthesis, conductivity, and application in electrochemical CO2 capture*, Under review. Preprint DOI: 10.26434/chemrxiv-2023-3ml48.

4. L. B. Zasada, P. H. Le, A. M. Hill, R. T. Shafranek, D. J. Xiao. *Controlling the crystal packing and morphology of metal–organic macrocycles through side-chain modification,* ACS Materials Lett. **6**, 3043 (2024).

Publications

1. L. B. Zasada, L. Guio, A. A. Kamin, D. Dhakal, M. Madison, G. T. Seidler, C. K. Luscombe, D. J. Xiao, *Conjugated Metal–Organic Macrocycles: Synthesis, Characterization, and Electrical Conductivity,* J. Am. Chem. Soc. **144**, 4515 (2022).

2. K. M. Snook, L. B. Zasada, D. Chehada, D. J. Xiao, *Oxidative control over the morphology of $Cu_3(HHTP)_2$, a 2D conductive metal–organic framework*, Chem. Sci. **13**, 10472 (2022).

3. A. A. Kamin, I. P. Moseley, J. Oh, E. J. Brannan, P. M. Gannon, W. Kaminsky, J. M. Zadrozny, D. J. Xiao, *Geometry-dependent valence tautomerism, magnetism, and electrical conductivity in 1D iron–tetraoxolene chains*, Chem. Sci. **14**, 4083 (2023).

4. A. A. Kamin, T. D. Clayton, C. E. Otteson, P. M. Gannon, S. Krajewski, W. Kaminsky, R. Jasti, D. J. Xiao. *Synthesis and metalation of polycatechol nanohoops derived from fluorocycloparaphenylenes,* Chem. Sci. **14**, 9724 (2023).

5. L. B. Zasada, P. H. Le, A. M. Hill, R. T. Shafranek, D. J. Xiao. *Controlling the crystal packing and morphology of metal–organic macrocycles through side-chain modification,* ACS Materials Lett. **6**, 3043 (2024).

6. P. H. Le, A. Liu, L. B. Zasada, J. Geary, A. A. Kamin, A. M. Hill, Y. Liu, D. J. Xiao. *Nitrogen-rich conjugated macrocycles: Synthesis, conductivity, and application in electrochemical CO2 capture*, Under review. Preprint DOI: 10.26434/chemrxiv-2023-3ml48.

Understanding Interfacial Chemistry and Cation Order-Disorder in Mixed-Phase Complex Sodium Metal Oxide Cathodes for Sodium Ion Batteries

Hui (Claire) Xiong (Principal Investigator), Micron School of Materials Science and Engineering, Boise State University

Yan-Yan Hu (Co-Investigator), Department of Chemistry & Biochemistry, The National High Magnetic Field Laboratory, Florida State University

Keywords: Sodium-ion batteries, heterostructures, interface engineering, positive electrode materials, electrochemical energy storage

Research Scope The overarching goal of this project is to test the hypothesis that interfacial properties and cation ordering in intergrown phases play a pivotal role in suppressing detrimental host rearrangement during electrochemical cycling. Therefore, strategically designed intergrown phases can enhance the structural, electrochemical, and mechanical stability of mixed-phase complex sodium metal oxide cathodes for Na-ion storage. Specifically, the *Research Objectives* are to: (1) understand the nucleation and growth of intergrown phases within complex sodium metal oxides (CSMOs) through controls over composition, structure, and synthesis approach; (2) determine the structural, electrochemical, and mechanical stability of intergrown phase interfaces; (3) identify the characteristics of the intergrown phases such as structure, composition, domain size, and microstrain and understand their effects on host rearrangement, defect evolution (e.g., cation ordering), charge transport and transfer; and (4) obtain a mechanistic understanding toward interfacial properties of intergrown phases in mixed-phase CSMOs across different length scales through a holistic experimental and theoretical approach.

Recent Progress

The Role of Li in Intergrown Na-O3/Li-O'3 $Li_xNa_{0.87}Ni_{0.4}Fe_{0.2}Mn_{0.4}O_{2+\delta}$ (LSNFM) We previously reported the influence of intergrown Na-O3 and Li-O'3 structures on the electrochemical behavior of Li-substituted $Li_{0.25}Na_{0.87}Ni_{0.4}Fe_{0.2}Mn_{0.4}O_{2+\delta}$ (LSNFM).[1] Using neutron and synchrotron X-ray diffraction characterization, it is found that the lithium-free material adopts the typical O3 structure (Na-O3). As the Li content increases, an additional Li-rich, distorted O3 (Li-O'3) starts to evolve. Electron microscopy reveals that the Na-O3 and Li-O'3 phases are intergrown at the nanometer scale, which allows for a strong interaction between the phases. Examination by x-ray absorption spectroscopy (XAS) identifies the oxidation state of the transition metals does not change as a function of lithium content, which

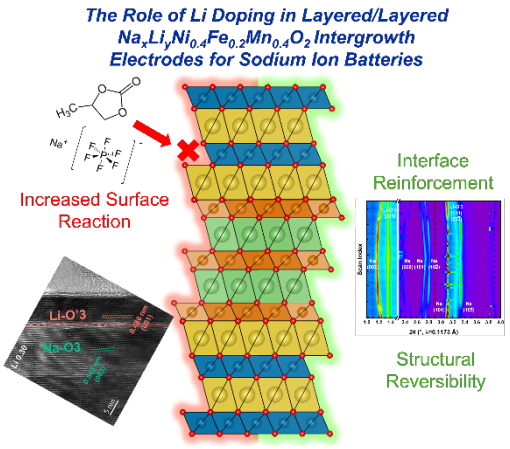

Figure 1. Schematic that represents the role of Li doping in the intergrown $Li_xNa_{0.87}Ni_{0.4}Fe_{0.2}Mn_{0.4}O_{2+\delta}$ (LS-NFM).

implies that the Li and Na within the layered structures predominantly occupy the alkali layers. Further, detailed structure modeling of the extended fine structure region of the XAS spectra identifies that Ni and Fe are concentrated within the Li-O'3 phase. The application of solid-state nuclear magnetic resonance (NMR) reveals an increasing amount of diamagnetic Na species as the Li content increases. The electrochemical properties are systematically investigated to determine the role of the layered/layered intergrowth as a function of Li content. Operando x-ray diffraction identified that the chemomechanical reinforcement of the Na-O3/Li-O'3 intergrowth can suppress the phase transformation that occurs on the initial cycle of the undoped material, leading to improved short-term stability. However, accelerated side-reaction at higher Li contents is identified with high-precision static leakage current measurements. *Ex situ* nuclear magnetic resonance measurements reveal that the instability of the cathode-electrolyte interphase is the primary cause of the side reaction. These **side reactions ultimately dominate the long-term cycling stability of the material, despite the better structural reversibility of the intergrowth structure.** Atomic layer deposition of alumina is shown to provide substantial improvement in the cycling stability, which results from the surface protection provided by the comparatively inert coating. **In this work, we show that while Li doping can promote and modify the intergrowth structure to improve the structural stability during cycling, it results in accelerated parasitic side reaction that dominates the long-term cycle stability (Fig. 1).** While the low level of Li doping provides the best performance among tested materials, further optimization of coatings or electrolyte formation for stable interphase, and the total alkali content and Na/Li ratio might maintain the stable intergrowth structure and better protect the surface by stabilizing the cathode electrolyte interphase (CEI). This class of layered/layered intergrowth electrode materials is a promising avenue for the development of high-performance sodium ion batteries.

Structure-Property Relationship of P2/P3 $Na_xNi_{0.25}Mn_{0.75}O_2$ (NM13) A series of $Na_xNi_{0.25}Mn_{0.75}O_2$ materials were prepared to identify the effect that the sodium content has on the P2/P3 intergrowth structure. The structures with $Na_{0.5}$ (P3-NM13), $Na_{0.6}$ (P2/P3-NM13), and $Na_{0.7}$ (P2-NM13) were all identified by XRD. Over 100 cycles, P2/P3-NM13 maintained a higher capacity than P2-NM13 and a greatly enhanced stability compared to P3-NM13. Operando sXRD of P2-NM13 demonstrated no phase transformation, while P2/P3-NM13 and P3-NM13 exhibit a series of distortions of the P3 phase while the P2 phase is maintained. P3-NM13 suffered from poor rate performance while P2-NM13 displayed a stable rate performance. P2/P3-NM13 exhibited increase rate capabilities than P3-NM13 and maintained a higher capacity than P2-NM13, even at high current rates (5C). Galvanostatic intermittent titration technique (GITT) found that the loss in diffusional capabilities at high- and low-voltages due to P3 structural transitions were significantly suppressed in the P2/P3 intergrowth material when compared to the pure P3 material.

References

1. C. Deng, P. Skinner, Y. Liu, M. Sun, W. Tong, C. Ma, M. Lun Lau, R. Hunt, P. Barnes, J. Xu, H. Xiong. *Li-Substituted Layered Spinel Cathode Material for Sodium Ion Batteries.* Chem. Mater. **30**, 8145-8154 (2018).

Publications

1. J. Park, K. Ku, J. Gim, S.-b. Son, H. Jeong, L. Cheng, H. Iddir, D. Hou, H. Xiong, Y. Liu, E. Lee,* C. Johnson, *Multifunctional Effect of Fe Substitution in Na Layered Cathode Materials for Enhanced Storage Stability*, ACS Appl. Mater. & Interfaces, **15**, 32, 38454–38462, (2023).
2. L. Tao, J. A. Russell, D. Xia, B. Ma, S. Hwang, Z. Yang, A. Hu, Y. Zhang, P. Sittisomwong, D. Yu, P. A. Deck, L. A. Madsen, H. Huang, H. Xiong, P. Bai, K. Xu, F. Lin, *Reversible Switch in Charge Storage Enabled by Selective Ion Transport in Solid Electrolyte Interphase*, *J. Amer. Chem. Soc.*, **145**, 30, 16538–16547, (2023).
3. E. Gabriel, C. Ma, K. Graff, A. Conrado, D. Hou, H. Xiong, *Heterostructure engineering in electrode materials for sodium ion batteries: recent progress and perspectives*, eScience, 100139 (2023).
4. X. Zhou, L. Stan, D. Hou, Y. Jin, H. Xiong, L. Zhu, and Y. Liu, *Operando study of mechanical integrity of high-volume expansion Li-ion battery anode materials coated by Al_2O_3*, Nanotechnology **34**, 235705 (2023).
5. C. Ma, J. Jiang, Y. Fan, X. Li, Z.-F. Ma, H. Ben, and H. Xiong, *Elucidating the Synergic Effect in Nanoscale MoS_2/TiO_2 Heterointerface for Na-ion Storage*, Adv. Sci. 2204837 (2022).
6. C. Wang, A.C. Thenuwara, J. Luo, P.P. Shetty, M.T. McDowell, H. Zhu, S. Posada-Pérez, H. Xiong, G. Hautier & W. Li, *Extending the low-temperature operation of sodium metal batteries combining linear and cyclic ether-based electrolyte solutions*, Nat. Commun. **13**, 4934 (2022).
7. E. Gabriel, D. Hou, E. Lee, and H. Xiong, *Multiphase layered transition metal oxide positive electrodes for sodium ion batteries,* Energy Sci. Eng. **10**, 1672-1705 (2022).
8. D. Hou, E. Gabriel, K. Graff, T. Li, Y. Ren, Z. Wang, Y. Liu, H. Xiong, *Thermal dynamics of P2-$Na_{0.67}Ni_{0.33}Mn_{0.67}O_2$ cathode materials for sodium ion batteries studied by in situ analysis*, J. Mat. Res. **37**, 1156-1163 (2022).

Emerging Properties through Controlled Phase Transformations for High Energy Sodium Ion Batteries

Hui (Claire) Xiong (Principal Investigator), Micron School of Materials Science and Engineering, Boise State University

Wanli Yang (Partner), Advanced Light Source, Lawrence Berkeley National Laboratory

Keywords: Sodium-ion batteries, layered transition metal oxide positive electrode materials, emerging properties, thermal treatment

Research Scope This proposal aims to ***elucidate the emerging properties through controlled phase transformations in layered sodium transition metal oxide (LSTMO) cathode materials for high-energy Na-ion batteries (SIBs).*** The ***research objectives*** are to (1) synthesize P-type Mn-rich LSTMO ($Na_xNi_yMn_{1-y}O_2$, x=0.5-0.7, y=0.33 and 0.25) cathodes with controlled phase transformations during cycling through heat treatment and Li substitution; (2) quantify cationic and oxygen redox reactions through state-of-the-art synchrotron-based soft X-ray spectroscopy; (3) track transition metal (TM) interlayer ordering, migration, and Na^+/vacancy ordering through neutron scattering and advanced analytical electron microscopy; and (4) clarify the fundamental mechanism of oxygen redox and develop design strategy for high energy cathode materials.

Recent Progress

Controlled phase transformation of $Na_{2/3}Ni_{1/3}Mn_{2/3}O_2$ toward stable cycling of layered oxides for sodium ion batteries

We utilized a simple low-temperature heat treatment method to modulate the charge compensation behavior and stabilize the structure of the P2-type $Na_{2/3}Ni_{1/3}Mn_{2/3}O_2$ (NNMO) positive electrodes. The O2-phase formed through desodiation is converted to nanostructured P2 phase (H-P2) after a short heating procedure, which manifests a unique structure with Ni/Na mixed at the interlayer. Strikingly, such a simple treatment process leads to a complete change of the redox behaviors across the whole-voltage-range, with negligible chemical state variations in both the cationic and anionic activities, sharply contrasting the charge compensation mechanism in original NNMO electrodes. This leads to not only inspirations on fundamental viable redox chemistry, but also, the material displays minimal lattice displacement and much improved cycling stability.

Formation of O2-$Ni_{1/3}Mn_{2/3}O_2$ during charging and its thermal stability

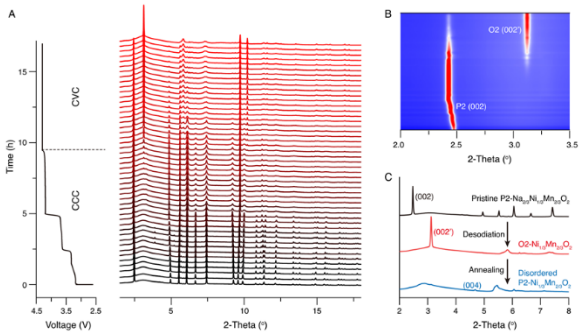

Fig 1. Formation of O2-$Ni_{1/3}Mn_{2/3}O_2$ during charging and its thermal stability. **A**, V-t curve of P-P2 and corresponding operando XRD. **B**, Contour plot highlighting the P2-O2 phase transition in P-P2. **C**, XRD patterns of the $Na_xNi_{1/3}Mn_{2/3}O_2$ at different conditions.

For the layered P2-type $Na_{2/3}Ni_{1/3}Mn_{2/3}O_2$ (NNMO), the P2-O2 transition occurs above 4.2 V. The Na-free O2-$Ni_{1/3}Mn_{2/3}O_2$ structure is metastable as it experiences strong electrostatic repulsion between TMs when Na^+ ions are extracted, which suggests the instability of NNMO at high voltage. Although the O2 to P2 phase transition can be mitigated through different routes, the key to improving the structural stability is to suppress the phase transition at high voltage or even minimize the lattice changes during the whole cycling process. Through a simple heating process on the desodiated O2-$Ni_{1/3}Mn_{2/3}O_2$ structure, we were able to **transform the structure to a nanocrystalline P2 phase, which no longer goes through P2-O2 transition in subsequent cycles and maintains superb structural stability with minimum lattice variation (Fig. 1).**

The Effect of Heat Treatment on Electrochemical Properties in NNMO Electrodes

We conducted galvanostatic charge/discharge cycling in the electrodes. A series of plateaus at different voltage ranges are observed in pristine NNMO (P-P2) during the first cycle, which corresponds to different redox reactions and rearrangement of Na^+/vacancy ordering. When the electrode is charged above ~4.2 V, the phase transition between P2 and O2 occurs, accompanied by anionic redox. The P2–O2 two-phase region contributes around half of the capacity but induces large lattice variations, leading to rapid capacity decay. Upon further cycling, the quick decrease in the ~4.2 V plateau indicates an irreversible structural transition. In the H-P2 electrode, the ~ 4.2 V plateau disappears upon charging, implying the first-order P2-O2 phase transition is suppressed in the H-P2 structure. Compared to P-P2, the H-P2 samples show significant improvement in long-term cycling stability**.**

The Microscopic Structural Difference of P-P2 and H-P2

We further elucidate the microscopic structural difference of P-P2 and H-P2 through high-angle annular dark-field scanning transmission electron microscopy (HAADF-STEM) imaging. The clearly defined bright and dark columns in the P-P2 correspond to atomic columns of Ni-Mn ions and Na ions, which are confirmed in the energy dispersive X-ray spectroscopy (EDS) scans. Compared to P-P2, weaker bright Z-contrast between adjacent TM atomic layers is observed in H-P2, indicating increased cation mixing. By examining the corresponding elemental distribution, it is identified that Mn is mainly concentrated in the TM layer, while Ni can be found in both TM and Na layers. This indicates the Ni migration to the Na layer in the H-P2 sample.

References

1. Dai, K. *et al. Negligible voltage hysteresis with strong anionic redox in conventional battery electrode*. Nano Energy, **74**, 104831 (2020).

Publications

9. E. Gabriel, Z. Wang, V. V. Singh, K. Graff, J. Liu, C. Koroni, D. Hou, D. Schwartz, C. Li, J. Liu, X. Guo, N. C. Osti, S. P. Ong, H. Xiong, *Influence of Interlayer Cation Ordering on Na Transport in P2-type* $Na_{0.67-x}Li_y\ Ni_{0.33-z}Mn_{0.67+z}O_2$ *for Sodium-Ion Batteries* (Front Cover), *J. Amer. Chem. Soc.*, **146**, 22, 15108–15118 (2024).

A New Paradigm for Water Splitting in Layered Materials by Modulation of Catalyst Oxidation State

Michael J. Zdilla and Eric Borguet, Temple University

John P. Perdew, Tulane University

Keywords: List up to 5 keywords using this font (Calibri 12 pt)

Heterogeneous catalysis, layered materials, Scanning Tunneling Spectroscopy, Density Functional Theory

Research Scope

Heterogenous redox catalysis is a cornerstone of industrial chemistry and energy science, though much development of heterogenous catalysts is achieved through serendipity and trial and error. Rare insights into the underlying electronic-structure basis for heterogeneous redox catalysis can serve to advance the field rapidly by informing design and narrowing elemental and structural space to be searched. Among the most important reactions to future energy supplies and industrial chemistry is water splitting, which requires catalysts or electrocatalysts that operate near the thermodynamic potentials for the hydrogen evolution reaction (HER) and oxygen evolution reaction (OER). For low-cost first-row transition metal (hydr)oxide catalysts, a unifying feature of high-performance catalysts is an unequally populated eg^1 electronic state on the metal ion, such as Mn^{III}, Co^{II}, and Ni^{III}(Figure).(*11*) Numerous explanations(*1, 3, 5-8*) have been offered, each of which presumes that the higher the density of these states, the more effective the catalysis.

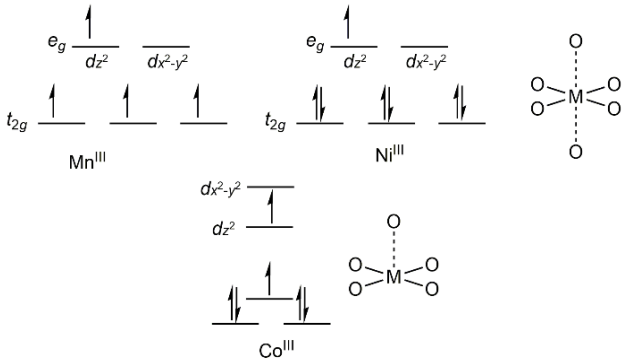

Figure. *d*-orbital splittings demonstrating the partial occupation of the e_g orbitals (dz^2, but not dx^2-y^2) in Mn^{III},(*1-8*) Co^{III},(*1, 9*) and Ni^{III}.(*10*)

We have recently discovered a phenomenon in layered manganese oxide OER catalyst materials that demonstrates that this previously held assumption about eg^1 states is false: that it is not the density of eg^1 states, but the periodic distribution of these states that gives the best catalysts. In layered catalysts, this is manifest in alternating structures where eg^1-rich layers are adjacent to eg^1-poor layers. The alternating presence and absence of these states in adjacent layers yields catalysts superior to systems of eg^1-rich manganese ions.

In this proposal we build on this finding and present preliminary results on other metal-based systems (Co and Ni) that demonstrate that this is not a phenomenon isolated to manganese, but that rather a paradigm across materials. We propose to elucidate the electronic structure basis for the activity in these new Co and Ni catalysts by a combined experimental and theoretical examination of density of states (DOS) using scanning tunneling spectroscopy (STS) and quantum

mechanical calculations (mostly density functional theory, DFT) respectively. We will widen the scope of the chemistry to include a newer class of layered materials: the layered double hydroxides (LDH) which are already excellent OER catalysts and enhance them by the use of our alternating high-low oxidation state layering strategy. We will examine DOS using STS and DFT, and prepare few-layer catalysts on electrode substrates (fluorine-doped tin oxide, FTO), and demonstrate the electrocatalytic performance of these materials. Finally, we will expand the study to a different reaction, HER, using related LDH materials for reduction of protons to H2. These will also be studied by DFT, STS, and electrocatalytic evaluation

Recent Progress

We have completed our first suite of measurements on modulated Co^{II}/Co^{III}, Ni^{II}/Ni^{III}, and Co^{II}/Ni^{II} materials with layer-by-layer modulation and associated control experiments. All three systems show an improvement in catalytic activity in the system with alternating layered structures. We have submitted a revised manuscript to *ACS Catalysis*. From the theoretical perspective, a new student has successfully reproduced the computations on our Mn^{III}/Mn^{IV} system and has completed an extensive study on Ni^{II}/Ni^{III} Ni^{III}/Ni^{IV} and Co^{II}/Co^{III} system for optimization of computational methods for DOS determinations. This has been submitted as a manuscript to *Phys. Rev. Mater.* These methods will also constitute papers to be submitted in the coming year on oxidation state modulation of catlysts in $KCoO_2$ and $KNiO_2$ based layered materials.

Extension and generalization of paradigm to other materials - enhancement of layered double hydroxide (LDH) OER catalysts by potential steps. So far we have a suite of data on variable compositions of NiFe and CoFe LDH in pure form and as layer-mixed materials. So far, we have not identified enhancement of catalysis by layer-by-layer modulation. Computational studies on these materials are underway, and we are working to understand the electronic-structure origins of this divergent behavior from the layered metal oxide materials.

We have obtained and cleaned the gold substrates for STM analysis and confirmed their stability over time using STM/STS. Next steps are to drop cast bilayers of Co and Ni oxides for the measurement of density of states for comparison to those calculated in Objective 1A.

Two additional papers with ancillary relationship to our proposal—and worked on by our students—have been submitted or published. First, a paper on the use of layered manganese dioxide (birnessite) and cobalt-dopped birnessite as precatalysts for Fischer Tropsch catalysis has been published in *ACS Omega.* Second, a manuscript on the effect of strain on bandgap in MoS_2 is in preparation for *Phys. Rev. Mater.*

References

1. U. Maitra, B. S. Naidu, A. Govindaraj, C. N. R. Rao, Importance of trivalency and the eg1 configuration in the photocatalytic oxidation of water by Mn and Co oxides. *Proceedings of the National Academy of Sciences* **110**, 11704-11707 (2013).
2. Z. Morgan Chan *et al.*, Electrochemical trapping of metastable Mn3+ ions for activation of MnO2 oxygen evolution catalysts. *Proceedings of the National Academy of Sciences* **115**, E5261 (2018).
3. P. F. Smith *et al.*, Coordination Geometry and Oxidation State Requirements of Corner-Sharing MnO6 Octahedra for Water Oxidation Catalysis: An Investigation of Manganite (γ-MnOOH). *ACS Catalysis* **6**, 2089-2099 (2016).
4. Y. Gorlin, T. F. Jaramillo, A Bifunctional Nonprecious Metal Catalyst for Oxygen Reduction and Water Oxidation. *J. Am. Chem. Soc.* **132**, 13612-13614 (2010).
5. C. W. Cady *et al.*, Tuning the Electrocatalytic Water Oxidation Properties of AB2O4 Spinel Nanocrystals: A (Li, Mg, Zn) and B (Mn, Co) Site Variants of LiMn2O4. *ACS Catalysis* **5**, 3403-3410 (2015).
6. D. M. Robinson *et al.*, Photochemical Water Oxidation by Crystalline Polymorphs of Manganese Oxides: Structural Requirements for Catalysis. *J. Am. Chem. Soc.* **135**, 3494-3501 (2013).
7. N. Birkner *et al.*, Energetic basis of catalytic activity of layered nanophase calcium manganese oxides for water oxidation. *Proceedings of the National Academy of Sciences* **110**, 8801-8806 (2013).
8. K. P. Lucht, J. L. Mendoza-Cortes, Birnessite: A Layered Manganese Oxide To Capture Sunlight for Water-Splitting Catalysis. *Journal of Physical Chemistry C* **119**, 22838-22846 (2015).
9. S. Levasseur *et al.*, Oxygen Vacancies and Intermediate Spin Trivalent Cobalt Ions in Lithium-Overstoichiometric LiCoO2. *Chem. Mater.* **15**, 348-354 (2003).
10. L.-F. Li, Y.-F. Li, Z.-P. Liu, Oxygen Evolution Activity on NiOOH Catalysts: Four-Coordinated Ni Cation as the Active Site and the Hydroperoxide Mechanism. *ACS Catalysis* **10**, 2581-2590 (2020).
11. E. Fabbri, A. Habereder, K. Waltar, R. Kötz, T. J. Schmidt, Developments and perspectives of oxide-based catalysts for the oxygen evolution reaction. *Catalysis Science & Technology* **4**, 3800-3821 (2014).

Publications

5. R. K. Bhullar, W. Xu, M. J. Zdilla. Hydrocarbon formation from syngas with in-operando monitoring of cobalt- and manganese-based (pre)catalysts using X-ray diffraction. *ACS Omega* **2024**, 9, 29917–29927.
6. R. Ding, D. Maldonado-Lopez, J. Mendoza-Cortes, J. E. Henebry, M. J. Zdilla, Enhanced activity in layered-metal-oxide-based oxygen evolution catalysts by layer-by-layer modulation of metal ion identity. *ACS Catal*. Under Revision.
7. R. K. Sah, M. J. Zdilla, E. Borguet., J. P. Perdew. Meta-GGAs vs. Hybrid Functionals for Point Defects: The Best of Both Worlds Applied to Layered MnO_2, NiO_2 and $KCoO_2$. *Phys. Rev. Mater.* Submitted. arXiv:2404.14317
8. R. K. Sah, J. P. Perdew. Effect of Strain on the Band Gap of Monolayer MoS2. *Phys. Rev. Mater.* In preparation.

Intrinsically Porous Polyoxometalate-Based Frameworks for Critical Metal Recovery

Zhonghua Peng,[1] Praveen Thallapally,[2] and Mohammadreza Momenitaheri[1]

[1]University of Missouri-Kansas City, [2]Pacific Northwest National Laboratory

Keywords: donut-shaped polyoxometalates, porous frameworks, adsorbents, critical metal recovery

Research Scope

The project's overall objective is to develop polyoxometalate (POM) molecular clusters and POM-derived frameworks (POMFs) with precisely controllable pore and chemical environments for selective and efficient capture and subsequent electrochemically or photochemically triggered release of targeted critical metal ions from saline sources. To limit the research scope, the project will explore POMs and POMFs that selectively recover Li^+ and two rare earth elements (REEs), Ce^{3+} and Eu^{3+}, representing light and middle REEs, respectively. The project combines data science and theoretical and experimental studies to gain a fundamental understanding of the interactions between porous POMs/POMFs and metal ions in aqueous saline solutions. Since the hydrated ionic sizes of the three targeted critical metal ions are in the 1 to 4 Å range,[1] the proposed work scope will focus on POM clusters and POM-based frameworks with pore sizes smaller than 10 Å. More specifically, two types of POMs with accessible intrinsic pores, namely doughnut-shaped POMs (ds-POMs) - the Preyssler anion (PA) $\{P_5W_{30}\}$ family[2] and the $\{P_8W_{48}\}$ series[3] – and their assembled POMFs will be systematically studied both experimentally and theoretically on their binding properties with the three metal ions under different POM reduction conditions. The specific objectives of the proposed project are 1) theoretical exploration that combines data science and molecular modeling to predict the most promising ds-POMs and POMFs for each targeted metal ion and to understand the contributing factors underlining the binding selectivity, capacity, and kinetics. 2) Experimental preparation and structural characterization of ds-POMs predicted by theoretical studies. 3) Design and synthesize POM-derived porous frameworks (POMFs) using ds-POMs as the building blocks or POM precursors as starting clusters, with or without the incorporation of interpenetrating polymers. 4) Physical property studies of the prepared POMs and POMFs, including hydrolytic stability studies under different pH, salt (NaCl) concentration and temperature, thermal stability, and electrochemistry. 5) Systematic and quantitative adsorption (selectivity, capacity, efficiency, adsorption energy, and rate) and desorption (efficiency and rate) studies of ds-POMs and POMFs under different extents of POM reductions.

Recent Progress

The proposed project encompasses theoretical prediction, materials preparation, and adsorption evaluation. During the past year, research efforts have therefore been directed towards 1) theoretical electronic structure calculations and classical and quantum molecular dynamic

simulations of ds-POMs in aqueous solutions, 2) Experimental preparation and structural characterization of ds-POMs (including metal-free PA) and POMFs. 3) Physical property studies of the prepared POMs and POMFs. Specific research progress includes:

1) A highly parallelized general-purpose software platform coined DL_POLY Quantum 2.0 for predictive classical and quantum molecular dynamic simulations in condensed phases has been developed.[4] This open-source software infrastructure, freely available to the scientific community, will be used for some of the proposed theoretical studies on structural, thermodynamic, dynamical, and spectroscopic properties of different considered POMs and POMFs in aqueous solutions of the targeted critical metal ions.

2) *Ab initio* molecular dynamic (AIMD) simulations were performed on PA with centrally encapsulated Na^+-H_2O, 14 Na^+ ions and 149 water molecules randomly added (using PACKMOL[5]) to the exterior of PA. Our calculated W-O_{PA} (oxygen of PA), Na-O_{PA}, and Na-O_W (oxygen of water) radial distribution functions (RDFs) agree very well with those of the experiment,[6] validating the level of theory employed. Theoretical simulations to calculate the free energy of the adsorption/desorption of the targeted ions on the outside vs. inside of the PA's internal cavity were carried out. Here, bias potentials were added within the context of the (well-tempered) meta-dynamics to simulate this adsorption/desorption process and calculate the free energy changes along the defined collective variable (CV) coordinates. The free energy barrier for exiting the Na^+ ion is estimated to be 41.1 kcal/mol, which agrees well with the reported value of 39.4 kcal/mol.[6]

3) Metal-free PA was synthesized by trapping the cation (Ag^+) through precipitation. Specifically, the Na^+ sitting in the doughnut hole of the parent PA was first exchanged by Ag^+ to realize the [Ag^+-PA]: $K_{14}[AgP_5W_{30}]$.[7] The counter cations (K^+) were then replaced by H^+ through an acidic resin to give $H_{14}[AgP_5W_{30}]$. The Ag^+ in the pore was then captured by Br^- as AgBr precipitates under hydrothermal conditions. The metal-free PA was confirmed by ^{31}P NMR, and efforts are being made to grow single crystals for crystal structure determination.

4) The parent $\{P_8W_{48}\}$ anion with a molecular formula $K_{28}Li_5H_7[P_8W_{48}O_{184}]\cdot xH_2O$ has been prepared. The synthesis involved a simple assembly approach using hexalacunary tungstophosphate $K_{12}[H_2P_2W_{12}O_{48}]$ as the building block and reacting it with glacial acetic acid, LiOH, and LiCl in DI water at room temperature. Exchanging external metal ions with tetrabutylammonium (TBA) cations led to its water-insoluble analog TBA-P_8W_{48}.

5) Using heptamolybdate as the starting cluster, Mo-V-based POMFs have been prepared, which are known to possess open channels with a 4 Å aperture diameter.[8] We have attempted to modify the pore sizes of the resulting POMFs by varying the Mo/V ratios of the starting materials. Mo/V feeding ratios of 8:1, 16:3, 4:1, 3:1 and 2:1 have been explored. Increasing Mo/V ratios decreased the product yield. Mo/V ratios of 4:1 and 3:1 resulted in Mo-V oxides with the orthorhombic structure, while the 2:1 ratio led to the trigonal structure.

References

1. P. D'Angelo, A. Zitolo, V. Migliorati, G. Chillemi, M. Duvail, P. Vitorge, S. Abadie, R. Spezia, *Revised Ionic Radii of Lanthanoid(III) Ions in Aqueous Solution*. Inorg. Chem. **50** (10), 4572-4579 (2011).
2. M. H. Alizadeh, S. P. Harmalker, Y. Jeannin, J. Martin-Frère, M. T. Pope, *A heteropolyanion with fivefold molecular symmetry that contains a nonlabile encapsulated sodium ion. The structure and chemistry of* $[NaP_5W_{30}O_{110}]^{14-}$. J. Am. Chem. Soc. **107**, 2662-2669 (1985).
3. S. Sasaki, K. Yonesato, N. Mizuno, K. Yamaguchi, K. Suzuki, *Ring-Shaped Polyoxometalates Possessing Multiple 3d Metal Cation Sites:*$[\{M_2(OH_2)_2\}_2\{M(OH_2)_2\}_4P_8W_{48}O_{176}(OCH_3)_8]^{16-}$(M= Mn, Co, Ni, Cu, Zn). Inorg. Chem. ***58***(12), 7722-7729 (2019).
4. N. London, D. K. Limbu, M. R. Momeni, F. A. Shakib, *DL_POLY Quantum 2.0: A Modular General-Purpose Software for Advanced Path Integral Simulations*. J. Chem. Phys. **160**, 132501 (2024).
5. L. Martinez, R. Andrade, E. G. Birgin, EJ. M. Martinez, *PACKMOL: A Package for Building Initial Configurations for Molecular Dynamics Simulations*. *J. Comput. Chem.* **30**, 2157-2164 (2009).
6. X. A. Fernandez, X. Lopez, C. Bo, C. de Graaf, E. J. Baerends, J. M. Poblet, *Polyoxometalates with Internal Cavities: Redox Activity, Basicity, and Cation Encapsulation in* $[X^{n+}P_5W_{30}O_{110}]^{(15-n)-}$ *Preyssler Complexes, with* $X = Na^+, Ca^{2+}, Y^{3+}, La^{3+}, Ce^{3+}$, *and* Th^{4+}. J. Am. Chem. Soc. **129**, 12244-12253 (2007).
7. J. Du, M.-D. Cao, S.-L. Feng, F. Su, X.-J. Sang, L.-C. Zhang, W.-S. You, M. Yang, Z.-M. Zhu, *Two New Preyssler-Type Polyoxometalate-Based Coordination Polymers and Their Application in Horseradish Peroxidase Immobilization*. Chem. Enr. J. **23**, 14614-14622 (2017).
8. M. Sadakane, K. Kodato, T. Kuranishi, Y. Nodasaka, K. Sugawara, N. Sakaguchi, T. Nagai, Y. Matsui, Y. Uedaet, *Molybdenum–Vanadium-Based Molecular Sieves with Microchannels of Seven-Membered Rings of Corner-Sharing Metal Oxide Octahedra*. Angew. Chem. Int. Ed. **47**, 2493 (2008).

Publications

None yet

Uncovering the mechano-electro-chemo mechanism of fresh Li in sulfide based all solid-state batteries through operando studies

Hongli Zhu, Department of Mechanical and Industrial Engineering, Northeastern University

Keywords: All solid state batteries, Fresh Li, In operando studies, Nucleation, Mechano-electro-chemo mechanism

Research Scope

1. Task 1 Investigation of the atomic structure, interatomic bonding, and crystalline structure of the fresh Li
   - Subtask 1.1 Ex situ Cryo-EM characterizing the nuclear structure of Li metal
   - Subtask 1.2 Phase diagram study of Li metal through experimental method
2. Task 2 Investigation of Li metal atomic structure-mechanical behavior correlation during electrochemical plating and stripping
   - In situ electrochemical atomic force microscopy investigating the mechanical properties of the fresh Li metal.
3. Task 3 Strategies to stabilize the Li metal in sulfide based all solid state batteries through coupling mechanical and electrochemical mechanisms
   - Subtask 3.1 Investigation of the fresh Li effect on the Li dendrite formation and soft short in all solid-state batteries
   - Subtask 3.2 Nondestructively visualizing and understanding "Soft Short" and Li creeping in All-solid-state Lithium-Metal batteries through neutron imaging

Recent Progress

This study investigated the morphology of fresh lithium plating and stripping on different current collectors (copper, nickel, and gold) using cryo-EM and SEM-EDX techniques. The research found that Ni and Au current collectors promote more uniform Li deposition compared to Cu, likely due to their higher work function and more compatible lattice structure. Higher current densities (0.25C vs 0.04C) resulted in more irregular and dendritic structures. SEM-EDX mapping revealed a significant presence of chlorine on the plated Li surface, forming localized patches or clusters. Additionally, the study explored the effect of silver particles and film on lithium nucleation and growth using neutron imaging and nano-CT. While neutron imaging showed clear lithiation/delithiation processes on the cathode side, nano-CT revealed that Ag particles act as nucleation sites for Li deposition, creating a composite Ag-Li anode, whereas Ag film provided a more uniform surface for Li deposition. These findings contribute to understanding the complex interplay between current collector materials, plating conditions, and Li morphology in battery anodes, which is crucial for developing high-performance, stable, and safe Li metal batteries.

In another study, we investigated Li dynamics in a graphite interlayer, a typical mixed ionic-electronic conductor (MIEC), using operando neutron imaging and Raman spectroscopy. Our findings revealed that intercalation-extrusion-dominated mechanochemical reactions during cell assembly transform graphite into a Li-graphite interlayer consisting of solid electrolyte (SE), Li^0, and graphite-intercalation compounds. During charging, Li^+ preferentially deposited at the Li-graphite|SE interface. Further plating led to Li^0-dendrite formation, inducing short circuits and

reverse migration of Li^0, Figure 1. Modeling indicates that the interface has the lowest nucleation barrier, governing lithium transport paths. Our study elucidates intricate mechano-chemo electrochemical processes in mixed conducting interlayers. The behavior of Li^+ and Li^0 in the interlayer is governed by multiple competing factors.

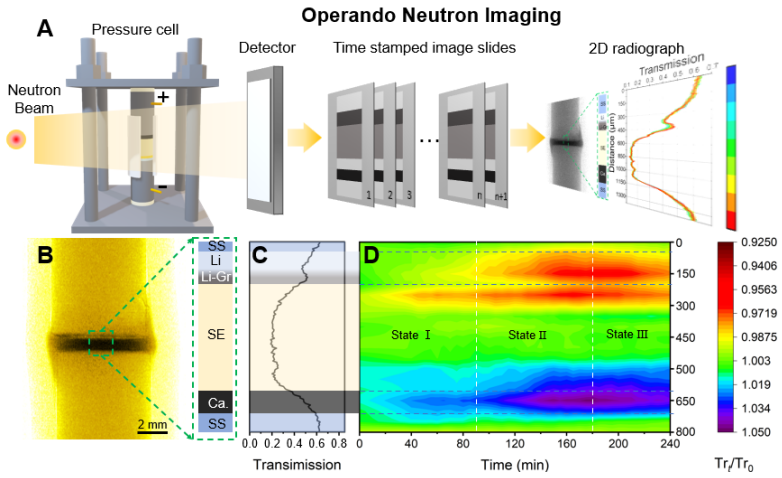

Figure 1: (A) Schematic of the operando neutron imaging. (B) Normalized neutron radiography image of the ASLMB to identify each component based on the neutron attenuation differentiation. The inset schematic displays the cell configuration. (C) Quantified neutron transmission in the labeled region along the cross section of the ASLMB. The inset schematic assigns the neutron transmission to different components. (D) Dynamic transmission evolution during charging. The green, warm, and cold colors represent no obvious changes, enriched Li, and Li depletion, respectively, compared to the pristine state.

In another work, We used the operando neutron imaging and X-ray computed tomography (XCT) to nondestructively visualize Li behaviors within ASLMBs. This approach offers real-time observations of Li evolutions, both pre- and post-occurrence of a "soft short". The coordination of 2D neutron radiography and 3D neutron tomography enables charting of the terrain of Li metal deformation operando. Concurrently, XCT offers a 3D insight into the internal structure of the battery following a "soft short". Despite the manifestation of a "soft short", the persistence of Faradaic processes is observed. To study the elusive "soft short", phase field modeling was coupled with electrochemistry and solid mechanics theory. The research unravels how external pressure curbs dendrite growth, potentially leading to dendrite fractures and thus uncovering the origins of both "soft" and "hard" shorts in ASLMBs. [1]

Future Plans

Building on our current findings, we propose a comprehensive research plan to further optimize Li metal anodes. We will start by developing quantitative image analysis algorithms to precisely characterize Li morphology across different conditions. Concurrently, we'll design an in-situ cryo-EM setup for real-time observation of Li plating/stripping, correlated with electrochemical measurements. We'll explore surface modifications of Cu current collectors and investigate alloy alternatives to improve Li deposition uniformity. Electrolyte engineering will focus on understanding and controlling the Cl-rich SEI formation, including testing new additives. For Ag-Li composite anodes, we'll optimize Ag particle characteristics and assess long-term cycling stability. Additionally, we will perform pressurized DSC and in operando electrochemical AFM studies on fresh Li to gain deeper insights into its thermal behavior and surface dynamics.

References

1 Cao, D. et al. Nondestructively Visualizing and Understanding the Mechano-Electrochemical Origins of “Soft Short” and “Creeping” in All-Solid-State Batteries. Advanced Functional Materials 33, 2307998, doi:https://doi.org/10.1002/adfm.202307998 (2023).

Publications

1 Cao, D. et al. Li Dynamics in Mixed Ionic-Electronic Conducting Interlayer of All-Solid-State Li-metal Batteries. Nano Letters 24, 1544-1552, doi:10.1021/acs.nanolett.3c04072 (2024).
2 Cao, D., Zhang, Y., Ji, T. & Zhu, H. In operando neutron imaging characterizations of all-solid-state batteries. MRS Bulletin 48, 1257-1268, doi:10.1557/s43577-023-00611-7 (2023).
3 Wang, H., Ozkan, C. S., Zhu, H. & Li, X. Advances in solid-state batteries: Materials, interfaces, characterizations, and devices. MRS Bulletin 48, 1221-1229, doi:10.1557/s43577-023-00649-7 (2023).
4 Cao, D. et al. Enhancing Lithium Stripping Efficiency in Anode-Free Solid-State Batteries through Self-Regulated Internal Pressure. Nano Letters, doi:10.1021/acs.nanolett.3c02713 (2023).

Author
Index